USGS
science for a changing world

Prepared in cooperation with the St. Johns River Water Management District,
South Florida Water Management District, and Southwest Florida Water Management District

Groundwater Flow and Water Budget in the Surficial and Floridan Aquifer Systems in East-Central Florida

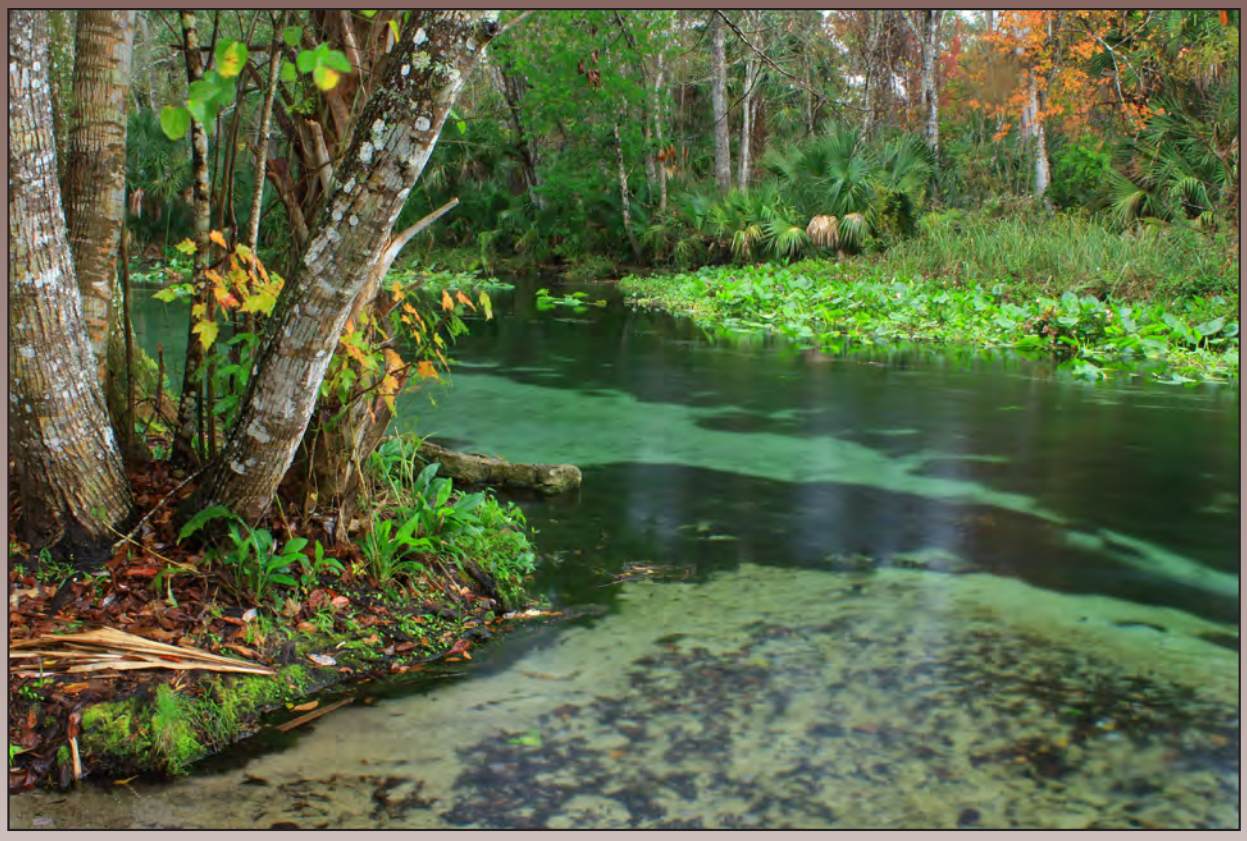

Scientific Investigations Report 2012–5161

U.S. Department of the Interior
U.S. Geological Survey

Cover. Wekiva River, Wekiwa Springs State Park, Orange and Seminole Counties, Florida. Photograph by Alan M. Cressler, USGS. Used with permission.

Groundwater Flow and Water Budget in the Surficial and Floridan Aquifer Systems in East-Central Florida

By Nicasio Sepúlveda, Claire R. Tiedeman, Andrew M. O'Reilly, Jeffrey B. Davis, and Patrick Burger

Prepared in cooperation with the St. Johns River Water Management District, South Florida Water Management District, and Southwest Florida Water Management District

Scientific Investigations Report 2012–5161

U.S. Department of the Interior
U.S. Geological Survey

U.S. Department of the Interior
KEN SALAZAR, Secretary

U.S. Geological Survey
Marcia K. McNutt, Director

U.S. Geological Survey, Reston, Virginia: 2012

Suggested citation:
Sepúlveda, Nicasio, Tiedeman, C.R., O'Reilly, A.M., Davis, J.B., and Burger, Patrick, 2012, Groundwater flow and water budget in the surficial and Floridan aquifer systems in east-central Florida: U.S. Geological Survey Scientific Investigations report 2012–5161, 214 p.

Acknowledgments

The authors want to express the most sincere gratitude to Wei Jin (St. Johns River Water Management District) for executing alternate parameter estimation runs in the St. Johns River Water Management District computer facilities.

The water-use data from Jill Hood (Southwest Florida Water Management District) and the stream network of the upper St. Johns River from Tom Jobes (St. Johns River Water Management District) are greatly appreciated as well as the expertise provided by hydrologists Brian McGurk (St. Johns River Water Management District), and Ron Basso and Mark Barcelo (Southwest Florida Water Management District) that helped improve the understanding of the flow system in east-central Florida.

Contents

Figures

Tables

Conversion Factors and Abbreviations

Inch/Pound to SI

Multiply	By	To obtain
	Length	
inch (in.)	2.54	centimeter (cm)
inch (in.)	25.4	millimeter (mm)
foot (ft)	0.3048	meter (m)
mile (mi)	1.609	kilometer (km)
	Area	
square mile (mi^2)	2.590	square kilometer (km^2)
	Volume	
gallon (gal)	0.003785	cubic meter (m^3)
million gallons (Mgal)	3,785	cubic meter (m^3)
	Flow rate	
cubic foot per second (ft^3/s)	0.02832	cubic meter per second (m^3/s)
gallon per day (gal/d)	0.003785	cubic meter per day (m^3/d)
million gallons per day (Mgal/d)	0.04381	cubic meter per second (m^3/s)
Recharge, evapotranspiration, and water exchange		
inch per year (in/yr)	25.4	millimeter per year (mm/yr)
Hydraulic conductivity		
foot per day (ft/d)	0.3048	meter per day (m/d)
	Leakance	
foot per day per foot [(ft/d)/ft]	1	meter per day per meter
inch per year per foot [(in/yr)/ft]	83.33	millimeter per year per meter [(mm/yr)/m]

Temperature in degrees Celsius (°C) may be converted to degrees Fahrenheit (°F) as follows:

$°F = (1.8 \times °C) + 32$

Temperature in degrees Fahrenheit (°F) may be converted to degrees Celsius (°C) as follows:

$°C = (°F - 32)/1.8$

Vertical coordinate information is referenced to the National Geodetic Vertical Datum of 1929 (NGVD 29).

Horizontal coordinate information is referenced to the North American Datum of 1983 (NAD 83).

Altitude, as used in this report, refers to distance above the vertical datum.

Concentrations of chemical constituents in water are given in milligrams per liter (mg/L).

Abbreviations

AFSIRS	Agricultural Field Scale Irrigation Requirement Simulation
APPZ	Avon Park permeable zone
CFCA	Central Florida Coordination Area
CFWI	Central Florida Water Initiative
DEM	digital elevation model
DWRM	District Wide Regional Model
ECFT	East-Central Florida Transient
ET	evapotranspiration
FAS	Floridan aquifer system
FDEP	Florida Department of Environmental Protection
GAI	Green-Ampt infiltration
GHB	General head boundary (MODFLOW-2005 Package)
GIS	geographical information system
GOES	Geostationary Operational Environmental Satellite
IAS	intermediate aquifer system
ICU	intermediate confining unit
LAK	Lake (MODFLOW-2005 Package)
LFA	Lower Floridan aquifer
MCU	middle confining unit
MOR	Monthly Operating Report
NEXRAD	Next Generation Weather Radar
NOAA	National Oceanic and Atmospheric Administration
OLPZ	Ocala low-permeable zone
OMR	overall mean residual
OPZ	Ocala permeable zone
RIB	rapid infiltration basin
RMSR	root-mean-square residual
ROMP	Regional Observation and Monitor-well Program
SAS	surficial aquifer system
SFR	Streamflow-Routing (MODFLOW-2005 Package)
SFWMD	South Florida Water Management District
SJRWMD	St. Johns River Water Management District
SWFWMD	Southwest Florida Water Management District
UFA	Upper Floridan aquifer
USGS	U.S. Geological Survey
UTM	Universal Transverse Mercator
UZF	Unsaturated zone flow (MODFLOW-2005 Package)

Groundwater Flow and Water Budget in the Surficial and Floridan Aquifer Systems in East-Central Florida

By Nicasio Sepúlveda[1], Claire R. Tiedeman[1], Andrew M. O'Reilly[1], Jeffrey B. Davis[2], and Patrick Burger[2]

Abstract

A numerical transient model of the surficial and Floridan aquifer systems in east-central Florida was developed to (1) increase the understanding of water exchanges between the surficial and the Floridan aquifer systems, (2) assess the recharge rates to the surficial aquifer system from infiltration through the unsaturated zone, and (3) obtain a simulation tool that could be used by water-resource managers to assess the impact of changes in groundwater withdrawals on spring flows and on the potentiometric surfaces of the hydrogeologic units composing the Floridan aquifer system. The hydrogeology of east-central Florida was evaluated and used to develop and calibrate the groundwater flow model, which simulates the regional fresh groundwater flow system.

The U.S. Geological Survey three-dimensional groundwater flow model, MODFLOW-2005, was used to simulate transient groundwater flow in the surficial, intermediate, and Floridan aquifer systems from 1995 to 2006. The East-Central Florida Transient model encompasses an actively simulated area of about 9,000 square miles. Although the model includes surficial processes—rainfall, irrigation, evapotranspiration (ET), runoff, infiltration, lake water levels, and stream water levels and flows—its primary purpose is to characterize and refine the understanding of groundwater flow in the Floridan aquifer system. Model-independent estimates of the partitioning of rainfall into ET, streamflow, and aquifer recharge are provided from a water-budget analysis of the surficial aquifer system. The interaction of the groundwater flow system with the surface environment was simulated using the Green-Ampt infiltration method and the MODFLOW-2005 Unsaturated-Zone Flow, Lake, and Streamflow-Routing Packages.

The model is intended to simulate the part of the groundwater system that contains freshwater. The bottom and lateral boundaries of the model were established at the estimated depths where the chloride concentration is 5,000 milligrams per liter in the Floridan aquifer system. Potential flow across the interface represented by this chloride concentration is simulated by the General Head Boundary Package. During 1995 through 2006, there were no major groundwater withdrawals near the freshwater and saline-water interface, making the general head boundary a suitable feature to estimate flow through the interface.

The east-central Florida transient model was calibrated using the inverse parameter estimation code, PEST. Steady-state models for 1999 and 2003 were developed to estimate hydraulic conductivity (K) using average annual heads and spring flows as observations. The spatial variation of K was represented using zones of constant values in some layers, and pilot points in other layers. Estimated K values were within one order of magnitude of aquifer performance test data. A simulation of the final two years (2005–2006) of the 12-year model, with the K estimates from the steady-state calibration, was used to guide the estimation of specific yield and specific storage values.

The final model yielded head and spring-flow residuals that met the calibration criteria for the 12-year transient simulation. The overall mean residual for heads, defining residual as simulated minus measured value, was -0.04 foot. The overall root-mean square residual for heads was less than 3.6 feet for each year in the 1995 to 2006 simulation period. The overall mean residual for spring flows was -0.3 cubic foot per second. The spatial distribution of head residuals was generally random, with some minor indications of bias.

Simulated average ET over the 1995 to 2006 period was 34.47 inches per year, compared to the calculated average ET rate of 36.39 inches per year from the model-independent water-budget analysis. Simulated average net recharge to the surficial aquifer system was 3.58 inches per year, compared with the calculated average of 3.39 inches per year from the model-independent water-budget analysis. Groundwater withdrawals from the Floridan aquifer system averaged about 920 million gallons per day, which is equivalent to about 2 inches per year over the model area and slightly more than half of the simulated average net recharge to the surficial aquifer system over the same period. Annual net simulated recharge rates to the surficial aquifer system were less than the total groundwater withdrawals from the Floridan aquifer system only during the below-average rainfall years of 2000 and 2006.

[1] U.S. Geological Survey.

[2] St. Johns River Water Management District.

Introduction

The total population of Lake, Orange, Osceola, Polk, and Seminole Counties in east-central Florida (fig. 1) has increased by about 70 percent from 1990 to 2010 (Florida Office of Economic and Demographic Research, 2012). This growth has increased the demand for groundwater from the Floridan aquifer system (FAS), which is the primary source of water supply in the region. Declines in groundwater levels, spring flows, and water-surface altitudes at lakes, as well as increases in groundwater chloride concentrations, have occurred in an area of concern designated as the Central Florida Coordination Area (CFCA). The CFCA includes southern Lake County and all of Orange, Osceola, Polk, and Seminole Counties (fig. 1). Declines in groundwater levels have been reported in wells penetrating the Upper Floridan aquifer (UFA), the primary source of water for potable, industrial, and agricultural purposes in the CFCA. These declines have been attributed to groundwater withdrawals and long-term below-average rainfall (Spechler and Halford, 2001). More recently, a statistical analysis of 115 sites by Murch and Tara (2010) indicated that 31 of 62 wells, 4 of 6 springs, and 13 of 47 lakes have exhibited statistically significant (80-percent confidence level) declines in water levels and flows during their respective periods of record, which collectively ranged from 1941 to 2009. A rise in groundwater levels has been observed in some areas, particularly in Polk County, and is attributed to a reduction in groundwater withdrawals associated with improved phosphate mining practices (Spechler and Kroening, 2007; Murch and Tara, 2010).

The cumulative effects of changes to the hydrologic system in the CFCA caused by natural or anthropogenic factors may alter the long-term balance between recharge and discharge. Over time, such changes could cause movement of the freshwater and saline-water interface. Multi-year, cyclic variations in rainfall may contribute to observed periods of generally increasing or decreasing lake levels (German and Adamski, 2005). Groundwater chloride concentrations have increased near well fields in eastern Seminole and Orange Counties, suggesting an upward movement of saline water that may have been caused by groundwater withdrawals (Spechler and Halford, 2001; Adamski and German, 2004). In addition to changes in rainfall or groundwater withdrawals, land application of reclaimed water has been shown to increase water-table altitudes, as well as UFA water levels (O'Reilly, 1998; Adamski and German, 2004). The construction of drainage ditches to reclaim land for development could increase groundwater seepage to streams, as suggested by German and Adamski (2005) for some streams in Orange County exhibiting long-term increases in 7-day flow. Based on a conceptual model developed by Tibbals (1978), expansion of paved surfaces could increase recharge to the FAS if a number of assumptions implicit in the model are satisfied. Where the water table is near land surface and subject to evapotranspiration (ET), such as occurs throughout much of the CFCA, small changes in depth to the water table can affect the availability of water for recharge (Knowles and others, 2002).

The St. Johns River Water Management District (SJRWMD), South Florida Water Management District (SFWMD), and Southwest Florida Water Management District (SWFWMD), manage the groundwater resources in the CFCA to ensure water resources are sufficient to satisfy demand associated with future population growth (Central Florida Water Initiative, 2011). To address these concerns, SJRWMD, SWFWMD, and SFWMD are coordinating resource management efforts within the CFCA with the creation of the Central Florida Water Initiative (CFWI). The initiative is a collaborative process between stakeholders to manage groundwater resources in the CFCA. The main goals of the CFWI are to develop a planning tool to evaluate water-resource management strategies in the CFCA and to develop a regional water-supply plan.

In 2008, the U.S. Geological Survey (USGS) initiated a 3 1/2-year study, in cooperation with SJRWMD, SFWMD, and SWFWMD, to determine the long-term effects on the hydrologic budget caused by changes in climate, groundwater withdrawals, and land-use practices. The CFWI has incorporated the USGS modeling study as part of its planning initiatives.

To date, several groundwater flow models have been developed for areas within central Florida but none represent consistent conceptualizations of the CFCA hydrologic system. Water management decisions within CFCA consider the effects of land use and land cover change, including the development of new well fields, withdrawals from existing well fields, reclaimed water applications, and expansion of urban land use. To address study objectives, the USGS developed a fine-resolution, areally extensive groundwater flow model of the aquifer system in the CFCA and adjacent areas of east-central Florida (fig. 1). The model may be used to evaluate the effects of future groundwater withdrawal scenarios in the CFCA and assess the impact of changes in groundwater withdrawals on the potentiometric surfaces of the FAS.

Purpose and Scope

The purpose of this report is to describe the hydrologic flow system and water budget in east-central Florida (fig. 1) from 1995 to 2006, a time period associated with a wide range in hydrologic conditions in east-central Florida. Specifically, this report documents the development of the groundwater flow model used to (1) refine the conceptual understanding of the water exchanges between the surficial aquifer system (SAS) and the FAS and (2) improve the estimates of the recharge rates to the SAS from infiltration through the unsaturated zone.

This report describes exchange of water within the SAS, intermediate aquifer system (IAS), and FAS, including the intervening confining or semiconfining units and their interaction with surface-water systems (lakes, streams, rivers, and springs), and external aquifer stresses including ET, rainfall,

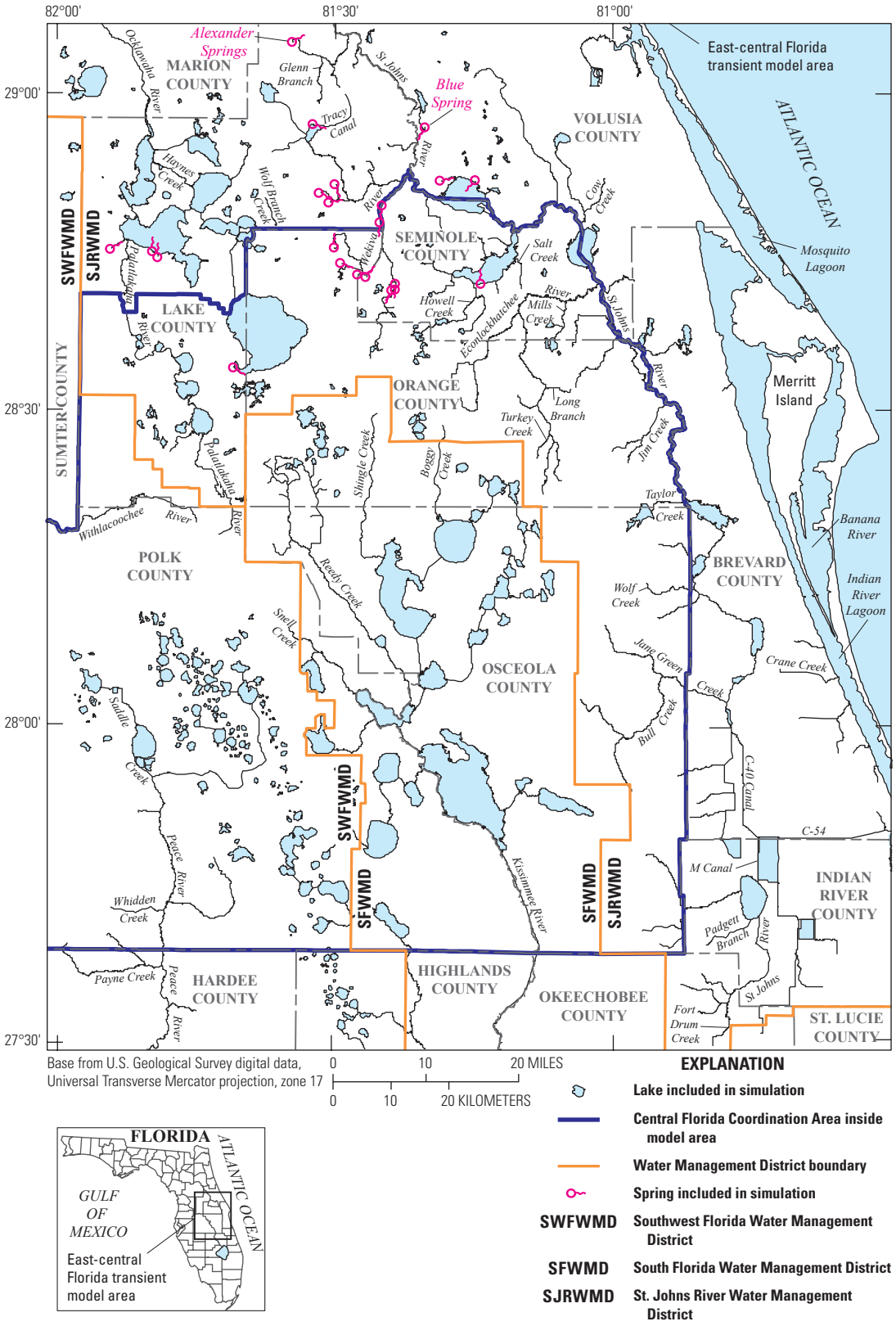

Figure 1. Areal extent of the East-Central Florida Transient (ECFT) model area (study area) and Central Florida Coordination Area.

well withdrawals, artificial recharge and irrigation systems. Also discussed are the hydrologic budget, model construction, calibration procedures, parameter sensitivity analyses, simulated potentiometric surfaces, analyses of vertical flow directions, and estimates of fluxes between model units and boundaries.

The model presented herein simulates regional flow in the freshwater-bearing part of the groundwater flow system, flow between the groundwater and surface-water systems, and flow in the surface-water system in the CFCA. Although the model simulates the surficial processes of runoff, infiltration, water-level fluctuation in lakes and streams, and streamflow, emphasis is placed on simulation of the groundwater flow system and its interaction with the surface-water system. The model is not an integrated surface-water/groundwater model, nor is intended to model surface-water processes in detail. Simulation of the saline groundwater flow system or potential interaction between the freshwater and saline-water flow systems was beyond the scope of the modeling effort.

Geographical information system databases (Environmental Systems Research Institute, Inc., 2010) were developed to manage spatially distributed information about hypsography, hydrography, land use, soil types, hydrostratigraphy, and hydrogeologic properties within the study area. To achieve consistency of coordinate systems, geographical information system files used the Universal Transverse Mercator (UTM) projection, zone 17 of the Florida coordinate system, west zone (Snyder, 1983). The North American Datum of 1983 was used for all data generated in this study.

Previous Studies

Several groundwater flow models have been developed for areas within central Florida. Models having subregional to regional extent were summarized by Sepúlveda (2002), who developed a steady-state quasi-three-dimensional model of the IAS and FAS for peninsular Florida using a grid cell size of 5,000 × 5,000 feet (ft). Using the Sepúlveda (2002) model, Environmental Simulations Inc. (2004) developed a steady-state, quasi-three-dimensional model of the SAS, IAS, and FAS that encompasses SWFWMD lands, and is referred to as the District Wide Regional Model (DWRM) version 1. This model developed into the DWRM version 2 (Environmental Simulations Inc., 2007) transient model, calibrated to 1996–2002 hydrologic conditions. More finely discretized (2,500 × 2,500-ft cell size) steady-state quasi-three-dimensional models of the SAS and FAS were developed by Knowles and others (2002) covering Lake County and the Ocala National Forest, and by McGurk and Presley (2002) covering east-central Florida. The SFWMD used the model by McGurk and Presley (2002) to develop a transient quasi-three-dimensional groundwater flow model of the SAS and FAS for the same east-central Florida area. That model, the East-Central Florida Transient (ECFT) version 1 (David Butler, South Florida Water Management District, written commun., 2012), is calibrated to 1995–1999 hydrologic conditions and uses an application designed to simulate wetland flows in areas where the water-table altitude rises above land surface. A panel of scientists evaluated the ECFT version 1 model objectives, flow conceptualization and model design, assumptions, and documentation to assess whether the model was a suitable tool to evaluate future impacts on the hydrologic system (Andersen and others, 2007). The model described herein was developed to address, to the degree possible, the main recommendations of the review panel based on availability of data.

Description of Study Area

The simulated onshore area of the model encompasses about 9,000 square miles (mi^2) (fig. 1). The study area spans approximately 112 miles (mi) on its eastern and western sides, approximately 92 mi on its northern and southern sides, and includes all but the westernmost edge of the CFCA (fig. 1). The land surface area simulated in the model excludes actively simulated lakes, as well as coastal estuaries and islands (Banana River, Indian River Lagoon, Mosquito Lagoon, Merritt Island, and other barrier islands). Land-surface altitudes range from NGVD 29 along the coast of the Atlantic Ocean to more than 300 ft above NGVD 29 in Polk and Lake Counties. Numerous karst features, including sinkholes and springs, are present in the study area. Sinkholes in all stages of development are common throughout much of the area and range from small depressions to large lakes. Many of these sinkholes can be areas of high recharge to the underlying aquifers. The springs in the northern half of the study area discharge water from the UFA into rivers and streams that eventually flow into the Atlantic Ocean.

The physiographic delineation previously defined by White (1970) and based on topography was used to subdivide the study area into 21 distinct regions (fig. 2) and refined for this study based on hydrologic features. The Green Swamp (region 21, fig. 2) was delineated in place of the physiographic regions in this area because of its unique hydrogeologic nature. In addition, the Lake Wales Ridge was subdivided into northern (region 15), central (region 19), and southern (region 20) regions based on differences in hydrogeologic properties (fig. 2).

Land Use

Land cover and land-use areas were available for 1995, 2000, and 2004, and generalized into eight categories based on detailed classifications provided by SJRWMD (Jill A. Stokes, St. Johns River Water Management District, written commun., 2010). In 1995, agriculture was the most areally extensive land use, covering 28 percent of the study area, followed by wetlands (24 percent), forest (15 percent), and urban (14 percent) (fig. 3). The remaining 19 percent of the study area consisted of water (9 percent), shrubs/grass (7 percent), mining (3 percent), and barren land (0.4 percent) in 1995.

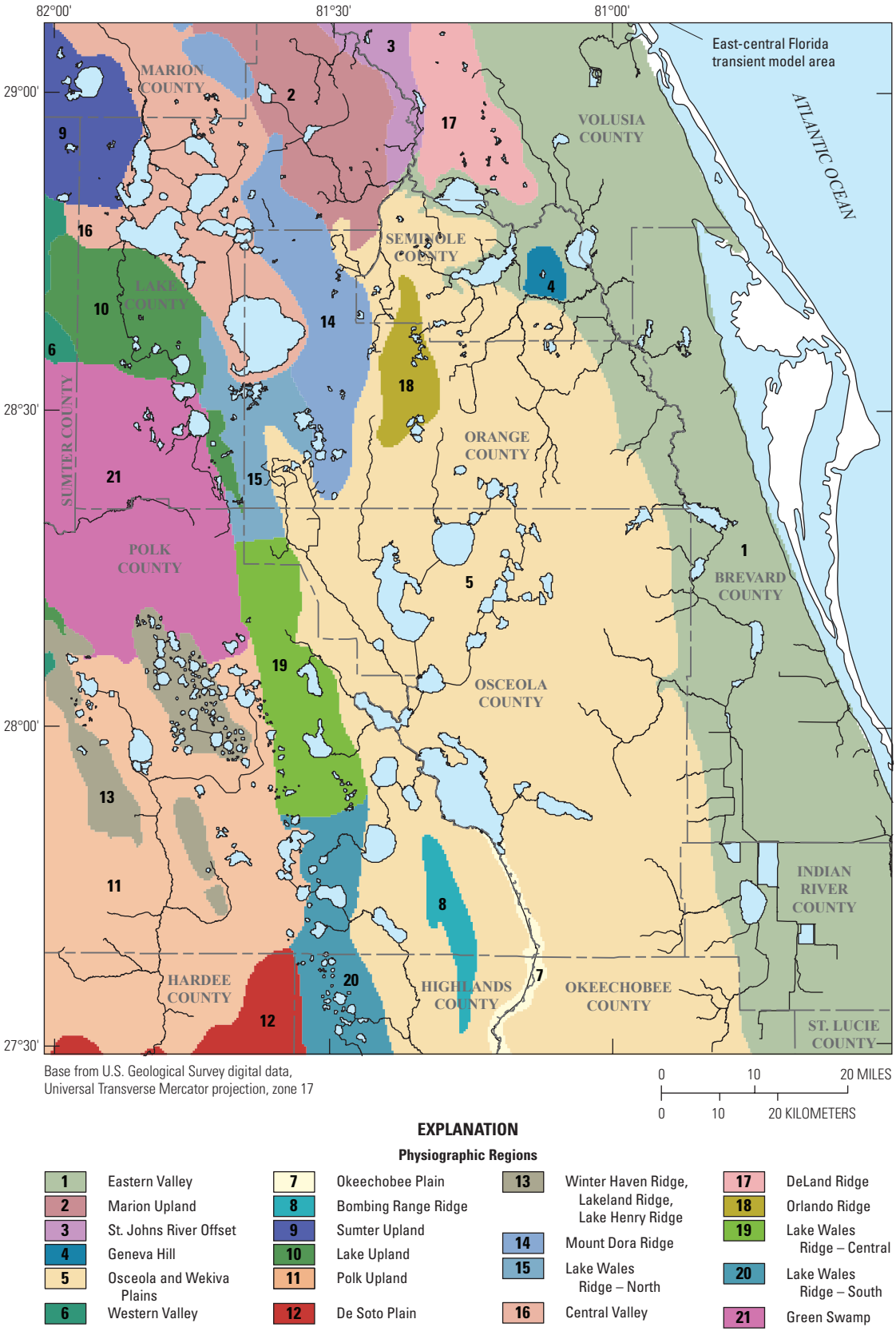

Figure 2. Areal extent and spatial distribution of grouped physiographic regions and the Green Swamp in the study area.

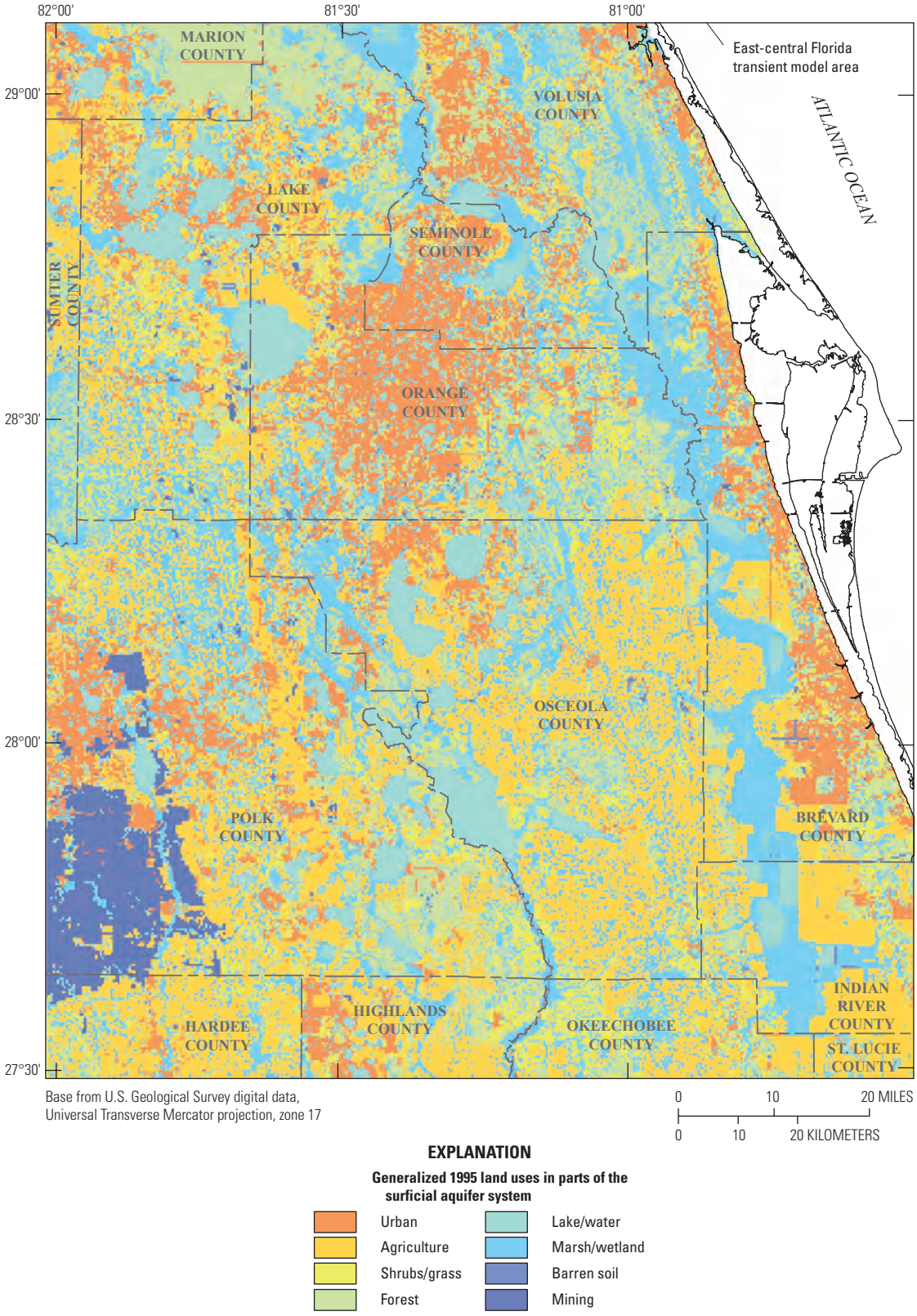

Figure 3. Generalized 1995 land use in the study area.

Land-use data were used to infer where urbanization occurred and could have affected the partitioning of rainfall into runoff and infiltration. Urbanization levels increased in about 4 percent of the study area from 1995 to 2004 (fig. 4, Jill A. Stokes, St. Johns River Water Management District, written commun., 2010), ranging from a change in low-density to high-density population areas or from non-urban land cover to urban land use. Transitions from non-urban land cover to urban land use are particularly important because such changes could increase the runoff potential caused by reduced infiltration associated with impervious surfaces, soil compaction during development, or stormwater drainage systems. However, depending in part on stormwater-management system type, such as the use of stormwater infiltration basins rather than surface-water discharge, urbanization could result in an increased average infiltration over the study area.

Soil Groups

Soils in the study area range from having low runoff potential (high infiltration) to high runoff potential (low infiltration). The runoff/infiltration potential is based on hydrologic soil groups delineated by the Natural Resources Conservation Service (2011). Hydrologic soil groups are based on the intake of water when the soils are saturated and receive rainfall from long-duration storms (Schellentrager and Hurt, 1990, p. 71). Soils are assigned to four hydrologic groups designated by letters, where "A" indicates high infiltration rate, "B" indicates a moderate infiltration rate, "C" indicates a low infiltration rate, and "D" indicates a very low infiltration rate (Schellentrager and Hurt, 1990, p. 71). A dual designation is assigned to soils—A/D, B/D, and C/D—in areas where a high water table may limit infiltration; in such cases, the first letter applies to the drained condition and the second letter applies to the undrained condition.

Soils in the study area have predominantly moderate infiltration rates that may be further limited by a shallow water table, with 56 percent of the area classified as B/D soils (fig. 5). The next most prevalent hydrologic soil group is A (19 percent); these well drained, high infiltration soils are commonly present in the ridge and upland physiographic regions (figs. 2 and 5). The third most prevalent hydrologic soil group is D (16 percent); these poorly drained soils generally have moderately fine to fine texture or have a layer that impedes downward water movement and are often associated with wetland areas (fig. 3 and 5). The remaining 9 percent of the study area consists of A/D (1 percent), B (1 percent), C (6 percent), and C/D (1 percent) soils.

Drainage Basins

The study area encompasses the headwaters of the four major river basins of peninsular Florida, namely, the St. Johns, Kissimmee, Withlacoochee, and Peace River Basins (fig. 1). Drainage basins delineating the land surface area (watershed) contributing runoff to a nearby stream or lake were derived based on topographic divides as provided by SJRWMD. The area of the drainage basin for a stream depends on the length of the stream segment and the surrounding topography. For example, the basin for Soldier Creek in Seminole County (fig. 6*A*) has an area of 12.2 mi^2, whereas the drainage basin area for Wekiva River is 152.4 mi^2. The area of the drainage basin for a large lake can be quite extensive. For example, an area of 130 mi^2 drains directly into Lake Tohopekaliga in Osceola County (fig. 6*B*). The delineation of drainage basins in an area of low relief, such as Florida, can be difficult. The effective drainage basin can change temporally and be influenced by anthropogenic changes to the surface drainage system or even by meteorological conditions (rainfall and wind patterns in flat terrains may change the direction of overland flow). Well-drained soils and karst terrain occur in some areas, and 9 percent of the study area consists of noncontributing areas where runoff is lost to ET or is retained and infiltrates in topographic depressions or closed-basin lakes (fig. 7).

Climate

The climate of the study area is classified as subtropical and is characterized by warm, normally wet summers and mild, dry winters. Maximum temperatures usually exceed 90 degrees Fahrenheit (°F) during the summer, but may fall below freezing for several days in the winter. The mean annual air temperatures are 72.7 °F and 73.6 °F for the cities of Sanford and Bartow (locations shown on fig. 8*A*), respectively, for 1981–2010 (National Oceanic and Atmospheric Administration, 2011). In January, mean monthly air temperatures are 59.7 °F at Sanford and 61.8 °F at Bartow, and in July, are 83.3 °F at Sanford and 82.8 °F at Bartow. Mean annual rainfall at Sanford and Bartow is 53.04 and 52.08 inches (in.), respectively, for 1981–2010 with 55 and 59 percent (station locations shown on fig. 8*A*) occurring from June through September (National Oceanic and Atmospheric Administration, 2011). During the summer and early fall, tropical storms and hurricanes can produce substantial rainfall in the area. Winter rainfall generally is associated with large frontal systems that move from the northern latitudes southward.

Rainfall

The spatial and temporal distributions of rainfall over the study area from 1995 to 2006 were obtained from the National Oceanic and Atmospheric Administration (NOAA), SJRWMD, SWFWMD, and SFWMD rainfall stations. Total measured rainfall for 1995 at 40 stations ranged from 40.97 to 74.08 inches per year (in/yr) (fig. 8*A*). Because these rainfall values were available only at site-specific locations, the spatial distribution of rainfall over the study area was based on NOAA Next Generation Weather Radar (NEXRAD) data. The methodology used to calculate the initial spatial distribution of NEXRAD rainfall data was presented by Hoblit and others (2003); however, the calculated 1995 total

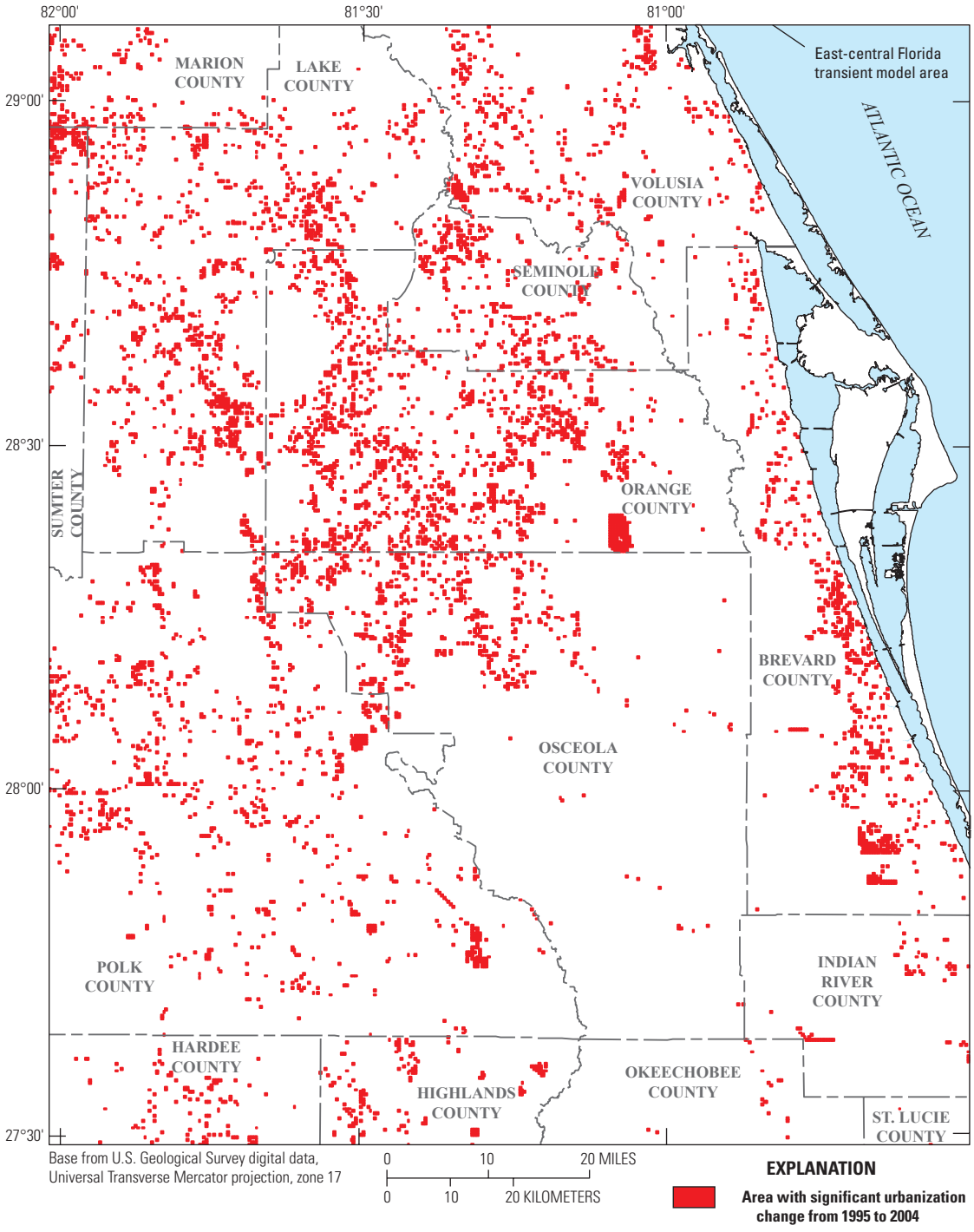

Figure 4. Areas of increased urbanization levels from 1995 to 2004.

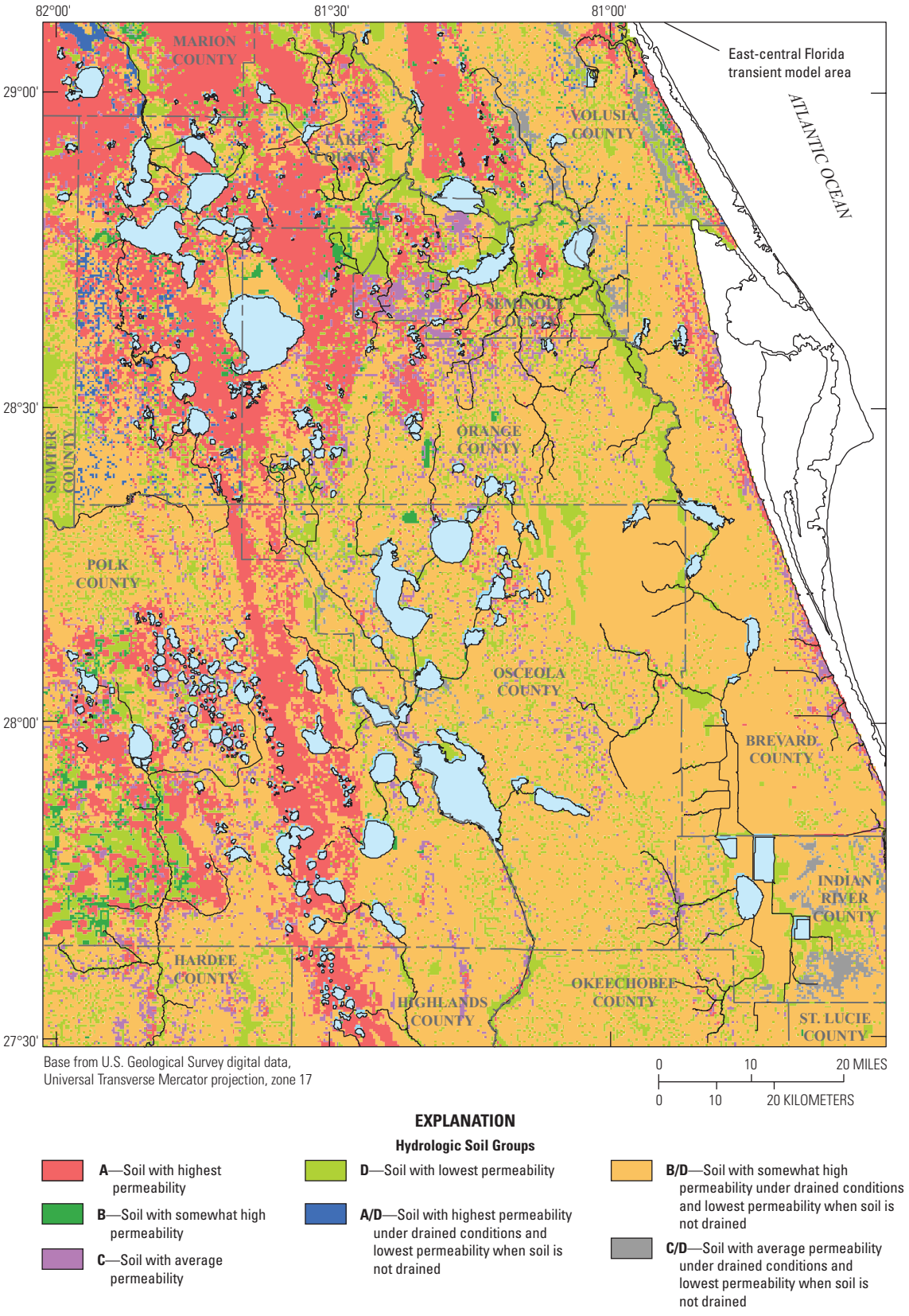

Figure 5. Areal extent and spatial distribution of hydrologic soil groups as classified by the Natural Resources Conservation Service.

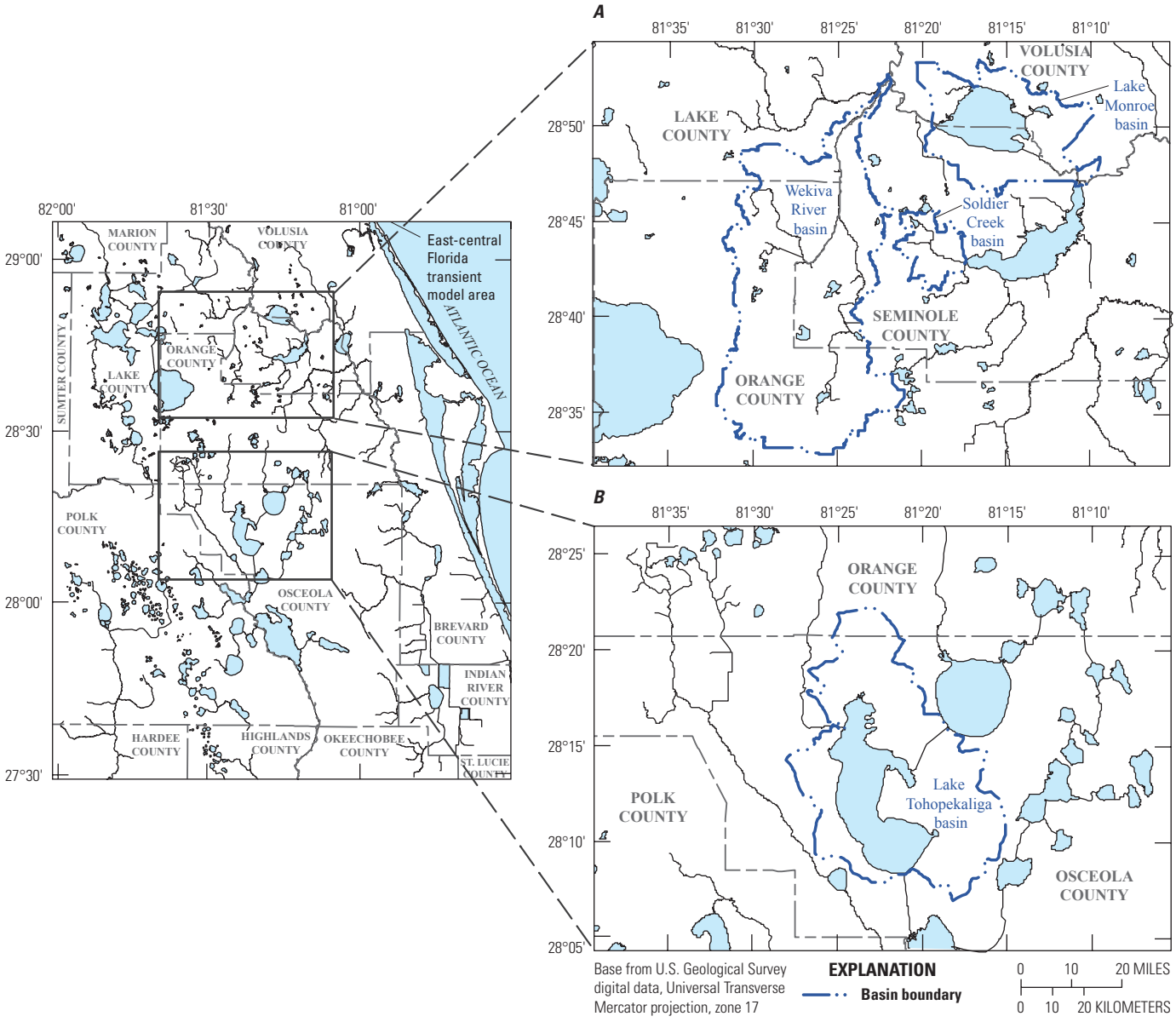

Figure 6. Drainage basins used to delineate the drainage fields for selected streams and lakes near *A*, Seminole and *B*, Orange Counties.

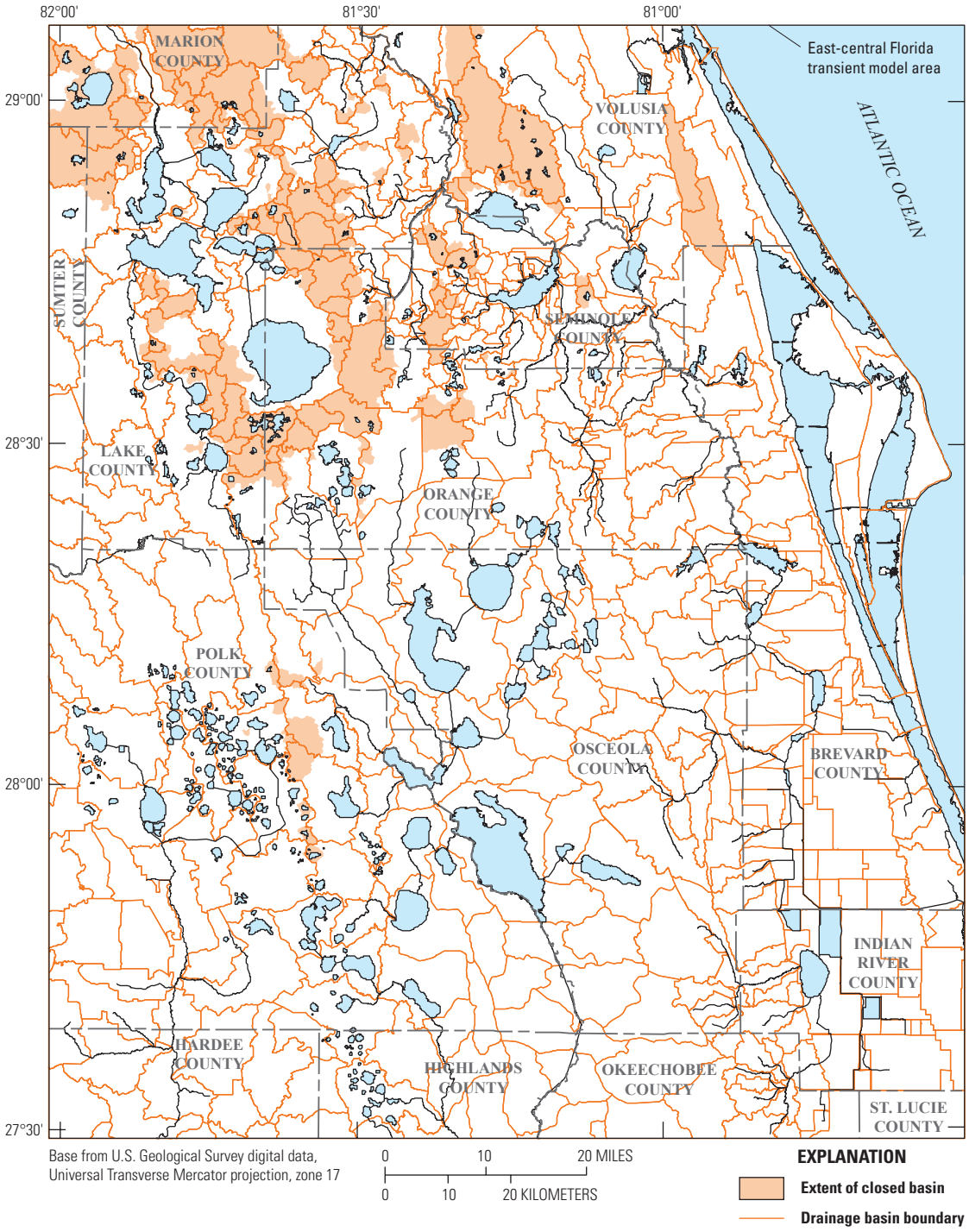

Figure 7. Basin delineation in the study area showing closed basins not contributing runoff to the stream network.

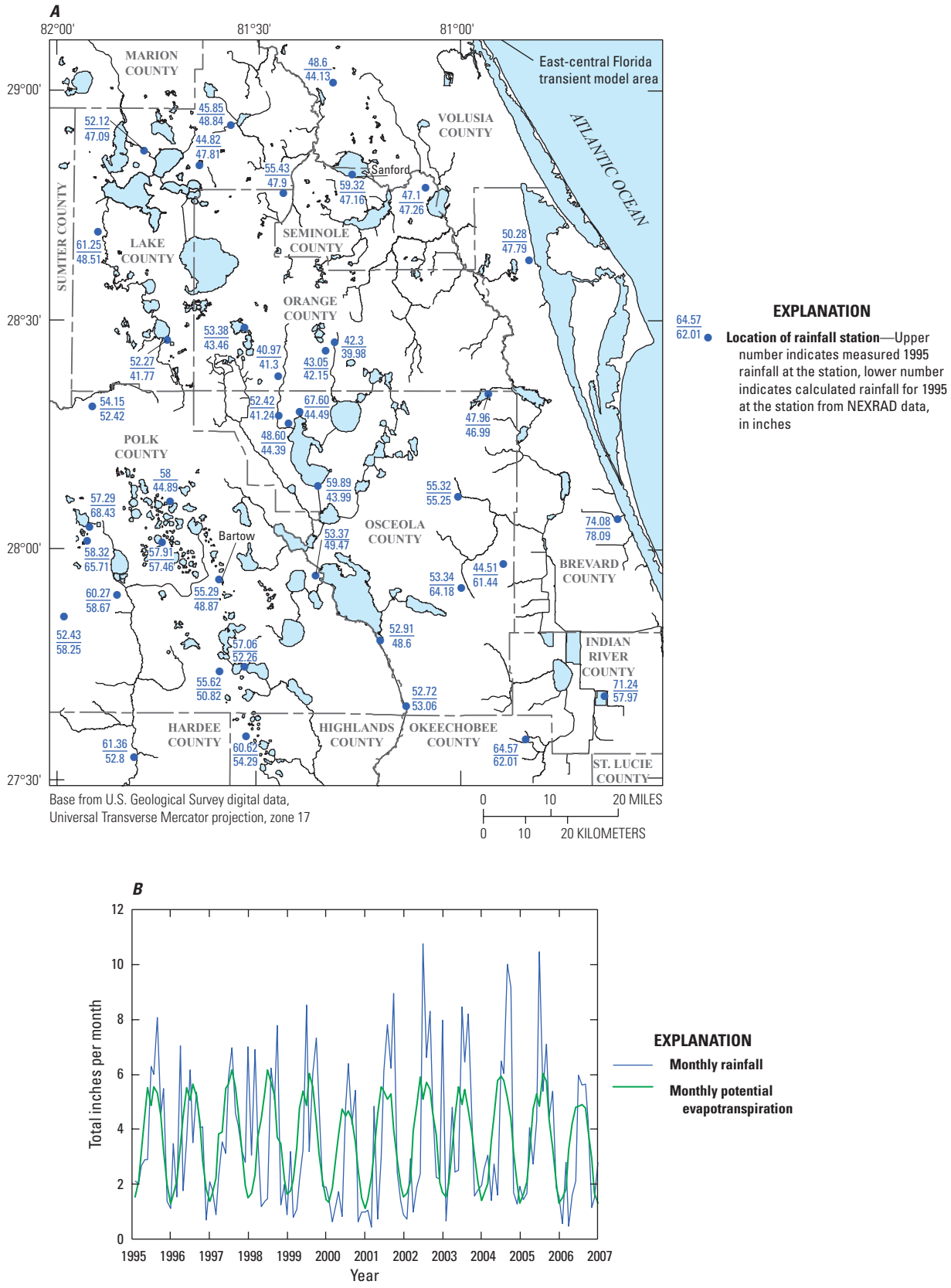

Figure 8. *A*, Locations of rainfall stations, measured 1995 rainfall at the stations, and calculated rainfall from Next Generation Weather Radar (NEXRAD) data, and *B*, monthly rainfall and potential evapotranspiration (ET) totals from 1995 to 2006.

NEXRAD rainfall at the stations differs from the measured totals (fig. 8*A*). The 1995 rainfall totals from NEXRAD varied from about 40 to 78 in., ranging from a 23-in. underestimate to an 11-in. overestimate compared to measured totals. Changes in monthly rainfall from 1995 to 2006 indicate the seasonal pattern of higher rainfall monthly totals during the second and third quarters of the year and lower during the first and fourth quarters (fig. 8*B*).

To account for differences between measured and NEXRAD rainfall, multiplicative factors were introduced to make the spatially available NEXRAD rainfall values equal to measured rainfall. An array of multiplicative factors was calculated as the arithmetical ratio of the rainfall values shown in figure 8*A*, resulting in factors that ranged from about 0.8 to 1.5 for 1995. A surface of multiplicative factors was generated using splines based on continuously differentiable quintic polynomials between any two observed points, and constrained at the model boundary by adding a set of unity values along the study area boundary. These multiplicative factor surfaces were multiplied by the corresponding NEXRAD daily point data to derive the final adjusted spatial rainfall distribution, which were summed to yield the spatial distribution of 1995 annual rainfall (fig. 9). Similarly, independent interpolations for the 11 years from 1996 to 2006 were made to adjust NEXRAD rainfall data so that they equaled the measured annual rainfall at the stations. The application of these multiplicative factor adjustments resulted in rainfall totals ranging from 41 to about 63 in. for 1999, and from about 46 to 62 in. for 2003. The general spatial distribution of rainfall data from NEXRAD was retained, although adjustment to the daily rainfall values was made using the multiplicative factors to agree with measured rainfall values at the rainfall stations.

Based on the adjusted NEXRAD data, the average annual rainfall over the ECFT study area from 1995 to 2006 ranged from about 31 in/yr during 2000 to about 61 in/yr during 2005, averaging about 51 in/yr over the 12-year period. Annual average rainfall for 2006 was 36.5 in/yr over the ECFT study area, making 2000 and 2006 years with below average rainfall. Annual average rainfall was above average in 2002, 2004, and 2005, exceeding 58 in/yr.

Evapotranspiration

Whereas rainfall provides the greatest input of water to the hydrologic system in central Florida, the greatest annual water loss occurs through ET. The fraction of annual precipitation returned as ET in Florida ranges from about 50 percent in settings of relatively deep water table, shallow rooted vegetation, and sandy soils (Sumner and Bradner, 1996) to almost 110 percent from lakes (Swancar and others, 2000).

ET may be difficult to quantify, because of the paucity, cost, and labor of ET measurements (Sumner, 2006), necessitating the use of approximations. Such approximations commonly incorporate more easily derived potential ET data, which is then scaled by a factor or factors (typically derived empirically) to approximate ET (O'Reilly, 2007). The USGS Florida Water Science Center provides State-wide coverage, at a 2-kilometer pixel resolution, of daily potential ET derived from satellite and ground-based data from June 1995 to the near-present (U.S. Geological Survey, 2012). As an approximation, potential ET rates for January to May 1995 were set equal to the potential ET rates for January to May 1996. Potential ET is computed by using the Priestley-Taylor equation (Sumner and Jacobs, 2005). Potential ET represents the rate for freely available water and thus would approximate evaporation from a free water surface such as a lake, river, or a lush green, actively growing landscape. Potential ET is independent of land cover type and ranged from about 47 to 62 in/yr in 1995 (fig. 10*A*).

Potential ET was used to estimate ET at six sites across central Florida where ET measurements were available (fig. 10*B*). These sites cover a range of environmental settings, from dry areas having well drained, sandy soil with a relatively deep water table to wetlands having poorly drained soils (Sumner, 1996; Sumner, 2001; Knowles, 2005; Sumner, 2006; O'Reilly, 2007). Using monthly data and the results of multilinear regressions, ET was estimated as a function of potential ET and rainfall, yielding potential ET coefficients ranging from 0.39 to 0.87 and rainfall coefficients ranging from 0 to 0.08. The estimated ET is strongly correlated with potential ET and weakly correlated with rainfall, and regression coefficients are consistent with those reported by Cheng and others (2011) for humid and subtropical watersheds.

Based on land cover and water-table depth, the study area was subdivided into ET zones. Each zone was assigned an ET rate corresponding to a site, having similar physical characteristics for which ET was calculated. Regions characterized by marsh, forest, shrub, or ridge each had an associated site from which multiple linear regressions could be performed to estimate ET from potential ET and rainfall (figs. 3 and 10*B*). For example, marsh areas were assigned ET rates derived from the regression coefficients calculated for the Blue Cypress Marsh ET station, and forest areas having a deep water table were assigned ET rates derived from regression coefficients calculated for the Lyonia Preserve ET station (fig. 10*B*). Potential ET and rainfall regression coefficients could not be calculated for some land cover categories because of the lack of measured ET rates. These categories include agricultural, mining, barren soil, or urban land cover. Thus, ET zones are modified from the land cover distribution map (fig. 3) to adapt the existing data to estimate ET rates. Lakes were also designated as an ET zone. The ET rate at each lake was set equal to the potential ET at the nearest lake for which potential ET was estimated from the Statewide Evapotranspiration Database (U.S. Geological Survey, 2012). In total, the study area was divided into nine regions for which ET rates were assigned, including eight regions based on land-use types as identified in figure 3 and one region for the Lakes Wales Ridge (fig. 2). Annual ET rates estimated for 1995 ranged from about 35 to 62 in/yr (fig.10*B*). The spatial

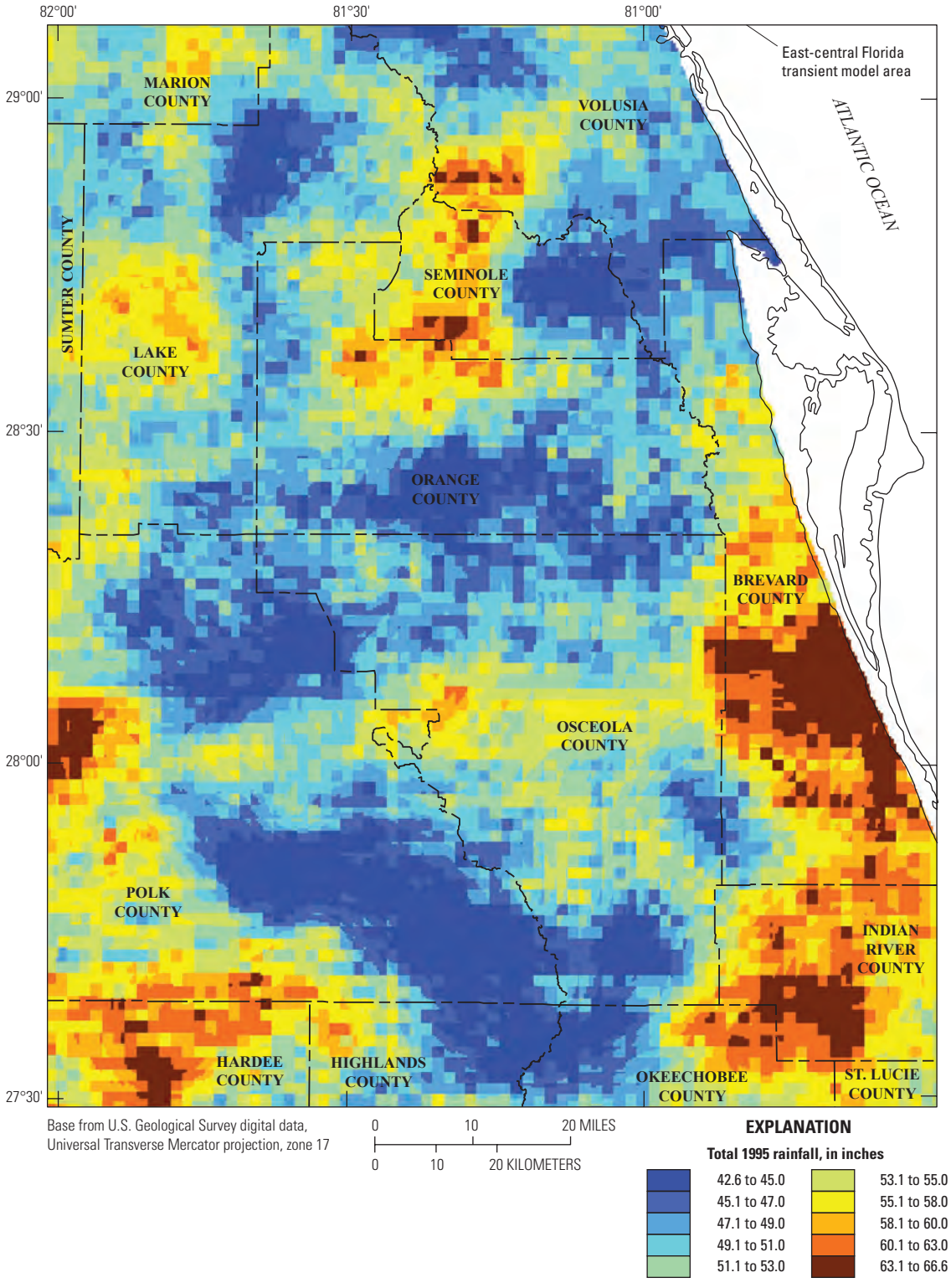

Figure 9. Spatial distribution of total 1995 rainfall derived from Next Generation Weather Radar (NEXRAD) data and the measured 1995 rainfall at the stations shown in figure 8*A*.

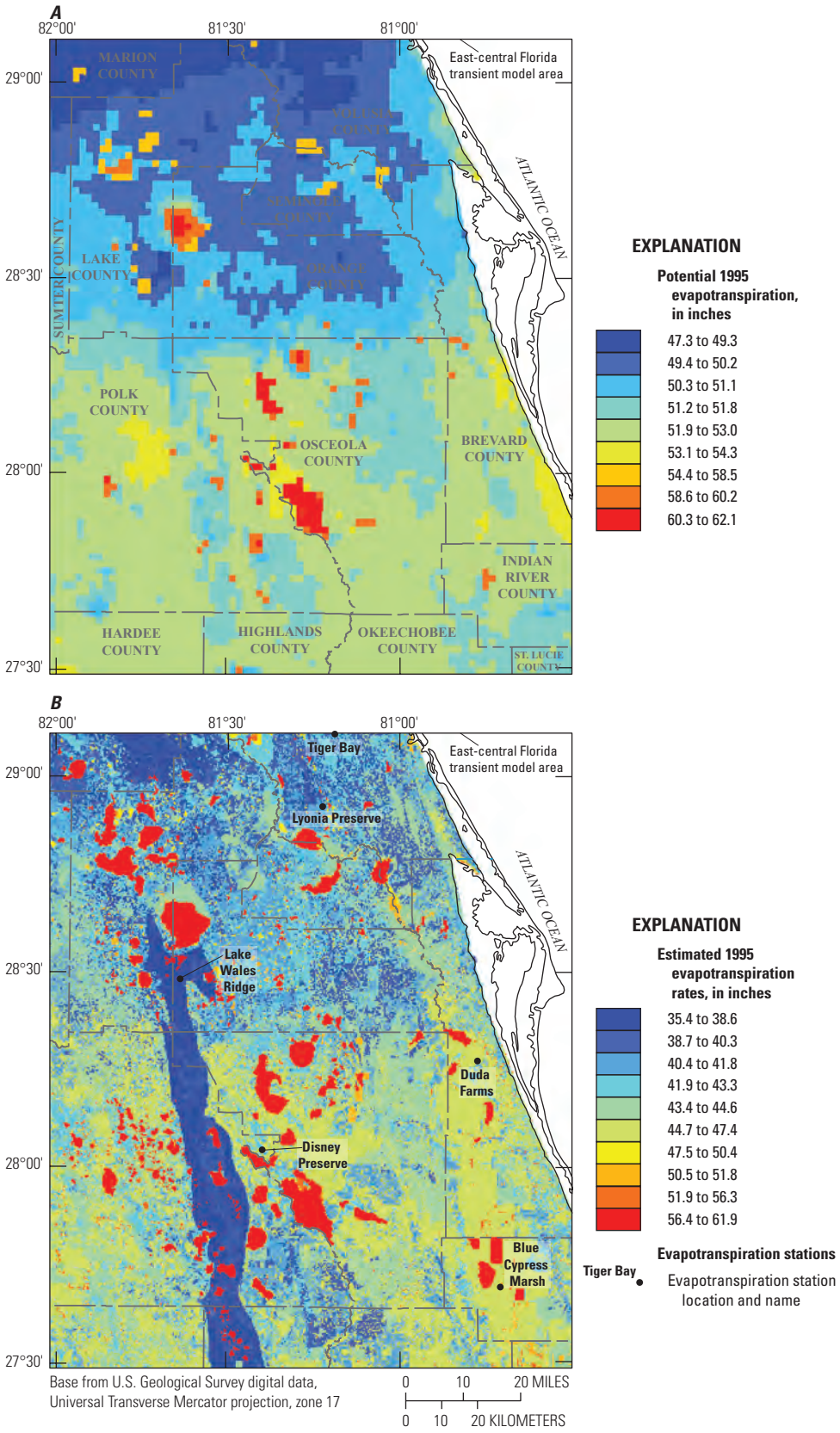

Figure 10. *A*, Spatial distribution of potential evapotranspiration (ET) for 1995 calculated from USGS Florida Water Science Center Statewide Evapotranspiration Database, and *B*, spatial distribution of estimated ET for 1995.

distribution of estimated ET rates for 1995 is an initial distribution, subject to refinements from model calibration because simulation of ET depends on physical features of the land surface such as soil permeability, changes in land cover, and drainage characteristics. From 1995 to 2006, the largest potential ET rate was 63.67 in/yr in 2000 and the smallest was 34.25 in/yr in 2001.

Differences between the annual maximum and minimum estimated ET rates over the 1995–2006 study period, namely the range of annual estimated ET rates, were nearly constant between years. For example, the ET range in 1999 was about 22 in/yr, while in 2003 this range was about 23 in/yr.

Hydrology of the Study Area

The principal hydrologic components of the study area are the surface-water flow system, groundwater flow system, and the major sources of water that enter and exit the system. These components are discussed within the context of study area hydrogeology and subsurface areas containing freshwater.

Surface-Water Flow System

The rivers that form the major surface-water flow system in the study area are the St. Johns, Palatlakaha, and Ocklawaha Rivers, which flow north; the Peace and Kissimmee Rivers (fig. 1), which flow south; the Withlacoochee River, which flows west; and several streams that flow east and discharge at locations along the eastern Atlantic coastline.

For the purpose of numerical model discretization, each stream segment was identified by a unique number, and identifiers numerically increase in the downstream direction. Each stream segment begins either at the most upstream point of a river, a lake, or the confluence of one or more streams and ends at another stream confluence, a lake, or outside the model (fig. 11). The stream discharge and water-surface altitude data are available from stations located along several of the stream segments (fig. 11). In addition, the stream discharge recorded at stream segments along the ECFT model boundaries provide estimates of flows exiting the study area and were used in the water-budget analysis. In total, there are 320 stream segments in the ECFT study area.

The highest monthly average streamflow in the time period from 1995 to 2006 was about 12,000 cubic feet per second (ft^3/s), measured in October 2004 at station number 02236000 on the St. Johns River (figs. 11 and 12). The lowest monthly average streamflow for the same period at this station was -119 ft^3/s, measured in May 2002 (fig. 12). Negative discharge indicates wind effects or tidal flow of water upstream that reverse the flow direction when the surface-water hydraulic gradient is small.

Measured monthly average upstream discharge of the Kissimmee River is generally higher than downstream during certain periods, suggesting well withdrawals may induce surface-water recharge to the aquifer. A small part of this loss can be attributed to streamflow leakage to the groundwater system; a larger fraction of this decrease could be associated with the operation of structures and storage of water along the Kissimmee River. An example of such a structure is located within stream segment number 253, upstream from station number J9202 (fig. 11). Similarly, the Peace River has several discharge stations with greater flows measured at upstream locations. In general, the Kissimmee River and the Peace River exhibit greater evidence of stream-aquifer interaction than does the St. Johns River.

Most lakes considered in this study are directly connected to streams or have a water-surface altitude station (fig. 13). Of the 351 lakes considered in this study, 287 lakes had monthly average water-surface altitudes measured for at least 1 month from 1995 to 2006. Ungaged lakes having a surface area less than 0.1 mi^2 were not considered in the study because these were smaller than the area of one model cell.

Water-surface altitude at lakes at gaged stations and water levels at nearby wells provide an assessment of surface-water and groundwater interactions. During the 1995–2006 period of study, the average water-surface altitude of gaged lakes was lowest at the close of 2000, which was slightly more than 3 ft below the water-surface altitudes measured at the beginning of 1995. This is consistent with 2000 representing a below-average rainfall year. By the close of 2005, average water-surface altitudes at gaged lakes were about 0.25 ft above the water altitudes at the beginning of 1995. The drought of 2006 caused average water-surface altitudes at lakes to drop again to about 1.5 ft below those measured at the beginning of 1995.

Flow occurs between the surface-water and the groundwater flow systems through areas of recharge and discharge. Drainage well inflows are a type of recharge to the UFA. Rapid infiltration basins are a means of land application of reclaimed water that also recharge the groundwater system. The calculated monthly average rate of recharge to the SAS from rapid infiltration basins (RIBs) during 1995 to 2006 was 33 million gallons per day (Mgal/d). Drainage wells capture surface-water runoff and recharge the upper zone of the UFA. These drainage wells are found predominantly in the Orlando metropolitan area. Calculated monthly average recharge rates to the UFA from drainage wells during 1995 to 2006 was 19.6 Mgal/d. The drainage areas of these wells, delineated based on the digital elevation model (DEM) for the ECFT study area, were used to identify model cells that contribute runoff as recharge to the UFA. These runoff volumes were not directed to lakes or streams and were mainly limited to the Orlando metropolitan area (fig. 14). The locations of the drainage wells were identified by Bulmer (2003) and RIB locations were obtained from databases of the SJRWMD (fig. 14).

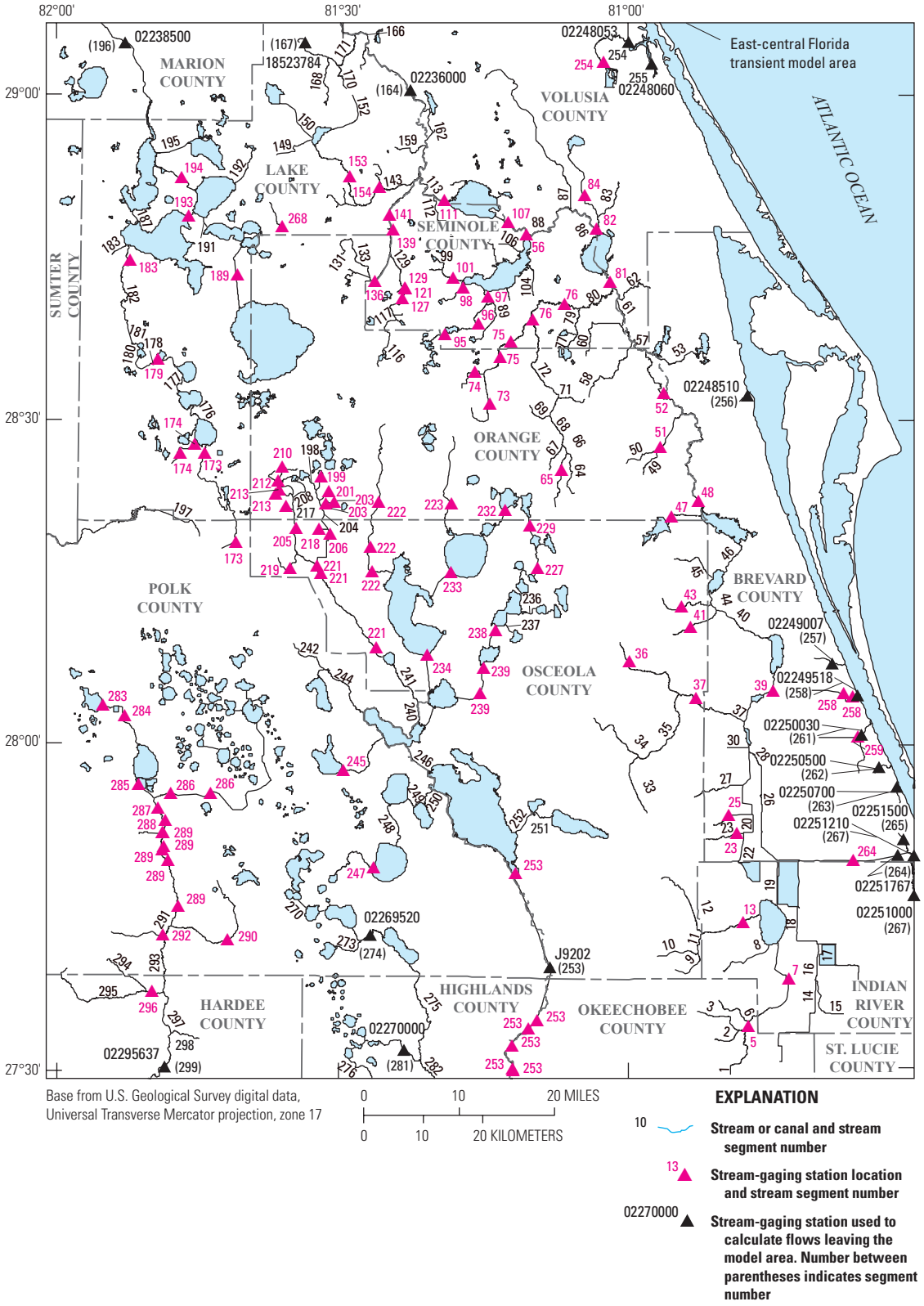

Figure 11. Stream-gaging stations, ungaged stream segments, segment numbers, and stream-gaging stations used to calculate streamflows discharging outside the East-Central Florida Transient (ECFT) study area.

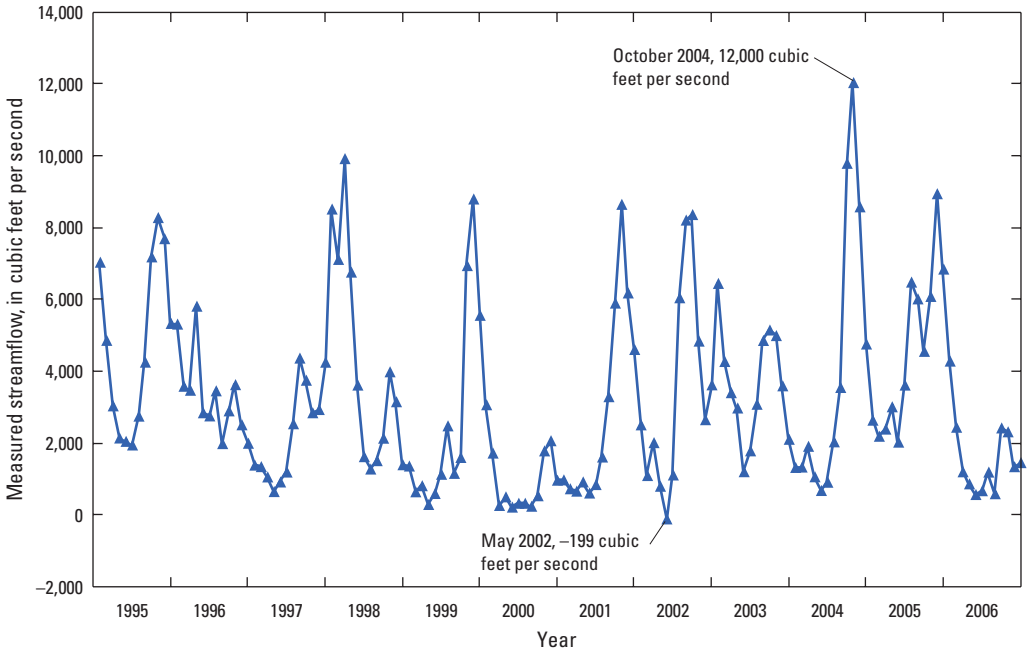

Figure 12. Measured streamflow for St. Johns River, station number 02236000 in figure 11.

Groundwater Flow System

Horizontal groundwater flow is controlled mainly by the horizontal hydraulic conductivity of the UFA and Lower Floridan aquifer (LFA) (fig. 15). Vertical groundwater flow is mainly controlled by the water levels in the SAS, the potentiometric surfaces of the UFA and LFA, and the vertical hydraulic conductivity of the intermediate confining unit (ICU), which underlies the SAS. The SAS generally is recharged by rainfall, irrigation, and by diffuse upward leakage in areas where the hydraulic head of the UFA is higher than the water-table altitude. The assessment of vertical flow between the UFA and the LFA and flow within the LFA itself could be conducted only at a few sites due to the paucity of LFA water-level data. UFA recharge or discharge occurs mostly through vertical ICU leakage. The vertical leakage rate to or from the UFA is a function of the hydraulic gradient between the SAS and UFA, the vertical hydraulic conductivity of the ICU, and the thickness of the ICU.

Hydrogeologic Framework

The hydrogeologic units that define the model layers have been correlated with regional lithostratigraphic units across the ECFT study area (fig. 15). Lithostratigraphic units are mappable bodies of bedded or unbedded rocks characterized on the basis of their lithologic properties or lithologic properties and stratigraphic position. Hydrogeologic units are defined by their ability to transmit or restrict flow, which is the result of both primary geologic characteristics, such as grain size distribution and composition, and secondary geologic characteristics, such as fracturing and dissolution-enhanced porosity or cementation. Hydrogeologic units may transgress lithostratigraphic boundaries, especially where fractures or secondary porosity enhancement features are present. Regional structural, depositional, and erosional trends may also affect the correlation between hydrogeologic and lithostratigraphic units.

The designation of the hydrogeologic units listed herein generally follows the regional designations of Miller (1986), integrated with important subunits within the UFA in the ECFT study area as designated by Davis and Boniol (2011). Some units described by Miller (1986) (for example, LFA subunits) are not included in this hydrogeologic framework because they either are not present within the study area or were not mapped or delineated for this study. The regional hydrogeologic units in the ECFT study area consist of the SAS, the ICU and IAS, and the units within the FAS. The FAS comprises the UFA, the middle confining units I and II (MCU I/II), and the LFA. Within the UFA, defined hydrogeologic units include the Ocala permeable zone (OPZ), the Ocala low-permeable zone (OLPZ), and the Avon Park permeable zone (APPZ) (fig. 15). The upper surfaces and thicknesses of the hydrogeologic units were mapped using the interpretations from Miller (1986), as well as additional borehole geophysical data, test-hole and core descriptions, and selected lithologic descriptions from water management district and Florida Geological Survey files that have been collected since that publication. Hydrogeologic surfaces were identified by comparing published interpretations with units identified in nearby boreholes. Geophysical log characteristics were compared between boreholes, and additional well data were used to help refine the interpreted hydrogeologic designations.

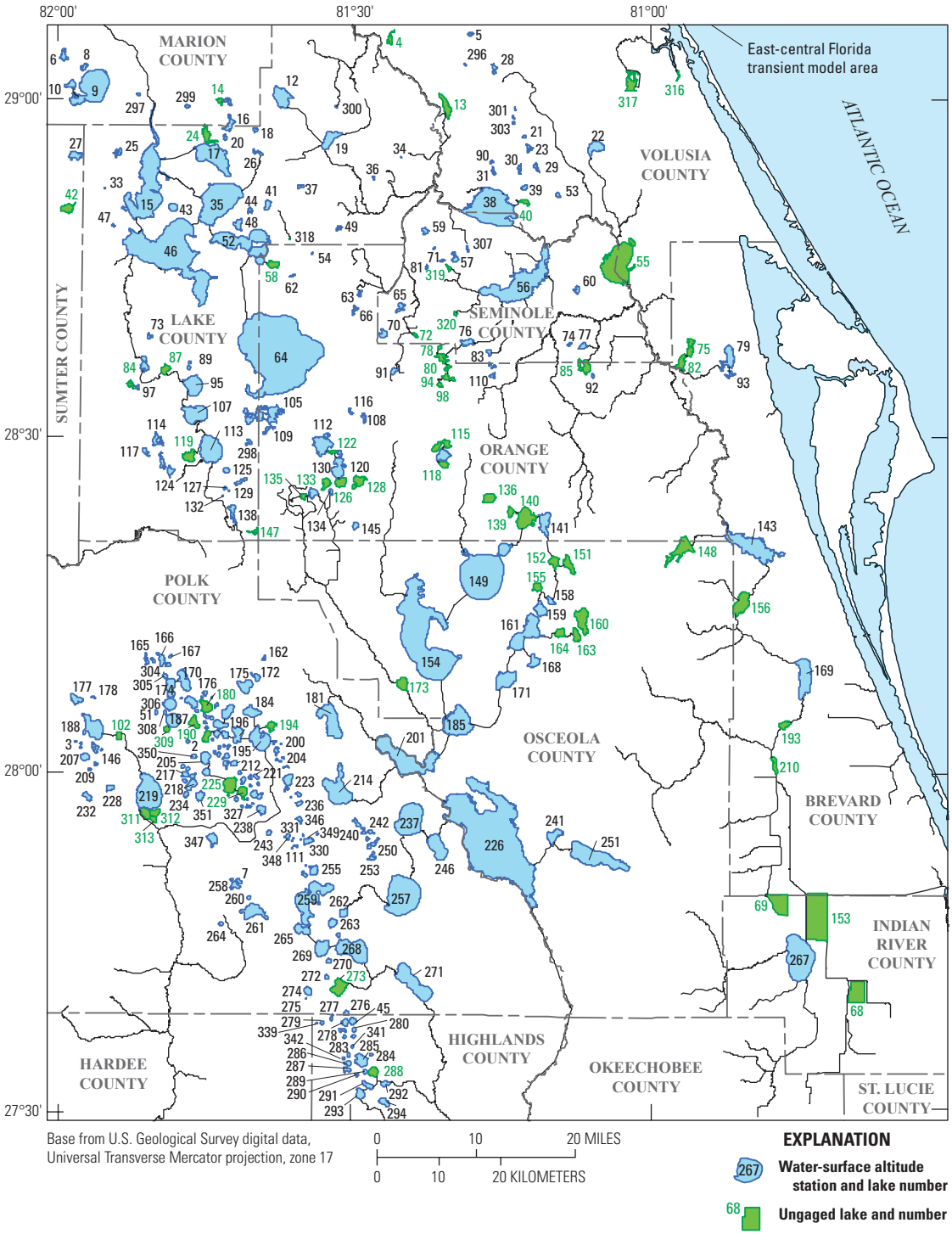

Figure 13. Lakes with water-surface altitude stations and selected ungaged lakes.

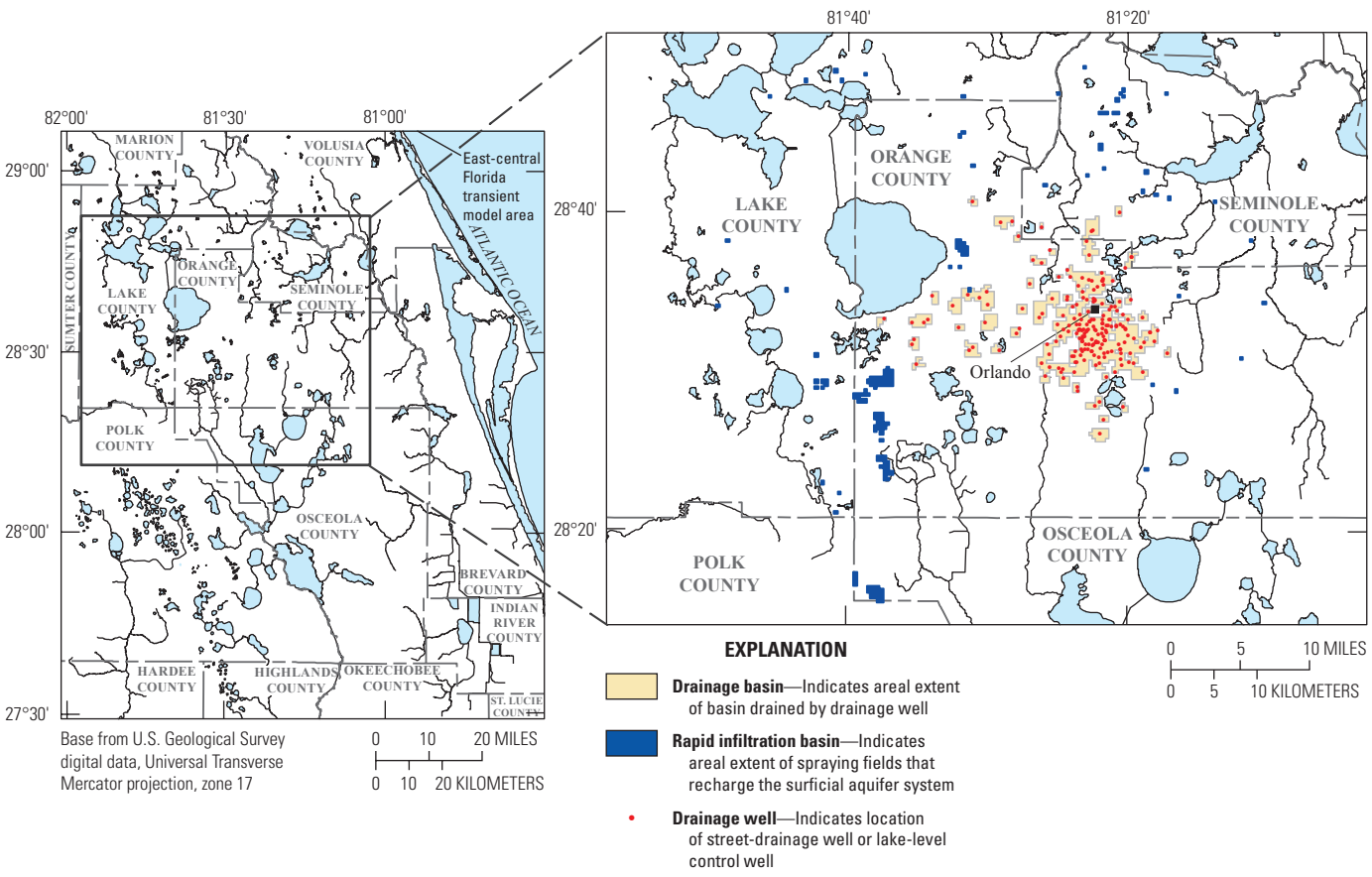

Figure 14. Locations of drainage wells, areal extent of drainage wells basins, and locations of rapid infiltration basins.

The altitude of the top of each hydrogeologic unit was mapped using geostatistical estimation techniques available in the software ISATIS (Geovariances, 2011). A geostatistical analysis was performed to estimate the altitude of the top of the FAS and the top of the ICU, which had substantially more well control than the other hydrogeologic units. This geostatistical analysis utilized kriging and a moving geostatistics procedure to account for local variability of the data, the uneven spatial distribution of data points, and the long-range drift related to structural or depositional features. Because strong correlation was identified between the global trend of the altitude of the top of the FAS and the deeper units, a thickness filtering approach was used to guide the estimation of the deeper hydrogeologic units that had less well control. The thickness between the interpreted top surface of the FAS and each lower hydrogeologic unit was calculated at each sampled location. The thickness values were then used in an ordinary kriging process to map the thickness across the area. This thickness map displays a more stationary behavior than could be derived by kriging only the data values available for the top of a given hydrogeologic unit. The upper surface of a hydrogeologic unit was then computed by subtracting the mapped thickness from the mapped altitude of the top of the FAS across the ECFT study area. This technique maintained consistency between hydrogeologic surfaces, and prevented unrealistic estimations of altitude or thickness in areas having limited well control. These procedures captured the large-scale geologic structures and local karst features, while honoring actual data values.

Surficial Aquifer System

In the study area, the unconfined to semiconfined SAS consists of unlithified sediments of variable permeability comprising Holocene undifferentiated sediments and Pliocene to Pleistocene formations (post-Hawthorn Group sediments). The sediments are primarily composed of clean sands and intermittent clay beds occurring mostly as discontinuous lenses. The lithology of the surficial sediments can vary substantially both vertically and laterally across short distances. The shell and sand beds of the Pleistocene Anastasia Formation and the sand beds of the Okeechobee, Nashua, and Cypresshead Formations compose the water-producing zones of the SAS. Where surficial sediments are absent due to erosion, the SAS is thin or non-existent at land surface. In other areas, surficial sediments can be greater than 100 ft thick, such as in upland

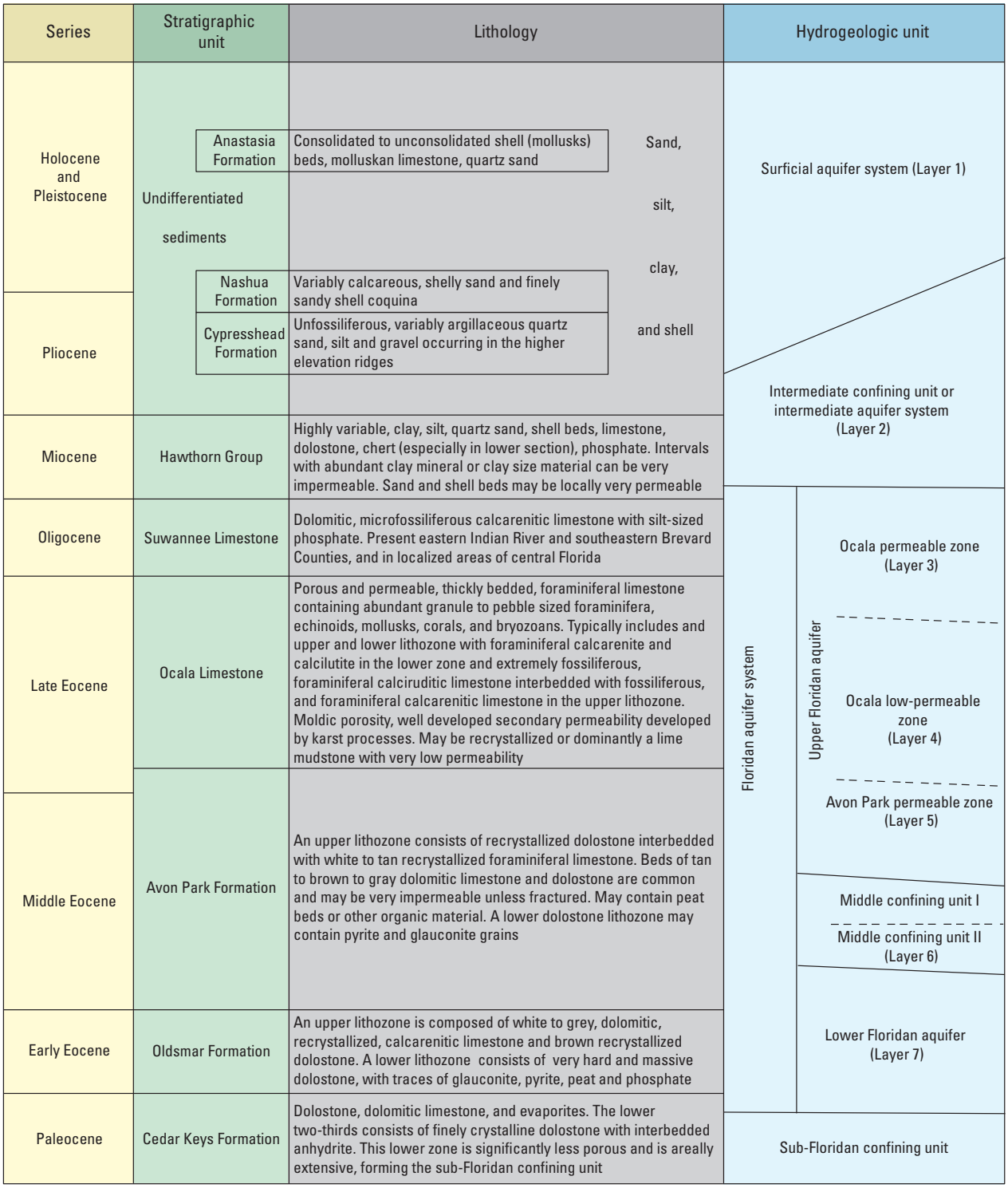

Figure 15. Relation between stratigraphic and hydrogeologic units in the East-Central Florida Transient (ECFT) study area.

ridge areas underlain by recent terrace deposits. The surficial siliciclastic sediments may be thicker than at the nearby mantle that infills karst collapse features.

The mapped upper surface of the SAS in the study area directly corresponds with land surface altitude (fig. 16), which ranges from 0 to 302 ft NGVD 29 in the ECFT study area. The thickness of the SAS in the ECFT study area ranges from 5 to 240.6 ft (fig. 17). Across most of the study area the SAS is underlain by the ICU/IAS, but in some western parts of the study area, the SAS may directly overlie the UFA. The base of the SAS may be marked by a distinct clay unit or a gradational increase in clay or other fine-grained sediment.

Generally, groundwater within the SAS is unconfined, although in some areas, beds of low permeability cause semi-confined or locally confined conditions in deeper parts of the aquifer. Hydraulic conductivity data for the SAS were selected from databases of the USGS, SJRWMD, SWFWMD, and SFWMD. According to these data, the horizontal hydraulic conductivity in the SAS in the ECFT study area ranges from 6 to 55 feet per day (ft/d) (fig. 18). McGurk and Presley (2002) and Sepúlveda (2002) describe the prevailing hydraulic gradients in the SAS, its correlation with land-surface altitude, and maps of the water-table altitude.

The utility of the SAS for water supply depends on sufficient thickness and lateral extent of permeable zones to provide consistent groundwater storage and transmission. The SAS is thickest in the south-central portion of the ECFT study area (fig. 17). Areas in the northwest may also be thick enough to provide sufficient production for specific uses. In some areas, localized, low permeable clay, silt, or very fine sand layers may limit use of the SAS. Although withdrawals from the SAS are greatest in Polk, Indian River, and Highlands Counties, the SAS is used to some extent everywhere within the ECFT study area.

Intermediate Confining Unit and Intermediate Aquifer System

The ICU/IAS comprises the largely clastic sediments of the Miocene Hawthorn Group that generally restrict the movement of water between the overlying SAS and underlying FAS (fig. 15). Generally, the ICU acts as a confining unit for the FAS, but where there are multiple permeable zones, the sequence of hydrogeologic units is referred to as the IAS. In this report, these units are referred to collectively as the ICU/IAS, and are conceptualized for simulation purposes as a single composite unit.

The top of the ICU/IAS is defined by the uppermost, laterally extensive, and vertically continuous sediments of lower permeability below the SAS or, where the surficial sediments are eroded, by land surface. In areas where the Hawthorn Group sediments are thin or absent, such as northern Brevard County and parts of Volusia and Lake Counties, erosional remnants of the Hawthorn Group and Pliocene sediments act as a semiconfining unit. In the northeastern part of the ECFT study area, fine-grained Pliocene-aged or reworked Hawthorn Group sediments above or in place of the Hawthorn Group are considered part of the ICU/IAS. The base of the ICU/IAS is at the top of the vertically continuous, permeable carbonate section of the FAS. In the study area, the altitude of the top of the ICU/IAS ranges from -136.8 to 135.4 ft (fig. 19), and ICU/IAS thickness ranges from 3.3 to 412.1 ft (fig. 20)

The IAS is present throughout most of the southwestern part of the ECFT study area and is characterized by clastic sediments interbedded with carbonate rocks of Miocene age that generally coincide with the Hawthorn Group (fig. 21). Although the IAS is less permeable than the underlying UFA, the carbonate strata within the IAS are sufficiently permeable and productive to constitute a groundwater supply. Two main permeable zones are present in the IAS in the ECFT study area (Basso, 2003; Basso and Hood, 2005; Knochenmus, 2006); where these are present, the IAS is confined above and below by confining zones of the ICU.

The horizontal hydraulic conductivity of the IAS from aquifer tests obtained from databases of the SWFWMD ranged from 1 to 230 ft/d (fig. 21). The only hydraulic conductivity value found for the ICU (23 ft/d, fig. 21) was from an aquifer test performed in east-central Orange County. This production zone in the ICU is outside the extent of the IAS, and the hydraulic conductivity value obtained is not typical of the ICU and therefore not considered representative.

Floridan Aquifer System

The FAS comprises a thick sequence of layered, carbonate rocks of varying permeability. The limestones, dolomitic limestones, dolostones, and evaporites that compose the FAS were deposited in marine carbonate shelf environments, resulting in variable mineralogy and depositional characteristics. Post-depositional processes, including cementation and dissolution, as well as fracturing, karst processes and larger-scale structural features, have subsequently altered the original physical characteristics of the sediments and resulted in highly variable lithology and permeability within the FAS (Miller, 1986). Vertically and laterally extensive zones of enhanced porosity and permeability are present in the aquifer units and alternate with extensive zones of relatively lower porosity and permeability that compose the confining units.

The FAS generally corresponds to the Paleocene upper Cedar Keys Formation, the early Eocene Oldsmar Formation, the middle Eocene Avon Park Formation, the late Eocene Ocala Limestone, and the Oligocene Suwannee Limestone (fig. 15). The top of the FAS generally coincides with a distinct downward transition from the largely clastic, fine-grained Miocene-aged sediments, to a permeable carbonate section that is vertically and laterally extensive. Throughout most of the study area, the uppermost surface of the FAS coincides with the top of the Ocala Limestone, yet where present, the Suwannee Limestone forms the top of the FAS. In localized areas of central peninsular Florida, the Suwannee Limestone and Ocala Limestone are absent due to erosion or

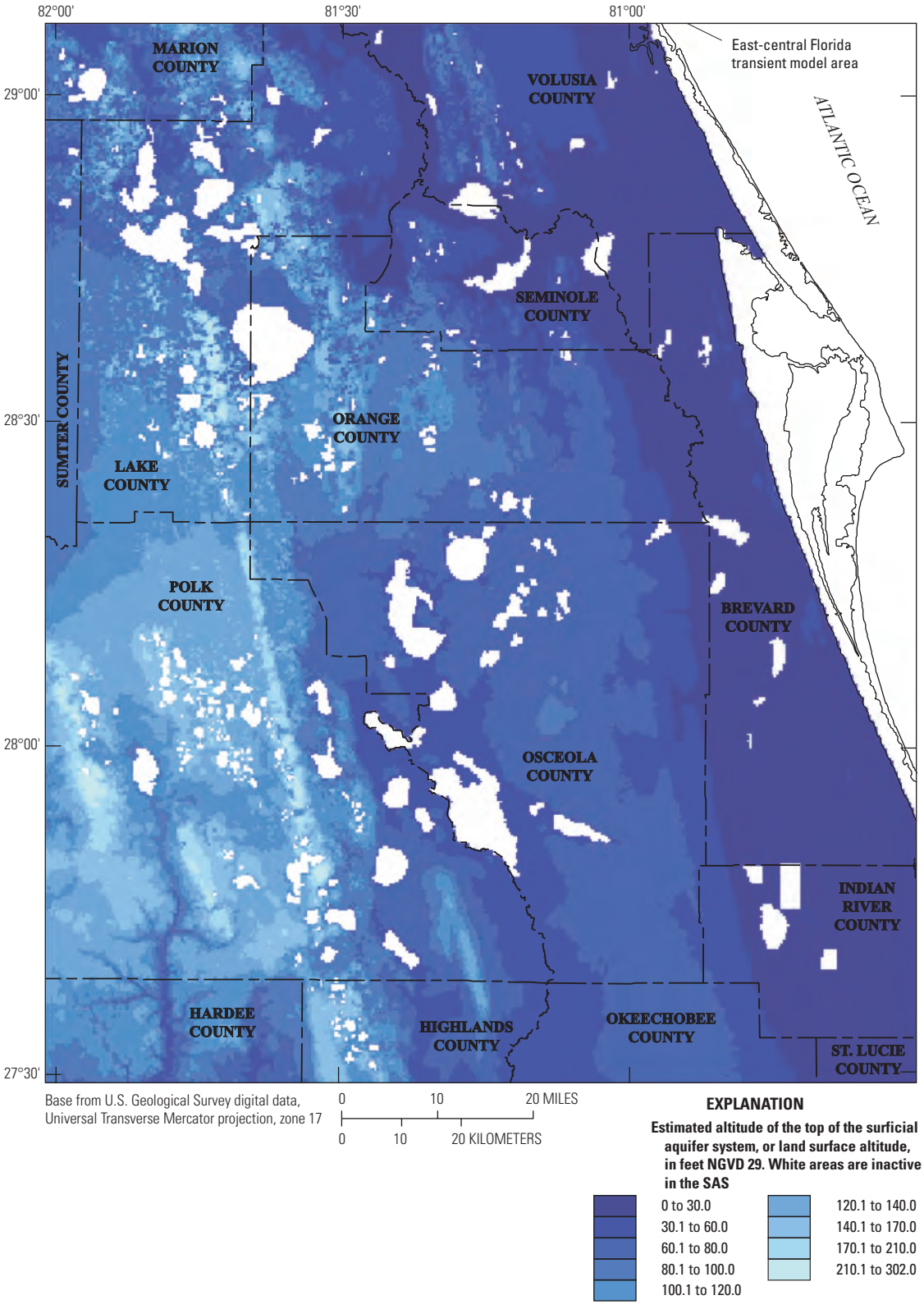

Figure 16. Altitude of land surface (top of the surficial aquifer system) in the East-Central Florida Transient (ECFT) study area.

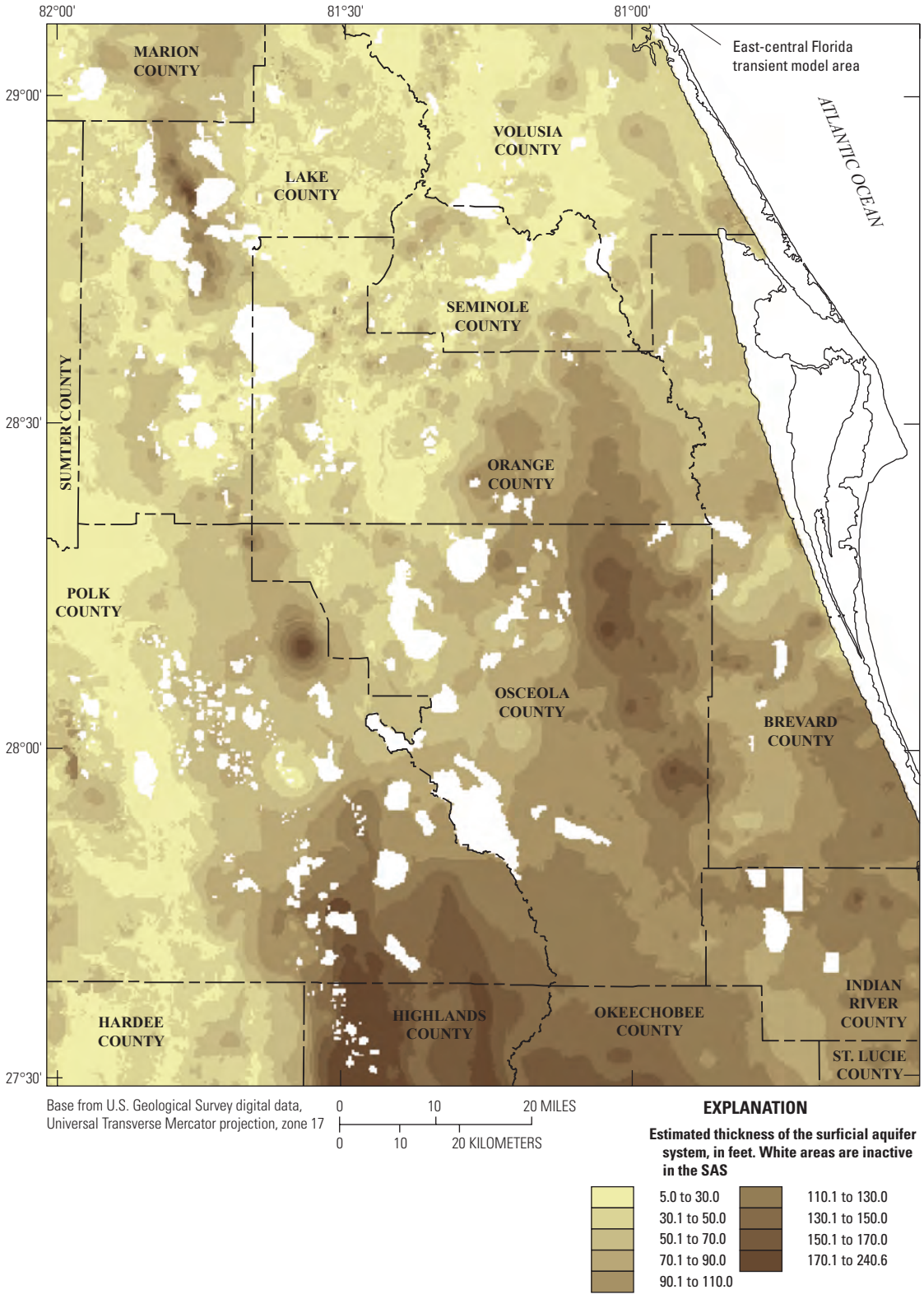

Figure 17. Thickness of the surficial aquifer system in the East-Central Florida Transient (ECFT) study area.

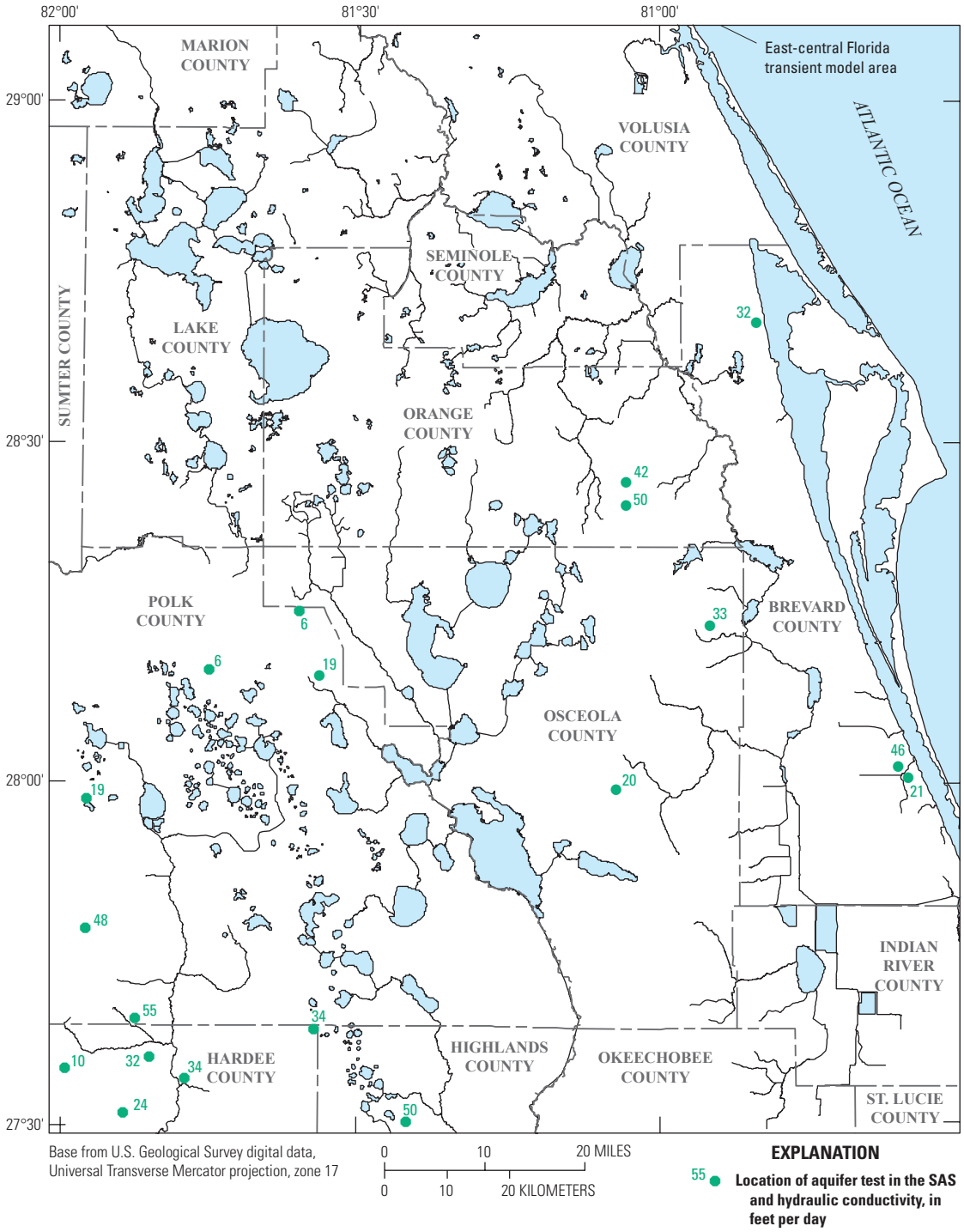

Figure 18. Hydraulic conductivity in the surficial aquifer system (SAS) from selected aquifer tests.

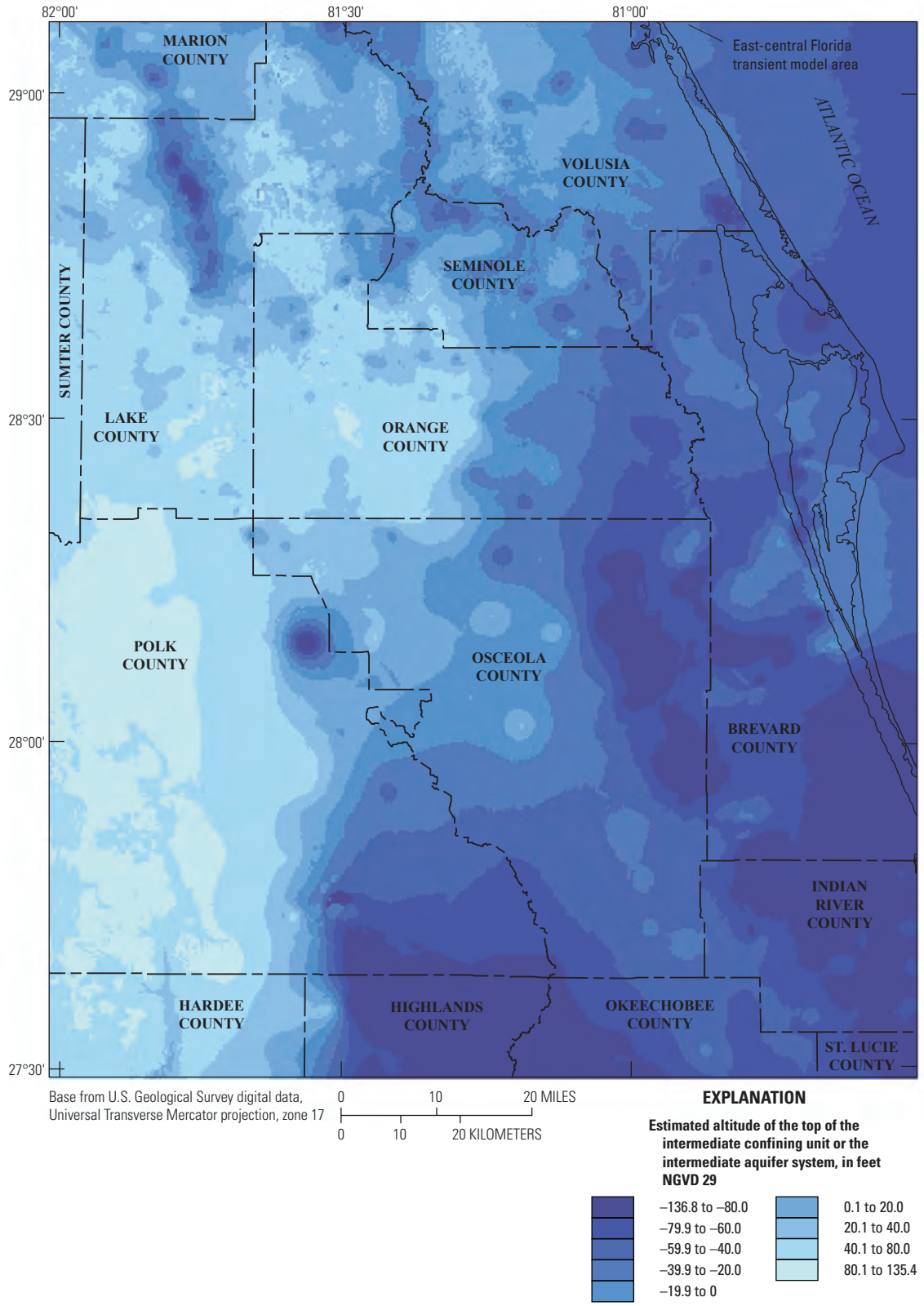

Figure 19. Altitude of the upper surface of the intermediate confining unit/intermediate aquifer system in the East-Central Florida Transient (ECFT) study area.

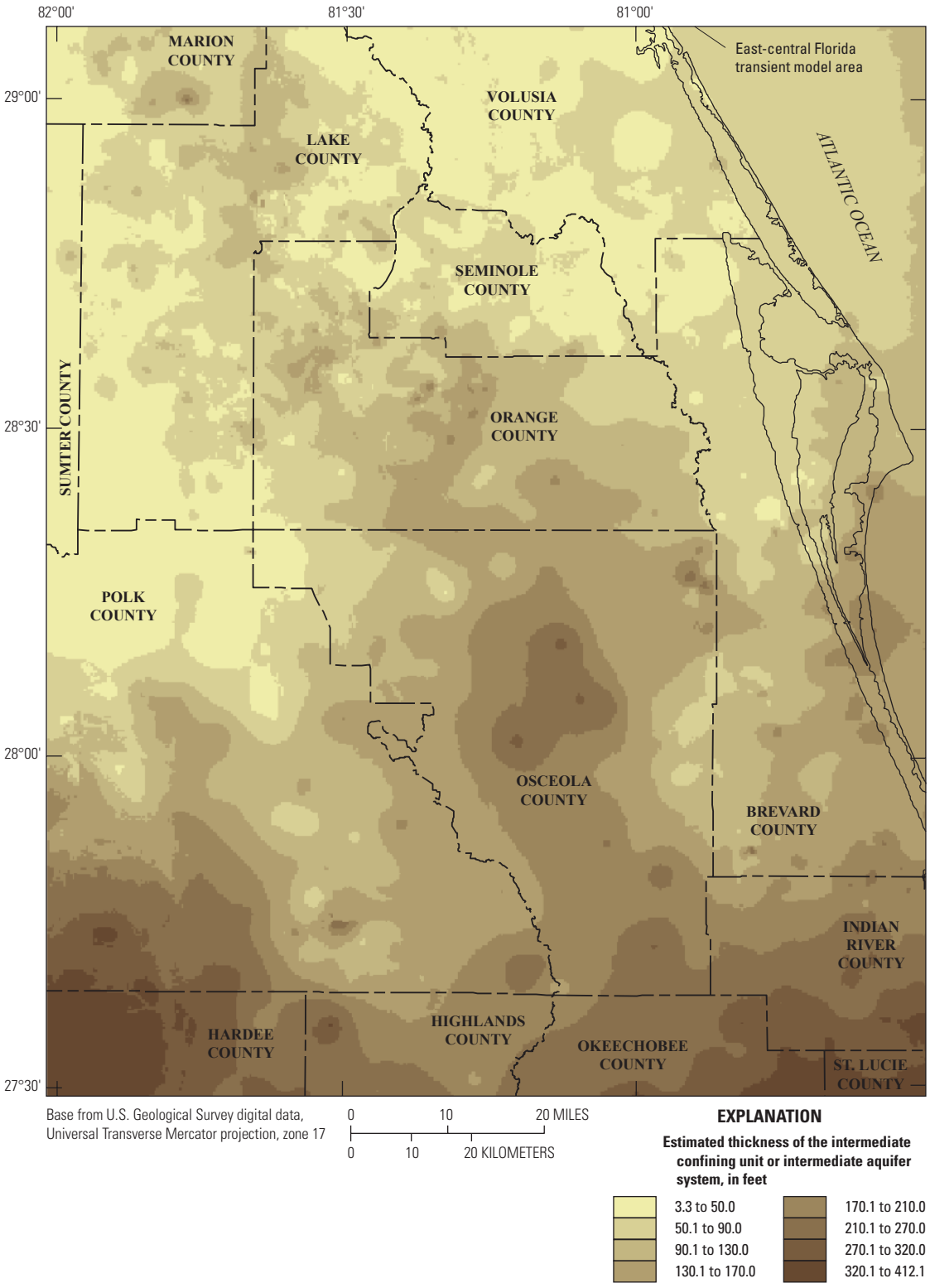

Figure 20. Thickness of the intermediate confining unit/intermediate aquifer system in the East-Central Florida Transient (ECFT) study area.

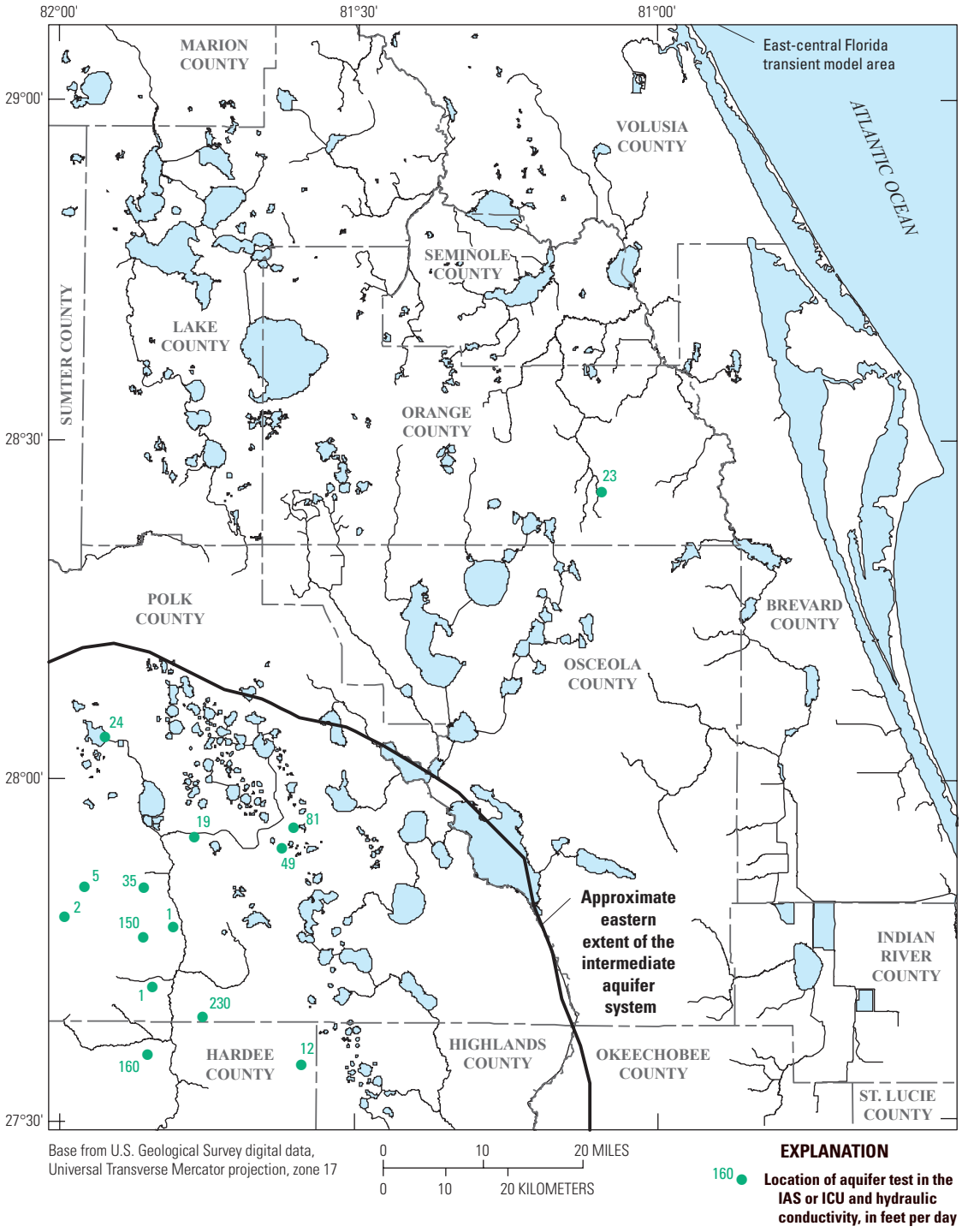

Figure 21. Hydraulic conductivity in the intermediate aquifer system (IAS) and the intermediate confining unit (ICU) from selected aquifer tests.

nondeposition, and the Avon Park Formation is the uppermost geologic unit of the FAS. The base of the FAS is within the Cedar Keys Formation and is characterized by a regionally continuous sequence of anhydrite beds interlayered with dolostone.

The FAS is subdivided into regionally extensive aquifers and confining units, including the UFA, MCU I/II, and LFA. The UFA is further subdivided into the regionally extensive OPZ, OLPZ, and APPZ (fig. 15). All of these units are explicitly represented in the ECFT model. The permeable zones of the UFA are characterized by variable porosity and permeability, depending on the depositional texture and mineralogy of the rocks and on the presence of fractures and secondary dissolution features. Within each hydrogeologic unit, local zones of contrasting permeability may be present, but these contrasting zones generally do not affect the regional hydraulic characteristics of a unit.

The configuration, dip, and thickness of the OPZ, OLPZ, and APPZ are influenced by regional and local structural features, as well as karst and erosional processes. The altitude of the top of each unit follows regional structures, and the thickness of each unit tends to be greater in structurally low areas and less in the structurally high areas. The subregional to localized highs and lows in the ECFT study area are probably erosional or karst features superimposed on the regional structural features. The bottom of the UFA is marked by a regionally extensive confining unit of lower permeability, corresponding either to MCU I in most of the study area or to MCU II in the southwestern part of the study area.

The Ocala Permeable Zone

The OPZ is a highly productive zone at the top of the FAS, characterized by intergranular, moldic, and vuggy primary porosity and well-developed secondary porosity (Davis and Boniol, 2011); the zone corresponds to the Ocala Limestone and the Suwannee Limestone (where present) lithostratigraphic units. The OPZ is equivalent to zone A of the UFA (O'Reilly and others, 2002) and the upper permeable zone of the UFA (Spechler, 2010). Zones of enhanced permeability are characterized by cavities, caves, and other dissolution features likely formed by karst processes. The OPZ is the primary groundwater production zone for many areas of Florida, except for those areas having poor water quality. The altitude of the top of the OPZ in the study area ranges from 426.2 to 85.6 ft NGVD 29 (fig. 22). The thickness of the OPZ ranges from 50.1 to 519 ft (fig. 23). Horizontal hydraulic conductivity values derived from aquifer tests selected from USGS, SJRWMD, SWFWMD, and SFWMD databases ranged from 6 to 14,000 ft/d in the OPZ and show large spatial variability (fig. 24).

A potentiometric surface was estimated for the OPZ for average 1995 conditions from monthly average heads (fig. 25). The data for most of the sites used to generate the surface include 12 average monthly head values, but about 10 percent of the sites had fewer data. For each of these sites, average annual head was estimated using multiple linear regressions that relate the average annual head to two monthly average heads.

The potentiometric surface of the OPZ shows a groundwater high in Polk County that groundwater would flow radially away from. This high corresponds to a topographic high in the southern Green Swamp physiographic area (figs. 2 and 16). The shape of the potentiometric mound around this high is oblong, creating an approximately north/south divide in the western part of the study area, from Marion County through the high in Highlands County that approximately follows the Lake Wales Ridge (fig. 25). Groundwater flows away from the divide and generally in a direction perpendicular to the potentiometric surface contours. The 10-ft closed depression contour in the northeastern area shown in figure 25 corresponds to the location of Blue Spring (table 2–1, figs. 25 and 2–1), the spring with the greatest flow rate in the model area. The absence of a corresponding depression in the potentiometric surface map for Alexander Springs (figs. 1 and 25) is likely the result of the 5-ft contour interval, which is larger than the depression in local heads caused by the spring. Closely spaced contours in the west-central section of the model area reflect a transition zone in hydraulic conductivity (figs. 24 and 25).

The Ocala Low-Permeable Zone

The OLPZ is a zone of relatively lower permeability than that of the overlying OPZ and underlying APPZ, and consists of micritic limestone, dolomitic limestone, and dolostone within the Ocala Limestone and the upper Avon Park Formation. This zone is equivalent to the middle confining unit I separating the UFA from the APPZ as defined by Reese and Richardson (2008). The OLPZ is characterized by the lack of enhanced dissolution features or fractures that are prevalent in permeable units of the UFA. Although intervals of moderate permeability or thin cavities can be present within the OLPZ, this unit is not a major source of groundwater, and generally acts as a semiconfining zone. The term "Ocala low-permeable zone" used herein replaces nomenclature previously used to describe the Ocala semiconfining zone (Mallams and Lee, 2005). The OLPZ has, however, been used in some recent SWFWMD Regional Observation and Monitor-well Program (ROMP) reports (LaRoche, 2007). The altitude of the OLPZ in the study area ranges from -929.7 to -90.3 ft NGVD 29 (fig. 26). The thickness of the OLPZ ranges from 10 to 715.1 ft (fig. 27).

The Avon Park Permeable Zone

The APPZ consists of thick beds of dolostone with thinner interbedded limestone and dolomitic limestone that are present within the middle to upper Avon Park Formation (O'Reilly and others, 2002). This hydrogeologic unit has been alternatively defined as zone B of the UFA (O'Reilly and others, 2002), and the dolostone zone (McGurk and Presley, 2002). The dolostone texture varies from poorly to moderately consolidated,

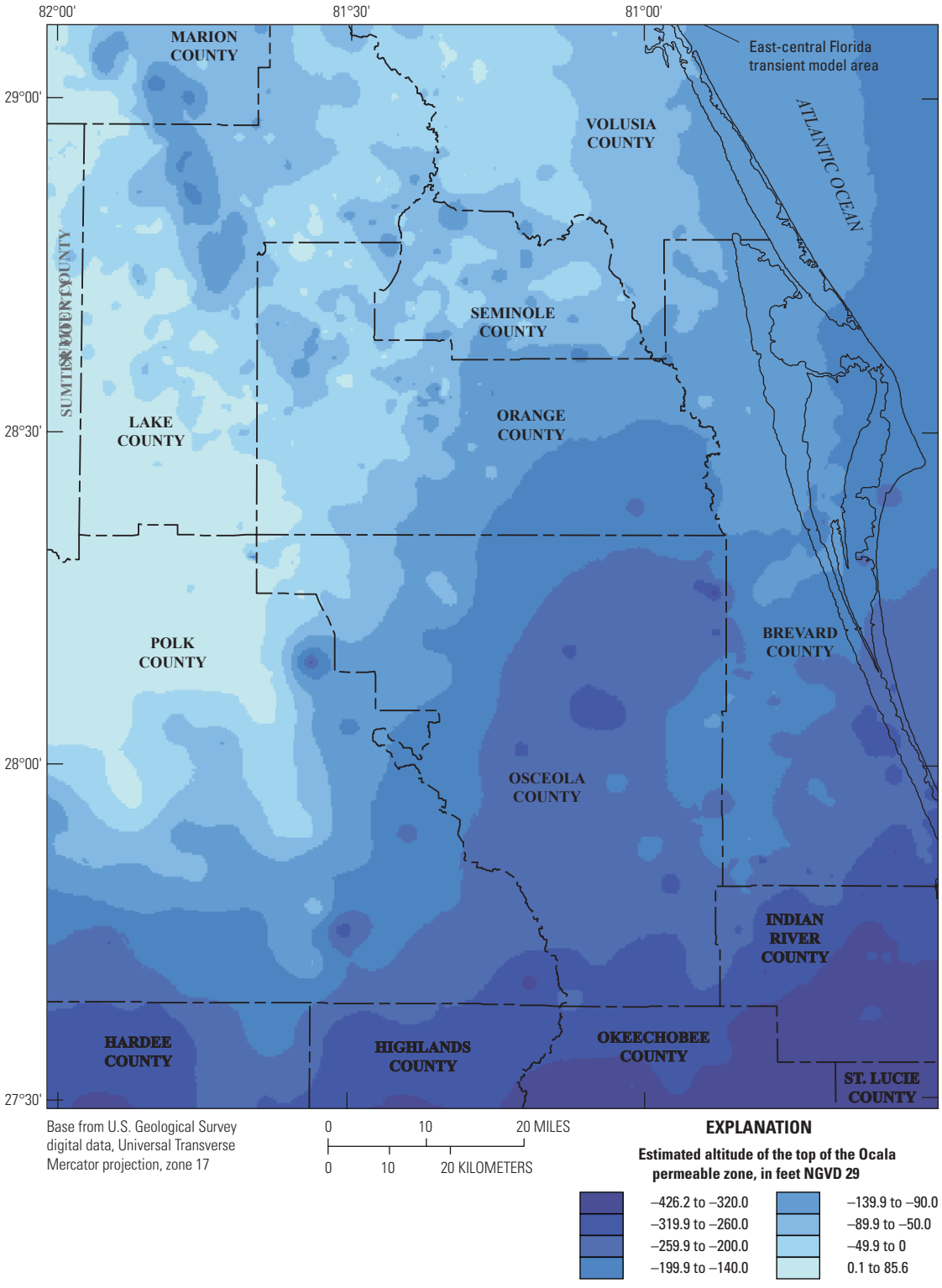

Figure 22. Altitude of the upper surface of the Ocala permeable zone (top of the Upper Floridan aquifer) in the East-Central Florida Transient (ECFT) study area.

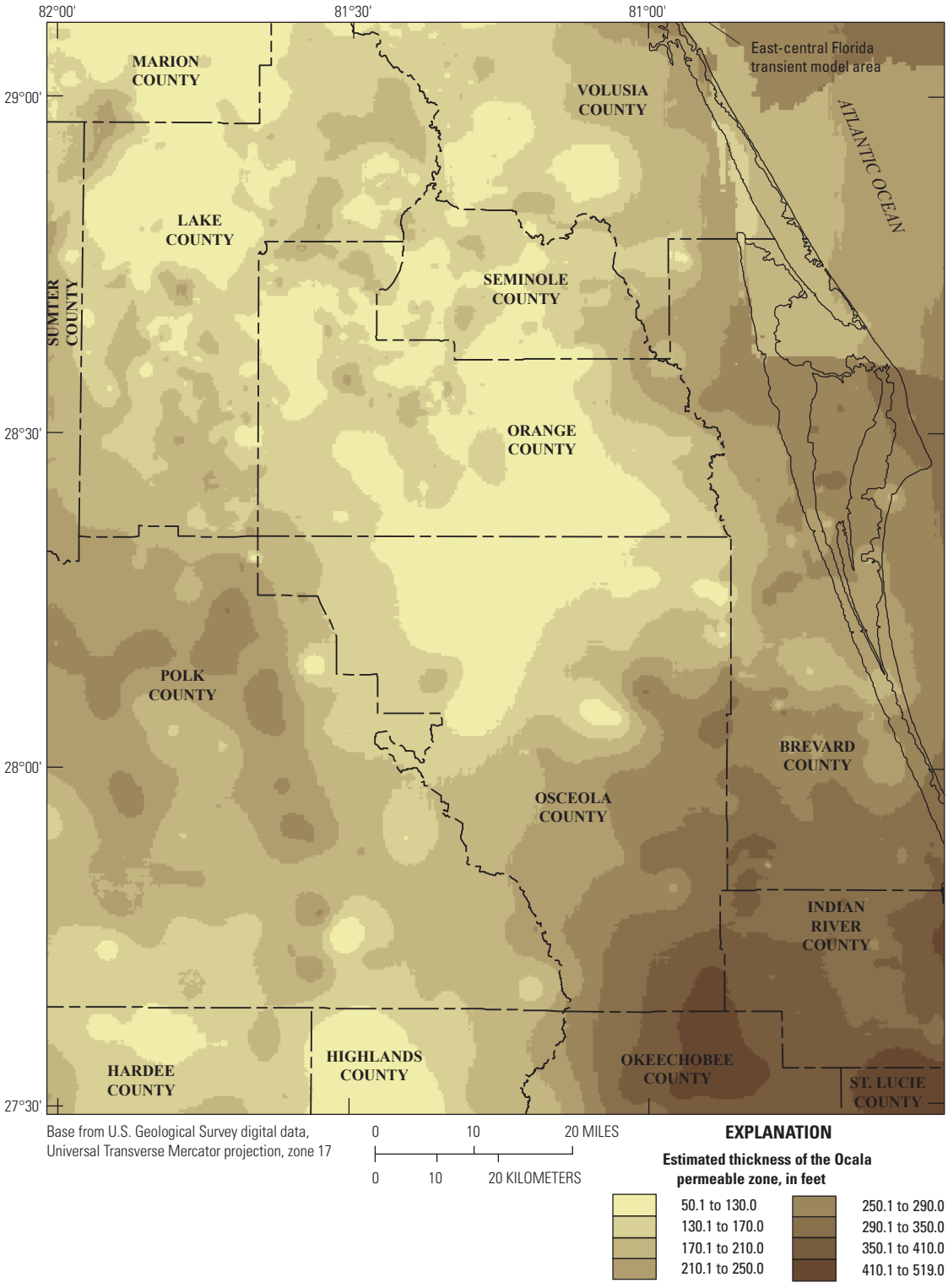

Figure 23. Thickness of the Ocala permeable zone in the East-Central Florida Transient (ECFT) study area.

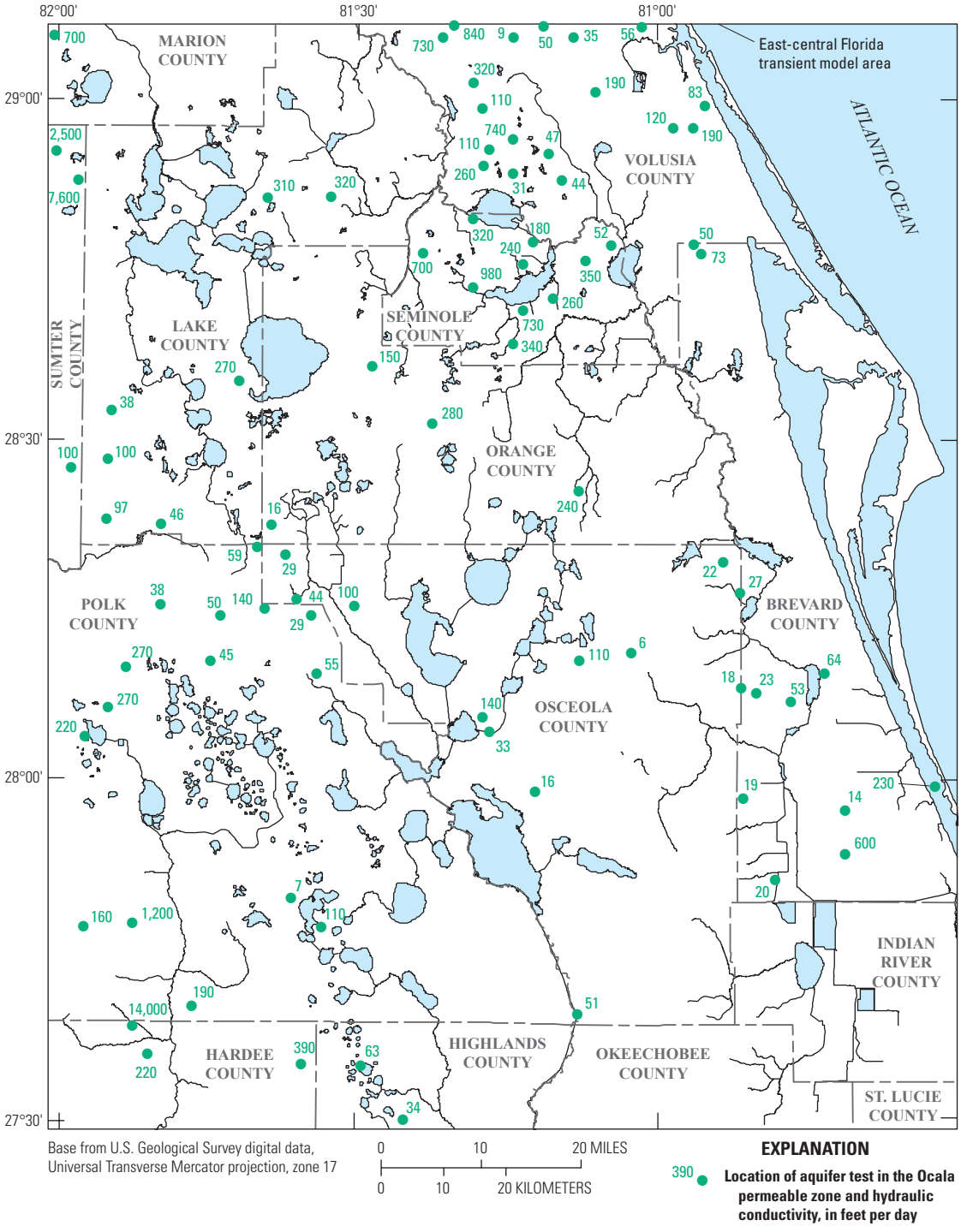

Figure 24. Hydraulic conductivity in the Ocala permeable zone from selected aquifer tests.

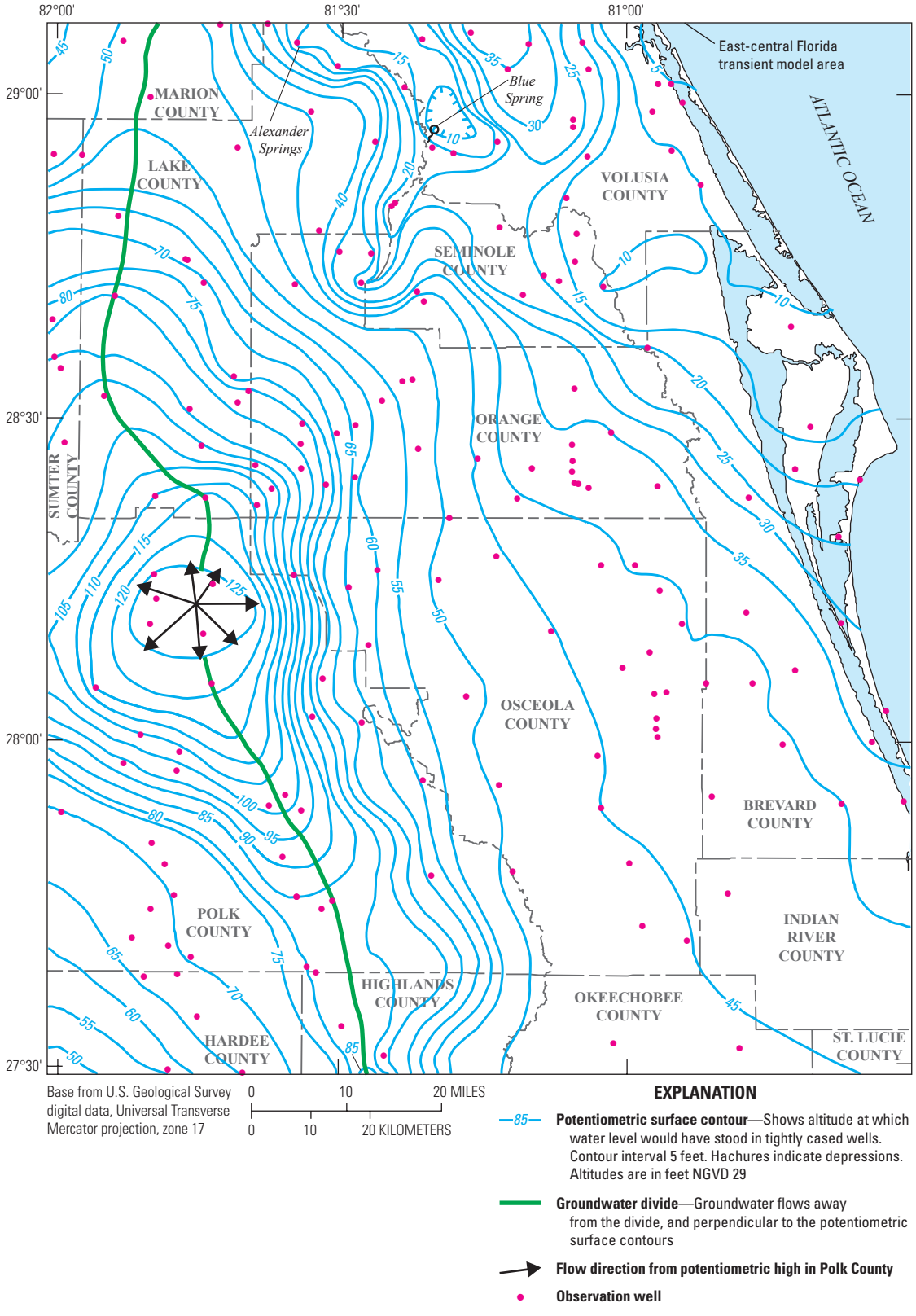

Figure 25. Estimated potentiometric surface of the Ocala permeable zone (Upper Floridan aquifer), average 1995 conditions.

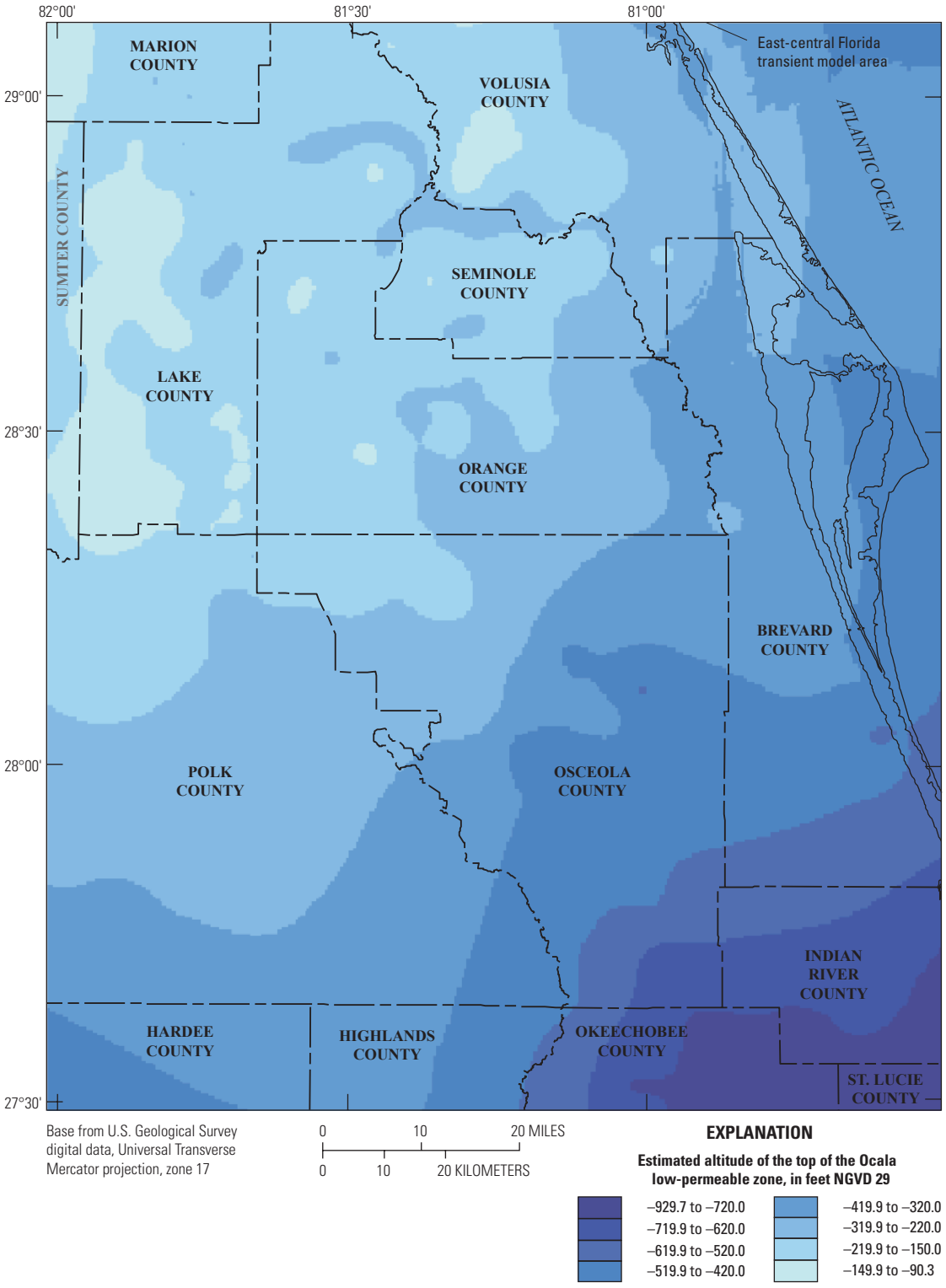

Figure 26. Altitude of the upper surface of the Ocala low-permeable zone in the East-Central Florida Transient (ECFT) study area.

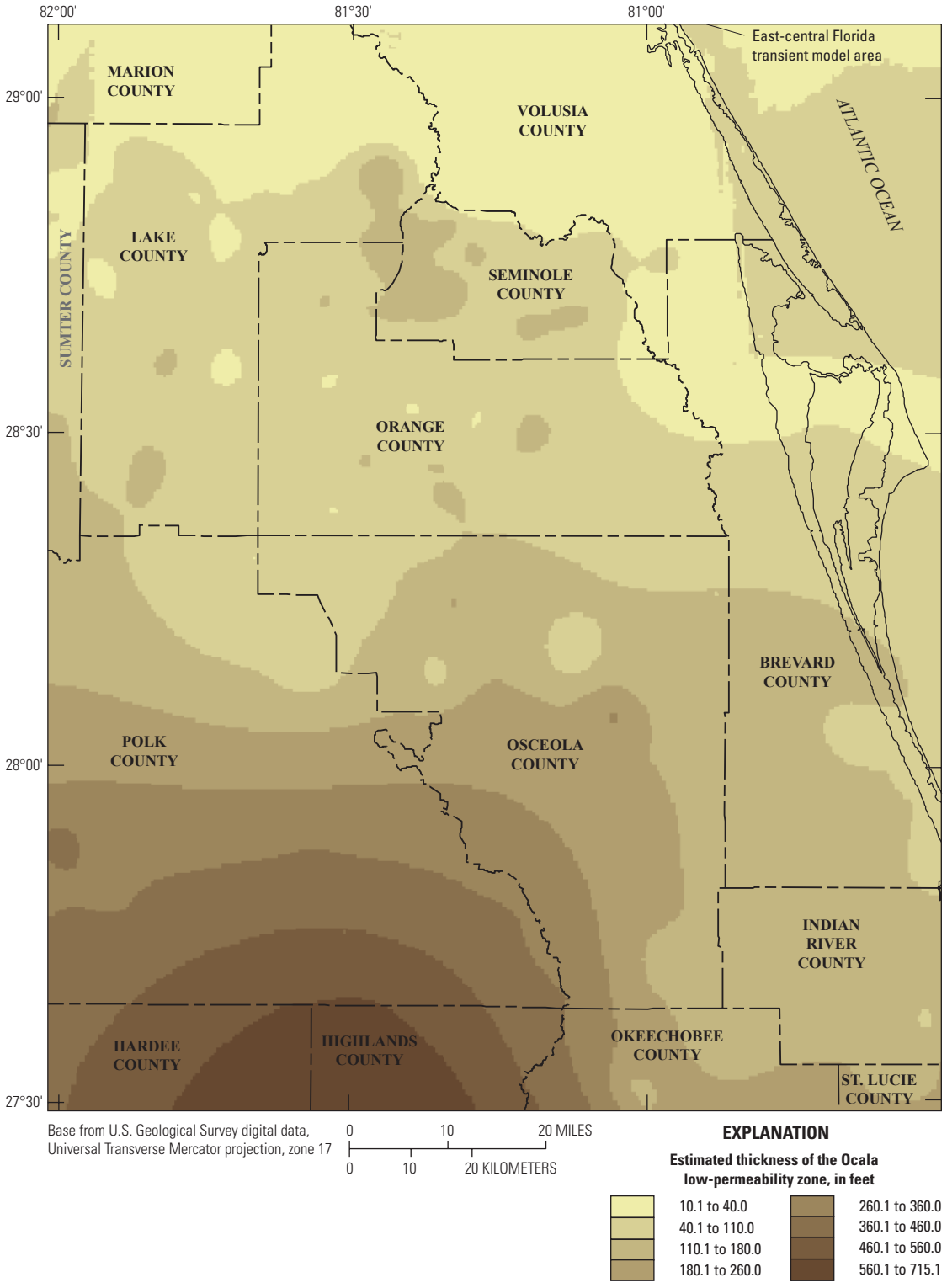

Figure 27. Thickness of the Ocala low-permeable zone in the East-Central Florida Transient (ECFT) study area.

to dense, hard, and massive. The dolostones typically have low intergranular primary porosity, with high secondary porosity and permeability caused by fracturing and dissolution cavities. Zones of fractured and cavernous dolostone in the APPZ are a major source of water supply. The degree of hydraulic connectivity between productive zones is uncertain and dependent upon the presence of interconnected fractures and caverns. Layers of dense, unfractured dolostone provide a degree of confinement between the flow zones.

APPZ wells are commonly characterized by numerous abrupt borehole enlargements when drilled into carbonate rock affected by dissolution, fracturing, and downhole sloughing of rock material. Characteristic borehole geophysical data include an increase in gamma-ray activity associated with the dolostone, high resistivity except where affected by borehole enlargement, and erratic neutron detection activity or acoustic velocity suggesting substantial porosity variability. Borehole flowmeter data indicate the presence of large flow zones marked by large temperature or fluid resistivity changes (Reese and Richardson, 2008; O'Reilly and others, 2002). Video logs also show the presence of distinct fracture and cavernous zones. Within the study area, many of the wells utilized for public supply and agricultural purposes are completed into this zone. In the ECFT study area, the altitude of the upper surface of the APPZ ranges from -1,131 to -104 ft NGVD 29 (fig. 28) and APPZ thickness ranges from 50 to 629.4 ft (fig. 29).

Selected horizontal hydraulic conductivity values compiled for the APPZ ranged from 30 to 3,400 ft/d (fig. 30), a narrower range than that compiled for the OPZ, but this may be at least partly the result of fewer data. Because of the leakiness of the OLPZ, head differences between the OPZ and the APPZ are relatively small and range from about -3 ft in southwestern Volusia County, indicating an upward gradient, to almost 4 ft in eastern Seminole County, indicating a downward gradient (fig. 31).

Middle Confining Unit I and Middle Confining Unit II

The MCU I and MCU II are two distinct regional confining units that correlate with the Avon Park Formation and separate the UFA from the LFA. MCU I corresponds to the middle semiconfining unit I in the eastern half of peninsular Florida, and MCU II corresponds to the middle semiconfining unit II in west-central Florida, as designated by Miller (1986). MCU I consists of dolostone, micritic limestone, and dolomitic limestone, locally containing some gypsum and chert, and corresponds to the middle to lower part of the Avon Park Formation. This confining unit is characterized and distinguished from the overlying UFA and underlying LFA by secondary mineralization in the pore spaces and a lack of secondary porosity. MCU I can be identified in borehole logs by a consistent temperature and fluid resistivity relative to overlying and underlying permeable zones, suggesting intra-borehole flow and the lack of substantial flow zones (O'Reilly and others, 2002). MCU II is present in the southwestern part of the study area at a lower altitude than MCU I and is composed of hard, crystalline dolomitic limestone and gypsiferous dolomite corresponding to the middle to lower parts of the Avon Park Formation. MCU II is characterized by the presence of gypsum as beds or infilling of pore spaces, and by dense, unfractured dolomite that exhibits a decrease in formation resistivity and a sharp decrease in flow compared to the overlying and underlying permeable zones.

MCU I and MCU II are offset, and the former areally overlaps the latter within the study area, so these units are considered together herein. The altitude of the upper surface of the MCU I/II in the study area ranges from -1,604.3 to -153.9 ft NGVD 29 (fig. 32) and its thickness ranges from 115.8 to 743.7 ft (fig. 33).

The Lower Floridan Aquifer

The Lower Floridan aquifer (LFA) comprises a sequence of alternating zones of relatively higher and lower permeability. The top of the LFA is identified by a substantial increase in permeability relative to the overlying MCU I/II as indicated by borehole flow, temperature, and fluid resistivity logs (O'Reilly and others, 2002). The upper permeable zone of the LFA consists largely of dolostone and dolomitic limestone, with abundant fractures and dissolution features corresponding to the lower part of the Avon Park Formation and the upper part of the Oldsmar Formation. Some chert, peat, and minor amounts of gypsum and anhydrite may be present in lower parts of this zone. Enhanced permeability occurs in intervals containing fractured dolostone. The upper permeable zone of the LFA can be highly productive in some locations and is the source for a large number of public water-supply utilities in the study area.

The altitude of the top of the LFA in the study area ranges from -1,854.1 to -435.1 ft NGVD 29 (fig. 34). The hydrogeologic framework presented herein does not differentiate permeable zones below the LFA upper permeable zone. The number of wells for which identification of the lower units is possible is limited and insufficient for regional mapping. The altitude of the base of the FAS as mapped by Miller (1986, plate 33) was used to estimate the thickness of the LFA in the study area, which ranged from 922 to 1,944 ft (fig. 35).

The limited information available concerning the lithology, permeability, and water-bearing characteristics of the LFA generally pertains to the upper permeable zone. Selected values of horizontal hydraulic conductivity from aquifer tests in the LFA, compiled from databases of the USGS, SJRWMD, SWFWMD, and SFWMD, ranged from 23 to 7,700 ft/d (fig. 36).

Where average monthly head data are available for both the UFA and LFA, the head differences between the aquifers range from more than 37 ft in northeastern Polk County, indicating a downward gradient, to almost -9 ft in southwestern Volusia County, indicating an upward gradient. The MCU II has characteristically low permeability in the southwestern portion of the ECFT study area, and likely causes the large head differences between the UFA and the LFA observed near the boundary of the eastern extent of the MCU II (fig. 31) (B.E. McGurk, St. Johns River Water Management District, written commun., 2010).

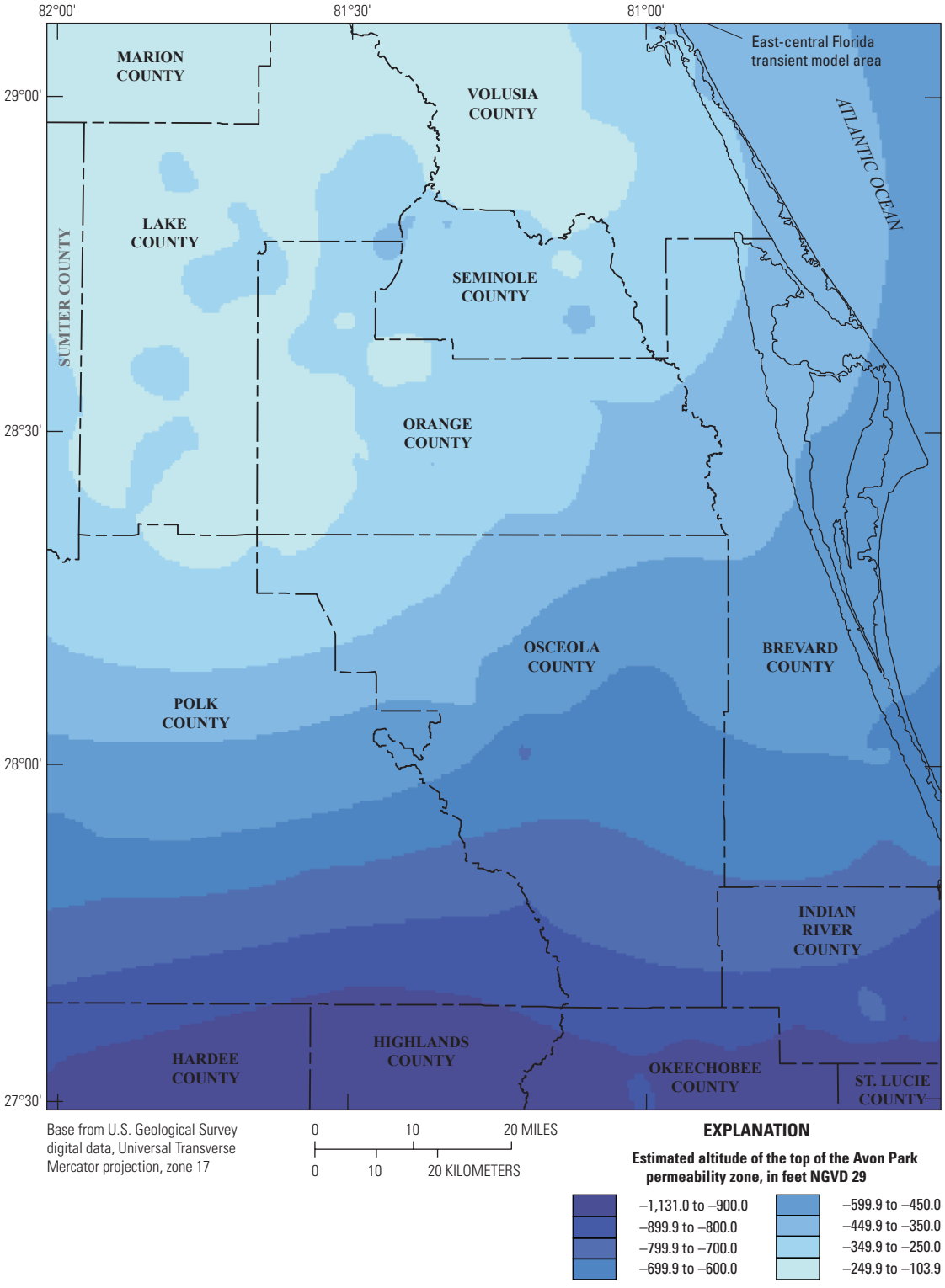

Figure 28. Altitude of the upper surface of the Avon Park permeable zone in the East-Central Florida Transient (ECFT) study area.

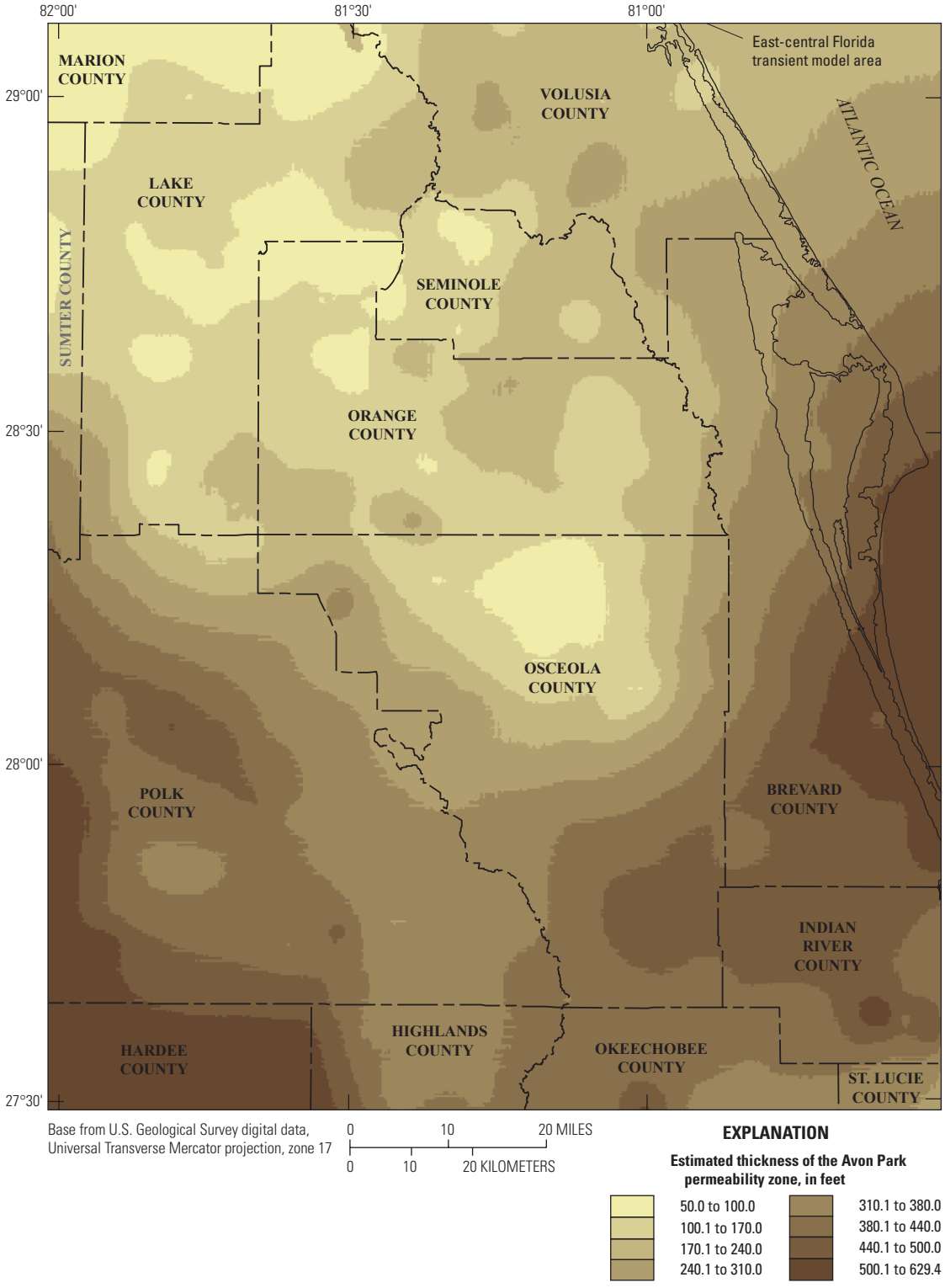

Figure 29. Thickness of the Avon Park permeable zone in the East-Central Florida Transient (ECFT) study area.

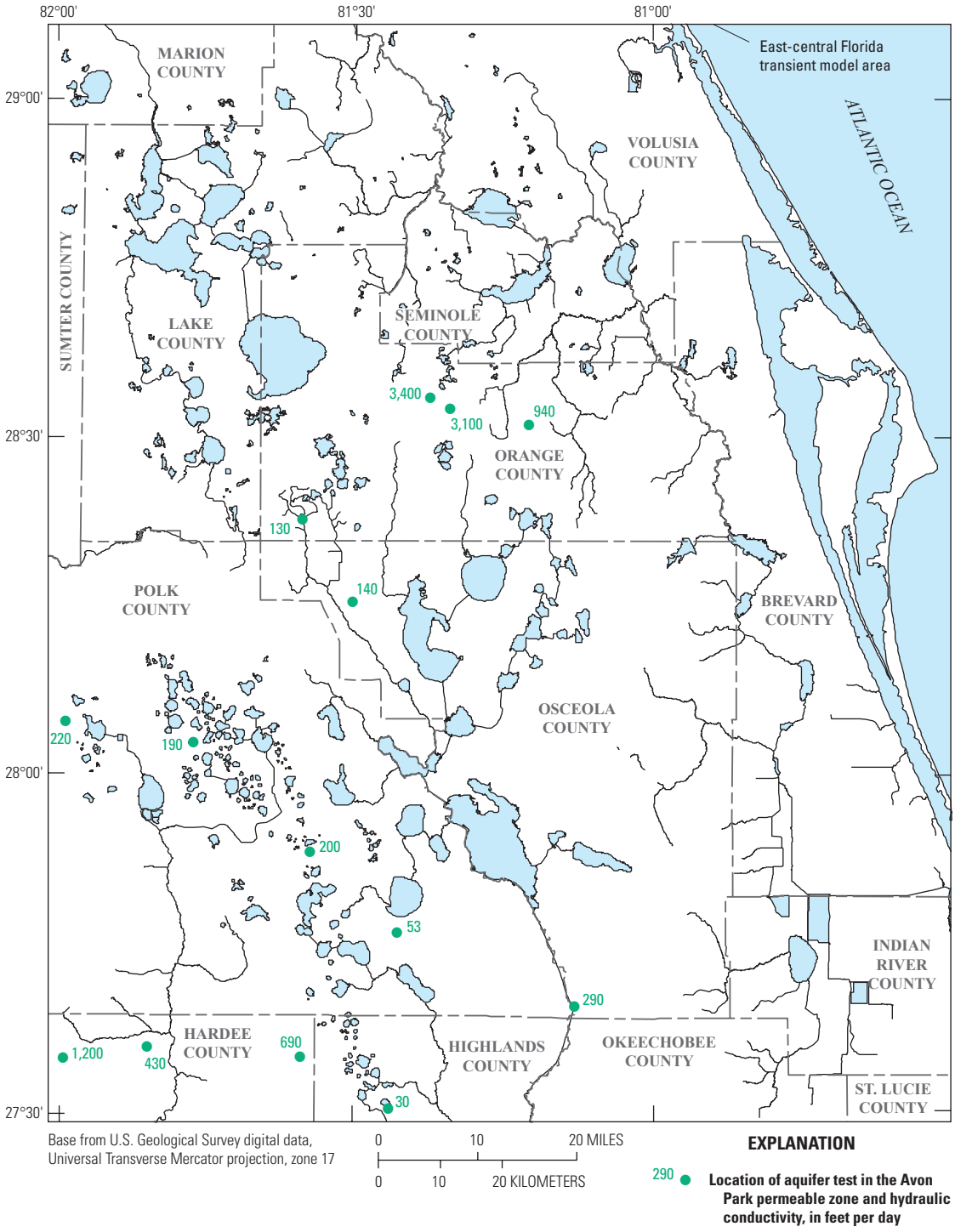

Figure 30. Hydraulic conductivity in the Avon Park permeable zone from selected aquifer tests.

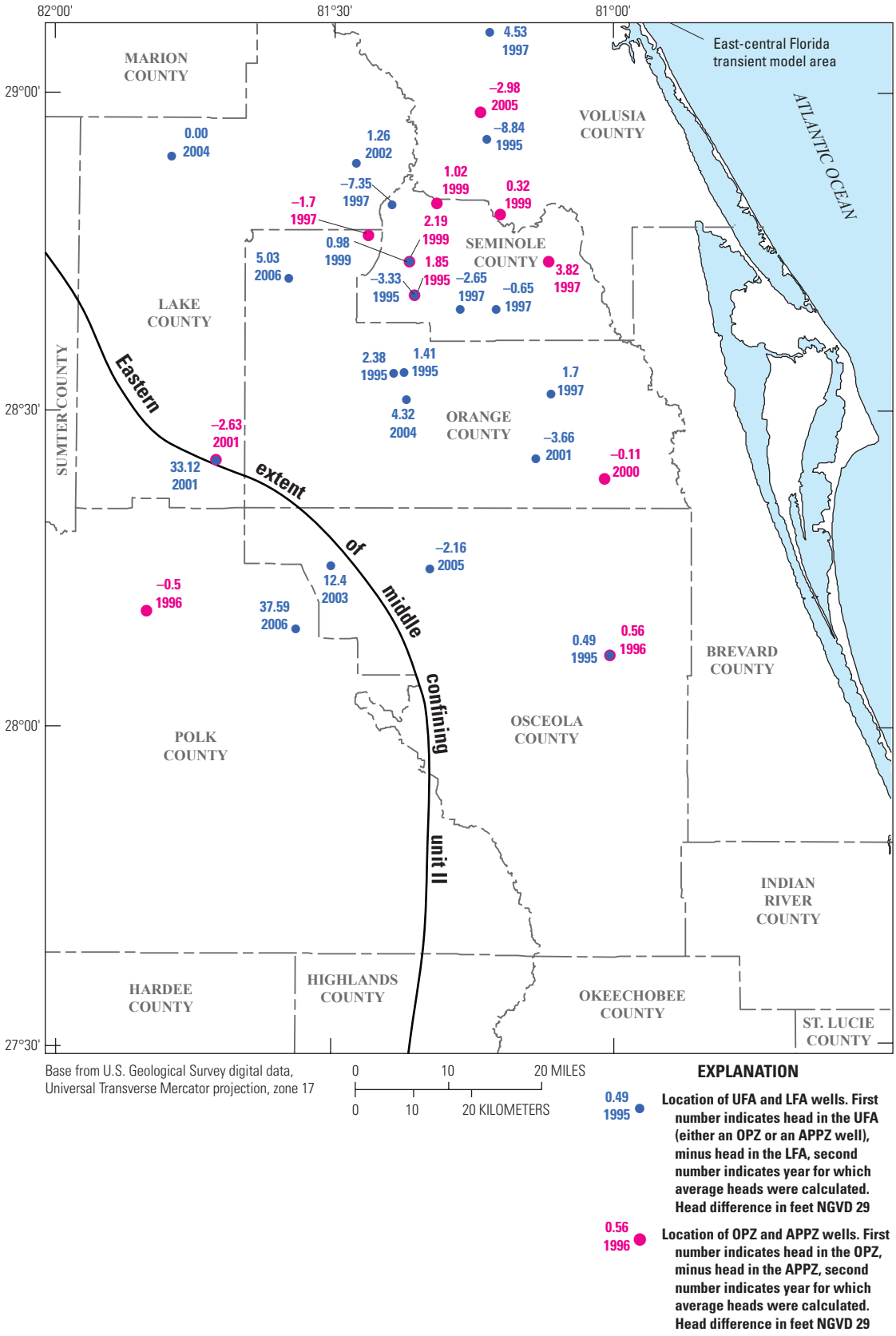

Figure 31. Differences in average annual heads between the Ocala and Avon Park permeable zones (OPZ and APPZ) and between the Upper and Lower Floridan aquifers (UFA and LFA).

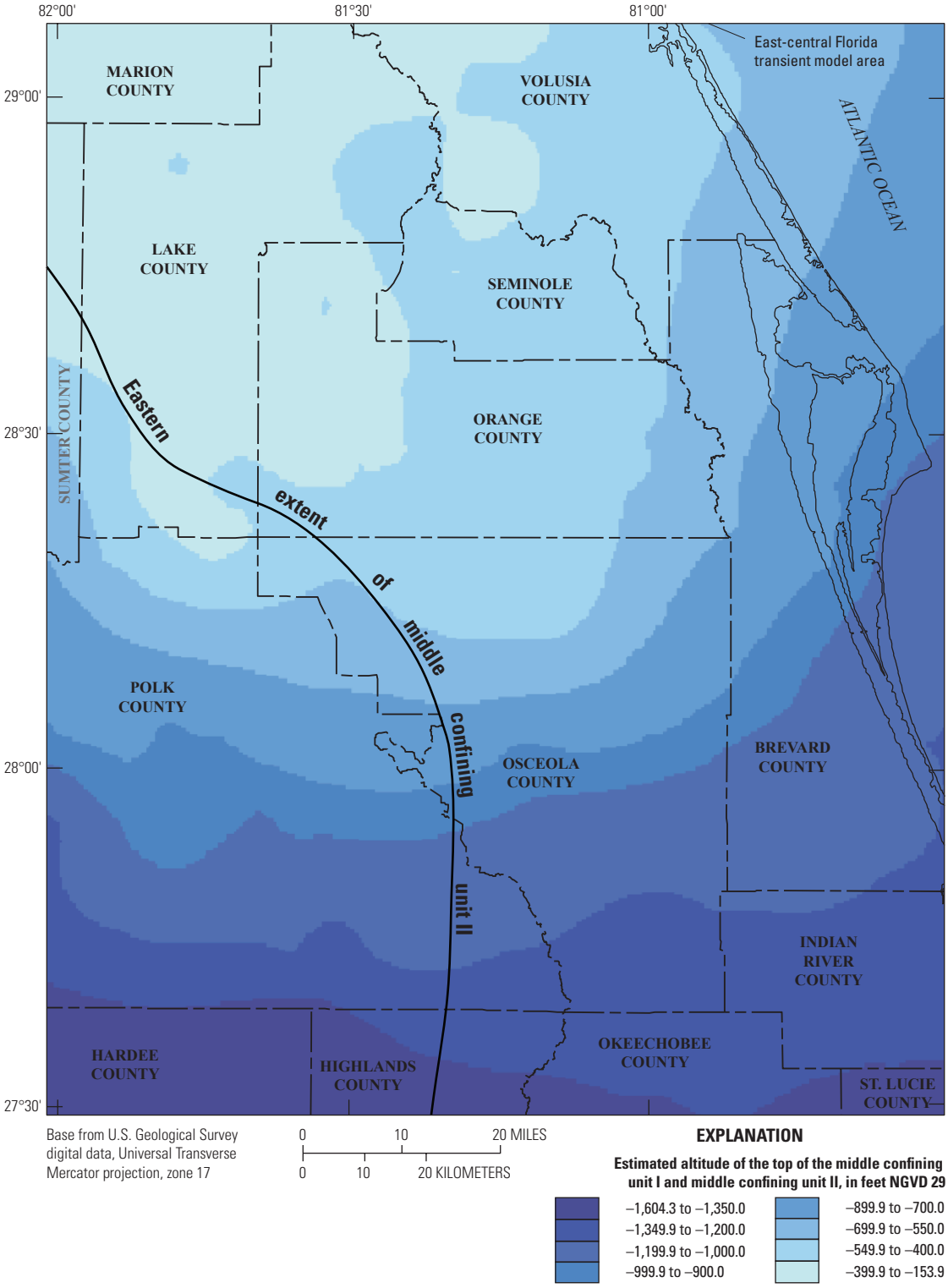

Figure 32. Altitude of the upper surfaces of the middle confining units I/II (MCU I/II) in the East-Central Florida Transient (ECFT) study area.

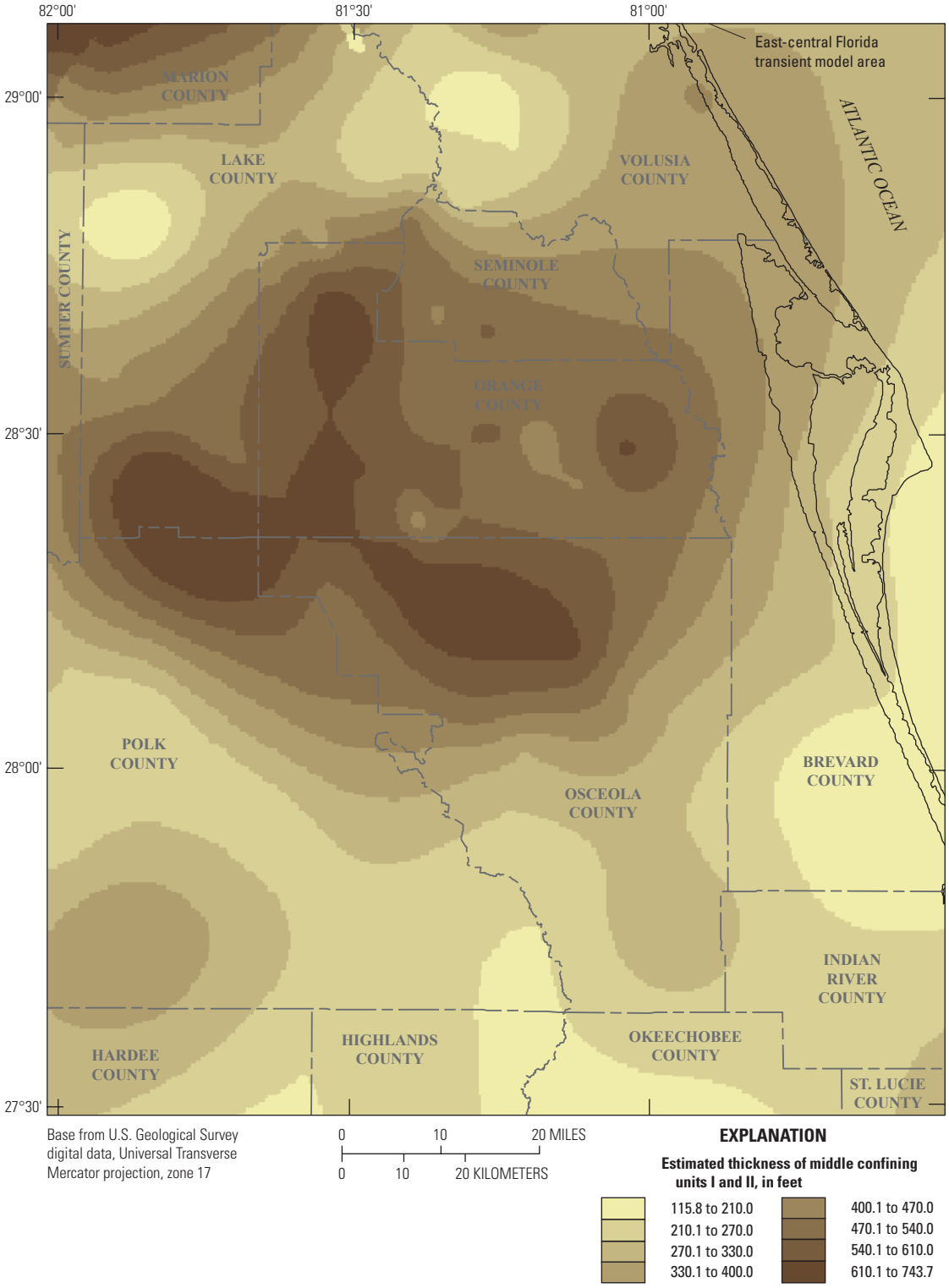

Figure 33. Thickness of the middle confining units I/II (MCU I/II) in the East-Central Florida Transient (ECFT) study area.

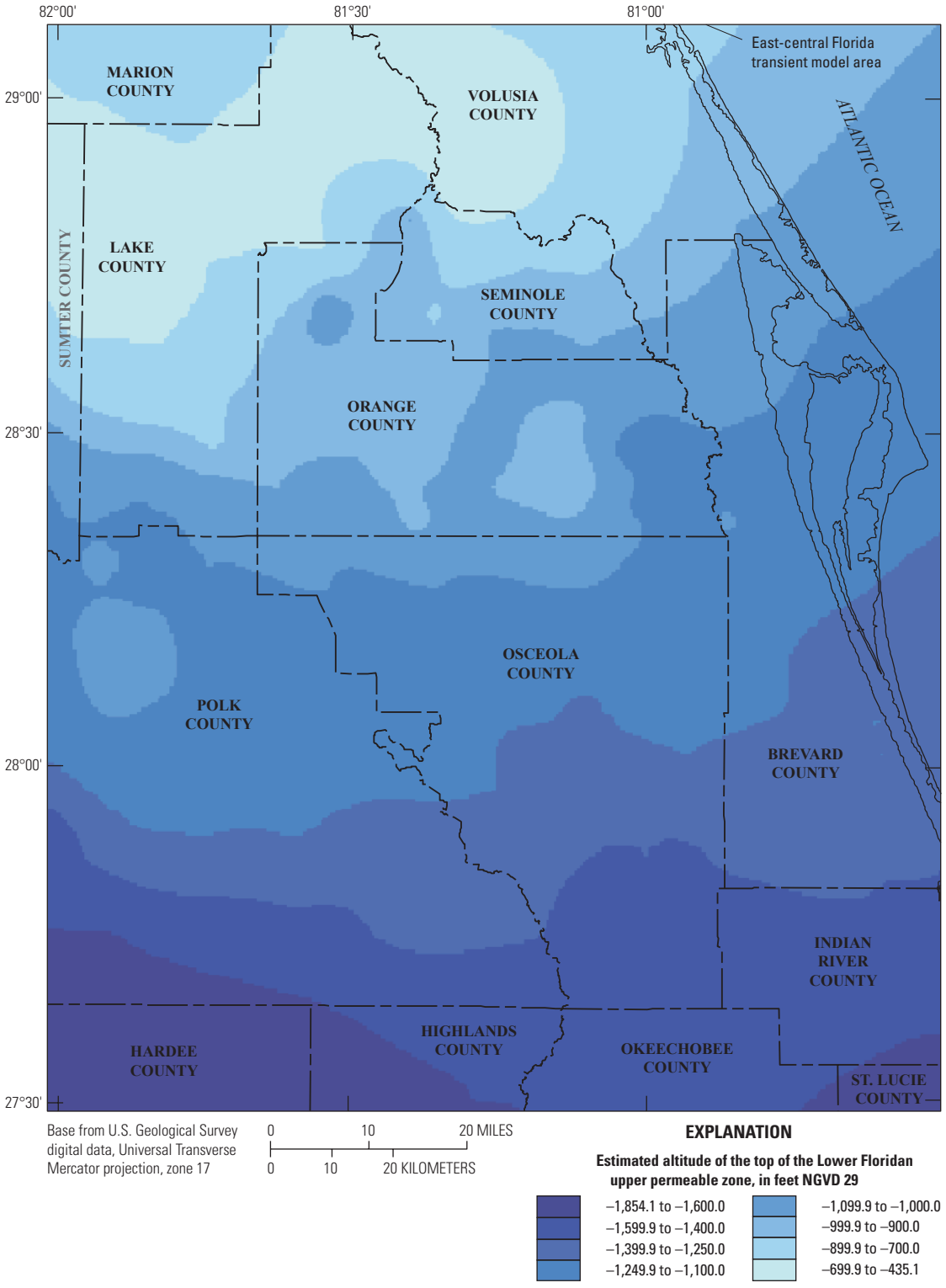

Figure 34. Altitude of the upper surface of the Lower Floridan aquifer in the East-Central Florida Transient (ECFT) study area.

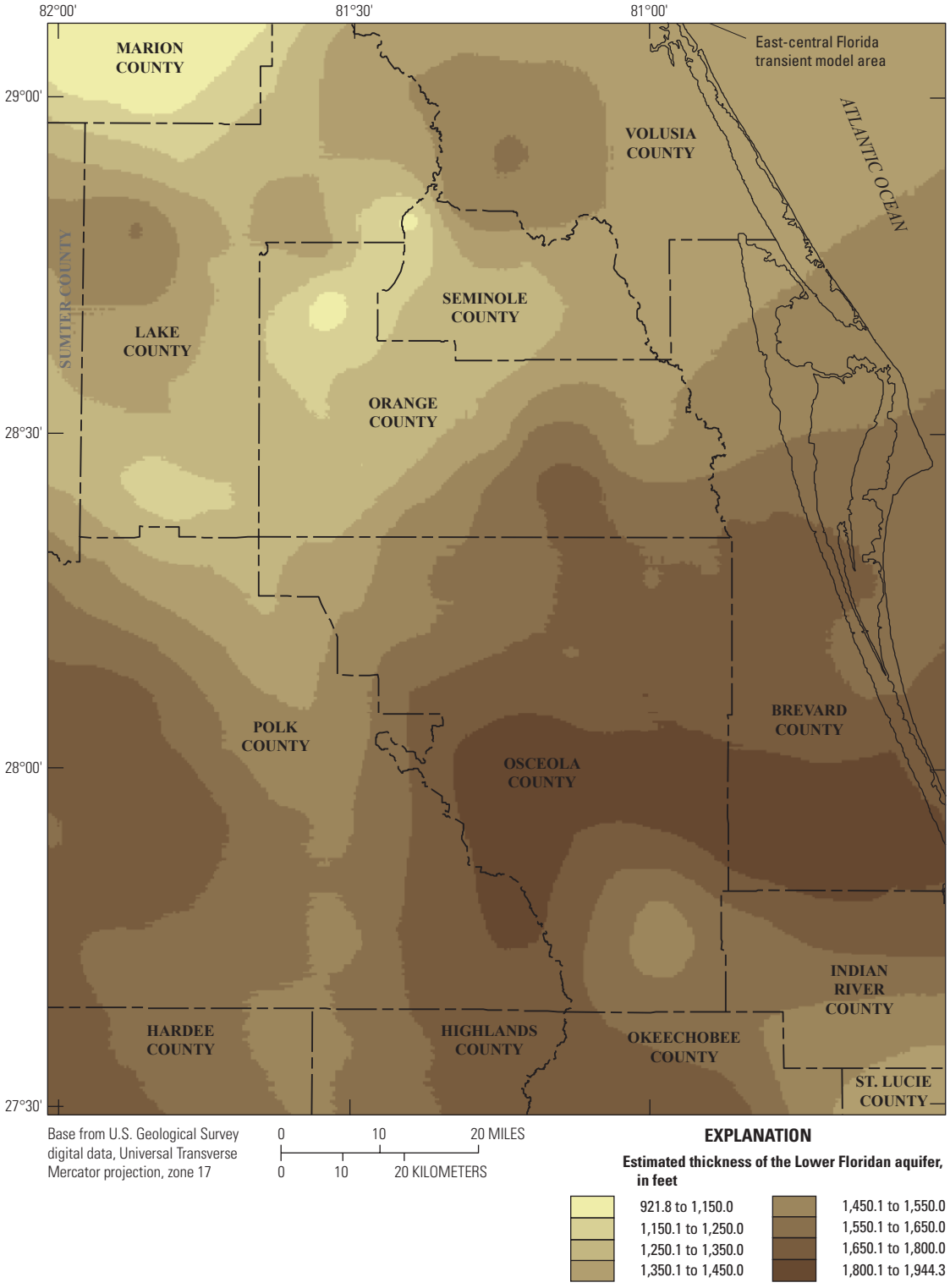

Figure 35. Thickness of the Lower Floridan aquifer in the East-Central Florida Transient (ECFT) study area.

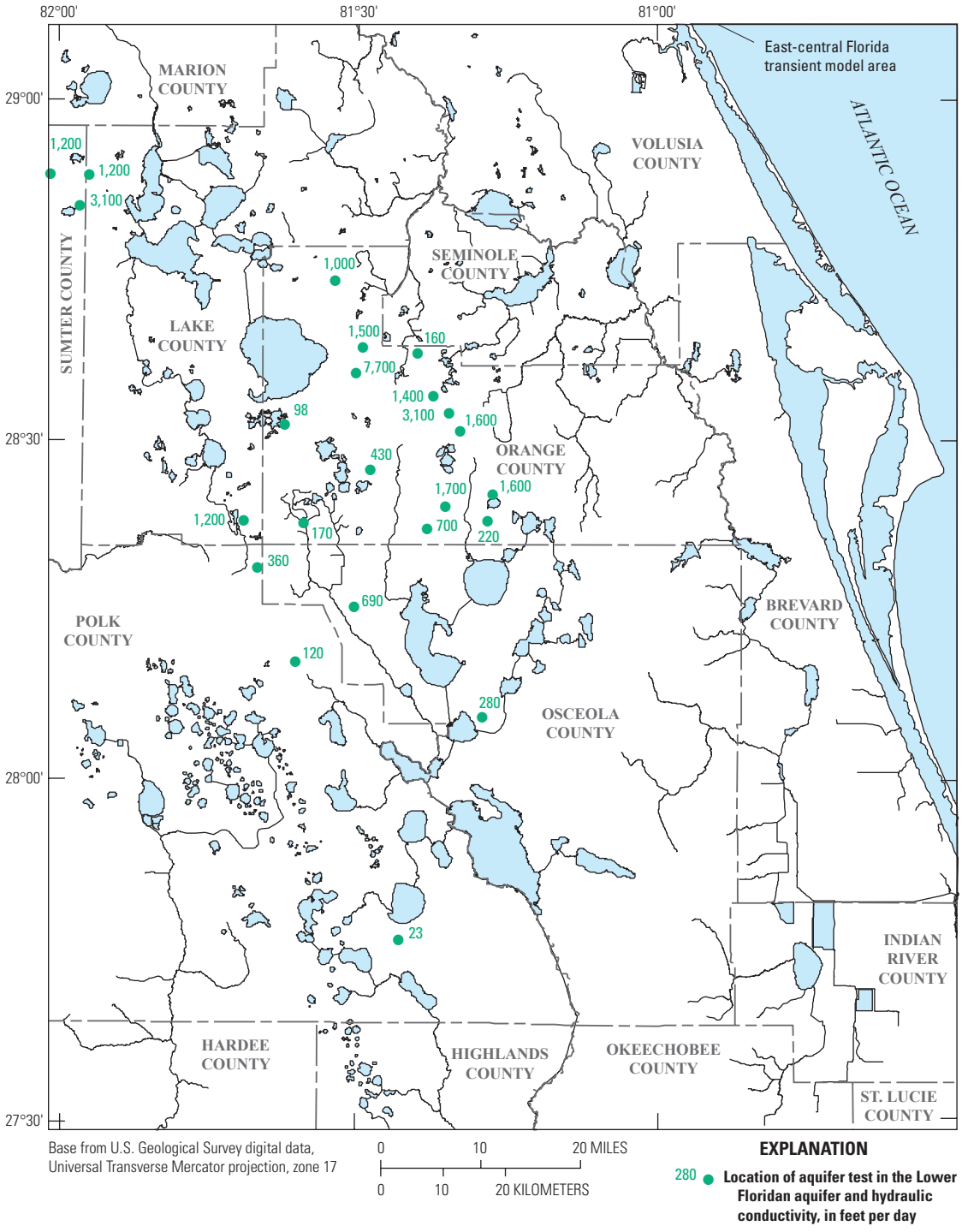

Figure 36. Hydraulic conductivity in the Lower Floridan aquifer from selected aquifer tests.

Chloride Distribution

The surface representing 5,000 milligrams per liter (mg/L) of chloride in groundwater, or the 5,000 mg/L isochlor, was estimated to determine where the freshwater/saltwater transition zone was likely to act as a barrier to flow because of vertical density differences, and thus represented the lower boundary of the simulated part of the groundwater system. Flow across the interface between the freshwater and saline-water flow systems can be assumed to be negligible where the transition and consequent density disparity occur abruptly and in the absence of any large nearby stress, such as a pumping well (Reilly, 2001, p. 11). The 5,000 mg/L isochlor was chosen as the base of the freshwater flow system in east-central Florida because (1) it approximately represents the boundary between moderately brackish water and very brackish to saline water (Sprinkle, 1989), and (2) the thickness of the transition zone between the 5,000 and 10,000 mg/L isochlors is relatively thin (McGurk and Presley, 2002). UFA water levels near the study-area coastlines lie above NGVD 29 and decrease seaward, indicating an onshore-to-offshore flow gradient that minimizes the movement of seawater inland (Todd, 1980).

To construct the 5,000 mg/L isochlor, a database containing site locations, water-sample depths, and chloride concentrations of groundwater samples from FAS wells was created from data compiled by the SJRWMD, SFWMD, SWFWMD, and USGS. The chloride data were used to estimate the altitudes in the FAS where chloride concentrations were approximately 5,000 mg/L. The SJRWMD mapped the altitude where the 5,000-mg/L isochlor was present in the FAS in east-central Florida (McGurk and Presley, 2002 and Sepúlveda, 2002). The altitude of the 5,000 mg/L isochlor was based on measured groundwater chloride concentrations and Sprinkle's (1989) map showing the altitude of water having a 10,000 mg/L chloride concentration (fig. 37). In the western part of the study area, chloride concentrations were extrapolated based on chloride trends in the eastern part because of the paucity of available data.

Water Use

Water use is categorized as (1) groundwater withdrawals from the SAS, IAS, OPZ, OLPZ, APPZ, MCU I/II, and the LFA; (2) artificial recharge systems, including drainage wells that directly recharge confined aquifers and rapid infiltration basins (RIBs) that recharge the SAS; and (3) irrigation, which recharges the SAS. The various types of groundwater withdrawal rates or direct water-recharge (inflows) data were provided for the years 1995 to 2006 by the SJRWMD, SWFWMD, SFWMD, and the Florida Department of Environmental Protection (FDEP); these data represent the best available data at the time of this study. The reported and estimated water withdrawals and inflows represent amounts for all of Seminole, Orange, Brevard, and Osceola Counties and parts of Lake, Marion, Volusia, Sumter, Polk, Indian River, Hardee, Highlands, Okeechobee, and St. Lucie Counties (fig. 38*A*).

Groundwater Withdrawals

Groundwater withdrawals included public water supply, commercial or industrial, agricultural, domestic self-supply, and a small component from free-flowing wells. Total estimated annual average groundwater withdrawals for all uses for the period 1995 to 2006 ranged from 819 to 1,146 Mgal/d. Annual average withdrawals by water use category for all years were 456 Mgal/d for public water supply (49 percent of the total); 351 Mgal/d for agricultural use (38 percent of the total); 61 Mgal/d for commercial and industrial uses; 54 Mgal/d for domestic self-supply use; and less than 1 Mgal/d for free-flowing wells (table 1). Monthly variation in water use for each water use category for the period 1995 to 2006 showed the peaks of the two largest categories (public supply and agricultural) generally coincided in time (fig. 38*B*). Based on consideration of well construction data, more than 95 percent of groundwater withdrawn within the ECFT study area for the 12-year study period was from the FAS, with the following average values the other hydrogeologic units: 10 Mgal/d from the SAS; 13 Mgal/d from the IAS; 722 Mgal/d from the UFA (including 3 Mgal/d from MCU); and 121 Mgal/d from the LFA.

Public-water-supply groundwater-withdrawal data for the SJRWMD and SFWMD were gathered from FDEP Monthly Operating Reports (MORs) for 1995 through 2006. Annual average public-supply water use for the study area ranged from 371.6 Mgal/d in 1995 to 549 Mgal/d in 2006. This category represents all water sent to service from the water-treatment facilities for public water supply on a monthly basis. Total monthly water amounts delivered from a water treatment plant were distributed equally to active wells that supply the plant. Some exceptions to this approach included assigning specific well distributions determined from permitting compliance reports submitted to the three Water Management Districts (WMDs) by the utilities. Water accounted as public water supply includes all permit holders that pump from wells with a casing at least 4 inches in diameter at a rate equal to or greater than 100,000 gallons per day (gal/d). Groundwater withdrawals for public water supply in the SWFWMD area were compiled from metered data for most production wells or from estimates for a few wells within the SWFWMD area. Public-supply water use by county shows Orange County having the largest withdrawal rates from 1995 to 2006 (appendix 1, table 1–1).

In cases where groundwater withdrawals from individual public supply wells were unknown, each active well was assigned a withdrawal amount equal to the total withdrawal multiplied by the ratio of the well capacity to the sum of well capacities for all active wells in the well field. Many production wells withdraw from more than one discrete aquifer unit within the FAS. To apportion the groundwater withdrawals between hydrogeologic units within the FAS, the assigned groundwater withdrawal for each unit was set equal to the total withdrawal rate multiplied by the ratio of the transmissivity of the interval open to a particular aquifer to the transmissivity of

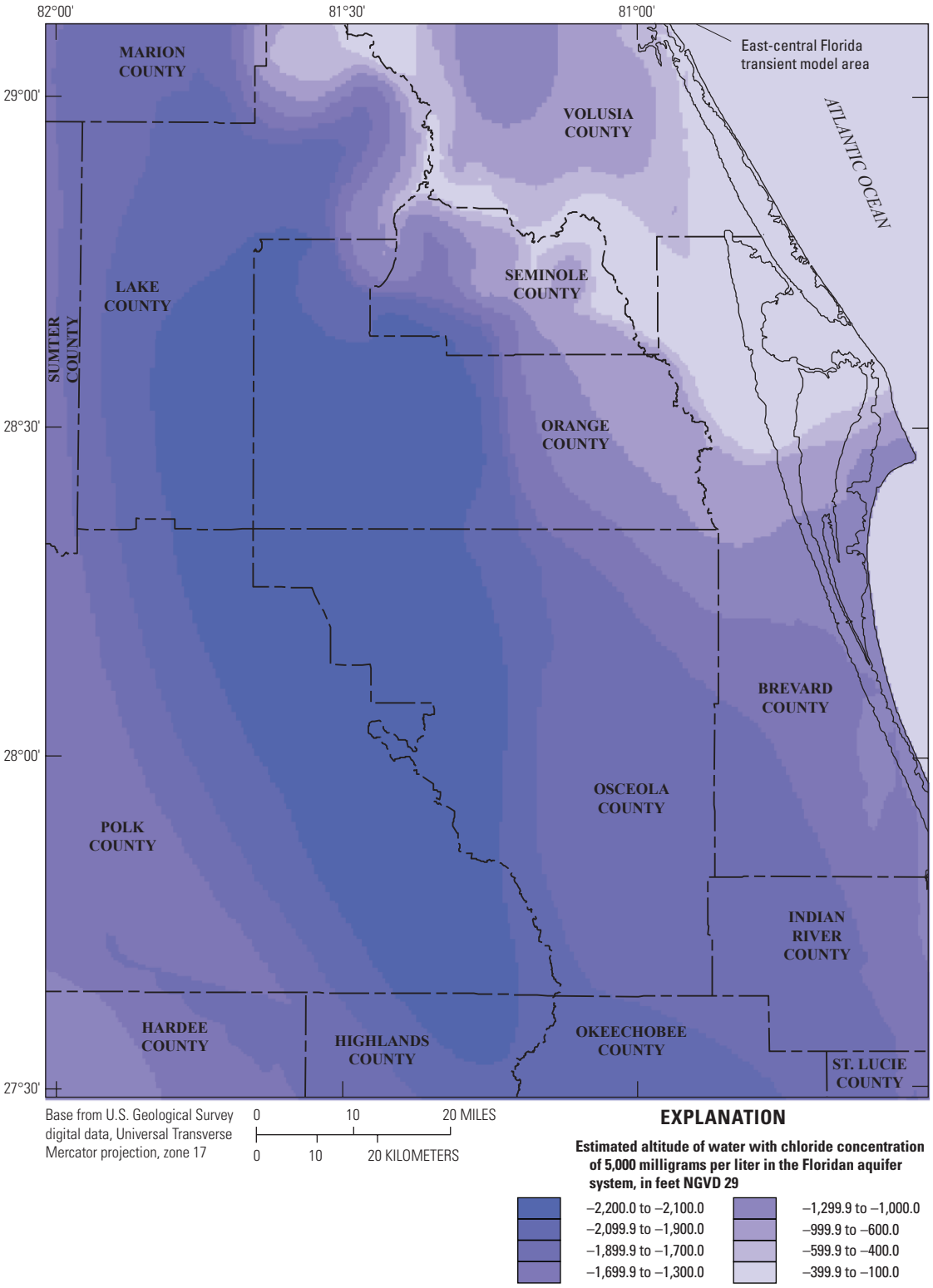

Figure 37. Estimated altitude of water containing a chloride concentration of 5,000 milligrams per liter in the East-Central Florida Transient (ECFT) study area of the Floridan aquifer system.

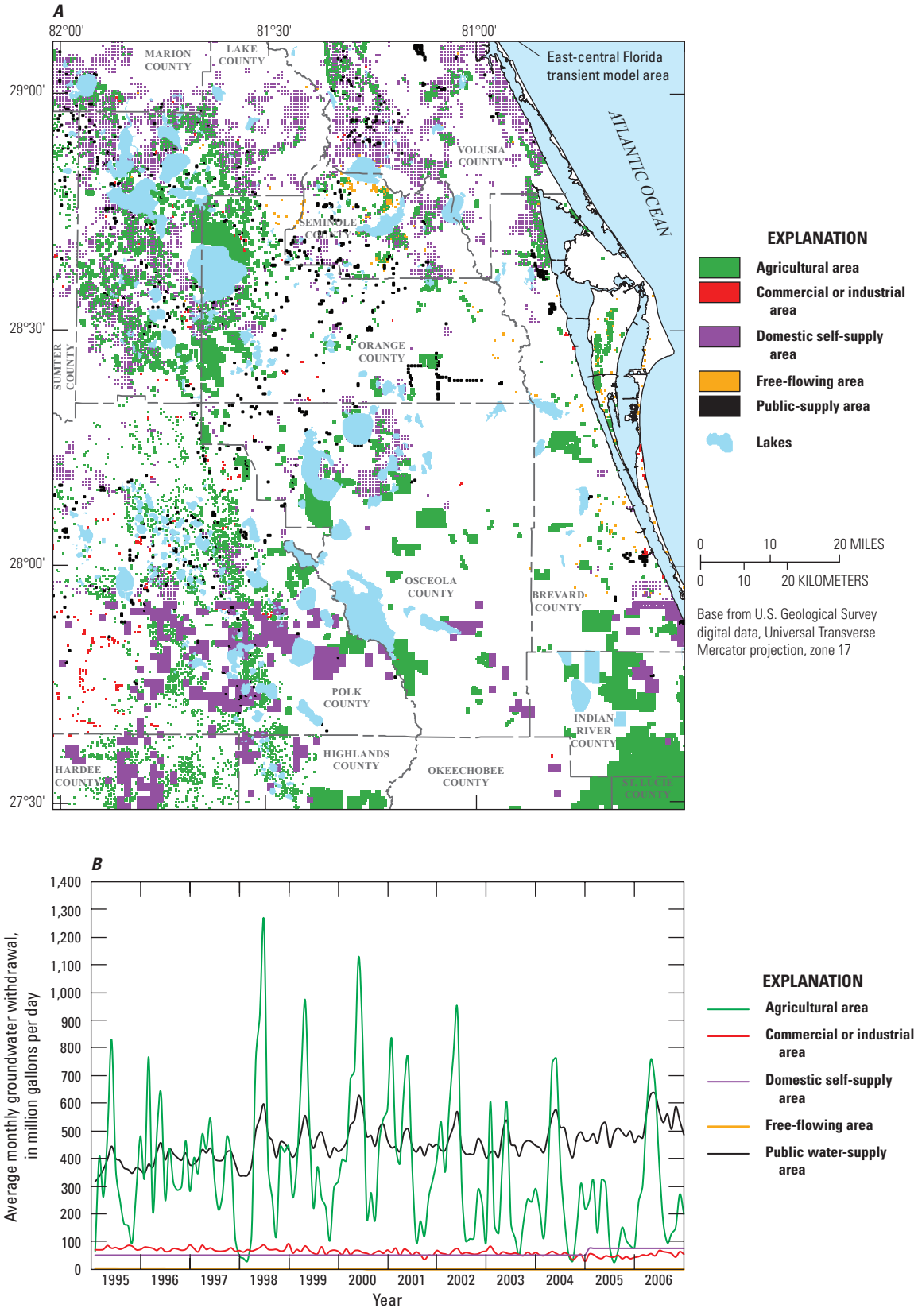

Figure 38. *A*, Groundwater uses by area, and *B*, estimated average monthly groundwater withdrawals in the East-Central Florida Transient (ECFT) study area by water use.

Table 1. Average groundwater withdrawals by water use category and year.

[PWS, public-water supply; AG, agricultural; CI, commercial or industrial; DSS, domestic self-supply; FFW, free-flowing well; Ave, average rate from 1995 to 2006; all rates are in million gallons per day]

Use	1995	1996	1997	1998	1999	2000	2001	2002	2003	2004	2005	2006	Ave
PWS	371.6	402.6	403.2	450.6	458.7	506.6	449.0	453.9	452.5	482.8	487.0	549.0	455.6
AG	320.6	396.3	340.4	431.4	385.0	528.7	400.7	370.1	264.6	291.6	159.4	328.9	351.4
CI	74.8	72.5	69.5	71.8	64.8	60.0	56.5	58.8	57.7	48.9	43.9	53.9	61.1
DSS	49.6	49.6	49.6	49.6	49.6	49.6	49.6	49.6	49.6	49.6	75.1	75.1	53.9
FFW	2.2	1.8	1.4	1.2	1.1	0.6	0.0	0.0	0.0	0.0	0.0	0.0	0.7
Total	818.8	922.8	864.1	1,004.6	959.2	1,145.5	955.8	932.4	824.4	872.9	765.4	1,006.9	922.7

the entire open interval of the well. Transmissivity was calculated from the thickness of the open interval and the simulated hydraulic conductivity of the unit.

Groundwater withdrawals for commercial or industrial uses from SJRWMD and SFWMD areas were compiled from either FDEP MORs, or from water use reports submitted by well-field operators to the WMDs for 1995 through 2006. SWFWMD either measures or estimates groundwater withdrawals from commercial and industrial wells within their district. Water use for commercial or industrial uses varied from a high of 74.8 Mgal/d in 1995 to a low of 43.9 Mgal/d in 2005 (table 1). Annual averages of commercial or industrial uses were highest in Polk County (appendix 1, table 1–2). Water use for each commercial entity was distributed among active wells based on the well radius listed in the permit. Secondary users for commercial or industrial purposes, which are supplied water from public water supply, are not included in the groundwater withdrawals listed in table 1 or appendix 1, table 1–2.

Two approaches were taken to account for agricultural water use. Information supplied by SWFWMD was used directly and consisted of either measured or estimated monthly pumping rates from wells at known locations. Monthly pumping rates from wells and locations used for agricultural purposes in SJRWMD and SFWMD were estimated using the Agricultural Field Scale Irrigation Requirement Simulation (AFSIRS) model (Smajstrla, 1990) and land-use data. These estimates were further refined with actual water-use data collected from the SJRWMD Benchmark Farms agricultural meter data program. The Benchmark Farms program consists of a group of farms that provide a statistical sampling of various agricultural commodity groups through the monitoring of water use at metered wells (Portier, 1988, Singleton, 1996).

For SJRWMD and SFWMD, the AFSIRS model was used to estimate monthly crop water requirements in response to climatic data for the calibration period. AFSIRS incorporates crop type, soil type, irrigation method, rainfall, and evapotranspiration (ET) to develop these monthly irrigation requirements. In order to determine the spatial extent of agriculture within the ECFT study area, SJRWMD developed data for irrigated lands within its area using land-use data from 1995, 1999, and 2004. The 1995 land-use data were used for 1995 to 1999, the 1999 land-use data were used for 1999 to 2004, and the 2004 land-use data were used for 2004 to 2006. Field observations were then made by SJRWMD to estimate the crop type and irrigation methods. Similar information for SFWMD was taken from land-use data, where available, or estimated based on similar practices in the region for the same land-use years. Rainfall data were obtained from SJRWMD NEXRAD rainfall database, and the ET data were obtained from the USGS (2012) as derived from Geostationary Operational Environmental Satellite (GOES) satellite data using the methodology of Mecikalski and others (2011). These data were compiled for each agricultural area and input files for the AFSIRS program were developed. The AFSIRS estimates of crop irrigation demands were used as initial values and then adjusted to better represent the average irrigation observed from the Benchmark Farms meter data (appendix 1, table 1–3). When Benchmark Farms information was not available, specific crop types from AFSIRS data were used. Data for agricultural well locations within SJRWMD and SFWMD were estimated based on the irrigated crop locations. Total groundwater withdrawals for agriculture represent the sum of pumping rates for all crop types or for the dominant crop associated with the irrigated project. All well withdrawals were assumed to be from the OPZ, unless otherwise specified in the available data. When surface water was the known source of irrigation water, the rates were not included in the agricultural water-use category. Agricultural water use ranged from a maximum of 528.7 Mgal/d in 2000 to a minimum of 159.4 Mgal/d in 2005 (table 1). Annual averages of agricultural use show that Polk County has the largest groundwater withdrawals for each year within the ECFT study area (appendix 1, table 1–4). Agricultural water use has a clearly discernible seasonal variation (fig. 38*B*).

Estimated groundwater withdrawals from domestic self-supply wells for 1995 to 2006 were provided by SJRWMD in the ECFT study area. Withdrawal rates were estimated using a geographical information system (GIS) approach that incorporated land use and per-capita use rate for each county. Residential land uses outside public-water-supply service areas were identified from appropriate databases for 1995 and

2004, and per capita use rates were multiplied by the estimated residential capacities to develop estimated water-use volumes for 1995 and 2005. Estimates for 1995 were applied to rates from 1995 to 2004, inclusive, and estimates for 2005 were applied to rates from 2005 to 2006. Domestic self-supply water use was estimated to be 49.6 Mgal/d from 1995 to 2004, and 75.1 Mgal/d for 2005 and 2006 (table 1).

Discharge rates from free-flowing wells in SJRWMD were estimated to decrease from 2.2 Mgal/d in 1995 to 0.6 Mgal/d in 2000 (table 1). These estimates were obtained from the SJRWMD artesian well plugging program (St. Johns River Water Management District, 2004). There have been no known free-flowing wells in the SJRWMD since 2000, and no information was available for free-flowing wells, if any, outside the SJRWMD.

Artificial Recharge

Direct inflow to the OPZ occurs through 210 active drainage wells that are mostly concentrated in the Orlando metropolitan area (fig. 14). The status and locations of these wells were verified by Bulmer (2003). These wells, which are cased to the top of the OPZ and then drilled open-hole into the OPZ, either discharge street runoff from storm drains (street drainage wells) or control lake levels (lake-level control wells). The estimated total recharge to the OPZ through drainage wells in the study area ranged from a maximum of 32.7 Mgal/d in 1997 to a minimum of 4.8 Mgal/d in 2000 (table 2) and is based on rainfall for the delineated basins in figure 14 for the period 1995 to 2006, and the permeability of the top soils in the basins of these drainage wells. The recharge rates to the OPZ at drainage wells are strongly correlated to the amount of total rainfall for any period. The method used to derive the recharge rates is the same as that used to compute surface runoff throughout the model, which is explained later in this report.

RIBs provide a direct means of recharge to the SAS, and the SJRWMD has collected information about the locations of these basins and their applied rates of flow to the SAS through these basins. The data for RIBs were provided from multiple sources, including the FDEP and several utilities that operate these facilities. These recharge-rate data were reviewed for accuracy by the utility. Average monthly recharge flows from RIBs were calculated for the 1995 to 2006 period. Annual average inflows to the SAS from RIBs in the ECFT study area showed these recharge rates were highest during 2005 and lowest during 1999 (table 3). An

Table 2. Annual average of inflows to the Ocala permeable zone from street drainage and lake-level control wells by county.

[All rates are in million gallons per day]

County	1995	1996	1997	1998	1999	2000	2001	2002	2003	2004	2005	2006	Ave
Orange	26.5	25.4	31.1	17.2	12.0	4.6	15.5	22.2	18.6	29.4	16.0	6.1	18.7
Seminole	1.4	1.3	1.6	0.9	0.6	0.2	0.8	1.2	0.4	1.5	0.8	0.3	0.9
Total	**27.9**	**26.7**	**32.7**	**18.1**	**12.6**	**4.8**	**16.3**	**23.4**	**19.0**	**30.9**	**16.8**	**6.4**	**19.6**

Table 3. Annual average of inflows to the surficial aquifer system from rapid infiltration basins by county.

[Ave, average rate from 1995 to 2006; all rates are in million gallons per day]

County	1995	1996	1997	1998	1999	2000	2001	2002	2003	2004	2005	2006	Ave
Brevard	0.0	0.0	0.0	0.0	0.0	1.4	0.7	0.6	0.6	0.4	0.6	0.2	0.4
Lake	0.0	0.0	0.0	0.0	1.1	8.1	1.5	1.9	2.3	2.7	2.1	0.6	1.7
Orange	25.9	27.0	22.3	22.0	20.7	22.0	21.4	26.3	23.1	25.7	28.0	26.1	24.2
Osceola	2.6	3.7	4.1	2.5	2.5	2.5	2.5	2.6	4.1	2.5	3.7	2.6	3.0
Polk	0.2	1.6	0.7	2.3	1.0	1.0	1.0	0.2	0.7	1.0	1.6	0.2	1.0
Seminole	1.3	1.1	1.3	1.2	1.0	3.7	3.2	4.1	3.8	3.1	3.3	1.9	2.4
Sumter	0.0	0.0	0.0	0.0	0.0	0.1	0.1	0.1	0.1	0.0	0.0	0.0	0.0
Volusia	0.0	0.0	0.0	0.0	0.0	0.4	0.8	0.8	0.9	0.5	0.5	0.2	0.3
Total	**30.0**	**33.4**	**28.4**	**28.0**	**26.3**	**39.2**	**31.2**	**36.6**	**35.6**	**35.9**	**39.8**	**31.8**	**33.0**

additional source of recharge to the SAS was inflow from septic tanks, simulated as infiltration to the unsaturated zone. The estimated inflow from septic tanks was assumed to be 50 percent of domestic self-supply well withdrawals.

Net average groundwater withdrawal and recharge rates from production wells, drainage wells, and RIBs were calculated for 1999 and 2006 to illustrate the spatial distribution of these rates. The spatial distribution patterns observed for the other years were similar. Drainage wells in the ECFT study area (fig. 14) are responsible for the observed net recharge the UFA, including both OPZ and APPZ, in central Orange County (figs. 14, 39*A*, and 40*A*). There is an extensive area of agricultural groundwater withdrawals in the UFA although the rates are not as large as those for many public-supply wells (figs. 38*A*, 39*A*, and 40*A*). The largest measured rates of groundwater withdrawal were in the Lower Floridan aquifer, concentrated in central Orange County, although at fewer wells than those with relatively large withdrawal rates in the UFA (figs. 39*A–B,* 40*A–B*).

Irrigation

Agricultural irrigation was applied based on the estimated crop needs presented in the Groundwater Withdrawals section. Recharge to the SAS resulting from agricultural irrigation rates in SJRWMD and SFWMD was applied to irrigated crop parcels identified in the SJRWMD and to agricultural lands for SFWMD based on the 1995, 2000, and 2005 data. Irrigation rates for the years 1996 to 1999 were applied based on 1995 land-use data, rates for 2000 to 2004 were applied based on 2000 land-use data, and rates for 2005 to 2006 were applied based on 2005 land-use data. Agricultural irrigation for SWFWMD was derived using data from metered wells and applied to the agricultural areas found in land-use parcels closest to the metered location. To account for the lack of 100 percent irrigation efficiency, annual agricultural irrigation rate estimates were added to rainfall to account for potential recharge to the SAS.

There is no direct measurement of landscape irrigation from publicly supplied water, commercial or industrial water, or domestic self-supplied water. Landscape irrigation rates were estimated by using the aesthetic irrigation application rates and applying these rates to appropriate land uses. Average monthly water-requirement application rates were derived from the AFSIRS model. The AFSIRS model was applied for sod production under various soil characteristics as mapped by the Natural Resource Conservation Service for typical residential and commercial size parcels in each county of the ECFT study area. Because the AFSIRS model utilizes long-term climate data, these rates reflect 30-year annual average use rates for sod production in each of the counties based on soil type. These rates were then applied to the residential and commercial land-use categories (as established in the land-use database) within each county, independent of the source of irrigation water.

In order to account for changes in land use, the method just described was applied to the 1995, 1999, and 2004 land-use maps provided by the WMDs. Because of the lack of land-use data for other years, 1995 land-use data were used to calculate 1995 to 1998 irrigation estimates, 1999 land-use data were used to calculate 1999 to 2003 irrigation estimates, and 2004 land-use data were used to calculate 2004 to 2006 irrigation estimates. The 30-year annual average rates determined by AFSIRS were used and variations in monthly applications were taken from the 30-year annual average information. Because AFSIRS calculates an amount for sod production purposes, these amounts were then further reduced to represent a range of 40 to 75 percent of the county's total for public water supply, commercial industrial, and domestic self-supply use amounts in the ECFT study area. The monthly volumes were proportioned by the total available irrigation area, incorporating the percentage of impervious land for the appropriate land uses receiving irrigation. These rates, determined for the ECFT study area, were then incorporated into the model as additional rainfall to calculate runoff and infiltration rates.

No specific reuse irrigation rates were considered because of a lack of reuse irrigation data. Irrigation rates for the reuse category were assumed to be represented by the public water supply, commercial or industrial, and domestic self-supply use categories as described earlier, which do not identify specific sources. A nominal rate at which residential and commercial land uses are irrigated was used.

Estimated Recharge and Evapotranspiration Rates in the Surficial Aquifer System

An approximation of a water-balance equation that considers all inflows and outflows over the SAS domain can be used to calculate ET rates by solving for ET after estimating or measuring the remaining parameters in the balance equation. Rainfall to the SAS domain is an inflow and considered positive, whereas the total measured streamflow leaving the model through the lateral stream cells and the estimated ET rates are outflows and considered negative. The leakage rates between the streams and the SAS occur within the same domain of interest and thus are not considered flows leaving or entering the SAS domain. By convention, rates of flow entering the SAS are positive whereas those leaving the SAS are negative. The net groundwater basin flows to the SAS through the lateral boundaries and the net vertical leakage between the SAS and the ICU or IAS were initially estimated using a regional groundwater flow model (Sepúlveda, 2002). Both quantities were mostly negative, indicating outflows from the SAS; these rates apply to the entire SAS area, including lakes. Groundwater injections from the RIBs were inflows to the SAS. Changes in storage in the SAS were calculated using measured water levels in SAS wells and measured water-surface altitudes at lakes. Average rainfall is the largest inflow to the SAS domain.

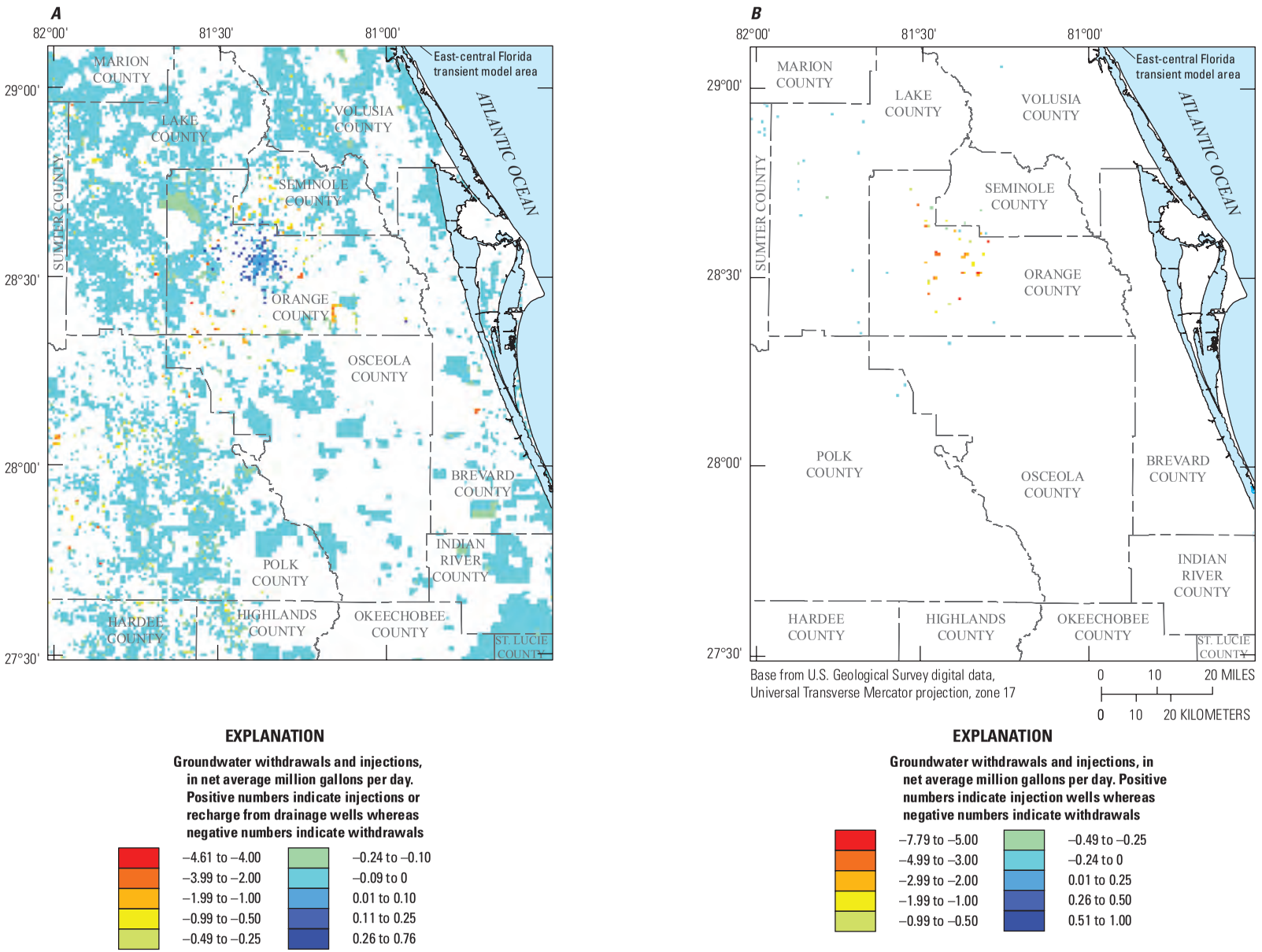

Figure 39. Estimated net average 1999 groundwater withdrawal rates in the *A*, Upper Floridan aquifer, and *B*, Lower Floridan aquifer.

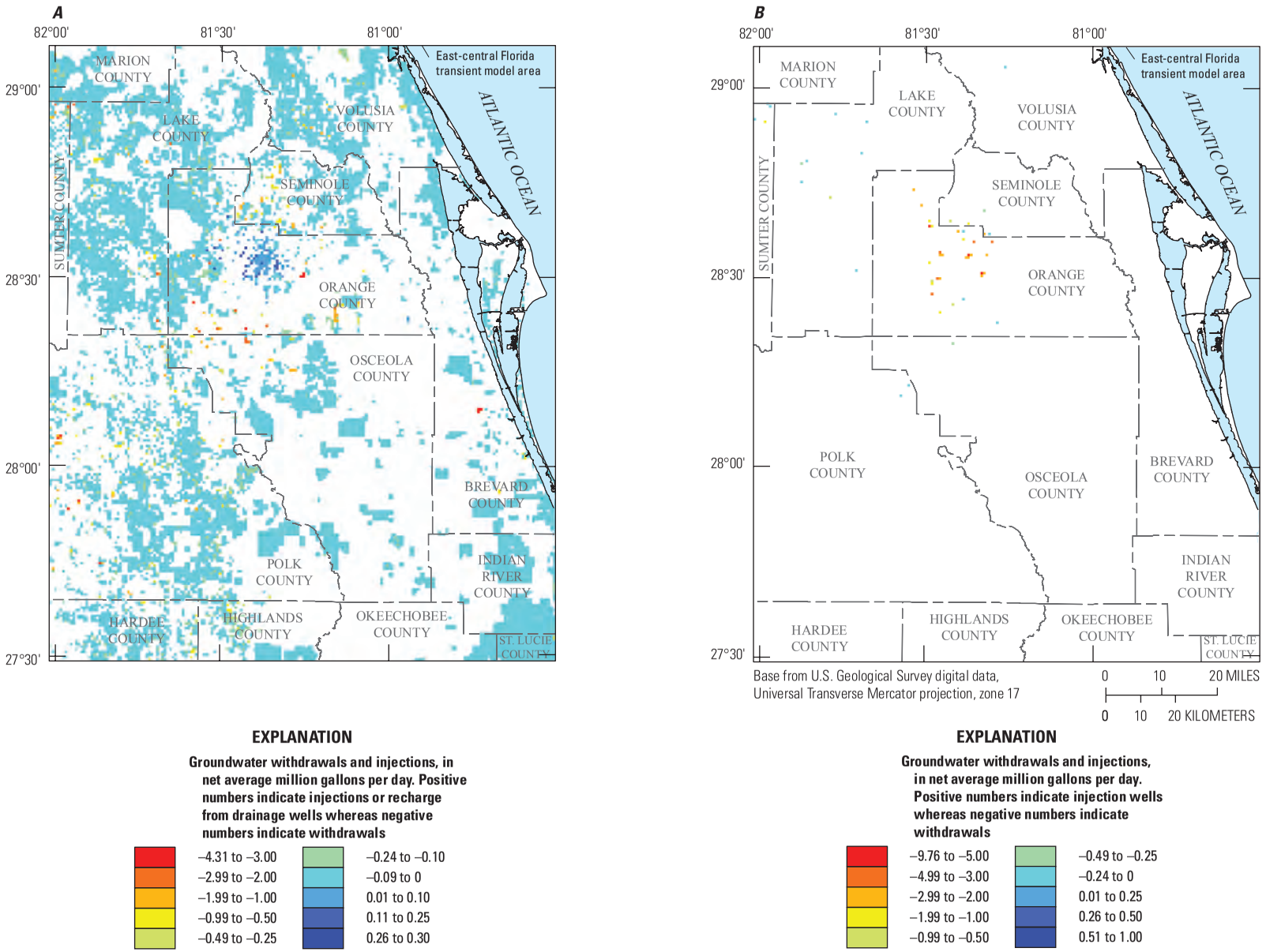

Figure 40. Estimated net average 2006 groundwater withdrawal rates in the *A*, Upper Floridan aquifer and *B*, Lower Floridan aquifer.

The water balance equation can be written as

$$\text{RAIN} + \text{SFG} + \text{SFU} + \text{GWBF} + \text{VLICU} + \text{GWSAS} + \text{EET} = \text{Sy}\frac{\Delta h}{\Delta t} \approx 0.9387\,\text{Sy}\frac{\Delta h_w}{\Delta t} + 0.0613\frac{\Delta L}{\Delta t} \quad (1)$$

where

RAIN	is the total rainfall into the SAS, including irrigation,
SFG	is the total stream flow leaving the SAS through gaged streams,
SFU	is the total stream flow leaving the SAS area through ungaged streams,
GWBF	is the net groundwater basin flow through the lateral boundaries of the SAS,
VLICU	is the net vertical leakage between the underlying ICU/IAS and the SAS,
GWSAS	is the net groundwater withdrawals and injections to and from the SAS,
EET	is the estimated ET,
Sy	is the specific yield,
0.9387	is a coefficient equal to the percentage of the SAS area not covered by lakes,
0.0613	is the percentage of the SAS area covered by lakes,
$\frac{\Delta h_w}{\Delta t}$	is the change in water levels at the wells over a period of time Δt, and
$\frac{\Delta L}{\Delta t}$	is the change in water-surface altitudes at lakes over a period of time Δt.

The potential changes in percentages of the SAS covered by lakes during the 12-year period resulted in changes in estimated ET rates within a few tenths of an inch, which is generally smaller than the error associated with the measurements of the flow parameters in equation 1. The estimated ET rates are used to calculate recharge rates to the SAS by subtracting ET rates and streamflow from rainfall.

Average annual ET and recharge rates to the SAS were calculated to provide guidelines for model calibration by allowing a comparison between annual estimated and simulated ET rates, and to identify the years for which the calculated changes in storage are smallest to select the most appropriate periods to approximate steady-state conditions without introducing significant errors to the model. During model calibration, it was recognized that the margin of error in some of the estimated rates in equation 1 imply that an exact match between measured and simulated ET rates and recharge to the SAS is not practical.

The evaluation of the right-hand side of equation 1 was accomplished by (1) assuming a specific yield value of 0.14; (2) calculating the average change in lake altitudes from the gaged lakes in the ECFT study area (fig. 13) for each year; and (3) calculating the average change in water-table altitudes from the wells withdrawing from the SAS. Temporal changes in the water-table altitude and in lake altitudes were calculated from monthly average data for each year from 1995 to 2006. All changes were calculated by subtracting the value at the beginning of the year from the value at the end of the year; negative rates thus indicate a loss in storage relative to conditions at the beginning of the year and positive rates indicate a gain in storage. Results from these calculations showed that the smallest absolute values for the right-hand side of equation 1 were for 1999 and 2003 (table 4). Based on the cumulative rates of $\Delta L/\Delta t$, it was observed that the average water-surface altitudes at lakes at the end of 2006 were about 1.5 ft lower than corresponding levels at the beginning of 1995. Only in 2005 did average water-surface altitudes at lakes exceed those at the beginning of 1995 (table 4). The calculation of the $\text{Sy}\frac{\Delta h}{\Delta t}$ terms in table 4 for the SAS results in the largest possible values when compared to confined units or aquifers because the Sy values are always larger than those for storage coefficients.

The calculation of each term in the left-hand side of equation 1 was accomplished by (1) using the NEXRAD rainfall data with the adjustment made explained in the Rainfall section of this report; (2) calculating the total streamflow measured at stream-gaging stations in figure 11 leaving the SAS in the ECFT study area; (3) using a regional groundwater flow model (Sepúlveda, 2002) to estimate the horizontal flows entering and leaving the SAS through the lateral boundaries of the SAS area and the vertical flows through the ICU or IAS; and (4) calculating the average groundwater withdrawals

Table 4. Annual storage changes in lakes and surficial aquifer system wells from 1995 to 2006.

[Values in bold represent storage changes for steady-state model years. CCIS, cumulative changes in storage; refer to equation 1 for the definition of column headers; all rates are in inches per year]

Year	$\frac{\Delta L}{\Delta t}$	$\frac{\Delta h_w}{\Delta t}$	$\text{Sy}\frac{\Delta h}{\Delta t}$	CCIS
1995	–10.06	–1.39	–0.80	–10.06
1996	–2.00	–3.86	–0.63	–12.06
1997	8.66	3.88	1.04	–3.40
1998	–13.09	–4.57	–1.40	–16.49
1999	5.24	2.00	**0.58**	–11.25
2000	–26.47	–15.96	–3.72	–37.72
2001	13.02	6.64	1.67	–24.70
2002	14.00	4.98	1.51	–10.70
2003	–4.29	–2.31	**–0.57**	–14.99
2004	12.52	2.77	1.13	–2.47
2005	5.93	2.71	0.72	3.46
2006	–21.94	–7.46	–2.33	–18.48

from the SAS. The calculation of the first six terms in equation 1 and the data in the fourth column of table 4 allows the estimation of EET for each year. Results from these calculations showed that EET ranged from about 27 to 44 in/yr (table 5) from 1995 to 2006. These results required estimating the SFU term, the streamflow leaving the SAS area through ungaged streams. The estimation of SFU was based on the product of the measured streamflow at stations shown in figure 11 (or SFG in table 5) and the ratio of the drainage area of ungaged streams leaving the SAS in the ECFT study area to the drainage area of the gaged streams leaving the SAS. The ratio of these two drainage areas was calculated to be 0.221 and it was assumed to be constant for all years. In addition, independent measurements or estimates of VLICU and GWBF in equation 1 cannot be made. Initial estimates of GWBF and VLCIU were derived from Sepúlveda (2002), representing average steady-state conditions (August 1993 through July 1994). Annual average values simulated by the ECFT model were used in table 5, and are similar in magnitude to those from Sepúlveda (2002). Values for GWBF are negligible, and any error can be disregarded. Values for VLICU are within 0.4 in/yr of that (-3.6 in/yr) from Sepúlveda (2002). Because flows in table 5 represent an approximation of inflows and outflows for the SAS, the ET and recharge rates to the SAS in table 5 are estimates, not measured rates.

Simulation of Groundwater Flow System

The conceptual model of the flow system in the ECFT study area (hereafter called the model area) represents the same area where the flow system is simulated and can be presented in terms of the interactions among (1) the surface-water system represented by lakes and streams, (2) the unconfined (SAS), and (3) the confined groundwater system (FAS). Rainfall and irrigation are the sources of runoff to lakes and streams and of infiltration to the unsaturated zone. Infiltration is routed to the SAS through the unsaturated zone, and water that is not lost to ET recharges the SAS. The exchange of water between streams and the SAS can occur through the streambed, whereas interaction between the lakes and the SAS or ICU/IAS can occur through the lakebed because lakes are assumed to penetrate the entire thickness of the SAS. Water exchange between the unconfined SAS and the confined FAS occur through the confining units as upward leakage in discharge areas and as downward leakage in recharge areas. Lateral flows through the boundaries are assumed to leave or enter the model area in all hydrogeologic units: SAS, ICU/IAS, OPZ, OLPZ, APPZ, MCU I/II, and LFA. Flow through the freshwater and saline-water interface, assumed to be

Table 5. Estimation of groundwater flow terms for 1995–2006 in the surficial aquifer system of the East-Central Florida Transient (ECFT) study area.

[RAIN, rainfall plus irrigation; SFG, streamflow leaving the SAS through gaged streams; SFU, streamflow leaving the surficial aquifer system (SAS) area through ungaged streams; GWBF, groundwater flow leaving the study area; VLICU, net downward leakage from the SAS to the underlying intermediate confining unit (ICU); GWSAS, net groundwater withdrawals and injections to and from the SAS; EET, estimated ET; RCH, recharge rate to the SAS, equal to SFG+SFU+EET+RAIN; Ave, average rates for the 1995–2006 period; negative flows indicate outflows to the SAS whereas positive flows indicate inflows; all rates are in inches per year]

Year	RAIN	SFG	SFU	GWBF	VLICU	GWSAS	EET	RCH
1995	53.12	–12.08	–2.67	–0.02	–3.44	0.05	–35.77	2.60
1996	50.13	–8.46	–1.87	–0.01	–3.64	0.06	–36.84	2.96
1997	54.78	–7.20	–1.59	–0.02	–3.49	0.04	–41.49	4.50
1998	49.39	–12.61	–2.78	0.00	–3.72	0.05	–31.72	2.28
1999	49.60	–6.65	–1.47	–0.05	–3.86	0.04	–37.03	4.45
2000	31.72	–3.32	–0.73	–0.06	–4.05	0.07	–27.35	0.32
2001	50.96	–7.95	–1.75	–0.05	–3.71	0.05	–35.87	5.39
2002	60.41	–9.31	–2.05	–0.02	–3.69	0.07	–43.90	5.15
2003	53.04	–11.51	–2.54	0.00	–3.49	0.07	–36.13	2.86
2004	58.78	–11.71	–2.58	–0.01	–3.48	0.07	–39.94	4.55
2005	61.46	–14.17	–3.13	0.01	–3.46	0.09	–40.08	4.08
2006	37.14	–4.15	–0.92	–0.03	–3.90	0.08	–30.54	1.53
Ave	**50.88**	**–9.09**	**–2.01**	**–0.02**	**–3.66**	**0.06**	**–36.39**	**3.39**

located at altitudes where the 5,000-mg/L chloride isochlor is present, depends on the hydraulic conductivity of the interface between the aquifer cell and the boundary and specified heads along the interface.

The rainfall and irrigation rates were partitioned to calculate surface runoff and infiltration based on soil properties. The surface runoff was directed to streams, lakes, outside the model, or in the case of closed basins, back to the cell as infiltration, based on the drainage basins. Infiltration was routed through the unsaturated zone to become recharge to the SAS after considering ET losses in the unsaturated zone and at the water table if the extinction depth was below the water table (fig. 41). Additionally, in areas having a relatively thin unsaturated zone (fig. 41*A*) and a shallow water table, groundwater ET occurs and is withdrawn directly from the saturated zone whenever the extinction depth is below the water table, whereas in areas with a thick unsaturated zone (fig. 41*B*), total ET equals the unsaturated ET because groundwater ET is zero.

The hydrogeologic framework, conceptual groundwater flow system, and other hydrologic information presented in the previous sections were used to construct a numerical groundwater flow model of the SAS, ICU/IAS, OPZ, OLPZ, APPZ, MCU I/II, and LFA. The ECFT model simulates transient groundwater flow in the study area (fig. 1) for a period of 12 years, starting in 1995, based on the hydrologic and hydraulic properties derived from both steady-state and transient model calibration.

Model Construction

The USGS three-dimensional finite-difference groundwater flow model code MODFLOW-2005 (version 1.8) was used to simulate the flow system (Harbaugh, 2005). Interaction of the groundwater flow system with the surface environment (rainfall, irrigation, ET, lakes, and streams) was simulated using the Green-Ampt infiltration (GAI) method (Chow and others, 1988), Unsaturated-Zone Flow (UZF1) Package (Niswonger and others, 2006), Lake (LAK7) Package (Merritt and Konikow, 2000), and Streamflow-Routing (SFR2) Package (Niswonger and Prudic, 2006). Integration of the GAI method and the UZF1, LAK7, SFR2 Packages in MODFLOW-2005 ensures a water mass balance in surface water and groundwater.

Spatial and Temporal Model Discretization

The model area was horizontally discretized into a uniform grid with a cell size of 1,250 by 1,250 ft. The grid consists of 472 rows and 388 columns and is oriented along a north-south axis for simplicity, because the majority of stresses or boundary conditions were not oriented in any specific direction. The UTM coordinates of the model grid corners, specifying the extent of the model area, are provided in table 6. The resolution of the model grid is depicted in the expanded views of two grid corners (shown in fig. 42). Vertical discretization involved partitioning the model into seven layers: the SAS, ICU, OPZ, OLPZ, APPZ, MCU I/II, and LFA.

Temporal discretization involved dividing the 12-year simulation period into 144 monthly stress periods, over each of which boundary conditions remain constant, and each stress period comprises 10 time steps that are uniform in duration. The simulation period begins in January 1995 and ends in December 2006. Average monthly water levels for this 12-year simulation were calculated for wells, lakes, and streams; average monthly flows were calculated for springs and streams. Average monthly groundwater withdrawals were calculated for all water use types.

Flow-model development included assigning or estimating specific yield, storage coefficients, and horizontal and vertical hydraulic conductivity for each aquifer and confining unit, resulting in a fully three-dimensional groundwater flow model. Although the IAS includes vertically stratified permeable zones (Basso, 2003; Basso and Hood, 2005; Knochenmus, 2006), which may affect local groundwater flow, the IAS in the southwestern corner of the model area (fig. 21) is simulated as a single model layer representative of regional flow conditions in this aquifer system.

Initial Conditions

Initial conditions for the 12-year transient model were equal to the head distribution solution for steady-state conditions for January 1995. Because the true head distribution is not known with certainty, an approximation was derived from a separate steady-state forward model run for January 1995. Boundary conditions for this run are based on average hydrologic conditions in the ECFT model area in January 1995, and the run uses calibrated hydraulic conductivity values discussed later in this report. This model-derived set of initial conditions eliminated the effects of head interpolation over large areas where few measured heads are available. There is some error associated with the assumption of steady-state conditions for January 1995, however, because actual conditions were transient and influenced by antecedent hydrologic conditions. Different initial conditions could lead to different simulated heads and flows at later times. To test the effect of the initial conditions, forward runs of the 12-year transient model were done with two different sets of initial conditions to determine the time at which simulated heads in both runs became nearly equal. The first set is that derived from the steady-state model run representing January 1995 conditions, described earlier. The second set of initial heads was derived from the head solution for a steady-state model representing annual average 1995 conditions.

Comparison of results from the 12-year transient model runs with the two different sets of initial conditions showed that by stress period 7 (representing July 1995) the maximum absolute value in head difference was 0.05 ft in layer 1 and 0.01 ft in layers 2 to 7. By the end of 1995, the maximum head difference in layer 1 was 0.01 ft. Because the goal was to calculate the number of simulated stress periods required for

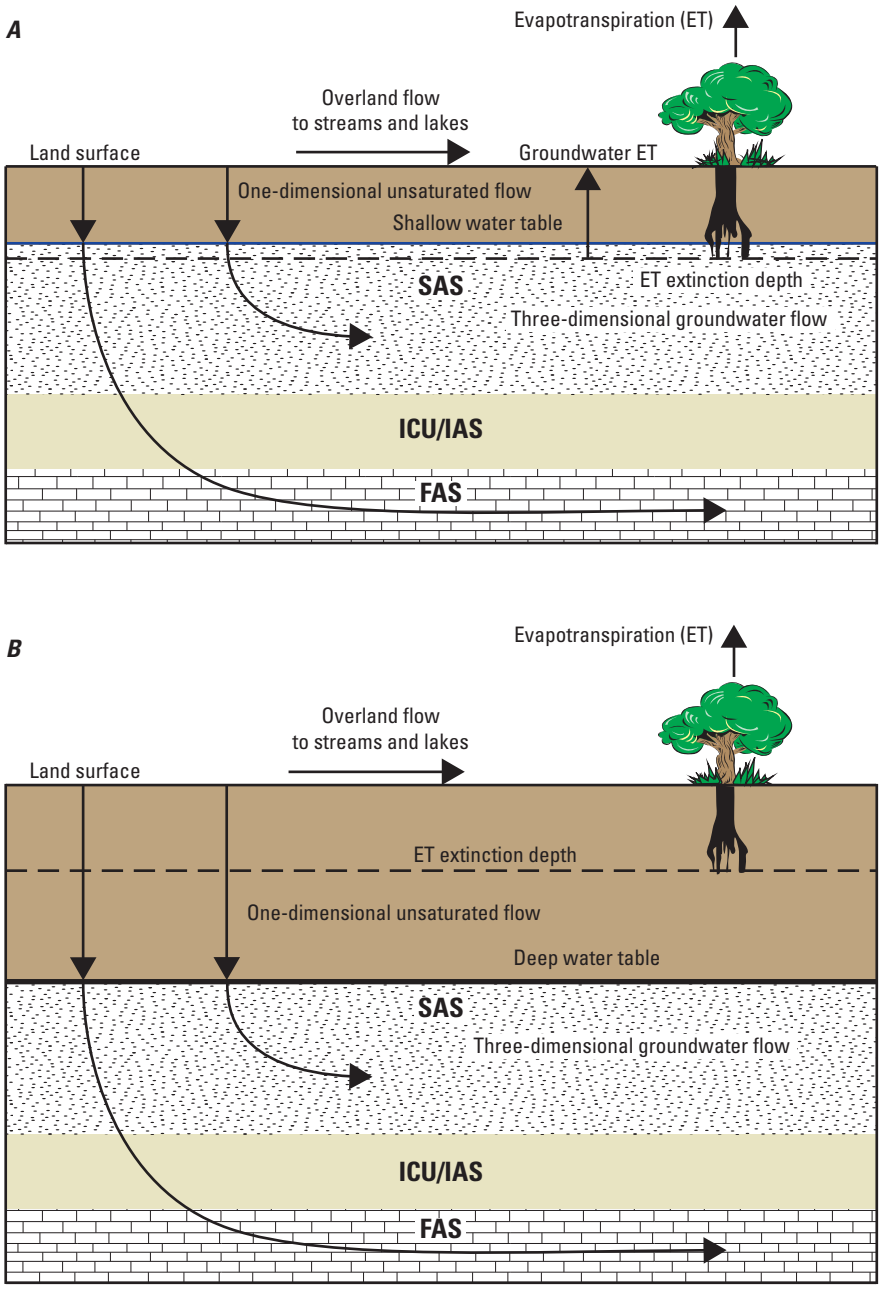

Figure 41. One-dimensional unsaturated-zone flow coupled with three-dimensional groundwater flow for the *A*, shallow water table, and *B*, deep water table. Modified from Niswonger and others (2006).

Table 6. Geographical information system coordinates of the corners of the groundwater flow model grid.

[XUTM and YUTM coordinates refer to Universal Transverse Mercator projection, North American Datum 1983, Zone 17N, in meters (Snyder, 1983)]

Grid corner	XUTM	YUTM
Upper left	401023.75	3220231.0
Upper right	548470.75	3220231.0
Lower left	401023.75	3040780.0
Lower right	548470.75	3040780.0

two different initial head distributions to coincide, the effects of the differences in initial conditions dissipate in at most one year of simulation.

Boundary Conditions

The main boundary conditions imposed in the ECFT model are (1) head-dependent flux at lateral boundary cells (using the General Head Boundary (GHB) Package), (2) head-dependent flux at springs, (3) head-dependent flux between lakes and the SAS, and between the lakes and the ICU/IAS through representation of vertical leakance of both lakebed and ICU/IAS, (4) head-dependent flux between streams and the SAS through the vertical hydraulic conductivity of the streambed, and (5) the no-flow condition imposed at the bottom of the LFA.

The model simulates the freshwater flow system, and cells representing areas where the OPZ, OLPZ, APPZ, MCU I/II, or LFA (layers 3 to 7) contained water with chloride concentrations exceeding 5,000 mg/L were made inactive. This minimized potential errors introduced by simulating aquifer areas containing water having variable density. By definition, the base of the simulated freshwater flow system coincides with the base of the LFA (Sepúlveda, 2002), or the altitude at which chloride concentrations of 5,000 mg/L occur (fig. 37), whichever is shallower. GHB cells along the bottom of the simulated freshwater interface allow potential flux to occur across this interface. The active portions of each model layer were delineated by intersecting the surfaces representing the top of each hydrogeologic unit (figs. 22, 26, 28, 32, and 34) with the altitude of the 5,000 mg/L chloride concentration isochlor (fig. 37) to generate the lateral extent of active cells in each layer (fig. 43). The thickness of the hydrogeologic units in active cells near the lateral boundary cells is thinner than that of active cells away from the lateral boundaries because the freshwater and saline-water interface is shallower near the lateral boundaries.

Model boundaries were assigned to approximate the actual groundwater flow system as accurately as possible. Head-dependent flow boundary conditions were simulated using the GHB Package and were applied to the lateral boundaries shown in figure 43 for the seven layers in the model. Simulation of the freshwater and saline-water interface is a simplified approximation of the physical system, which could be more accurately simulated by a variable-density flow model. The GHB Package was used to represent potential flow across the 5,000 mg/L chloride concentration boundary. The magnitude of this flow depends on the specified heads estimated from measured heads near the boundary cells and on the conductance calculated from hydraulic conductivity. Such conceptualization is a common approach for simulating the freshwater parts of the aquifer system on a regional scale. Specified heads used in the GHB Package were interpolated along the lateral boundaries based on measured water levels at nearby wells. Where needed, heads were interpolated based on hydraulic gradients between hydrogeologic units (fig. 31). The specified heads at the GHB cells were varied annually for the 1995–2006 simulation period. Boundary conductance values used in the GHB Package were computed as the product of the horizontal hydraulic conductivity of the model layer for the cell at the lateral model boundary and the cross-sectional area of the cell, divided by an internode distance of 1,250 ft (Harbaugh, 2005). The base of the simulated flow system was assigned a no-flow boundary condition and coincided with the 5,000 mg/L isochlor (fig. 37) or the base of the LFA as shown in Sepúlveda (2002), whichever was shallower.

Flow at 22 springs in the northern part of the ECFT model area (fig. 1, appendix 2, table 2–1) was simulated using estimated spring-pool altitudes and the assumption of increased hydraulic conductivity near springs. A major component spring flow is the net aquifer recharge from rainfall; however, spring response is delayed by aquifer-matrix storage. Higher spring flows are common in late fall after the rainy season, whereas lower flows occur in late spring when rainfall is low. Spring flows from the UFA tend to create depressions in the potentiometric surface, the areal extent of which depends on the magnitude of the spring flow and aquifer and the confining-unit properties near the spring. The GHB Package was used to simulate spring flow by specifying an estimated head at the spring that best represented the spring-pool altitude and specifying a conductance value calculated from the horizontal hydraulic conductivity estimated by calibration. The estimated pool altitudes at the springs were varied annually for the 1995–2006 simulation period.

Lakes were simulated as another boundary condition on the model. All gaged lakes in the ECFT model area, as well as ungaged lakes that were part of the stream network, were included in the simulation. Ungaged lakes smaller than a single grid cell were not considered in the model. The main consequence of not considering a lake in a flow simulation is that recharge to the SAS is simulated by routing infiltration through the unsaturated zone instead of simulating leakage to or from the unit beneath the lake through the lakebed material. As a conceptual simplification, a few ungaged lakes with surface areas up to 0.25 mi^2 were not considered in the study because of a lack of corresponding water-surface altitude data. Ungaged

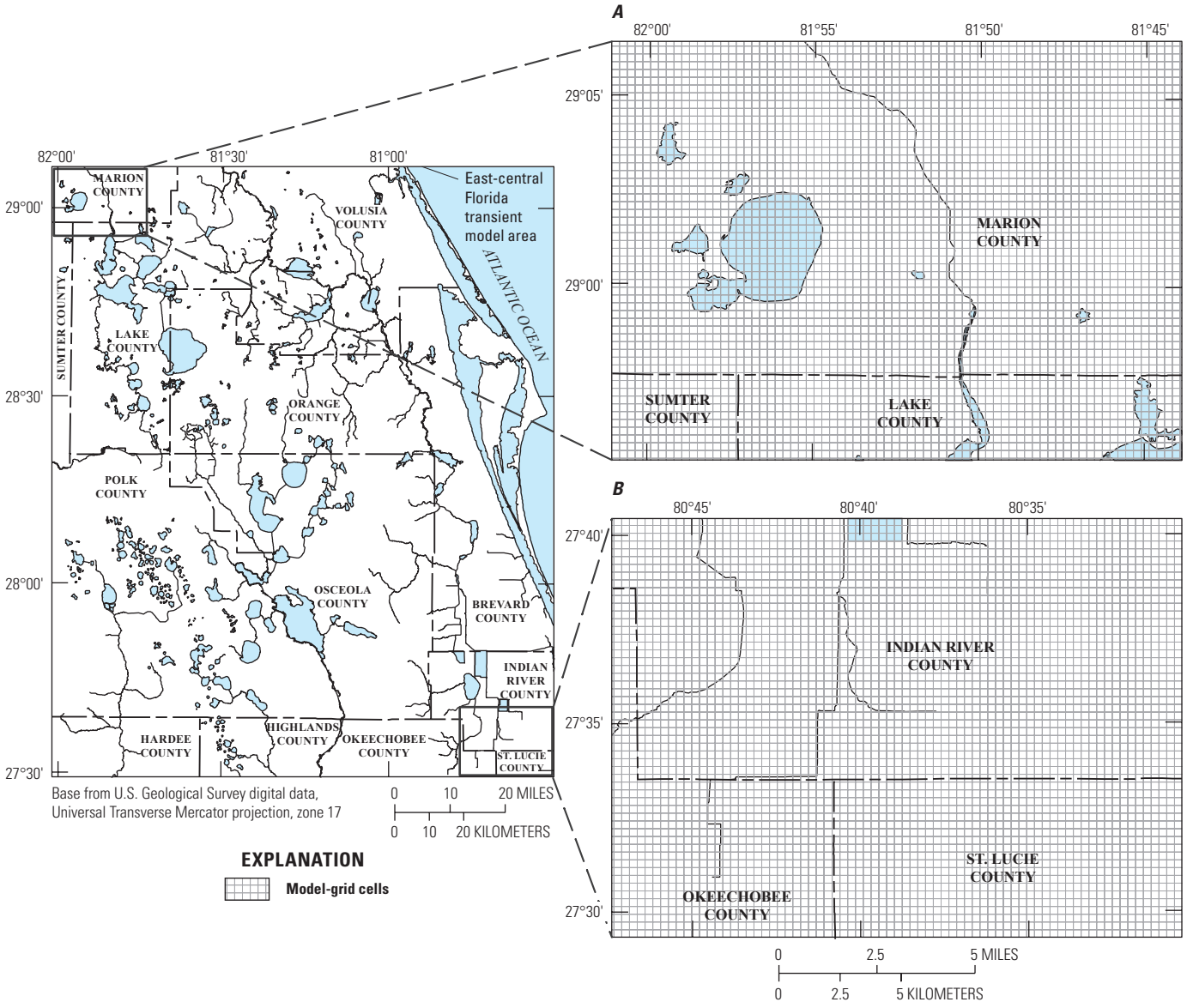

Figure 42. Expanded view of the groundwater flow model for the East-Central Florida Transient (ECFT) study area displaying the model grid in portions of *A*, Marion, and *B*, Indian River Counties.

lakes with parts of their drainage areas lying outside the model area were not considered in the study because the calibration of fluxes at such lakes would have required an overestimation of runoff from the part of the drainage area within model bounds. Regardless of whether or not an ungaged lake was considered, water exchanges were considered either by simulating leakage through the lakebed material or by simulating recharge to the SAS. The water-surface altitudes at the 351 lakes included in the ECFT model (fig. 13) were simulated using the LAK7 Package developed by Merritt and Konikow (2000). As is shown for Lake Apopka (fig. 44), lakes in figure 13 were intersected with the model grid to generate the lake cells, which are considered to be inactive cells in the SAS. Lake cells were, in general, those grid cells with at least 50 percent of their represented area occupied by a lake. Initial water-surface altitudes at the lakes were either estimated from the DEM or assigned from measured values near the beginning of the simulation, namely January 1995. For ungaged lakes discharging to streams, the initial 1995 water-surface altitude was assigned a value based on the water-surface slope continuity between the stream and the lake. Selected lakes and lake names, with the number of average monthly measured water-surface altitudes close to the total number of stress periods (144), are shown in appendix 3.

The main parameters that control the changes in water-surface altitudes at the lakes are the land-surface runoff, the vertical hydraulic conductivity of the lakebed, the streambed slope and channel width of the first stream reach of the lake's

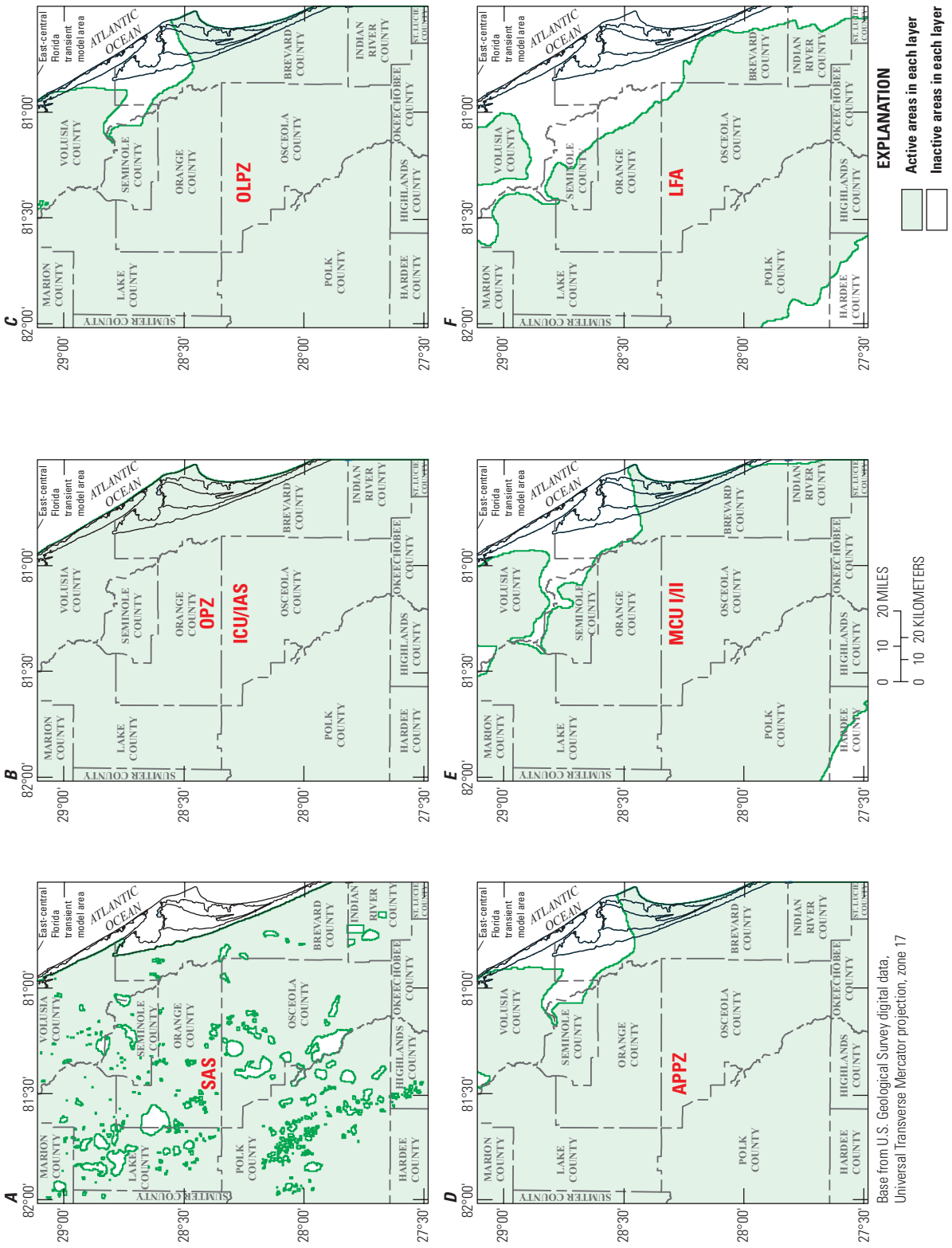

Figure 43. Areal extent of active areas simulated in *A*, layer 1, the surficial aquifer system (SAS); *B*, layers 2 and 3, the intermediate confining unit or intermediate aquifer system (ICU/IAS) and the Ocala permeable zone (OPZ), which coincided in the extent of active areas; *C*, layer 4, the Ocala low-permeable zone (OLPZ); *D*, layer 5, the Avon Park permeable zone (APPZ); *E*, layer 6, the middle confining units I/II (MCU I/II); and *F*, layer 7, the Lower Floridan aquifer (LFA) in east-central Florida. Shading indicates active areas simulated in each layer.

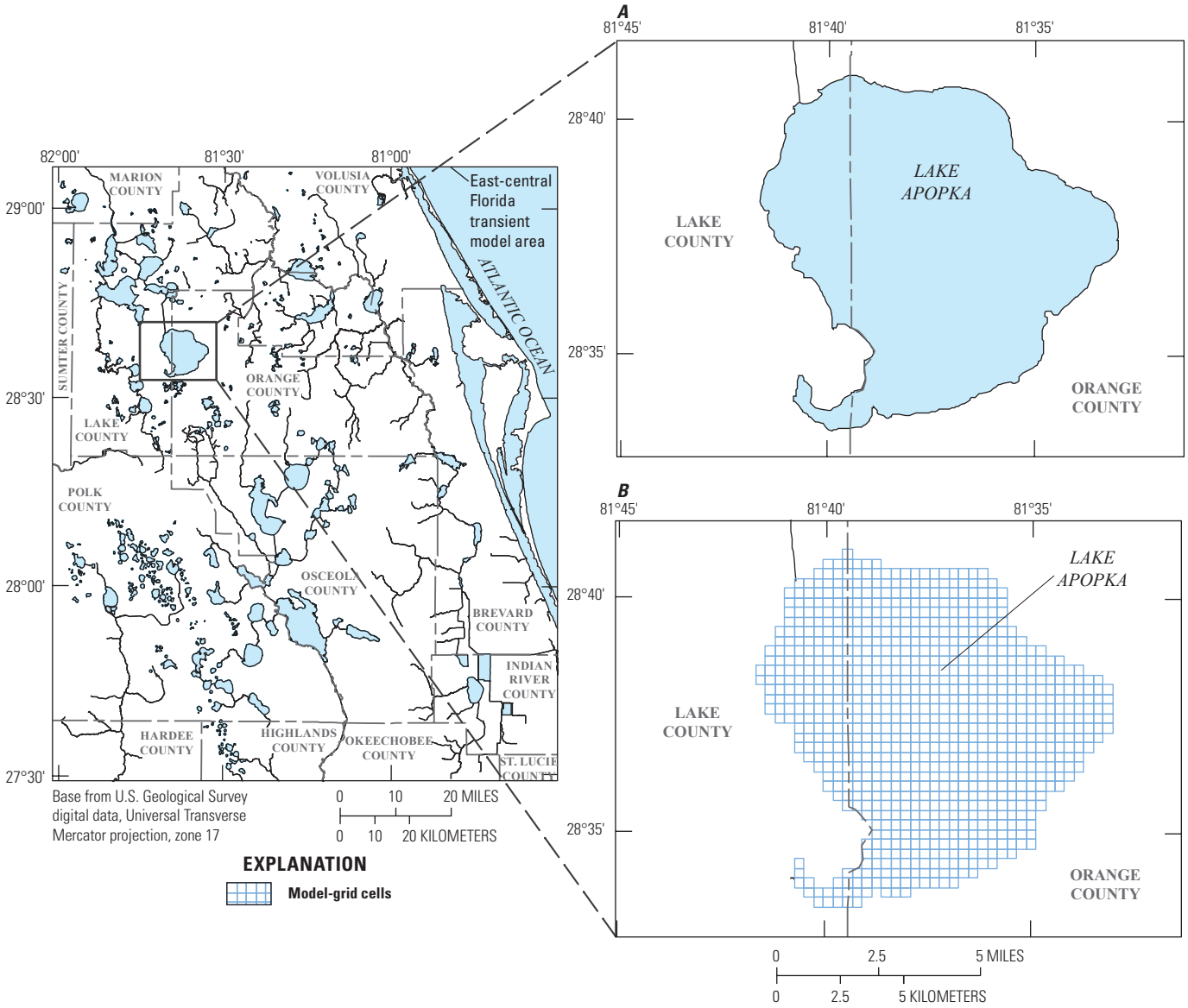

Figure 44. *A*, Lake Apopka, and *B*, the corresponding lake cells after intersection with the grid.

outlet, the rainfall, and the potential ET at the lake surface. The vertical hydraulic conductivity of the lakebed and the difference between water-surface altitude and head determined the lateral flow to or from the SAS and the vertical flow to or from the ICU/IAS, depending on the lake location. The streambed slope of the first stream reach of the lake's outlet was adjusted as needed during the calibration of the water-surface altitudes at the lakes.

The streamflow routing was performed using the SFR2 Package developed by Niswonger and Prudic (2006). All gaged streams in the ECFT model area were included in the simulation. All perennial streams, whether ungaged or gaged, were also included in the simulation. The main streams in the ECFT model area, and included in the simulation, are the St. Johns River, the Kissimmee River, the Peace River, and the Palatlakaha River (fig. 1). As illustrated in figure 45 for the Peace River and some of its tributaries, the streams in figure 11 were intersected with the model grid to subdivide the 320 stream segments into cell-specific reaches within each segment. Initial flow at the uppermost reach of each stream was specified for the first three stress periods of 1995 and for each stress period where the uppermost reach of the stream is a spring. Examples of measured streamflows at selected stream-gaging stations are shown in appendix 4.

The parameters that determine the magnitude and the routing of the streamflow are the surface runoff applied to each stream, the stream-channel width, the stream water-surface altitude slope, the streambed slope, the thickness of the streambed, the vertical hydraulic conductivity of the streambed, the potential ET, the rainfall applied to the stream surface area, and

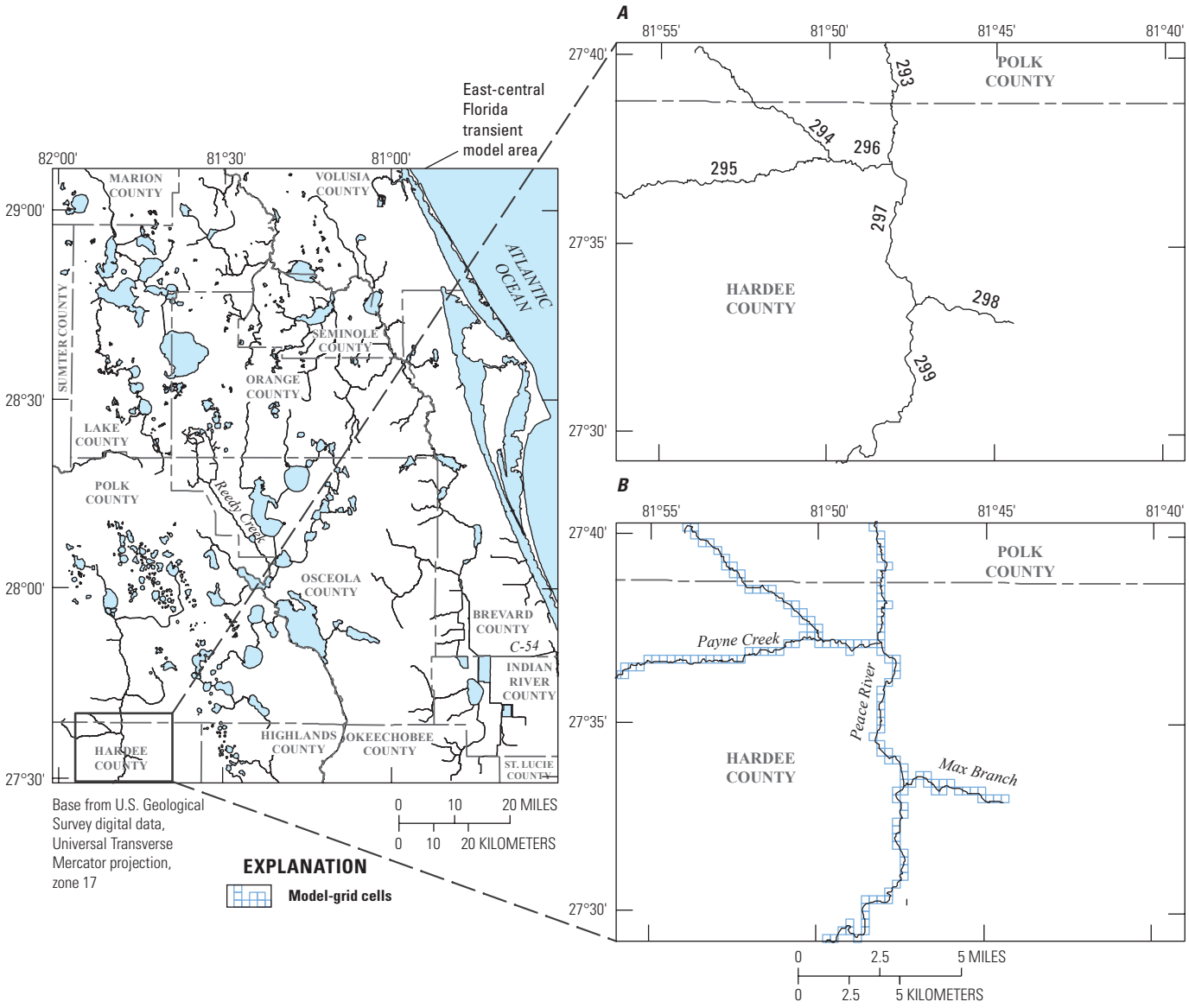

Figure 45. *A*, Peace River, some tributaries, and stream segment numbers; and *B*, the corresponding stream cells after the intersection with the grid.

Manning's dimensionless roughness coefficient. The roughness coefficient, assigned a value of 0.05 for all streams, is a measure of the resistance to flow in the channel. The surface runoff applied to each stream depended on the drainage area of each stream, which was estimated from the basin delineation in databases of the SJRWMD, SWFWMD, and SFWMD (Brian McGurk, St. Johns River Water Management District, written commun., 2008). The stream channel width was approximated using aerial photographs available from GIS (Environmental Systems Research Institute, ArcMap, version 10.0, 2010). The stream water-surface altitude slope was assigned the value of 0.0001, 0.0002, or 0.0003, depending on the calculated slope between operating water-surface stations, where available, or in the absence of gaged stations, estimated from the DEM developed by Arthur and others (2007). The water-surface altitude slopes at streams estimated from the DEM were adjusted following the general rule that water-surface slopes are generally lower than terrain slopes.

The streambed slope was calibrated at the point where a lake discharges to streams based on the net flow to the lake and the water-surface altitude at the lake. Because of the lack of data for streambed thickness, all stream segments were assumed to have a streambed thickness of 5 ft. The vertical hydraulic conductivity of the streambed, under the 5-ft streambed thickness assumption, was set to a uniform calibrated value of 0.02 ft/d for all stream segments. The ratio of the vertical hydraulic conductivity to its streambed thickness controls the groundwater flux between the stream and the aquifer, and thus, if a streambed is actually thicker than 5 ft, then the calibrated vertical hydraulic conductivity should be larger than 0.02 ft/d.

The uniform value of 0.02 ft/d was modified only for stream segments 268 and 283 to 289 (fig. 11), where measured downstream flow was measured to be less than the measured upstream flow for specific stress periods, suggesting a strong stream-aquifer hydraulic connection. This was observed for stream-segment numbers 287 and 289 of Peace River (figs. 1 and 11). Stream segment 268 corresponds to Wolf Branch Creek (figs. 1 and 11), which discharges to a sinkhole and therefore needs to have a greater streambed vertical hydraulic conductivity, guided by those values that reduce the residuals between simulated and measured streamflows. The remaining stream segments that had a calibrated streambed vertical hydraulic conductivity different from 0.02 ft/d were stream segments 283 to 286, 288, and 290 to 299 (fig. 11).

Potential ET rates and rainfall were applied directly to stream-surface areas. The following flows are hydraulically routed using the SFR2 Package: land-surface runoff to streams segments, rainfall (falling on the stream surface area), and lake outflow to streams where it occurs. Groundwater interactions between the streams and the SAS are also simulated by the SFR2 Package.

Rainfall and irrigation at cells within closed basins was treated as infiltration because runoff is assumed not to drain out of the closed basins. Irrigation rates consisted of landscape and agricultural irrigation, which were added to rainfall before partitioning total rainfall and irrigation into surface runoff and infiltration. Landscape and agricultural irrigation generally was much smaller than rainfall. For example, total 2003 landscape and agricultural irrigation ranged from 0.1 to 35 in. (fig. 46), whereas total 2003 rainfall ranged from 46.5 to 62.3 in.

Flow in the Unsaturated Zone

Conceptually, the unsaturated zone is the link between infiltration, resulting from rainfall and irrigation applied at land surface and computed by the GAI method, and the saturated groundwater flow system (fig. 47). The effects of flow, ET, and storage in the unsaturated zone were simulated using the UZF1 Package. This Package solves the one-dimensional form of the Richards' equation, which is approximated by a kinematic-wave equation by assuming vertical flux is only driven by gravitational forces (Niswonger and others, 2006). This formulation neglects capillary processes.

When the rainfall rate exceeds the infiltration rate, it results in surface runoff known as Hortonian runoff (Horton, 1933). When the water-table altitude is at, near, or above land surface, rainfall becomes mostly runoff, and this type of runoff is referred to as Dunnian runoff (Dunne and Black, 1970). Hortonian runoff is not simulated by the UZF1 Package in this model because the maximum rainfall intensity over the stress period of any month was always less than the infiltration rate, which is the hydraulic conductivity in the unsaturated zone calculated from Brooks-Corey equation (Niswonger and others, 2006). One of the primary reasons for the application of the UZF1 Package, as opposed to simpler conceptualizations, is its ability to simulate the time lag incurred during percolation of surface infiltration through a thick unsaturated zone, such as occurs in many of the local ridge or upland physiographic regions (for example, Lake Wales Ridge and Marion Upland; fig. 2). Additionally, the UZF1 Package simulates groundwater seepage to land surface (sometimes referred to as surface leakage) when the simulated water table is near, at, or above land surface, which may occur in topographic depressions. Both groundwater seepage and Dunnian runoff are added instantaneously to the specified streams or lakes according to the drainage field (fig. 7).

Dunnian runoff is calculated by the UZF1 Package (Niswonger and others, 2006). The rate of infiltrated water is reduced by the ET simulated by the UZF1 Package in the unsaturated zone, ultimately resulting in the net recharge to the SAS. The calculation of Hortonian runoff using the GAI method was applied to cells draining to streams or lakes outside the model area, cells draining to streams, including stream cells, and cells draining to lakes (cell types 2, 3, 4, fig. 47). The GAI method was not applied to lake cells or cells in closed basins because rainfall over lakes goes directly to the water surface and closed basins are characterized by topography in which runoff does not leave the basin, causing runoff to become additional infiltration (cell types 1 and 5, fig. 47).

The Brooks-Corey function (Brooks and Corey, 1966) is used in the UZF1 Package to characterize the water storage and transmission properties of the unsaturated zone, which requires specification of the following parameters: saturated hydraulic conductivity, residual water content θ_r, saturated water content θ_s, and the Brooks-Corey exponent ε (Niswonger and others, 2006). Saturated hydraulic conductivity values were set equal to a few feet per day less than the calibrated horizontal hydraulic conductivity of the SAS, which was obtained from model runs. Although θ_r and ε can vary depending on soil type, constant average values of 0.10 and 3.50, respectively, were used for all active cells in the SAS. In order to maintain water mass balance between the unsaturated and saturated zones, specific yield Sy of the SAS was specified to be equal to $\theta_s - \theta_r$ (Niswonger and others, 2006, p. 6). Values of Sy were estimated by model calibration, and θ_s values used in the UZF1 Package and those used in the GAI method were adjusted accordingly.

ET from the unsaturated and saturated zones was simulated using the UZF1 Package. The specified ET rate is a function of the extinction depth and the extinction water content, below which no ET can be removed from the unsaturated zone. The ET losses are withdrawn from the unsaturated zone until the water content is reduced to the extinction water content or the ET demand is met. If insufficient water is available in the unsaturated zone to meet the ET demand and the water table is above the extinction depth, then ET is removed from groundwater by the UZF1 Package using the same algorithm as in the MODFLOW ET Package (McDonald and Harbaugh, 1988). Otherwise, if the water table is below the extinction depth, the simulated ET is limited to that withdrawn until the unsaturated zone water content is reduced to the extinction water content. The ET rate specified in the

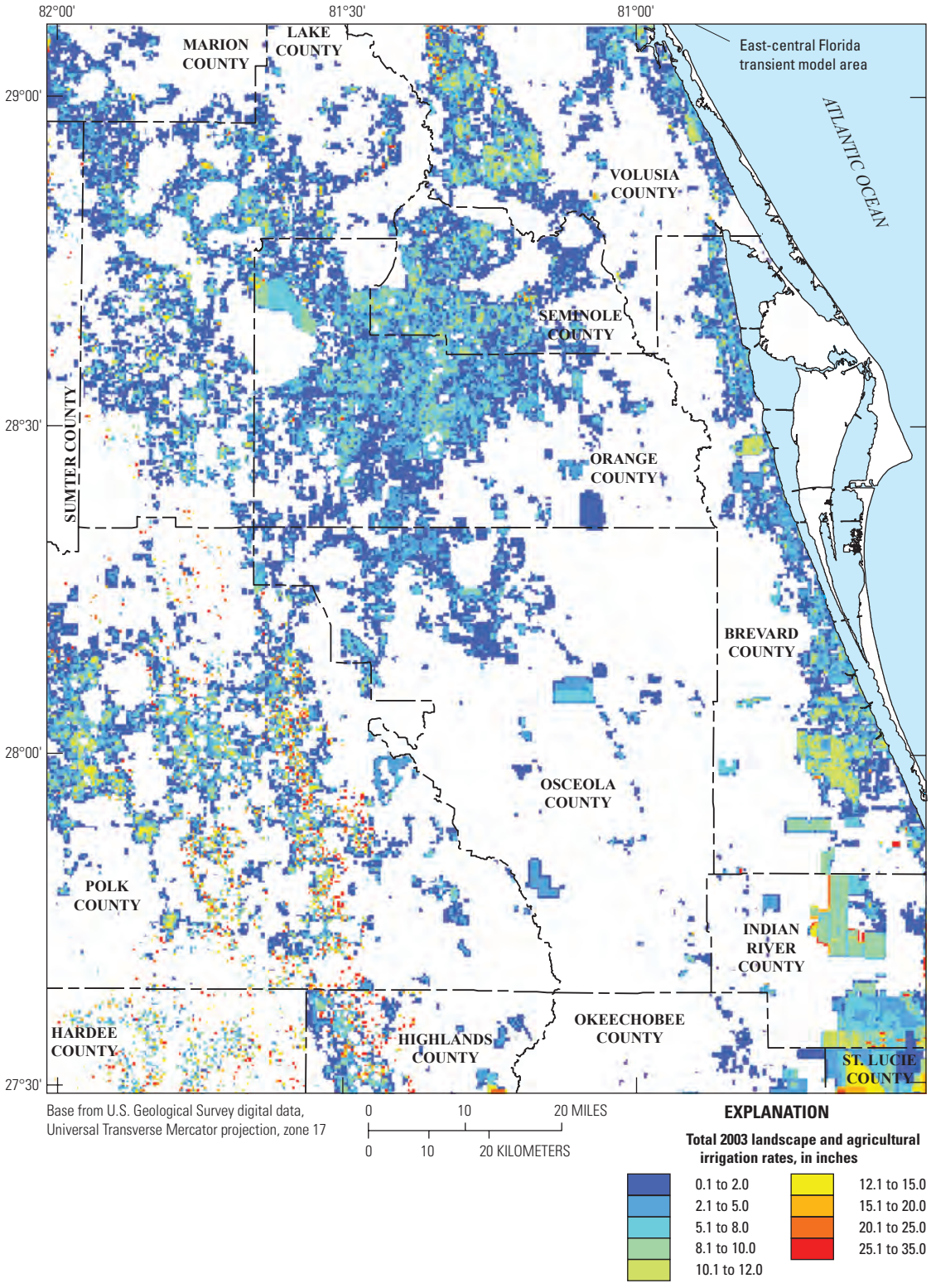

Figure 46. Landscape and agricultural irrigation rates used to calculate infiltration by the Green-Ampt method for 2003.

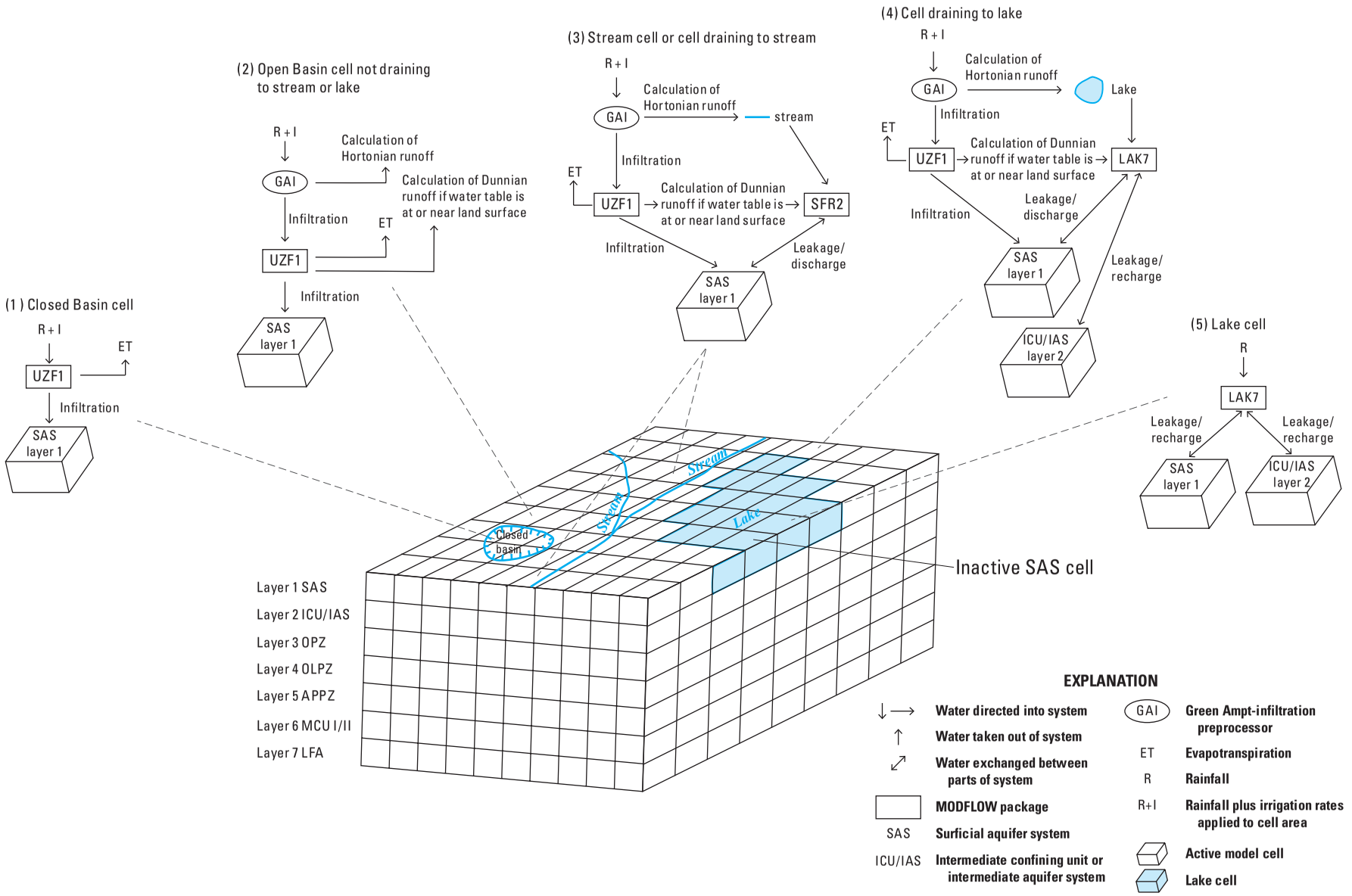

Figure 47. Implementation of flow processes in the shallow part of the hydrologic system.

UZF1 Package was set equal to the estimated ET, as described previously in the Evapotranspiration section; monthly values of estimated ET were used. Extinction water content, required to be between θ_r and θ_s, was set equal to $\theta_r + 0.01$ as a result of model calibration. Greater values than $\theta_r + 0.01$ for the extinction water content result in the underestimation of simulated ET; setting the extinction water content equal to θ_r results in numerous dry cells and an overestimation of ET. Extinction depth was specified based on values reported by Shah and others (2007) for generalized soil texture classes and a grass-land cover (table 7), where values are listed with the same accuracy published in their paper.

Table 7. Evapotranspiration extinction depths based on values from Shah and others (2007).

Soil texture class	Extinction depth, in feet below land surface
Sand	4.76
Loamy sand	5.58
Sandy loam	7.55
Sandy clay loam	7.55[a]
Sandy clay	7.55[a]
Muck	7.55[a]
Urban	4.76[b]
Greater than 50 percent Water	4.76[b]
Wetlands	4.76[b]

[a] The value for sandy loam was used.

[b] The value for sand was used.

Partitioning of Rainfall and Irrigation into Runoff and Infiltration

The main variables used in the GAI method are the hydraulic conductivity of the top soil K; the initial water content θ_i; the residual water content θ_r; the saturated water content θ_s; the difference between saturated and initial water content $\Delta\theta$; and the wetting front capillary pressure head Ψ; and the thickness of the wetting front L (fig. 48). Although θ_r can vary depending on soil type, a constant average value of 0.10 was used for all active cells in the SAS. The downward movement of the wetting front causes increases in water content, ranging from the residual water content θ_r to the saturated water content θ_s (fig. 48). The θ_s values were derived from calibration of the groundwater flow model and conceptually represent the water content when the soil is effectively saturated. Thus, θ_s excludes the effect of gas bubble entrapment and is less than porosity. Gas bubbles trapped beneath a

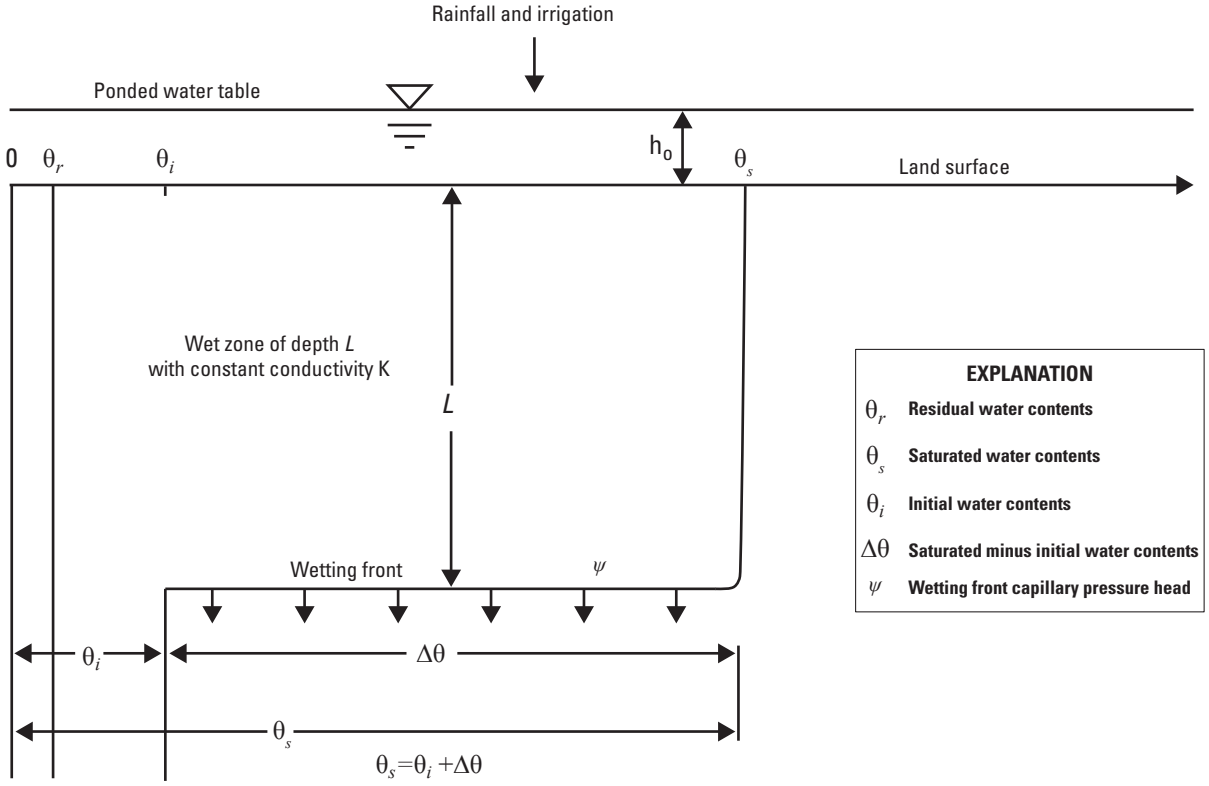

Figure 48. Vertical movement of the wetting front through the unsaturated zone and the relation between soil moisture content variables used in the Green-Ampt infiltration method.

descending wetting front or generated by microorganisms are common and can effectively reduce θ_s (Fayer and Hillel, 1986; Faybishenko, 1995). The effects of entrapped gas have been observed in central Florida during laboratory wetting of sand and clayey-sand cores representing flooded conditions in a RIB (Sumner and Bradner, 1996, p. 12, 18), and during natural water-table fluctuations (Nachabe and others, 2004).

The following steps are used to calculate infiltration and Hortonian runoff from rainfall and irrigation; further details are provided in Chow and others (1988).

1. At time $t = 0$, or just before rainfall begins, it is assumed that the cumulative infiltration F_0 is zero. The infiltration rate, f_0, is thus assumed to be a hypothetical maximum to avoid division by zero. At time $t > 0$, the cumulative infiltration F_t at time t and the rainfall intensity i_t are assumed to be known from the previous time step. For any time $t > 0$, the infiltration rate f_t at time t is calculated from:

$$f_t = K\left(\frac{\psi\Delta\theta}{F_t}+1\right). \quad (2)$$

2. If the infiltration rate f_t is less than or equal to the rainfall intensity i_t, then ponding occurs throughout the interval $t+\Delta t$ and $F_{t+\Delta t}$ is calculated from:

$$F_{t+\Delta t} = F_t + K\,\Delta t + \psi\Delta\theta\,\ln\left(\frac{F_{t+\Delta t}+\psi\Delta\theta}{F_t+\psi\Delta\theta}\right); \quad (3)$$

proceed to step 5 below to calculate runoff and infiltration.

3. If the infiltration rate f_t is greater than i_t, then no ponding occurs at the beginning of the time interval $t+\Delta t$ and a tentative value $F'_{t+\Delta t} = F_t + i_t\,\Delta t$ is calculated, deriving $f'_{t+\Delta t}$ from $F'_{t+\Delta t}$ using equation 2. If $f'_{t+\Delta t}$ is less than or equal to i_t, then ponding occurs during interval $t+\Delta t$. The cumulative infiltration at ponding F_p is calculated from i_t and equation

$$F_p = \frac{K\psi\Delta\theta}{(i_t - K)}, \quad i_t < K. \quad (4)$$

4. The time at which ponding first occurs within time interval Δt is calculated from $\Delta t' = \left(F_p - F_t\right)/i_t$. The cumulative infiltration $F_{t+\Delta t}$ is calculated by replacing F_t and Δt in equation 3 with F_p and $\Delta t'$. If $f'_{t+\Delta t}$ is greater than i_t, then no ponding occurs throughout interval $t+\Delta t$, and $F_{t+\Delta t}$ is calculated from $F_{t+\Delta t} = F_t + i_t\,\Delta t$.

5. Cumulative runoff is calculated by subtracting cumulative infiltration from cumulative rainfall. Runoff for each time step is calculated from cumulative runoff. Infiltration for each time step is calculated by subtracting runoff from rainfall. Current time t is then increased by Δt, and the process is continued at step 1 above.

Variability in antecedent moisture conditions required the adjustment of θ_i for each rainfall event. Defining the duration of each rainfall event as the number of consecutive days with nonzero rainfall, total rainfall was calculated for each event. Values of θ_i, calculated empirically as a variation between θ_r and θ_s, were adjusted as part of the calibration of measured and simulated streamflows. Rainfall events preceded by greater rainfall events with relatively few days in between had a larger θ_i than those preceded by a large number of days without rainfall. The capability of the soil to drain is considered in the value of K used in equations 2 through 4; and not in θ_i because the sensitivity of the GAI method to θ_i was low for daily rainfall.

Values for the wetting front capillary pressure head, ψ, were obtained from average values (log mean) of soil horizons reported by Rawls and others (1983) for each generalized soil texture class in the ECFT model area (fig. 49, table 8). Because the units of ψ are independent of time, values listed in table 8 were not changed during the calibration of infiltration and runoff rates.

The calibrated K values used in equation 3 compensate for using a coarse temporal resolution for rainfall data (day) in the model to describe rainfall/infiltration/runoff processes that have large intra-day variability. The calibrated hydraulic conductivity of the top soil used for the GAI method is different than the saturated hydraulic conductivity values used in the UZF1 Package or the hydraulic conductivity values used for the SAS. The smaller the time interval of the rainfall, the closer K would be to field values as the need for parameter compensation of coarse temporal resolution declines. Field values for K would only be attained when using instantaneous rainfall. Effective K values were derived by matching observed groundwater levels, water-surface altitudes at lakes, and streamflows, thereby yielding proper partitioning of rainfall and irrigation into runoff and infiltration in accordance with these regional-scale observations. The calibration of K in the GAI method was performed based on the hydrologic soil groups (fig. 5), the steps shown in figure 50, and adhering to decreasing values from the most permeable soil group, A, to the least permeable, D (table 9). However, many factors other than Darcian-derived K values affect infiltration processes—such as two-phase flow (water and soil gas), macropore flow, and biological and chemical characteristics of the top soil—leading to the need for "composite" or "effective" parameter values to simulate these processes at the scale of a regional model.

Representation of Hydraulic Conductivity

Several model parameters were defined to represent the distribution of horizontal (Kh) and vertical (Kv) hydraulic conductivity for the seven model layers (tables 10 and 11, respectively). Generally, Kh and Kv are represented as spatially variable

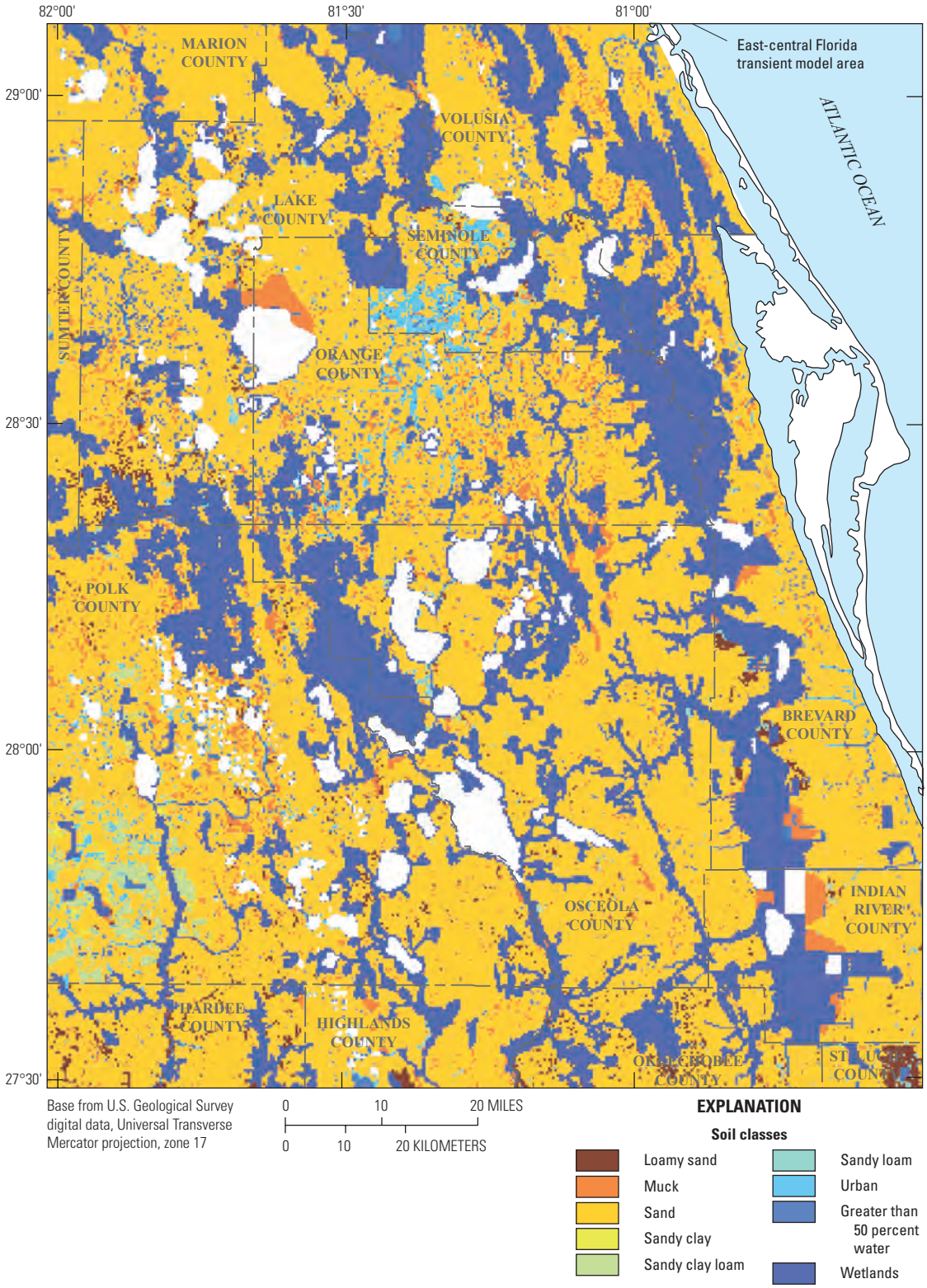

Figure 49. Spatial distribution of soil texture classes in the active cells of the surficial aquifer system.

Table 8. Wetting front capillary pressure head values used in the Green-Ampt infiltration method based on values from Rawls and others (1983).

Soil texture class	Wetting front capillary pressure head, in feet
Sand	0.162
Loamy sand	0.201
Sandy loam	0.361
Sandy clay loam	0.717
Sandy clay	0.784
Muck	1.037[a]
Urban	0.162[b]
Greater than 50 percent Water	0.162[b]
Wetlands	0.292[c]

[a] The value for clay (Rawls and others, 1983) was used.

[b] The value for sand (Rawls and others, 1983) was used.

[c] The value for loam (Rawls and others, 1983) was used.

Table 9. Average calibrated hydraulic conductivity of the hydrologic soil groups used in the Green-Ampt infiltration method.

Hydrologic soil group	Average K value used over all active cells, in feet per day
A	0.085
B	0.067
C	0.055
D	0.038
A/D	0.080
B/D	0.060
C/D	0.045

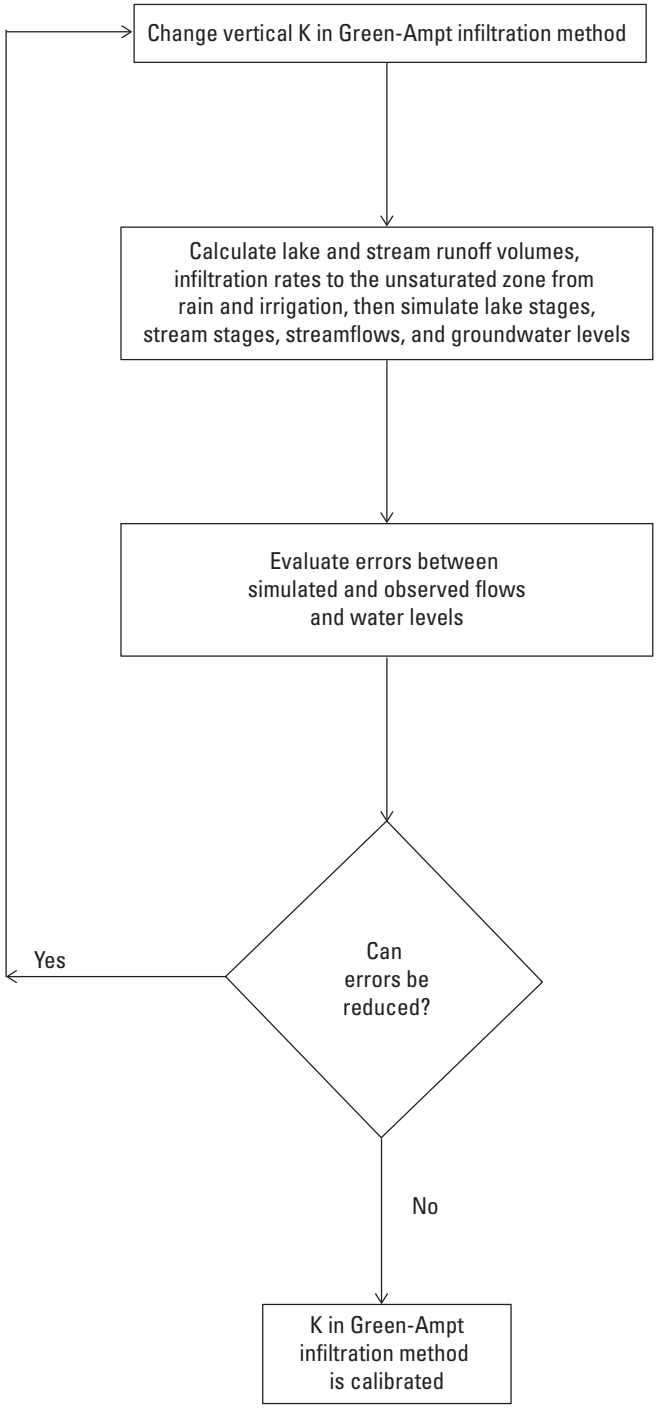

Figure 50. Steps used to calibrate the hydraulic conductivity of the top soil used in the Green-Ampt infiltration method.

Table 10. Model parameters defined to represent horizontal hydraulic conductivity.

[SAS, surficial aquifer system; ICU/IAS, intermediate confining unit and intermediate aquifer system; OPZ, Ocala permeable zone; OLPZ, Ocala low-permeable zone; APPZ, Avon Park permeable zone; MCU, middle confining units I and II; LFA, Lower Floridan aquifer; Kh, horizontal hydraulic conductivity; ft/d, feet per day; —, not applicable]

Model layer	Hydrogeologic unit	Method used to represent spatial variability in Kh	Number of defined parameters	Number of estimated parameters	Number of specified parameters	Number of tied parameters
1	SAS	Zones of uniform values	21	21	—	—
2	ICU/IAS	Regional Pilot Points	285	59 (IAS)	226 (ICU; Kh=7 ft/d)	—
3	OPZ	Regional Pilot Points and Spring Pilot Points	285 96	285 22	— —	— 74
4	OLPZ	Uniform Value	1	—	1; Kh=20 ft/d	
5	APPZ	Regional Pilot Points and Spring Pilot Points	275 96	275 —	— —	— 96
6	MCU	Uniform Value	1	—	1; Kh=1 ft/d	—
7	LFA	Regional Pilot Points	228	228	—	—
Total			**1,288**	**890**	**228**	**170**

Table 11. Model parameters defined to represent vertical hydraulic conductivity.

[SAS, surficial aquifer system; ICU/IAS, intermediate confining unit and intermediate aquifer system; OPZ, Ocala permeable zone; OLPZ, Ocala low-permeable zone; APPZ, Avon Park permeable zone; MCU, middle confining units I and II; LFA, Lower Floridan aquifer; Kh, horizontal hydraulic conductivity; Kv, vertical hydraulic conductivity; Direct, Kv defined; Calculated, α defined and Kv=Kh/α; α, vertical anisotropy; —, not applicable]

Model layer	Hydrogeologic unit	Method of defining Kv	Method used to represent spatial variability in Kv	Number of defined parameters	Number of estimated parameters	Number of specified parameters	Number of tied parameters
1	SAS	Direct	Zones of uniform values	21	—	21; Kv=0.15–0.95	—
2	ICU/IAS	Direct	Regional Pilot Points	285	285	—	—
3	OPZ	Calculated	Uniform Value	1	—	1; α=100	—
4	OLPZ	Direct	Regional Uniform Value Spring Pilot Points	1 96	1 —	— —	— 96
5	APPZ	Calculated	Uniform Value	1	—	1; α=100	—
6	MCU	Direct	Zones of uniform values	2	2	—	—
7	LFA	Calculated	Uniform Value	1	—	1; α=125	—
Total				**408**	**288**	**24**	**96**

in layers where the calibration observations are sensitive to these aquifer properties and field data indicate spatial variability, and as spatially uniform in layers where the calibration observations are not sensitive to the aquifer properties and field data provide little or no information on spatial variability. Kh is spatially variable in the aquifers (layer 1, the IAS of layer 2, and layers 3, 5, and 7), and is constant in the confining units (layer 4, the ICU of layer 2, and layer 6). Kv is represented directly, and independently of Kh, in layers 1, 2, 4, and 6 by defining its spatial distribution. In layers 3, 5, and 7, Kv is represented by defining vertical anisotropy (α = Kh/Kv); MODFLOW then internally calculates Kv (equal to Kh/α) using the spatially variable Kh for these layers.

Sets of regional-scale pilot-point parameters are used to represent the regional-scale variability of Kh for layers 2, 3, 5, and 7 (table 10), and of Kv for layer 2 (table 11). Pilot points are a method for estimating the spatial distribution of a hydraulic property that varies smoothly over all or part of a model layer. The inverse modeling code PEST (Doherty, 2010a, b), which was used to estimate parameters of the ECFT model, includes a suite of programs that facilitates use of the pilot-points method (Doherty, 2008). By this method, pilot points are placed at some of the model cells in the region where a smooth parameter distribution is to be estimated. Parameter values at some or all pilot points are estimated at all iterations of the nonlinear regression, and parameter values at all model cells in the region are interpolated from the values at the pilot points. In this way, parameter values at all cells are estimated, but the computational expense of calculating parameter sensitivities is limited to the pilot point parameter locations. PEST supports kriging as the interpolation method, using a variogram that is specified *a priori*.

Zones of constant parameter value are used to represent the spatial variability of Kh or Kv in some layers (tables 10 and 11). For layer 1, zones corresponding to the 21 physiographic regions shown in figure 2 are used to represent both Kh and Kv, because the hydrogeologic properties of the SAS are thought to vary by these regions. For Kv of layer 6, two zones are defined, one corresponding to the region where MCU I is present, and the other corresponding to the region where MCU II is present. The Kv of the MCU II, in the southwestern part of the ECFT area (fig. 32), is expected to be substantially smaller than that of the MCU I, owing to the widespread occurrence of the permeability limiting gypsum mineralization within the MCU II.

Model results, geologic data, and aquifer test data supported the need to represent Kh of layers 2, 3, 5, and 7, and Kv of layer 2 using a spatially variable distribution instead of zones with uniform values. Geologic data provide only sparse information about the variability of rock properties within the hydrogeologic units represented by each of these layers. There are a large number of aquifer test data from the OPZ (model layer 3), but the variability in the Kh values from these tests precludes using these data to delineate zones of constant hydraulic conductivity (fig. 24). There are few aquifer test data available for guiding the delineation of zones in the IAS (layer 2), the APPZ (layer 5), and the LFA (layer 7) (figs. 21, 30 and 36). Furthermore, in each of these hydrogeologic units, aquifer test data vary over short distances, which can confound use of these data to delineate zones of equal Kh. For the ICU (layer 2), there is thought to be a high degree of spatial variability in Kv, but again there are very few geologic or hydraulic test data to guide constructing zones of constant Kv. The occurrence of sinkholes indicates locations where the vertical hydraulic conductivity of the ICU may be presumed to be relatively large. However, for a groundwater flow model in the Lake Wales Ridge area of west Orange and southeast Lake Counties, O'Reilly (1998, p. 51) reported unsatisfactory results when attempting to calibrate ICU leakance based on sinkhole density inferred from land-surface depressions. Because of these difficulties with delineating zones, the pilot-points approach was used for representing Kh of layers 2, 3, 5, and 7, and Kv of layer 2.

For the layers in which regional-scale variability of Kh or Kv is represented using the pilot point method, a regularly-spaced grid of regional pilot points was placed over the extent of the model area in each layer. The grid of points in layer 3 (fig. 51) shows that the distance between pilot points in the row or column direction is 25 grid cells, representing a distance of 31,250 ft (5.9 mi). This spacing allowed an appropriate degree of variability to be estimated given the scale of the flow model. It produced a total of 1,358 pilot points for the entire model, and Kh or Kv was estimated at 1,156 of these points. An exponential variogram, recommended by Doherty and others (2010), was used for the kriging procedure to interpolate Kh or Kv values for all model cells in a given layer:

$$\gamma(h) = C_0\left[1 - \exp\left(-h / a\right)\right], \tag{5}$$

where $\gamma(h)$ is the variogram, C_0 is the sill, h is the separation distance between points, and the range is given by $3a$ (where the variogram reaches 95 percent of the sill). The sill does not affect interpolated values. For the regional variogram, the value of a is denoted a_r and is set to 49,213 ft (15,000 meters), which is about 1.6 times the pilot point separation distance. This is consistent with the recommendation of Doherty and others (2010) that for uniformly spaced pilot points, the value of a should be set equal to 1 to 2 times the pilot point separation distance. Ordinary kriging, in which the mean of the interpolated values is not specified *a priori*, is used for interpolation of the regional pilot points.

An additional 288 spring pilot points were used to represent the distribution of a hydraulic conductivity (K) multiplier that allows for increased hydraulic conductivity near the springs because of the commonly observed state of enhanced dissolution of carbonate rocks near the springs (fig. 52). The springs emanate from the UFA, which is composed of the OPZ, OLPZ, and APPZ. Thus, the K multipliers are used to define Kh in the corresponding layers 3

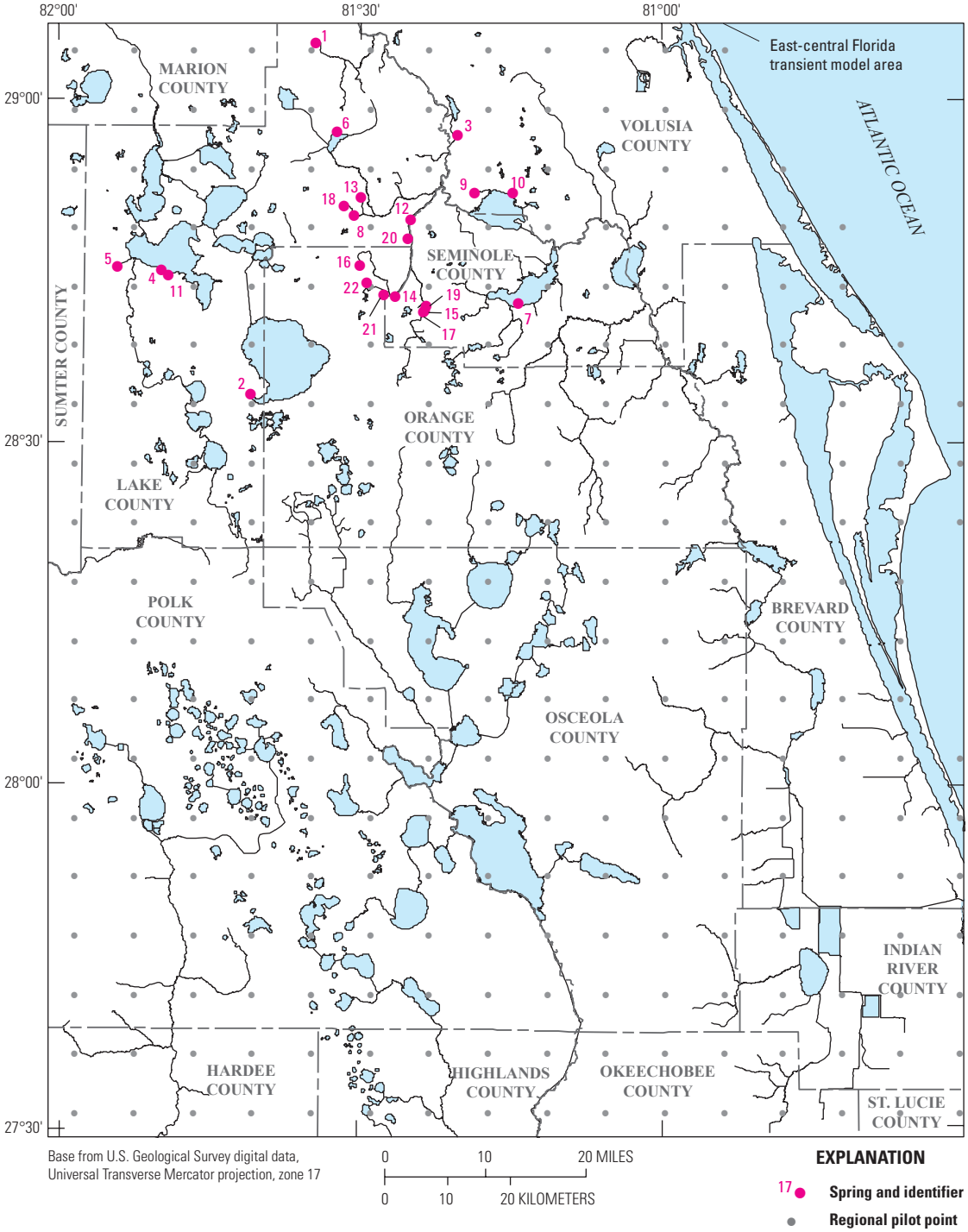

Figure 51. Locations of regional pilot points used for the Ocala permeable zone (OPZ, layer 3). The spring name corresponding to the identifier shown is given in table 2–1.

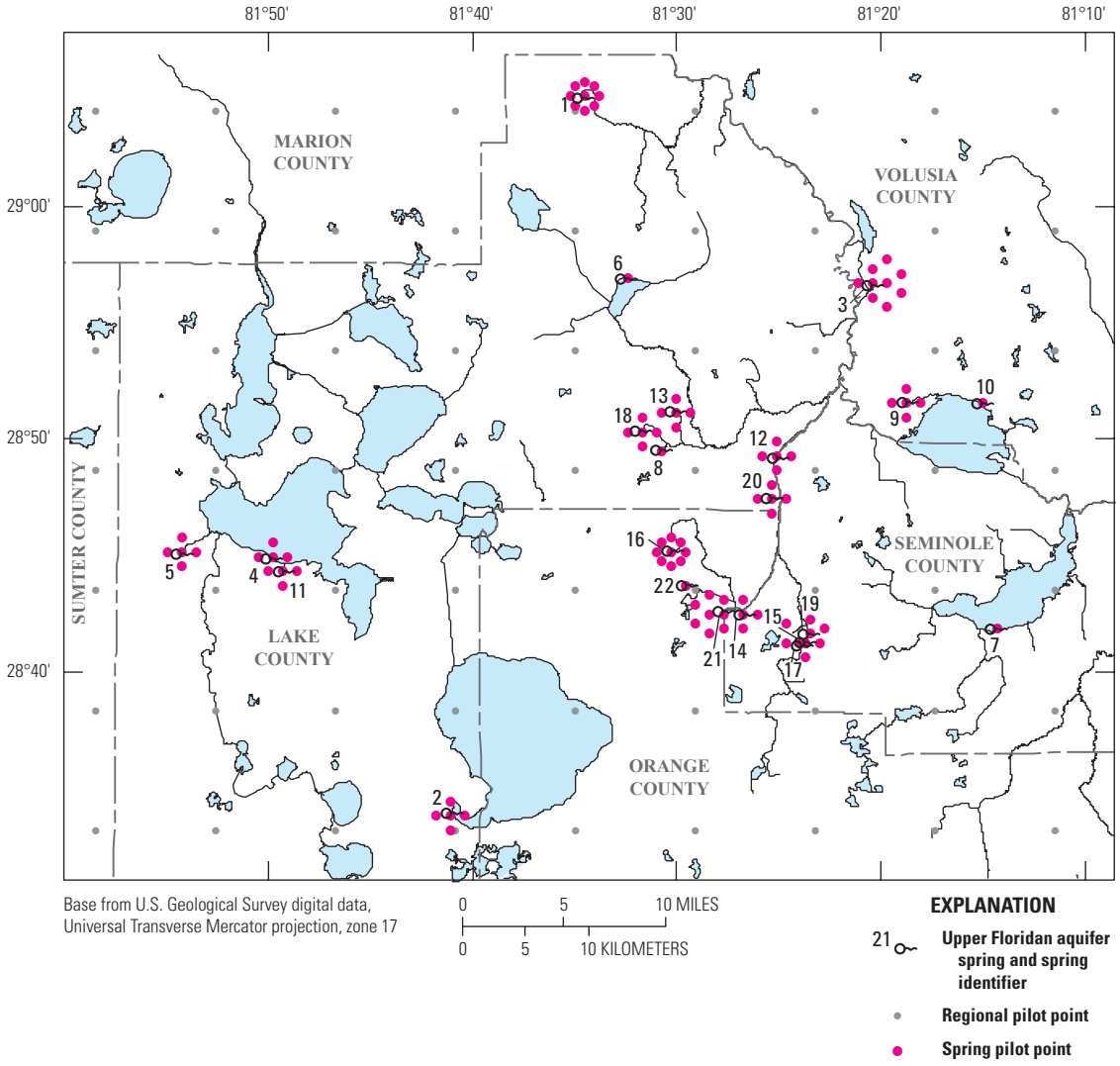

Figure 52. Locations of spring pilot points and regional pilot points in the northern section of the East-Central Florida Transient (ECFT) study area. The spring name corresponding to the identifier shown is given in table 2–1.

and 5, and Kv in corresponding layer 4. A set of 96 spring pilot points was applied to each of these 3 layers to represent the K multipliers, with the pilot-point configuration identical in each layer (fig. 52). Simple kriging, in which the mean of the interpolated values is specified *a priori*, and an exponential variogram (equation 5) are used for interpolation of the K multipliers. The mean K multiplier value is set to 1.0 and the multiplier variogram parameter a, denoted a_s, is set to 4,921 ft (1,500 meters), a deliberately small value, so that the effect of the estimated multiplier parameters does not extend far from the location of the springs.

The regional pilot points and the spring pilot points are used together to obtain the Kh of layer 3 according to the following instructions:

1. Using the Kh parameter values at the regional pilot points in layer 3 at the start of a PEST run or at the start of an optimization iteration of a PEST run, interpolate the regional Kh values over all model cells in layer 3 using the exponential variogram with range $3a_r$.

2. Using the K multiplier parameter values at the spring pilot points in layer 3 at the start of a PEST run or at the start of an optimization iteration of a PEST run, interpolate the spring K multiplier values over all model cells in layer 3 using the exponential variogram with range $3a_s$. Because the mean value of the multiplier is set to 0, the K multiplier will equal 0 at all cells that are further than $3a_s$ from any spring pilot point.

3. Multiply the regional Kh values for layer 3 by the *K* multiplier values for layer 3, on a cell-by-cell basis. This produces the Kh of layer 3.

The same procedure is used to estimate the Kh of layer 5. For layer 4, a uniform value of Kv applies at the regional scale, rather than spatially variable values (table 11). Thus, in step 3, this value of Kv is multiplied by the multiplier values at each cell of layer 4 to produce the Kv of layer 4.

These approaches to parameterizing the horizontal and vertical hydraulic conductivity values resulted in 1,696 defined parameters, including 1,288 defined Kh parameters (table 10) and 408 defined Kv parameters (table 11). Of these defined parameters, 1,178 were estimated, including 890 Kh parameters and 288 Kv parameters. The rationale for selecting the subset of parameters to be estimated is explained later in the discussion of sensitivities.

Representation of Specific Yield and Specific Storage

The specific yield Sy of layer 1 was parameterized in the same manner as Kh of layer 1, using zones corresponding to the physiographic regions shown in figure 2. This resulted in 21 S_y parameters (Sy_1, Sy_2, Sy_3, …, Sy_21). Because of the lack of data concerning the spatial variability of specific storage Ss within the other aquifers and confining units, this property was assumed to be uniform within each layer. One Ss parameter was defined for layer 2 (Ss_2) because of the greater clay content of the ICU compared to the deeper layers. A second Ss parameter (Ss_3-7) was defined to represent S_s in layers 3, 4, 5, 6, and 7, because of the similar carbonate lithology of the hydrogeologic units constituting the FAS.

Calibration

The model was calibrated by estimating values of hydraulic conductivity K, specific yield Sy, and specific storage Ss parameters to match observed groundwater heads and spring flows within specified targets. The vertical hydraulic conductivity of the streambed, leakance of the lakebeds, hydraulic conductivity of the top soil used for the GAI method, and the streambed slopes were updated after every calibration run. The computer execution time for a forward simulation of the 1995–2006 transient model varied from about 6 to 12 hours (depending on input values) using a state-of-the-art computer workstation. This execution time was prohibitively long for the 12-year model to be used as the basis for parameter estimation by inverse methods. With the software used in this study (presented later), the minimum simulation time for one parameter estimation iteration is equal to about four times the forward simulation time, even if an unlimited supply of computer processors are available. Commonly, at least seven iterations are needed, and thus for an 8-hour forward run time, the minimum parameter estimation run time is 224 hours, or about 9 days. For the ECFT model, calibration involved numerous parameter estimation runs, because model development and calibration proceeded concurrently. The 9-day run time would have substantially impeded progress on completing the model.

Based on the aforementioned concerns, model calibration was achieved by iteratively (1) estimating K parameters using inverse modeling with steady-state approximations of the model that represent average annual conditions in 1999 and 2003, then (2) estimating Sy and Ss using inverse modeling for the final 2 years (2005–2006) of the transient model, and finally (3) using model fit results of a forward simulation of the 12-year transient model to guide manual adjustments of the conceptual model and (or) boundary conditions. This iterative procedure repeats until parameter estimates are within reasonable ranges defined on the basis of independent information about the hydraulic and storage properties of the aquifers, boundary conditions do not violate known or estimated information about the flow system, and model fit targets are met for the simulation results of step 3.

The inverse modeling code PEST (Doherty, 2010a, b) is used in steps 1 and 2 of the model calibration approach to estimate ECFT model parameters. PEST uses a modified Gauss-Newton nonlinear regression method to estimate parameters that minimize a sum of squared weighted residuals objective function. For this study, the objective function, Φ, can be expressed as:

$$\Phi = \sum_{i=1}^{N_d}\left[\omega_i\left(y_i' - y_i\right)\right]^2 + \mu\sum_{k=1}^{N_{pr}}\left[\omega_k\left(P_k' - P_k\right)\right]^2 \qquad (6)$$

where

N_d is the number of observations,
y_i is a head or spring-flow observation,
y_i' is the simulated equivalent of that observation,
ω_i is the weight on y_i,
N_{pr} is the number of prior values,
P_k is the k^{th} prior information value,
P_k' is the simulated value of P_k,
ω_k is the weight on P_k, and
μ is the regularization weight factor.

The difference $y_i' - y_i$ is the observation residual, and $P_k' - P_k$ is the prior information residual. Conventionally, these residuals are usually defined as $y_i - y_i'$ and $P_k - P_k'$, but a different convention is used here so that a positive residual indicates simulated values are too high, and a negative residual indicates simulated values are too low.

In PEST, observation weights are defined as

$$\omega_i = 1/\sigma_i \qquad (7)$$

where σ_i is the standard deviation of the observation error.

Similarly, prior weights are defined as

$$\omega_k = 1/\sigma_k \quad (8)$$

where σ_k is the standard deviation of the error in the prior value. Observations, prior information, and weights for the ECFT model are discussed later. The value of μ is estimated by PEST if prior information is used as regularization, and equals 1.0 otherwise.

Regularization was used in calibrating the ECFT model and is a method of stabilizing the inverse problem when aquifer properties are represented in the model by a larger number of parameters than can be estimated with the available observations. Models in which a large number of parameters are used to represent the variability of an aquifer property are commonly called "highly parameterized". For such models, two potential issues are that (1) multiple combinations of such parameters can produce an equally good fit to the observations, and (2) the parameter estimation procedure might achieve a very close fit to the observation data at the expense of producing unrealistic variability in the distribution of a parameter field, for example, unrealistic hydraulic conductivity values. These issues also can arise when using small numbers of parameters in model calibration, but they tend to be exacerbated when using a highly parameterized approach. The first issue can be explored by evaluating parameter uncertainty, discussed later therein. To illustrate how PEST addresses the second issue, the objective function in equation 6, can be rewritten as:

$$\Phi = \Phi_m + \mu\Phi_r \quad (9)$$

where

$\Phi_m = \sum_{i=1}^{N_d}\left[\omega_i\left(y_i - y_i'\right)\right]^2$ is the measurement objective function and $\Phi_r = \sum_{k=1}^{N_{pr}}\left[\omega_k\left(P_k - P_k'\right)\right]^2$ is the regularization objective function. When regularization is used, PEST incorporates a user-defined variable denoting the "limiting measurement objective function" (PHIMLIM), into the algorithm for minimizing the total objective function Φ. PHIMLIM is the smallest allowable value of the measurement objective function and is used to prevent the regression from overfitting the observation data. To estimate parameters when regularization is used, PEST minimizes Φ of equation 9 while constraining Φ_m to be greater than or equal to PHIMLIM. As part of this process, PEST calculates the regularization weight factor μ (equations 6 and 9) and uses this variable to implement an appropriate degree of regularization strength.

If weights on the observations used in the measurement objective function reflect all sources of observation error as well as model error, then theoretically PHIMLIM equals the number of observations (Fienen and others, 2009). However, sources of error, particularly model error, can be difficult to quantify and observation weights consequently might not reflect all error components. This is the case for observation weights in the ECFT models; therefore, a trial and error procedure was used to determine an appropriate value of PHIMLIM, with the goal of selecting a value that produces an acceptable fit to the observation data and estimated parameter values that are within the reasonable ranges.

Observation Data

This section explains the determination of annual and monthly average spring flows, monthly average streamflows, and monthly average water levels from wells used as targets for calibration. Also discussed are the multiple linear regressions used to calculate annual water levels at wells used for the steady-state models. Several calibration criteria that were used to achieve calibration for the 12-year transient model are also presented.

Spring Flows

For each of the 22 springs, average annual flows used to calibrate the steady-state models were calculated from the average monthly spring-flow measurements. The limited availability of spring-flow measurements potentially increases the error associated with computing representative average annual spring-flow observations. The calibration of the 2005–2006 transient model used average monthly flows from July 2005 to December 2006 at the 22 springs; explanation for excluding the observed flows from January 2005 to June 2005 is given later in the section Water Levels at Wells. To assess the fit to spring flows in the 12-year transient model, average monthly flows from January 1995 through December 2006 were used. Examples of measured spring-flow hydrographs for selected springs and the locations of the selected springs are provided in the Model Fit section of this report and in appendix 2 (figs. 2–1 to 2–7). After calibration was completed using the GHB Package for the springs, the same spring conductance and spring-pool altitude data were used to generate the Drain Package for the 22 springs, obtaining the same results for the 12-year transient simulation as generated when simulating the springs with the GHB Package. The Drain Package is a practical feature to predict spring flow because if the simulated aquifer head drops below the pool altitude, then the discharge is set to zero, making this a head-dependent flow boundary condition and a non-linear function of simulated head. The GHB Package is an efficient boundary condition for model calibration of spring flow when using parameter estimation because the head-dependent flow is a linear function of the simulated aquifer head and the specified spring-pool altitude.

Weights on spring-flow measurements for both the steady-state and transient calibrations were calculated using equation 7, expressed as $\omega_i = 1/(cv_i \times y_i)$, where

Table 12. Coefficients of variation used to calculate weights on spring-flow measurements.

[Number of spring flow observations provided for the steady-state simulation years to provide changes in spring magnitude; ft^3/s, cubic foot per second]

Spring magnitude (ft^3/s)	Coefficient of variation (cv)	Number of 1999 springflow observations	Number of 2003 springflow observations
0 to 3	0.2	5	5
3 to 10	0.1	7	5
10 to 100	0.05	8	10
>100	0.02	2	2

$\sigma_i = (cv_i \times y_i)$ and cv_i is the discharge error coefficient of variation for spring-flow observation y_i. The values for cv_i varied by spring magnitude (table 12). The product $100 \times cv$ can be thought of as the percent error in observed discharge. The percent errors are somewhat smaller than the likely errors associated with field measurements of discharge, particularly for the larger magnitude flows, but were used because of the small number of spring-flow observations compared to the head observations, and the consequently smaller influence on the objective function. The spring-flow observations were matched poorly by the model when larger *cv* values were used. The total number of spring-flow observations used for each steady-state model was equal to the number of springs, which allowed all springs to be considered in the calibration (table 12).

Water-Surface Altitudes at Lakes and Streamflows

Monthly average water-surface altitudes calculated for gaged lakes (fig. 13) were used to calibrate the GAI parameters that determine the land-surface runoff to lakes and the lakebed leakance, which is defined as the hydraulic conductivity of the lakebed material divided by the thickness of the lakebed. The steps followed to achieve calibration of the water-surface altitudes at the lakes were to (1) adjust the extent of the drainage field of each lake, based on the DEM values, to estimate realistic surface runoff volumes to arrive at the lakes, (2) adjust the K value used in equation 3 for cells in the drainage field of each lake to achieve consistency between soil types and infiltration parameters, (3) calibrate the streambed slope at lake outlets (where it applies), and (4) increase or decrease lakebed leakance incrementally to systematically reduce the water-surface altitude residuals at the lakes while still simulating realistic leakage rates between the gaged lakes and the underlying ICU. Measured water-surface altitude hydrographs and the locations of these gaged lakes are shown in the Model Fit section of this report and in appendix 3 (figs. 3–1 to 3–19).

The lakebed leakances were calibrated iteratively between parameter estimation runs. After several runs of the steady-state models, it was clear that there was a limited range of values on lakebed leakances that were sensitive to water-surface altitudes at lakes. The range of calibrated lakebed leakances was, for all but two lakes, two orders of magnitude. The two lakes outside the 0.002 to 0.00002 d^{-1} lakebed leakance range were lake numbers 318 and 346 (fig. 13). Wolf Branch Creek (fig. 1) discharges to a sinkhole simulated as lake number 318 in Lake County (fig. 13). The calibrated lakebed leakance of lake number 318 was 0.1 d^{-1}, establishing a high hydraulic connection between the sinkhole and the aquifer. Lake number 346 in Polk County (fig. 13), which receives water for augmentation from a nearby well, had a calibrated lakebed leakance of 0.01 d^{-1}.

Monthly streamflow averages calculated for stream-gaging stations (fig. 12) were used to calibrate the GAI parameters that determine the land-surface runoff to streams and the vertical hydraulic conductivity of the streambed. Because tidal effects cannot be simulated with the SFR2 Package, flow residuals are expected to be larger for the stress periods where measured streamflows were negative. Examples of measured streamflow hydrographs and the locations of these stations are shown in the Model Fit section of this report and in appendix 4 (figs. 4–1 to 4–9).

The UZF1 Package distributes the generated land-surface runoff along the streams reaches composing a stream segment, with no time delay because of overland routing. This implies that the time delay associated with routing overland runoff is not simulated because runoff is instantaneously distributed along the corresponding stream reaches of the stream segment. Thus, for large basins, the simulated time of a peak streamflow may be offset from the measured hydrograph peak depending on when in the month the rainfall event occurred. The time difference between the simulated and measured stream hydrograph peaks should be smaller for small basins than for large basins.

Water Levels at Wells

Average annual or monthly water levels were used as observations during parameter estimation for calibrating the hydraulic conductivity distributions for the steady-state conditions of 1999 and 2003 and the storativity properties for the transient conditions of 2005 and 2006. Average monthly water levels for 1995–2006 were used to quantitatively assess the fit of the transient model over the 12-year simulation period.

The average annual heads used to calibrate the model for steady-state conditions were calculated from average monthly data. Sets of 442 and 505 wells, respectively, were used in the calibration of the 1999 and 2003 steady-state models. The number of wells differed because of (1) variations in the availability of head measurements and (2) drilling of new wells between 1999 and 2003 (figs. 53 to 55).

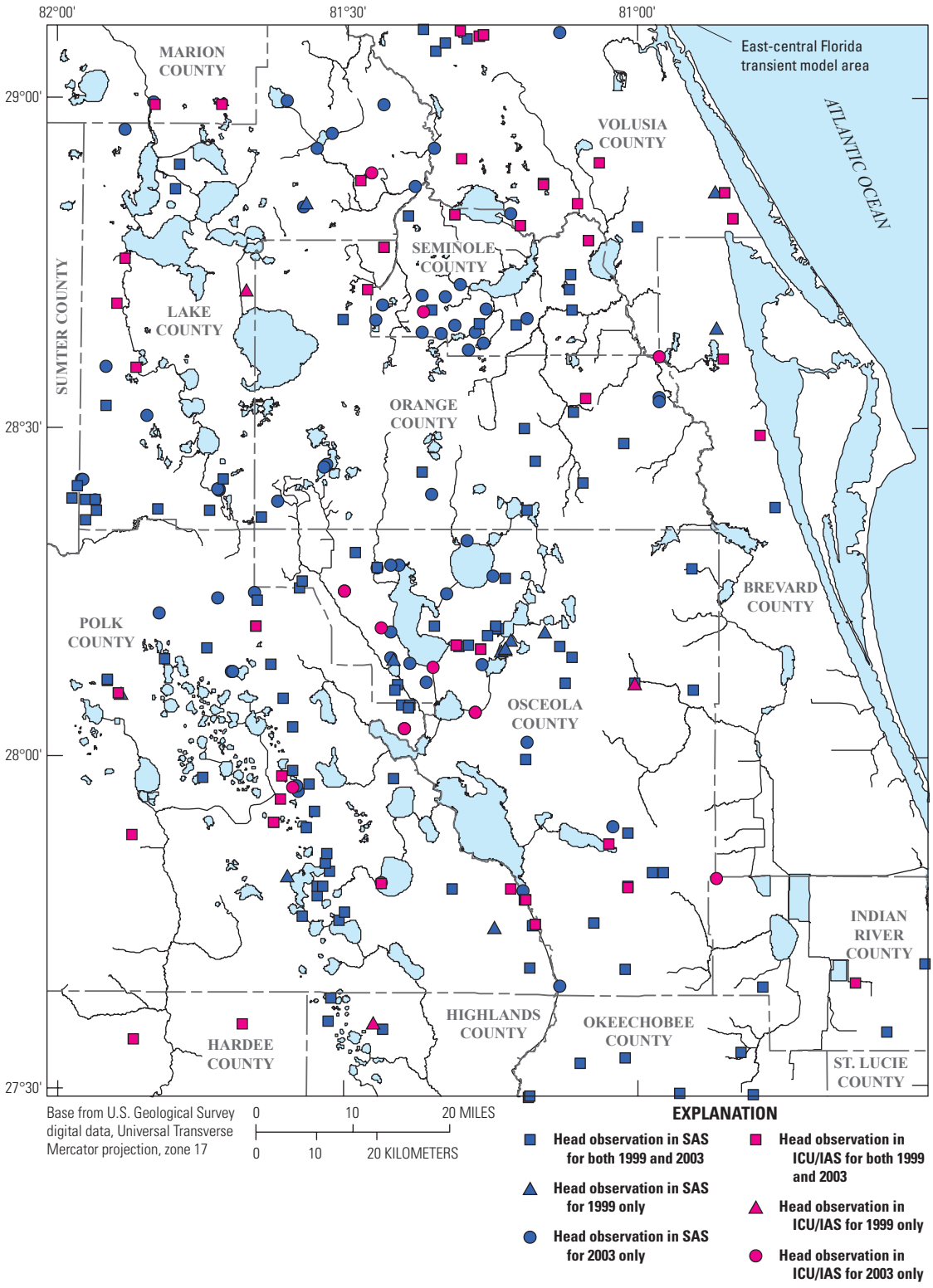

Figure 53. Locations of wells in the surficial aquifer system (SAS, layer 1) and intermediate confining unit/intermediate aquifer system (ICU/IAS, layer 2) for which average annual head observations in 1999 and 2003 were used to calibrate the steady-state models.

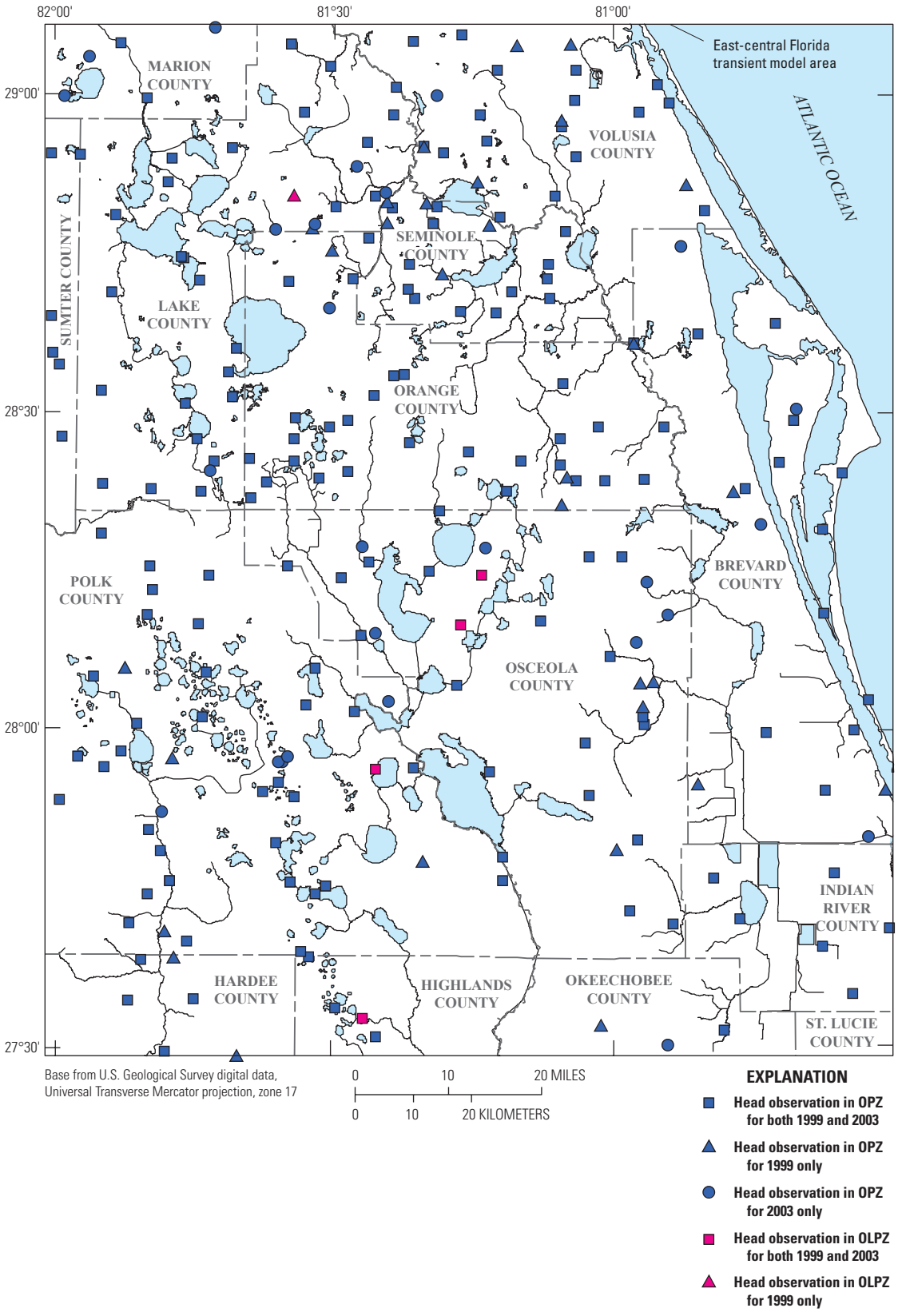

Figure 54. Locations of wells in the Ocala permeable zone (OPZ, layer 3) and Ocala low-permeable zone (OLPZ, layer 4) for which average annual head observations in 1999 and 2003 were used to calibrate the steady-state models.

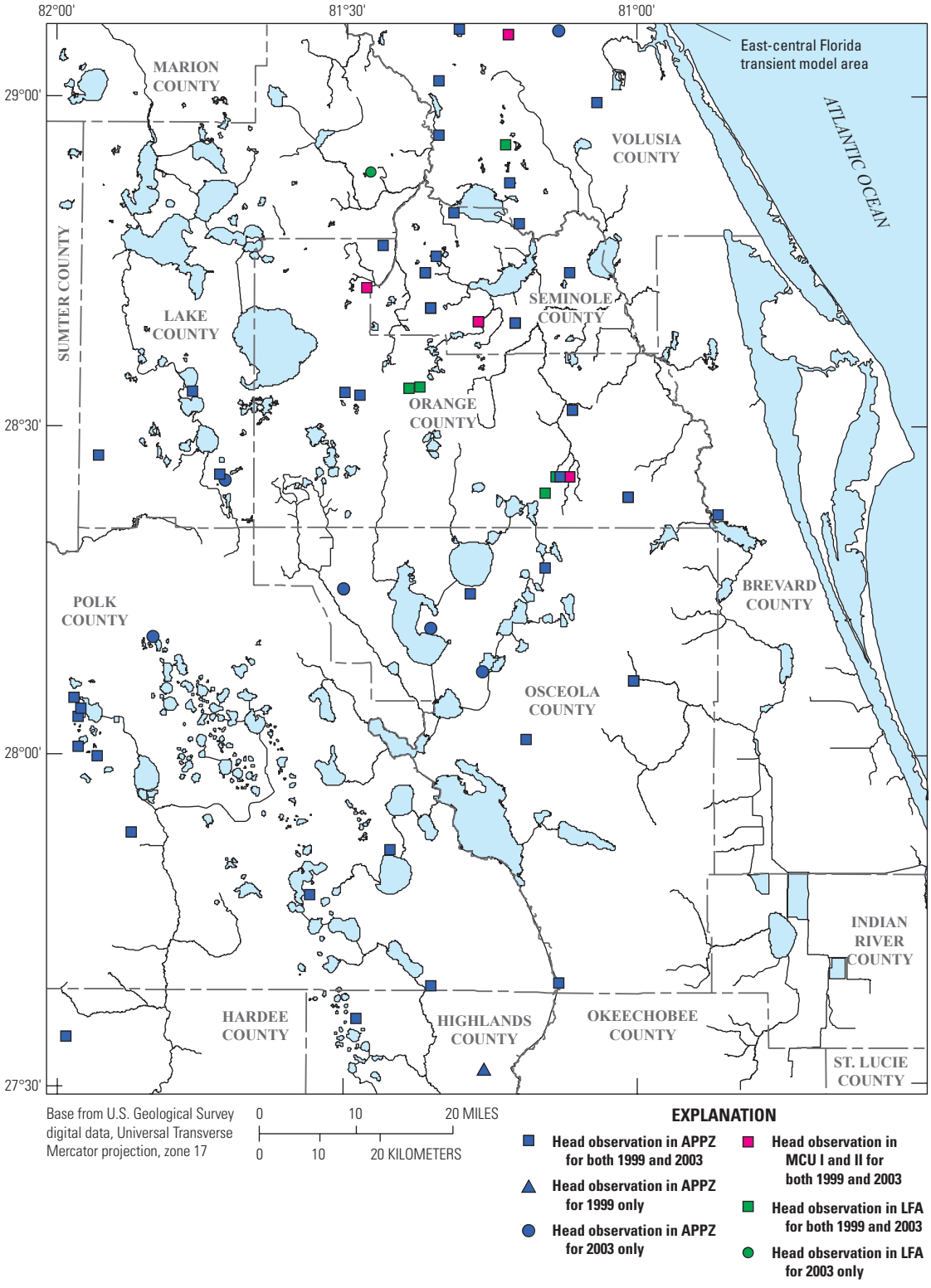

Figure 55. Locations of wells in the Avon Park permeable zone (APPZ, layer 5), middle confining unit I/II (MCU I/II, layer 6), and Lower Floridan aquifer (LFA, layer 7) for which average annual head observations in 1999 and 2003 were used to calibrate the steady-state models.

Head observations for the steady-state simulations were calculated at wells for which at least two average monthly heads were available in a given year. Average annual heads were first calculated at wells for which all 12 average monthly heads were available for the year. These average annual heads for a given model layer were then used to obtain dimensionless linear regression coefficients $\hat{\beta}_{M1}$ and $\hat{\beta}_{M2}$ for any two months, M1 and M2, using the multiple linear regression:

$$\overline{h_{year}} = \hat{\beta}_{M1}\overline{h_{M1}} + \hat{\beta}_{M2}\overline{h_{M2}} + \varepsilon \qquad (10)$$

where

$\overline{h}_{M1}$ and $\overline{h}_{M2}$ are the average monthly heads (in ft) at the well for months M1 and M2,

ε is the regression error, and

$\overline{h}_{year}$ is the annual average head at the well.

For wells with fewer than 12 but with at least two average monthly heads for a given year, average annual heads were then estimated using equation 10. The correlation coefficient of the multiple linear regressions was always at least 0.98, implying a strong correlation between the annual head averages and the average monthly head averages calculated for the wells. Monthly average heads for the full 12-year period of the transient simulation were used to calculate measures of model fit, which included root-mean-square and overall mean residuals.

Monthly average heads from July 2005 through December 2006 were used to calibrate the Sy and Ss for transient conditions during 2005 to 2006. Before starting a regression run using the 2005–2006 model, the 1995–2006 transient model was simulated with the starting Sy and Ss values used for the regression run. Simulated heads in the 1995–2006 model at the end of 2004 were then used as initial heads for the 2005–2006 model simulation. However, even though the initial heads for this estimation run were consistent with the starting Sy and Ss values for the run, they became inconsistent when these values changed during the parameter estimation procedure. Tests discussed previously (see Initial Conditions section) showed that transient forward model runs with different initial head distributions take about 6 months simulation time for simulated heads and flows to become consistent with the model parameters. Therefore, the first 6 months of observation data for the 2005-06 transient model were excluded from the model calibration.

Error-based weighting is a recommended procedure for defining weights on observations used in model calibration (Hill and Tiedeman, 2007, p. 291). By this method, the weight for the i^{th} observation is defined as in equation 7 when using PEST, where the total standard deviation of observation error, σ_i, is computed from all components of observation error. For the 1999 and 2003 average annual hydraulic head observations, these components include error related to: (1) temporal variability in the monthly values used to compute the annual average hydraulic head at a well, (2) the location of the well, (3) the well measuring-point altitude, and (4) the depth-to-water measurement. The four observation-error components listed were used to determine that σ_i for 1999 head observations ranged from 0.22 to 18.3 ft, with a median of 1.5 ft, and that for 2003, σ_i ranged from 0.20 to 12.4 ft, with a median of 0.96 ft. Error component 1, related to the temporal variability of monthly values used to calculate the annual average, dominates the total error in the head observations. Some types of model error can be included in the calculation of observation weights by equation 7 (Hill and Tiedeman, 2007, p. 300), but model error is difficult to quantify and was not included in the calculations.

Using uniform head weights produced a better fit to observations from the 12-year transient simulation than did using K values estimated using error-based weights. Using the error-based weights de-emphasized average annual head observations at wells with substantial temporal variability. However, in the transient simulation, all monthly head observations are implicitly considered to have equal weights, for purposes of calculating the measures of model fit used in this study. Therefore, the final weighting strategy for calibration of the steady-state model was to set all head standard deviations of error for the steady-state model calibration to 1 ft, with the corresponding weights equal to 1 ft^{-1}. This value was selected because 1 ft is (1) roughly equal to the median standard deviation computed from error components (1) to (4) above, and (2) conceptually is a reasonable error assumption for a flow system where the total range in observed heads is from about 0 to 130 ft. Weights for the monthly head observations from July 2005 to December 2006 were specified using the same approach, and also were set to 1.0 ft^{-1}.

Examples of hydrographs from wells open to hydrogeologic units corresponding to model layers 1 to 7 and the locations of these wells are shown in the Model Fit section of this report and in appendix 5 (figs. 5–1 to 5–73). The heads shown in these hydrographs for the 12-year transient model are the result of the calculation of monthly averages. The calculation of annual average heads from multiple linear regressions was used only to determine average annual heads for the steady-state calibrations.

Calibration Criteria

Data used to calibrate the model for steady-state conditions during 1993 and 2003 were the annual average measured heads at the wells, the annual average measured spring flows, the monthly average measured streamflows (used to calibrate annual average recharge rates to the SAS and riverbed vertical hydraulic conductivity), and the average monthly water-surface altitudes at lakes (used to calibrate annual average recharge rates to the SAS and lakebed vertical hydraulic conductivity). Data used to calibrate the model for transient conditions for the 12-year simulation period were the monthly average measured heads at the wells, the monthly average measured spring flows, the monthly average streamflows, and the monthly average water-surface altitudes at lakes.

For the 12-year transient model, calibration criteria were established on the basis of the residuals (defined after equation 6) and the root-mean-square residual (RMSR) for monthly average heads at wells, spring flows, water-surface altitudes at lakes, and streamflows. The RMSR for a set of residuals is defined as $RMSR = \left(\sum_{i=1}^{n} \left(y_i' - y_i \right)^2 / n \right)^{1/2}$, where y_i' and y_i are defined following equation 6, and n is the number of residuals used in the calculation.

The overall goal for heads at wells was to have a minimum of 50 percent of wells with a residual less than or equal to 2.5 ft in absolute value, a minimum of 80 percent of wells with a residual less than or equal to 5 ft in absolute value, an RMSR for all wells of less than 5 ft for each of the 12 simulated years, and a maximum overall mean residual (OMR), defined as $\mathrm{OMR} = \sum_{i=1}^{n} \left(y_i' - y_i \right) / n$, of less than 1 ft in absolute value for each of the 12 simulated years. These calibration criteria are based on the potential sources of error in the head observations, which are related to the (1) accuracy of the calculated average annual water levels for 1999 and 2003 used in the steady-state simulations, (2) accuracy of the measured water levels, and (3) model error in general. The combination of these factors was generalized into the calibration criteria listed above. An additional calibration criterion for head residuals was to achieve, as much as possible, a random spatial distribution of residuals.

The calibration criterion for spring flows, over the 12-year period of simulation, was to have an RMSR within 10 percent of the measured flows for spring flows larger than or equal to 10 ft^3/s, and within 20 percent for smaller springs. The calibration criterion for the water-surface altitudes at lakes was to have an annual RMSR, calculated over all lakes and for each of the 12 years of simulation, of less than 3 ft. The reason for the 3-ft maximum RMSR at lakes is because control structures near lake outlets are not simulated because these structures control the flow leaving the lake under otherwise natural conditions and such flow data were not available. Examples of these control structures are at stream segments 178 and 253 (fig. 11).

Stream control structures also limit the ability to simulate streamflows because flow downstream of a structure depends on the altitude of the structure. The presence of these control structures precluded establishing a calibration criterion for streamflow residuals. Therefore, the calibration criterion for streamflow was that the volumes under the hydrograph curves for the simulated and observed flows be as close as possible.

Calibration of K Parameters for Steady-State Conditions during 1993 and 2003

The model was used to represent annual stressed steady-state conditions during 1999 and 2003 for the purpose of estimating the distributions of hydraulic conductivity (K) values with PEST. Steady-state models were developed for 1993 and 2003 because the estimated absolute value of the storage term of the groundwater flow equation was smallest for these two years (table 4), thus reducing the model error associated with the approximation of steady-state conditions. Modifications of the model to represent steady-state conditions were made with the goal of keeping the representation of boundary conditions as close as practical to that of the transient model. Adjustments included replacing the SFR2, LAK7, and UZF1 Packages used for transient 1995–2006 conditions as follows: (1) using the River Package (Harbaugh, 2005) in place of the SFR2 Package; (2) using constant-head cells at the locations of lake cells in place of the LAK7 Package; and (3) using the Recharge and Evapotranspiration Packages (Harbaugh, 2005) in place of the UZF1 Package.

For the 1999 and 2003 steady-state simulations, annual average water-surface altitudes at rivers and lakes were calculated from monthly averages. Monthly average water-surface altitudes at rivers were calculated from stream-gage measurements or estimated from the DEM. Similarly, water-surface altitudes at the lakes were calculated from lake-gage measurements or estimated from the DEM. Annual average heads used as general-head boundaries along the lateral boundaries of the model for steady-state simulations are the same as those used to represent 1999 and 2003 conditions for the transient simulation. Annual average recharge rates to the SAS for 1999 and 2003 were calculated from the net effects of infiltration, unsaturated zone ET, and groundwater seepage (surface leakage), all of which are simulated by the UZF1 Package in the transient simulation. Surface leakage was simulated in the steady-state models by subtracting surface leakage from net recharge rates if these resulted in positive recharge rates. If these resulted in negative rates, recharge rates were set to zero and the negative rates were included in the Well Package. Annual average estimated ET rates for the 1999 and 2003 steady-state simulations were calculated from the groundwater ET simulated by the UZF1 Package in the transient simulation.

Hydraulic conductivities around and beneath the constant-head cells representing the lakes were adjusted so that leakance values calculated internally in the steady-state simulations equaled leakance values specified for the LAK7 Package in the transient simulation. The horizontal hydraulic conductivities of the active cells in the SAS along the perimeter of the constant-head cells were calculated by multiplying the lakebed leakance in the transient simulation by half the width of the cell (625 ft). Additionally, the vertical hydraulic conductivity of the active cells in layer 2 that underlie the constant-head cells was calculated by multiplying the lakebed leakance in the transient simulation by half the thickness of the constant-head cell.

PEST was used with the steady-state simulations for 1999 and 2003 to estimate the hydraulic conductivity parameters. Observations from multiple simulations can be used in a single PEST run to estimate parameters that are common to the simulations. Here, the representation of K in both of the

Table 13. Definition of sensitivity parameters.

[Kh, horizontal hydraulic conductivity; Kv, vertical hydraulic conductivity; ghb, general-head boundary]

Sensitivity parameter	Definition
Kh1_m	Factor that multiplies Kh of all cells in layer 1
Kv1_m	Factor that multiplies Kv of all cells in layer 1
Kh2_m	Factor that multiplies Kh of all cells in layer 2
Kv2_m	Factor that multiplies Kv of all cells in layer 2
Kh3_m	Factor that multiplies Kh of all cells in layer 3
Kv4_m	Factor that multiplies Kv of all cells in layer 4
Kh5_m	Factor that multiplies Kh of all cells in layer 5
Kv6_m	Factor that multiplies Kv of all cells in layer 6
Kh7_m	Factor that multiplies Kh of all cells in layer 7
Ghb1c_m	Factor that multiplies conductance of all ghb cells in layer 1
Ghb2c_m	Factor that multiplies conductance of all ghb cells in layer 2
Ghb3c_m	Factor that multiplies conductance of all ghb cells in layer 3
Ghb4c_m	Factor that multiplies conductance of all ghb cells in layer 4
Ghb5c_m	Factor that multiplies conductance of all ghb cells in layer 5
Ghb6c_m	Factor that multiplies conductance of all ghb cells in layer 6
Ghb7c_m	Factor that multiplies conductance of all ghb cells in layer 7
Riv_m	Factor that multiplies conductance of all river cells
Rch99_m	Factor that multiplies recharge rate in all cells of the 1999 steady-state model
Rch03_m	Factor that multiplies recharge rate in all cells of the 2003 steady-state model
Evtr99_m	Factor that multiplies evapotranspiration rate in all cells of the 1999 steady-state model
Evtr03_m	Factor that multiplies evapotranspiration rate in all cells of the 2003 steady-state model

steady-state simulations is identical to that of the 1995–2006 transient simulation, and the same parameters related to K are defined in each of the simulations. In essence, the separate MODFLOW-2005 simulations for 1999 and for 2003 together constitute a single simulation with respect to PEST.

Parameter Sensitivities

Composite scaled sensitivities (*css*) are used to guide selection of parameters to be estimated by PEST. The *css* for parameter b_j is calculated as follows (Hill and Tiedeman, 2007, p. 50, modified to use weight definition in PEST):

$$css_j = \left[\left(\sum_{i=1}^{N_d} \frac{\partial y_i'}{\partial b_j} \left| b_j \right| \omega_i \right) / N_d \right]^{1/2} \qquad (11)$$

where $\partial y_i' / \partial b_j$ is the sensitivity of the simulated equivalent of observation y_i' with respect to parameter b_j (hereafter denoted observation sensitivities), and ω_i is defined in equation 7. Each css_j is a measure of the information provided by all the observations about parameter b_j. Typically, only parameters with large *css* relative to other parameters can be estimated by the regression.

For the steady-state models, the large number of parameters related to K precludes evaluating the *css* for each parameter defined in tables 10 and 11. Instead, for purposes of calculating *css*, sets of these hydraulic conductivity parameters were lumped together using multiplier parameters, as defined in table 13. These multiplier parameters are denoted "sensitivity parameters" to distinguish them from the K multiplier parameters at the spring pilot points. There is one sensitivity parameter related to the Kh for each model layer in which this property is spatially variable, and one sensitivity parameter related to Kv for each model layer in which this property is spatially variable. For model layers where a uniform Kh parameter is defined (layers 4 and 6; table 10), the *css* is calculated for the Kh parameter. Similarly, for layers

in which a uniform value of α is used to define Kv (layers 3, 5, and 7; table 11), the *css* is calculated for α . Additional sensitivity parameters were defined that relate to recharge and ET rates and to the conductance specified for GHB and river cells (table 13).

The *css* calculated with all head and flow observations from both the 1999 and 2003 steady-state models are shown in figure 56*A*. These *css* are derived using the final parameter estimates. Among the sensitivity parameters of the hydraulic conductivity, the *css* values are largest for Kh1_m, Kv2_m, Kh3_m, Kh5_m, Kv6_m, and Kh7_m (fig. 56*A*). This set includes parameters related to the Kh of all aquifers and the Kv of most confining units. The *css* are very small for all sensitivity parameters related to the general head boundary and riverbed conductance. The *css* for the recharge and ET rate sensitivity parameters lie in the same range as the largest *css* values for the sensitivity parameters related to hydraulic conductivity.

The *css* were calculated for subsets of the head and spring-flow observations, including observations from both 1999 and 2003 (figs. 56*B–D*). For these *css* calculations, N_d in equation 11 is equal to the number of observations in the subset. The maximum *css* for any observation subset with respect to any general-head-boundary sensitivity parameter is about 0.8, and the maximum *css* for any subset with respect to the riverbed sensitivity parameter is about 0.2, so these parameters are excluded from the figures.

On the basis of the *css* magnitudes (fig. 56), all Kh parameters defined for layers 1, 3, 5, and 7 (table 10) and all Kv parameters defined for layers 2 and 6 (table 11) were selected for estimation by PEST. In PEST, such parameters are denoted "adjustable." The Kv of layer 4 also was adjustable, so that the vertical properties of all confining units were allowed to be estimated. With regularization included as discussed in the next section, the regression method can accommodate adjustable parameters with small sensitivities through the use of prior information. In addition, for layer 2, Kh parameters representing the IAS (fig. 21) were adjustable, whereas the Kh parameter representing the ICU was specified at 7 ft/d, which is within the same order of magnitude of the only aquifer test value in the ICU away from the IAS (table 10, fig. 21). Much smaller values than 7 ft/d for Kh in the ICU would lead to an unrealistically large drawdown near this aquifer test value (fig. 21). The general-head boundaries and riverbed conductances were specified because of the very small *css* for their respective sensitivity parameters. The hydraulic conductivity parameters for the remaining hydrogeologic units, for layers 2 to 7, were specified at reasonable values based on field knowledge (tables 10 and 11).

The recharge and ET rate sensitivity parameters have large *css*, indicating that the simulated values at the observation locations are moderately to highly sensitive to the rates. However, the rates were not included as adjustable parameters. As discussed previously, the approach to development and calibration of the 1995–2006 ECFT model involved calculating recharge and ET rates by using extensive physical and hydrologic data, and by considering the physical and hydrologic processes that affect the movement of water at land surface and within the unsaturated zone. This procedure resulted in spatially variable estimates of the rates that are likely more realistic than could be obtained by the regression method used for flow-model parameter estimation. Furthermore, estimating both recharge rate and hydraulic conductivity parameters in model calibration is often problematic because of parameter correlations and non-unique solutions; therefore, the independent recharge and ET rate estimates were specified, rather than estimated, in the regression.

Parameters related to the spring pilot points are not included in the *css* graphs because the sensitivity parameters defined for calculating the *css* (table 13) apply to distributions of Kh in layers 3 and 5 and Kv of layer 4 that already account for the effects of the K multipliers estimated at these pilot points. Initial regression runs explored observation sensitivities for the K multiplier parameters. These runs showed that the observations do not support estimation of spatial variability in the K multipliers within any layer, nor do they support estimation of different K multipliers in layers 3, 4, and 5. Therefore, a single K multiplier was adjustable for one of the pilot points associated with each spring, and the K multipliers at all other pilot points associated with that spring were "tied" to this estimate.

Preferred Value Regularization

Preferred value regularization was used for all adjustable parameters in the calibration of the steady-state simulations. By this method, the prior information that serves as regularization is of the form

$$\log_{10}\left(P_k'\right) = \log_{10}\left(P_k\right) \tag{12}$$

where $\log_{10}$ is the base-10 logarithm and P_k' and P_k are defined following equation 6. In equation 12, P_k' is a Kh, Kv, or K-multiplier parameter and P_k is the preferred value of this parameter, also referred to as its prior value. In equation 12, $\log_{10}$ is used because all parameters were log-transformed in the regression. Log-transforming prevents the parameters from becoming negative, is consistent with substantial evidence that the distribution of hydraulic conductivity in aquifers tends to be lognormal, and can make nonlinear regression for groundwater systems behave more linearly.

The preferred values represent information about the parameters from field data and expert knowledge. These values are based on aquifer-performance test data (figs. 18, 21, 24, 30, and 36), maps of the potentiometric surface that provide indirect evidence of low or high horizontal hydraulic conductivity (for example, fig. 25), and knowledge from USGS, SJRWMD, SFWMD, and SWFWMD personnel familiar with the hydrogeology of the flow system. In addition

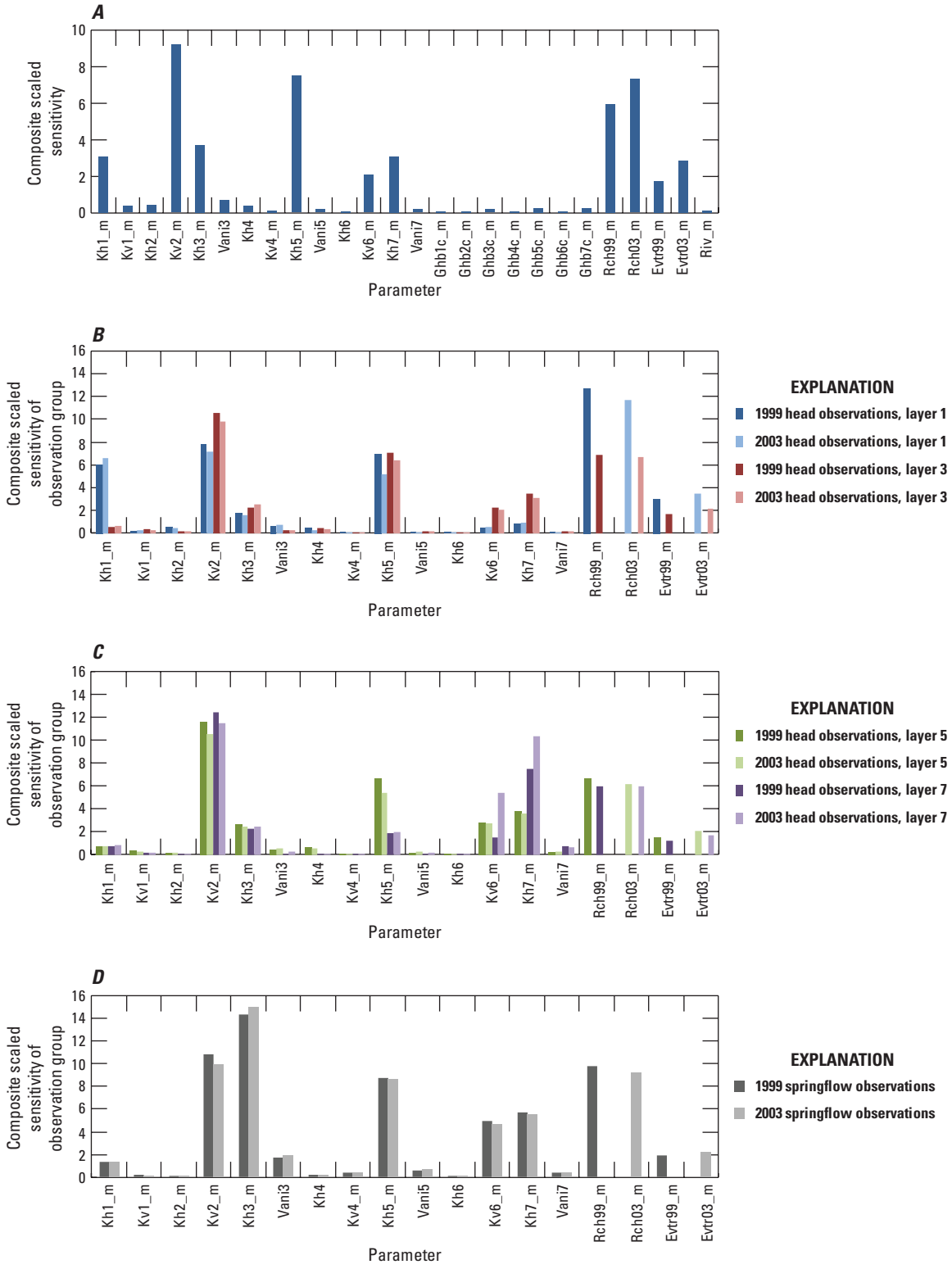

Figure 56. Composite scaled sensitivities for physical and sensitivity parameters of the steady-state models for *A*, all observations, *B*, head observations in layers 1 and 3, *C*, head observations in layers 5 and 7, and *D*, spring-flow observations. Parameters Vani3, Vani5, and Vani7 are the vertical anisotropy of layers 3, 5, and 7, respectively. Parameters Kh4 and Kh6 are the horizontal hydraulic conductivity of layers 4 and 6, respectively. Sensitivity parameters ending in "_m" are defined in table 13.

to being used as regularization, the preferred values are used as the initial values in parameter estimation runs.

Preferred value regularization adds a penalty to the objective function when an estimated parameter value deviates from its preferred value (equations 6 and 9). A parameter will deviate if doing so improves the total objective function Φ, subject to the constraint that Φ_m remains equal to or larger than PHIMLIM (discussed following equation 9). An improvement in Φ occurs when the decrease in Φ_m, representing the fit to observations, is greater than the increase in $\mu\Phi_r$, the penalty term. For parameters to which the simulated values at observations are not very sensitive, the preferred value regularization ensures that the estimates will remain near values that are based on field data and expert knowledge. When using preferred value regularization (and an appropriate PHIMLIM) for a set of spatially distributed pilot point parameters representing an aquifer property, the estimated values of the property will change in locations where doing so improves Φ, and will remain near the preferred values in other areas. Therefore, despite the large number of parameters defining the spatial distribution, the procedure allows deviations from the preferred values only when such changes are supported by the observation data.

Preferred values of Kh in layer 1 range from 8 to 60 ft/d (fig. 57). The lowest value corresponds to Green Swamp (fig. 2) where fine-grained sediments are abundant (Grubb and Rutledge, 1979). The highest values are associated with Polk Upland, Lake Wales Ridge, Winter Haven Ridge, Lakeland Ridge, and Lake Henry Ridge (fig. 2). In these areas, coarse sediments generally cause the water table to be relatively flat and deep beneath hills and upland areas (Sumner and Bradner, 1996; O'Reilly, 1998).

Preferred values for Kh of layers 2, 3, 5, and 7 and for Kv of layer 2 are assigned at the pilot point locations. These values are then interpolated using the kriging procedure described previously. Preferred values of Kh in layer 2 are largely guided by aquifer test data (fig. 58). Away from areas with aquifer test data, the preferred Kh value in the IAS and the specified Kh value in the ICU are 7 ft/d. Preferred values of Kv in layer 2 are largest along Lake Wales Ridge, where the prevalence of sinkholes and the observation of similar water-level fluctuations in SAS and UFA wells suggest that the ICU is highly leaky in this area (fig. 59; Tihansky and others, 1996; Yobbi, 1996; O'Reilly, 1998). Data for the Kv of the ICU are limited, and the data available are highly variable; however, lithologic information indicates a greater prevalence of clayey, fine-grained, or otherwise lower permeability sediments composing the ICU throughout the Osceola and Wekiva Plains and Eastern Valley (fig. 2) where preferred values were less than 0.005 ft/d (fig. 59).

In layer 3, preferred values of Kh are low in Polk and southern Lake Counties, where a high in the potentiometric surface of the OPZ (fig. 25) is thought to be related to the presence of low Kh values (fig. 60). An area of low Kh also is present in the northeastern part of layer 3, because of another high in the potentiometric surface of the OPZ (fig. 25). This area in Volusia County generally coincides with an area of karst topography (Wyrick, 1960) where sinkhole collapses possibly have caused reduced permeability by the filling of cavities with a mixture of overlying sand and clay, which is consistent with aquifer test results indicating lower Kh of the OPZ (fig. 24). The largest preferred values of Kh in layer 3 are near springs because of the effect of the K multipliers, which have preferred values ranging from 2 to 20, as discussed subsequently. For the regional Kv of layer 4, the preferred value is 5 ft/d, because the OLPZ is a semiconfining unit and allows fairly good vertical hydraulic connection with the APPZ.

Preferred values of Kh in layer 5 (fig. 61) generally are larger than those in layer 3 (fig. 60). A regionally extensive zone of fracture- or dissolution-enhanced permeability in the APPZ contributes to these high Kh values. The preferred values for Kv of the MCU I and MCU II in layer 6 are, respectively, 0.05 and 1×10^{-4} ft/d, because of the prevalence of gypsum mineralization in the MCU II.

In layer 7, preferred values of Kh are small in the region underlying the MCU II and thought to be attributable to less developed secondary porosity caused by relatively limited groundwater leakage through the low permeability MCU II (fig. 62). The areas with the largest preferred values of Kh in layer 7 are those in which several aquifer tests yielded a Kh value of more than 1,000 ft/d.

Preferred values of the K multipliers at the springs vary according to the magnitude of spring flow. There are few aquifer test data in the vicinity of most springs (fig. 60); however, K is likely to be larger near the springs with large discharge rates, because of the greater state of dissolution of the carbonate rock, than near springs with smaller discharge. Accordingly, the preferred value of the K multiplier for spring number 3 is 20 (Blue Spring in Volusia County, figs. 1, 51); this spring has the largest discharge among all springs in the ECFT model area. The preferred value of the K multipliers for springs with measured discharge between 30 and 100 ft^3/s is 10 (spring numbers 1, 16, 18, and 21, fig. 51), and that for springs with discharge between 9 and 29 ft^3/s (spring numbers 2, 5, 13, 17, 19, and 20, fig. 51) is 5. For the remainder of the springs, the preferred value of the K multiplier is 2.

Weights for the prior information were calculated by using an error-based approach. A reasonable range of values for each parameter was constructed using the same types of information that guided determination of the preferred values. This range was assumed to be a 95-percent confidence interval on the prior value. Using log transformation and assuming a normal distribution, the confidence interval was used to derive a standard deviation on each of the prior values. The weight for a prior information value was then calculated using equation 8.

The lower and upper limits of the reasonable parameter ranges also were used as bounds on the parameter values. PEST does not allow estimated parameter values to lie outside the range formed by the user-specified upper and lower bounds.

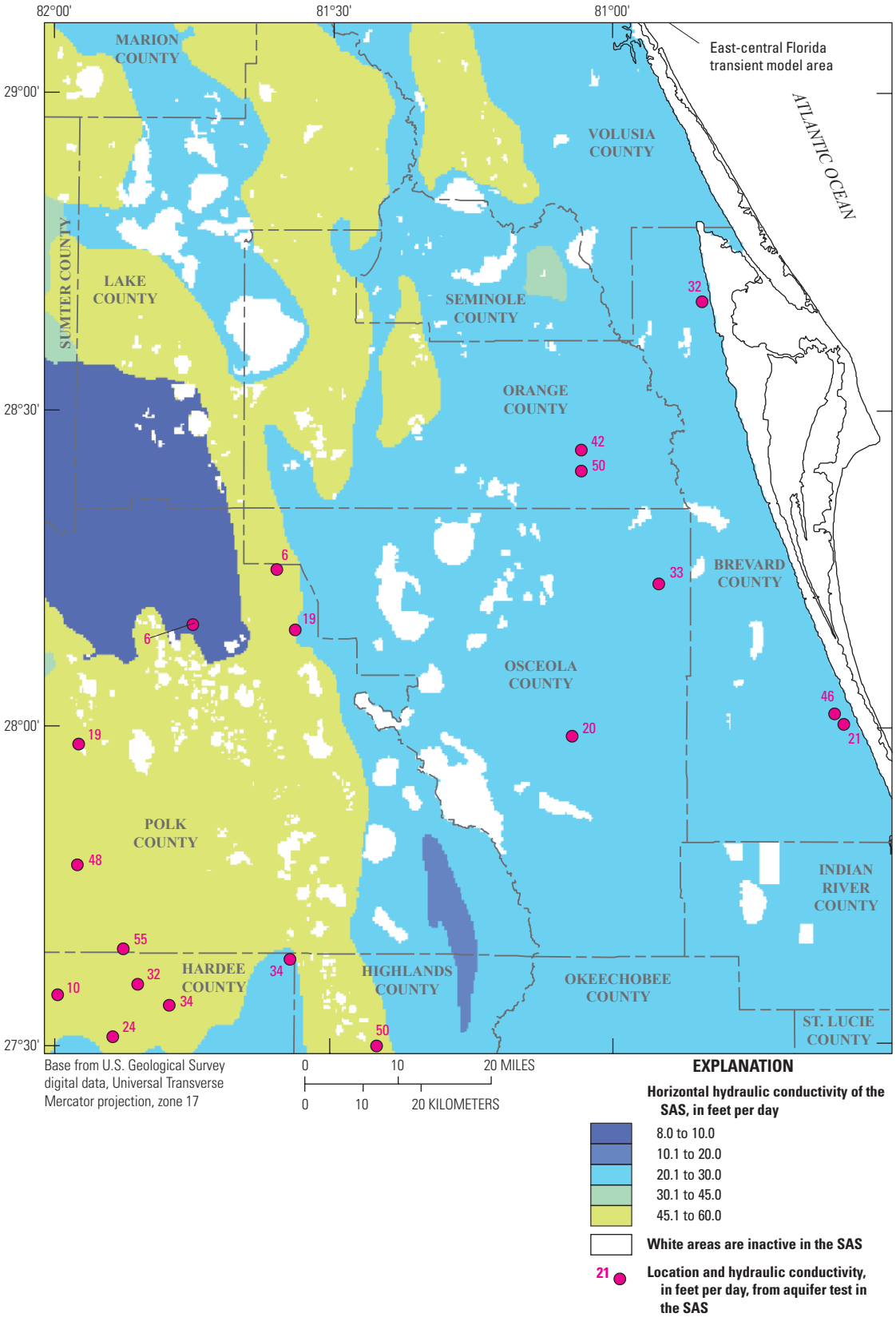

Figure 57. Preferred values of horizontal hydraulic conductivity (Kh) in the physiographic regions used to represent Kh in the surficial aquifer system (SAS, layer 1) and selected aquifer test values.

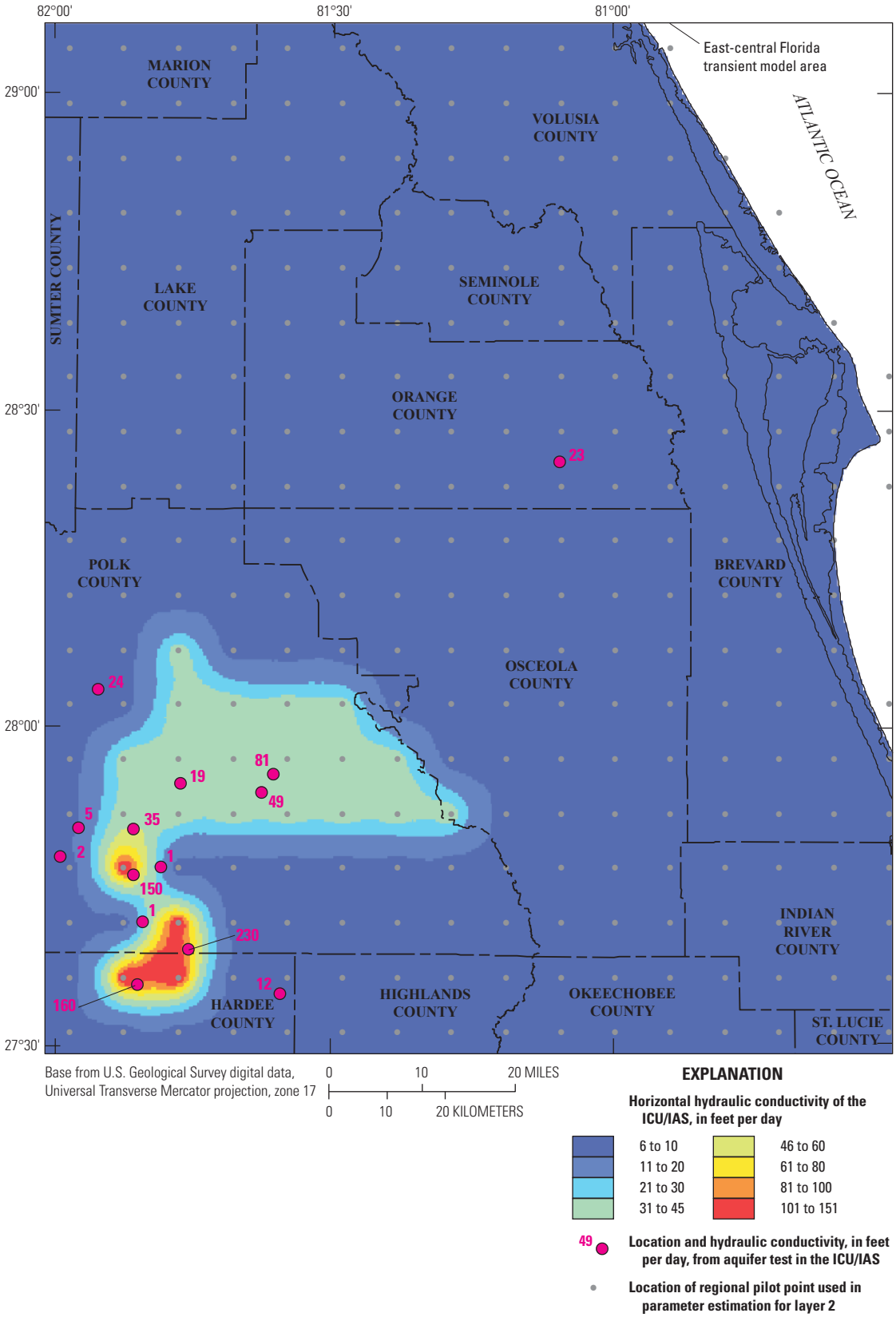

Figure 58. Interpolation of horizontal hydraulic conductivity from preferred values at pilot points in the intermediate confining unit/intermediate aquifer system (ICU/IAS, layer 2) and selected aquifer test values.

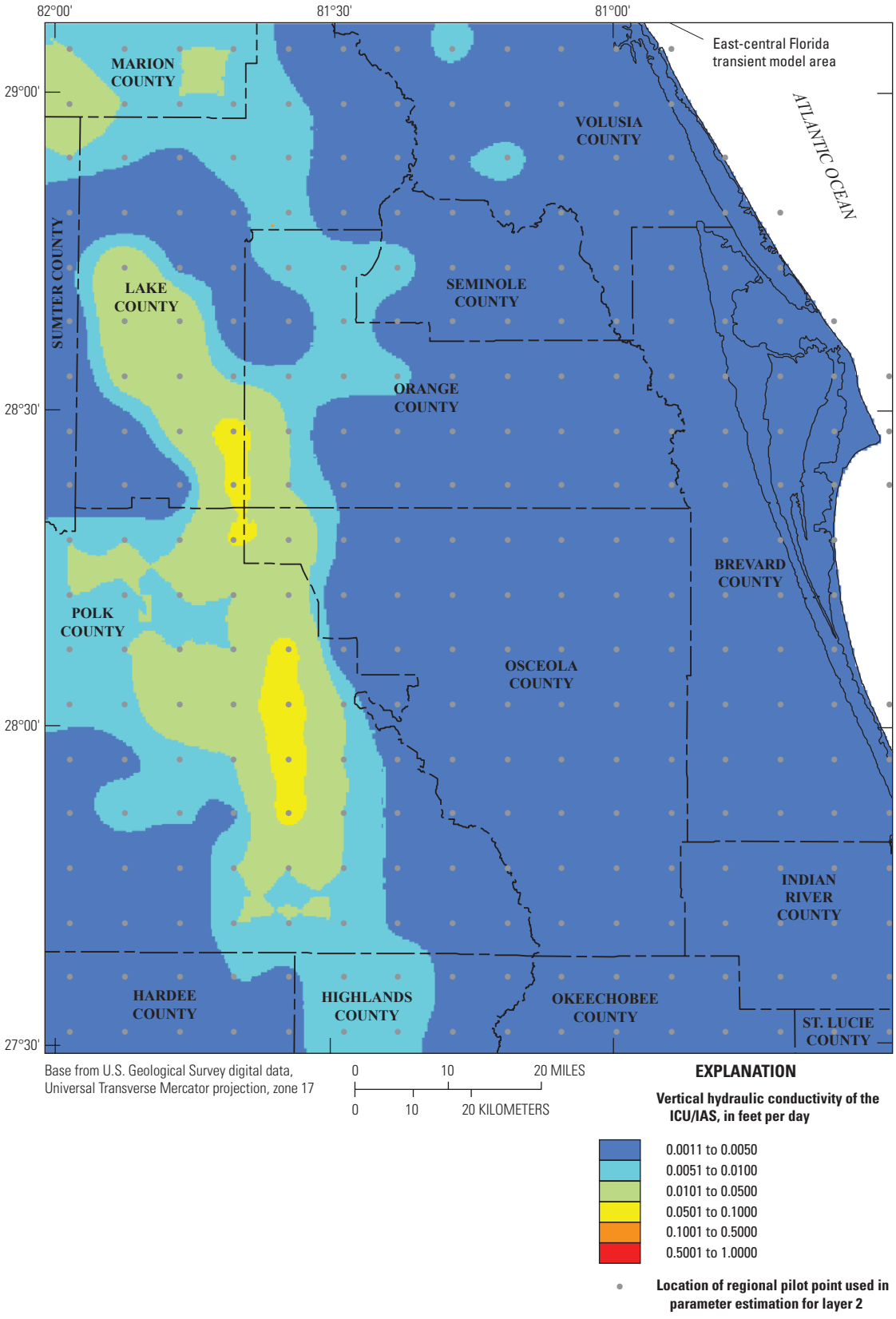

Figure 59. Interpolation of vertical hydraulic conductivity from preferred values at pilot points in the intermediate confining unit/intermediate aquifer system (ICU/IAS, layer 2) and selected aquifer test values.

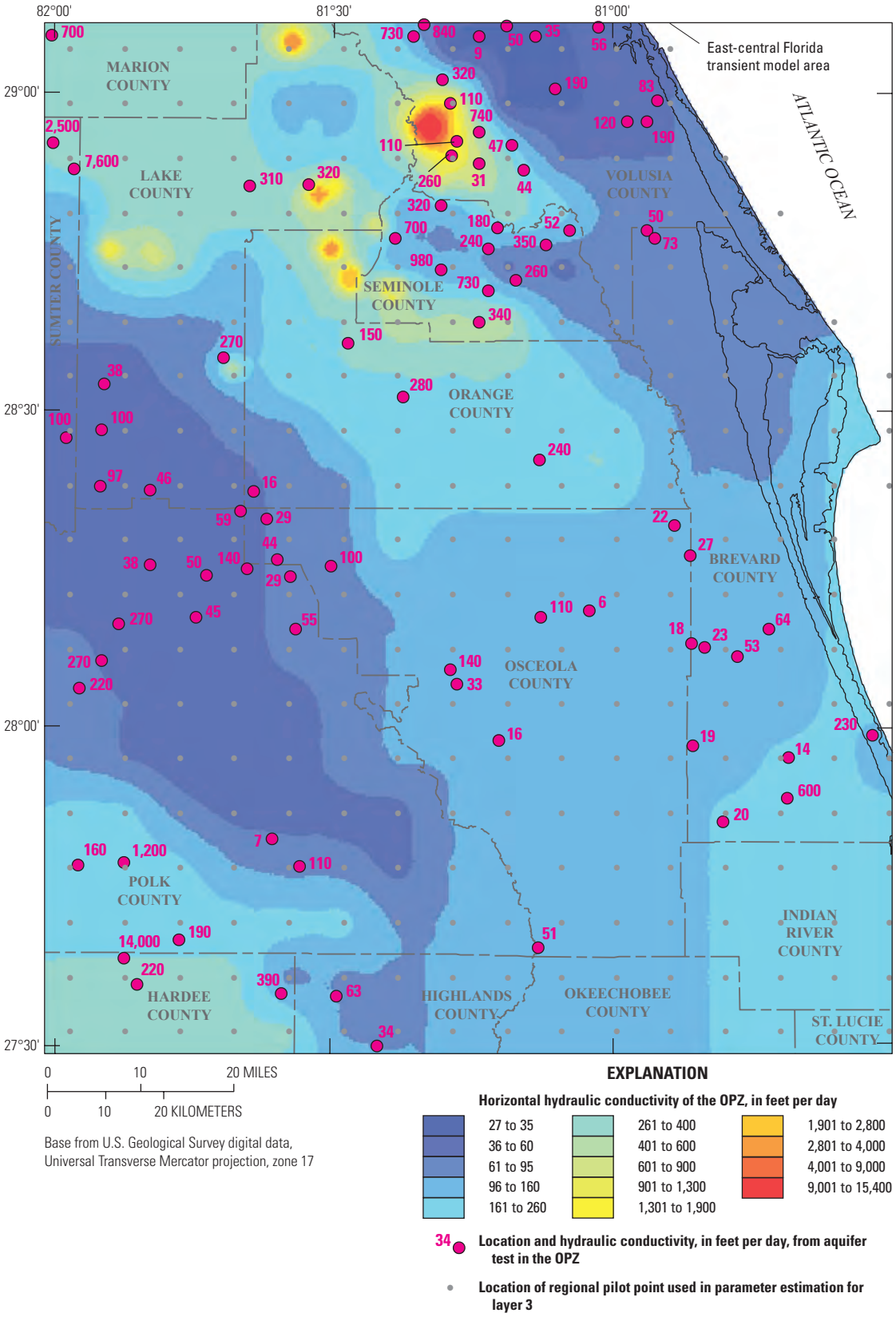

Figure 60. Interpolation of horizontal hydraulic conductivity from preferred values at pilot points in the Ocala permeable zone (OPZ, layer 3) and selected aquifer test values.

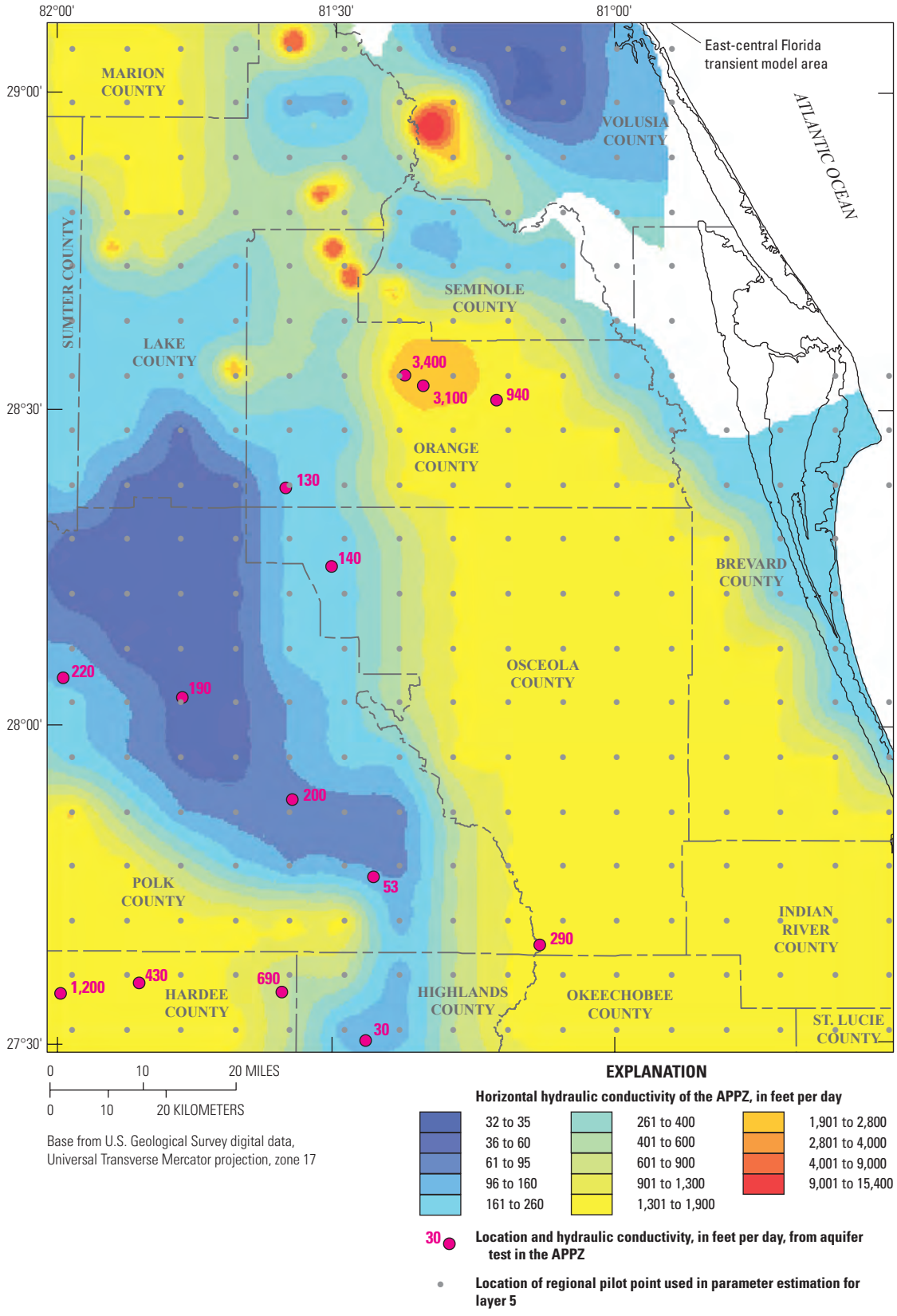

Figure 61. Interpolation of horizontal hydraulic conductivity from preferred values at pilot points in the Avon Park permeable zone (APPZ, layer 5) and selected aquifer test values.

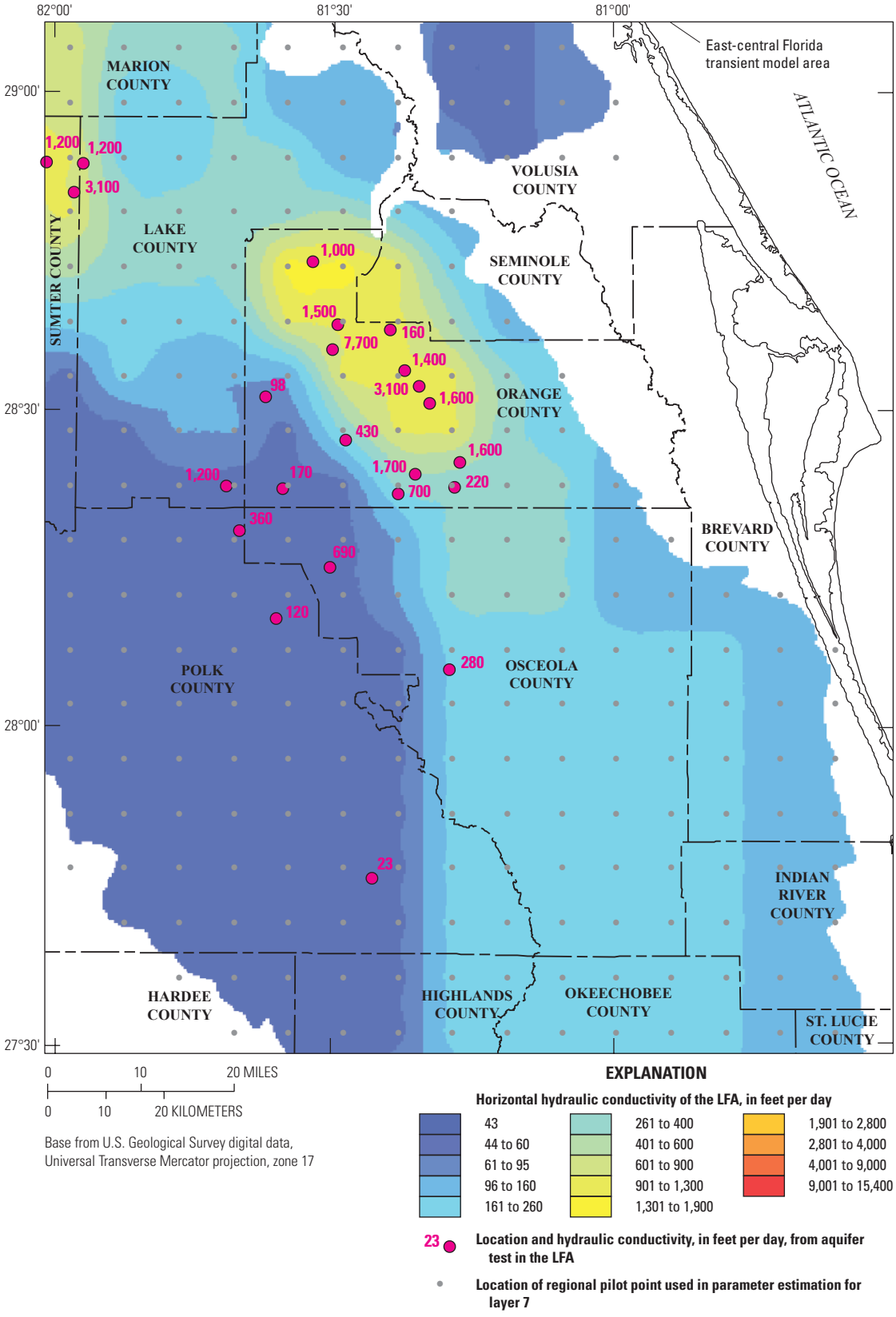

Figure 62. Interpolation of horizontal hydraulic conductivity from preferred values at pilot points in the Lower Floridan aquifer (LFA, layer 7) and selected aquifer test values.

The value of PHIMLIM for the regularized parameter estimation was set equal to 10,000. The starting objective function value for the steady-state model calibration, with the parameter values equal to the preferred values, was 45,400. Trial-and-error exploration of different PHIMLIM values showed that a measurement objective function value of 10,000 produced a realistic distribution of spatial variability in the Kh and Kv distributions governed by the pilot points approach and also yielded an acceptable model fit.

Calibrated Hydraulic Conductivities

PEST was used to estimate the 1,178 adjustable parameters, including Kh parameters for layers 1, 3, 5, 7, and part of layer 2; Kv parameters for layers 2, 4, and 6; and K multiplier parameters near springs (tables 9 and 10). The preferred value regularization and the variable PHIMLIM are important for keeping parameter estimates reasonable and preventing an unrealistically close fit to the observed values. Most Kh and Kv parameters do not differ significantly from the preferred values. For example, the estimates for only 82 of the 1,178 adjustable parameters differ from their respective preferred values by more than a factor of 2, which is a relatively small difference for a hydraulic conductivity value observed to vary by orders of magnitude. Only 14 estimates, mostly for Kv in layer 2, differ from the preferred values by more than an order of magnitude. Overall, compared to the preferred parameter values, the estimation procedure moderately adjusted the parameter values in areas where there are Kh and Kv parameters to which the calibration observations are sensitive, and only slightly or negligibly adjusted the parameter values elsewhere. The estimated Kh and Kv parameters from PEST are referred to next as calibrated parameters.

Most calibrated values of Kh in layer 1 are not significantly different than the interpolated preferred values (figs. 57 and 63). The largest differences are for zones corresponding to Mount Dora Ridge, Deland Ridge, and the southern part of Lake Wales Ridge, where the estimated values of Kh are smaller than the preferred values. The resulting Kh value for Mount Dora Ridge is equal to the lower bound for this parameter of 10 ft/d, indicating that lowering the value further would likely improve the measurement objective function. However, 10 ft/d is considered the lowest reasonable value for the SAS sediments in this area. The vertical hydraulic conductivity of layer 1 had almost negligible *css*, which supported assigning the Kv values chosen. The Kv values were assigned to be proportional to the preferred values of Kh for layer 1 (fig. 64).

The calibrated values of Kh in layer 2 are essentially equal to the interpolated preferred values (figs. 58 and 65). This is expected given the small *css* for sensitivity parameter Kh2_m (fig. 56). For Kv of layer 2, calibrated values in the western part of the model area are substantially different than preferred values (figs. 59 and 66). The calibrated Kv along Lake Wales Ridge is as large as 1 ft/d, and is greater than 0.1 ft/d over parts of the ridge. The calibrated Kv also is larger in the northern part of the ECFT area than the interpolated values. These areas of greater Kv generally coincide with more karstic terrain where sinkhole activity may have resulted in breaches of the ICU. Nine out of the 285 estimated layer 2 Kv parameters are equal to the value of a parameter bound. Five of these parameters are located along the Lake Wales Ridge, and their calibrated values equal an upper bound of 0.5 or 1.0 ft/d. Four of the parameters are equal to a lower bound of 0.004, 0.005, or 0.01 ft/d.

The calibrated values of Kh in layer 3 are not substantially different than the interpolated preferred values (figs. 60 and 67). For areas away from the springs, the primary difference is in the shape of the low-K region in the west-central part of the domain. This is consistent with the relatively small *css* for the head observations with respect to Kh3_m, compared to the *css* for the head observations with respect to Kv2_m and Kh5_m (figs. 56*B*–*C*). Kh values in layer 3 differ relative to the interpolated preferred values to a greater degree near the springs, which is consistent with the large value of *css* for the spring-flow observations with respect to Kh3_m (fig. 56*D*). Of the 11 small springs with a preferred value of 2 for the K multiplier, the calibrated value of this parameter is smaller at 10 springs, and for 4 of these, the calibrated value is the lower bound of 1; this lower bound is considered reasonable because it is unlikely that Kh is smaller at the few cells surrounding a spring, compared to its value further away.

The calibrated regional Kv of layer 4 is 6.5 ft/d, a slight difference compared to the uniform preferred value of 5 ft/d. Spatial variability in this layer occurs only where the K multipliers at the springs apply (fig. 68), allowing enhanced vertical hydraulic connection between the OPZ and APPZ. Because the regional Kv of layer 4 is uniform, the location and effects of the calibrated values of these K multipliers can be easily identified visually (fig. 68). For example, the calibrated K multiplier is 1.0 at all spring locations where Kv is 6.5 ft/d on this figure. The largest calibrated K multiplier is 19.5 for spring number 1 (fig. 51), the northernmost spring in the model area.

The calibrated values of Kh in layer 5 differ from their interpolated preferred values (figs. 61 and 69), consistent with the magnitude of the *css* values (fig. 56). There is a difference in the shape of the large high-K region in the east, and calibrated Kh values are greater within this region than the interpolated preferred values. The maximum calibrated Kh at the northern end of this region is 3,800 ft/d, and the maximum in the central part is about 2,800 ft/d. Similarly, Kh values are higher in the southwest high K region, to a maximum of about 3,800 ft/d. Minimum Kh values equal about 30 ft/d in the northeastern and the west-central parts of the model area. Two estimates of Kh at pilot points are equal to their bounds. The southernmost pilot point near the boundary between Hardee and Highlands Counties is equal to its lower bound of 500 ft/d. The pilot point in east-central Polk County is equal to its upper bound of 2,000 ft/d.

In layer 6, the calibrated value of Kv for the MCU I is about 0.12 ft/d, greater than its preferred value of 0.05 ft/d (fig. 70). The calibrated value of Kv for the MCU II is equal to its preferred value of 10^{-4} ft/d, indicating that the observations are insensitive to this parameter as long as it is sufficiently small.

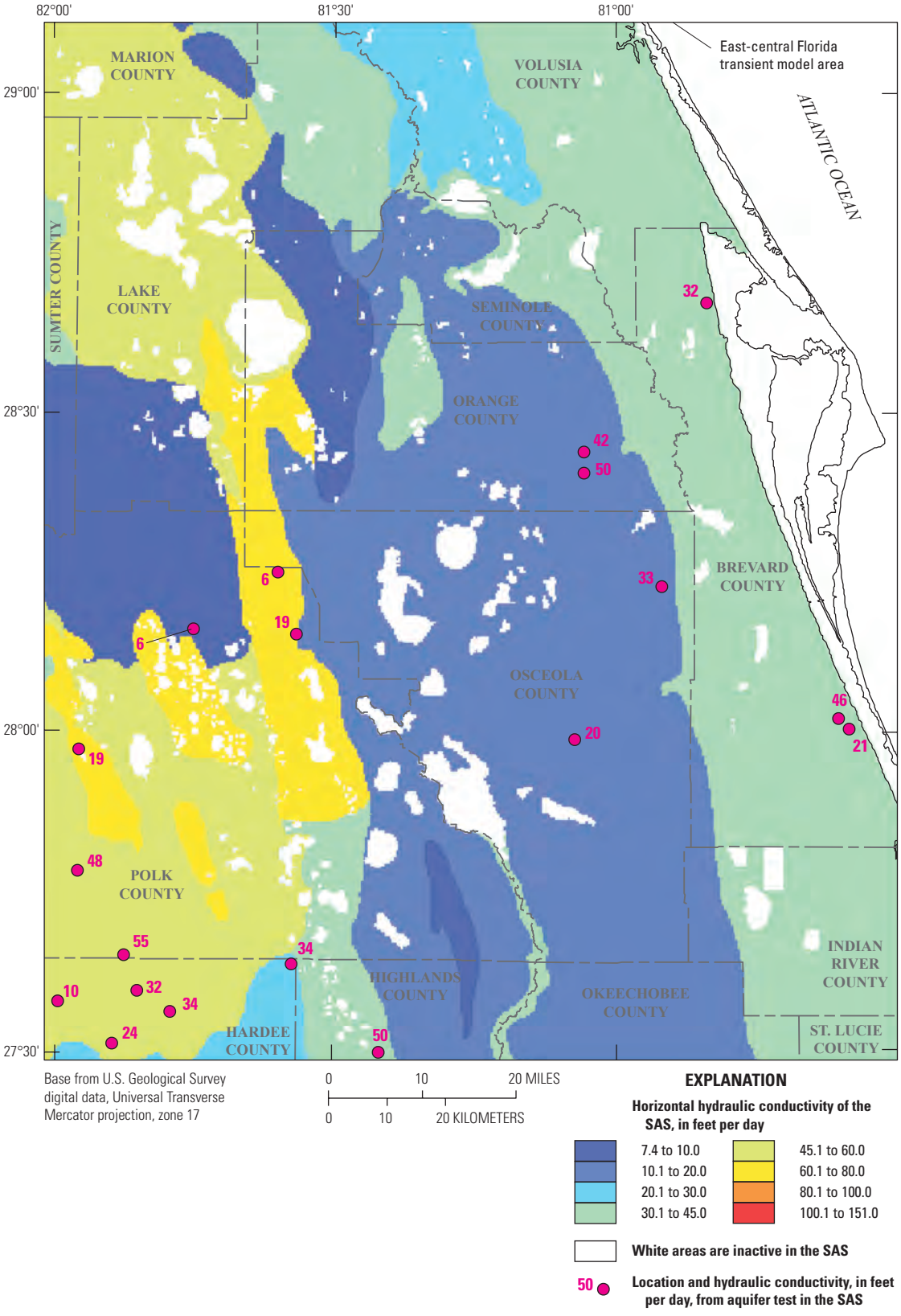

Figure 63. Calibrated horizontal hydraulic conductivity of the surficial aquifer system (SAS, layer 1) and selected aquifer test values.

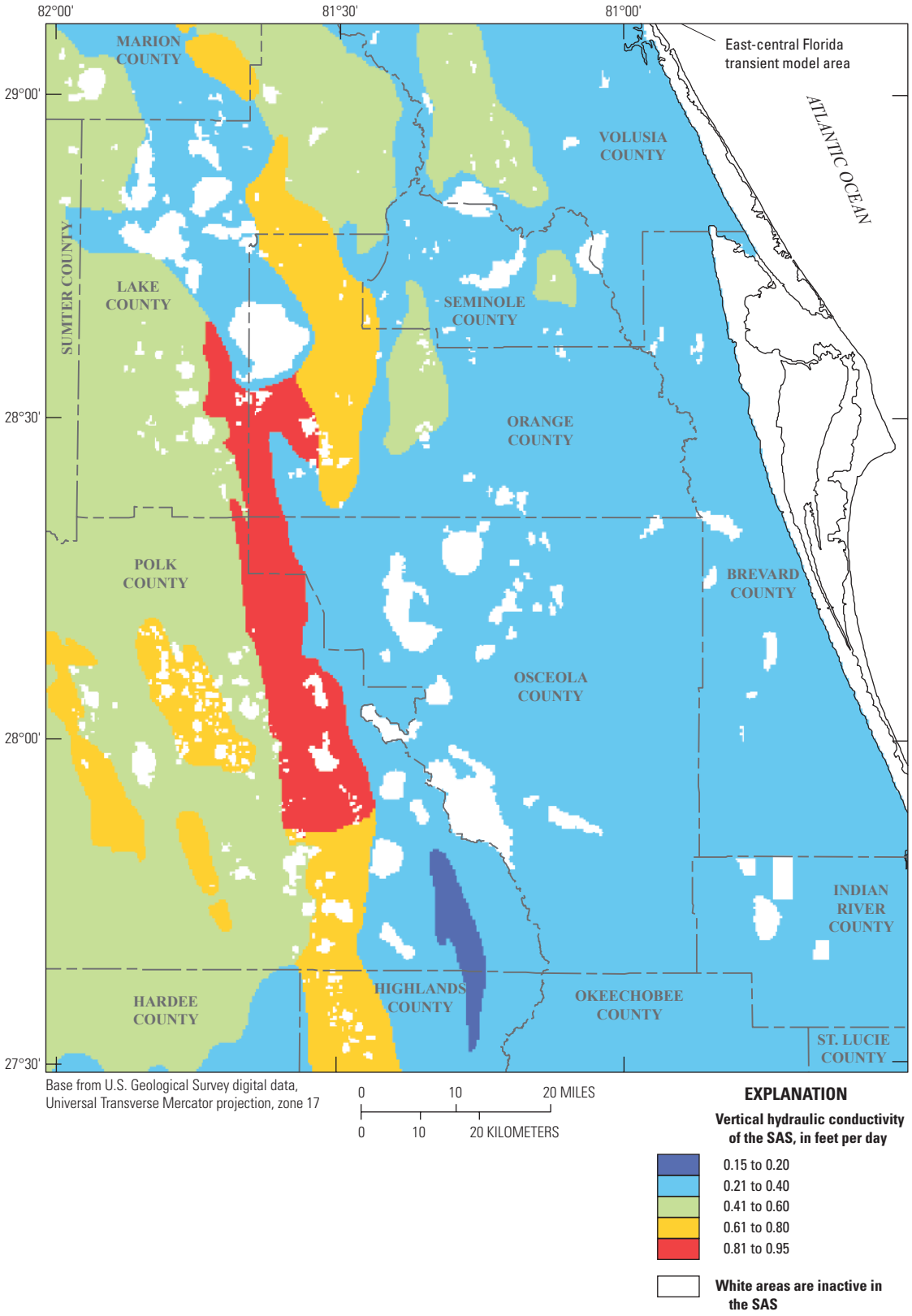

Figure 64. Specified vertical hydraulic conductivity of the surficial aquifer system (SAS, layer 1).

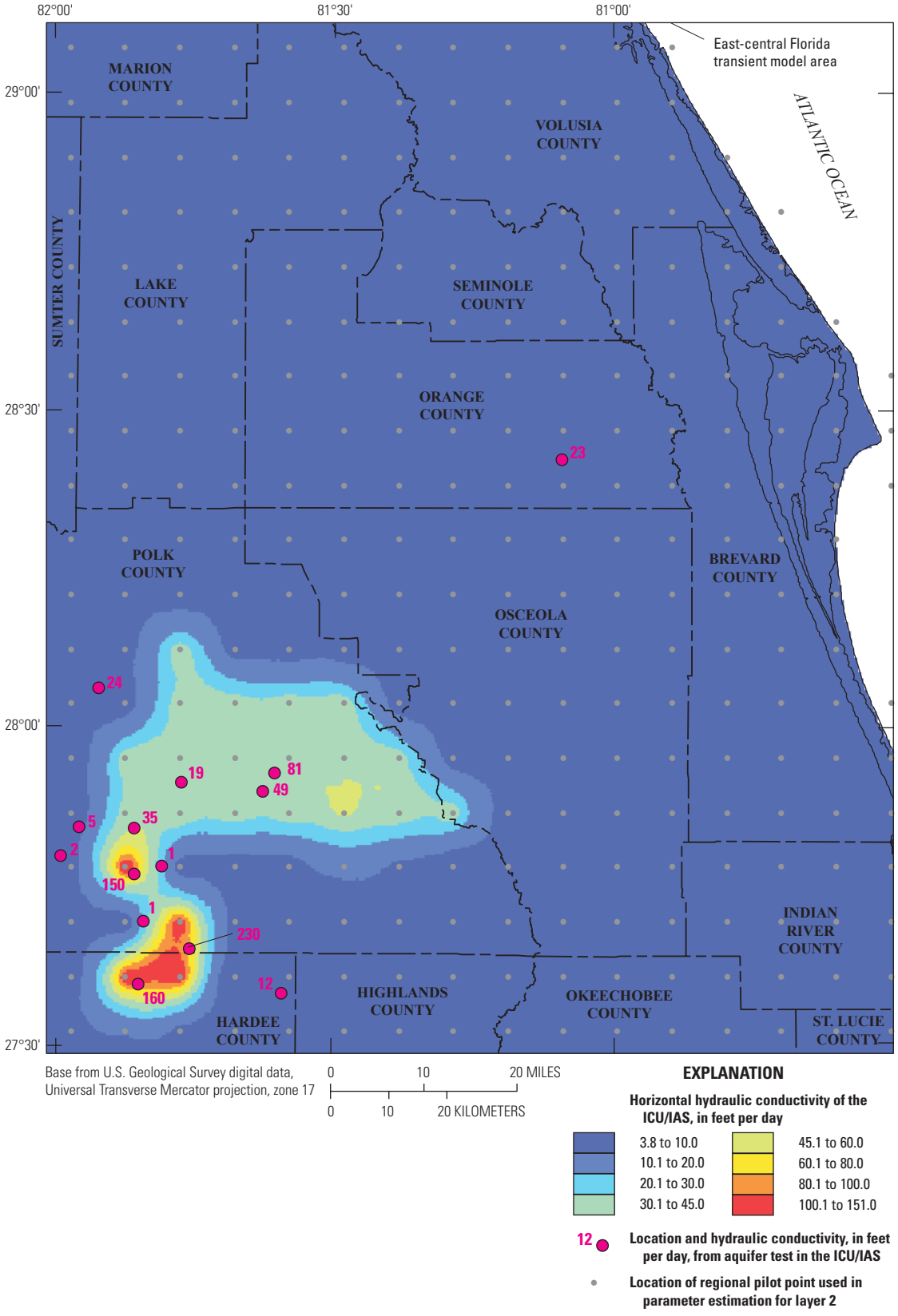

Figure 65. Calibrated horizontal hydraulic conductivity of the intermediate confining unit/intermediate aquifer system (ICU/IAS, layer 2) and selected aquifer test values.

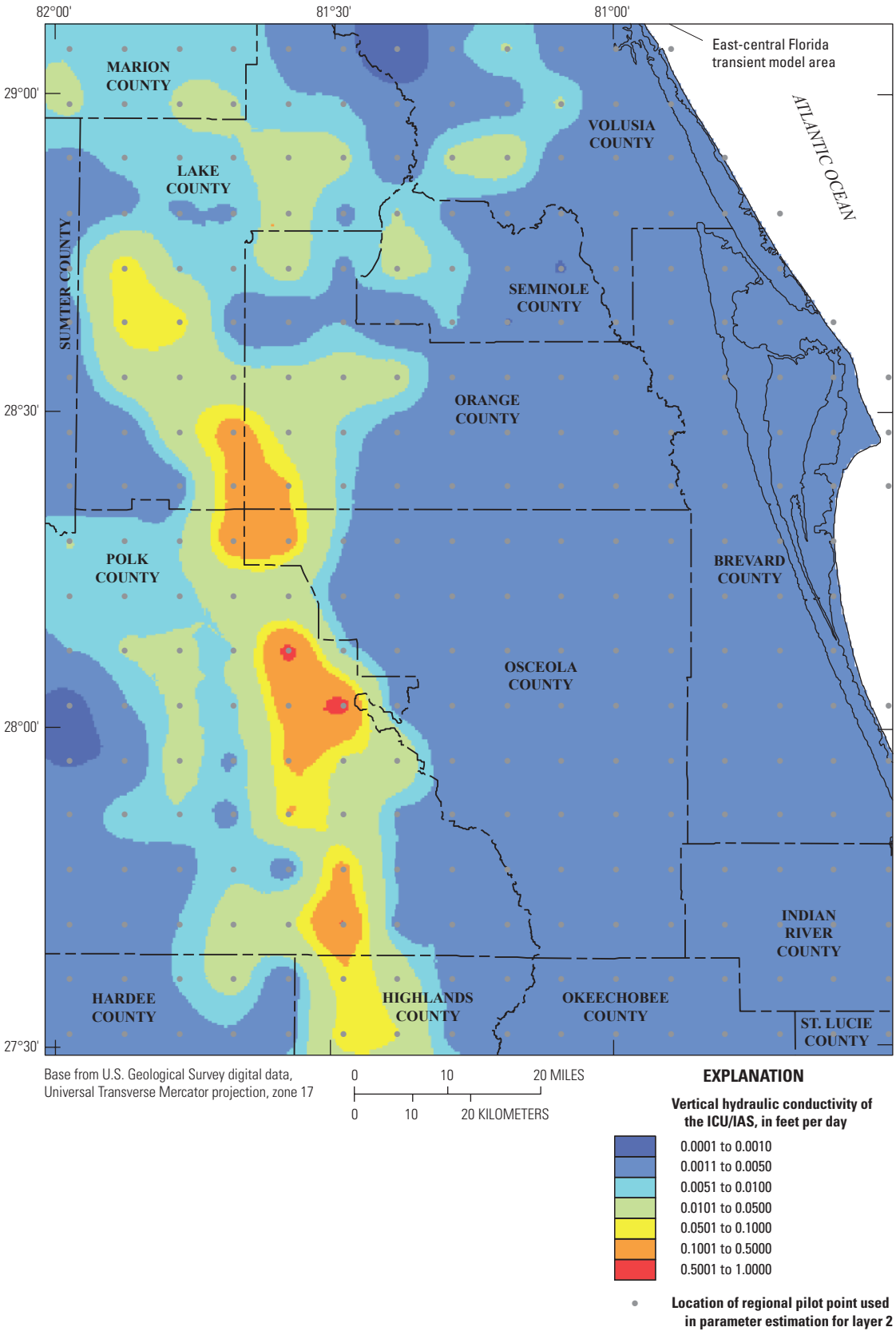

Figure 66. Calibrated vertical hydraulic conductivity of the intermediate confining unit/intermediate aquifer system (ICU/IAS, layer 2).

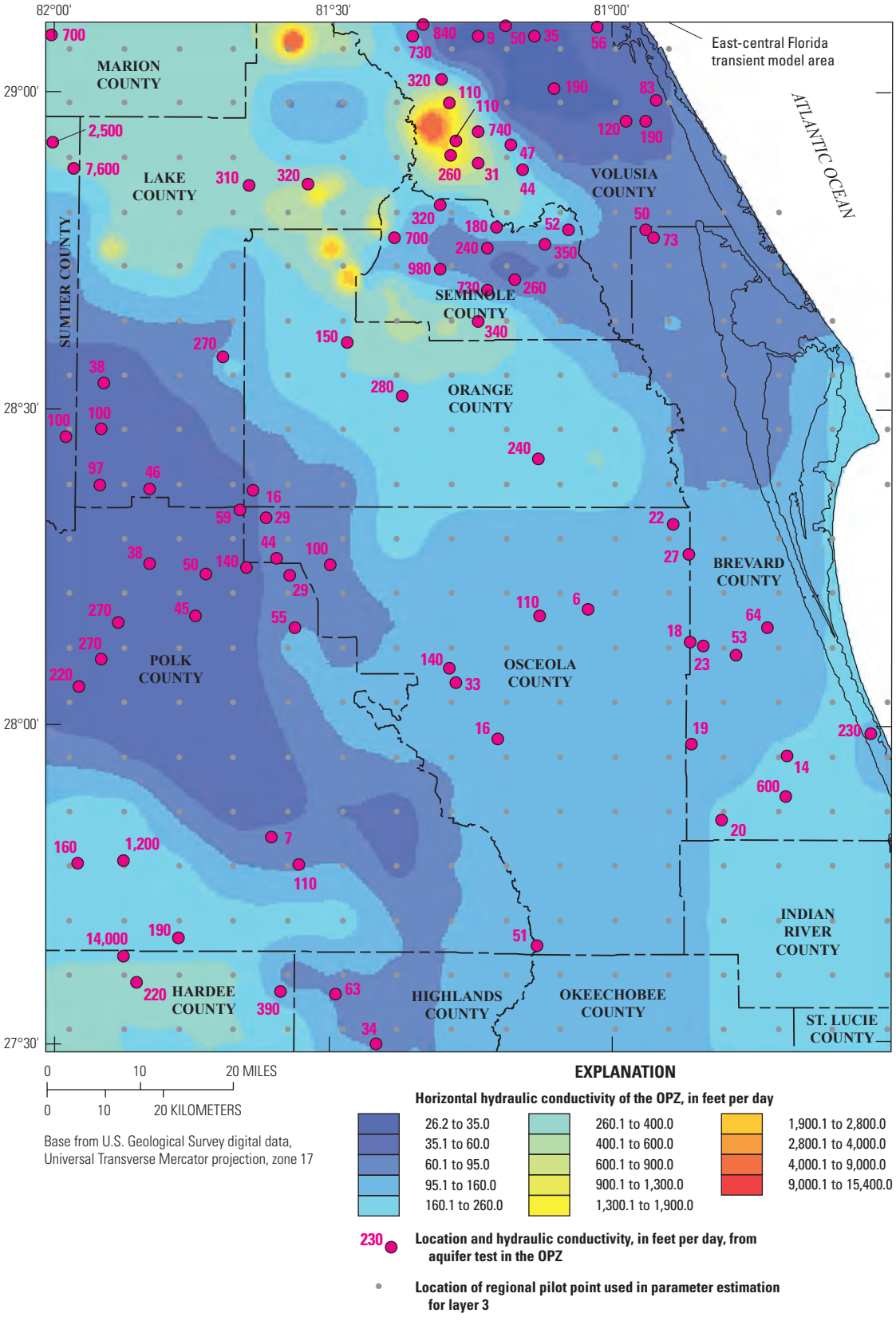

Figure 67. Calibrated horizontal hydraulic conductivity of the Ocala permeable zone (OPZ, layer 3) and selected aquifer test values.

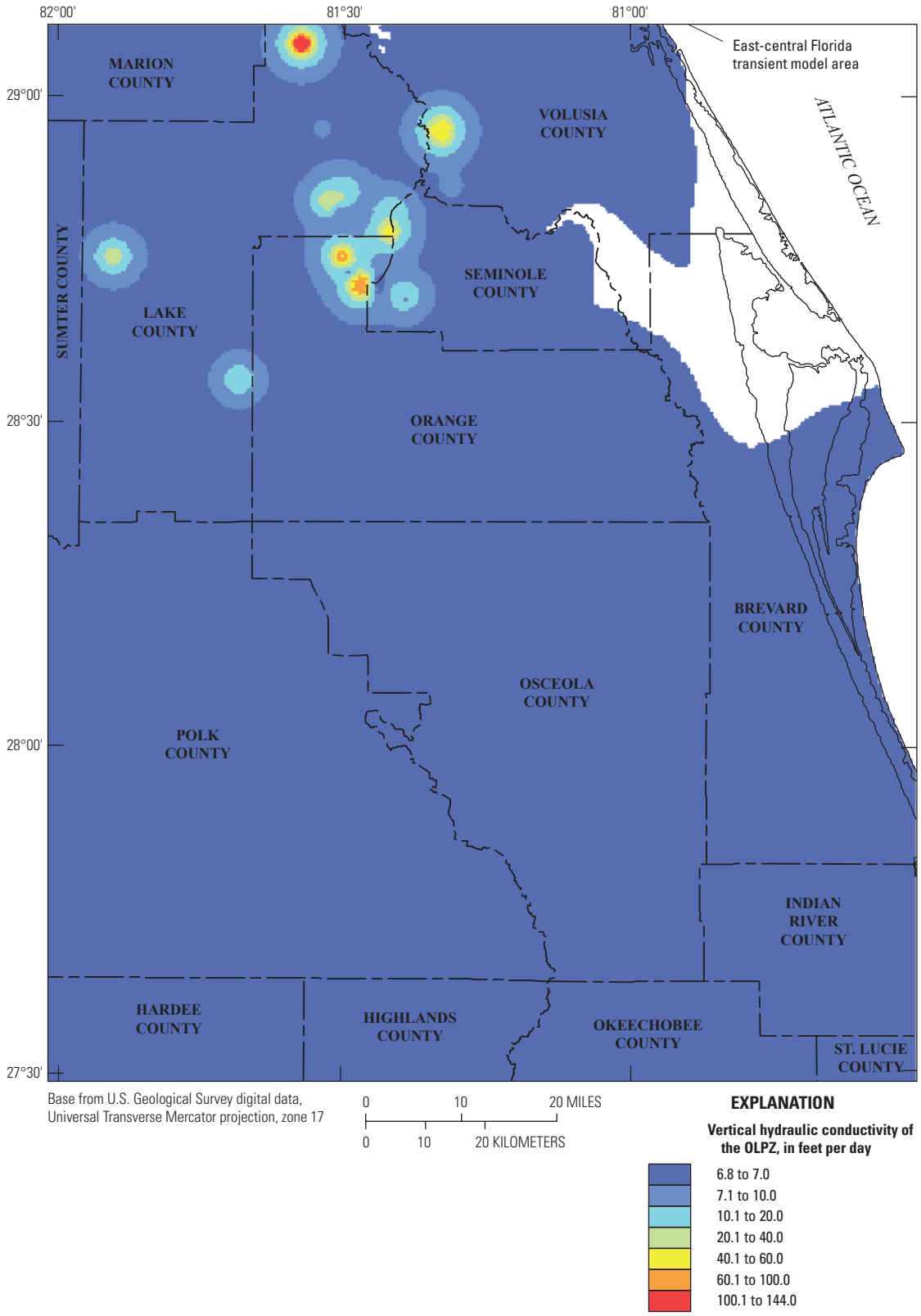

Figure 68. Calibrated vertical hydraulic conductivity of the Ocala low-permeable zone (OLPZ, layer 4).

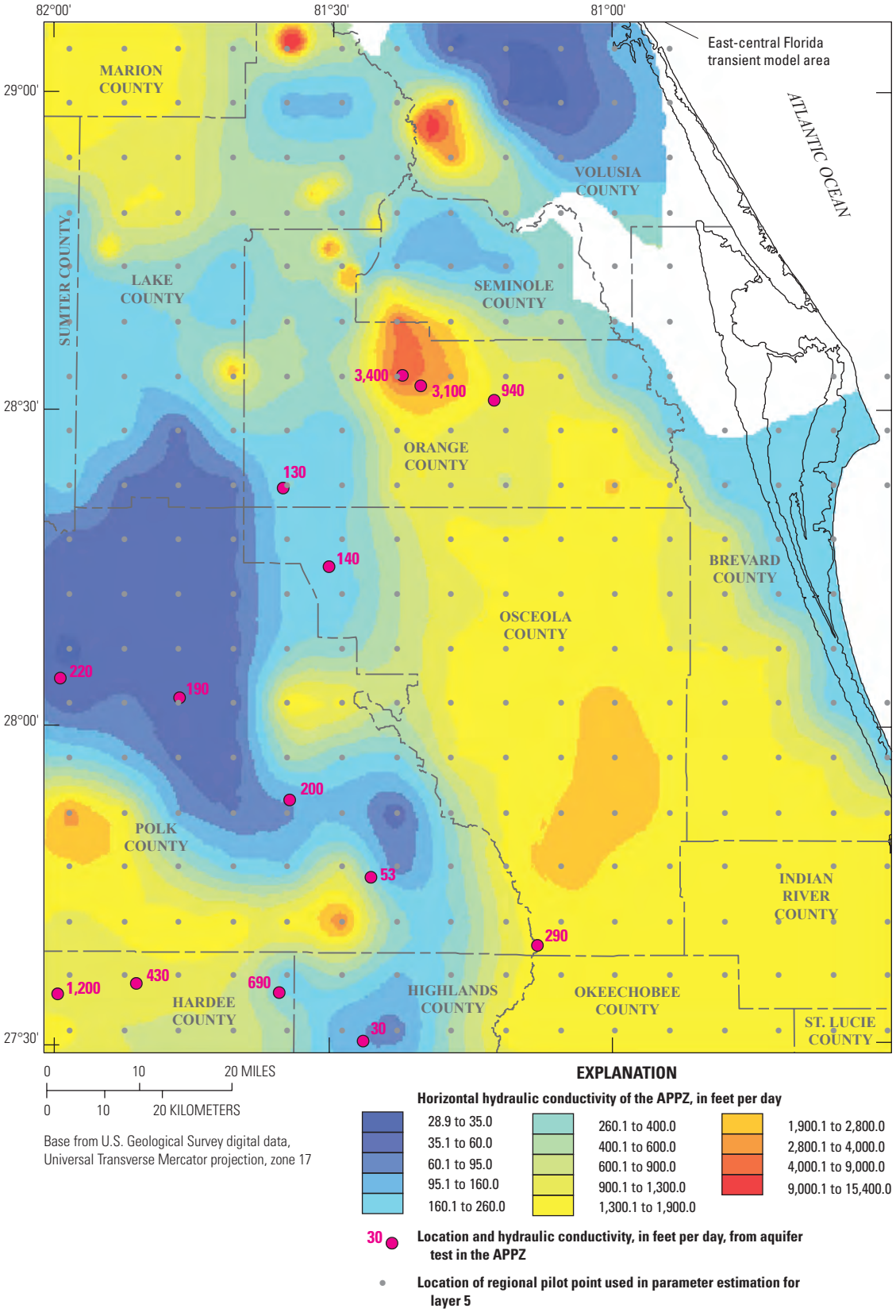

Figure 69. Calibrated horizontal hydraulic conductivity of the Avon Park permeable zone (APPZ, layer 5) and selected aquifer test values.

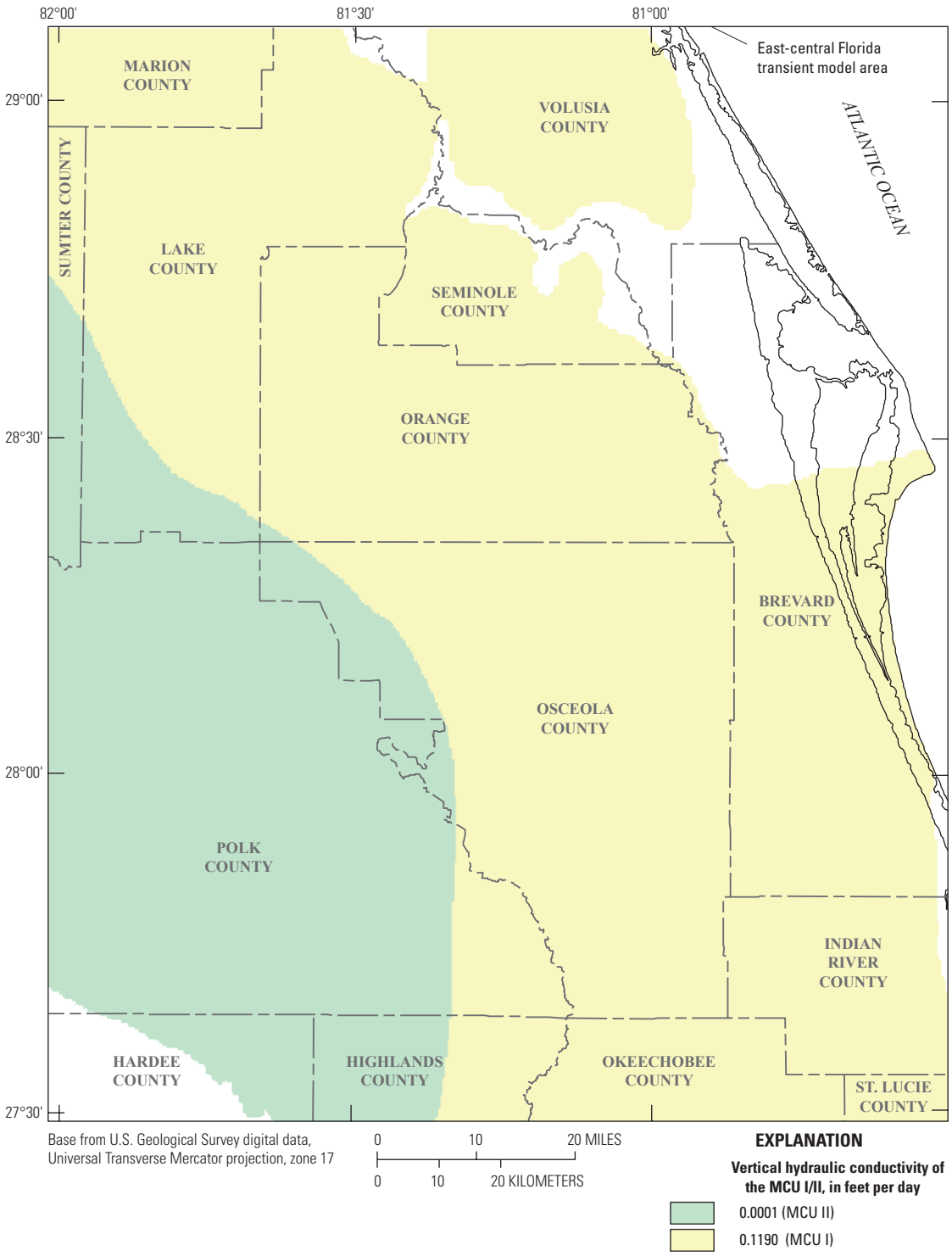

Figure 70. Calibrated vertical hydraulic conductivity of the middle confining units (MCU I/II, layer 6).

Calibrated values of Kh in layer 7 differ little compared to the preferred values (figs. 62 and 71). The minimum and maximum calibrated values of Kh are 33 ft/d and 1,900 ft/d, respectively.

Calibration of Storage Parameters Using Transient Conditions During 2005–2006

The model was used to estimate specific yield (Sy) of layer 1 and the specific storage (Ss) of layers 2 to 7 by fitting model output to measured heads and spring flows for transient conditions from July 2005 to December 2006. Only 2 years were simulated to calibrate storage parameters because the simulation time was prohibitively long for the necessary multiple iterations of the 12-year transient simulation required for regression of the parameters by PEST. In the transient regression simulations, the Kh and Kv distributions were fixed at the values estimated using the steady-state simulations. Simulated heads in the 12-year transient model at the end of 2004 were used as initial heads for the 2-year simulation.

Simulated equivalents of the transient measured heads are highly nonlinear with respect to Sy, as heads increase substantially with lower specific yield values. This is illustrated by differences of calculated *css* values for different Sy values (fig. 72). For each *css* calculation, the Sy parameter values for all zones were the same (0.11, 0.15, or 0.24). For most parameters, the *css* values are about 5 to 10 times larger when calculated using an Sy value of 0.11 than when calculated using 0.15 (fig. 72). The nonlinearity of heads is milder, but still evident, for Sy in the range of 0.15 to 0.24. The values of Ss_2 and Ss_3-7 in all *css* calculations were 3×10^{-6} ft^{-1} and 2×10^{-6} ft^{-1}, respectively. Values of *css* calculated at different Ss values showed that the simulated equivalents of the observations vary in a more linear manner with respect to Ss parameter values compared with Sy parameter values.

The relative magnitudes of the *css* among the 21 Sy parameters are similar for each of the three sets of Sy parameter values (fig. 72). For an Sy value of 0.15, parameters with the largest css are Sy_15, Sy_19, and Sy_20. These Sy parameters are associated with, respectively, the north, central, and south parts of Lake Wales Ridge. These large *css* for specific yield can be explained by the fact that the water table is below the ET extinction depth throughout most of the Lake Wales Ridge (fig. 2). Groundwater ET reduces water-table fluctuations because (1) as Sy decreases, the water table rises, and in turn, increases groundwater ET and limits the magnitude of the water-table fluctuations, and (2) as Sy increases, the water table declines, and in turn, decreases groundwater ET and limits the water-table decline. Because the water table is below the extinction depth throughout most of the Lake Wales Ridge, the corresponding absence of ET causes Sy to affect water-table fluctuations to a greater degree in this region than in other physiographic regions. Parameters with very small *css* values include Sy_3, Sy_6, Sy_12, and Ss_2.

The strategy for estimating Sy and Ss was to specify the values of the least sensitive parameters and then designate the remainder of the parameters with prior information. Parameters Sy_3, Sy_6, and Sy_12 were each set to 0.15, and Ss_2 was set to 3×10^{-6} ft^{-1}. Because of the nonlinearity with respect to Sy, the use of prior information helped stabilize the regression. If a parameter became insensitive during a regression simulation, its estimated value remained close to the prior value, which was 0.15 for all Sy parameters. This value is considered reasonable for the sandy sediments that compose the SAS. PEST's regularization capability of a highly parameterized approach was not used for the calibration to transient conditions because the storage properties are represented using 21 Sy zones and two Ss parameters. The value of μ was set to 1.0 in the objective function (equation 6) because prior information was used and regularization was not used.

During regression simulations, Sy tended to either stay near the prior value or decrease to the lower bound, which was initially set to 0.11. When Sy was as low as 0.11, this caused higher simulated heads than observed at many wells and lower simulated ET rates relative to the estimated minimum rate. To constrain model calibration to reasonable parameter values, the simulated ET rate generally was maintained, as much as possible, to be at least half the sum of rainfall and irrigation for the cell. Because of the tendency to estimate lower Sy values than was acceptable, the lower bound for all Sy parameters was increased to 0.14. Estimated specific yield parameters that remained similar to the prior value were set to 0.15 in the calibrated model, including those for physiographic regions 1, 2, 4, 7, 8, 9, 16, and 17, as well as regions 3, 6, and 12, which were not adjusted (fig. 2). Parameters with an estimated value equal to the lower bound of 0.14 included regions 5, 10, 11, 13, 14, 15, and 18 through 21 (fig. 2, table 14). The estimated value of Ss_3-7 tended to become larger than that of Ss_2 during the regression runs. However, because the sediments in layers 3 through 7 are less compressible than those in layer 2, it is expected that Ss_3-7 would be smaller than Ss_2. Accordingly, Ss_2 was set to 3×10^{-6} ft^{-1} and Ss_3-7 was set to 2×10^{-6} ft^{-1} in the calibrated model (table 14).

Model Fit for 1995–2006 Transient Conditions

Following calibration of hydraulic conductivity parameters for the steady-state 1993 and 2003 conditions, and calibration of storage parameters for 2005–2006 transient conditions, the estimated values were used as input for a forward simulation of transient conditions from 1995 to 2006. Simulated heads and spring flows from this forward simulation were used to assess model fit to the observed heads and spring flows.

The model fit satisfies all the calibration criteria for groundwater heads presented earlier. For each year simulated, almost 60 percent of the wells have an absolute value of head residual less than or equal to 2.5 ft, more than 85 percent of the wells have an absolute value of head residual less than or equal to 5 ft, the absolute value of the overall mean residual

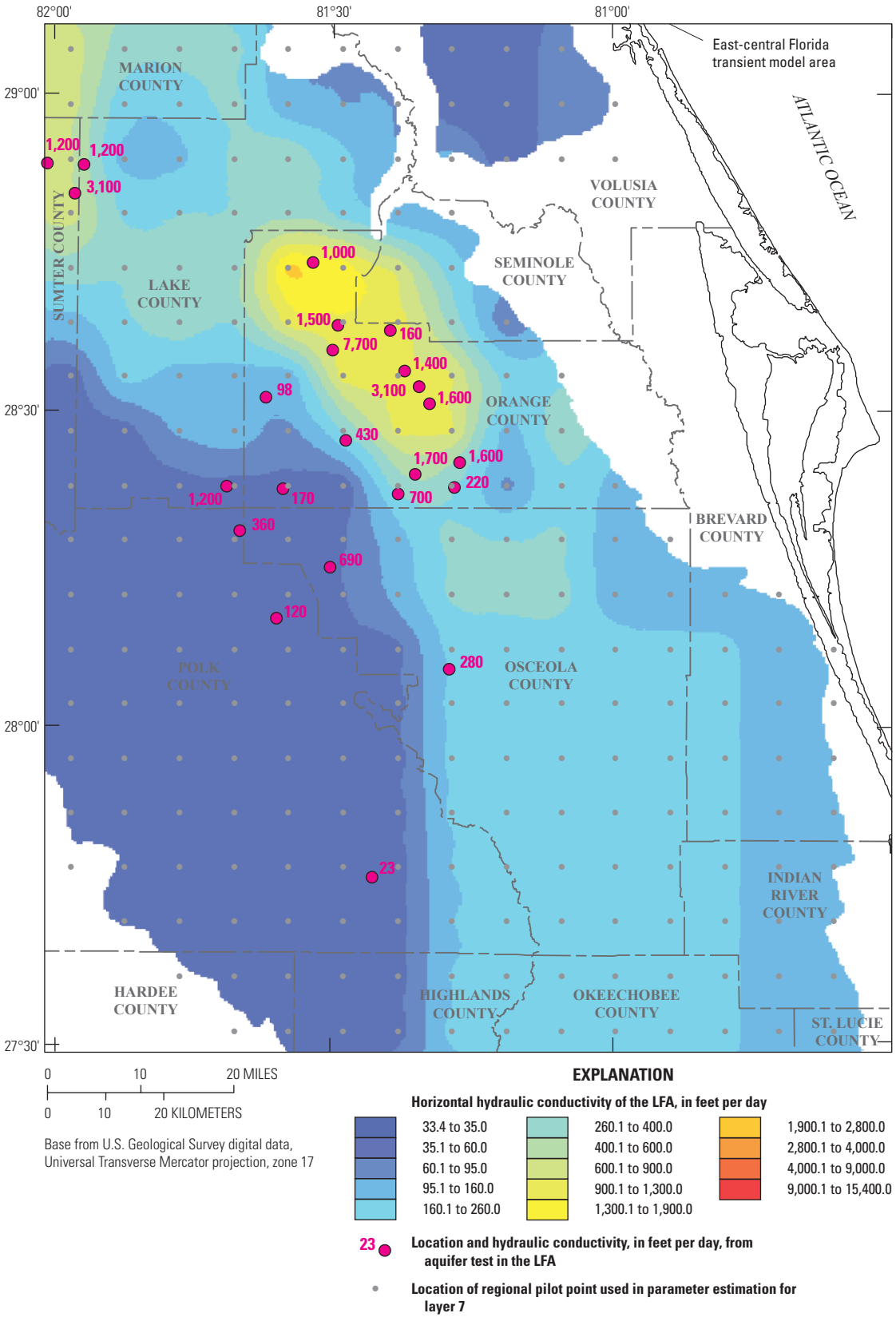

Figure 71. Calibrated horizontal hydraulic conductivity of the Lower Floridan aquifer (LFA, layer 7) and selected aquifer test values.

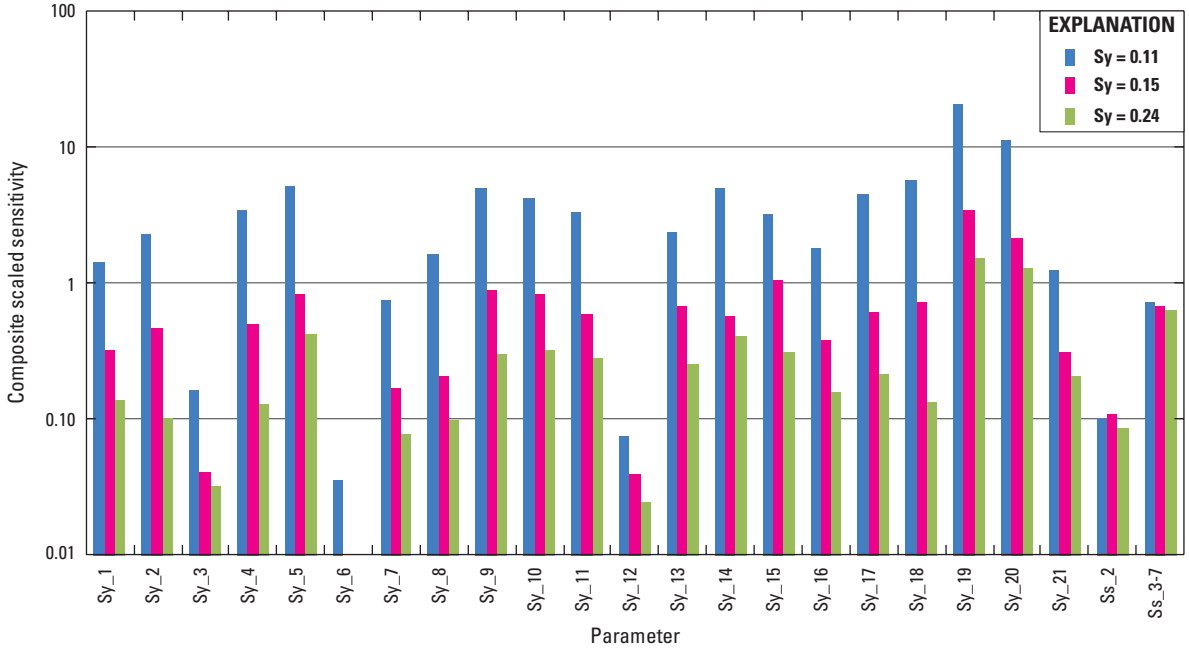

Figure 72. Composite scaled sensitivities for specific yield and specific storage parameters in the transient model, calculated using head and spring-flow observations from July 2005 through December 2006.

(OMR) is less than 1 ft, and the RMSR is less than 3.6 ft (table 15). For the entire simulation period of 1995 to 2006, the OMR is -0.04 ft and the RMSR is about 3.4 ft.

The transient 1995–2006 simulation results also satisfy the calibration criteria for spring flows. For each spring, average simulated flow and average observed flow were calculated over the entire simulated period. Residuals calculated for these averages are less than 10 percent of average observed flow for all springs (table 16). The spring with one of the highest residuals was spring number 8, which is also the spring with the lowest average observed flow among all springs (table 16). The overall mean residual between measured and simulated spring flow is about -0.3 ft^3/s.

In addition to satisfying the calibration criteria related to statistical measures calculated from the residuals, it is important that the weighted residuals be randomly distributed (Hill and Tiedeman, 2007). Randomness is evaluated using weighted residuals from selected years of the 12-year model, using two types of figures. First, on graphs of weighted residuals versus simulated values, randomness is indicated by an even spread of positive and negative weighted residuals for all simulated values. Second, on maps of weighted residuals displayed geographically, randomness is indicated by a visual mix of positive and negative residuals distributed randomly throughout the model area. Nonrandom weighted residuals indicate model bias and possible model error. A typical indicator of bias is a cluster of weighted residuals in a geographic area that are large and identical in sign.

Graphs of unweighted residuals of average annual heads (with all weights equal to 1.0) and spring flow weighted residuals versus monthly simulated flows are shown for 1999, 2003, and 2006 (figs. 73 and 74). These selected years include the 2 years for which steady-state conditions were calibrated by PEST, as well as the final year of the 12-year simulation. For 1999, the head residuals are evenly spread above and below the horizontal grid line corresponding to a residual value of zero (fig. 73*A*). For 2003 and 2006, head residuals each exhibit slight bias (fig. 73*C*), because there are more

Table 14. Estimated specific yield and specific storage values for the calibrated transient model of 1995 to 2006.

[Sy, specific yield; Ss, specific storage; PHYSR, physiographic region number shown in figure 2; Layer, layer number to which value was applied; —, not applicable]

Value	PHYSR	Layer
	Sy	
0.14	5, 10, 11, 13, 14, 15, 18, 19, 20, 21	1
0.15	1, 2, 3, 4, 6, 7, 8, 9, 12, 16, 17	1
	Ss	
3×10^{-6} ft^{-1}	—	2
2×10^{-6} ft^{-1}	—	3, 4, 5, 6, 7

Table 15. Statistics of head residuals for the calibrated 1995–2006 transient model.

[NW, number of wells; NE2.5, number of wells with absolute value of residual not exceeding 2.5 feet (ft); PNE2.5, percent of NW in NE2.5 category; NE5, number of wells with absolute value of residual not exceeding 5 ft; PNE5, percent of NW in NE5 category; LT-5, number of wells with residuals less than –5 ft; PLT-5, percent of NW in LT-5 category; GT5, number of wells with residuals greater than 5 ft; PGT5, percent of NW in GT5 category; OMR, overall mean residual, in feet; RMSR, root-mean-square residual, in feet]

Year	NW	NE2.5	PNE2.5	NE5	PNE5	LT-5	PLT-5	GT5	PGT5	OMR	RMSR
1995	379	243	64.1	331	87.3	24	6.3	24	6.3	0.04	3.56
1996	413	255	61.7	362	87.7	31	7.5	20	4.8	–0.25	3.59
1997	408	257	63.0	354	86.8	39	9.6	15	3.7	–0.32	3.51
1998	436	278	63.8	375	86.0	44	10.1	17	3.9	–0.66	3.51
1999	468	295	63.0	404	86.3	31	6.6	33	7.1	0.14	3.38
2000	434	258	59.4	374	86.2	24	5.5	36	8.3	0.51	3.48
2001	474	283	59.7	412	86.9	21	4.4	41	8.6	0.59	3.58
2002	476	305	64.1	412	86.6	38	8.0	26	5.5	–0.26	3.45
2003	519	338	65.1	459	88.4	35	6.7	25	4.8	0.17	3.22
2004	522	336	64.4	457	87.5	34	6.5	31	5.9	0.12	3.25
2005	523	338	64.6	461	88.1	49	9.4	13	2.5	–0.41	3.27
2006	529	307	58.0	458	86.6	45	8.5	26	4.9	–0.13	3.46
1995–2006										**–0.04**	**3.43**

Table 16. Statistics of spring-flow residuals for the calibrated 1995–2006 transient model.

[SN, spring number, refer to table 2–1 for spring name; SF, average simulated spring flow from 1995 to 2006, in ft^3/s; AF, average observed spring flow from 1995 to 2006 in ft^3/s; RES, residual equal to difference between average simulated and average observed flow, in ft^3/s; PD, percent difference between average simulated and average observed flows, calculated relative to average observed flow; OMR, overall mean residual; Ave, average PD]

SN	SF	AF	RES	PD	SN	SF	AF	RES	PD
1	103.18	103.02	0.16	0.16	13	16.00	16.04	–0.04	–0.25
2	26.16	26.85	–0.69	–2.57	14	5.47	5.61	–0.14	–2.50
3	152.08	153.49	–1.41	–0.92	15	5.40	5.61	–0.21	–3.74
4	2.71	2.77	–0.06	–2.17	16	55.58	56.13	–0.55	–0.98
5	10.74	10.93	–0.19	–1.74	17	17.93	18.78	–0.85	–4.53
6	0.82	0.83	–0.01	–1.20	18	33.43	34.43	–1.00	–2.90
7	1.39	1.31	0.08	6.11	19	12.94	13.44	–0.50	–3.72
8	0.75	0.81	–0.06	–7.41	20	19.63	19.65	–0.02	–0.10
9	9.66	9.82	–0.16	–1.63	21	63.63	64.41	–0.78	–1.21
10	1.75	1.71	0.04	2.34	22	1.95	1.97	–0.02	–1.02
11	3.41	3.45	–0.04	–1.16	**OMR**			**–0.29**	
12	8.14	8.09	0.05	0.62	**Ave**				**–1.39**

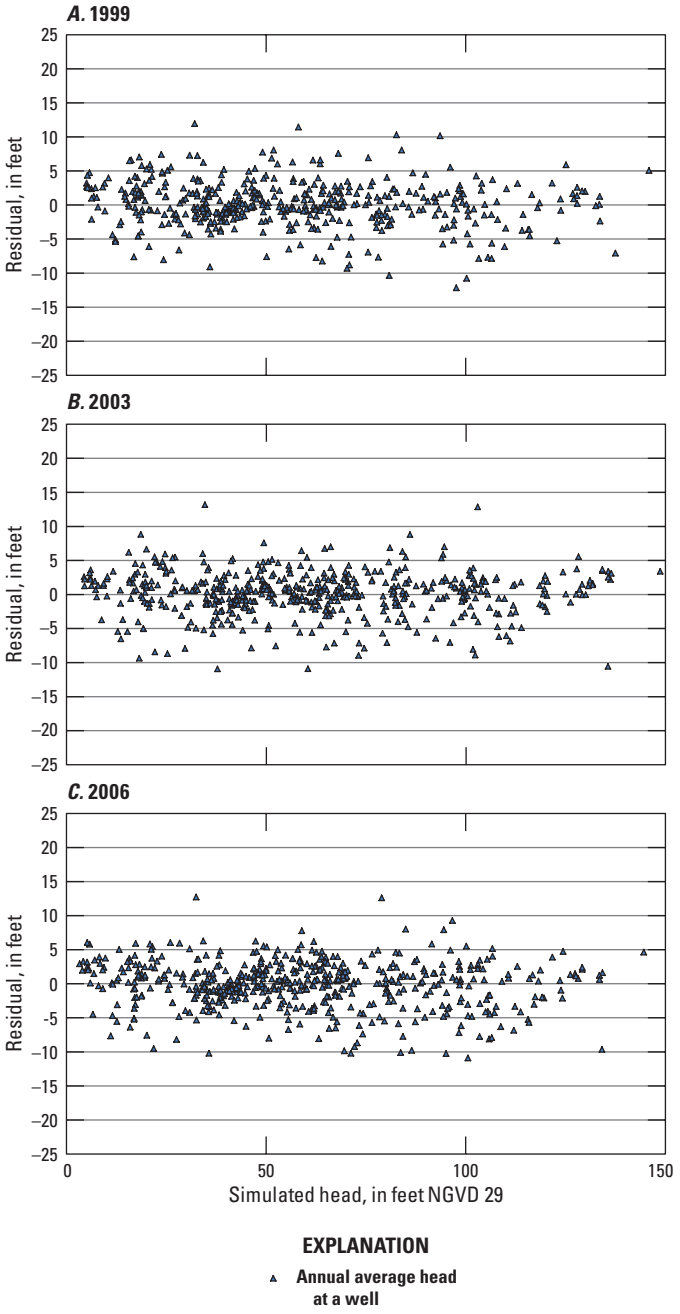

Figure 73. Annual average head residuals versus annual average simulated heads for *A*, 1999, *B*, 2003, and *C*, 2006. All values are calculated using the 12-year model.

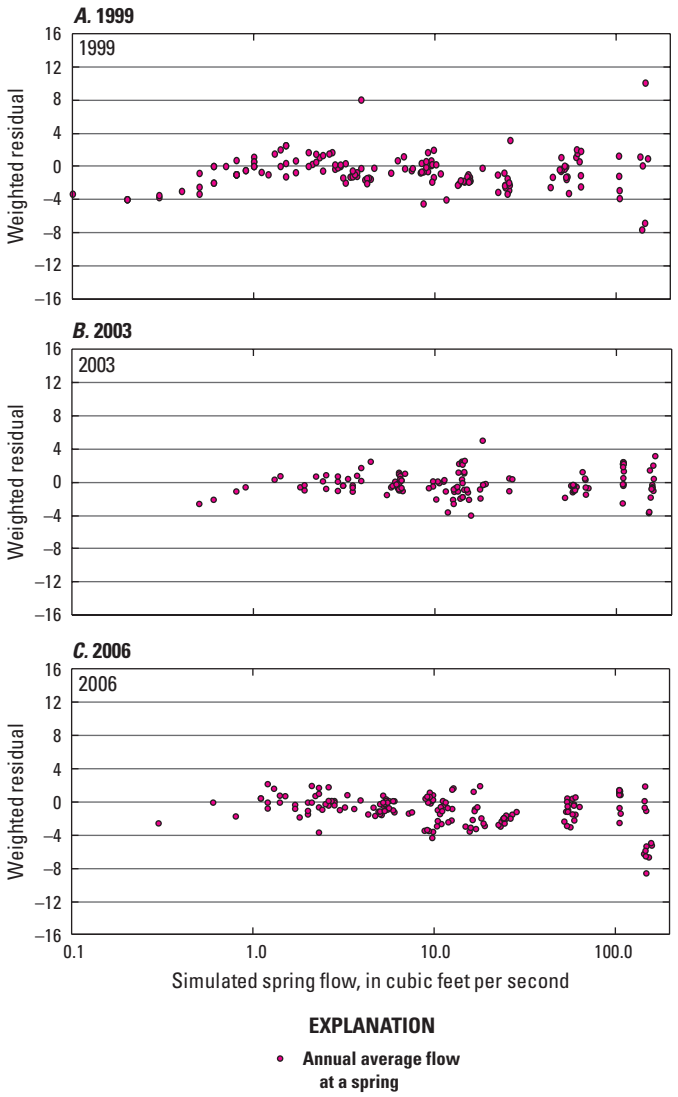

Figure 74. Weighted monthly average spring flow residuals versus monthly average simulated flows for *A*, 1999, *B*, 2003, and *C*, 2006. All values are calculated using the 12-year model.

negative than positive residuals for simulated heads of about 70 to 110 ft. Within this range, the majority of residuals less than -5 ft lie along the Lake Wales Ridge and in western Polk and Lake Counties.

For the spring-flow observations in 1999 and 2003, weighted residuals are evenly distributed about a value of zero, except for those associated with flows that are less than 1 ft^3/s (fig. 74*A*–*B*), which occur for springs 6, 7 (1999 only), and 8 (fig. 51). This bias is not a great concern because of the small magnitudes of flows and unweighted residuals at these springs. For simulated flows of about 8 to 60 ft^3/s in 2006, there are more negative weighted residuals less than -2 than positive weighted residuals greater than 2 (fig. 74*C*). The majority of the weighted residuals less than -2 are for springs 2, 5, 16, and 17 (fig. 51). In addition, the cluster of negative weighted residuals for spring 3, at a simulated flow of about 145 ft^3/s, is an outlier on fig. 74*C*. Springs 2, 3, 5, 16, and 17 are not concentrated in a specific area (fig. 51), and all but spring 2 are relatively near other springs, suggesting that any model error that is causing a bias in simulated flow at these springs for 2006 is relatively localized.

Average annual head residuals are displayed geographically for the four model layers corresponding to aquifers (the SAS, OPZ, APPZ, and LFA), for 1999 and 2006. These years represent 1 year for which a steady-state model was calibrated and the final year of the 12-year simulation. For 1999,

the head residuals in the SAS appear randomly distributed over much of the model area (fig. 75). An exception is in central Polk County, in the central and southern parts of the Lake Wales Ridge (figs. 2 and 75), where there is a cluster of negative residuals. Large simulated surface leakage rates along the eastern edge of Lake Wales Ridge are the result of relatively large differences in hydraulic conductivity and land-surface altitude between the Lake Wales Ridge and the Osceola and Wekiva Plains (figs. 2, 16, and 63). Large surface leakage rates reduce the recharge rates to layer 1 and thus the potential for larger leakage rates to the underlying layers representing aquifers. These reductions cause the aquifer heads to be underestimated, making adjustments to reduce residuals in this area difficult while using realistic K values, recharge, and ET rates.

In the underlying OPZ, the head residuals for 1999 are mostly randomly distributed, except in western Lake County where many residuals are negative and large in magnitude (fig. 76). At these locations, the residuals for 1999 steady-state conditions are randomly distributed. Therefore, it is likely that differences in boundary conditions between the steady-state and transient simulations produce differences in the residuals, causing annual average simulated heads in 1999 to be low for the 1995–2006 transient simulation. This result points out a limitation of the calibration approach, in that parameter estimates that produce a good fit for approximated steady-state conditions do not necessarily produce the same level of fit for transient conditions. As this discussion and the subsequent analyses of residuals show, this problem tends to be limited to local areas within the model.

In both the APPZ and LFA, there are few head observations (fig. 77), which makes assessing randomness more difficult because of the small sample size. In the APPZ simulated average annual heads are low at three wells in the south-central part of the domain; average annual heads also are low at these wells for 1999 steady-state conditions. Sensitivities from the 1999 steady-state simulation show that for several pilot points near the two southernmost wells for which residuals are in the lowest range, increasing Kh will increase the head at one well and decrease head at the other well. Therefore, one reason for the poor fit at both wells is that the regression cannot improve fit at one well without worsening it at the other. In the LFA, most residuals are between -2.5 and 2.5 ft. (fig. 77).

Comparison of 2006 average annual head residuals in each aquifer with those for 1999 shows that at most sites for which observations exist in both of these years, the model fit showed small differences in residuals between 1999 and 2006 (figs. 75 to 80). In addition, average annual head residuals that can be calculated only in 2006 tend to be a mix of positive and negative values. For the average annual head residuals that can be calculated only in 2006, there are slightly more residuals that are negative and of large magnitude than there are large positive residuals. However, the distributions of all average annual head residuals in 2006 do not show any additional areas of clusters of same-signed residuals, compared to those identified for 1999.

The ECFT model was used to generate simulated spring-flow hydrographs from 1995 to 2006, which is illustrated with Rock Springs (spring number 16) and Wekiwa Springs (or spring number 21) (fig. 52, table 2–1). Rock Springs and Wekiwa Springs, which had respective average measured flows of 56 and 64 ft^3/s over the simulation period, had overall mean flow residuals of less than 1 ft^3/s in absolute value (table 16). Simulated spring flow was greater during wet years than during dry years (figs. 81 and 82, table 5). Additional spring-flow hydrographs are shown in appendix 2.

The ECFT model was also used to generate simulated water-surface altitude hydrographs at lakes from 1995 to 2006, which are shown for Lake Monroe (lake number 38) and Lake Arbuckle (lake number 271) (fig. 13). Lakes Monroe and Arbuckle, which had respective average water-surface altitudes of 2.4 and 53.6 ft over the simulation period, had overall mean water-surface altitude residuals of about 0.06 and -0.28 ft, indicating a lack of bias in the simulated residuals. Fluctuations in water-surface altitudes over relatively short periods (figs. 83 and 84) were simulated. Additional water-surface altitude hydrographs for lakes are shown in appendix 3.

The capability of the model to simulate streamflows at stream-gaging stations was assessed by using data from St. Johns River station number 02236000 (stream segment number 164, fig. 11) and Peace River station number 02295637 (segment number 299, fig. 11). Respective average measured streamflows at these two stations (figs. 85 and 86) were 3,190 and 706 ft^3/s based on average monthly measurements from 1995 to 2006. The respective overall mean flow residuals at these two stations were about -270 and 8 ft^3/s over the simulation period, indicating a small bias in the flow residuals. The calibration of streamflows was limited to reducing, as much as possible, the differences between total simulated and measured water volumes over the simulation period. Additional streamflow hydrographs at stream-gaging stations are shown in appendix 4.

Measured and simulated well hydrographs in the SAS, IAS, OPZ, APPZ, and LFA were compared to assess the model fit over the entire simulation period. Well numbers 2 and 13, in figure 5–1, named Cocoa K and Ridge Wrap H-1, are SAS wells with respective average measured water levels of 57.51 and 104.47 ft from 1995 to 2006 (figs. 87 and 88). The respective overall mean residuals at these two wells were -0.19 and 0.31 ft, indicating a lack of bias in the residuals. These hydrographs show measured seasonal rises and declines in the water table. Additional hydrographs from SAS wells are shown in figures 5–2 to 5–16 in appendix 5.

Well numbers 1 and 4, in figure 5–17 (appendix 5), named Bithlo 2 ICU and L-0096 Groveland Fire Tower, are ICU wells with respective average measured heads of 47.43 and 81.85 ft for the entire 1995 to 2006 simulation period (figs. 89 and 90). The respective overall mean residuals at these two wells were 0.21 and -1.63 ft, suggesting a small bias in the water-table altitude residuals. Additional hydrographs from ICU wells are shown in figures 5–18 to 5–25 in appendix 5.

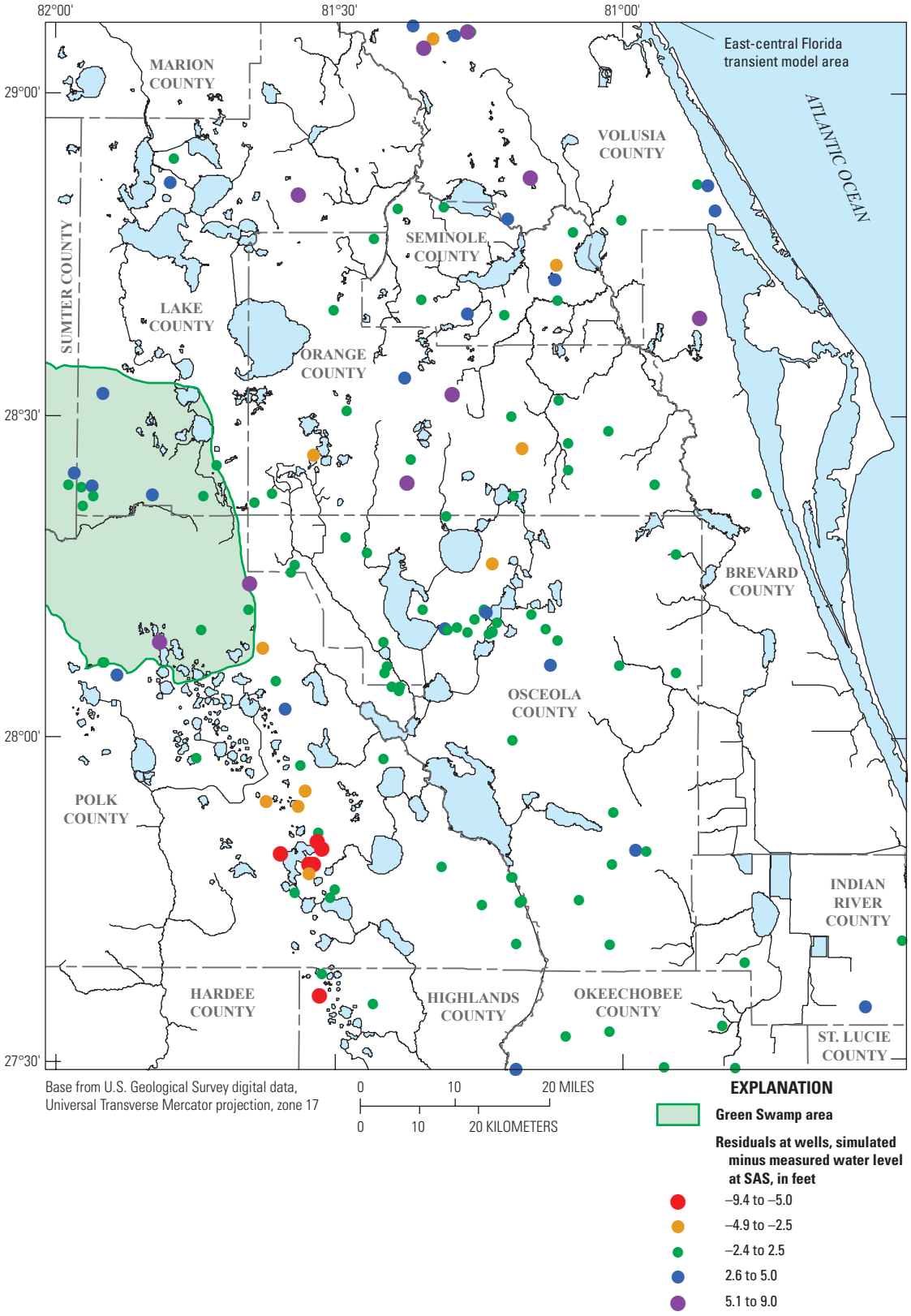

Figure 75. Head residuals for 1999 in surficial aquifer system (SAS, layer 1) wells, calculated using average annual simulated (from the 12-year model) and observed heads.

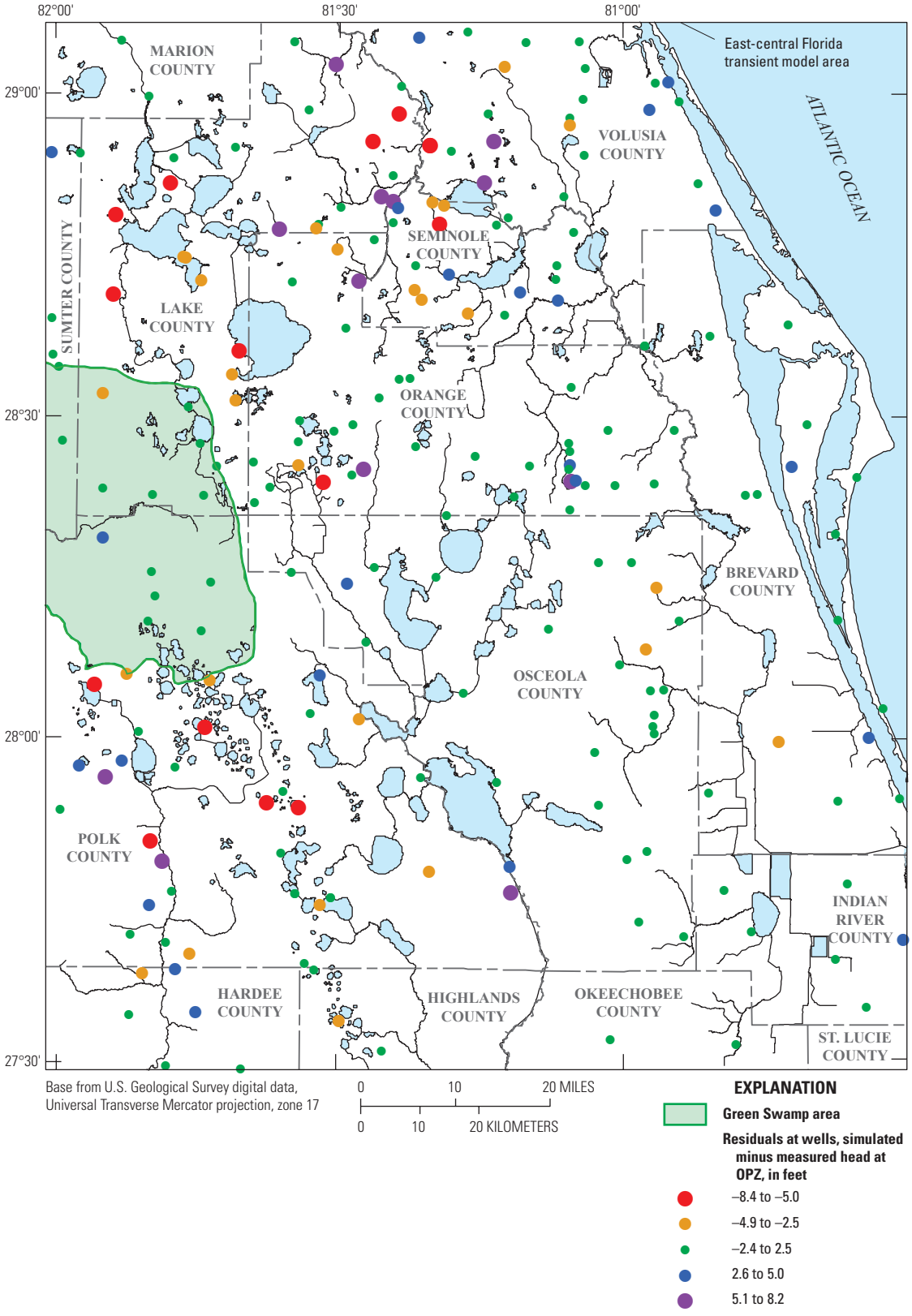

Figure 76. Head residuals for 1999 in Ocala permeable zone (OPZ, layer 3) wells, calculated using average annual simulated (from the 12-year model) and observed heads.

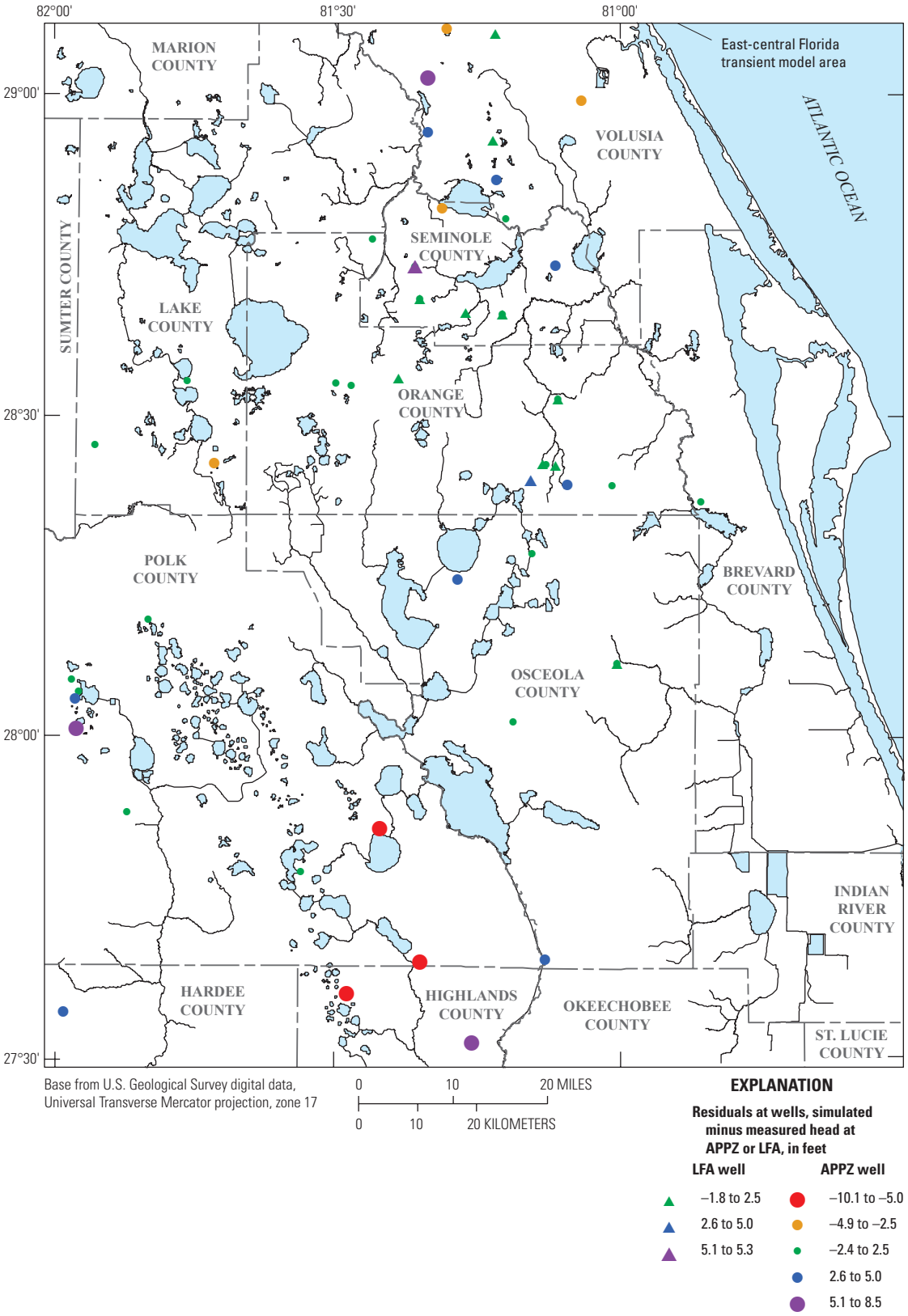

Figure 77. Head residuals for 1999 in Avon Park permeable zone (APPZ, layer 5) and Lower Floridan aquifer (LFA, layer 7) wells, calculated using average annual simulated (from the 12-year model) and observed heads.

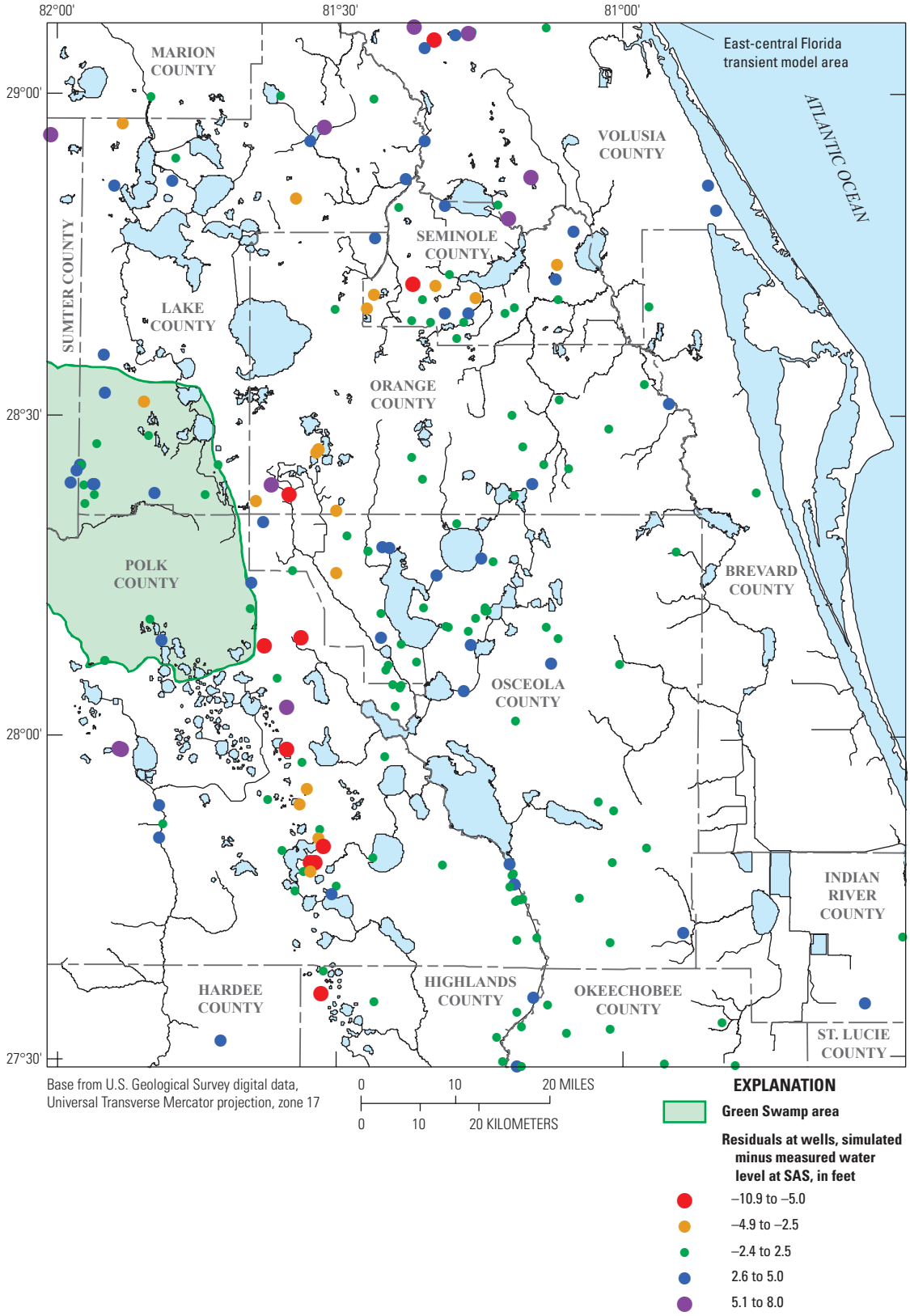

Figure 78. Head residuals for 2006 in surficial aquifer system (SAS, layer 1) wells, calculated using average annual simulated (from the 12-year model) and observed heads.

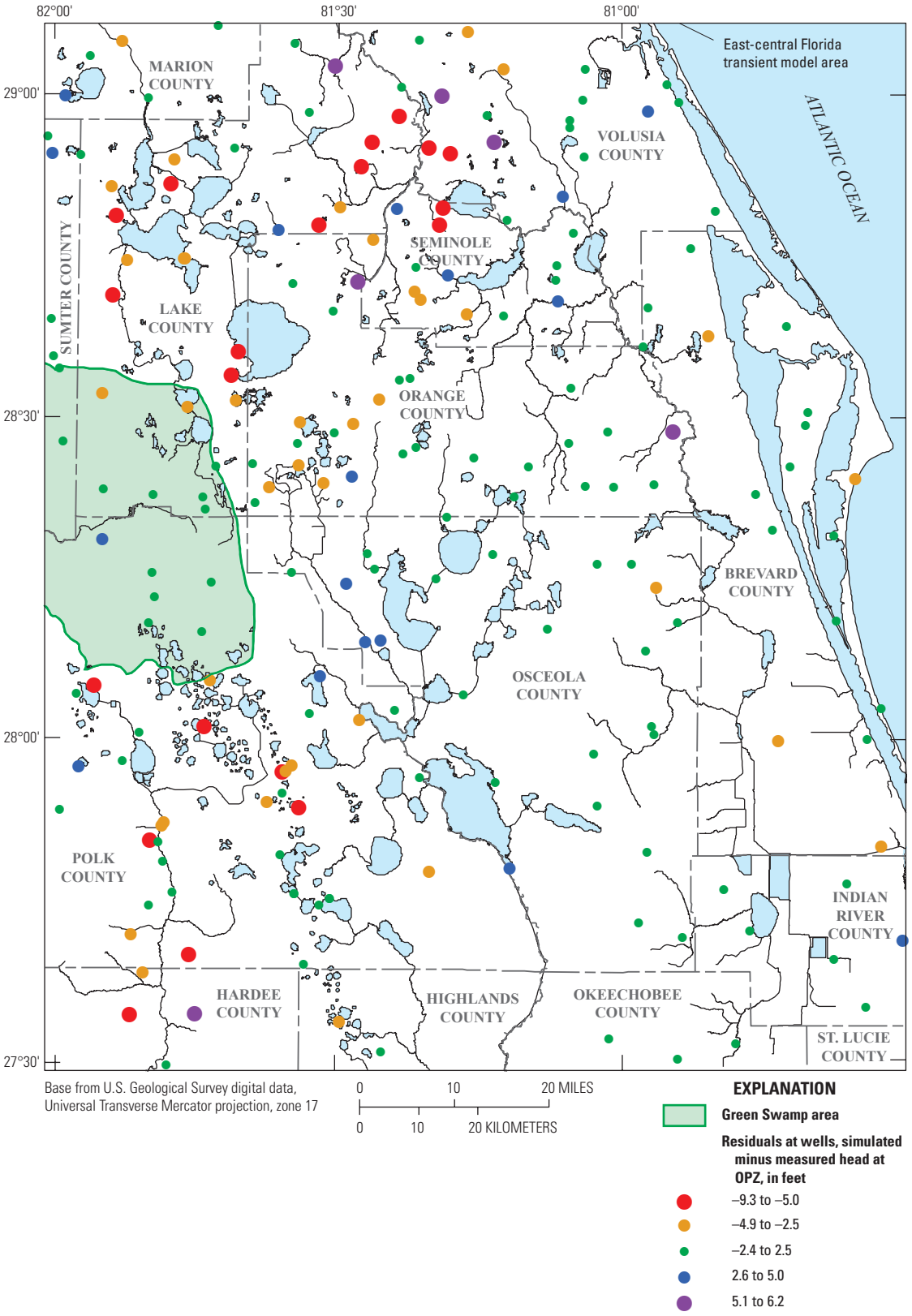

Figure 79. Head residuals for 2006 in Ocala permeable zone (OPZ, layer 3) wells, calculated using average annual simulated (from the 12-year model) and observed heads.

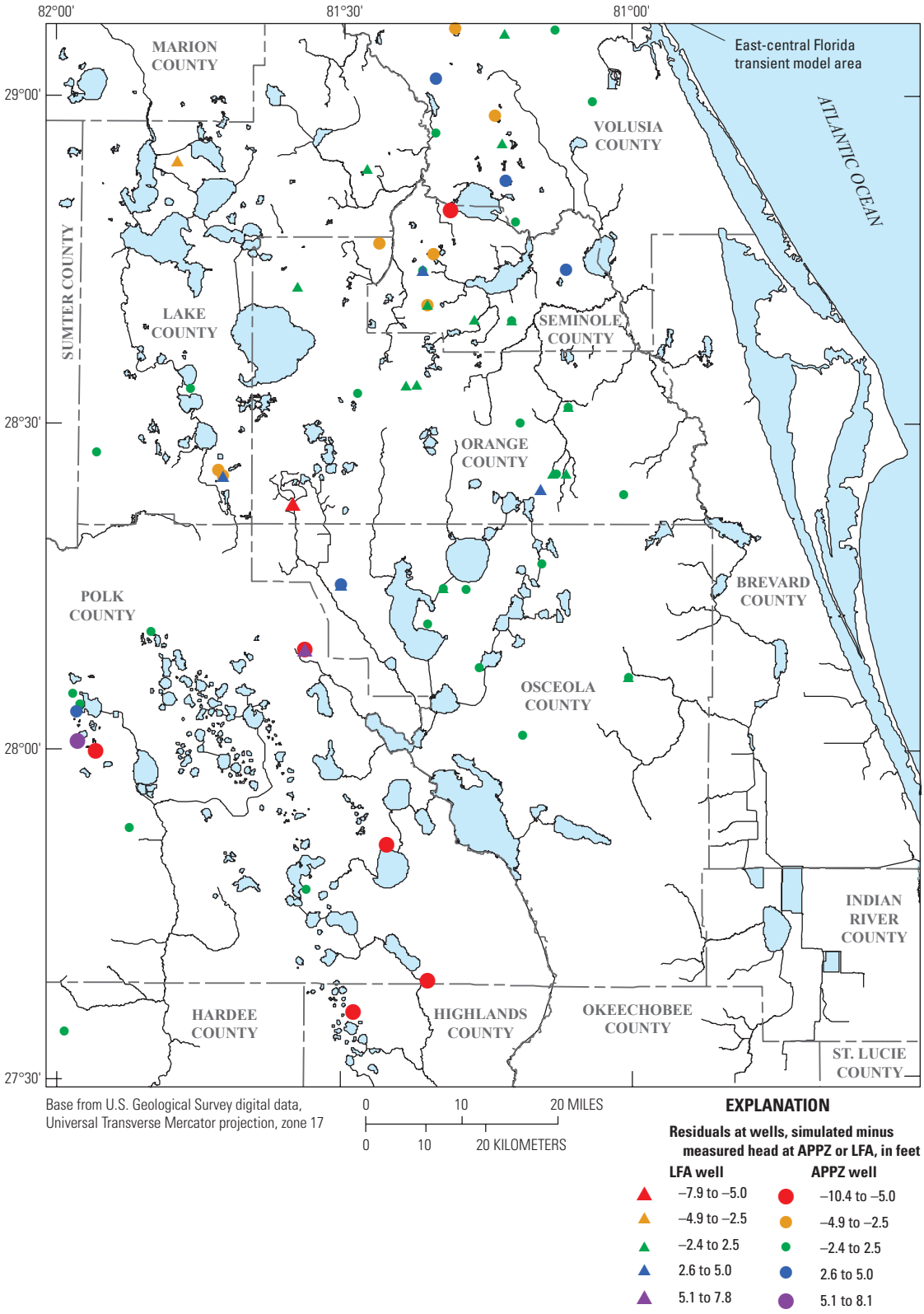

Figure 80. Head residuals for 2006 in Avon Park permeable zone (APPZ, layer 5) and Lower Floridan aquifer (LFA, layer 7) wells, calculated using average annual simulated (from the 12-year model) and observed heads.

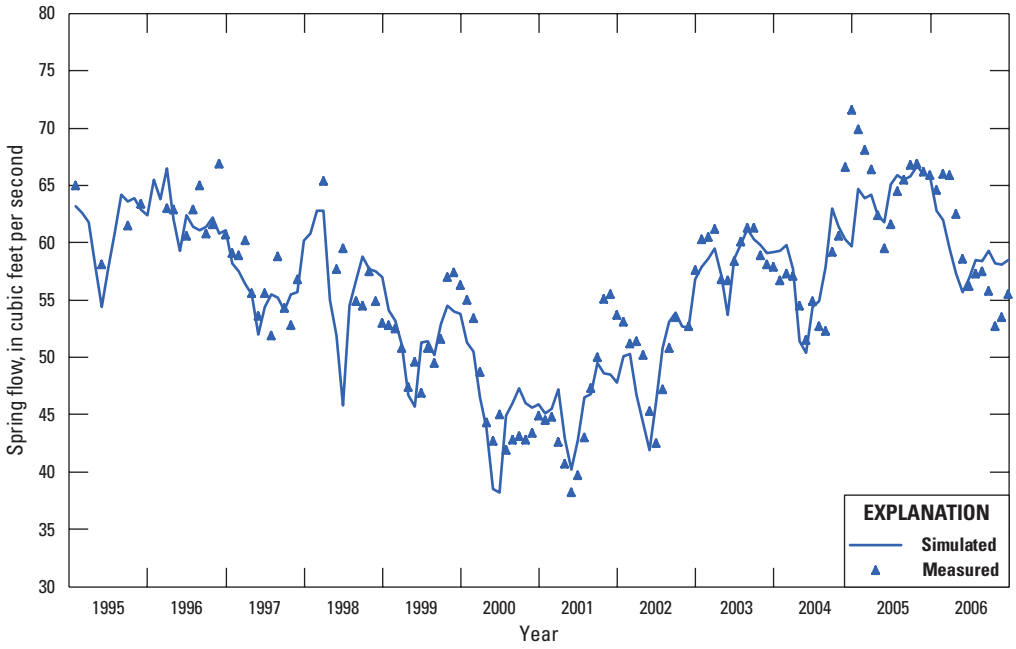

Figure 81. Measured and simulated flows for Rock Springs, spring number 16 in figure 51.

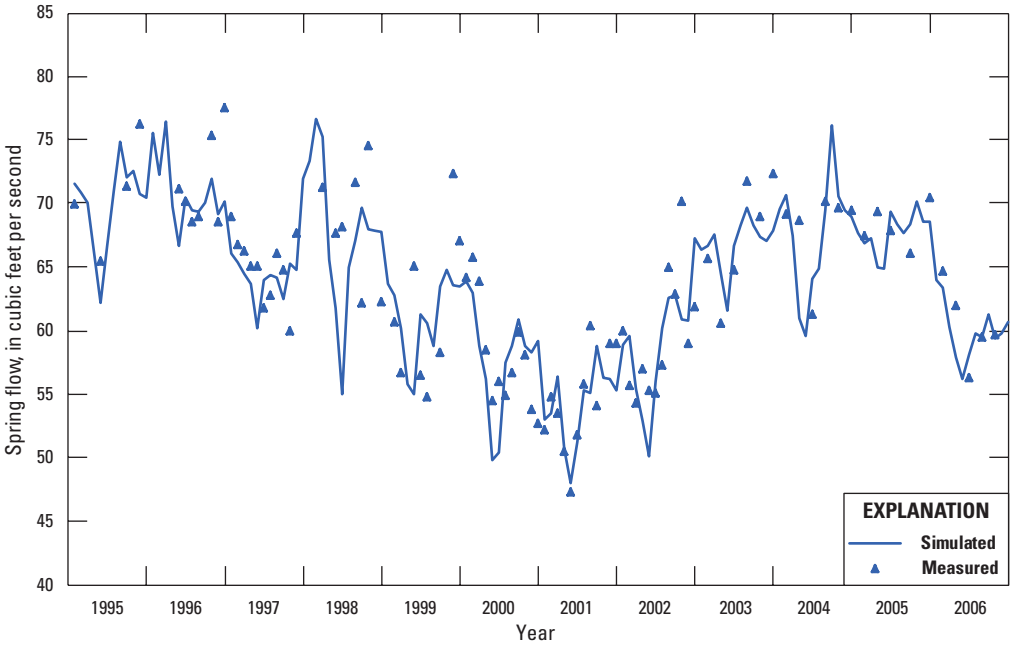

Figure 82. Measured and simulated flows for Wekiwa Springs, spring number 21 in figure 51.

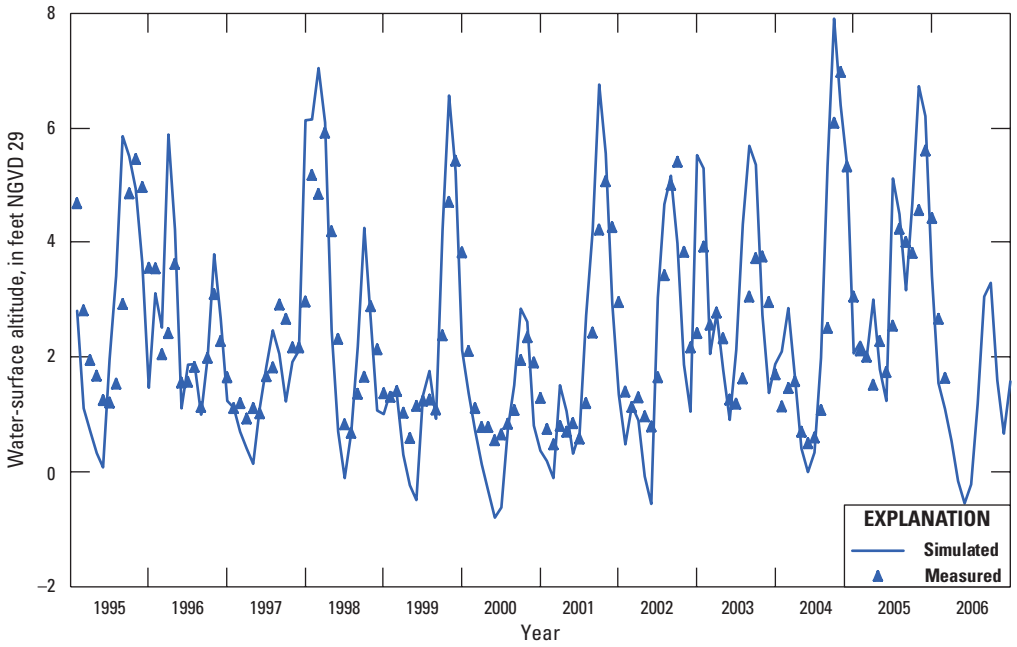

Figure 83. Measured and simulated water-surface altitude hydrographs for Lake Monroe, lake number 38 in figure 13.

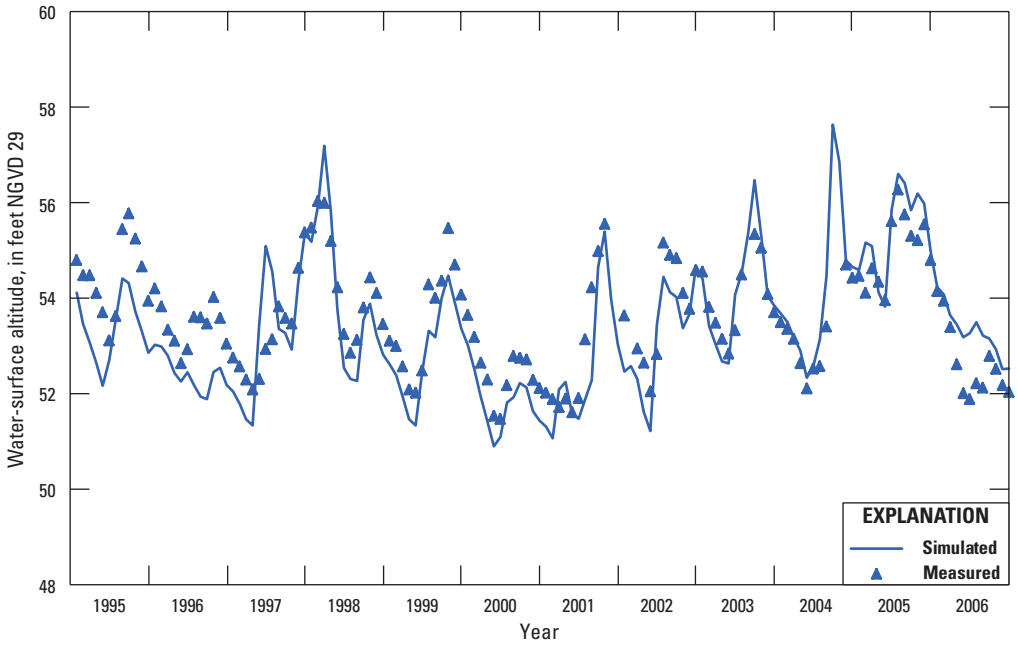

Figure 84. Measured and simulated water-surface altitude hydrographs for Lake Arbuckle, lake number 271 in figure 13.

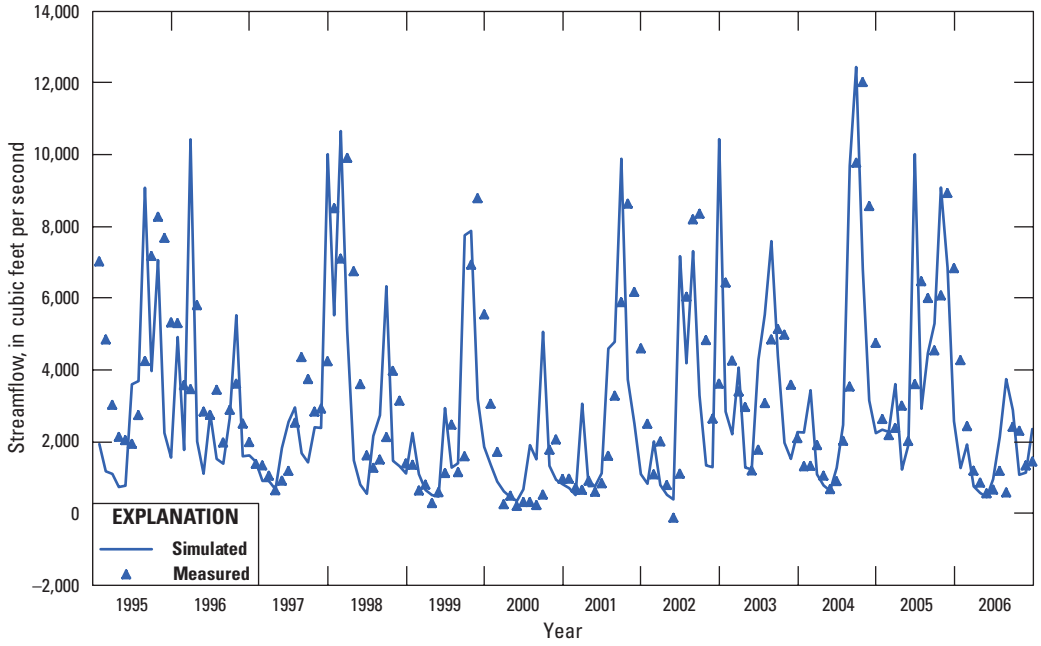

Figure 85. Measured and simulated flow hydrographs for St. Johns River station number 02236000 in figure 11.

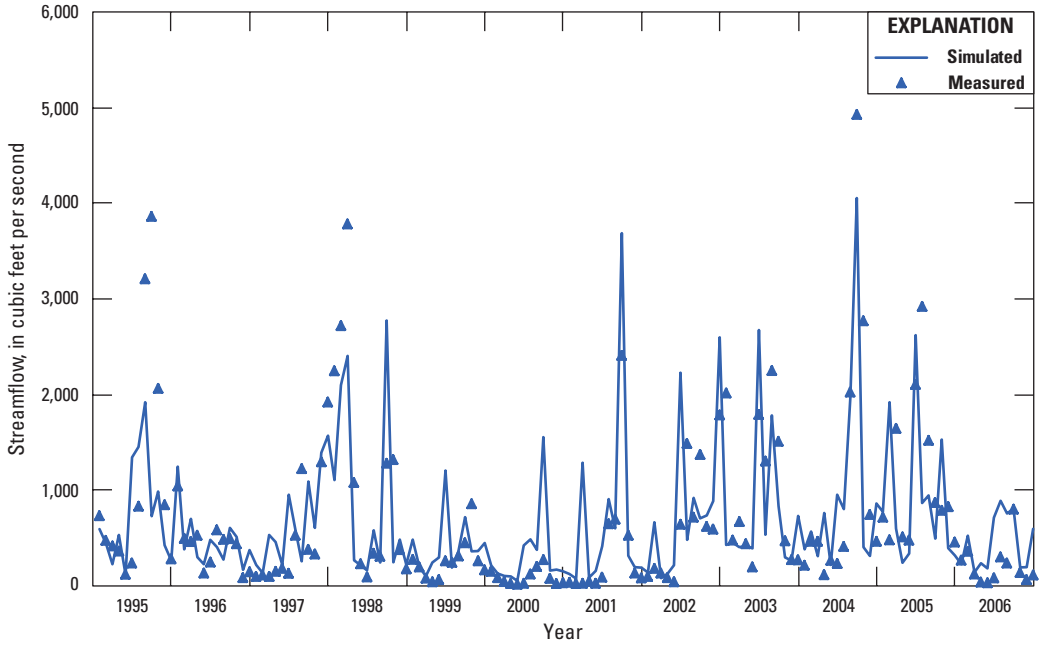

Figure 86. Measured and simulated flow hydrographs for Peace River station number 02295637 in figure 11.

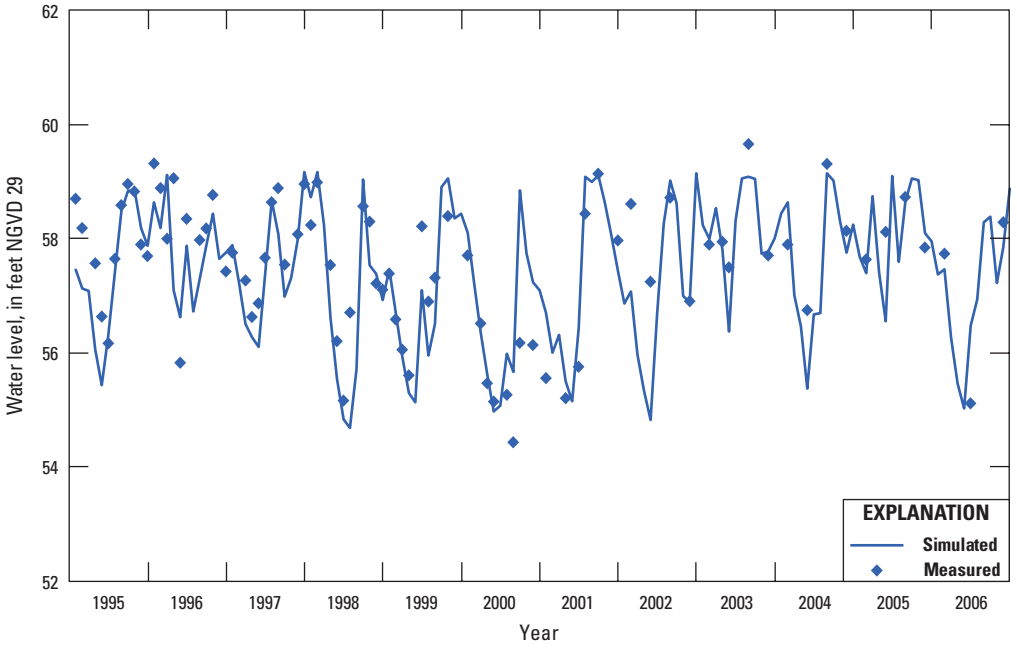

Figure 87. Measured and simulated water-level hydrographs for Cocoa K, well number 2 in figure 5–1.

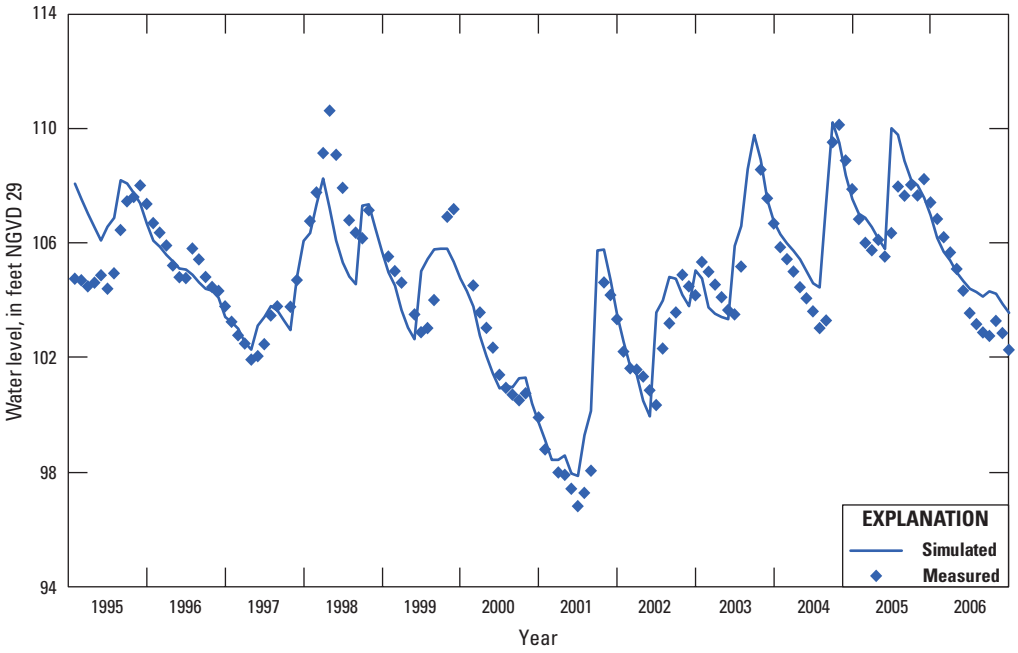

Figure 88. Measured and simulated water-level hydrographs for Ridge Wrap H-1, well number 13 in figure 5–1.

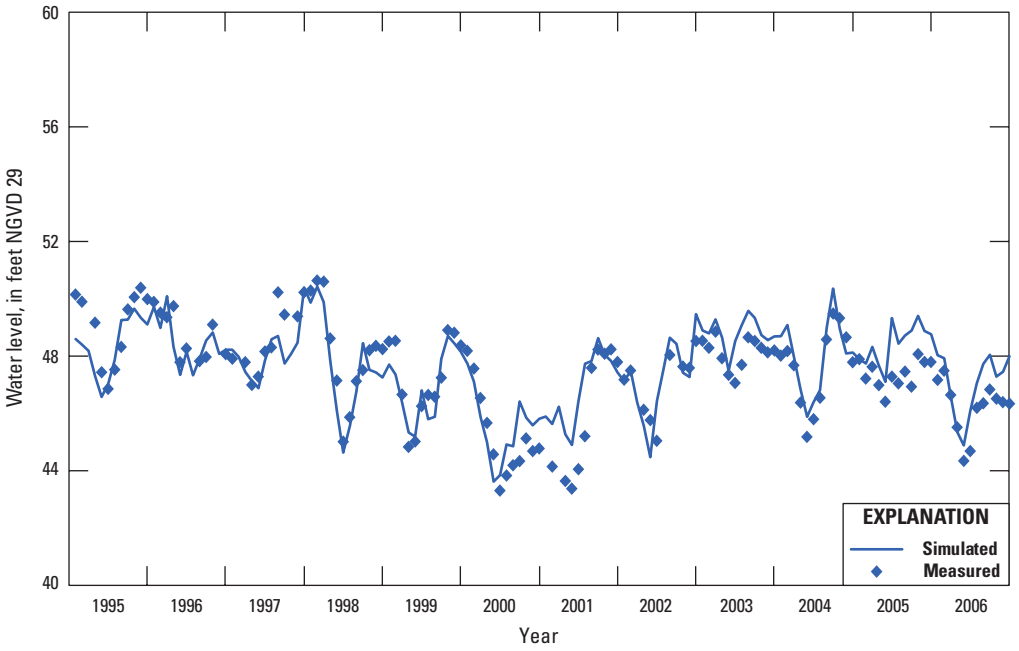

Figure 89. Measured and simulated water-level hydrographs for Bithlo 2 ICU, well number 1 in figure 5–17.

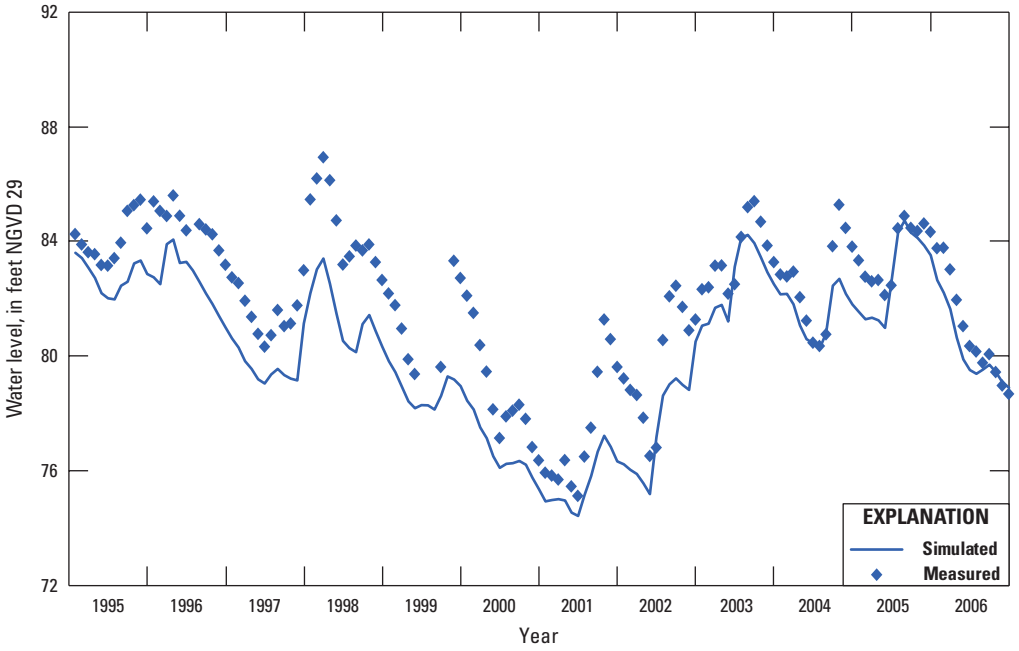

Figure 90. Measured and simulated water-level hydrographs for L-0096 Groveland Fire Tower, well number 4 in figure 5–17.

Well numbers 6 and 20, in figure 5–26 (appendix 5), named L-0059 Crows Bluff NFS and ROMP 58 Ocala, are OPZ wells with respective average measured heads of 17.35 and 97.96 ft for the entire 1995 to 2006 simulation period (figs. 91 and 92). The respective overall mean residuals at these two wells were 0.18 and -0.75 ft, suggesting a negligible bias in head residuals. Additional hydrographs from OPZ wells are shown in figures 5–27 to 5–50 in appendix 5. Hydrographs for the OLPZ are shown in figures 5–52 and 5–53.

Well numbers 1 and 5, in figure 5–54 (appendix 5), named OR-47at Orlo Vista and ROMP deep well 101, are APPZ wells with respective average measured heads of 58.95 and 97.46 ft for the entire 1995 to 2006 simulation period (figs. 93 and 94). The respective overall mean residuals at these two wells were -0.03 and 0.64 ft, suggesting a negligible bias in the head residuals. Additional hydrographs from APPZ wells are shown in figures 5–55 to 5–60 in appendix 5. Hydrographs from the MCU I are shown in figures 5–62 to 5–64.

Well numbers 3 and 7, in figure 5–65 (appendix 5), named OR0614 Cocoa WF Site S zone 3 and OS0025 Bull Creek APT TM2, are LFA wells with respective average measured heads of 36.24 and 41.51 ft from 1995 to 2006 (figs. 95 and 96). The respective overall mean residuals at these two wells were 0.99 and 0.28 ft, suggesting a small bias in the head residuals. Additional hydrographs from LFA wells are shown in figures 5–66 to 5–73 in appendix 5.

Parameter Uncertainty

Groundwater models commonly are developed and calibrated for purposes of making predictions, such as drawdown under conditions of increased pumping. In general, prediction uncertainty is of greater interest and importance than parameter uncertainty. This report, however, does not present predictions using the ECFT model. Therefore, parameter uncertainty, which is a component in the calculation of prediction uncertainty, is used to assess model uncertainty.

Uncertainty in the K values estimated for the ECFT model is calculated using a linear method that considers three types of information about the parameters: (1) information about the spatial variability of Kh, Kv, or the K multiplier in layers where pilot points are used, which is contained in the variograms (equation 5) used for interpolation of the K estimates at the pilot points; (2) information about the ranges of reasonable values for the parameters, which is quantified by the weights on the prior information, and (3) information from the calibration observations, which is represented by the observation sensitivities and weights. The PEST application PREDUNC6 (Doherty, 2010b) enables these sources of information to be included in the calculation of parameter uncertainty. PREDUNC6 is designed to calculate prediction uncertainty, but can be used to calculate parameter uncertainty by defining the model parameters as the predictions.

The types of information just described in (2) and (3) of the previous paragraph have been discussed previously. To include information about spatial variability (item 1 in the previous paragraph), the sill (C_0, equation 5) values of the variograms must be specified. The sill is the variance of the property that is interpolated using the variogram, and is the value of the vertical axis at which the variogram approaches a maximum. Whereas the value of the sill does not affect the interpolated values, it is used to calculate parameter uncertainty. In the context of calculating uncertainty using PREDUNC6, the sill reflects knowledge available prior to model calibration. In the variograms for Kh of layers 2, 3, 5, and 7, the sill is set to 0.68, 0.39, 0.37, and 0.34, respectively. These values are the variances of $\log_{10}$(K) calculated using aquifer test data from the respective layers (figs. 18, 21, 24, 30, and 36). For Kv of layer 2, no such field data are available. Because this property is highly variable, the variance was calculated assuming Kv of layer 2 varies over four orders of magnitude, which is consistent with the estimated values of this property that range from about 0.0001 to 1.0 ft/d. This produces a $\log_{10}$(K) variance of 1.0.

PREDUNC6 computes standard deviations as the measure of parameter uncertainty. These standard deviations are used to compute coefficients of variation that are not log-transformed. Coefficients of variation are dimensionless, and express uncertainty in a manner that can be compared among different parameters. The coefficient of variation cv_{b_j} for parameter b_j is calculated as $cv_{b_j} = \sigma_{b_j} / b_j$, where σ_{b_j} is the standard deviation of b_j. A *cv* of 1.0 indicates the parameter standard deviation is the same magnitude as its estimated value.

Figure 97 shows the range of cv_{b_j} values calculated for the Kh of zones in layer 1, the Kh or Kv of pilot point parameters by layer, and the K multipliers at the spring pilot points. The cv_{b_j} values for estimated parameters not displayed on this figure are as follows: Kv of layer 4, 0.51; Kv of the MCU I in layer 6, 0.08; and Kv of the MCU II in layer 6, 0.31. The coefficients of variation are best evaluated in a relative sense for comparing uncertainty across model layers. Coefficients of variation for layers 4 and 6 and figure 97 show that the uncertainty is smallest for Kh of layer 1, Kv of layer 6, and the K multipliers, and largest for Kh and Kv of layer 2.

The relatively small uncertainty for Kh of layer 1 reflects that (1) zonation is used to represent this property and (2) the reasonable range of values for Kh of the SAS is narrower than that for other hydrogeologic units. The relatively large uncertainty for Kh of layer 2 reflects the small sensitivities of simulated values to this property (fig. 56). The uncertainty for individual pilot points representing Kv of layer 2 is highly variable, as shown by the wide range spanned by the minimum and maximum values on figure 97. This wide range partly reflects the spatial variability of the observation sensitivities to this property. The majority of the cv_{b_j} values for Kv of layer 2 are relatively large compared to those for other layers, because the ranges of reasonable values, and the *a priori* variability, for Kv parameters in layer 2 are larger than those for other hydrogeologic units. For Kh of layers 3 and 5, the sill values are quite similar, and sensitivities to Kh of layer 5 tend to be larger than those to Kh of layer 3 (fig. 56).

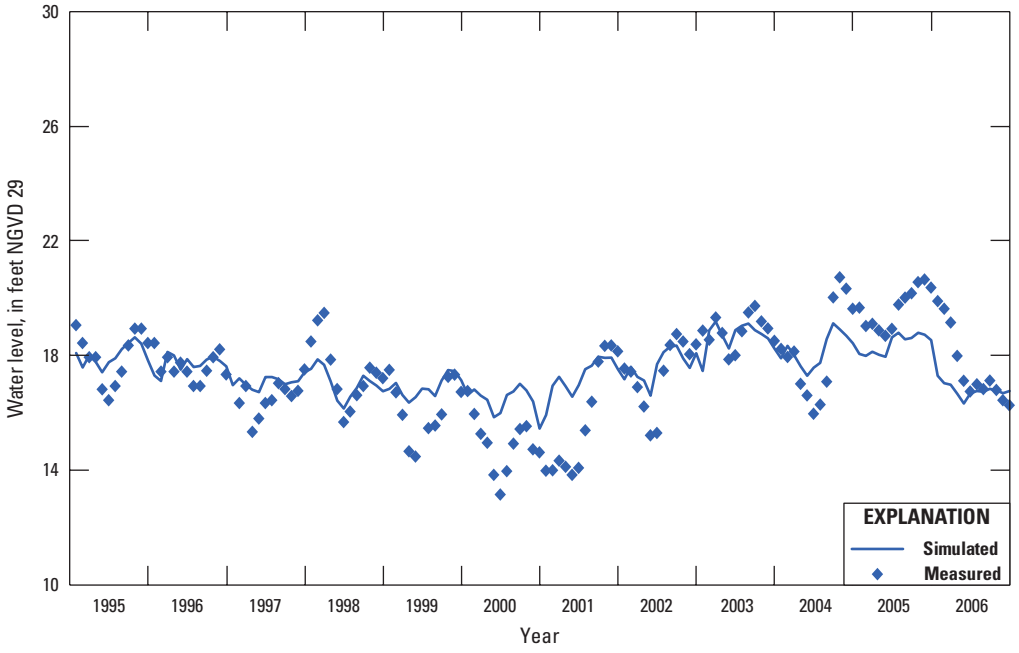

Figure 91. Measured and simulated water-level hydrographs for L-0059 Crows Bluff NFS, well number 6 in figure 5–26.

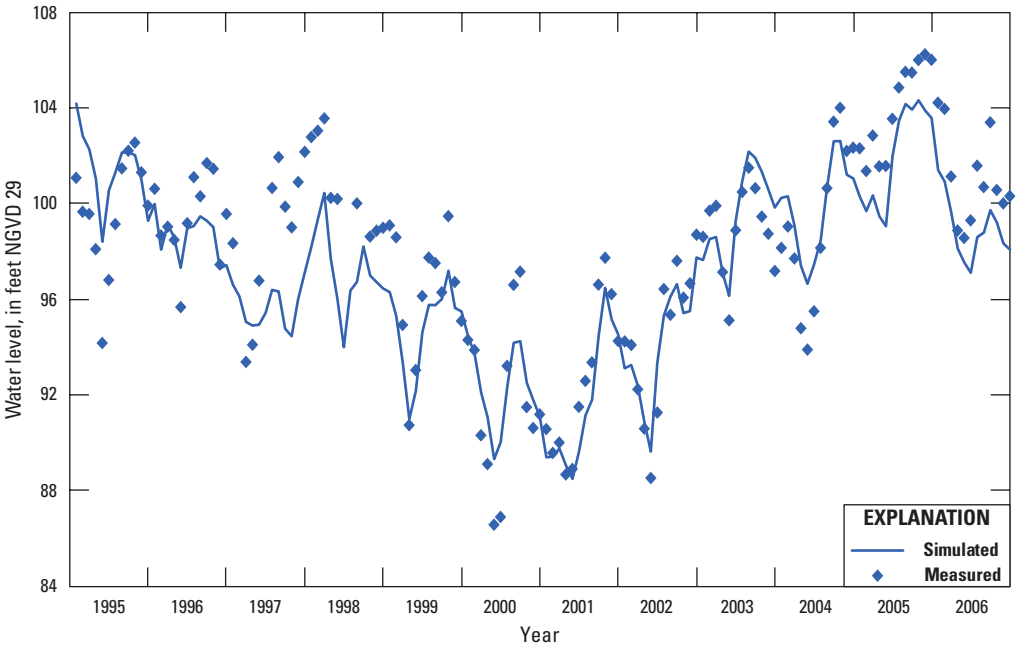

Figure 92. Measured and simulated water-level hydrographs for Regional Observation and Monitor-well Program 58 Ocala, well number 20 in figure 5–26.

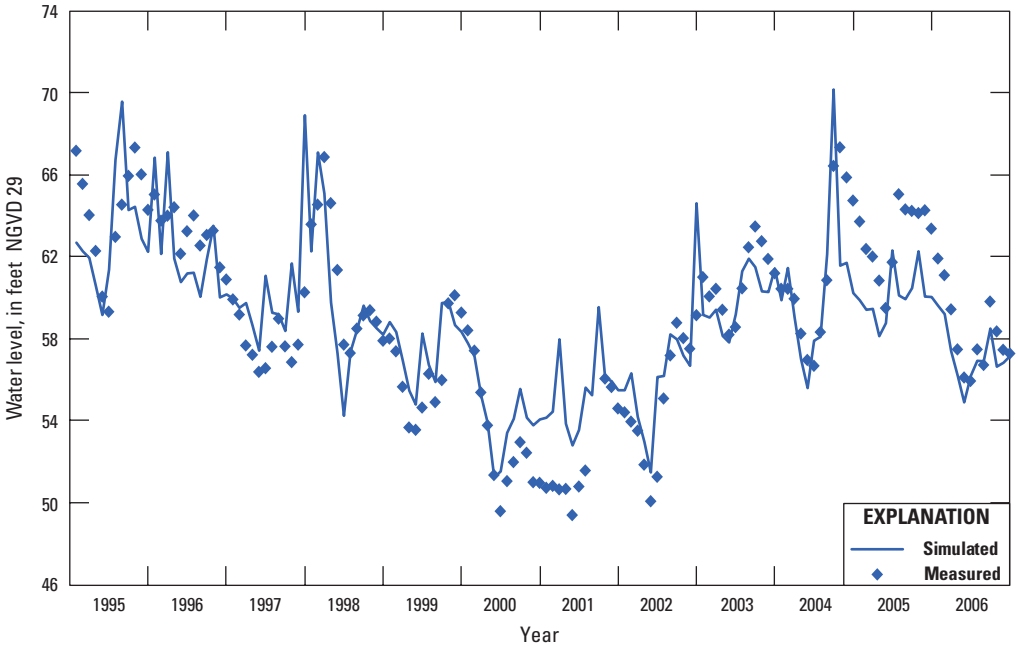

Figure 93. Measured and simulated water-level hydrographs for OR-47 at Orlo Vista, well number 1 in figure 5–54.

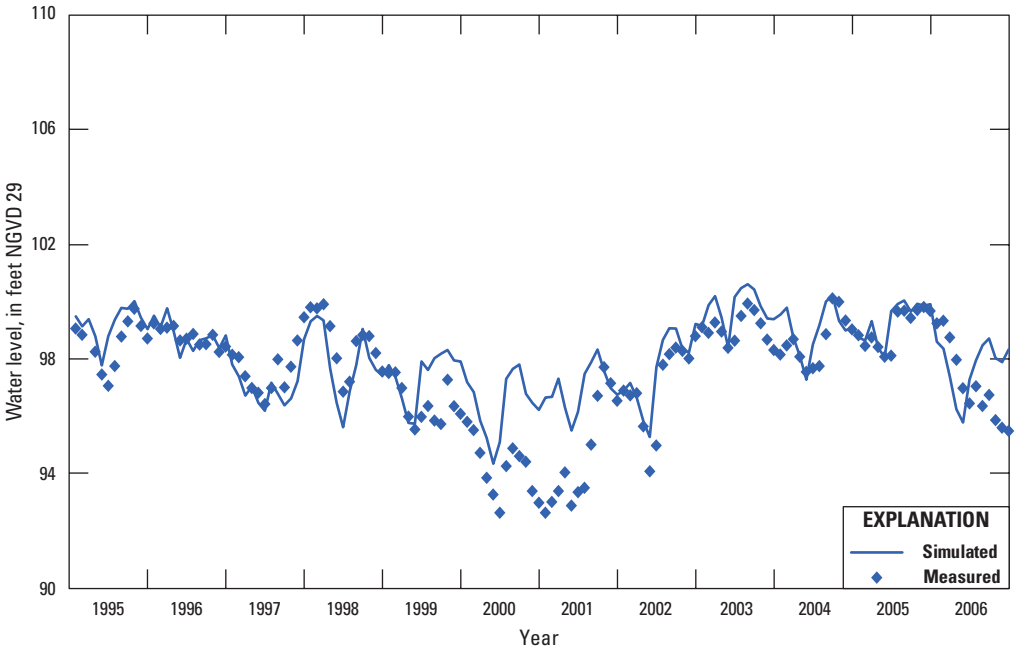

Figure 94. Measured and simulated water-level hydrographs for Regional Observation and Monitor-well Program deep well 101, well number 5 in figure 5–54.

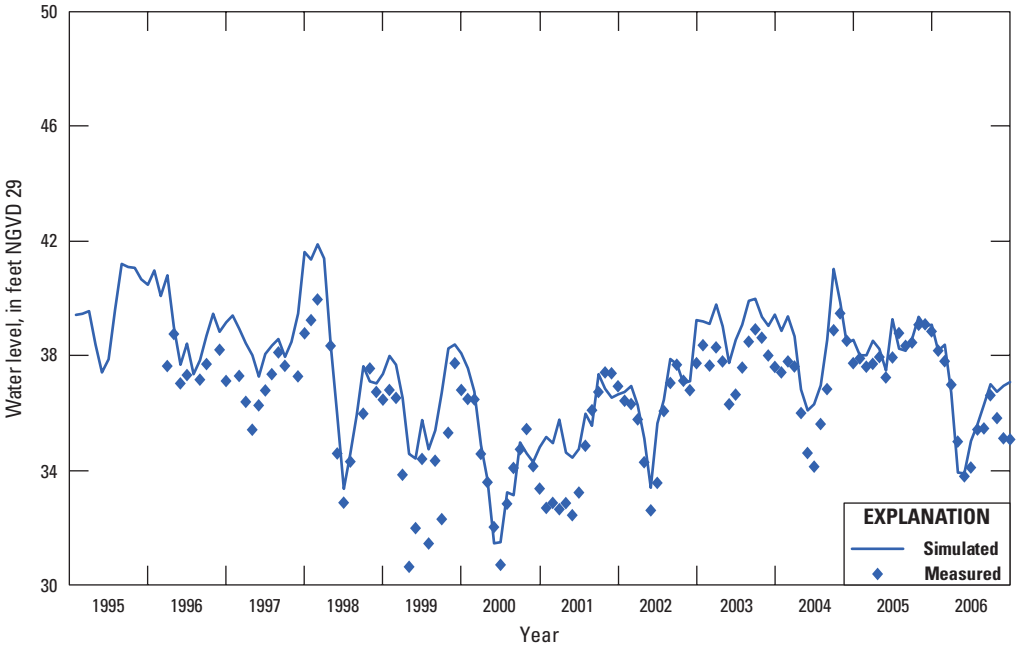

Figure 95. Measured and simulated water-level hydrographs for OR0614 Cocoa WF Site S zone 3, well number 4 in Figure 5–65. Refer to appendix 5 for figure 5–65.

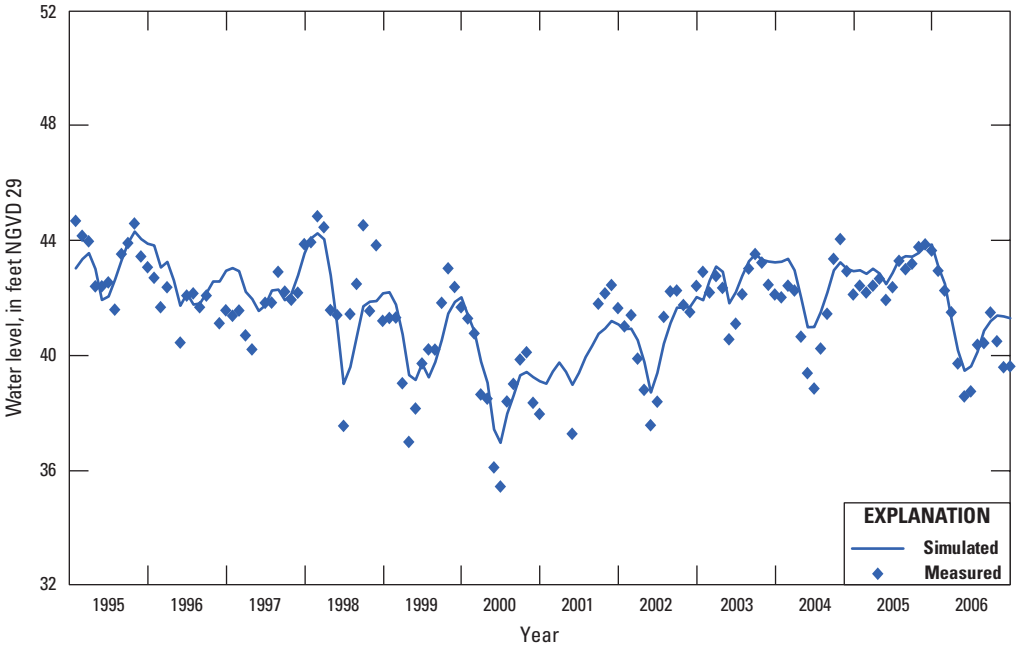

Figure 96. Measured and simulated water-level hydrographs for OS0025 Bull Creek APT TM2, well number 7 in Figure 5–65. Refer to appendix 5 for figure 5–65.

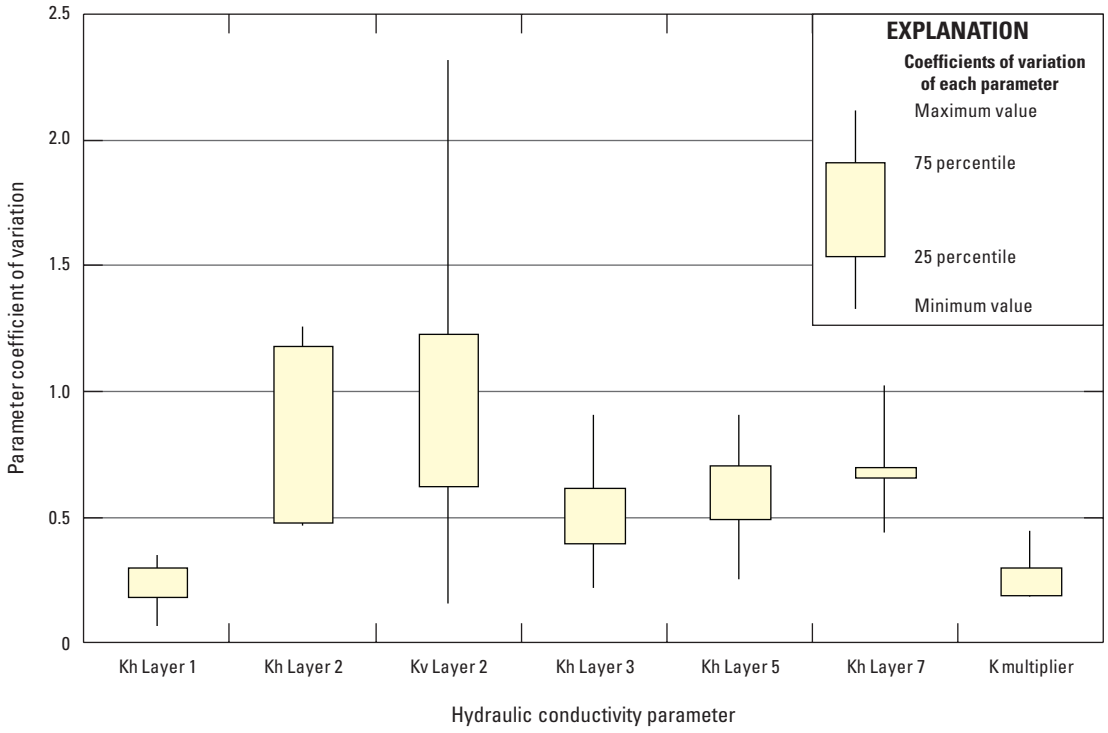

Figure 97. Parameter coefficients of variation. The data summarized by the box plots are Kh of zones in layer 1; Kh or Kv estimates for regional pilot points in layers 2, 3, 5, and 7; and K multiplier estimates for the spring pilot points.

The slightly larger cv_{b_j} for Kh of layer 5 than for Kh of layer 3 (fig. 97), as indicated by the larger values defining the interquartile range, is likely because of the generally wider ranges of reasonable values, and consequent smaller weights on prior information, for Kh of layer 5 compared to layer 3. Uncertainties for Kh of layer 7 are somewhat larger than those for layers 3 and 5, reflecting smaller sensitivities compared to layer 5, and wider ranges of reasonable values compared to layer 3.

It is important to assess the K estimates for the ECFT model in the context of the parameter uncertainty shown in figure 97. This uncertainty means that although the estimates presented herein are reasonable in the sense of not violating known or inferred information about the hydrogeologic properties of the model flow system, and produce a fit to the observations that meets the calibration criteria, it is highly likely that there are other distributions of model parameters or variations in the existing estimates that would also be reasonable and would fit the calibration data equally well. The existence of such alternative parameter distributions is especially likely when highly parameterized methods are used for representing flow system properties. Nonlinear uncertainty methods, such as Monte Carlo simulations, can be used to explore such alternative parameter distributions, but were beyond the scope of work for this study.

Simulated Potentiometric Surfaces

Simulated potentiometric surfaces for 1999, generated from the simulated heads from the 12-year transient simulation, are used to identify regional flow features. Simulated potentiometric surfaces for other years have the same general flow features present in the 1999 potentiometric surfaces. The average simulated water-table altitude for 1999, which is represented by the simulated head in layer 1 (SAS), generated from the 12-year transient model, reflects low water-table altitudes along the St. Johns River and extending to the eastern valley, along the Kissimmee River, and along the Peace River (figs. 1, 2, and 98). As expected, the altitude of the simulated water table was highest in the ridges (physiographic regions 8, 13, 14, 15, and 17 through 20) and uplands (regions 2 and 9 through 11, figs. 2 and 98).

The decline in the simulated water-table altitude from the eastern edge of the Lake Wales Ridge to the western edge of the Osceola and Wekiva Plains generates large horizontal hydraulic gradients in the SAS, given the magnitude of the water-level differences and the areal proximity between these two regions (figs. 2 and 98). The simulated west-to-east lateral flow in the SAS becomes surface leakage when such flow intercepts land surface along areas of the Osceola and Wekiva Plains. Surface leakage is also simulated elsewhere wherever

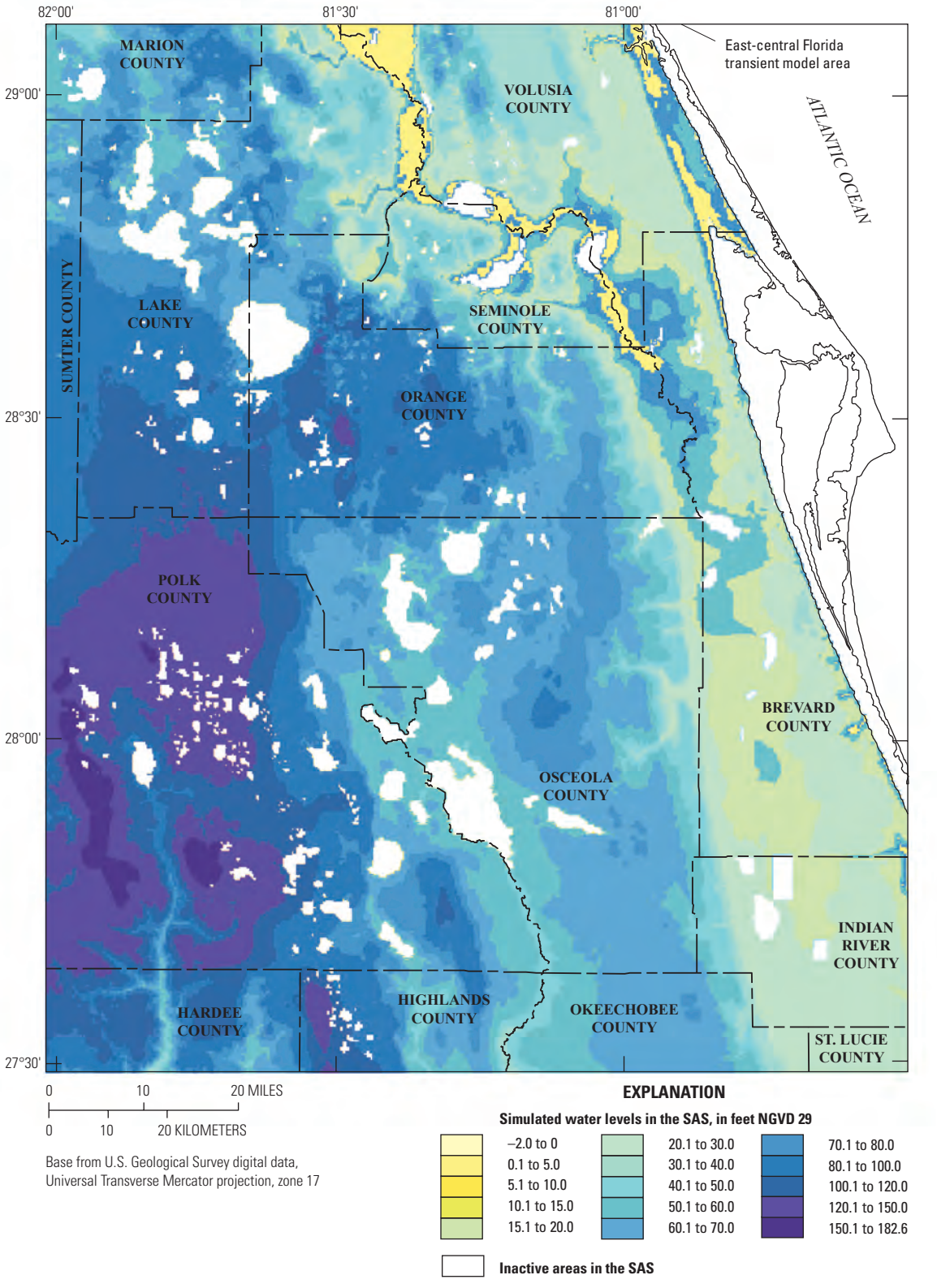

Figure 98. Average simulated water table in the surficial aquifer system (SAS, layer 1) for 1999, from the 12-year transient model.

similar horizontal hydraulic gradients exist in the SAS and flow intercepts land surface.

The simulated potentiometric surface of layer 3, which represents average annual conditions for the OPZ during 1999, reflects the main general features of the potentiometric surface of the OPZ for 1995 developed from observed water levels (figs. 25 and 99). The potentiometric-surface highs in north-central Polk County and in central Volusia County were reasonably well simulated, as was the configuration of the decreasing heads away from these potentiometric highs. The potentiometric-surface depressions along the St. Johns River are also present in the simulated potentiometric surface for layer 3 (OPZ, fig. 99). The depressions in the simulated potentiometric surface of layer 3 (OPZ) in the northern section of the model, along the St. Johns River, are the result of flow from Blue Spring leaving the OPZ. This feature is also present in the observed potentiometric surface of layer 3 (OPZ, fig. 25).

The differences in the simulated potentiometric surfaces between layers 3 and 5 (OPZ and APPZ) are generally small except in the northeastern section of the model area, explained in part by the differences in the extent of active areas between the two layers (figs. 99 and 100). A much larger calibrated Kh for layer 5 than for layer 3 along the southeastern part of the model area (figs. 67 and 69) could suggest a large resulting simulated hydraulic gradient between these units; however, the low simulated and measured hydraulic differences between these simulated potentiometric surfaces can be explained by the large Kv of layer 4, representing the OLPZ (fig. 68) compared, for example, to layer 2, representing the ICU (fig. 66).

The simulated potentiometric surface of layer 7, representing the LFA, reflects heads nearly 40 ft lower in the southwestern part of the model area (fig. 101) compared to the corresponding heads in layer 5, representing the APPZ; these differences were simulated but also are observed between the LFA and APPZ (fig. 31). Differences in simulated heads between the APPZ and the LFA (fig. 31), where MCU I is present, are smaller than in areas where these aquifers are separated by MCU II. The large vertical head differences between the two aquifers in the southwestern part of the model area are explained by the low permeability of the intervening MCU II (figs. 31 and 70). The dominant eastward flow component in the LFA along most of the eastern edge of the LFA is explained by the combination of (1) relatively greater hydraulic conductivity of the LFA in western and central Orange County (fig. 71), (2) a relatively permeable overlying MCU I unit, compared to the MCU II unit to the west, and (3) the induced flow caused by the large groundwater withdrawals that take place in the LFA in Orange County (figs. 39*B* and 40*B*). Although heads in the eastern edge of the LFA mimic the heads in the APPZ with differences of only several feet, heads throughout the southwestern part of the LFA are at least 20 ft below the corresponding heads in the APPZ.

Simulated Groundwater Flows and Water Budget

The calculation of simulated-flow terms in the unsaturated zone and in layer 1 allows the comparison between the simulated ET and recharge rates to layer 1 and those rates derived from both measured and estimated flows (table 5). This comparison is accomplished by using the cell-by-cell flow data generated from the 12-year transient model for layer 1 (representing the SAS). Simulated net recharge rates to the SAS (NRCH, table 17) and estimated net recharge to the SAS (RCH, table 5) differed by less than 1.2 in/yr for each simulated year. These differences in flow terms from one year to another between simulated and estimated rates are within the inaccuracies of estimated flows in the water-budget analysis of the SAS. The calibration process required the adjustment of the hydraulic conductivity of the soil used in the Green-Ampt infiltration (GAI) method to determine the infiltration rates to the unsaturated zone and the adjustment of the regression coefficients used to estimate actual ET rates from potential ET rates. Each one of these parameters was systematically adjusted to either increase or decrease recharge rates to the SAS to match the rates listed in table 5. These modifications to the recharge parameters preceded every PEST simulation of the steady-state models for 1999 and 2003. The adjustment of parameters that reduce the differences between simulated and estimated recharge rates to the SAS was limited to using only realistic parameter values. Surface leakage (ASL, table 17) is the simulated groundwater seepage in the SAS reduced by the difference between potential ET and simulated ET at closed basin cells (fig. 7). ET losses in the unsaturated zone (UZET, table 17) were increased by the same difference before net recharge rates were calculated. In addition, ASL was further reduced by the flows at cells draining to streams or to lakes because those flows are part of the total streamflow (STFL, table 17). Equivalently, ASL in table 17 refers to groundwater discharge (in the form of seepage) in closed basin cells or in cells draining to streams or lakes outside the model. Average net simulated recharge to the SAS for the 12-year period of simulation was 3.58 in/yr (NRCH, table 17).

The simulated changes in storage in the SAS (STO, table 18) show years 2000 and 2006 as those with the largest changes in storage, coinciding with being the driest periods of the 12 years simulated. Net leakage from the SAS to streams was at least five times greater than the net leakage from the SAS to the lakes (STRS and LKSP, table 18). The simulated net leakage between the SAS and ICU/IAS (FLN, table 18) was used as an estimate for net downward leakage from the SAS to the underlying ICU/IAS (VLICU, table 5) because of the lack of measured data to complete the estimation of ET rates and recharge rates for the SAS. The two flows, VLICU and FLN, are equivalent.

The differences between the estimated and simulated ET rates (EET, table 5; SET, table 17) and between estimated and

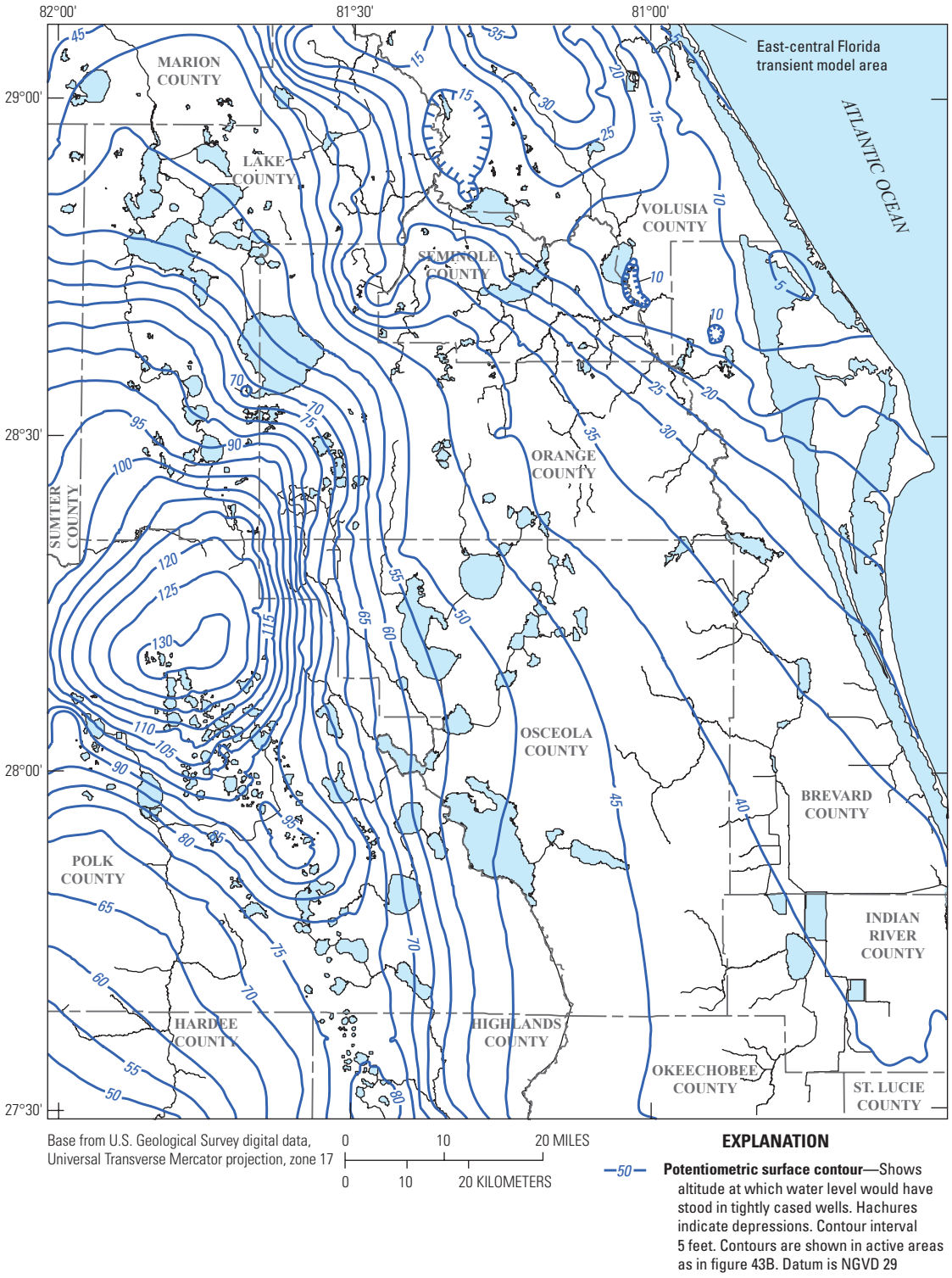

Figure 99. Average simulated potentiometric surface of the Ocala permeable zone (OPZ, layer 3) for 1999, from the 12-year transient model.

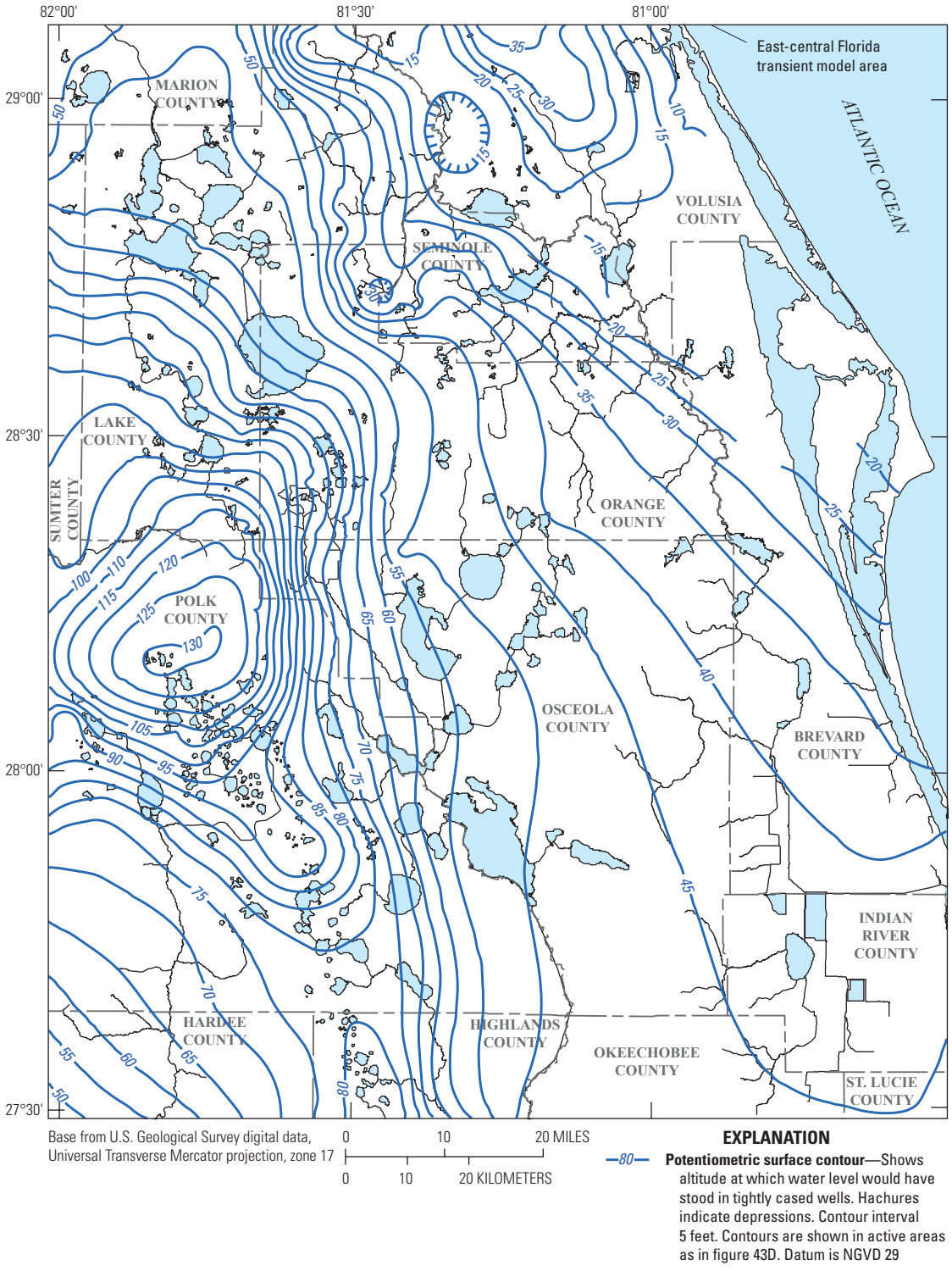

Figure 100. Average simulated potentiometric surface of the Avon Park permeable zone (APPZ, layer 5) for 1999, from the 12-year transient model.

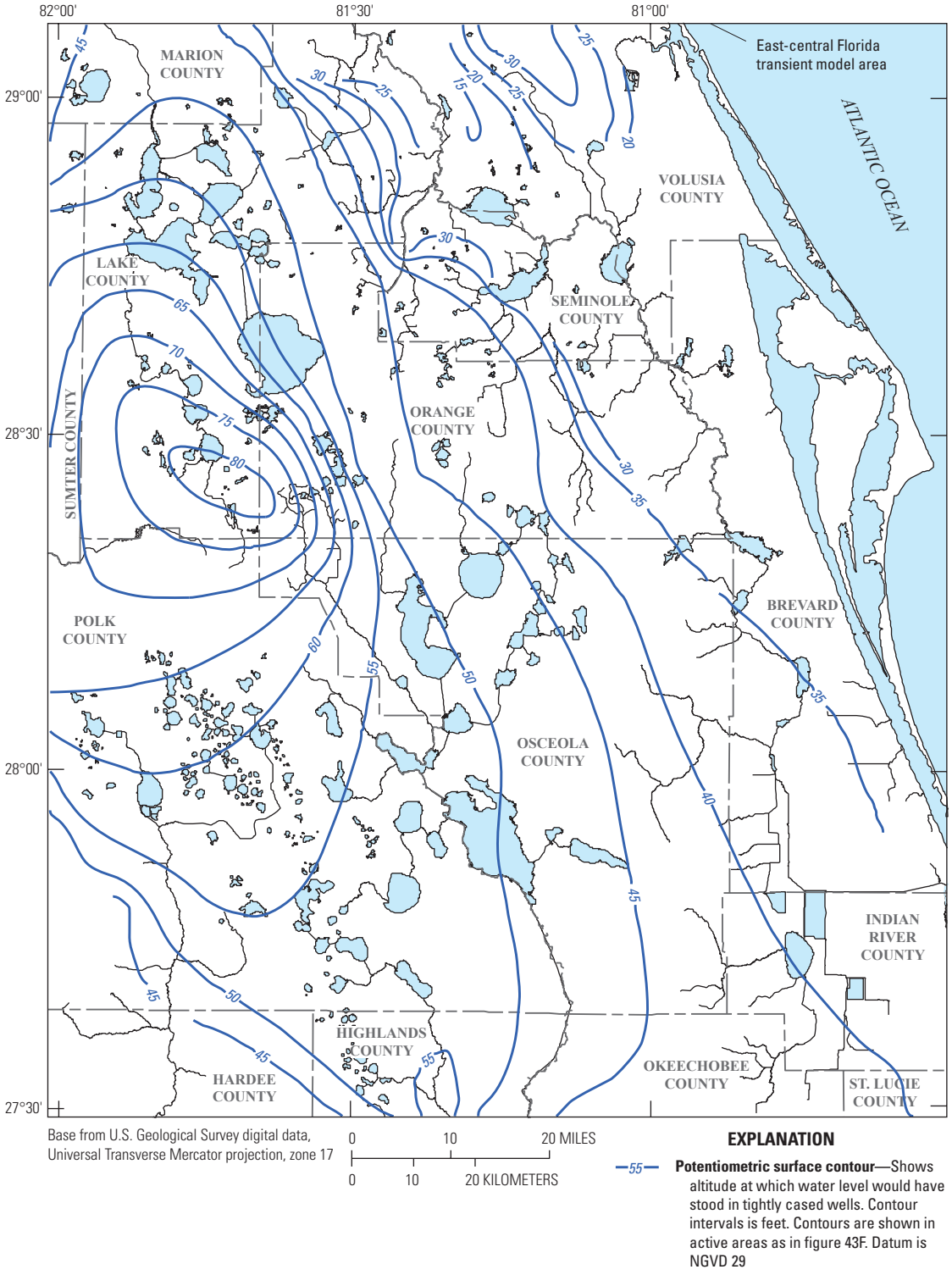

Figure 101. Average simulated potentiometric surface of the Lower Floridan aquifer (LFA, layer 7) for 1999, from the 12-year transient model.

Table 17. Simulated evapotranspiration (ET) and recharge rates to the surficial aquifer system (SAS, layer 1) from the calibrated transient model of 1995 to 2006.

[R, rainfall plus irrigation; LET, simulated ET at the lakes; STET, simulated ET at the streams; UZET, simulated ET in the unsaturated zone; GWET, simulated ET in the SAS; SET, total simulated ET, equal to LET+STET+UZET+GWET; STFL, streamflow leaving the model area; ASL, adjusted surface leakage after meeting potential ET in closed basins; NRCH, net recharge to the SAS, equal to R+SET+STFL+ASL; Ave, average rate for the 1995–2006 period; all rates are in inches per year; conversion to ft^3/s should use the combined 160,651 cells between 150,651 active cells in the SAS and 10,000 lake cells; negative flows indicate outflows to the model area, whereas positive flows indicate inflows]

Year	R	LET	STET	UZET	GWET	SET	STFL	ASL	NRCH
1995	53.12	–3.78	–0.02	–12.39	–20.53	–36.72	–11.48	–1.50	3.42
1996	50.13	–3.79	–0.02	–11.79	–19.82	–35.42	–10.50	–1.34	2.87
1997	54.78	–3.77	–0.02	–15.46	–17.66	–36.91	–11.29	–1.11	5.47
1998	49.39	–3.77	–0.02	–10.89	–17.73	–32.41	–13.49	–1.55	1.94
1999	49.60	–3.80	–0.02	–12.73	–18.38	–34.93	–8.54	–1.07	5.06
2000	31.72	–3.86	–0.02	–9.23	–13.29	–26.40	–4.87	–0.53	–0.08
2001	50.96	–3.57	–0.02	–12.24	–17.84	–33.67	–10.35	–1.14	5.80
2002	60.41	–3.67	–0.02	–12.46	–21.56	–37.71	–14.69	–1.71	6.30
2003	53.04	–3.51	–0.02	–9.16	–22.49	–35.18	–12.97	–2.04	2.85
2004	58.78	–3.64	–0.02	–13.06	–20.36	–37.08	–16.12	–1.77	3.81
2005	61.46	–3.65	–0.02	–10.95	–23.46	–38.08	–16.43	–2.37	4.58
2006	37.14	–3.91	–0.02	–9.39	–15.86	–29.18	–6.31	–0.82	0.83
Ave	**50.88**	**–3.73**	**–0.02**	**–11.64**	**–19.08**	**–34.47**	**–11.42**	**–1.41**	**3.58**

Table 18. Simulated flows entering and leaving the surficial aquifer system (SAS, layer 1) from the calibrated transient model of 1995 to 2006.

[SAS, surficial aquifer system; STO, amount of water from storage to/from the SAS; FLN, net downward flow to the ICU/IAS; GWW, net flow to the SAS from Rapid Infiltration Basins (RIBs) and wells; GHBF, net flow through the lateral boundaries of the model; GWET, simulated ET from the SAS; UZRCH, recharge from the unsaturated zone, before reducing it by GWET; SL, surface leakage, unreduced in closed basins; STRS, stream seepage; LKSP, lake seepage; Ave, average rate for the 1995–2006 period; all rates are in inches per year; negative flows indicate outflows to the SAS area,whereas positive flows indicate inflows]

Year	STO	FLN	GWW	GHBF	GWET	UZRCH	SL	STRS	LKSP
1995	0.68	–3.44	0.05	–0.02	–20.53	28.89	–5.55	–0.07	–0.01
1996	1.58	–3.64	0.06	–0.01	–19.82	27.53	–5.61	–0.08	–0.01
1997	–0.56	–3.49	0.04	–0.02	–17.66	26.61	–4.84	–0.07	–0.01
1998	1.81	–3.72	0.05	0.00	–17.73	26.59	–6.93	–0.06	–0.01
1999	0.18	–3.86	0.04	–0.05	–18.38	27.50	–5.34	–0.08	–0.01
2000	2.83	–4.05	0.07	–0.06	–13.29	17.68	–3.06	–0.11	–0.01
2001	–0.78	–3.71	0.05	–0.05	–17.84	27.58	–5.17	–0.07	–0.01
2002	–1.11	–3.69	0.07	–0.02	–21.56	33.62	–7.24	–0.06	–0.01
2003	1.62	–3.49	0.07	0.00	–22.49	32.52	–8.15	–0.07	–0.01
2004	0.97	–3.48	0.07	–0.01	–20.36	29.63	–6.76	–0.05	–0.01
2005	0.97	–3.46	0.09	0.01	–23.46	34.49	–8.58	–0.05	–0.01
2006	1.85	–3.90	0.08	–0.03	–15.86	22.25	–4.27	–0.11	–0.01
Ave	**0.84**	**–3.66**	**0.06**	**–0.02**	**–19.08**	**27.90**	**–5.96**	**–0.07**	**–0.01**

simulated recharge rates (RCH, table 5; NRCH, table 17) in the model area were the largest for the years 1997 and 2002. The parameters that determine the simulated ET rates were the same parameters used to modify the recharge rates to the SAS. Differences between simulated and estimated ET and recharge rates could be explained by the fact that the UZF1 Package simulates only ET from the subsurface and not direct evaporation of water at the canopy or at land surface. This simulation assumption could result in greater errors particularly during years when rainfall events result in extensive surface ponding causing actual ET rates to increase. If the estimated ET rates are increased by increasing the multiplicative factors applied to potential ET rates, then simulated recharge rates actually decrease. Thus, to avoid underestimating the water table, the simulated ET rates are mostly slightly lower than the estimated ET rates in table 5 for the SAS.

The simulated ET rates for 1999 were lowest in the ridges and upland physiographic regions and highest in lakes, in and near wetlands, and in areas where the water table is near land surface (figs. 98 and 102). Potential ET rates were applied at lakes, explaining the reason for the highest simulated ET rates. Low simulated ET rates in the ridges and uplands can be explained by the fact that ET losses at land surface (from surface-water bodies) are accounted for in the Lake and Streamflow Routing Packages of MODFLOW-2005 (Harbaugh, 2005), but not in the UZF1 Package.

The specified ET rates input to the UZF1 Package were generally greater than the simulated ET rates. These differences are mostly explained by the fact that simulated ET in the unsaturated zone, as calculated by the UZF1 Package, is limited by available water. This is particularly true during dry months when there is insufficient water in the unsaturated zone for evaporation or if the water table is below the extinction depth. The UZF1 Package simulates ET from specified rates, which are calculated by adjustments to the regression coefficients (less than 1) to potential ET rates from the USGS Florida Water Science Center Statewide Evapotranspiration Database (U.S. Geological Survey, 2012). Because the simulated ET rates (fig. 102) account only for ET from the unsaturated zone and from groundwater, they should be less than actual ET rates that account for ET losses from the canopy and land surface.

Simulated annual net recharge rates to layer 1, representing the SAS, in 1999 (fig. 103) were calculated by subtracting the simulated groundwater ET rates and the simulated surface leakage from the simulated recharge to the unsaturated zone. Recharge rates were greatest in areas where the sum of rainfall (fig. 9) and landscape and agricultural irrigation rates (fig. 46) were greatest. Recharge rates to layer 1 do not consider the inflow to the SAS from rapid infiltration basins (RIBs), because such rates were simulated as injection wells, and thus, were simulated in the Well Package. The ridge areas had larger recharge rates to the SAS than any other physiographic region. Large discharge rates in layer 1 were simulated along the eastern edge of the Lake Wales Ridge and the western edge of the Osceola and Wekiva Plains (figs. 2 and 103). These discharge rates correspond to the surface leakage simulated by the UZF1, where relatively large topographic/altitude gradients in the land-surface altitude occur, allowing lateral discharge from layer 1.

Average simulated net recharge for 1999 was almost twice that for 2003, although total rainfall was greater in 1999 than in 2003 (RCH, table 5; NRCH, table 17). The water-budget analysis presented in table 5 supports the simulation finding that one year with higher average rainfall had less average net recharge than another year with lower average rainfall. Measured streamflow for 1999 was about half the measured streamflow for 2003 (SFG+SFU values, table 5). Simulated streamflow in 1999 also was lower than that in 2003 (STFL, table 17). During wetter years, antecedent soil moisture is larger between rainfall events, resulting in greater runoff than during drier years. The year that preceded 2003 was wet, whereas the year that preceded 1999 was dry. Both measured and simulated streamflow during 2003 were greater than during 1999, which justifies why both estimated and simulated annual average recharge rates over the SAS were greater during 1999 than in 2003. This observation holds when the annual average recharge rates are calculated over the entire SAS. Recharge rates to the SAS in the ridges and uplands (fig. 2) were higher in 2003 than in 1999, but discharge zones in 2003 were more areally extensive than in 1999, which resulted in a lower average annual recharge rate for 2003 than for 1999 over all active cells in the SAS.

Calibrated lakebed leakance for lakes ranged from 0.00002 to 0.1 d^{-1} over the ECFT model area. Lakebed leakance affects the flow between layer 1, which represents the SAS, and layer 2, which represents the ICU/IAS. Lakebed leakance specified for lake cells along the perimeter of each lake and the difference between the water-table altitude and the water-surface altitude at the lake determined the lateral leakage rate between layer 1 and the lake. The average lateral leakage rate among cells with negative leakage rates (where flow is from layer 1 to the lakes) was -0.59 in/yr, the average lateral leakage rate among cells with positive leakage rates was 0.33 in/yr, and the overall average lateral leakage rate was -0.36 in/yr. When all 5,361 perimeter cells around lakes were considered, 3,360 lateral leakage rates were less than -0.1 in/yr, 704 rates were greater than 0.1 in/yr, and 1,297 rates were between -0.1 and 0.1 in/yr. The largest simulated lateral leakage rate to a lake from layer 1, 10.31 in/yr for 1999, was at lake number 263 in Polk County (figs. 13 and 104). The largest simulated lateral leakage rate to layer 1 from a lake, 12.32 in/yr for 1999, was simulated at lake number 318 in northeastern Lake County (fig. 13), where Wolf Branch Creek (fig. 1), represented by stream segment 268 in figure 11, discharges its flow (fig. 104).

The Lake Package in MODFLOW assumes that each lake is characterized by only a single value of lakebed leakance. Lakebed leakance specified for lake cells and the difference between the water-surface altitude at the lake and the head in layer 2, which represents the ICU/IAS, determined the simulated vertical leakage rate between the lake and layer 2. The

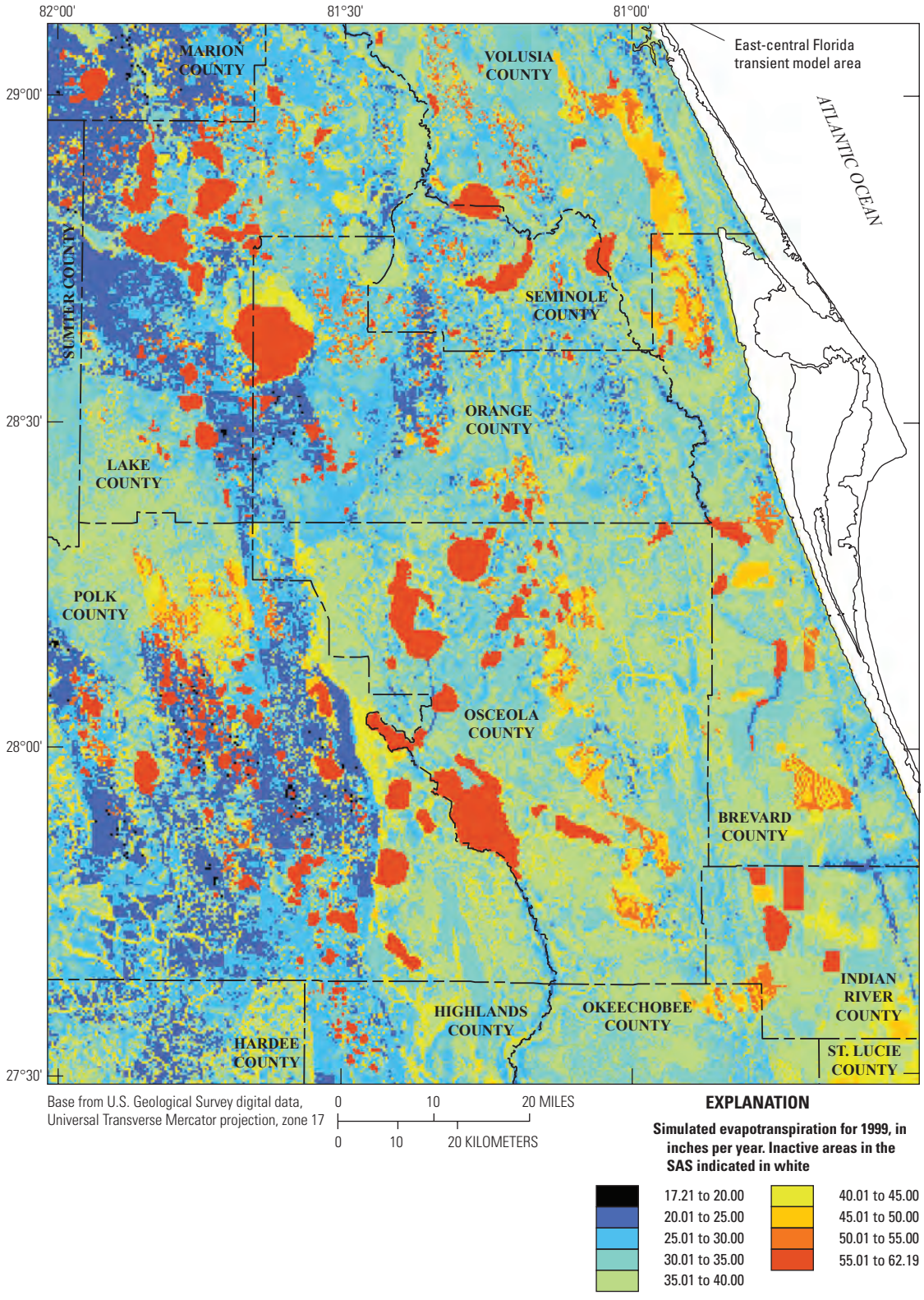

Figure 102. Simulated evapotranspiration rates for 1999 over active areas in the surficial aquifer system (SAS, layer 1) and in lakes, from the 12-year transient model.

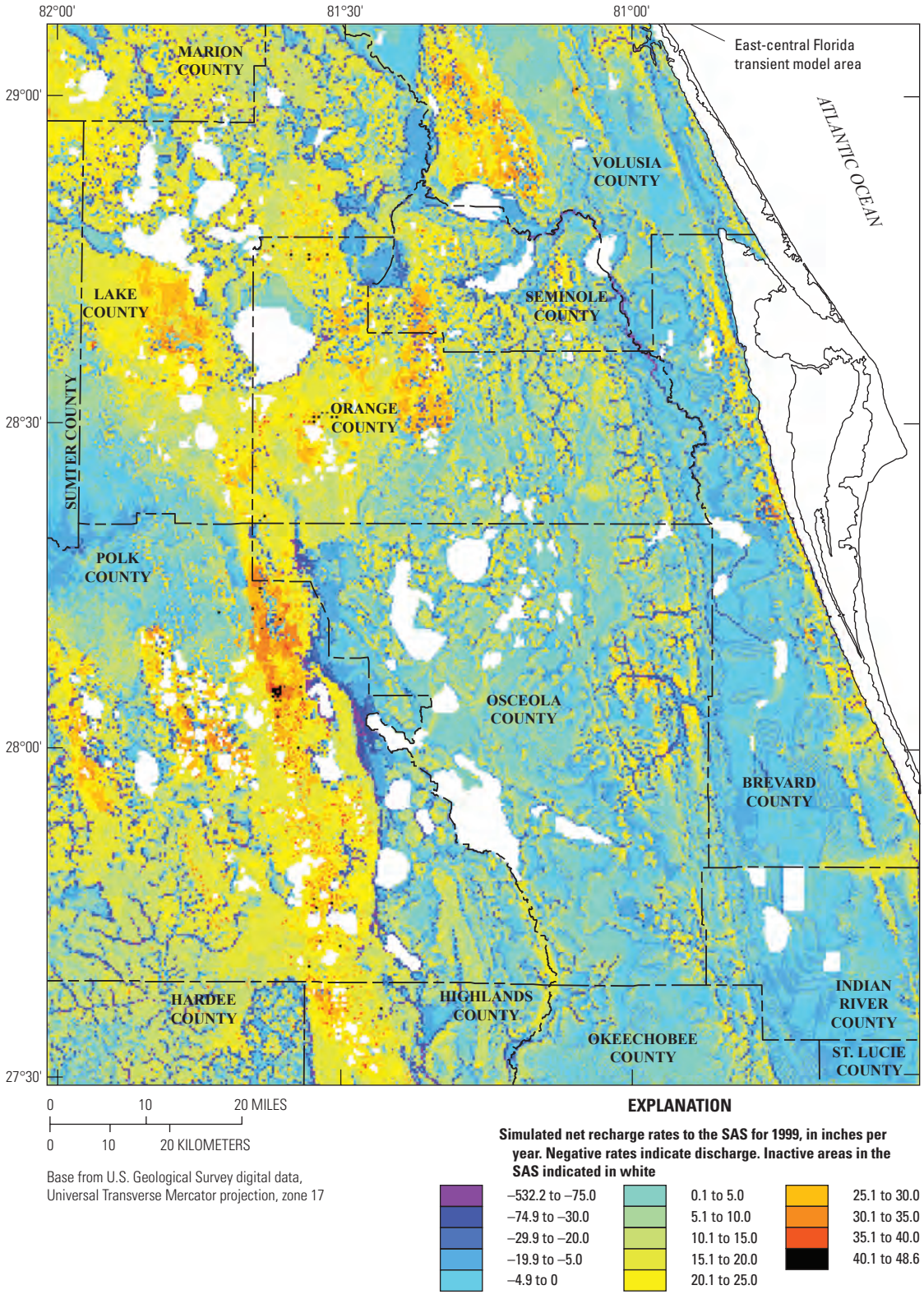

Figure 103. Simulated recharge and discharge rates over active areas of the surficial aquifer system (SAS, layer 1) in 1999, from the 12-year transient model.

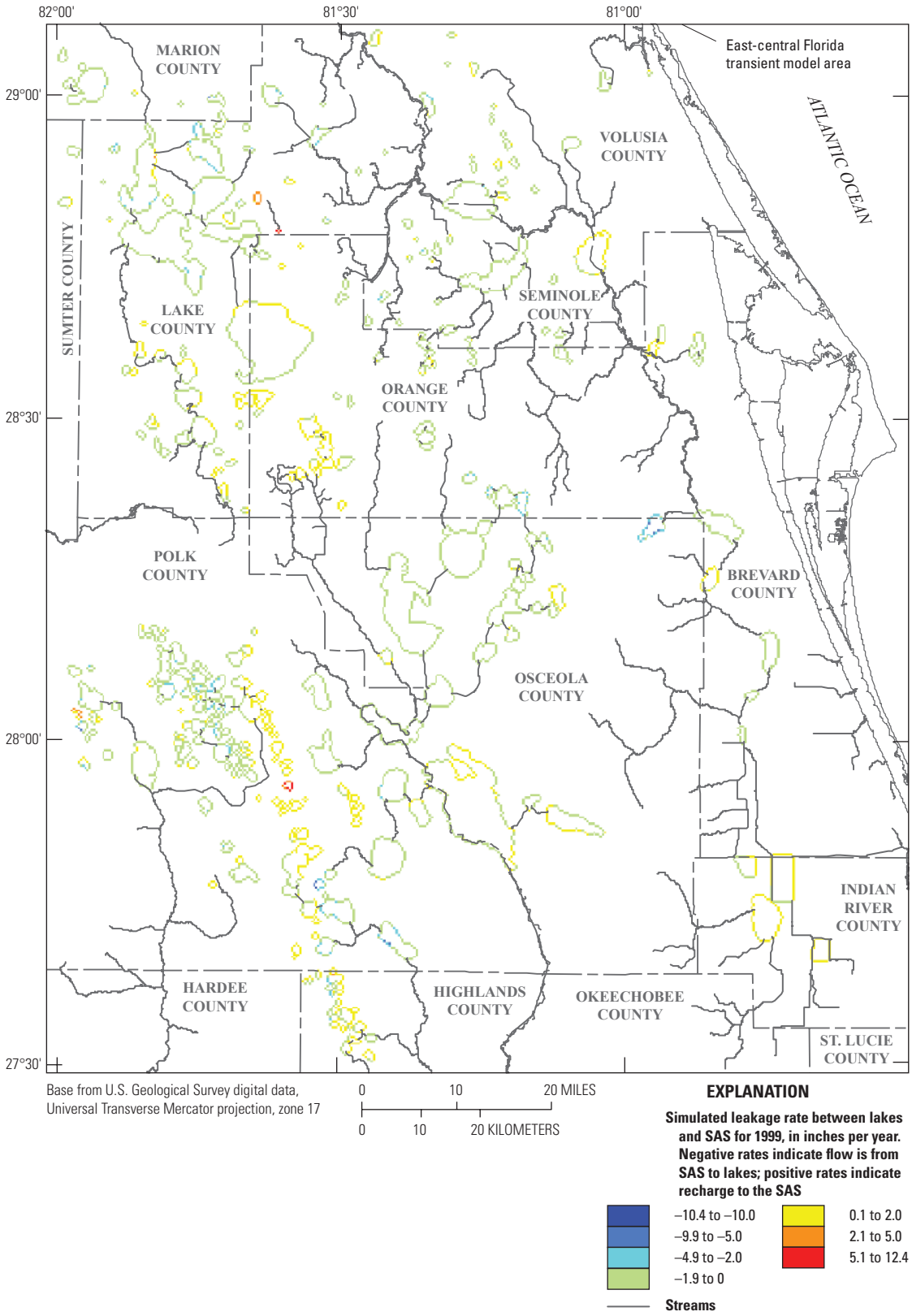

Figure 104. Simulated leakage rates between lakes and the surficial aquifer system (SAS, layer 1) based on the simulated lakebed leakance, average 1999 conditions.

average vertical leakage rate among cells with negative leakage rates (where flow is from layer 2 to the lakes) was -2.21 in/yr, the average vertical leakage rate among cells with positive leakage rates was 2.59 in/yr, and the overall average vertical leakage was 0.34 in/yr. When all 10,000 lake cells were considered, 4,120 vertical leakage rates were less than -0.1 in/yr, 5,160 rates were greater than 0.1 in/yr, and 720 rates were between -0.1 and 0.1 in/yr. The largest vertical leakage rate to a lake from layer 2, 19.2 in/yr, was simulated at lake number 56 in northeastern Seminole County (figs. 13 and 105). The largest vertical leakage rate to layer 2 from a lake, 438.9 in/yr, was simulated at the only lake cell corresponding to lake number 318. The next largest vertical leakage rates to layer 2 from a lake, which ranged from 44.06 to 34.82 in/yr, were simulated in the six lake cells that compose lake number 346 in central Polk County (figs. 13 and 105); the only lake in the ECFT model area with simulated augmentation from groundwater.

Calibrated vertical hydraulic conductivity values for streambeds were 0.08 ft/d for stream reaches of segment numbers 268, 287 and 289 (fig. 11), 0.05 ft/d for stream reaches of segment number 180 of the Palatlakaha River and the remaining stream segments of the Peace River and its tributaries (fig. 1), and 0.02 ft/d for all other stream segments.

The average simulated leakage rate through streambeds, among stream cells with negative leakage rates (where flow is discharge from layer 1 to the streams) was -4.24 in/yr; the average leakage rate through streambeds, among stream cells with positive leakage rates (representing recharge from the stream to layer 1) was 1.71 in/yr; and the overall average leakage rate was -2.60 in/yr. This overall average represents a discharge of 0.011 ft^3/s per stream cell from layer 1 to the streams or a total net discharge of 53.72 ft^3/s over all stream cells. When all 5,004 stream cells were considered, there were 3,467 leakage rates less than -0.1 in/yr, 1,226 rates greater than 0.1 in/yr, and 311 rates between -0.1 and 0.1 in/yr. Simulated leakage rates through the streambeds ranged from a maximum discharge from layer 1 to a stream of about 66 in/yr, to a maximum recharge from a stream to layer 1 of about 30 in/yr (fig. 106). Most stream segments composing the Peace River (figs. 1 and 106) simulated discharge from layer 1 to the stream. The largest simulated leakage rates to layer 1 from streams were simulated at stream segments 52, 56, 57, 59, and 61 of the St. Johns River, which are upstream from lake number 55 (figs. 1, 11, 13, and 106). The largest discharge rates to streams from layer 1 were simulated at stream segment 253 of the Kissimmee River and at stream segments 289, 293, 297, and 299 of the Peace River (figs. 1, 11, and 106). The direction of leakage (discharge compared to recharge) is generally governed by the simulated altitude of the water table relative to the water-surface altitude of the stream. Combined groundwater withdrawals from the Upper Floridan aquifer (figs. 1, 39*A*, and 40*A*) reduce upward leakage to the SAS, causing a decline in the water table that may consequently increase leakage from the stream to the SAS. This may be the reason for the simulation of leakage from the stream to the SAS along stream segments 52, 56, 57, 59, and 61 of the St. Johns River. In recharge areas of the SAS along the Kissimmee River and Peace River, the water table is generally higher than the water-surface altitude at the stream, which is the basis for the simulated direction of the flow.

Calibrated vertical hydraulic conductivity in layer 2, which represents the ICU/IAS, was the highest along the ridge physiographic regions (figs. 2 and 66), which resulted in the largest simulated downward vertical leakage rates between layer 1 and layer 2 for 1999 (fig. 107). Large upward leakage rates to layer 1 from layer 2, exceeding 45 in/yr, are simulated along the eastern perimeter of the Lake Wales Ridge, probably the result of cumulative lateral flow that leaks through areas of layer 2 that are relatively thin and permeable. The physiographic regions west of Lakes Wales Ridge, such as the De Soto Plain and the Polk Upland, and to the east, such as the Osceola Plain (figs. 2 and 107), show downward flow from layer 1; one exception is near the west-central part of the model area, where upward flow is simulated in some areas of the Green Swamp (figs. 2 and 107). Along the eastern edge of the ridges, and particularly along transitions in both the land-surface altitude and hydraulic conductivity of layer 1, flow to layer 1 from layer 2 was simulated along relatively narrow zones. Flow to layer 1 from layer 2 was also simulated along the boundary of the Lake Wales Ridge and the Green Swamp, where similar differences in land-surface altitude occur. The largest downward leakage rates to layer 2 were simulated in areas where artificial recharge occurs through RIBs (figs. 14 and 107). Leakage rates from layer 1 to layer 2 simulated for 1999 were not more than 5 in/yr in large sections of the Osceola Plain, De Soto Plain, and Polk Upland (figs. 2 and 107).

The simulated leakage-rate pattern between layer 2, representing the ICU/IAS, and layer 3, representing the OPZ, is similar to that between layer 1 and layer 2 (figs. 107 and 108). Upward flow occurs along most of the Eastern Valley, the St. Johns River, and the eastern edge of Lake Wales Ridge, whereas downward flow occurs along the ridges and uplands (figs. 2 and 108). Throughout most of the Osceola Plain, simulated leakage rates between the ICU and OPZ do not exceed 5 in/yr (figs. 2 and 108) because the calibrated vertical hydraulic conductivity of layer 2 is low in this physiographic region (fig. 66). The largest downward leakage rates to layer 3 were simulated in areas where artificial recharge occurs through RIBs (figs. 14 and 108).

The simulated leakage rates between the ICU/IAS and OPZ for 1999 are substantially larger in the ridges and uplands than in the neighboring valleys and plains; this is also the case for the simulated leakage rates between the OLPZ and the APPZ for the same year (figs. 108 and 109). The exceptions are (1) the large upward leakage rates near springs (figs. 1 and 109), (2) the downward leakage to layer 5 (APPZ) caused by the recharge to layer 3 from drainage wells (figs. 14 and 109), (3) the downward leakage to layer 5 caused by the downward leakage from the RIBS to layer 3, and (4) the upward flow from layer 5 induced by the pumping of agricultural and public-supply wells that pump from layer 3 (figs. 39*A* and 109).

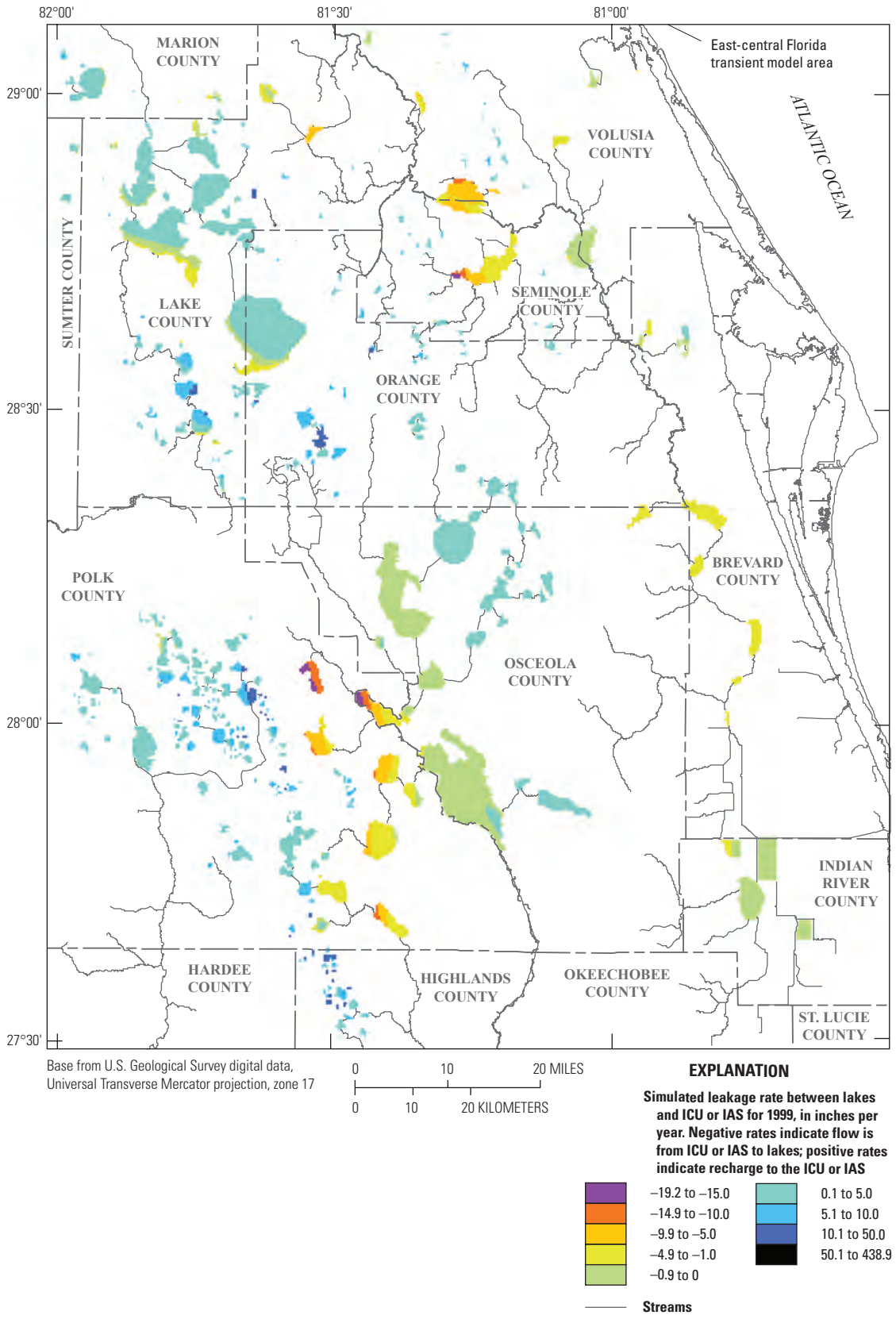

Figure 105. Simulated leakage rates between lakes and the intermediate confining unit/intermediate aquifer system (ICU/IAS, layer 2) based on the simulated lakebed leakance, average 1999 conditions.

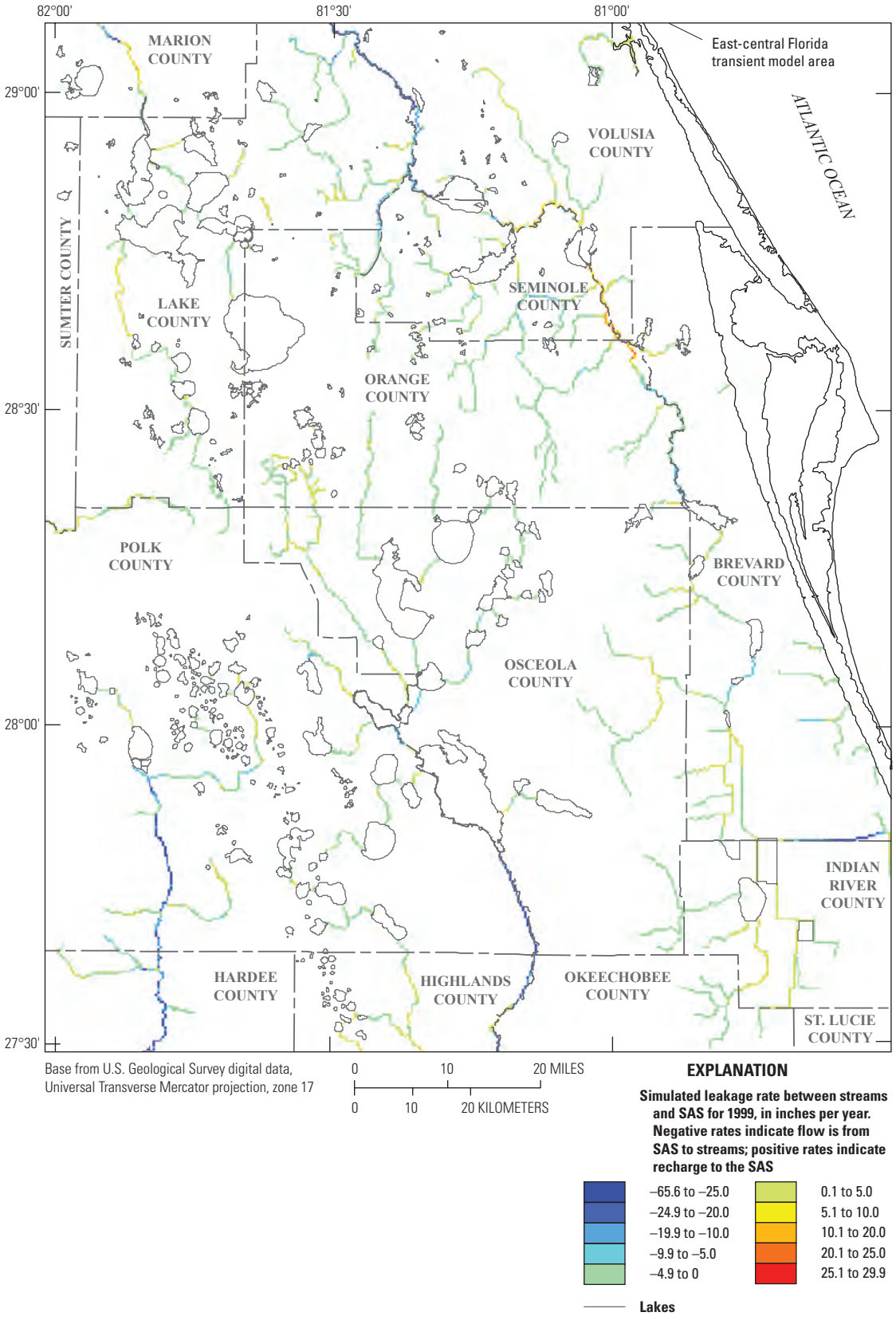

Figure 106. Simulated leakage rates between streams and the surficial aquifer system (SAS, layer 1) based on the simulated streambed vertical hydraulic conductivity, average 1999 conditions.

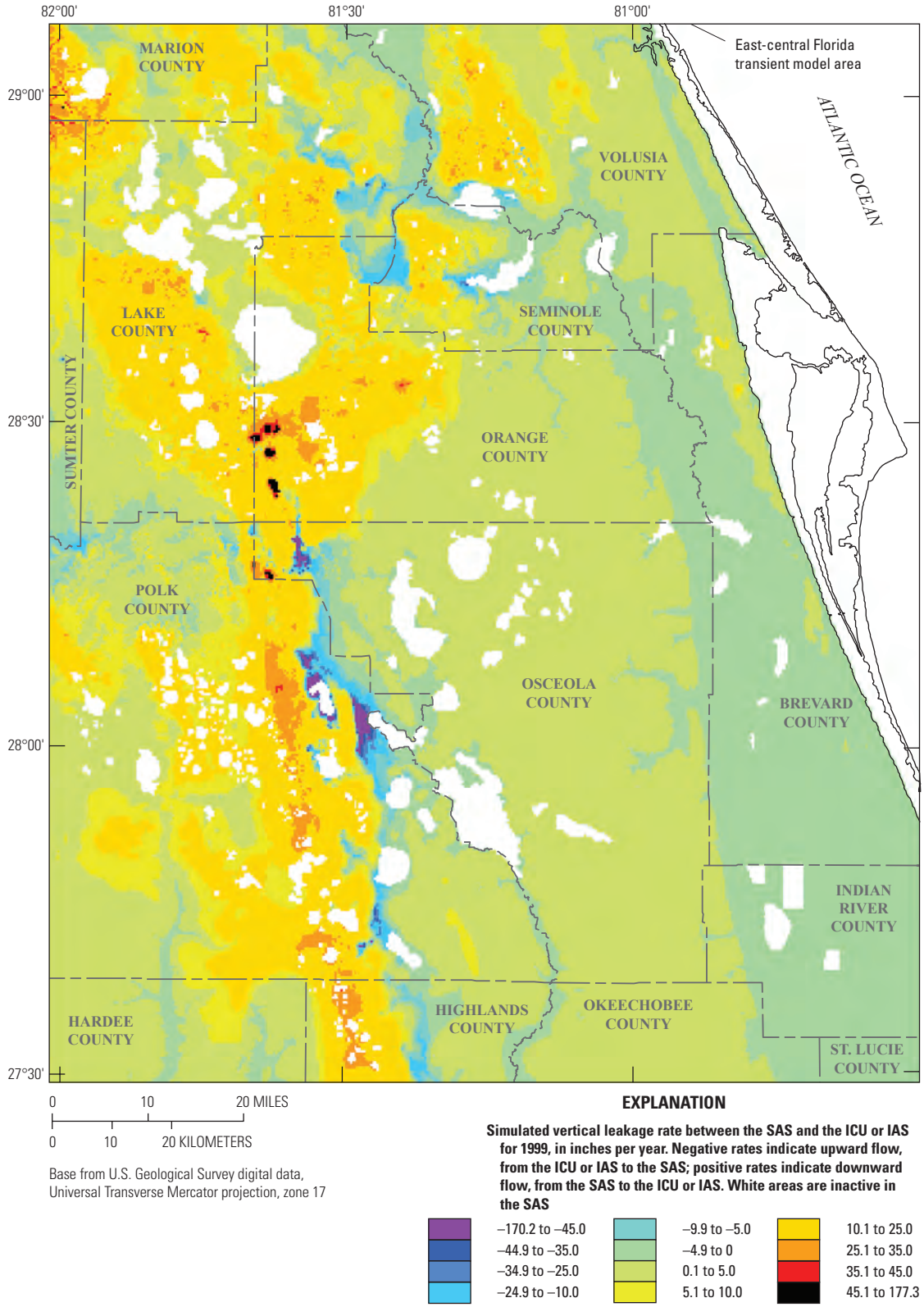

Figure 107. Simulated vertical leakage rates between the surficial aquifer system (SAS, layer 1) and the intermediate confining unit/intermediate aquifer system (ICU/IAS, layer 2), average 1999 conditions.

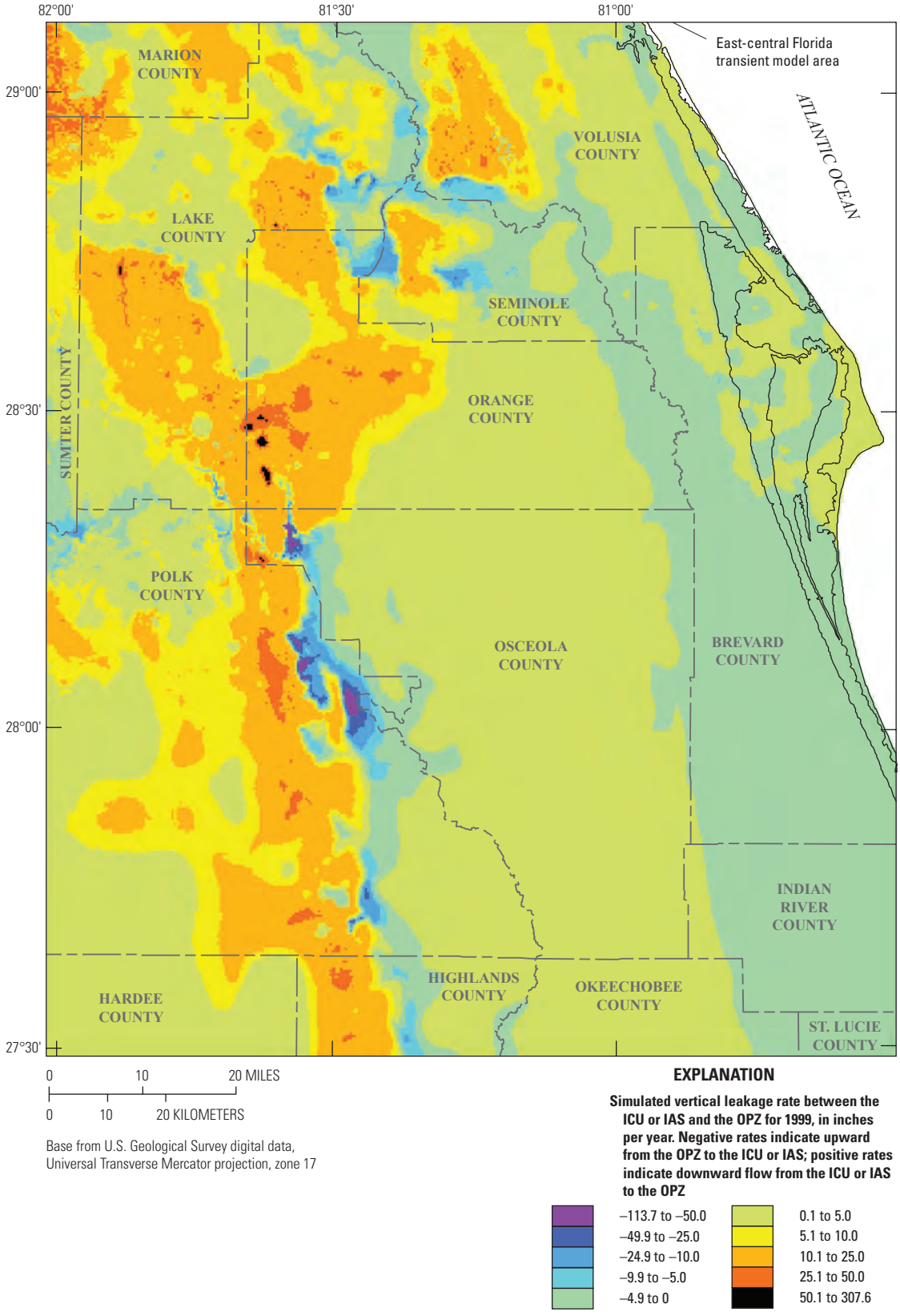

Figure 108. Simulated vertical leakage rates between the intermediate confining unit/intermediate aquifer system (ICU/IAS, layer 2) and the Ocala permeable zone (OPZ, layer 3), average 1999 conditions.

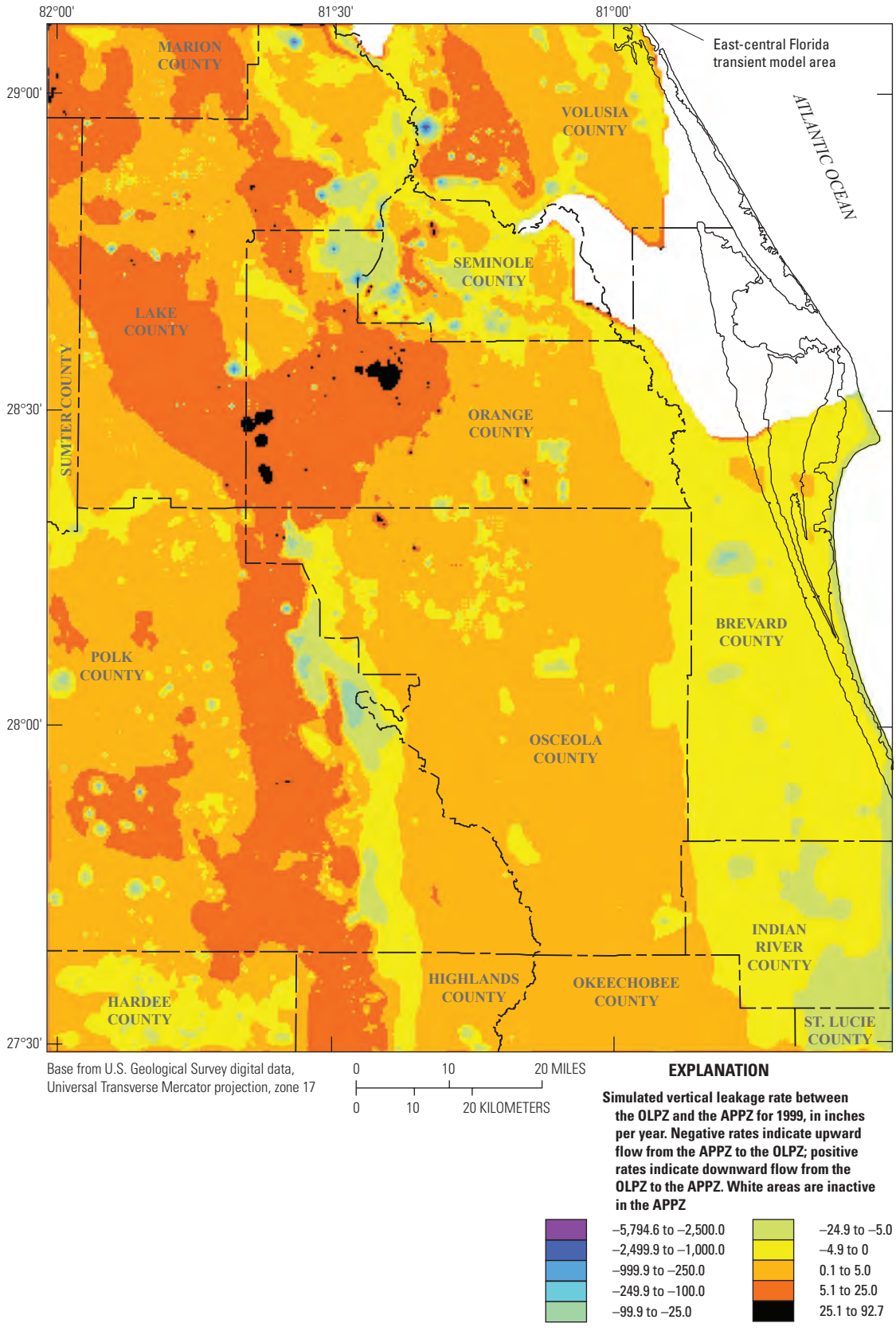

Figure 109. Simulated vertical leakage rates between the Ocala low-permeable zone (OLPZ, layer 4) and Avon Park permeable zone (APPZ, layer 5), average 1999 conditions.

The distribution of leakage between layers 6 and 7 is characterized by a region of very low rates of downward leakage in the southwestern part of the simulated area (fig. 110), which corresponds to areas where MCU II is present (fig. 32) and where a low value of Kv is assigned to layer 6 (fig. 70). The greatest downward leakage rates, from layer 6 (MCU I) to layer 7 (LFA), were simulated in the northwestern part of the model area and in the northeastern part of the eastern extent of the MCU II (figs. 32 and 110). Leakage rates were relatively small in most of the remaining areas, except along the southern and eastern boundaries of the model where simulated layers 6 and 7 are relatively thin as a result of the presence of the 5,000 mg/L isochlor.

Total flows leaving the simulated system from layers 3, 5, and 7 (representing the OPZ, APPZ, and LFA respectively) through the lateral boundaries were less than 0.7 in/yr for each of the 12 years of simulation (GHB3, table 19; GHB5 and GHB7, table 20). The rates corresponding to flux out of the model area from layers 3, 5 and 7 were 49, 131, and 304 ft^3/s, respectively. Average flow leaving the lateral boundaries of the model in the LFA was more than 2 times greater than the flow leaving the lateral boundaries of the model in the APPZ. About 90 percent of the total flow through the lateral boundaries of the LFA is along the northwestern corner of the model, where additional head data from the LFA could better define the specified heads for the GHB cells. Among the lateral boundary cells of the LFA, the northwestern corner of model had the highest calibrated hydraulic conductivity (fig. 71). Groundwater withdrawals from layer 3, which were greater for each of the 12 years than the combined withdrawals from the layers 5 and 7, induce greater net vertical flow to layer 3 (FLN3, table 19) than the combined net vertical flows to layers 5 and 7 (FLN5 and FLN7, table 20).

Simulated flows through the general-head boundaries allow the calculation of the outward flow through a wedge in the northwestern corner of the model (first 25 rows and first 25 columns in fig. 42*A*), and totaled about 14 ft^3/s for 1999 in layer 3, which represents the OPZ. Most of the flow during 1999 along these cells was simulated as flow out of the model. Outward flow through the northwestern corner of the model area totaled about 64 ft^3/s for 1999 in layer 5, which represents the APPZ. Total combined flow through the specified northwestern corner of the model area from layer 3 and layer 5 was 78 ft^3/s. Silver Springs is located about 40 mi northwest of the northwestern corner of the model area. Estimated average annual flow to Silver Springs for 1999 was about 700 ft^3/s (Sepúlveda, 2009). Because the drainage area of Silver Springs is almost radially symmetric, and because the ECFT model covers about one eighth of Silver Springs' drainage area, the outward flow simulated by the ECFT model should not exceed one eighth of the total flow to Silver Springs, or 87.5 ft^3/s. The combined layer 3 and layer 5 (OPZ and APPZ) outward flow simulated by the ECFT model through the northwestern corner of the model area does not exceed the reasonable limit of flow contribution to Silver Springs.

Average groundwater withdrawals from layers 3, 5, and 7 (OPZ, APPZ, and LFA respectively), over the 12-year period of simulation, were 1.22, 0.43, and 0.35 in/yr, respectively. The total of these withdrawals, 2 in/yr, was less than the 3.58 in/yr simulated average net recharge to layer 1 over the same period. Annual net simulated recharge to layer 1 was less than the total withdrawals from layers 3, 5, and 7 only during the dry years of 2000 and 2006 (tables 17, 19, and 20). The annual net simulated recharge to layer 1 was -0.08 in. (net loss) for 2000, and 0.83 in. for 2006 (table 17). Combined groundwater withdrawals from layers 3, 5, and 7 totaled 2.55 in. in 2000 and 2.22 in. in 2006.

Model Limitations

Groundwater flow simulations generally are based on conceptual models that are simplified representations of complex, heterogeneous groundwater flow systems. The lack of sufficient measurements to fully describe the spatial and temporal variability of hydrologic conditions and the spatial variability of hydraulic properties throughout the model area often necessitate these simplifications. Assumptions about hydraulic properties such as isotropy, spatial uniformity, and the absence of preferential flow zones are examples of simplified representations that can be sources of error in a groundwater flow model. Other examples of simplified representations are the use of a numerical model that yields inherent simplifications such as constant hydraulic properties, boundary values, and hydraulic head within each grid cell. These simplifications produce limitations on the model's simulation capabilities. It is important that these limitations are considered during application of the model.

The feasibility of the ECFT model to represent the hydrologic system during the simulation period is limited by the assumptions and simplifications associated with the (1) conceptualization of the flow system, (2) data available to represent the physical properties of the system, as well as observations of system conditions such as the measured heads, spring flows, water-surface altitudes at lakes, and streamflows, (3) temporal range of hydrologic and anthropogenic stresses and the spatial scale of the model grid, and (4) equations used to simulate components of the flow system. The ECFT model was shown to match springflow, streamflow, lake water levels and aquifer water levels over the wide range of hydrologic stresses and groundwater withdrawal conditions for monthly stress periods from 1995 to 2006, which included dry, wet, and average hydrologic conditions. Nonetheless, it may be inappropriate to use the model with hydrologic conditions outside of the range tested or to impose groundwater withdrawals greater than those used in the simulation or near the boundaries of the model area.

Simplifying the actual flow system with the selected conceptualizations does not invalidate model results, although model results should be interpreted at scales larger than the representative grid cell. The model is finely discretized for a

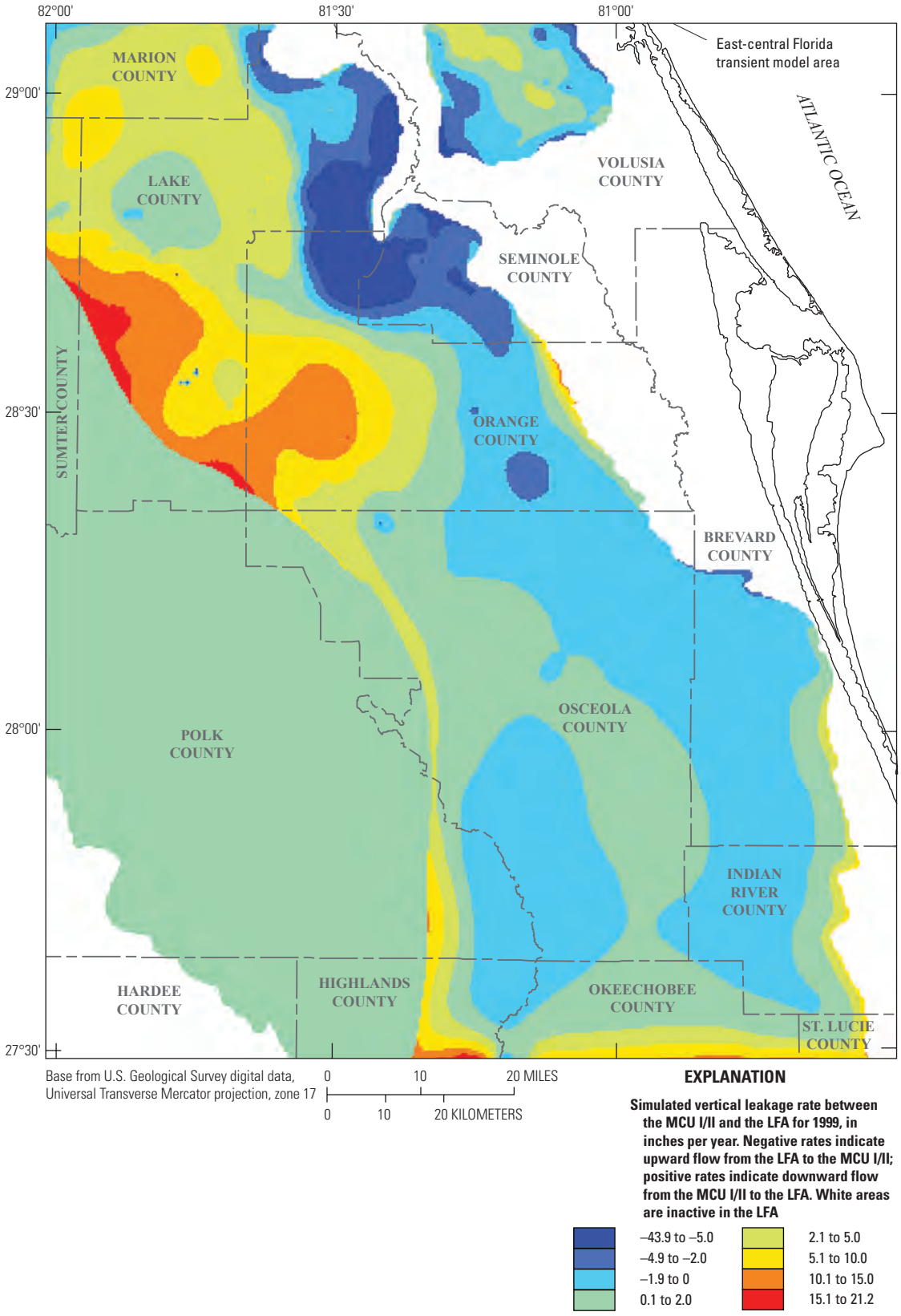

Figure 110. Simulated vertical leakage rates between middle confining unit I/II (MCU I/II, layer 6) and Lower Floridan aquifer (LFA, layer 7), average 1999 conditions.

Table 19. Simulated flows entering and leaving the Ocala permeable zone from the calibrated transient model of 1995 to 2006.

[STO3, amount of water from storage to/from the Ocala permeable zone (OPZ); FLN3, net vertical flow in the OPZ; GW3, groundwater withdrawals from the OPZ; GHB3, net flow through the lateral boundaries of the OPZ; DRN3, total spring flow leaving the OPZ; Ave, average rate for the 1995–2006 period; all rates are in inches per year; conversion to cubic feet per second should use the 169,552 active cells in the OPZ; negative flows indicate outflows in layer 3, whereas positive flows indicate inflows to layer 3]

Year	STO3	FLN3	GW3	GHB3	DRN3
1995	0.00	1.81	–1.09	0.08	–0.80
1996	0.00	2.20	–1.28	–0.06	–0.86
1997	0.00	2.03	–1.15	–0.10	–0.78
1998	0.00	2.30	–1.41	–0.06	–0.83
1999	0.00	2.17	–1.31	–0.10	–0.76
2000	0.01	2.42	–1.67	–0.08	–0.68
2001	–0.01	2.12	–1.31	–0.11	–0.69
2002	0.00	2.10	–1.24	–0.11	–0.75
2003	0.00	1.94	–1.01	–0.11	–0.82
2004	0.00	1.92	–1.04	–0.07	–0.81
2005	0.00	1.80	–0.83	–0.10	–0.87
2006	0.01	2.15	–1.28	–0.09	–0.79
Ave	**0.00**	**2.08**	**–1.22**	**–0.07**	**–0.79**

Table 20. Simulated flows entering and leaving the Avon Park permeable zone and the Lower Floridan aquifer from the calibrated transient model of 1995 to 2006.

[STO5, amount of water from storage to/from the Avon Park permeable zone (APPZ); FLN5, net vertical flow in the APPZ; GW5, groundwater withdrawals from the APPZ; GHB5, net flow through the lateral boundaries of the APPZ; STO7, amount of water from storage to/from the Lower Floridan aquifer (LFA); FLN7, net vertical flow in the LFA; GW7, groundwater withdrawals from the LFA; GHB7, net flow through the lateral boundaries of the LFA; Ave, average rate for the 1995–2006 period; all rates are in inches per year; conversion to ft^3/s should use the 159,139 active cells in the APPZ, and 129,441 active cells in the LFA; negative flows indicate outflows in layers 5 and 7, whereas positive flows indicate inflows to layers 5 and 7]

Year	STO5	FLN5	GW5	GHB5	STO7	FLN7	GW7	GHB7
1995	0.00	0.70	–0.37	–0.33	0.00	0.82	–0.27	–0.55
1996	0.01	0.52	–0.39	–0.14	0.02	0.86	–0.29	–0.59
1997	0.00	0.51	–0.37	–0.14	–0.01	0.90	–0.30	–0.59
1998	0.01	0.49	–0.41	–0.09	0.02	0.91	–0.36	–0.57
1999	0.00	0.70	–0.41	–0.29	0.00	0.99	–0.38	–0.61
2000	0.01	0.64	–0.46	–0.19	0.04	1.00	–0.42	–0.62
2001	–0.01	0.64	–0.41	–0.22	–0.02	0.93	–0.35	–0.56
2002	–0.01	0.68	–0.42	–0.25	–0.03	0.86	–0.35	–0.48
2003	0.00	0.58	–0.43	–0.15	–0.01	0.91	–0.35	–0.55
2004	0.00	0.58	–0.46	–0.12	0.01	0.95	–0.38	–0.58
2005	0.00	0.67	–0.46	–0.21	–0.01	0.97	–0.38	–0.58
2006	0.01	0.78	–0.52	–0.27	0.04	0.97	–0.42	–0.59
Ave	**0.00**	**0.63**	**–0.43**	**–0.20**	**0.00**	**0.92**	**–0.35**	**–0.57**

regional-scale model, with uniform cell size of 1,250 ft per side (0.056 mi^2). The groundwater flow equation solved by the model is based on Darcy's Law and the continuity equation for flow derived from the principle of mass conservation along with the assumption that fluid properties are constant in time and space. This equation is valid for groundwater flow conditions in which the velocity of groundwater is low and flow is laminar. In karstic terrains, however, it is possible for flow through caverns and solution channels to be turbulent. Consequently, the groundwater flow equation is not valid for the entire FAS. It was assumed herein that laminar flow prevailed throughout the model area; therefore, if laminar flow is not a valid assumption in parts of the model area, then the accuracy of model results would be compromised in such areas.

The simulation of the SAS as a single layer may be an additional model limitation because this assumption places the altitude of the bottom of the lakebed at the top of the underlying layer. This is generally not the case for lakes in or near the ridges. A study by O'Reilly (1998) concluded that using three layers to simulate the SAS and placing all lakes in the top layer, including the ones in the ridges, did not substantially change the horizontal flow component in the SAS. However, only modification of the ECFT model with enhanced vertical discretization of the SAS, where the lakes are placed in the upper layer, would identify the true impact of this model conceptualization on SAS flowpaths.

The assumption of uniform heads throughout the vertical extent of each grid cell is another possible source of model error. Vertical hydraulic gradients between the SAS and OPZ suggest that the value used for simulated heads in the ICU/IAS could be within the range of heads observed throughout the thickness of the ICU/IAS. Simulation of the observed hydraulic gradients within the ICU would require additional layering of this hydrogeologic unit.

The calibrated hydraulic conductivity obtained in this study for the ICU/IAS, OPZ, OLPZ, APPZ, MCU I/II, and LFA may vary from values in previously published local groundwater flow models. Final hydraulic conductivity values were constrained based on available aquifer test data and the expertise of the authors and water management district personnel. Although the calibrated hydraulic property maps are within acceptable ranges, it is highly likely that there are other distributions of hydraulic properties that would be reasonable and also fit the calibration criteria. Uncertainty analysis of this set of parameters indicates that the horizontal and vertical hydraulic conductivities of model layer 2 (which represents the ICU/IAS) are the most uncertain hydraulic properties given the current state of information and observations. Additionally, the lack of data for the MCU I/II and the LFA precludes a reliable estimation of their respective hydraulic conductivity distributions. The model simulates the decline in heads from the APPZ to the LFA in areas where the MCU II is present. However, additional hydraulic data for the MCU I could be used to improve the simulation of the upward head gradient between the APPZ and MCU I near Wekiwa Springs (spring number 21, fig. 51).

Areas in the IAS, OPZ, APPZ, or LFA where groundwater withdrawals were minimal may not be as well calibrated and may require changes to horizontal or vertical hydraulic conductivity as future aquifer stresses from increased groundwater withdrawals are applied and future observations and data are collected. The hydraulic properties were calibrated to conditions for specific stress periods, and model results may be incorrect if the system is stressed in ways outside of the conditions for which this model was calibrated.

The general-head boundaries specified along the perimeter of active cells were based on the assumption of minimal groundwater flow across the estimated surface beneath which the FAS contains water having chloride concentrations greater than 5,000 mg/L. The use of general-head boundaries at the lateral extent of the freshwater and saline-water interface to simulate flows and levels in central Florida will not affect the model results substantially as long as (1) conditions in the coastal areas are not changed and (2) the assumption holds that the freshwater and saline-water interface can be approximated as constant from 1995 to 2006. The estimated surface shown in figure 37 can be updated as more water-quality data become available. In addition, interaction of groundwater flow with the freshwater and saline-water interface in the LFA might be understood better as the potentiometric surface of the LFA becomes better defined by more head measurements as additional wells are drilled. The assumption of a stationary freshwater and saline-water interface also could introduce error in the model if groundwater withdrawals or lack of recharge induce movement of this interface.

Errors in initial conditions were shown to be far less than the accuracy of water-level observations after about a 6-month transient simulation period. Thus, any predictive runs for periods after 2006 that begin with the current 1995–2006 transient stress periods would not be affected by errors in initial conditions.

The transient model presented herein addresses the surface-water and groundwater interactions with a systematic and process-oriented approach in the ECFT area, using appropriate modeling tools available at the time. By providing estimates of hydraulic parameters, this model can be used to generate initial estimates of the hydraulic properties as well as boundary conditions needed for more localized studies.

Summary and Conclusions

A seven-layer, finite-difference, transient groundwater flow model of the surficial aquifer system (SAS), intermediate confining unit (ICU) or intermediate aquifer system (IAS), and Floridan aquifer system (FAS) in east-central Florida was developed and calibrated to increase the understanding of groundwater flow in the SAS and FAS; assess the recharge rates to the SAS from infiltration through the unsaturated zone, and obtain a simulation tool that could assess the impact of changes in groundwater withdrawals on the potentiometric

surfaces and flow in the FAS. The east-central Florida transient (ECFT) model area covers about 9,000 square miles, extending from about 4 miles west of the Lake-Sumter County line to the eastern shoreline of Florida and extending from northern Lake County to about 10 miles south of the Polk-Highland County line. The area includes more than 350 lakes and a network of major rivers and tributary streams. The model simulates groundwater flow from January 1995 to December 2006.

Hydrologic processes at land surface and in the unsaturated zone were simulated by using the Green-Ampt infiltration (GAI) method together with MODFLOW-2005. The GAI method was used to partition rainfall into runoff and infiltration, which provided surface-runoff estimates as input for the Lake (LAK7) and Streamflow-Routing (SFR2) Packages and infiltration to the Unsaturated Zone Flow (UZF1) Package. The combined usage of the GAI and these packages enabled routing of infiltration through the unsaturated zone, and thus the simulation of recharge rates to the SAS. This approach more closely represents the physical processes compared to the methods used to calculate recharge rates in previous modeling efforts.

The hydrogeologic framework of the study area includes sediments that form the SAS; the less permeable clay and carbonate rocks that form the ICU, as well as the correlative permeable carbonate rocks that form the IAS in the southwestern part of the model area; and a thick sequence of carbonate rocks of variable permeability that form the FAS. A uniformly spaced grid composed of 472 rows and 388 columns of 1,250-foot square cells was used to discretize the hydraulic properties of the SAS (layer 1), the ICU/IAS (layer 2), the Ocala permeable zone (OPZ, layer 3), the Ocala low-permeable zone (OLPZ, layer 4), the Avon Park permeable zone (APPZ, layer 5), the middle confining unit I/II (MCU I/II, layer 6), and the Lower Floridan aquifer (LFA, layer 7).

The regional horizontal hydraulic conductivity (Kh) was represented by zones in layer 1 (SAS); by a grid of pilot points uniformly spaced 25 model cells apart in the permeable area of layer 2 (representing the IAS), as well as in layers 3, 5, and 7; and by a uniform value in layers 4 and 6. The regional vertical hydraulic conductivity (Kv) was represented by zones in layers 1 and 6, by pilot points in layer 2, by a uniform Kv value in layer 4, and by a uniform value of vertical anisotropy in layers 3, 5, and 7. A set of irregularly spaced pilot points near springs also was used to calculate multiplicative factors that increase the Kh of layers 3 and 5 and the Kv of layer 4 to account for enhanced dissolution of rocks.

The ECFT model was calibrated by using PEST, an inverse modeling code that estimates model parameters by nonlinear regression with an objective function defined as the sum of squared weighted head and spring-flow residuals. The duration of a forward run for the 12-year model (more than 6 hours) required an iterative approach that included steady-state and transient simulations for subsets of the entire simulation period. Steady-state simulations for 1999 and 2003 were used to estimate hydraulic conductivity (K) parameters. Calibration observations included average annual heads and spring flows for 1999 and 2003. All head weights were specified as 1 $feet^{-1}$ (ft^{-1}); spring-flow weights varied in proportion to the magnitude of flow.

On the basis of sensitivity analysis, the Kh of layers 1, 3, 5, and 7, the Kh of the IAS in layer 2, and the Kv of layers 2, 4, and 6, were estimated by PEST. Estimated K distributions are reasonable compared to aquifer performance-test data, geologic information, and expert knowledge. The Kh of layer 1 ranged from about 7 to 71 feet per day (ft/d); the Kh of layer 2 ranged from about 4 to 150 ft/d; the regional Kh of layer 3, excluding the effects of the spring multiplicative factors, ranged from 26 to 1,440 ft/d; the regional Kh of layer 5 ranged from 29 to 3,860 ft/d; and the regional Kh of layer 7 ranged from 33 to 1,930 ft/d. Including the effects of the multiplicative factors near the springs, the maximum Kh values of layer 3 and layer 5 were 8,720 and 15,400 ft/d, respectively. The Kv of layer 2 ranged from 0.0001 to 1.0 ft/d, the regional Kv of layer 4 was 6.5 ft/d, and the Kv values for the two zones in layer 6 were 0.12 and 0.0001 ft/d. The multiplicative factors near the springs increased the maximum Kv of layer 4 from the regional value of 6.5 ft/d to 140 ft/d.

A transient simulation of the final 2 years (2005–2006) of the 12-year study period, incorporating the K values estimated from the steady-state simulations, was used with PEST to guide the estimation of specific yield and specific storage values. Values for specific yield were represented by zones corresponding to physiographic regions. Two specific storage parameters were defined, one for layer 2 and another for layers 3 to 7. Calibration observations included monthly average heads and flows. Nonlinear hydraulic processes confounded the estimation of the specific yield parameters for all zones, which resulted in setting values to either 0.14 or 0.15. The specific storage was set to 3×10^{-6} ft^{-1} for layer 2 and 2×10^{-6} ft^{-1} for layers 3 to 7.

The 12-year transient simulation yielded head and spring-flow residuals that met the calibration criteria for the 12-year transient simulation. The overall mean residual for heads (with residual defined as simulated minus measured value) was -0.04 ft. The overall root-mean square residual for heads was less than 3.6 feet (ft) for each year of the 1995–2006 simulation period. The overall mean residual for spring flows was about -0.3 cubic feet per second (ft^3/s). The spatial distribution of SAS head residuals in 1999 and 2006 shows a slight bias toward negative values along the Lake Wales Ridge. The distribution of OPZ head residuals in 2006 shows a bias towards negative values in the northwestern part of the model where simulated heads are generally lower than observed heads. Such bias is not present in the northwestern part of the model area for the 1999 residuals.

A comparison between the simulated water-budget components for the SAS and values derived from a water-budget analysis based on measured and estimated flows showed that the model can simulate recharge within 1 to 2 inches per year (in/yr) and evapotranspiration (ET) rates within several inches per year of independently estimated values.

Simulated ET rates ranged from an average of about 26 inches (in.) for the dry year of 2000 to about 38 in. for the wet year of 2005. Average ET over the simulated 12-year period was 34.47 in/yr, which accounts for 3.73 in. from lakes, 0.02 in. from streams, 11.64 in. from the unsaturated zone, and 19.08 in. from groundwater. The calculated average ET rate from a model-independent water-budget analysis over the same 12-year period was 36.4 in/yr. Simulated net recharge rates to the SAS ranged from a discharge of 0.08 in. for the dry year of 2000 to a net recharge of 6.30 in. for 2002. The average net recharge rate to the SAS over the simulated 12-year period was about 3.6 in/yr, compared with the calculated average of 3.4 in/yr from the model-independent water-budget analysis.

Groundwater withdrawals from the FAS over the 12-year period of simulation averaged 2 in/yr, which is less than the 3.58 in/yr simulated as average net recharge to layer 1 (SAS) over the same period. Annual net simulated recharge rates to layer 1 and net leakage rates to layer 3 (OPZ) were less than the total groundwater withdrawals from the layers representing the FAS only during the dry years of 2000 and 2006. The annual net simulated recharge to layer 1 was -0.08 in. (a net loss) for 2000 and 0.83 in. for 2006. Combined groundwater withdrawals from layers 3, 5, and 7 totaled 2.55 in. for 2000 and 2.22 in. for 2006. A direct comparison of net groundwater withdrawals and net recharge rates for the 12-year simulation period generally indicates a global positive net recharge in the ECFT area. However, a detailed local model would be needed to accurately assess the local effects of pumping.

The groundwater flow model presented here represents improvements from previous modeling efforts in the study area by (1) expanding the areas of active cells in the southwestern part of the model area, (2) fully representing three-dimensional flow by explicitly simulating the storativity and hydraulic conductivity for all confining units, (3) simulating the water-surface altitudes at lakes using the LAK7 Package, (4) routing streamflow using the SFR2 Package, (5) simulating the temporal distribution of recharge to the SAS using the GAI method and UZF1 Package, (6) using inverse modeling and head and spring-flow observations to estimate K parameters, and (7) using reliable estimates of rates from a model-independent water budget to compare against simulated recharge and ET rates. With these improvements, the numerical model more closely represents the physical processes governing groundwater flow and groundwater/surface-water interaction compared to previous models, and will help facilitate the management of the water resources in east-central Florida.

The calculation of the monthly infiltration and surface runoff rates from daily rainfall and irrigation rates, using the GAI method, proved to be a reliable tool for partitioning rainfall into infiltration and surface runoff. Dunnian runoff was calculated by the UZF1 Package using monthly stress periods and Hortonian runoff was calculated by the GAI method using daily rainfall data to calculate monthly infiltration and surface-runoff rates.

The simulated water exchanges between lakes and the SAS, between lakes and the ICU, and between streams and the SAS agreed within a few inches per year with corresponding estimated flows determined from a model-independent water-budget analysis. The simulated partitioning of rainfall and irrigation into surface runoff and infiltration yielded an acceptable match between measured and simulated water-table altitudes, water-surface altitudes at lakes, and streamflow rates. The agreement between the flows simulated by the model and flows calculated from the model-independent method affirms the advantages of the approach used in developing the model.

In addition to the regular set of pilot points, extra pilot points were added near springs to better simulate spring flow, and doing so proved to be an efficient method for reducing flow residuals. The additional set of densely distributed pilot points around the springs allowed the assignment of greater hydraulic conductivity near springs, a feature that could not have been achieved with the regularly spaced set of pilot points. The calibrated conductances at the spring cells were derived using the GHB Package. A Drain Package generated with the calibrated heads and conductances used in the GHB Package caused no changes when compared to the GHB Package for the 12-year transient model.

The small vertical head differences between the OPZ and the APPZ were simulated reliably well using the general knowledge that the APPZ is much more permeable than the OPZ and the OLPZ is a confining unit with a larger vertical hydraulic conductivity than that of the ICU and MCU I or II. These conditions allow the upward leakage to be induced from the APPZ to the OPZ through a relatively permeable OLPZ whenever large groundwater withdrawals occur in the OPZ.

The main components of groundwater flow in the LFA are towards the east and northeast. The higher hydraulic conductivity and larger groundwater withdrawals in Orange County induce lateral flow towards this area. The larger simulated flows leaving the model from the lateral boundaries occurred in the LFA, which could be based on the lack of head data in the LFA along these boundaries. As more head data along the lateral boundaries of the LFA become available, particularly along the eastern boundary, a more refined estimate of the flows leaving the model area could be made.

The feasibility of this model to represent the hydrologic system during the simulation period is limited by the assumptions and simplifications associated with the conceptualization of the flow system; the data available to represent the physical properties of the system as well as observations of system conditions such as measured heads, spring flows, water-surface altitudes at lakes, and streamflows; the temporal and spatial scale of the model; and the equations used to simulate components of the flow system. The ECFT model was shown to adequately match springflow, streamflow, lake water levels and aquifer water levels over the wide range of hydrologic stresses and groundwater withdrawal conditions for monthly stress periods from 1995 to 2006, which included dry, wet, and average hydrologic conditions. It may be inappropriate to use the model with hydrologic conditions outside of the range tested, however, or to impose groundwater withdrawals greater than those used in the simulation or near the boundaries of the model area.

References Cited

Adamski, J.C., and German, E.R., 2004, Hydrogeology and quality of groundwater in Orange County, Florida: U.S. Geological Survey Water Resources Investigations Report 03–4257, 113 p.

Andersen, P.F., Jacobs, B.L., and Konikow, L.F., 2007, Peer Review Report—East Central Florida Transient (ECFT) model, prepared for Resource Evaluation and Subregional Modeling Division: West Palm Beach, Fla., South Florida Water Management District, 70 p.

Arthur, J.D., Wood, A.R., Baker, A.E., Cichon, J.R., and Raines, G.L., 2007, Development and implementation of a Bayesian-based aquifer vulnerability assessment in Florida: Natural Resources Research, v. 16, no. 2, p. 93–107.

Basso, Ron, 2003, Predicted change in hydrologic conditions along the Upper Peace River Basin due to a reduction in ground-water withdrawals: Brooksville, Southwest Florida Water Management District, 53 p.

Basso, Ron, and Hood, Jill, 2005, Assessment of minimum levels for the intermediate aquifer system in the Southwest Florida Water Management District: Brooksville, Southwest Florida Water Management District, 217 p.

Brooks, R.H., and Corey, A.T., 1966, Properties of porous media affecting fluid flow: American Society of Civil Engineers, Journal of Irrigation and Drainage, v. 101, p. 85–92.

Bulmer, W.H., 2003, Drainage well inventory for Orange, Seminole, and Lake Counties: South Florida Water Management District, Orlando, Fla., 128 p.

Central Florida Water Initiative, 2011, Overview of the Central Florida Water Initiative: Accessed November 2011 at *http://cfwiwater.com*.

Cheng, Lei, Xu, Zongxue, Wang, Dingbao, and Cai, Ximing, 2011, Assessing interannual variability of evapotranspiration at the catchment scale using satellite-based evapotranspiration data sets: Water Resources Research, v. 47, W09509, 11 p.

Chow, V.T., Maidment, D.R., and Mays, L.W., 1988, Applied hydrology: New York, McGraw Hill, 243 p.

Davis, J. D., and Boniol, Don, 2011, Grids representing the altitude of top and/or bottom of hydrostratigraphic units for the ECFT 2012 groundwater model area: St. Johns River Water Management District, Bureau of Groundwater Sciences Geographic Information System, Electronic file archives.

Doherty, J., 2008, Groundwater data utilities: Brisbane, Australia, Watermark Numerical Computing.

Doherty, J., 2010a, PEST, Model-independent parameter estimation—User manual (5th ed., with minor revisions): Brisbane, Australia, Watermark Numerical Computing.

Doherty, J., 2010b, Addendum to the PEST manual: Brisbane, Australia, Watermark Numerical Computing.

Doherty, J., Fienen, M.N., and Hunt, R.J., 2010, Approaches to highly parameterized inversion: Pilot-point theory, guidelines, and research directions: U.S. Geological Survey Scientific Investigations Report 2010–5168, 36 p.

Dunne, T., and Black, R.G., 1970, An experimental investigation of runoff production in permeable soils: Water Resources Research, v. 6, p. 478–490.

Environmental Simulations, Inc., 2004, Development of the District Wide Regulation Model for Southwest Florida Water Management District: Reinholds, Penn., Environmental Simulations, Inc., 56 p.

Environmental Simulations, Inc., 2007, Refinement of the District Wide Regulation Model for Southwest Florida Water Management District: Reinholds, Penn., Environmental Simulations, Inc., 47 p.

Environmental Systems Research Institute, Inc., 2010, ArcGIS, version 10.0: Redlands, Calif.

Faybishenko, B.A., 1995, Hydraulic behavior of quasi-saturated soils in the presence of entrapped air: Laboratory experiments: Water Resources Research, v. 31, no. 10, p. 2421–2435.

Fayer, M.J., and Hillel, D., 1986, Air encapsulation: I. Measurement in a field soil: Soil Science Society of America Journal, v. 50, no. 3, p. 568–572.

Fienen, M.N., Muffels, C.T., and Hunt, R.J., 2009, On constraining pilot point calibration with regularization in PEST: Ground Water, v. 47, no. 6, p. 835–844 (also available at *http://onlinelibrary.wiley.com/doi/10.1111/j.1745-6584.2009.00579.x/full*)

Florida Office of Economic and Demographic Research, 2012, Historical data—Florida County Population Census Counts: 1900 to 2010: Accessed June 2012 at *http://edr.state.fl.us/Content/population-demographics/2010-census/data/index.cfm.*

Geovariances, 2011, ISATIS 2011: Avon-Fontainebleau, France.

German, E.R., and Adamski, J.C., 2005, Hydrogeology and water quality of lakes and streams in Orange County, Florida: U.S. Geological Survey Scientific Investigations Report 2005–5052, 103 p.

Grubb, H.F., and Rutledge, A.T., 1979, Long-term water supply potential, Green Swamp area, Florida: U.S. Geological Survey Water-Resources Investigations Report 78–99, 76 p.

Harbaugh, A.W., 2005, MODFLOW-2005, The U.S. Geological Survey modular ground-water model—The Ground-Water Flow Process: U.S. Geological Survey Techniques and Methods, book 6, chap. A16, 196 p.

Hill, M.C. and Tiedeman, C.R., 2007, Effective groundwater model calibration: With analysis of data, sensitivities, predictions, and uncertainty: New York, Wiley and Sons, 455 p.

Hoblit, B.B., Castello, Cris, Liu, Leiji, and Curtis, David, 2003, Creating a seamless map of gage-adjusted radar rainfall estimates for the state of Florida: Proceedings of the EWRI World Water and Environmental Congress, Philadelphia, Pa.

Horton, R.E., 1933, The role of infiltration in the hydrological cycle: American Geophysical Union Transactions, v. 23, p. 479–482.

Knochenmus, L.A., 2006, Regional evaluation of the hydrogeologic framework, hydraulic properties, and chemical characteristics of the intermediate aquifer system underlying southern west-central Florida: U.S. Geological Survey Scientific Investigations Report 2006–5013, 52 p.

Knowles, L., Jr., O'Reilly, A.M., and Adamski, J.C., 2002, Hydrogeology and simulated effects of ground-water withdrawals from the Floridan aquifer system in Lake County and in the Ocala National Forest and vicinity, north-central Florida: U.S. Geological Survey Water-Resources Investigations Report 02–4207, 140 p.

Knowles, L., Jr., Phelps, G.G., Kinnaman, S.L., and German, E.R., 2005, Hydrologic response in karstic-ridge wetlands to rainfall and evapotranspiration, central Florida, 2001–2003: U.S. Geological Survey Scientific Investigations Report 2005–5178, 82 p.

LaRoche, J.J., 2007, The geology, hydrology, and water quality of the ROMP 43–Bee Branch monitor-well site, Hardee County, Florida: Brooksville, Florida, Southwest Florida Water Management District, variously paged.

McDonald, M.G., and Harbaugh, A.W., 1988, A modular three-dimensional finite-difference ground-water flow model: U.S. Geological Survey Techniques of Water-Resources Investigations, book 6, chap. A1, 586 p.

Mallams, J.L., and Lee, R.A., 2005, Hydrogeology of the ROMP 29A Sebring monitor well site, Highlands County, Florida: Brooksville, Fla., South Florida Water Management District Report, variously paged.

McGurk, Brian and Presley, P.F., 2002, Simulation of the effects of ground-water withdrawals on the Floridan aquifer system in east-central Florida: Model expansion and revision: Palatka, Fla., St. Johns River Water Management District Technical Publication SJ2002–3, 196 p.

Mecikalski, J.R., Sumner, D.M., Jacobs, J.M., Pathak, C.S., Paech, S.J., and Douglas, E.M., 2011, Use of visible geostationary operational meteorological satellite imagery in mapping reference and potential evapotranspiration over Florida, *in* Labedzki, Leszek, ed., Evapotranspiration: Vienna, Austria, InTech Publishers, 446 p.

Merritt, M.L. and Konikow, L.F., 2000, Documentation of a computer program to simulate lake-Aquifer interaction using the MODFLOW ground-water flow model and the MOC3D solute-transport model: U.S. Geological Survey Water-Resources Investigations Report 00–4167, 146 p.

Miller, J.A., 1986, Hydrogeologic framework of the Floridan aquifer system in Florida and parts of Georgia, Alabama, and South Carolina: U.S. Geological Survey Professional Paper 1403–B, 91 p.

Murch, R.R., and Tara, P., 2010, Central Florida Coordination Area: statistical analysis: Special Publication SJ2010–SP13, Prepared for the St. Johns River Water Management District, Palatka, Fla., and the Southwest Florida Water Management District, Brooksville, Fla., 106 p., 2 appendixes.

Nachabe, M., Masek, C., and Obeysekera, J., 2004, Observations and modeling of profile water storage above a shallow water table: Soil Science Society of America Journal, v. 68, no. 3, p. 719–724.

National Oceanic and Atmospheric Administration, 2011, NOAA's 1981–2010 Climate Normals: Accessed November 2011 at *http://www.ncdc.noaa.gov/oa/climate/normals/usnormals.html.*

Natural Resources Conservation Service, 2011, Soil survey geographic (SSURGO) database for Florida: United States Department of Agriculture [cited November 2011] *http://soildatamart.nrcs.usda.gov*.

Niswonger, R.G., Prudic, D.E., and Regan, S., 2006, Documentation of the Unsaturated-Zone Flow (UZF1) Package for modeling unsaturated flow between the land surface and the water table with MODFLOW-2005: U.S. Geological Survey Techniques and Methods, book 6, chap. A19, 62 p.

Niswonger, R.G., and Prudic, D.E., 2006, Documentation of the Streamflow-Routing (SFR2) Package to include unsaturated flow beneath streams—A modification to SFR1: U.S. Geological Survey Techniques and Methods, book 6, chap. A13, 48.

O'Reilly, A. M., 1998, Hydrogeology and simulation of the effects of reclaimed-water application in west Orange and southeast Lake Counties, Florida: U.S. Geological Survey Water-Resources Investigations Report 97–4199, 91 p.

O'Reilly, A.M., 2007, Effects of the temporal variability of evapotranspiration on hydrologic simulation in central Florida: U.S. Geological Survey Scientific Investigations Report 2007–5100, 36 p.

O'Reilly, A.M., Spechler, R.S., and McGurk, B.E., 2002, Hydrogeology and water-quality characteristics of the Lower Floridan Aquifer in east-Central Florida: U.S. Geological Survey Water-Resources Investigations Report 02–4193, 60 p.

Portier, K.M., 1988, Statistical sample survey design for estimation of agricultural water use: Palatka, Fla., St. Johns River Water Management District Special Publication SJ88–SP8, 49 p.

Rawls, W.J., Brakensiek, D.L., and Miller, N., 1983, Green-Ampt infiltration parameters from soils data: Journal of Hydraulic Engineering, v. 109, no. 1, p. 62–70.

Reese, R.S. and Richardson, E., 2008, Synthesis of the hydrogeologic framework of the Floridan aquifer system and delineation of a major Avon Park permeable zone in central and southern Florida: U.S. Geological Survey Scientific Investigations Report 2007–5207, 60 p.

Reilly, T.E., 2001, System and boundary conceptualization in ground-water flow simulation: U.S. Geological Survey Techniques of Water-Resources Investigations, book 3, chap. B8, 29 p.

Schellentrager, G.W., and Hurt, G.W., 1990, Soil survey of Seminole County, Florida: U.S. Department of Agriculture, Soil Conservation Service, 164 p.

Sepúlveda, N., 2002, Simulation of ground-water flow in the intermediate and Floridan aquifer systems in peninsular Florida: U.S. Geological Survey Water-Resources Investigations Report 02–4009, 130 p.

Sepúlveda, N., 2009, Analysis of methods to estimate spring flows in a karst aquifer: Ground Water, v. 47, no. 3, p. 337–349.

Shah, N., Nachabe, M., and Ross, M., 2007, Extinction depth and evapotranspiration from ground water under land covers: Ground Water, v. 45, no. 3, p. 329–338.

Singleton, V.D., 1996, Benchmark farms project water use report on leatherleaf fern and potatoes (1999–94): Palatka, Fla., St. Johns River Water Management District Technical Publication SJ96–4, 57 p.

Smajstrla, A.G., 1990, Technical manual—Agricultural Field Scale Irrigation Requirements Simulation (AFSIRS) model—Version 5.5: St. Johns River Water Management District Special Publication SJ2008–SP17, 251 p.

Snyder, J.P., 1983, Map projections used by the U.S. Geological Survey: U.S. Geological Survey Bulletin B-1532, 313 p.

Spechler, R.M., and Halford, K.J., 2001, Hydrogeology, water quality, and simulated effects of ground-water withdrawals from the Floridan aquifer system, Seminole County and vicinity, Florida: U.S. Geological Survey Water-Resources Investigations Report 01–4182, 116 p.

Spechler, R.M., and Kroening, S.E., 2007, Hydrology of Polk County, Florida: U.S. Geological Survey Scientific Investigations Report 2006–5320, 114 p.

Spechler, R.M., 2010, Hydrogeology and groundwater quality of Highlands County, Florida: U.S. Geological Survey Scientific Investigations Report 2010–5097, 84 p.

Sprinkle, C.L., 1989, Geochemistry of the Floridan aquifer system in Florida and in parts of Georgia, South Carolina, and Alabama: U.S. Geological Survey Professional Paper 1403–I, 105 p.

St. Johns River Water Management District, 2004, Abandoned Artesian Well Plugging Program 2003: St. Johns River Water Management District Fact Sheet SJ2004–FS3, 4 p.

Sumner, D. M., 1996, Evapotranspiration from successional vegetation in a deforested area of the Lake Wales Ridge, Florida, U.S. Geological Survey Water-Resources Investigations Report 96–4244, 38 p.

Sumner, D. M., 2001, Evapotranspiration from a cypress and pine forest subjected to natural fires in Volusia County, Florida, U.S. Geological Survey Water-Resources Investigations Report 01–4245, 56 p.

Sumner, D.M., and Jacobs, J.M., 2005, Utility of Penman–Monteith, Priestley–Taylor, reference evapotranspiration, and pan evaporation methods to estimate pasture evapotranspiration: Journal of Hydrology, v. 308, p. 81–104.

Sumner, D.M., 2006, Adequacy of selected evapotranspiration approximations for hydrologic simulation: Journal of the American Water Resources Association, v. 42, no. 3, p. 699–711.

Sumner, D.M., and Bradner, L.A., 1996, Hydraulic characteristics and nutrient transport and transformation beneath a rapid infiltration basin, Reedy Creek Improvement District, Orange County, Florida: U.S. Geological Survey Water-Resources Investigations Report 95–4281, 51 p.

Swancar, A., Lee, T.M., and O'Hare, T.M., 2000, Hydrogeologic setting, water budget, and preliminary analysis of ground-water exchange at Lake Starr, Polk County, Florida: U.S. Geological Survey Water-Resources Investigations Report 00–4030, 65 p.

Tibbals, C.H., 1978, Effects of paved surfaces on recharge to the Floridan aquifer in east-central Florida—A conceptual model: U.S. Geological Survey Water-Resources Investigations Report 78–76, 42 p.

Tihansky, A.B., Arthur, J.D., and Dewitt, D.W., 1996, Sublake geologic structure from high-resolution seismic-reflection data from four sinkhole lakes in the Lake Wales Ridge, central Florida: U.S. Geological Survey Open-File Report 96–224, 71 p.

Todd, D.K., 1980, Groundwater hydrology (2d ed.), New York, John Wiley, 535 p.

U.S. Geological Survey, 2012, Florida Water Science Center evapotranspiration information and data [cited May 2012] *http://fl.water.usgs.gov/et/*.

White, W.A., 1970, The geomorphology of the Florida peninsula: Tallahassee, Florida Geological Survey Bulletin 51, 164 p.

Wyrick, G.G., 1960, The ground-water resources of Volusia County, Florida: Tallahassee, Florida Geological Survey Report of Investigations 22, 65 p.

Yobbi, D.K., 1996, Analysis and simulation of ground-water flow in Lake Wales Ridge and adjacent areas of central Florida: U.S. Geological Survey Water-Resources Investigations Report 94–4254, 82 p.

Appendixes 1–5

Appendix 1. Groundwater Withdrawals and Inflows

Table 1–1. Annual average of groundwater withdrawals from public-water supply wells by aquifer and by county.—Continued

[Counties: Bre, Brevard; Lak, Lake; Mar, Marion; Ora, Orange; Osc, Osceola; Pol, Polk; Sem, Seminole; Sum, Sumter; Vol, Volusia; Tot, total withdrawals for the aquifer; aquifers: SAS, surficial aquifer system; INT, intermediate confining unit or intermediate aquifer system; OPZ, Ocala permeable zone; OLPZ, Ocala low-permeable zone; APPZ, Avon Park permeable zone; MCU, middle confining units I and II; LFA, Lower Floridan aquifer; ALL, inclusion of all aquifers; Ave, average rate from 1995 to 2006; all rates are in million gallons per day]

Use	1995	1996	1997	1998	1999	2000	2001	2002	2003	2004	2005	2006	Ave
SAS-Bre	5.4	5.3	4.8	5.0	5.2	5.8	5.8	5.9	6.1	6.1	5.4	5.8	5.6
SAS-Lak	0.2	0.3	0.3	0.3	0.3	0.3	0.3	0.3	0.3	0.3	0.3	0.4	0.3
SAS-Ora	1.8	1.5	3.6	2.3	2.1	2.1	2.2	2.4	2.2	2.4	2.3	1.7	2.2
SAS-Pol	0.2	0.1	0.3	0.3	0.6	0.9	0.7	0.7	0.8	0.7	0.5	0.7	0.5
SAS-Tot	7.6	7.2	9.0	7.9	8.2	9.1	9.0	9.3	9.4	9.5	8.5	8.6	8.6
INT-Bre	5.5	5.1	3.7	4.3	3.8	4.1	4.2	4.4	4.7	4.9	4.8	4.8	4.5
INT-Lak	0.0	0.0	0.0	0.0	0.0	0.0	0.1	0.1	0.1	0.1	0.0	0.0	0.0
INT-Mar	0.0	0.0	0.0	0.0	0.0	0.0	0.0	0.0	0.0	0.0	0.0	0.0	0.0
INT-Ora	0.3	0.3	0.7	0.4	0.4	0.4	0.4	0.4	0.4	0.4	0.3	0.3	0.4
INT-Osc	0.0	0.0	0.0	0.0	0.0	0.0	0.0	0.0	0.0	0.0	0.0	0.0	0.0
INT-Pol	2.0	2.1	2.1	2.0	2.2	2.3	1.9	2.4	2.3	2.2	2.8	3.2	2.3
INT-Sem	0.1	0.3	0.3	0.4	0.4	0.2	0.2	0.2	0.2	0.2	0.2	0.0	0.2
INT-Vol	0.0	0.0	0.0	0.0	0.0	0.0	0.0	0.0	0.0	0.0	0.0	0.0	0.0
INT-Tot	7.9	7.8	6.8	7.1	6.8	7.0	6.8	7.5	7.7	7.8	8.1	8.3	7.5
OPZ-Bre	0.8	0.9	0.7	0.8	0.7	0.7	1.1	1.3	1.3	1.4	1.3	1.4	1.0
OPZ-Lak	10.5	11.5	11.3	13.2	14.0	15.2	13.3	13.2	13.0	13.3	12.9	15.6	13.1
OPZ-Mar	0.7	0.8	0.9	1.3	1.6	1.9	1.8	1.8	1.9	2.2	2.2	2.9	1.7
OPZ-Ora	15.0	18.6	19.1	19.9	18.0	20.3	17.6	18.8	17.9	17.5	18.5	19.5	18.4
OPZ-Osc	3.0	3.3	3.5	3.6	3.6	4.3	4.1	3.8	3.6	4.0	4.3	4.9	3.8
OPZ-Pol	28.4	30.3	30.6	31.3	32.9	35.3	32.3	34.3	32.4	34.2	37.5	40.6	33.3
OPZ-Sem	21.5	22.7	23.1	27.7	28.2	31.6	27.4	26.2	25.1	26.6	24.7	28.6	26.1
OPZ-Sum	1.2	1.6	1.8	3.0	3.7	4.3	5.5	6.4	6.2	6.4	5.6	8.6	4.5
OPZ-Vol	21.1	23.4	23.8	26.2	25.7	28.2	25.1	27.2	28.0	28.3	26.3	30.7	26.2
OPZ-Tot	102.2	113.1	114.8	127.0	128.4	141.8	128.2	133.0	129.4	133.9	133.3	152.8	128.2
OLPZ-Bre	0.0	0.0	0.0	0.0	0.0	0.0	0.0	0.1	0.1	0.1	0.1	0.1	0.0
OLPZ-Lak	1.3	1.3	1.5	1.7	1.8	2.2	1.8	1.7	1.7	2.0	2.1	2.7	1.8
OLPZ-Mar	0.2	0.2	0.2	0.5	0.5	0.5	0.5	0.6	0.6	0.6	0.5	0.6	0.5
OLPZ-Ora	1.5	1.8	1.5	1.3	1.3	1.3	1.2	1.2	1.1	1.1	1.1	1.2	1.3
OLPZ-Osc	0.5	0.6	0.6	0.6	0.7	0.8	0.8	0.7	0.7	0.8	0.8	0.9	0.7
OLPZ-Pol	10.1	11.1	11.9	12.2	12.4	13.0	11.9	10.3	9.2	9.1	9.7	11.0	11.0
OLPZ-Sem	3.8	3.9	4.0	4.9	5.5	5.5	4.2	4.4	3.7	3.7	3.9	4.4	4.3
OLPZ-Sum	0.0	0.0	0.0	0.0	0.0	0.1	0.1	0.1	0.2	0.2	0.2	0.2	0.1
OLPZ-Vol	0.0	0.1	0.1	0.1	0.1	0.1	0.1	0.1	0.1	0.1	0.1	0.1	0.1
OLPZ-Tot	17.4	19.0	19.8	21.3	22.3	23.5	20.6	19.2	17.4	17.7	18.5	21.2	19.8
APPZ-Bre	6.4	8.2	7.6	8.2	7.6	6.6	6.1	7.9	8.3	8.9	8.4	9.7	7.8

Table 1–1. Annual average of groundwater withdrawals from public-water supply wells by aquifer and by county.—Continued

[Counties: Bre, Brevard; Lak, Lake; Mar, Marion; Ora, Orange; Osc, Osceola; Pol, Polk; Sem, Seminole; Sum, Sumter; Vol, Volusia; Tot, total withdrawals for the aquifer; aquifers: SAS, surficial aquifer system; INT, intermediate confining unit or intermediate aquifer system; OPZ, Ocala permeable zone; OLPZ, Ocala low-permeable zone; APPZ, Avon Park permeable zone; MCU, middle confining units I and II; LFA, Lower Floridan aquifer; ALL, inclusion of all aquifers; Ave, average rate from 1995 to 2006; all rates are in million gallons per day]

Use	1995	1996	1997	1998	1999	2000	2001	2002	2003	2004	2005	2006	Ave
APPZ-Lak	10.4	11.6	11.8	13.6	14.6	16.7	14.9	16.5	17.0	20.0	20.5	24.4	16.0
APPZ-Mar	0.6	0.7	0.7	1.0	1.4	1.6	1.5	1.5	1.8	2.2	2.1	2.8	1.5
APPZ-Ora	63.0	71.2	60.5	63.4	61.8	69.1	63.4	61.8	62.3	68.8	69.0	72.9	65.6
APPZ-Osc	13.5	14.1	15.7	19.9	22.0	25.9	22.8	22.6	22.6	25.3	25.3	28.7	21.5
APPZ-Pol	19.8	20.6	21.1	22.2	22.1	24.2	21.2	21.6	21.8	22.8	24.7	31.7	22.8
APPZ-Sem	21.4	21.2	21.5	23.6	23.7	27.0	22.3	22.3	23.2	25.1	25.2	28.7	23.8
APPZ-Sum	0.4	0.4	0.8	0.9	0.9	1.5	2.6	2.2	2.4	2.9	3.0	3.9	1.8
APPZ-Vol	4.2	5.0	4.9	5.2	5.1	6.1	5.6	5.8	5.5	5.8	6.2	7.4	5.6
APPZ-Tot	139.7	153.0	144.6	158.0	159.2	178.7	160.4	162.2	164.9	181.8	184.4	210.2	166.4
MCU-Lak	1.6	1.5	1.6	2.0	2.1	2.3	1.6	1.5	1.4	1.6	1.6	1.8	1.7
MCU-Mar	0.0	0.0	0.0	0.0	0.0	0.0	0.0	0.0	0.0	0.0	0.0	0.0	0.0
MCU-Ora	0.9	2.0	1.0	0.3	0.1	0.0	0.0	0.0	0.0	0.0	0.0	0.0	0.4
MCU-Osc	0.0	0.0	0.0	0.0	0.0	0.0	0.0	0.0	0.0	0.0	0.0	0.0	0.0
MCU-Pol	0.0	0.0	0.0	0.0	0.0	0.0	0.0	0.0	0.0	0.0	0.0	0.0	0.0
MCU-Sem	0.3	0.3	0.3	0.4	0.5	0.5	0.4	0.5	0.6	0.6	0.5	0.5	0.5
MCU-Sum	0.0	0.0	0.0	0.0	0.0	0.0	0.0	0.0	0.0	0.0	0.0	0.0	0.0
MCU-Tot	2.8	3.8	2.9	2.7	2.7	2.8	2.0	2.0	2.0	2.2	2.1	2.3	2.5
LFA-Lak	1.0	1.3	1.4	1.5	1.5	1.6	1.3	1.3	1.2	1.3	1.3	3.3	1.5
LFA-Ora	88.5	93.4	99.7	120.3	125.1	136.8	115.7	115.1	115.1	121.4	124.9	132.4	115.7
LFA-Osc	0.1	0.2	0.2	0.3	0.5	0.5	0.5	0.5	0.6	0.6	0.6	0.7	0.4
LFA-Pol	0.0	0.0	0.0	0.0	0.0	0.0	0.0	0.0	0.0	0.0	0.0	0.0	0.0
LFA-Sem	2.3	2.1	2.1	2.2	2.2	2.7	2.4	2.4	2.4	2.9	2.6	2.5	2.4
LFA-Sum	0.0	0.0	0.0	0.0	0.0	0.0	0.0	0.0	0.9	1.8	0.2	4.7	0.6
LFA-Tot	91.9	97.0	103.4	124.3	129.3	141.6	119.9	119.3	120.2	128.0	129.6	143.6	120.7
ALL-Tot	369.5	400.9	401.3	448.3	456.9	504.5	446.9	452.5	451.0	480.9	484.5	547.0	453.7

Table 1–2. Annual average of groundwater withdrawals from commercial or industrial wells by aquifer and by county.

[Counties: Bre, Brevard; Har, Hardee; Hig, Highlands; Lak, Lake; Mar, Marion; Oke, Okeechobee; Ora, Orange; Osc, Osceola; Pol, Polk; Sum, Sumter; Vol, Volusia; Tot, total withdrawals for the aquifer; aquifers: SAS, surficial aquifer system; INT, intermediate confining unit or intermediate aquifer system; OPZ, Ocala permeable zone; OLPZ, Ocala low-permeable zone; APPZ, Avon Park permeable zone; MCU, middle confining units I and II; LFA, Lower Floridan aquifer; ALL, inclusion of all aquifers; Ave, average rate from 1995 to 2006; all rates are in million gallons per day]

Use	1995	1996	1997	1998	1999	2000	2001	2002	2003	2004	2005	2006	Ave
SAS-Bre	0.3	0.3	0.3	0.5	0.4	0.5	0.5	0.4	0.3	0.3	0.1	0.1	0.3
SAS-Hig	0.4	0.4	0.3	0.3	0.3	0.1	0.2	0.1	0.1	0.1	0.0	0.0	0.2
SAS-Lak	0.1	0.1	0.1	0.1	0.0	0.0	0.0	0.0	0.0	0.0	0.1	0.0	0.0
SAS-Ora	0.0	0.3	0.6	0.6	0.7	0.5	0.5	0.5	0.6	0.5	0.4	0.0	0.4
SAS-Pol	0.0	0.0	0.0	0.0	0.0	0.0	0.0	0.0	0.0	0.0	0.0	0.0	0.0
INT-Bre	1.3	0.9	0.9	0.7	0.6	0.5	0.2	0.2	0.2	0.1	0.0	0.1	0.5
INT-Har	0.0	0.0	0.0	0.0	0.0	0.0	0.0	0.0	0.0	0.0	0.0	0.0	0.0
INT-Lak	0.1	0.1	0.1	0.1	0.1	0.0	0.0	0.0	0.4	0.5	0.5	0.5	0.2
INT-Ora	0.0	0.0	0.0	0.0	0.0	0.0	0.0	0.0	0.0	0.0	0.0	0.0	0.0
INT-Osc	0.0	0.0	0.0	0.0	0.0	0.0	0.0	0.0	0.0	0.0	0.0	0.0	0.0
INT-Pol	4.4	5.1	4.1	4.7	4.2	4.6	4.5	6.5	4.8	4.8	3.9	5.6	4.8
OPZ-Bre	0.8	0.7	1.0	0.8	0.9	1.3	1.0	1.4	1.6	1.2	1.0	1.3	1.1
OPZ-Hig	0.2	0.2	0.2	0.2	0.2	0.1	0.1	0.1	0.1	0.1	0.0	0.0	0.1
OPZ-Lak	3.5	3.7	4.3	4.7	4.6	2.6	0.9	0.6	0.7	0.6	0.9	1.1	2.4
OPZ-Mar	0.0	0.0	0.0	0.0	0.0	0.0	0.0	0.0	0.0	0.0	0.0	0.0	0.0
OPZ-Oke	0.2	0.0	0.0	0.0	0.0	0.0	0.0	0.0	0.0	0.0	0.0	0.0	0.0
OPZ-Ora	0.0	0.0	0.0	0.0	0.0	0.0	0.0	0.0	0.0	0.0	0.0	0.0	0.0
OPZ-Pol	26.1	24.5	25.4	24.6	24.4	22.1	21.8	23.6	21.3	19.7	16.5	19.4	22.5
OPZ-Sum	0.0	0.0	0.0	0.0	0.0	0.0	0.0	0.0	0.0	0.0	0.0	0.0	0.0
OPZ-Vol	0.1	0.0	0.0	0.0	0.1	0.1	0.5	0.1	0.3	0.1	0.1	0.1	0.1
OLPZ-Hig	0.4	0.4	0.3	0.3	0.3	0.1	0.2	0.1	0.0	0.1	0.1	0.1	0.2
OLPZ-Lak	0.1	0.1	0.1	0.2	0.2	0.1	0.1	0.0	0.3	0.1	0.3	0.2	0.2
OLPZ-Ora	0.0	0.0	0.0	0.0	0.0	0.0	0.0	0.0	0.0	0.0	0.0	0.0	0.0
OLPZ-Pol	30.8	29.7	26.0	28.1	22.1	21.7	20.2	19.1	20.7	15.0	14.4	18.4	22.2
APPZ-Hig	0.1	0.2	0.1	0.1	0.1	0.0	0.1	0.0	0.0	0.1	0.0	0.0	0.1
APPZ-Lak	0.6	0.6	0.6	0.6	0.6	0.6	0.6	0.4	0.5	0.5	0.6	0.5	0.6
APPZ-Ora	0.0	0.0	0.0	0.0	0.0	0.0	0.0	0.0	0.0	0.0	0.0	0.0	0.0
APPZ-Pol	3.1	3.1	2.9	3.0	3.0	2.8	2.9	3.5	3.8	3.3	3.2	4.3	3.2
APPZ-Vol	0.1	0.1	0.1	0.1	0.2	0.2	0.1	0.1	0.0	0.0	0.0	0.0	0.1
MCU-Lak	0.5	0.5	0.5	0.7	0.7	0.7	0.8	0.9	0.6	0.6	0.5	0.6	0.6
MCU-Ora	0.0	0.0	0.0	0.0	0.0	0.0	0.0	0.0	0.0	0.0	0.0	0.0	0.0
LFA-Lak	0.0	0.0	0.0	0.0	0.0	0.0	0.0	0.0	0.0	0.0	0.0	0.0	0.0
LFA-Ora	0.0	0.0	0.0	0.0	0.0	0.0	0.0	0.0	0.0	0.0	0.0	0.3	0.0
LFA-Vol	0.2	0.1	0.1	0.1	0.2	0.3	0.2	0.1	0.0	0.1	0.1	0.1	0.1
ALL-Tot	73.4	71.1	68.0	70.5	63.9	58.9	55.4	57.7	56.3	47.8	42.7	52.7	59.9

Table 1–3. Summary of Benchmark Farms data used to estimate groundwater withdrawals for agricultural irrigation.

[Average irrigation is in inches per month]

Crop type	Number of projects	Average irrigation
Citrus	10,095	0.98
Flat wood citrus	4,851	0.78
Leather leaf	4,699	3.36
Nursery	5	2.72
Fern	942	1.17
Potatoes	5,077	1.45
Sod	1,068	1.11

Table 1–4. Annual average of groundwater withdrawals from agricultural wells by county.

[Ave, average rate from 1995 to 2006; all rates are in million gallons per day]

Use	1995	1996	1997	1998	1999	2000	2001	2002	2003	2004	2005	2006	Ave
Brevard	30.4	36.3	34.3	39.4	36.2	33.8	21.6	20.7	12.7	17.1	10.3	17.1	25.8
Hardee	24.2	29.2	29.3	31.6	33.4	38.1	35.0	33.2	21.1	24.0	14.0	27.5	28.4
Highlands	16.2	22.9	20.4	23.9	22.9	29.9	23.0	22.3	17.6	18.2	12.7	23.0	21.1
Indian River	36.3	51.6	38.4	51.5	52.2	97.3	58.1	60.5	41.5	40.2	16.6	43.7	49.0
Lake	27.8	31.2	25.2	38.8	28.5	41.3	41.2	26.9	27.5	22.8	11.1	27.7	29.2
Marion	2.2	3.1	2.5	3.5	3.0	2.6	2.9	1.9	2.1	1.5	0.6	1.9	2.3
Okeechobee	7.2	9.8	7.8	9.2	3.6	5.8	3.8	2.9	2.4	5.8	4.0	9.2	6.0
Orange	30.9	27.9	21.9	44.9	23.9	46.5	30.5	28.8	14.5	23.6	6.6	14.6	26.2
Osceola	11.4	15.6	13.3	16.4	13.8	22.3	15.0	13.2	10.7	11.1	6.7	15.8	13.8
Polk	92.9	116.5	110.5	121.0	123.5	153.8	128.6	121.1	83.0	93.3	60.5	109.4	109.5
Seminole	4.7	4.9	4.2	5.8	5.0	6.6	3.8	3.7	3.1	3.7	1.1	2.1	4.1
St. Lucie	21.9	30.9	20.2	30.1	24.2	29.9	23.5	20.4	18.3	19.4	9.7	27.3	23.0
Sumter	1.2	1.5	1.2	1.4	1.4	2.0	1.4	1.3	1.3	1.3	0.8	1.4	1.4
Volusia	13.3	14.9	11.3	14.0	13.4	18.8	12.5	13.4	8.8	9.6	4.9	8.3	11.9
Total	320.6	396.3	340.5	431.5	385.0	528.7	400.9	370.3	264.6	291.6	159.6	329.0	351.6

Appendix 2. Springs

Table 2–1. List of names and spring numbers in the East-Central Florida Transient (ECFT) model area.

[SN, Spring number; Row, Col, model grid row and column of spring; XUTM, YUTM, horizontal and vertical coordinates in NAD 83 Universal Transverse Mercator, zone 17N, in meters]

SN	Spring name	Row	Col	XUTM	YUTM
1	Alexander Spring	9	114	443965	3217088
2	Apopka (Gourdneck) Spring	159	86	433454	3160198
3	Blue Spring (Volusia County)	48	174	466913	3202228
4	Blue Springs (Lake County)	106	49	419175	3180423
5	Bugg Spring	104	30	411986	3180866
6	Camp La-no-che Springs	47	123	447399	3202657
7	Clifton Springs	120	200	476767	3174832
8	Droty Springs	83	130	450209	3189042
9	Gemini Springs	73	181	469694	3192839
10	Green Spring	73	197	475746	3192739
11	Holiday Springs	108	51	420141	3179484
12	Island Spring in Wekiva River	84	154	459428	3188456
13	Messant Spring	75	133	451299	3192153
14	Miami Springs	117	147	456754	3175969
15	Palm Springs	123	160	461624	3173844
16	Rock Springs	104	132	451035	3181095
17	Sanlando Springs	123	159	461352	3173581
18	Seminole Spring	79	126	448509	3190664
19	Starbuck Spring	121	161	461795	3174471
20	Wekiva Falls Resort (flowing 14-inch borehole)	93	153	458944	3185333
21	Wekiwa Springs	117	143	455056	3176192
22	Witherington Springs	111	135	452210	3178330

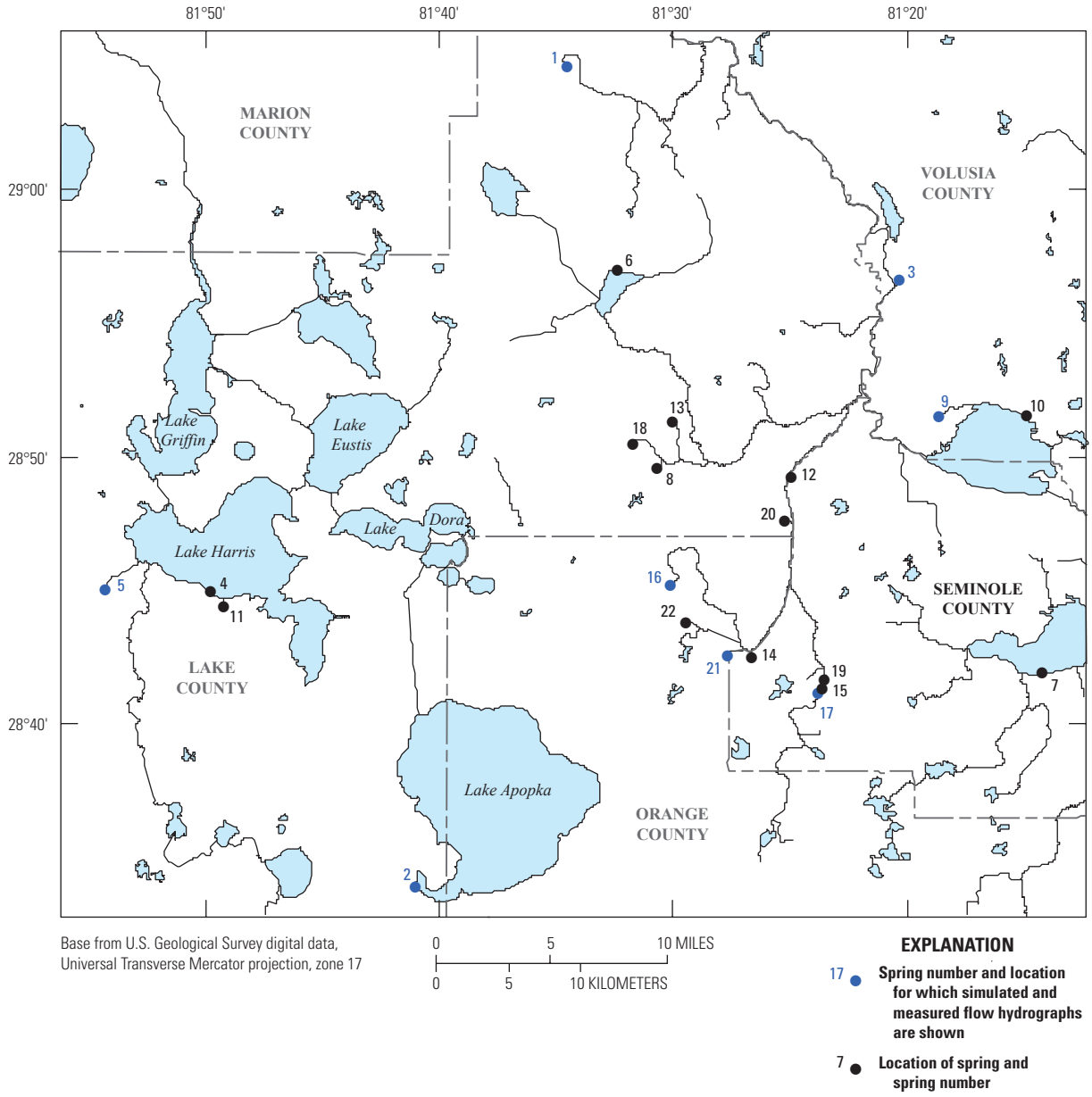

Figure 2–1. Selected springs for which simulated and measured spring-flow hydrographs are shown.

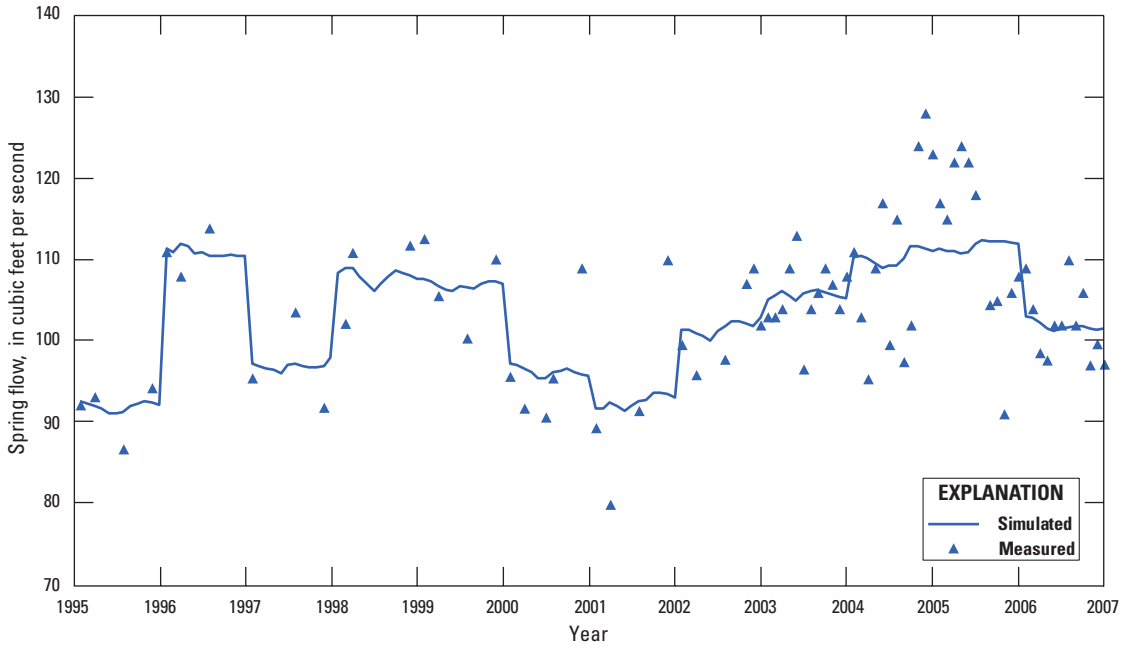

Figure 2–2. Measured and simulated flows for Alexander Spring, spring number 1 in figure 2–1.

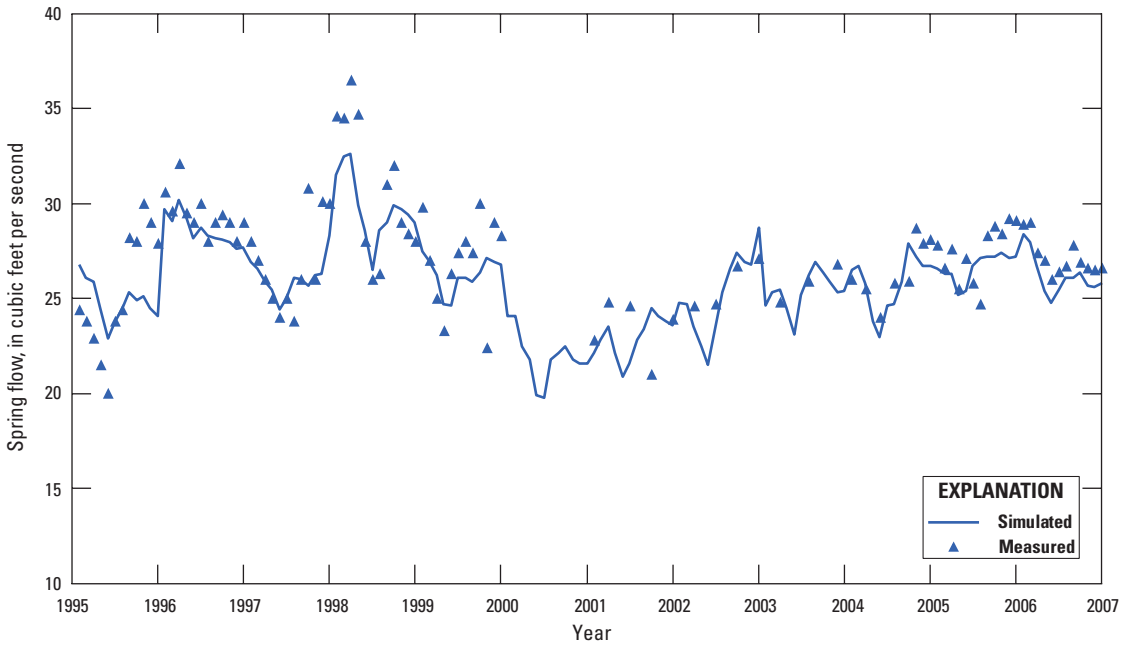

Figure 2–3. Measured and simulated flows for Apopka (Gourdneck) Spring, spring number 2 in figure 2–1.

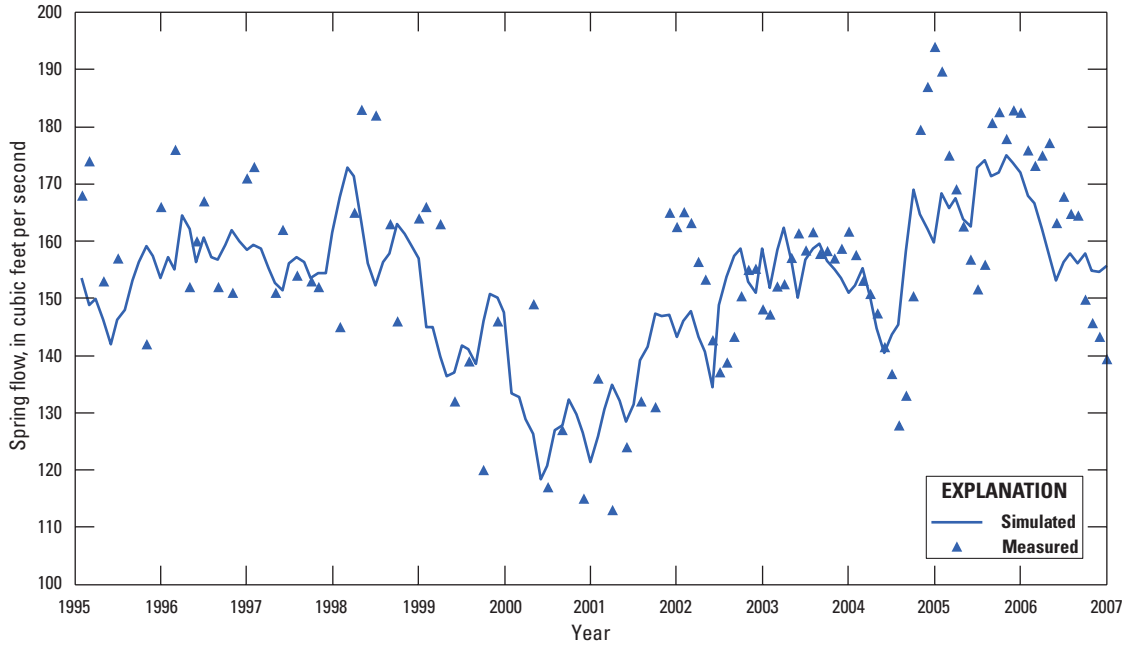

Figure 2–4. Measured and simulated flows for Blue Spring, spring number 3 in figure 2–1.

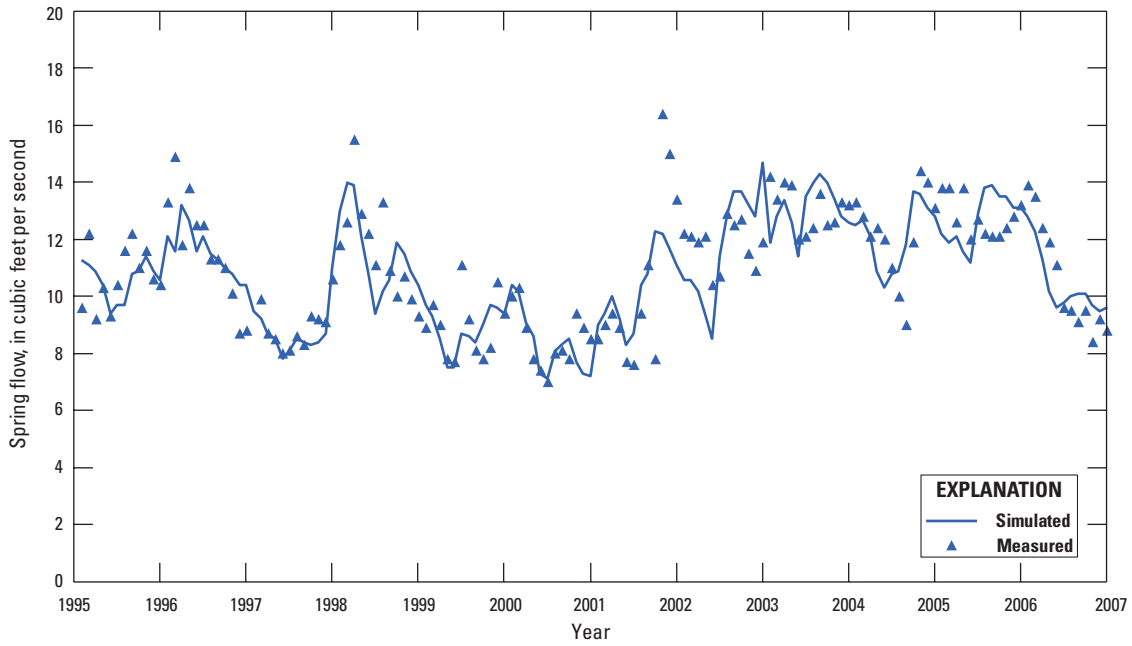

Figure 2–5. Measured and simulated flows for Bugg Spring, spring number 5 in figure 2–1.

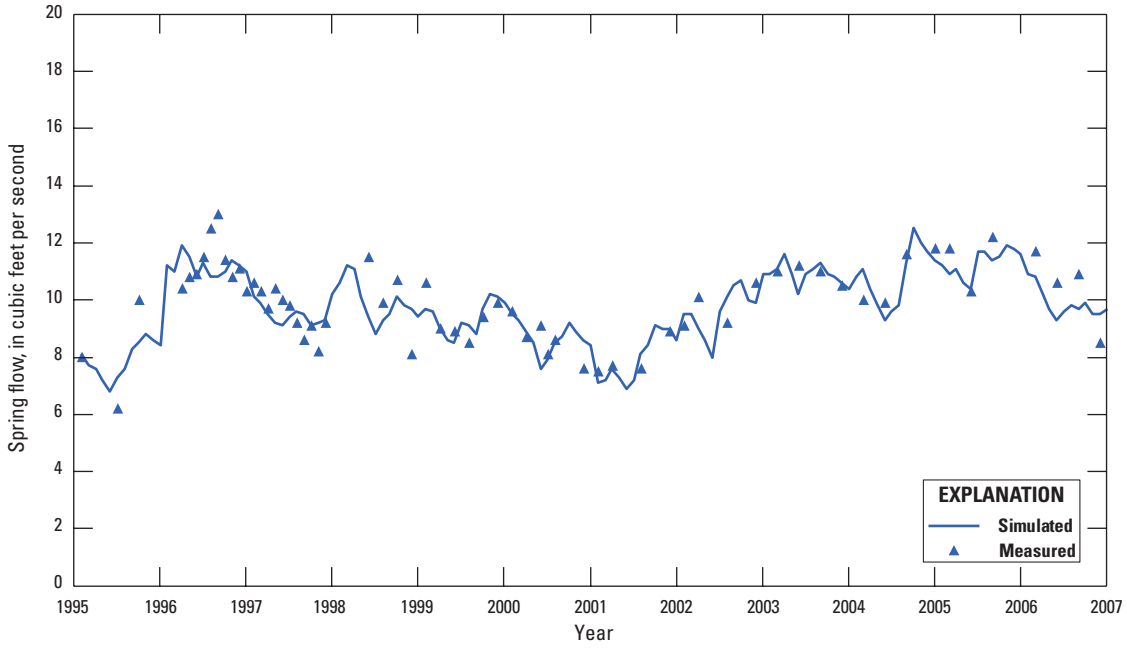

Figure 2–6. Measured and simulated flows for Gemini Springs, spring number 9 in figure 2–1.

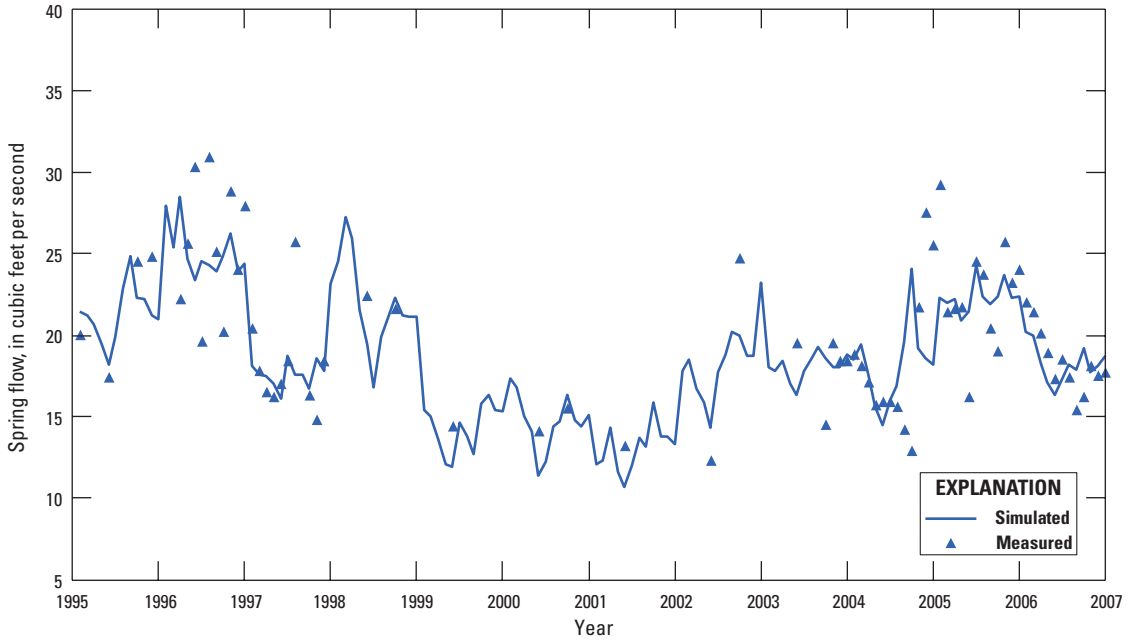

Figure 2–7. Measured and simulated flows for Sanlando Spring, spring number 17 in figure 2–1.

Appendix 3. Lakes

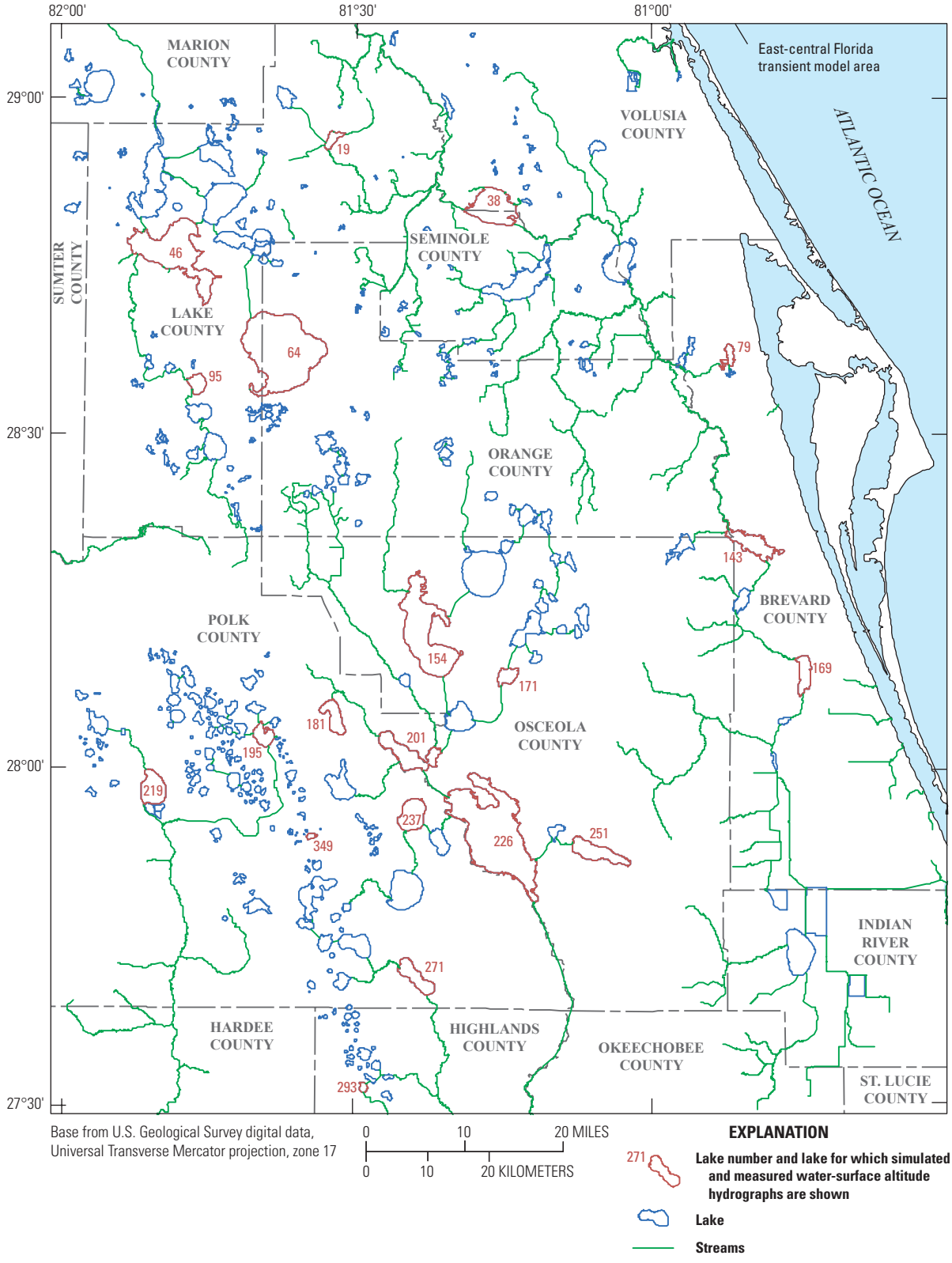

Figure 3–1. Selected lakes for which simulated and measured water-surface altitude hydrographs are shown.

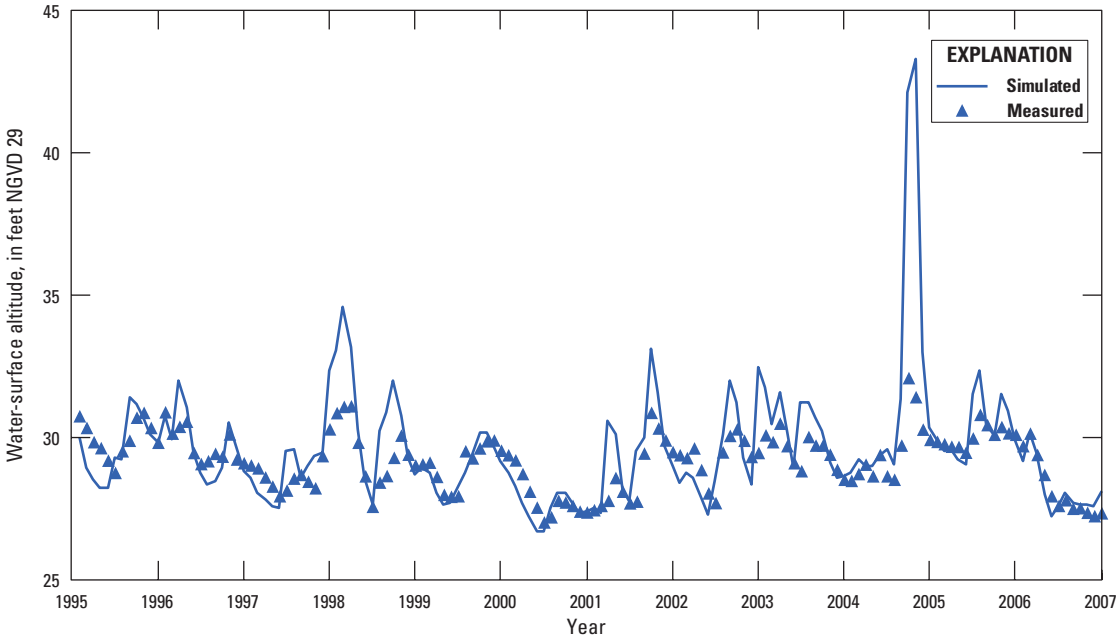

Figure 3–2. Measured and simulated water-surface altitude hydrographs for Lake Norris, lake number 19 in figure 3–1.

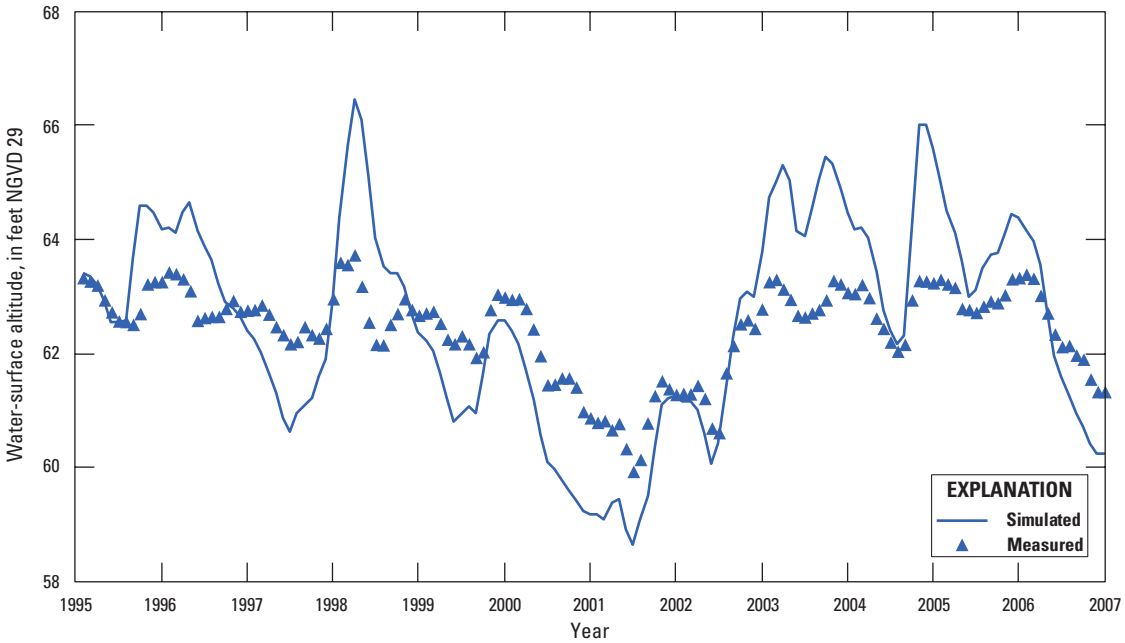

Figure 3–3. Measured and simulated water-surface altitude hydrographs for Lake Harris, lake number 46 in figure 3–1.

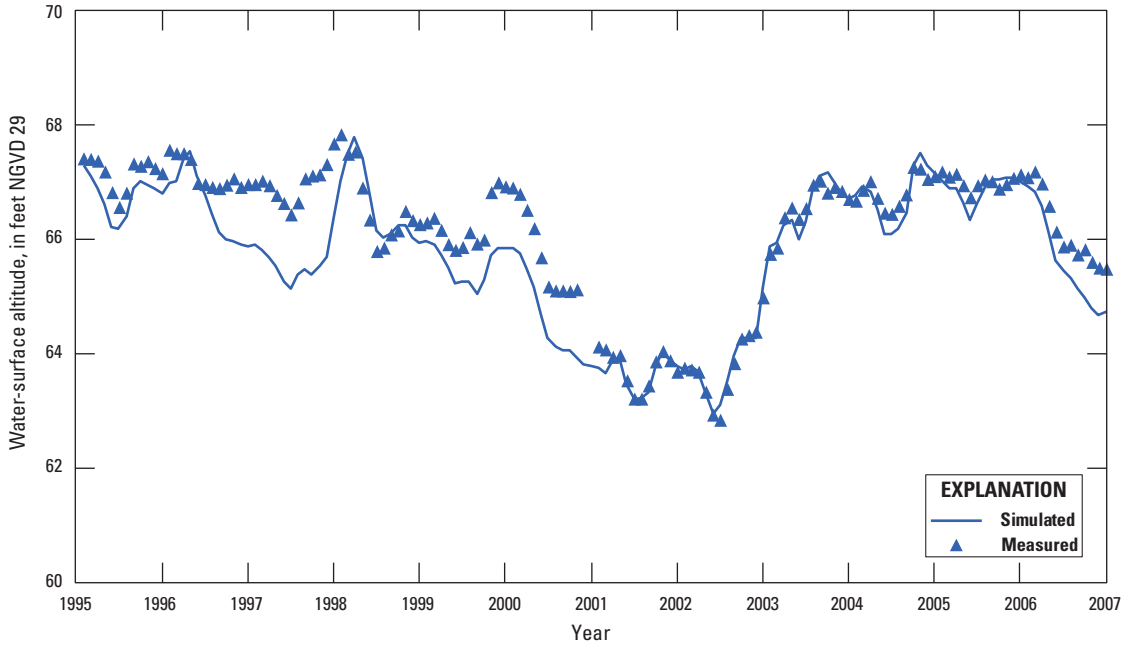

Figure 3–4. Measured and simulated water-surface altitude hydrographs for Lake Apopka, lake number 64 in figure 3–1.

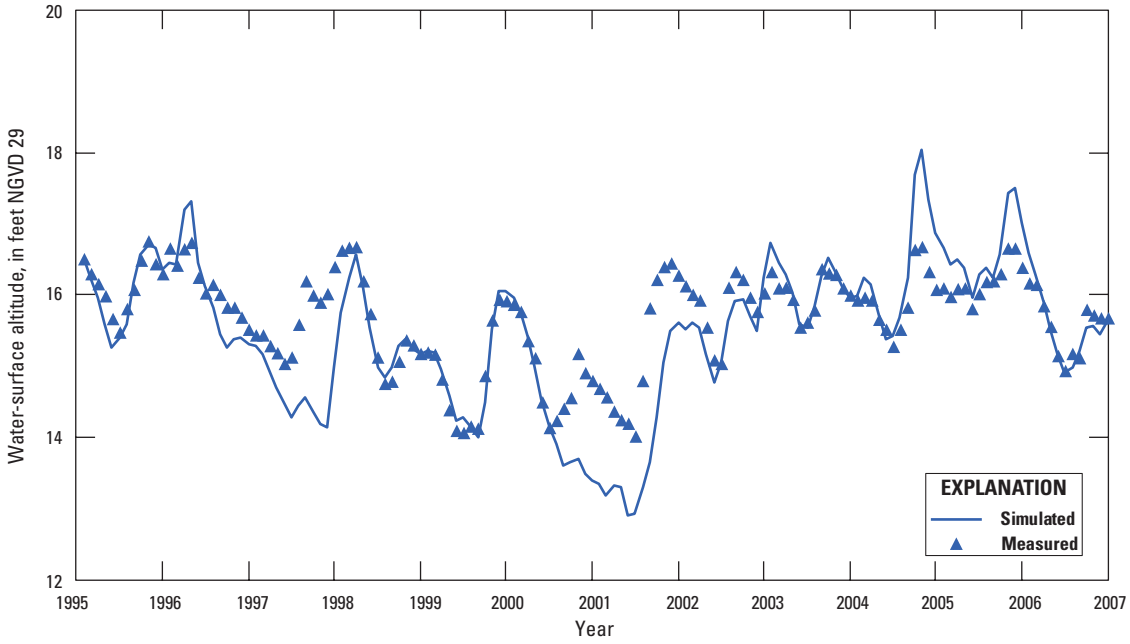

Figure 3–5. Measured and simulated water-surface altitude hydrographs for South Lake, lake number 79 in figure 3–1.

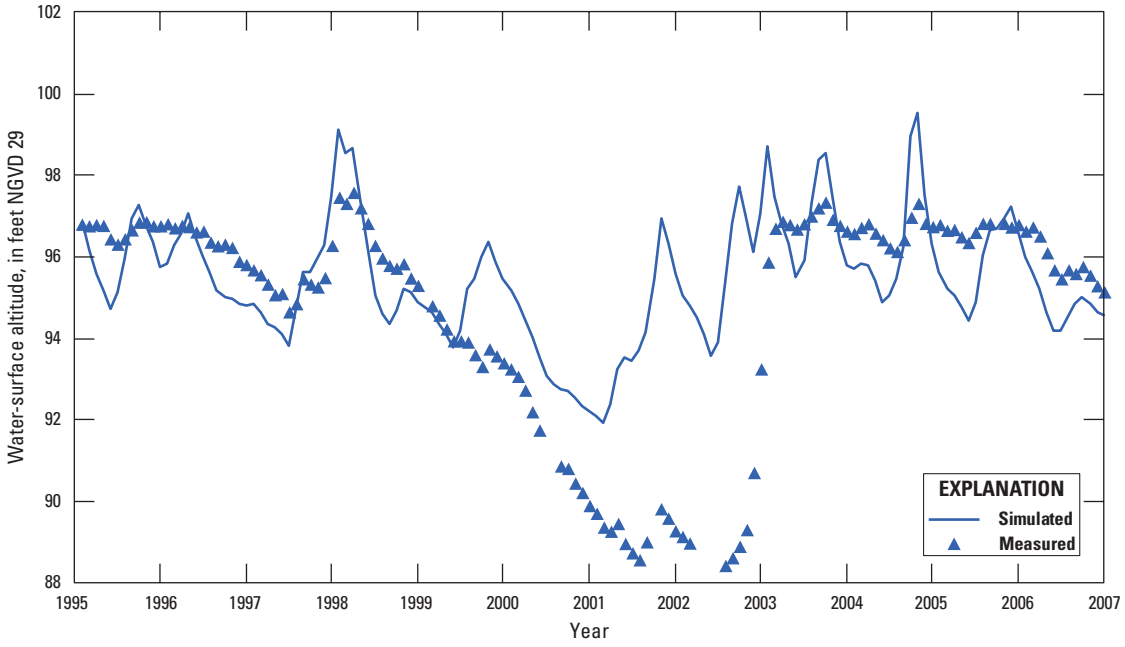

Figure 3–6. Measured and simulated water-surface altitude hydrographs for Lake Minneola, lake number 95 in figure 3–1.

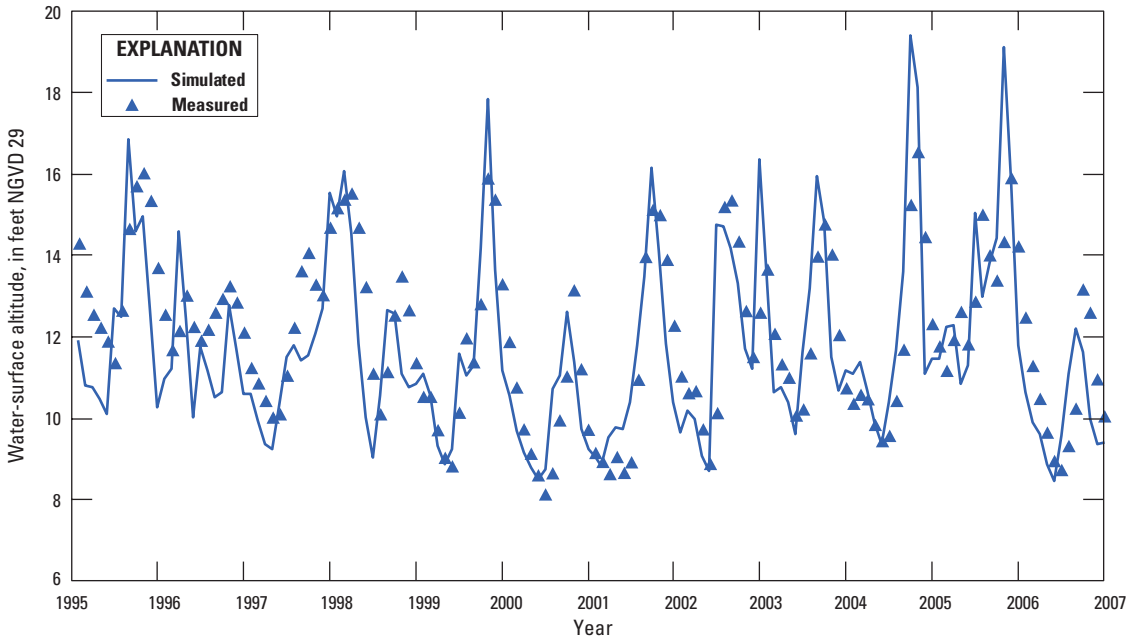

Figure 3–7. Measured and simulated water-surface altitude hydrographs for Lake Poinsett, lake number 143 in figure 3–1.

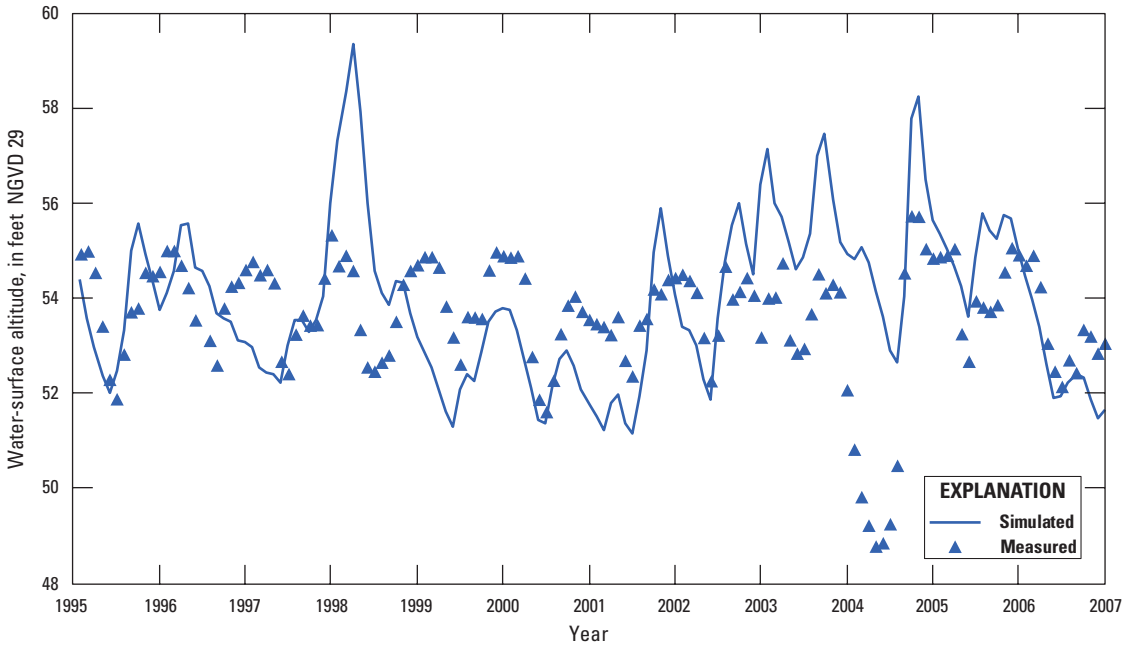

Figure 3–8. Measured and simulated water-surface altitude hydrographs for Lake Tohopekaliga, lake number 154 in figure 3–1.

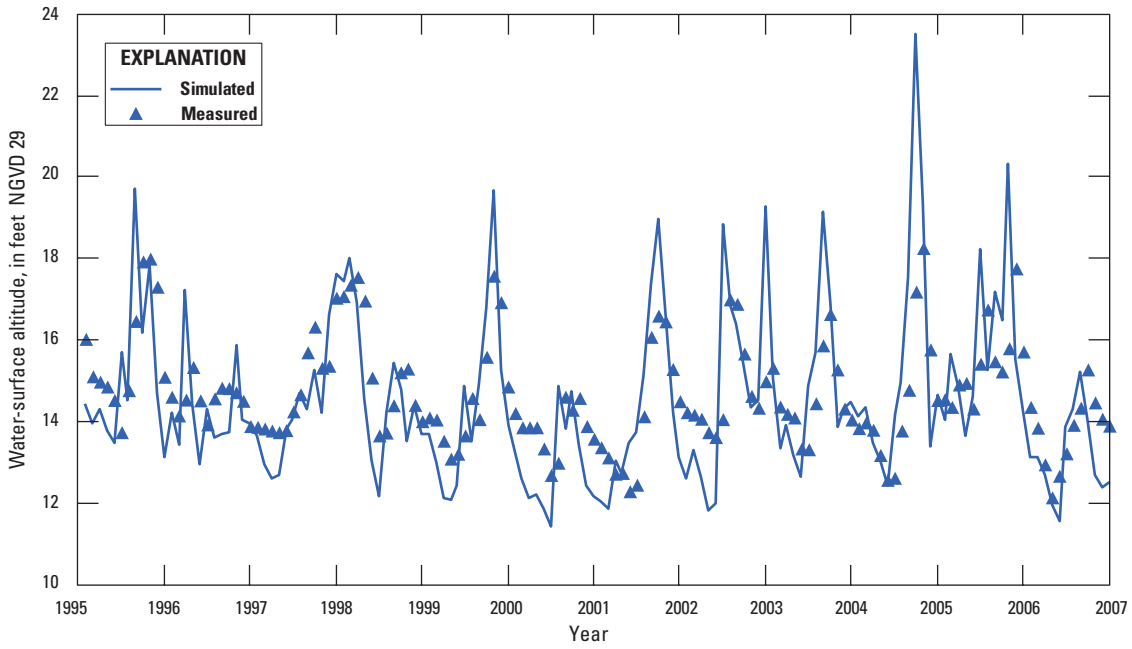

Figure 3–9. Measured and simulated water-surface altitude hydrographs for Lake Washington, lake number 169 in figure 3–1.

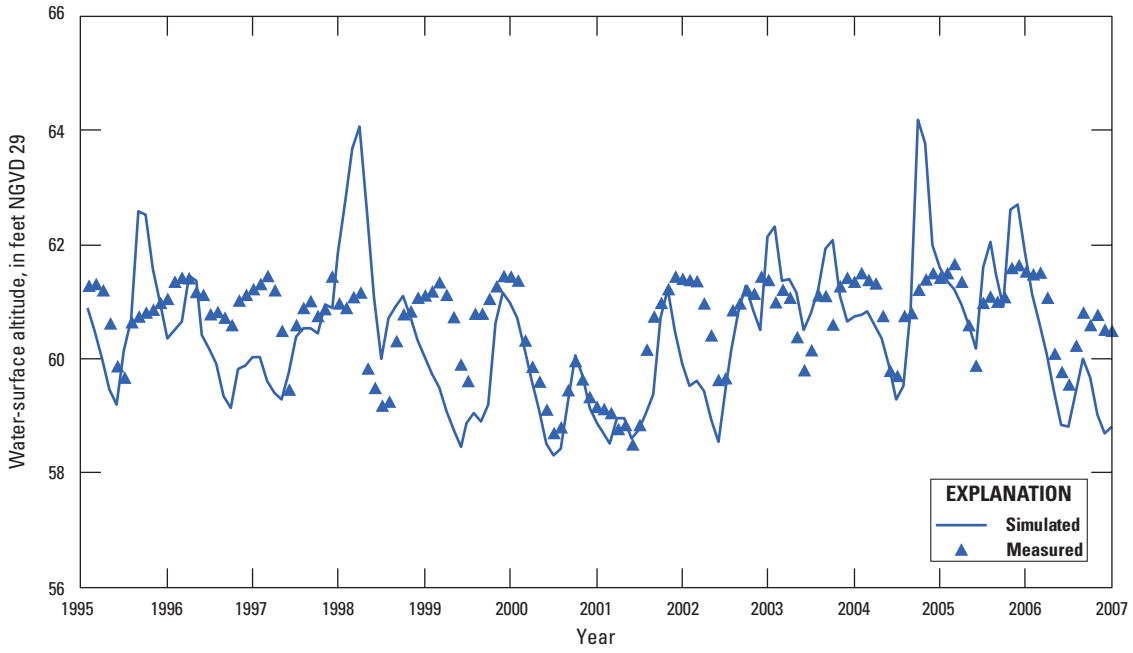

Figure 3–10. Measured and simulated water-surface altitude hydrographs for Lake Gentry, lake number 171 in figure 3–1.

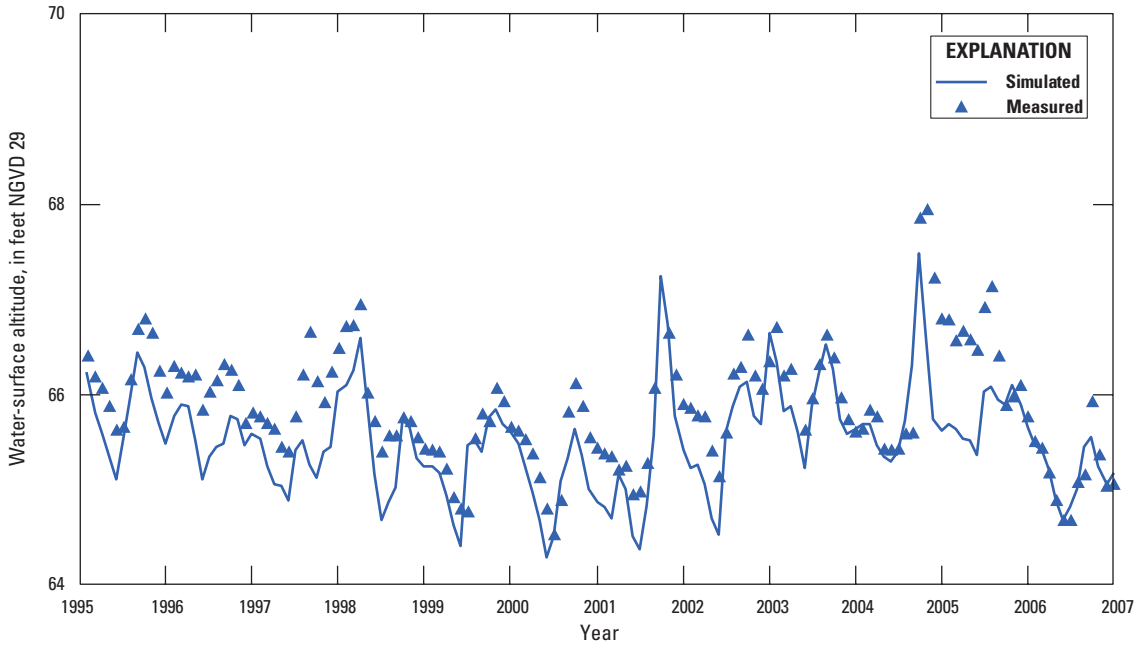

Figure 3–11. Measured and simulated water-surface altitude hydrographs for Lake Marion, lake number 181 in figure 3–1.

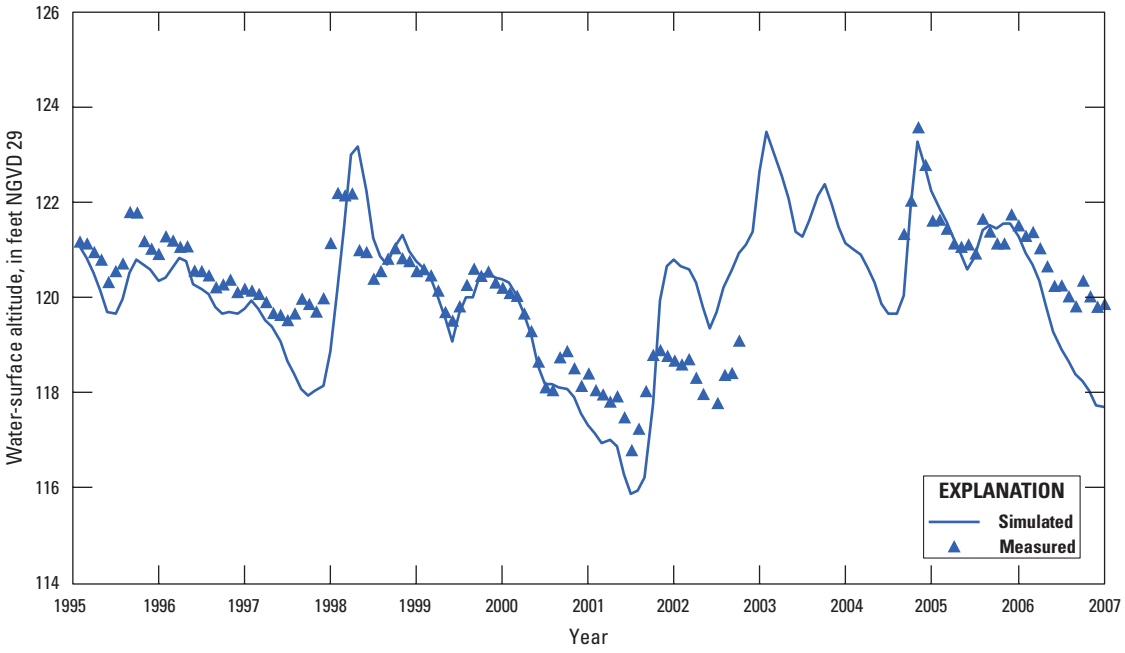

Figure 3–12. Measured and simulated water-surface altitude hydrographs for Lake Hamilton, lake number 195 in figure 3–1.

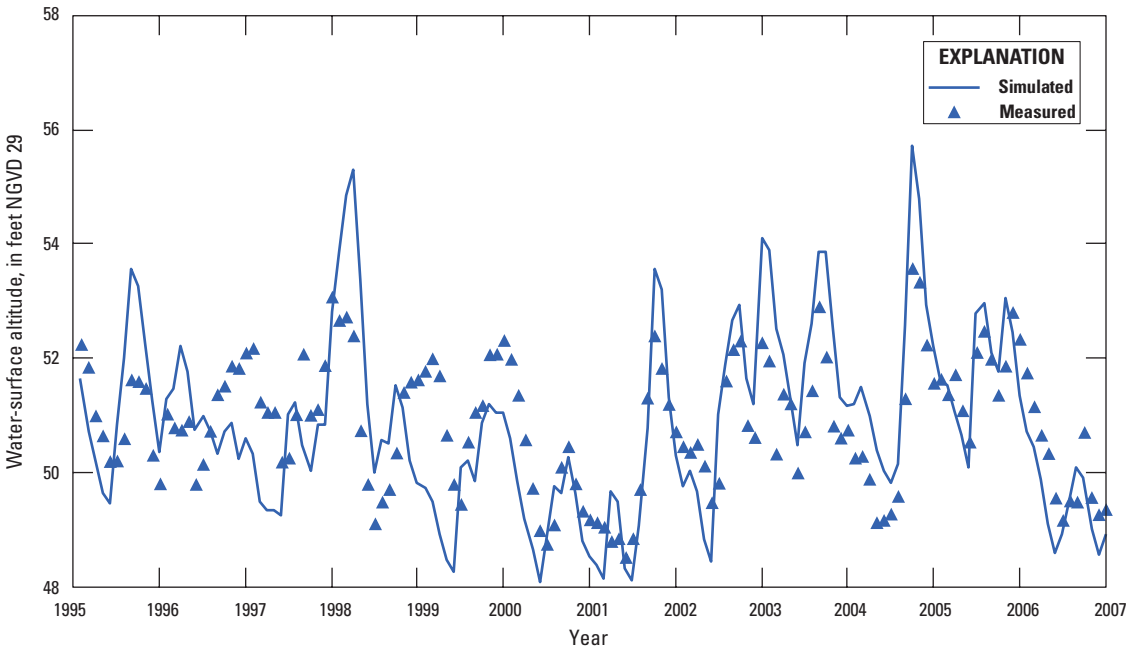

Figure 3–13. Measured and simulated water-surface altitude hydrographs for Lake Hatchineha, lake number 201 in figure 3–1.

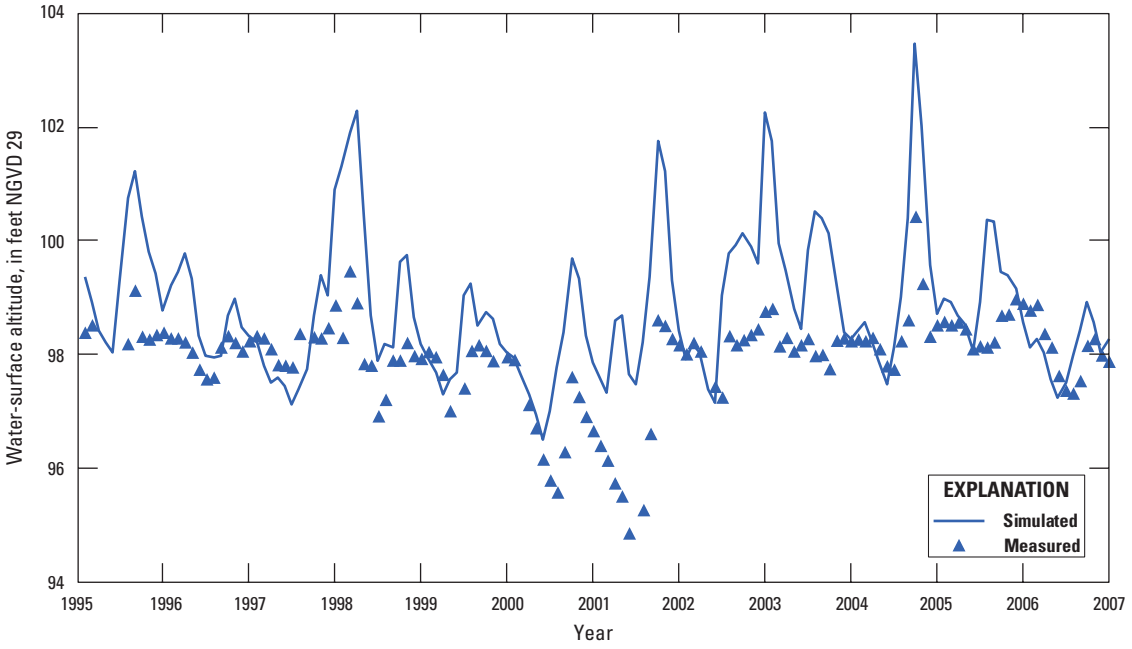

Figure 3–14. Measured and simulated water-surface altitude hydrographs for Lake Hancock, lake number 219 in figure 3–1.

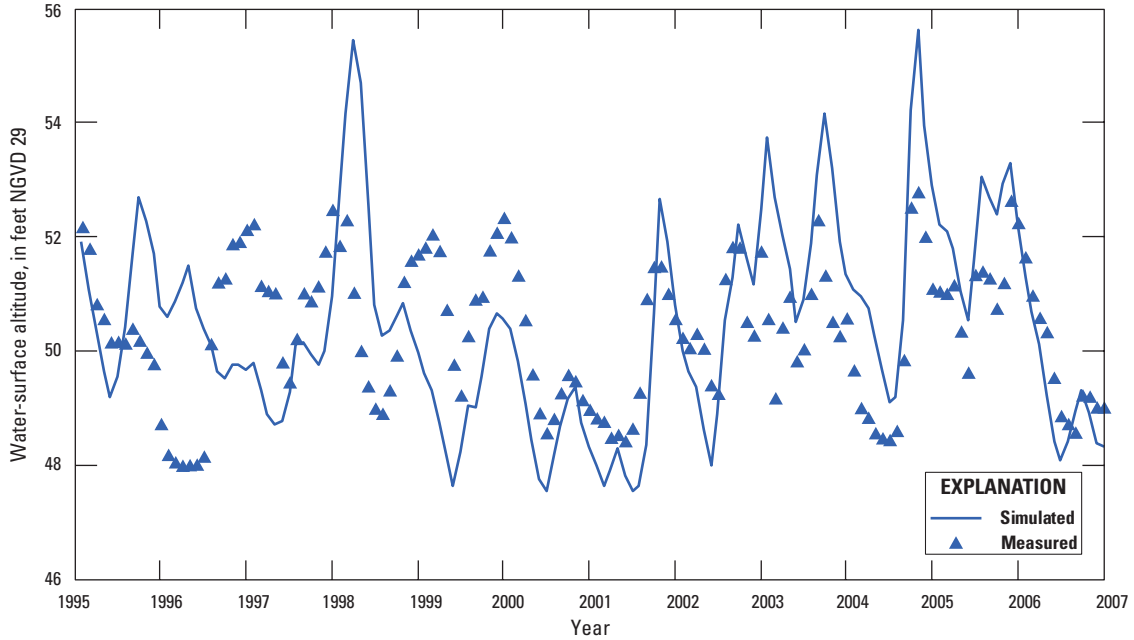

Figure 3–15. Measured and simulated water-surface altitude hydrographs for Lake Kissimmee, lake number 226 in figure 3–1.

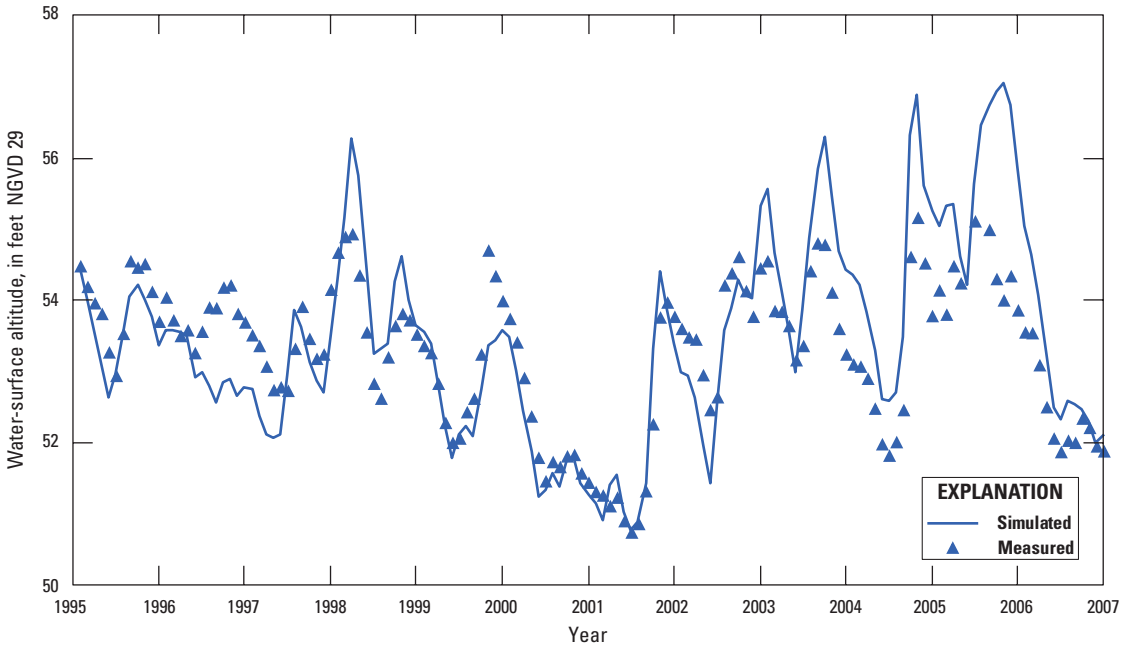

Figure 3–16. Measured and simulated water-surface altitude hydrographs for Lake Rosalie, lake number 237 in figure 3–1.

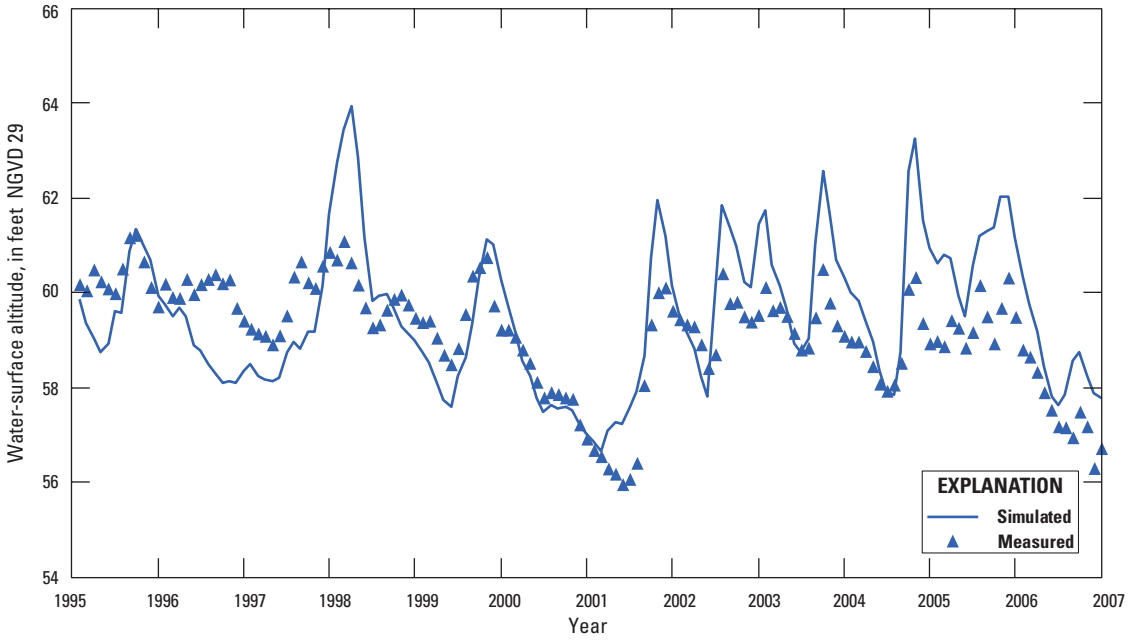

Figure 3–17. Measured and simulated water-surface altitude hydrographs for Lake Marian, lake number 251 in figure 3–1.

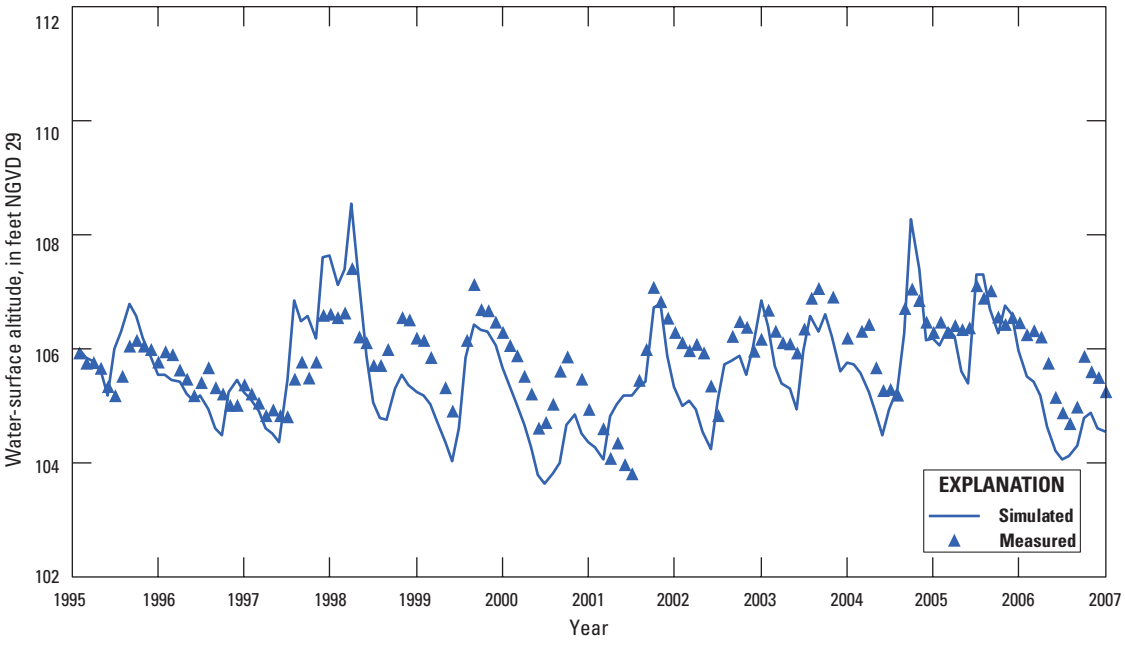

Figure 3–18. Measured and simulated water-surface altitude hydrographs for Lake Sebring, lake number 293 in figure 3–1.

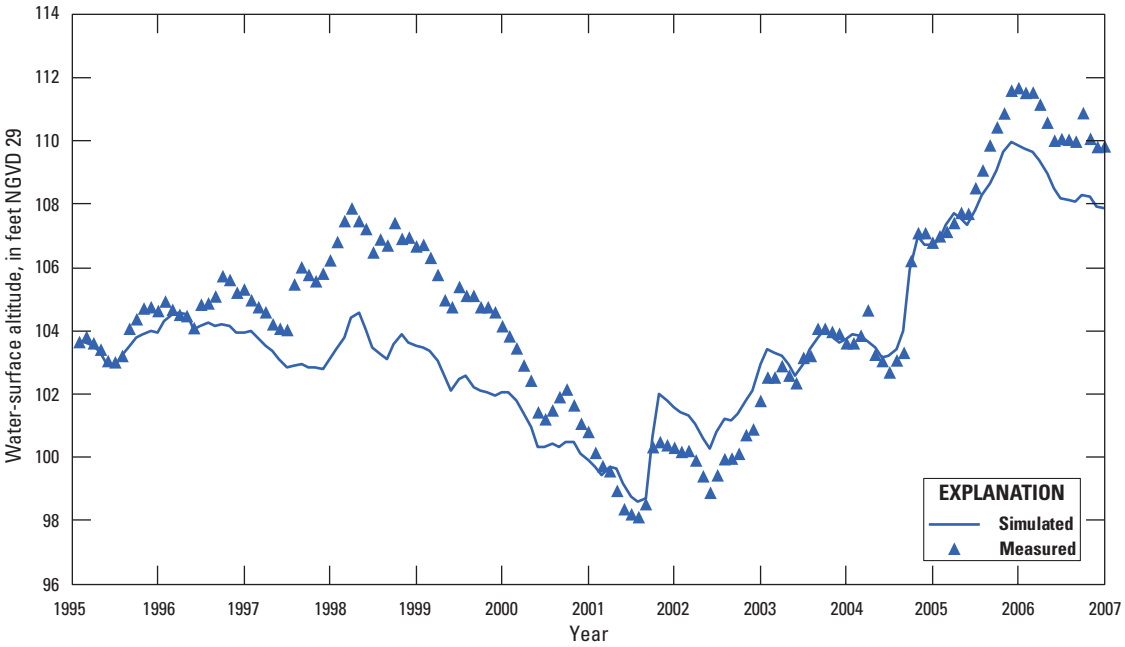

Figure 3–19. Measured and simulated water-surface altitude hydrographs for Lake Wales, lake number 349 in figure 3–1.

Appendix 4. Streams

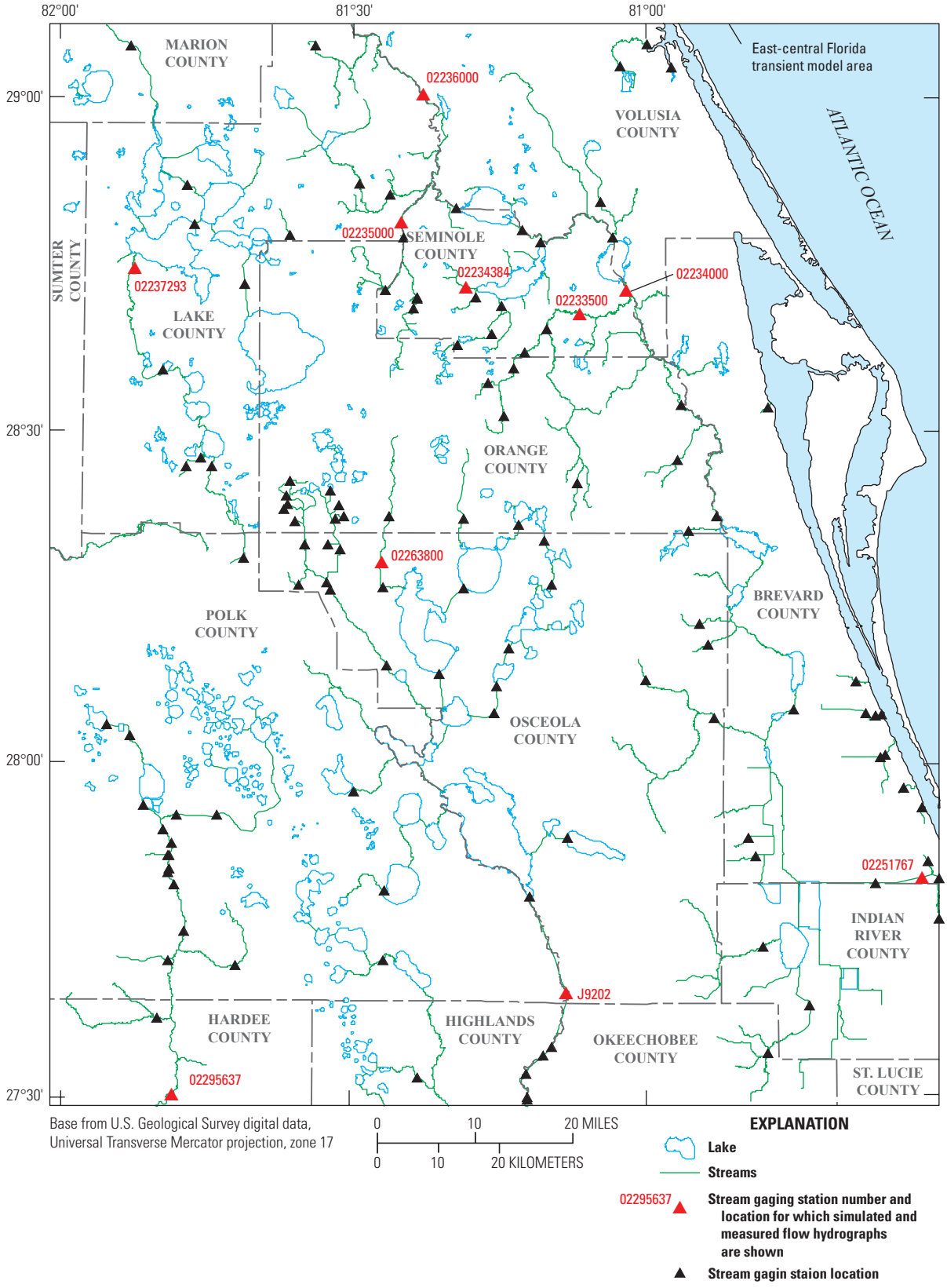

Figure 4–1. Selected stream-gaging stations for which simulated and measured flow hydrographs are shown.

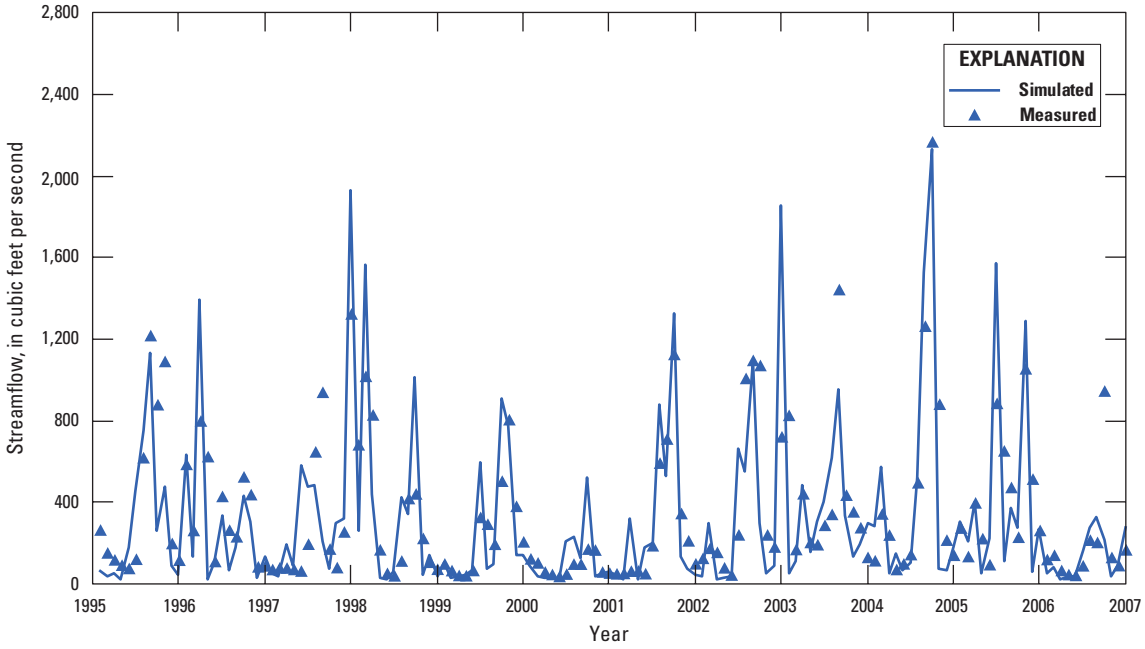

Figure 4–2. Measured and simulated flow hydrographs for Econlockhatchee River station number 02233500 in figure 4–1.

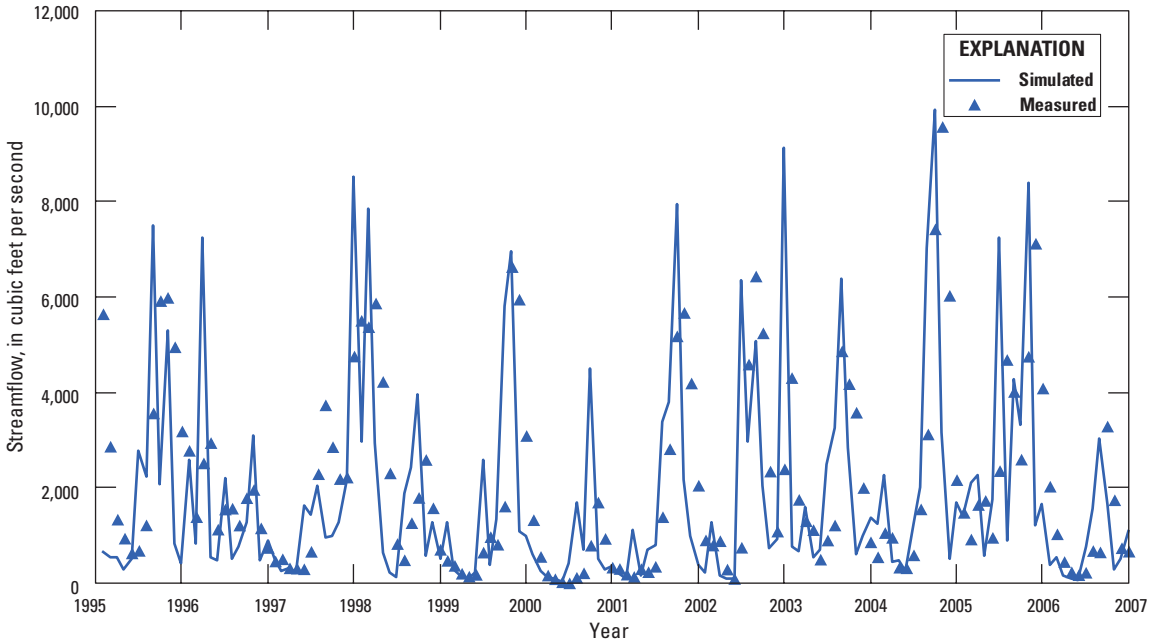

Figure 4–3. Measured and simulated flow hydrographs for St. Johns River above Lake Harney station number 02234000 in figure 4–1.

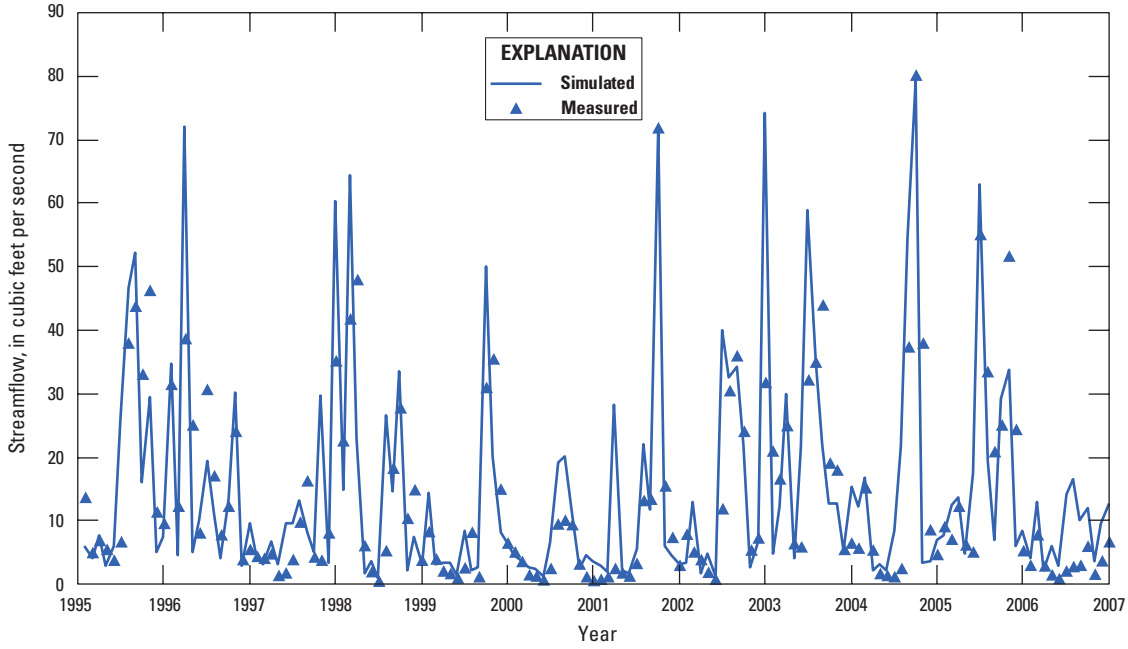

Figure 4–4. Measured and simulated flow hydrographs for Soldier Creek station number 02234384 in figure 4–1.

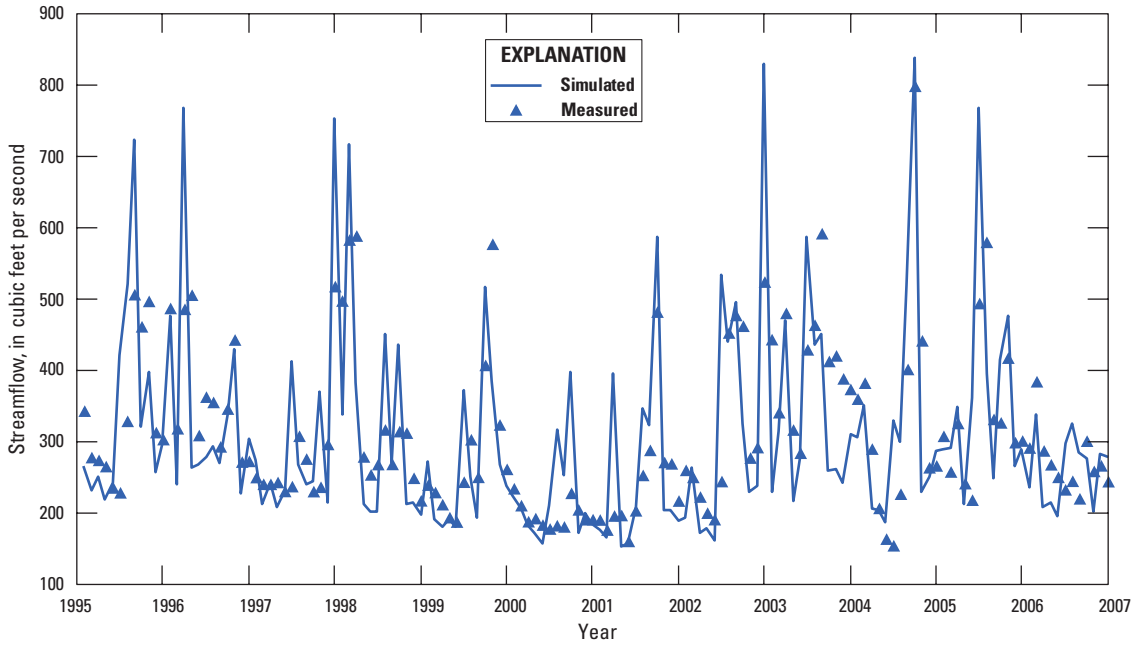

Figure 4–5. Measured and simulated flow hydrographs for Wekiva River station number 02235000 in figure 4–1.

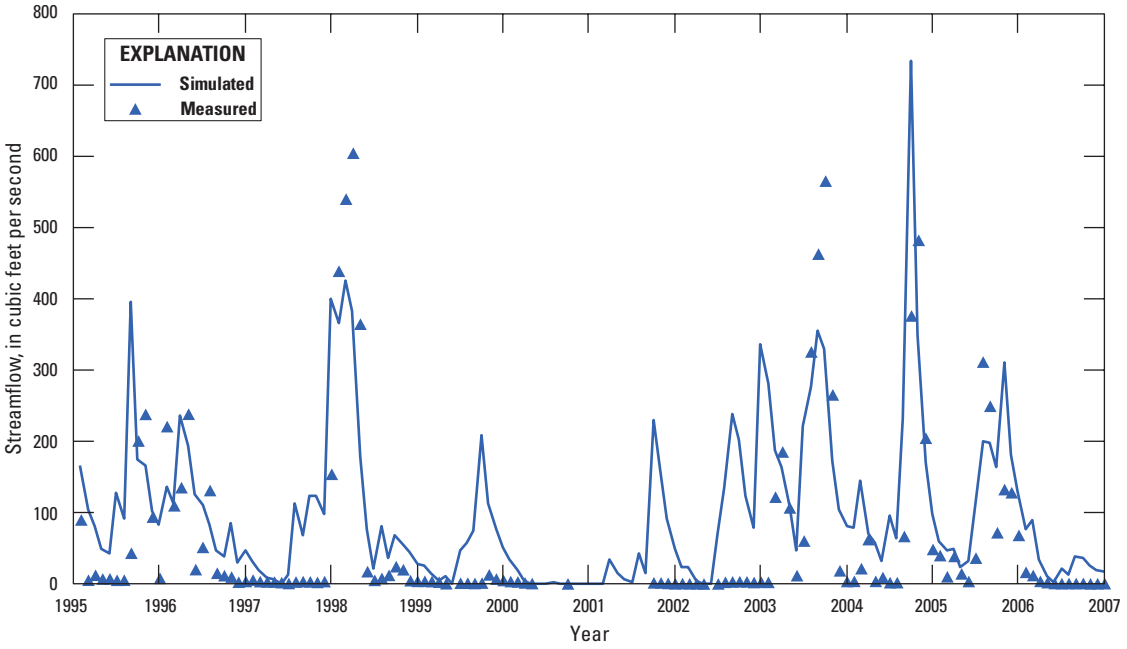

Figure 4–6. Measured and simulated flow hydrographs for Palatlakaha River station number 02237293 in figure 4–1.

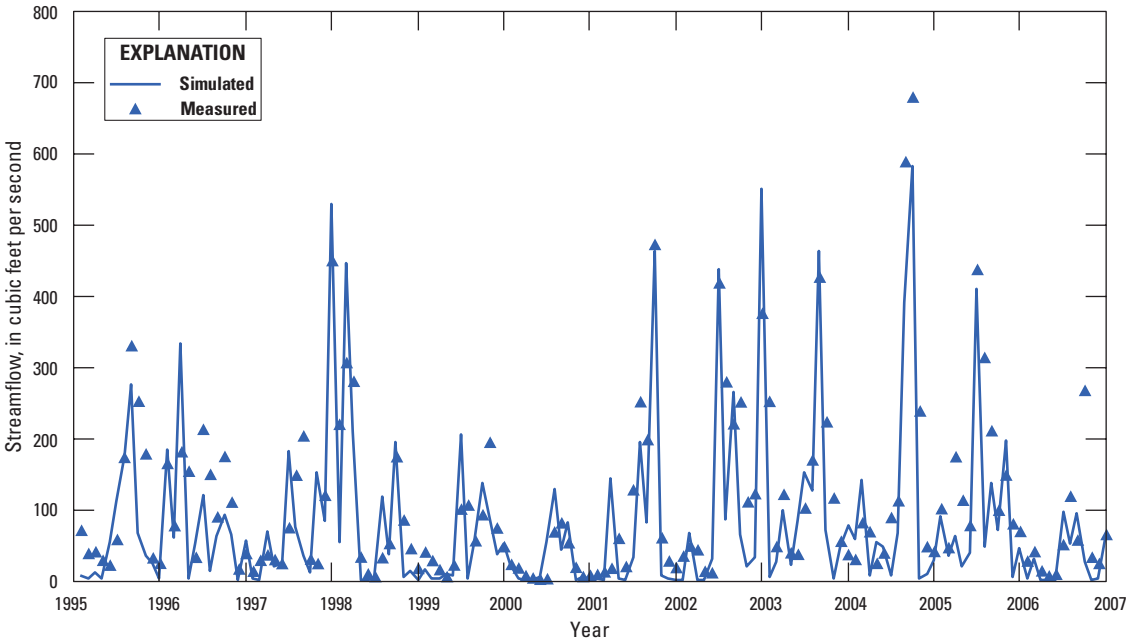

Figure 4–7. Measured and simulated flow hydrographs for Shingle Creek station number 02263800 in figure 4–1.

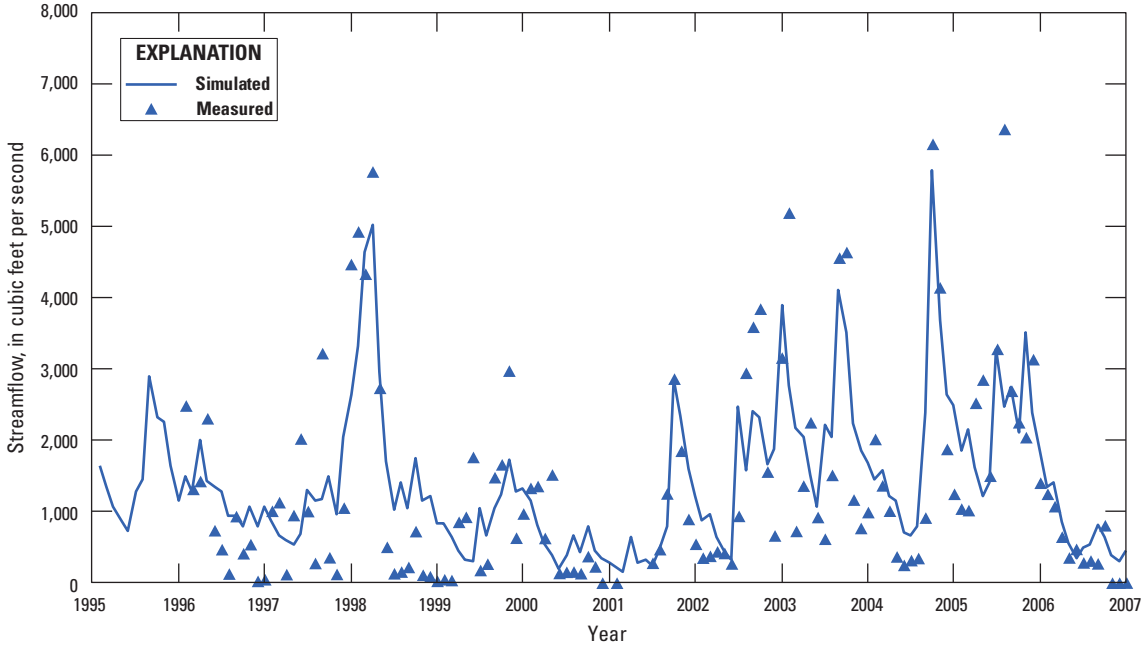

Figure 4–8. Measured and simulated flow hydrographs for Kissimmee River station identification J9202 in figure 4–1.

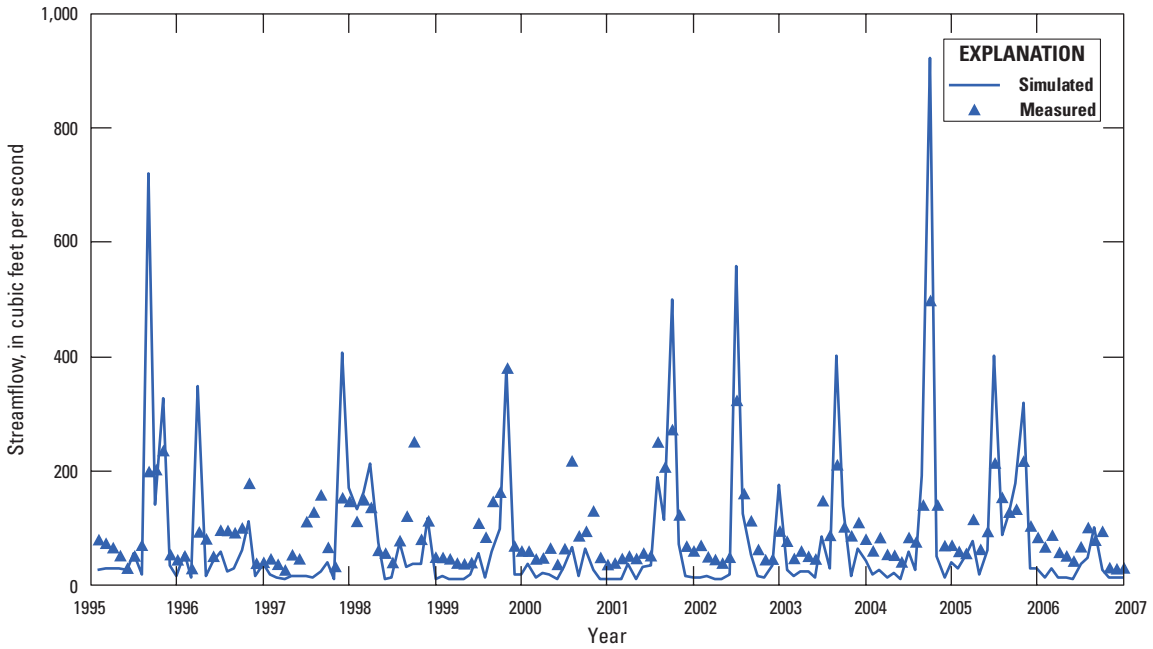

Figure 4–9. Measured and simulated flow hydrographs for Fellsmere Canal station number 02251767 in figure 4–1.

Appendix 5. Well Hydrographs

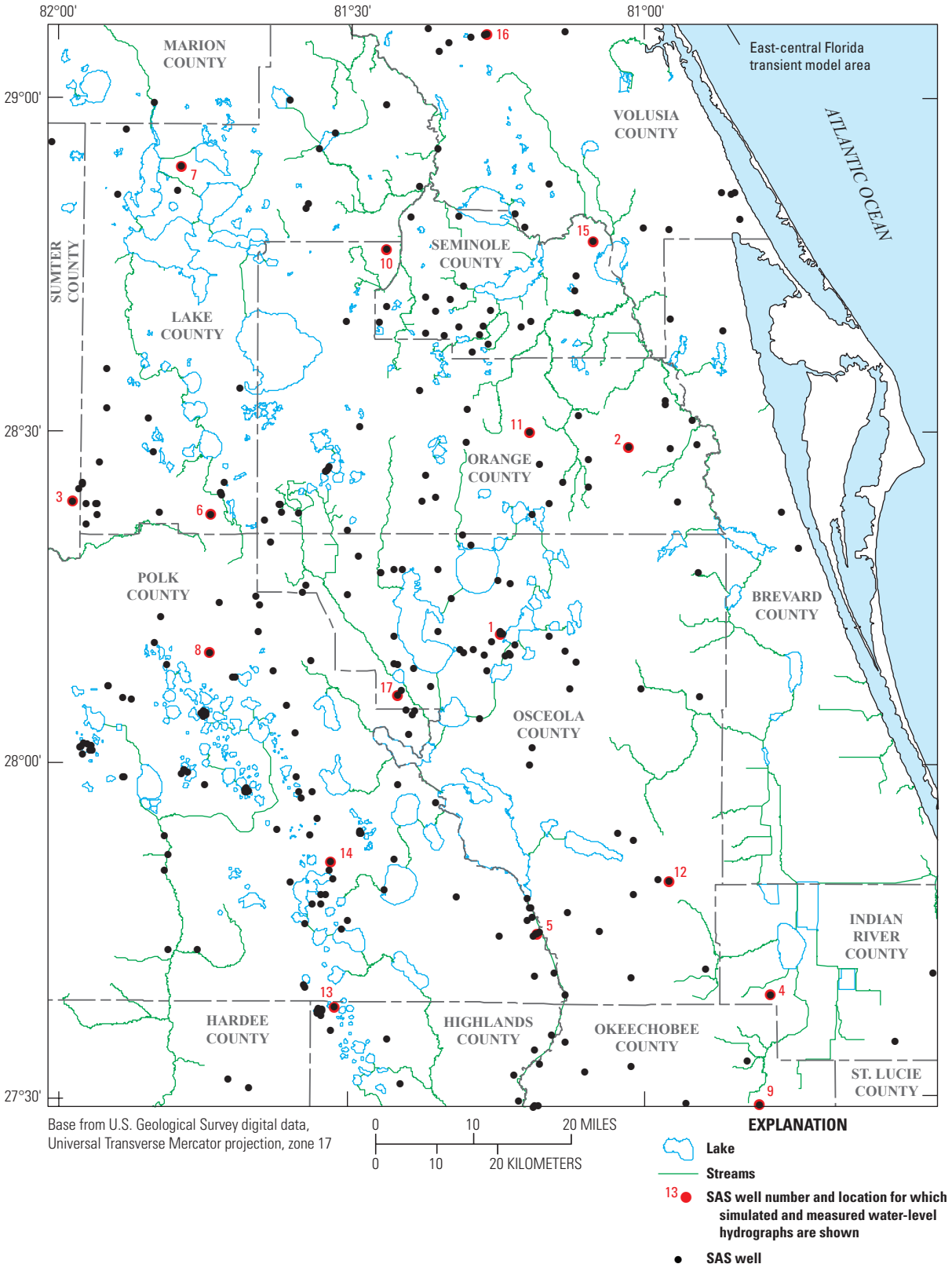

Figure 5–1. Selected surficial aquifer system (SAS) wells for which simulated and measured water-level hydrographs are shown.

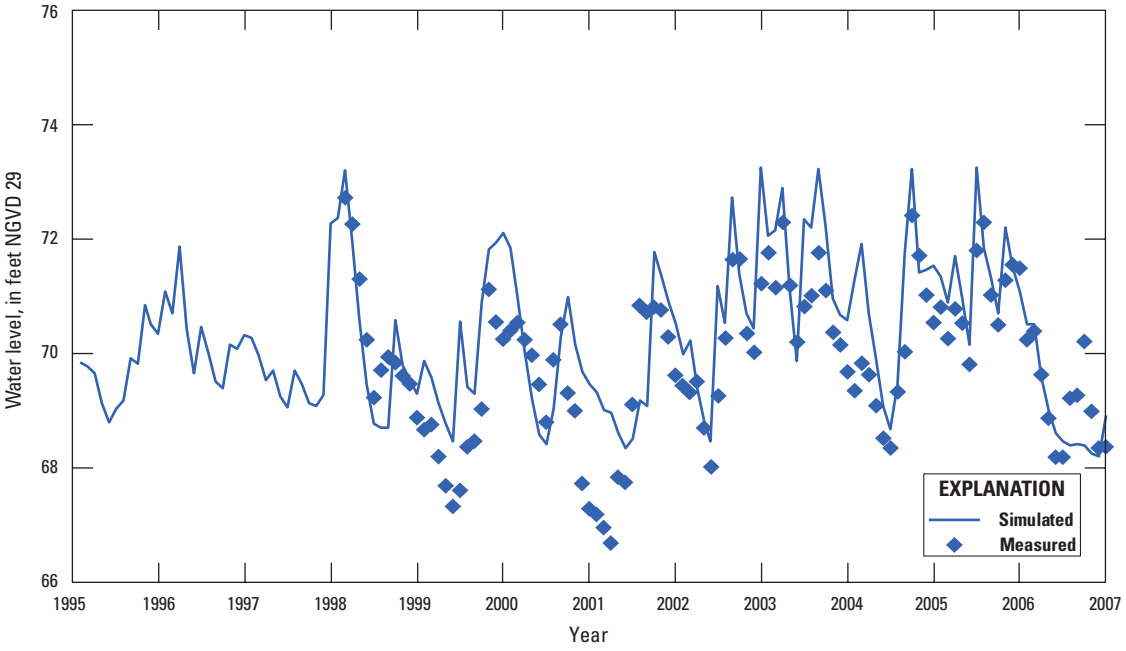

Figure 5–2. Measured and simulated water-level hydrographs for All1w2, well number 1 in figure 5–1.

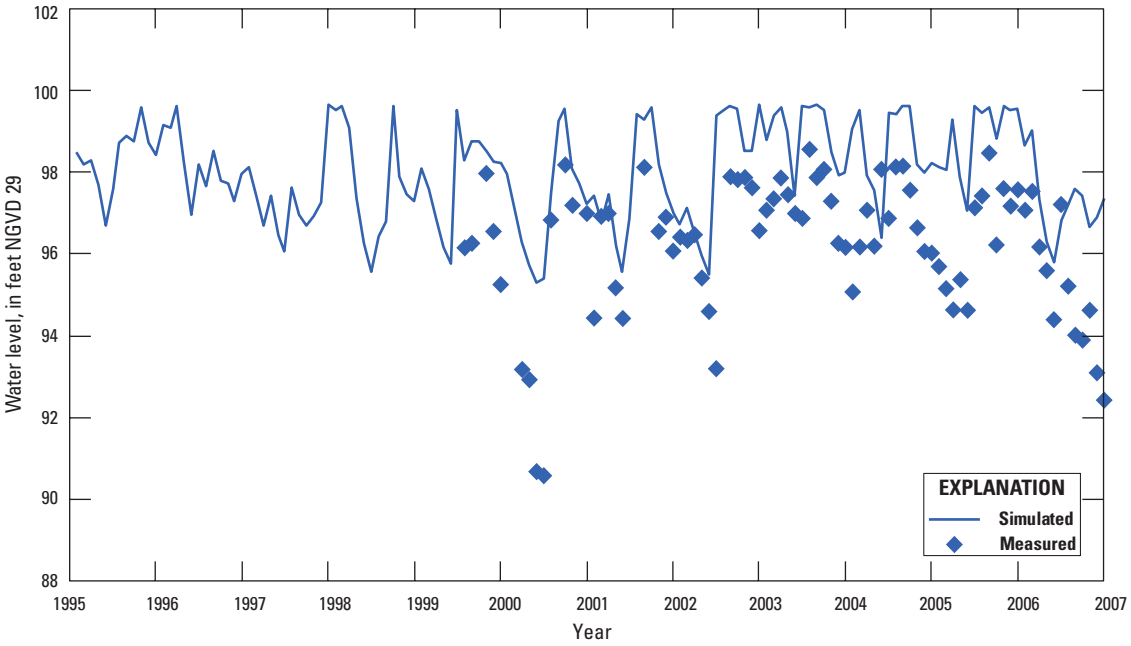

Figure 5–3. Measured and simulated water-level hydrographs for Green Swamp 6 Upland, well number 3 in figure 5–1.

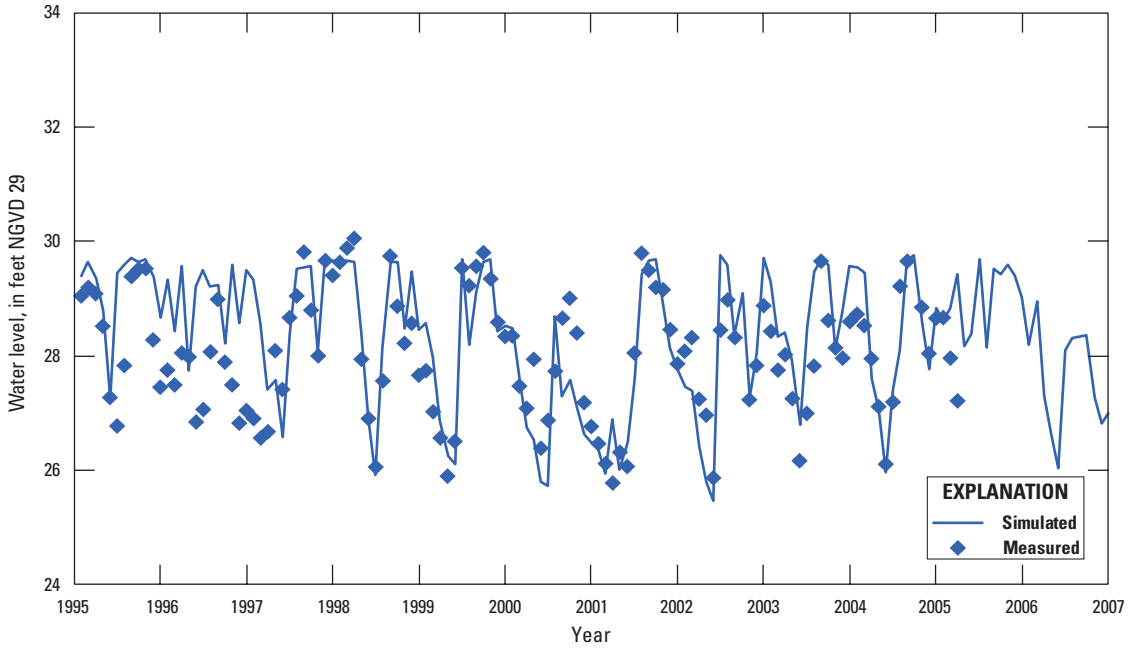

Figure 5–4. Measured and simulated water-level hydrographs for IR0025, well number 4 in figure 5–1.

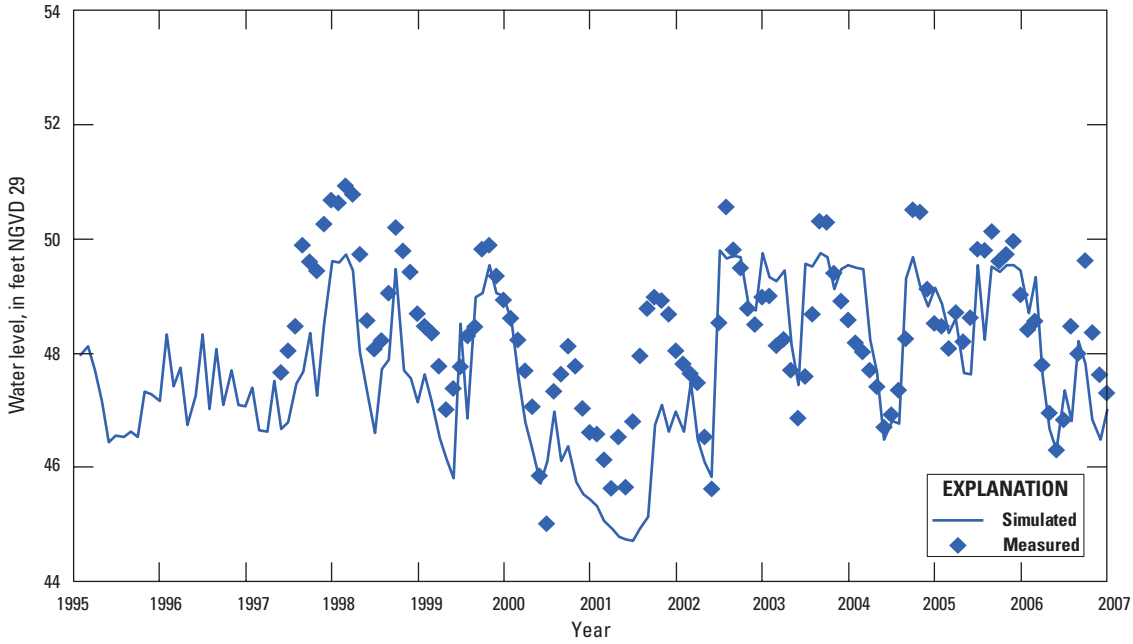

Figure 5–5. Measured and simulated water-level hydrographs for KREFFM, well number 5 in figure 5–1.

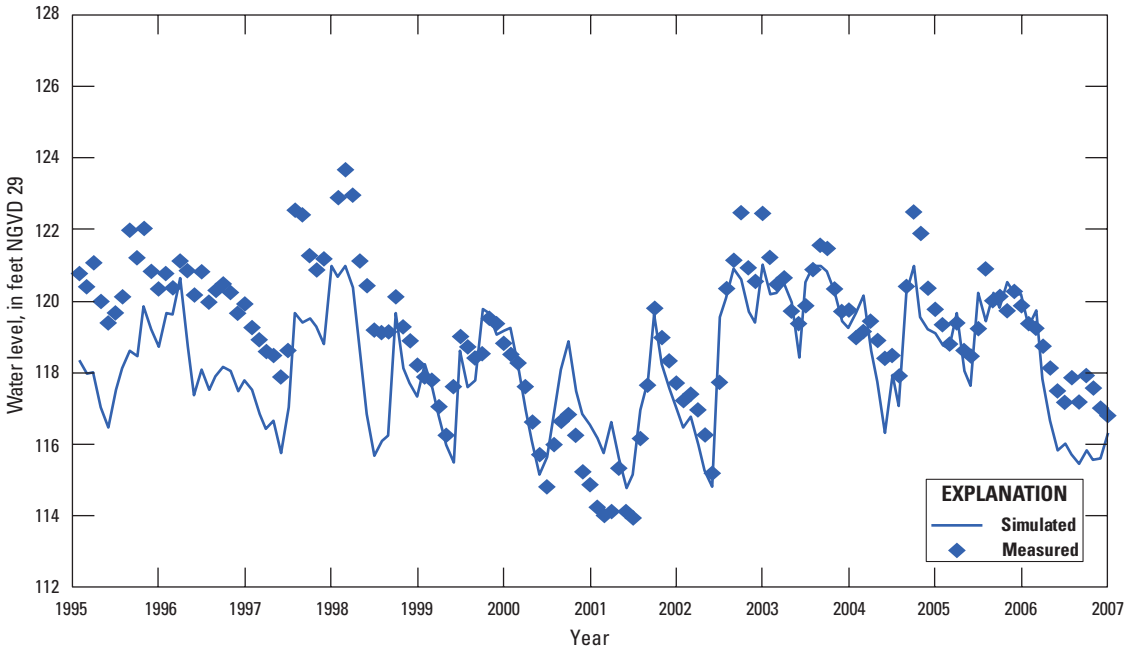

Figure 5–6. Measured and simulated water-level hydrographs for L–0050, well number 6 in figure 5–1.

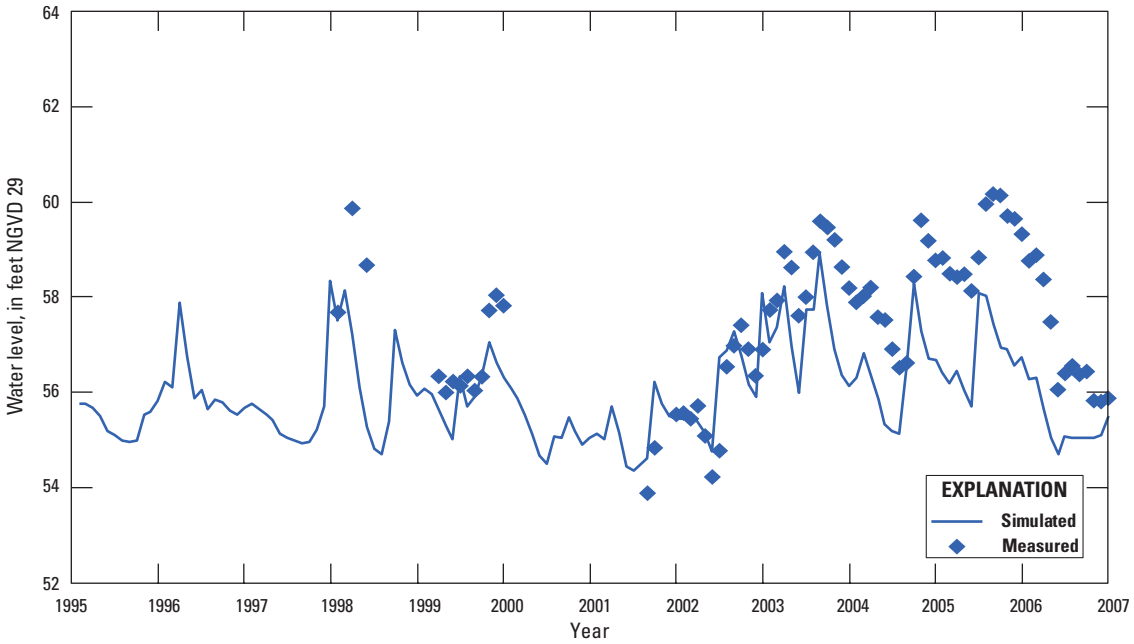

Figure 5–7. Measured and simulated water-level hydrographs for L–0703 Carrot Barn, well number 7 in figure 5–1.

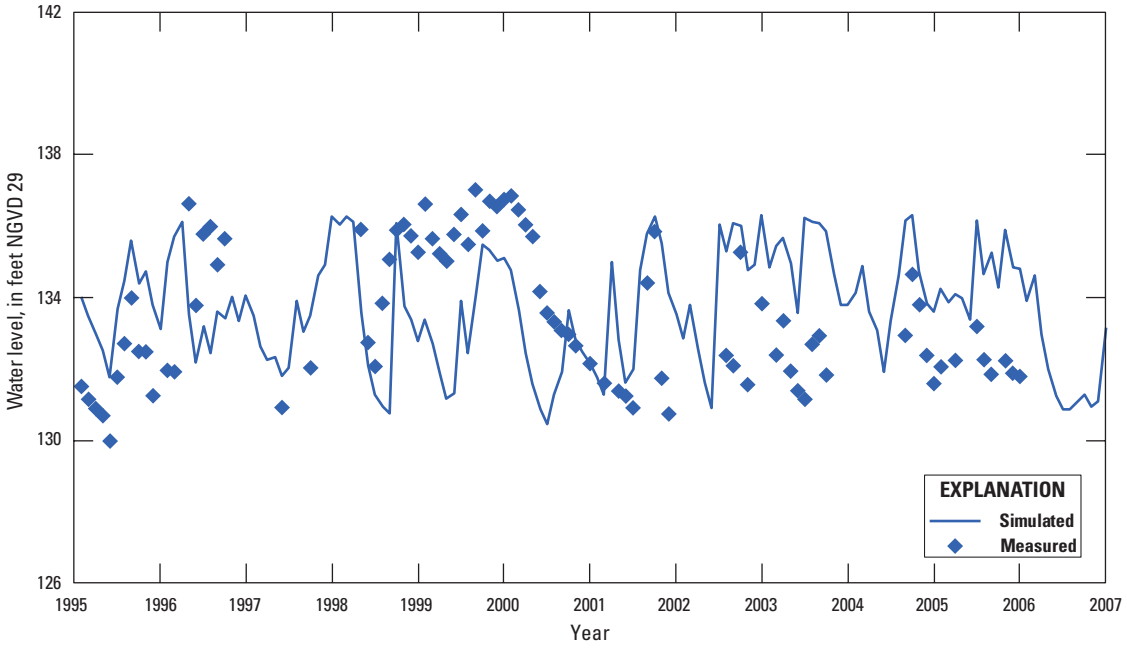

Figure 5–8. Measured and simulated water-level hydrographs for Lake Alfred shallow, well number 8 in figure 5–1.

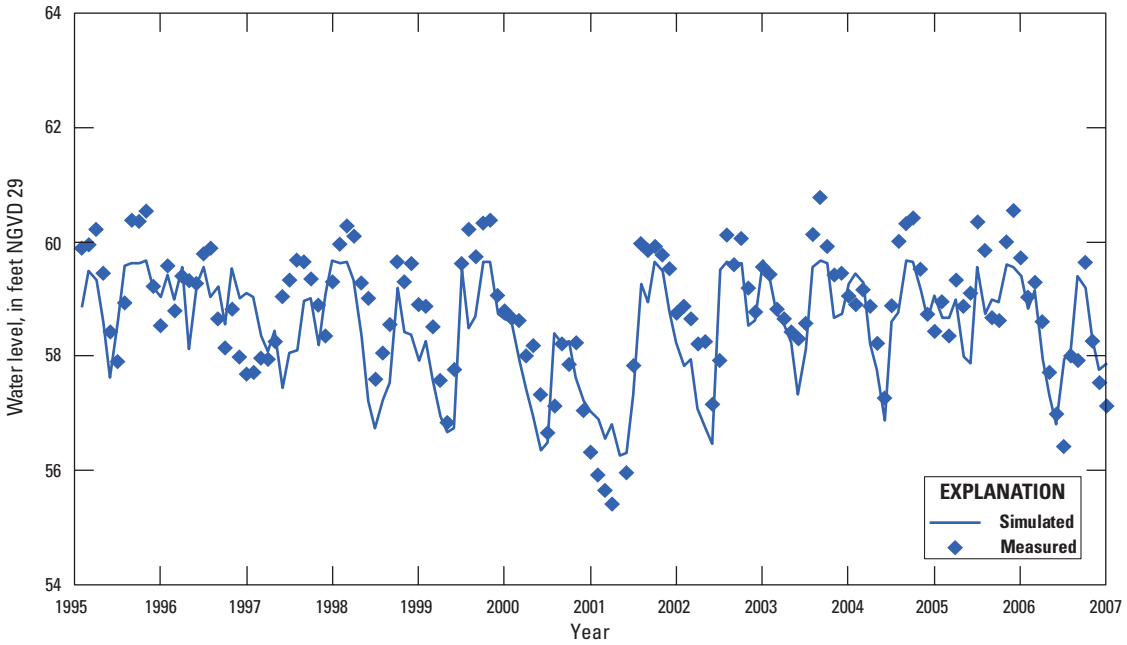

Figure 5–9. Measured and simulated water-level hydrographs for OK–3 G, well number 9 in figure 5–1.

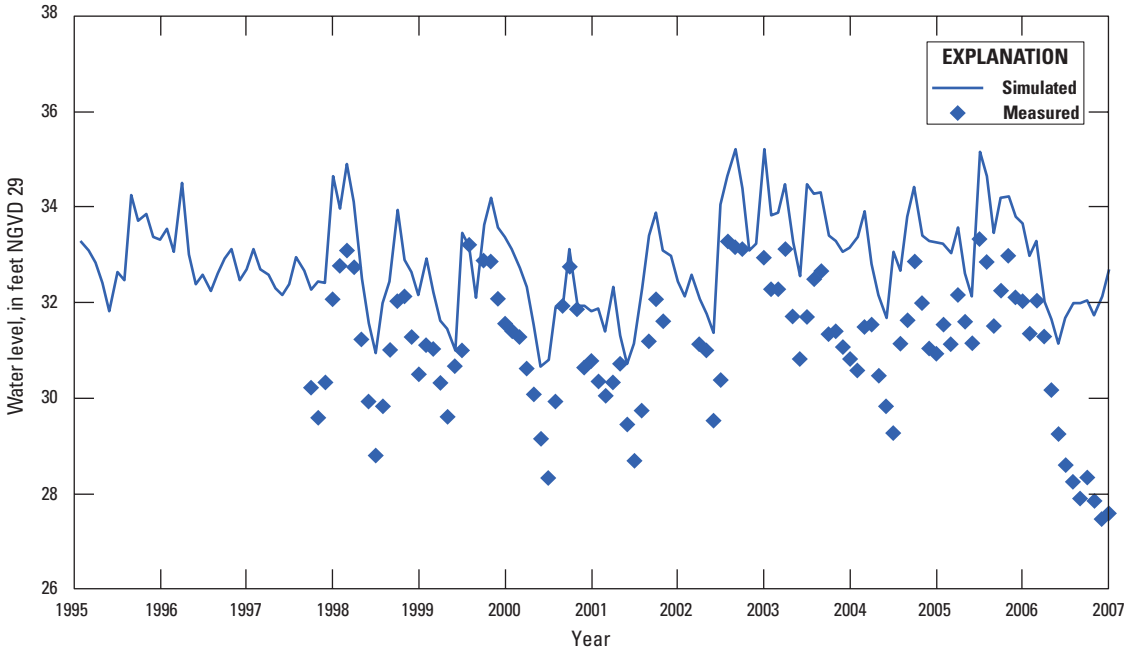

Figure 5–10. Measured and simulated water-level hydrographs for OR0650 Rock Springs, well number 10 in figure 5–1.

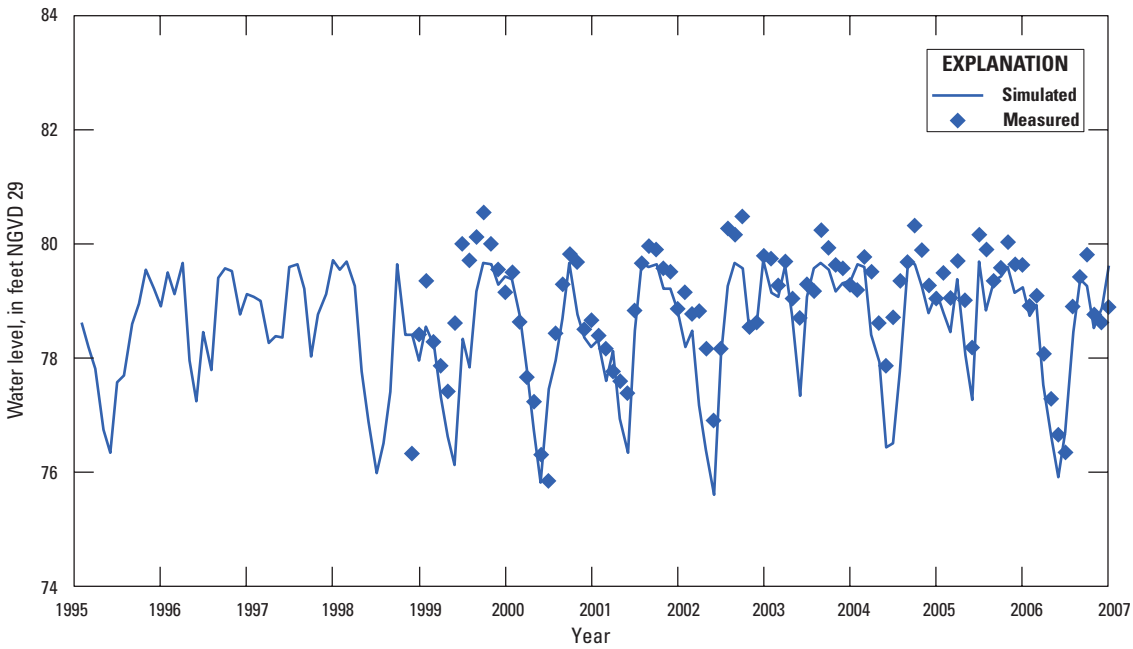

Figure 5–11. Measured and simulated water-level hydrographs for OR0665 Alafaya Trail WTP, well number 11 in figure 5–1.

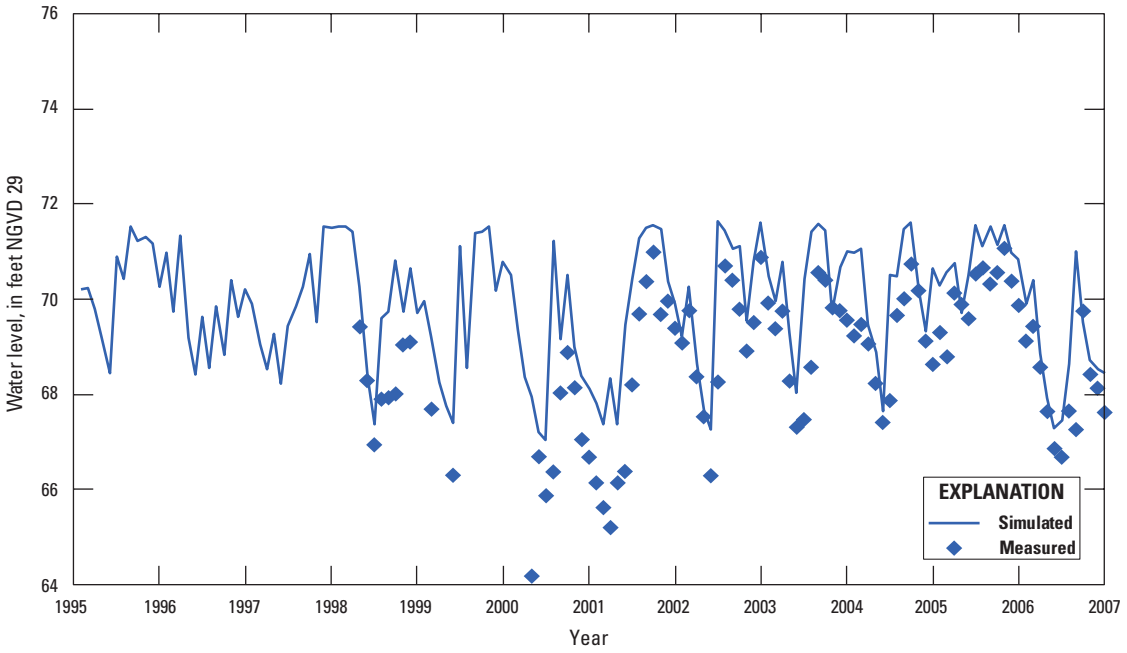

Figure 5–12. Measured and simulated water-level hydrographs for OS0232 Campbell Ranch, well number 12 in figure 5–1.

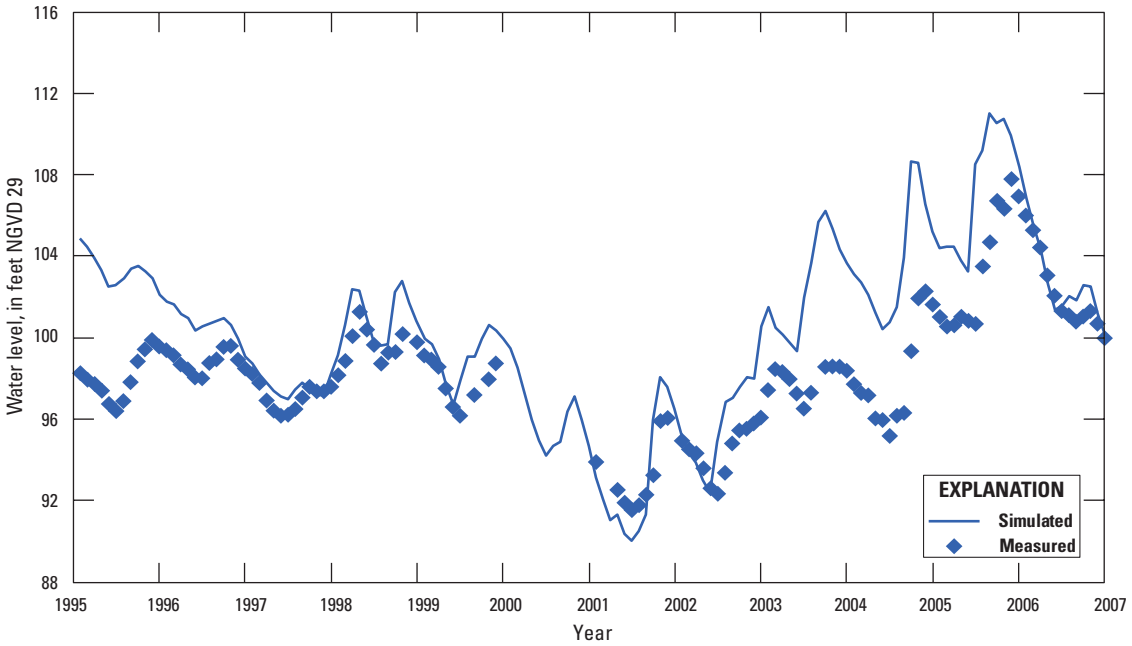

Figure 5–13. Measured and simulated water-level hydrographs for Ridge Wrap VC-1, well number 14 in figure 5–1.

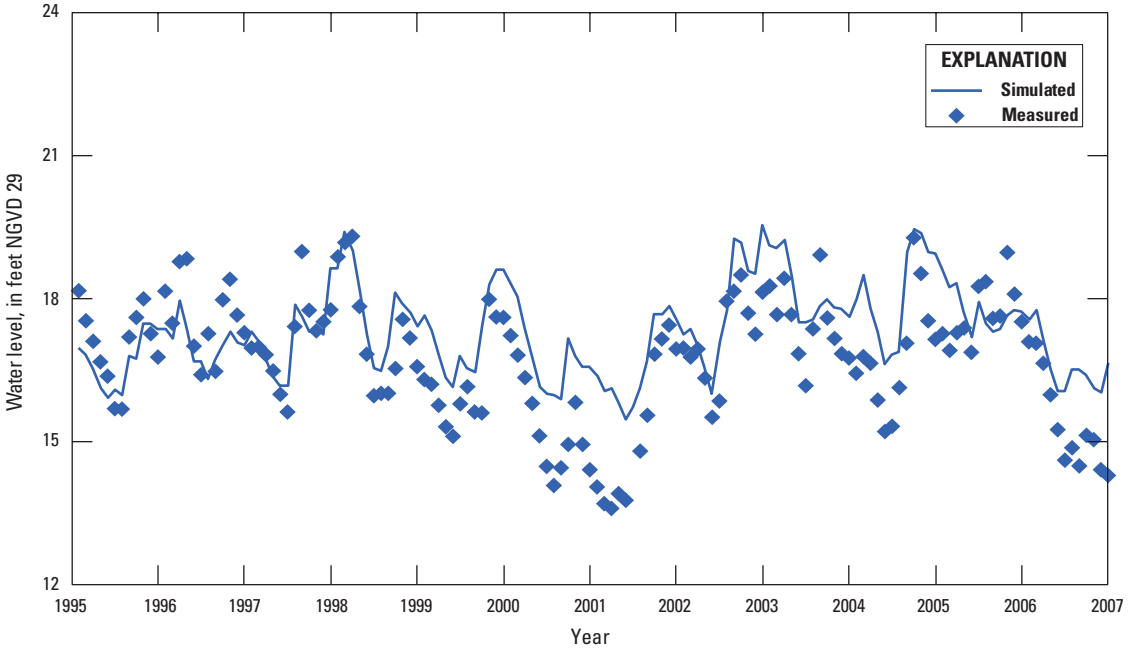

Figure 5–14. Measured and simulated water-level hydrographs for S-0266 at Osceola Landfill, well number 15 in figure 5–1.

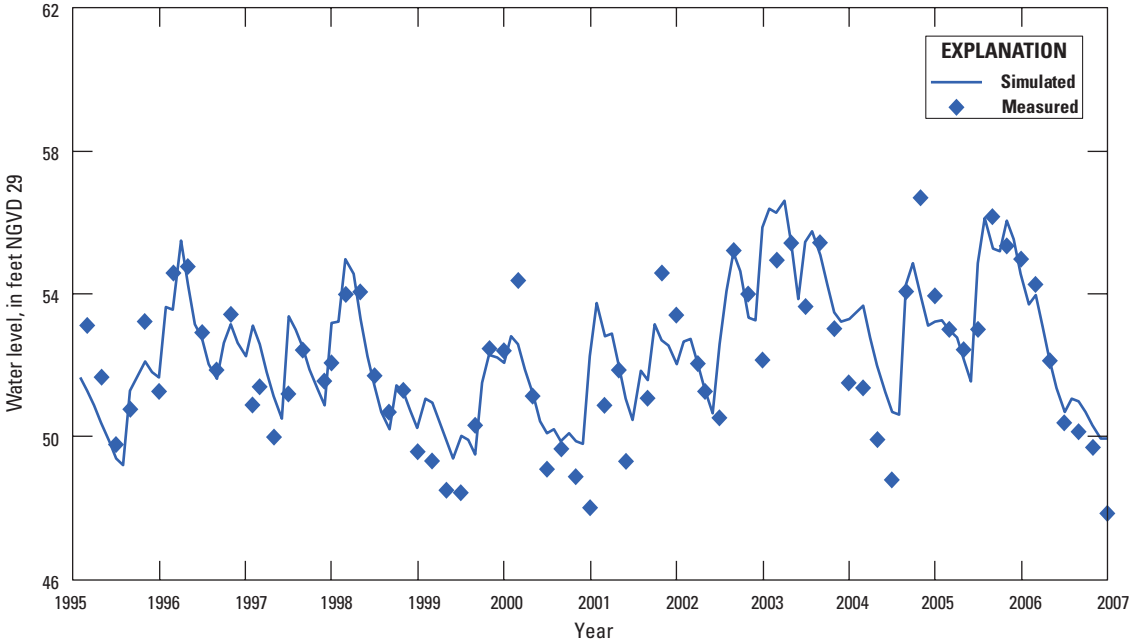

Figure 5–15. Measured and simulated water-level hydrographs for V-1062 at Lawrence Farms, well number 16 in figure 5–1.

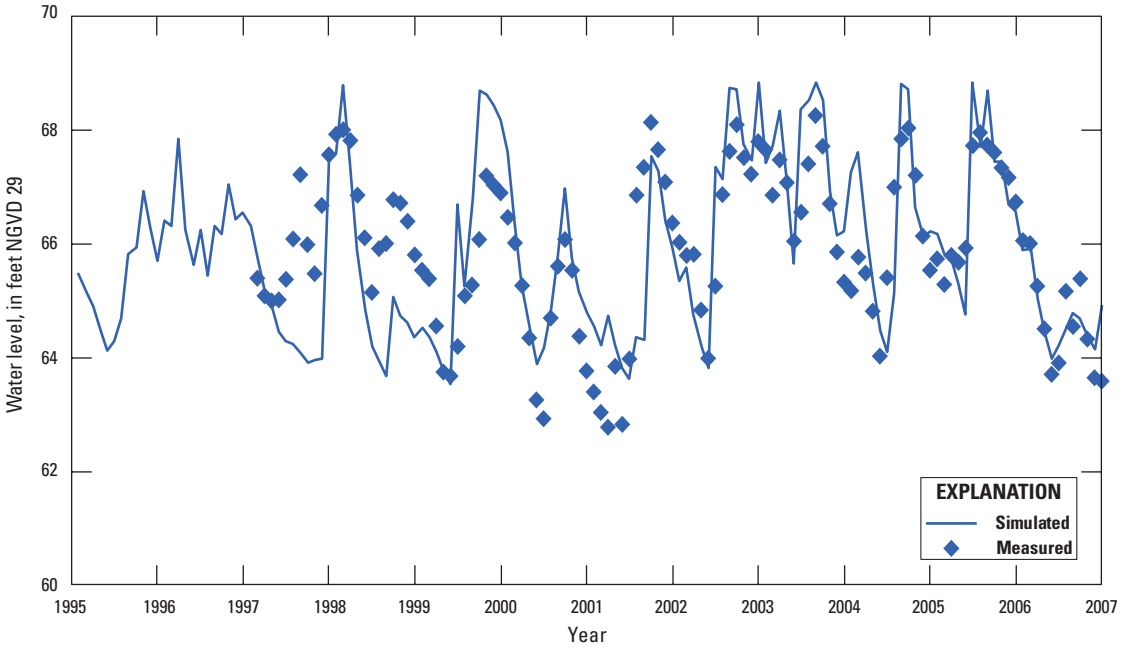

Figure 5–16. Measured and simulated water-level hydrographs for WR8 GW1, well number 17 in figure 5–1.

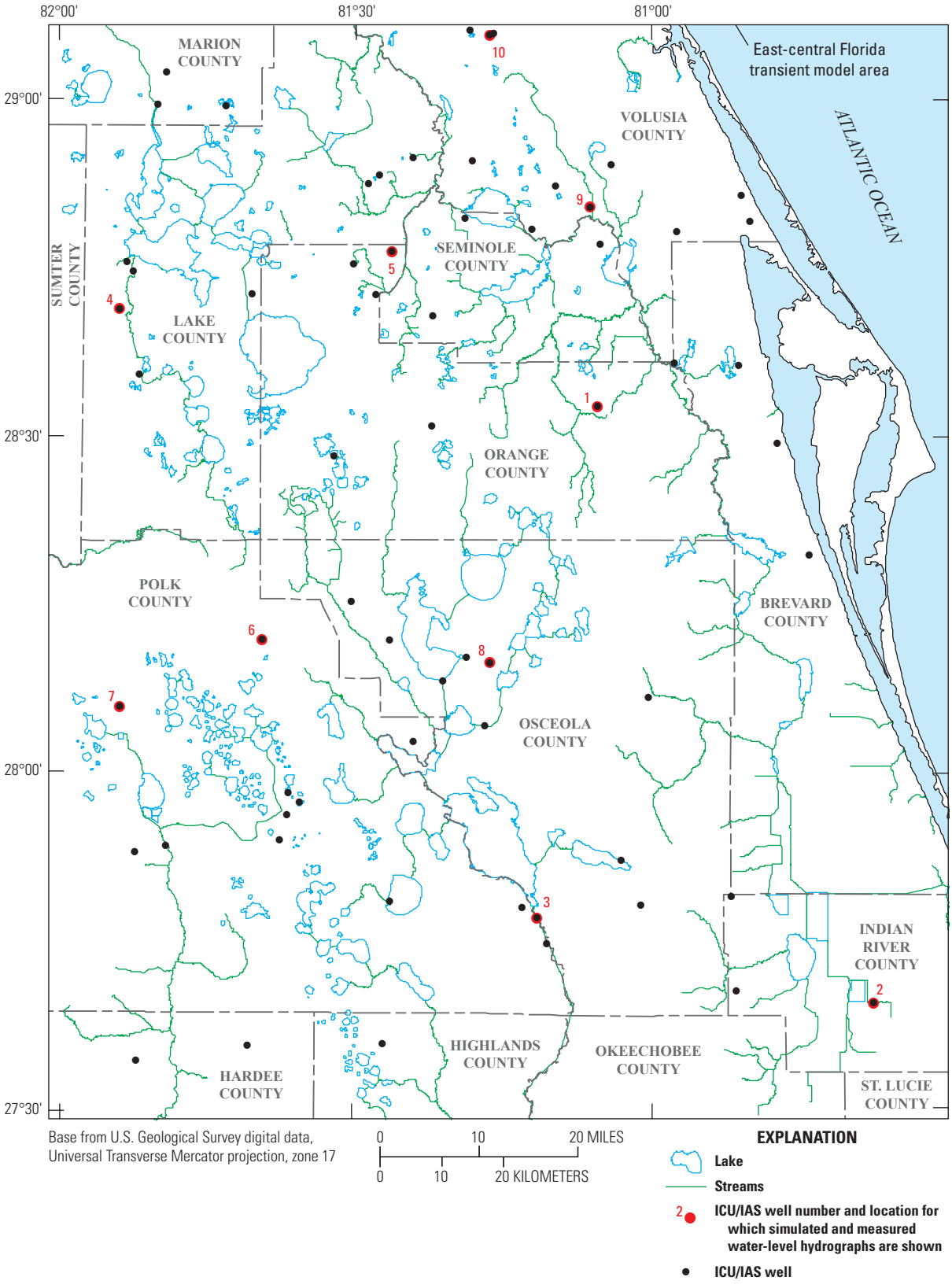

Figure 5–17. Selected intermediate confining unit/intermediate aquifer system (ICU/IAS) wells for which simulated and measured water-level hydrographs are shown.

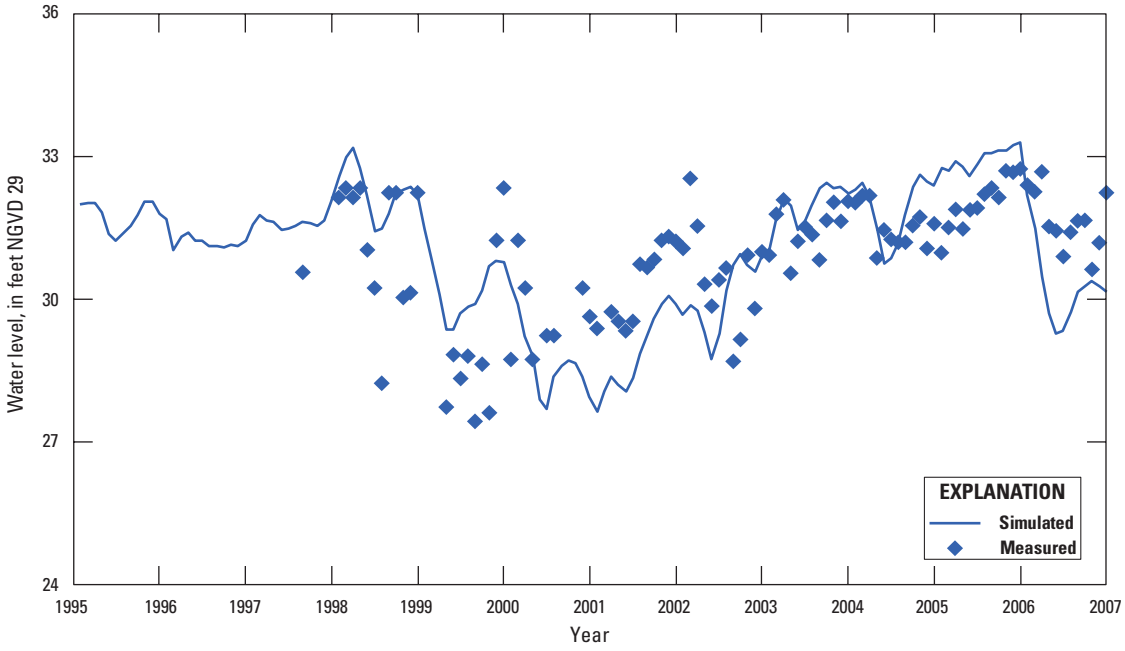

Figure 5–18. Measured and simulated water-level hydrographs for IR0956 Delta Farms, well number 2 in figure 5–17.

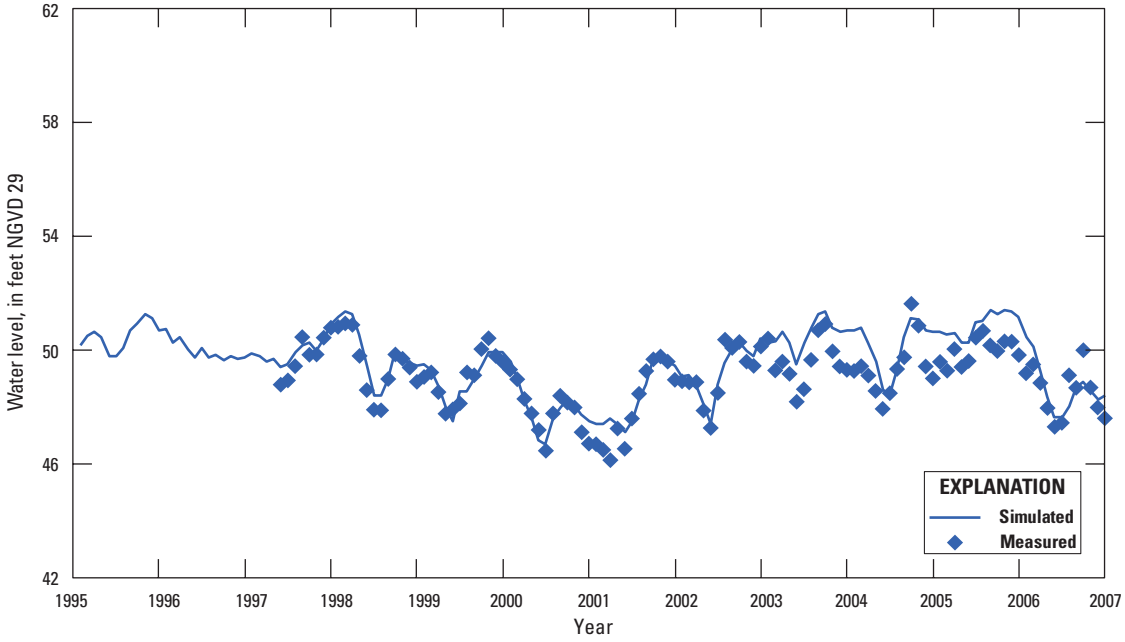

Figure 5–19. Measured and simulated water-level hydrographs for KRFNND, well number 3 in figure 5–17.

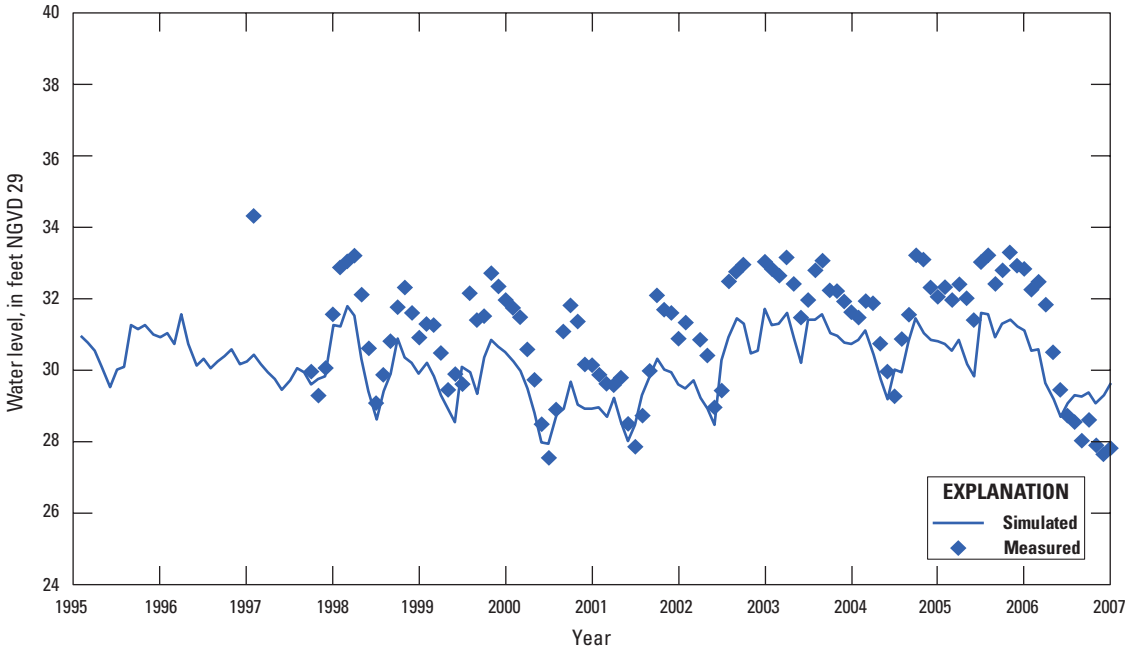

Figure 5–20. Measured and simulated water-level hydrographs for OR0651 Rock Springs intermediate, well number 5 in figure 5–17.

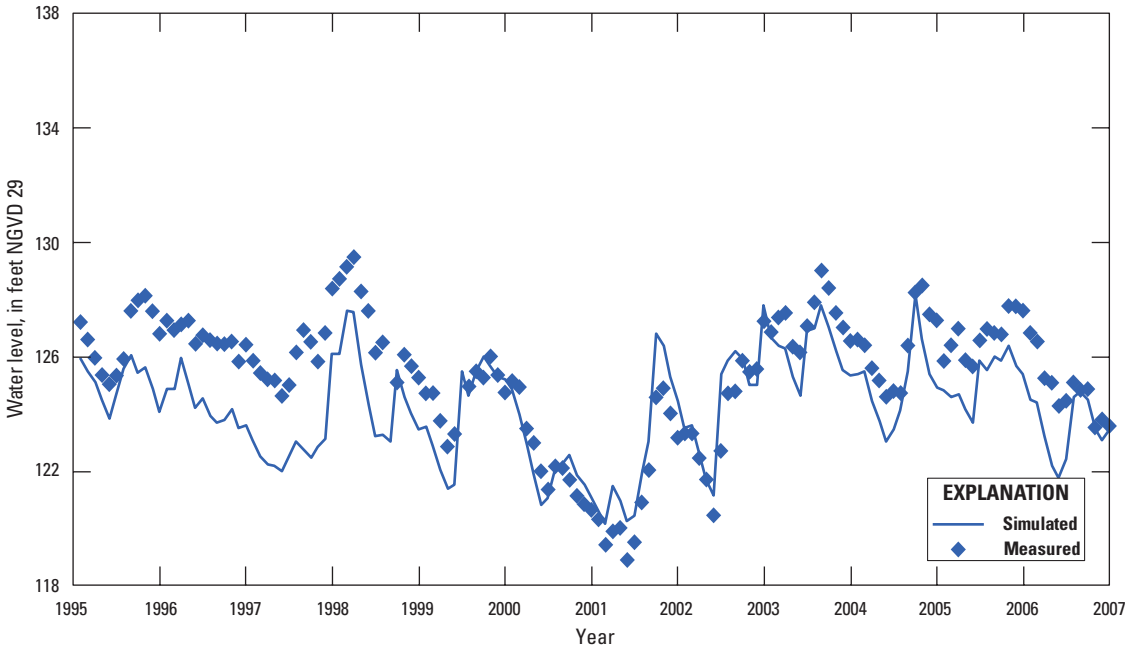

Figure 5–21. Measured and simulated water-level hydrographs for PO0001 Thornhill Ranch deep, well number 6 in figure 5–17.

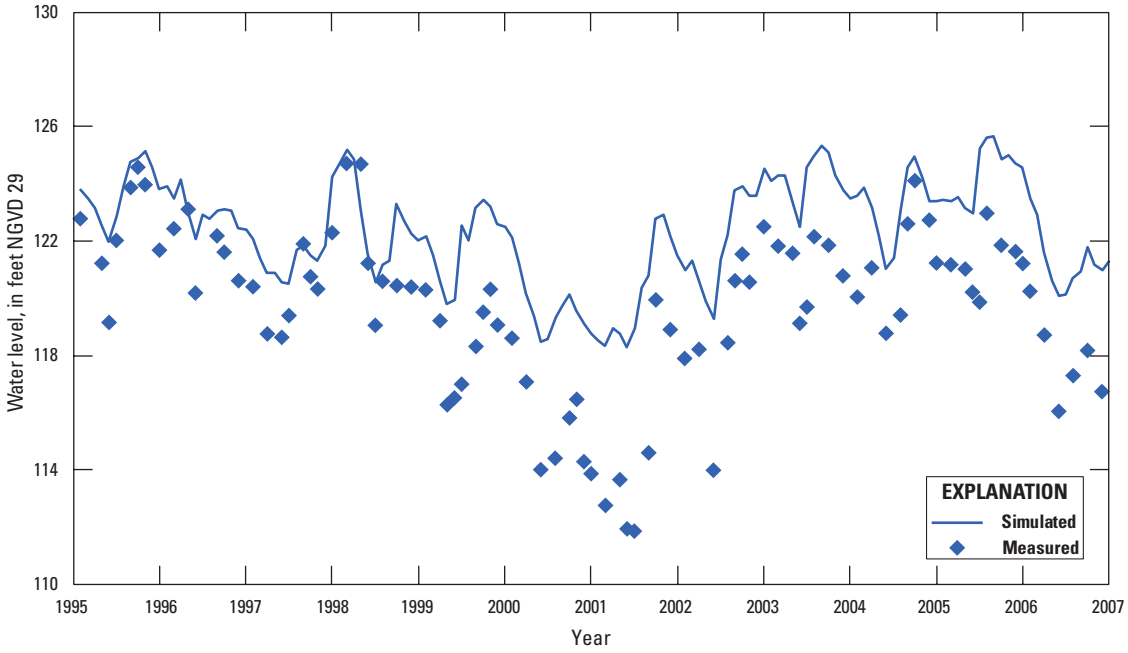

Figure 5–22. Measured and simulated water-level hydrographs for Tennorock Road well, well number 7 in figure 5–17.

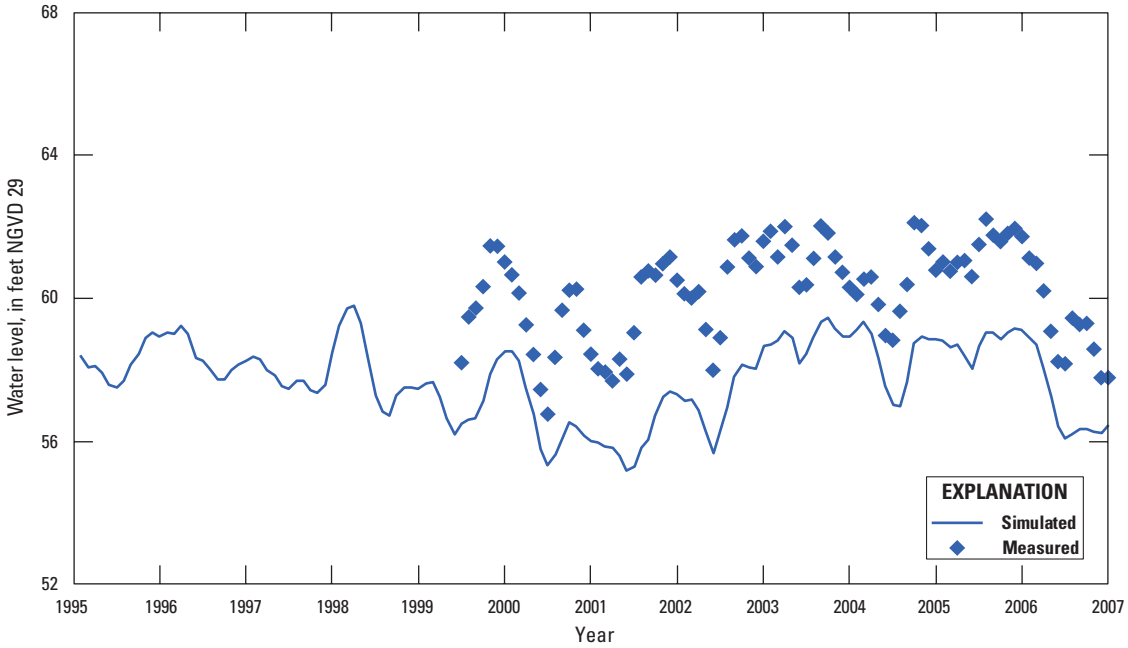

Figure 5–23. Measured and simulated water-level hydrographs for Toho16 W2, well number 8 in figure 5–17.

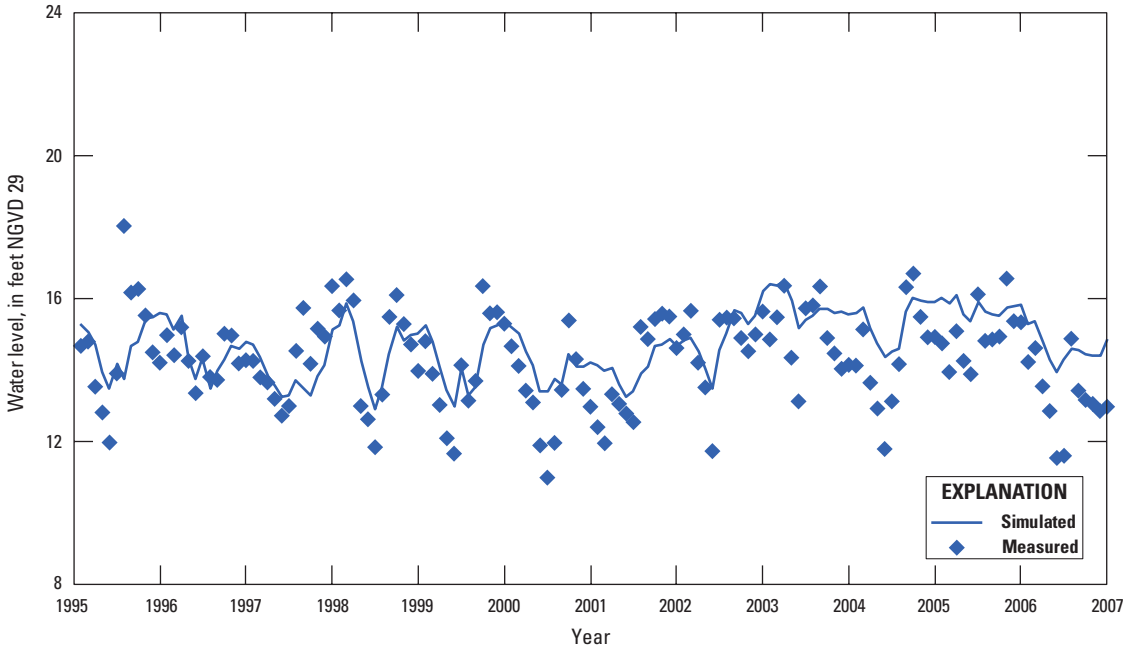

Figure 5–24. Measured and simulated water-level hydrographs for V-0166 Took Farm, well number 9 in figure 5–17.

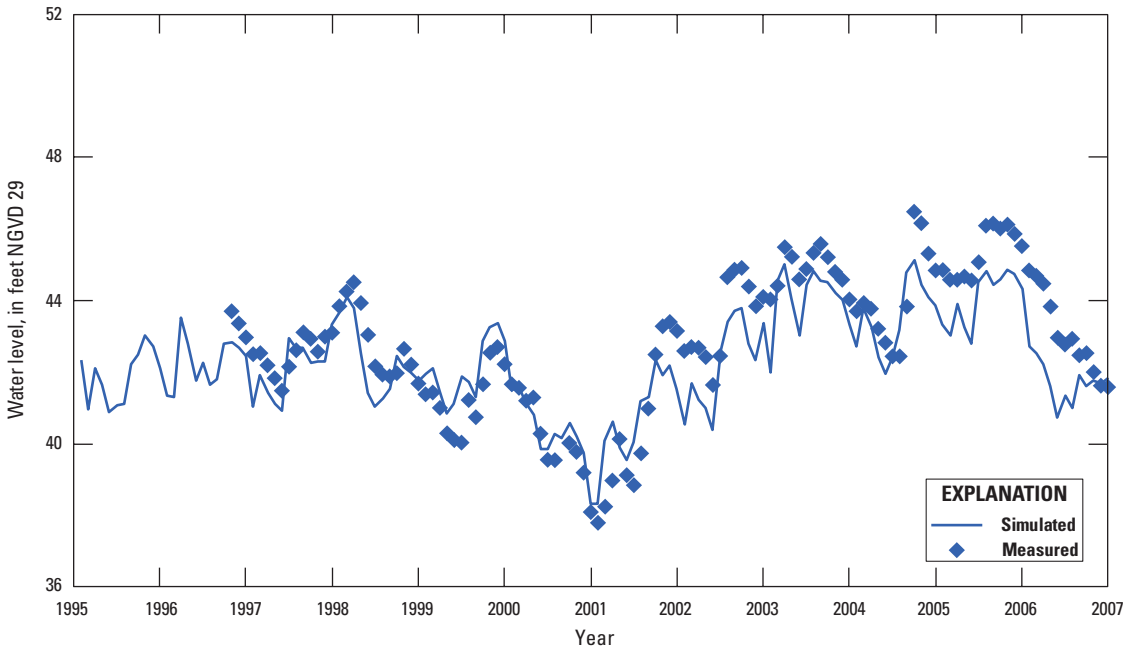

Figure 5–25. Measured and simulated water-level hydrographs for V-0812 Lake Daugharty, well number 10 in figure 5–17.

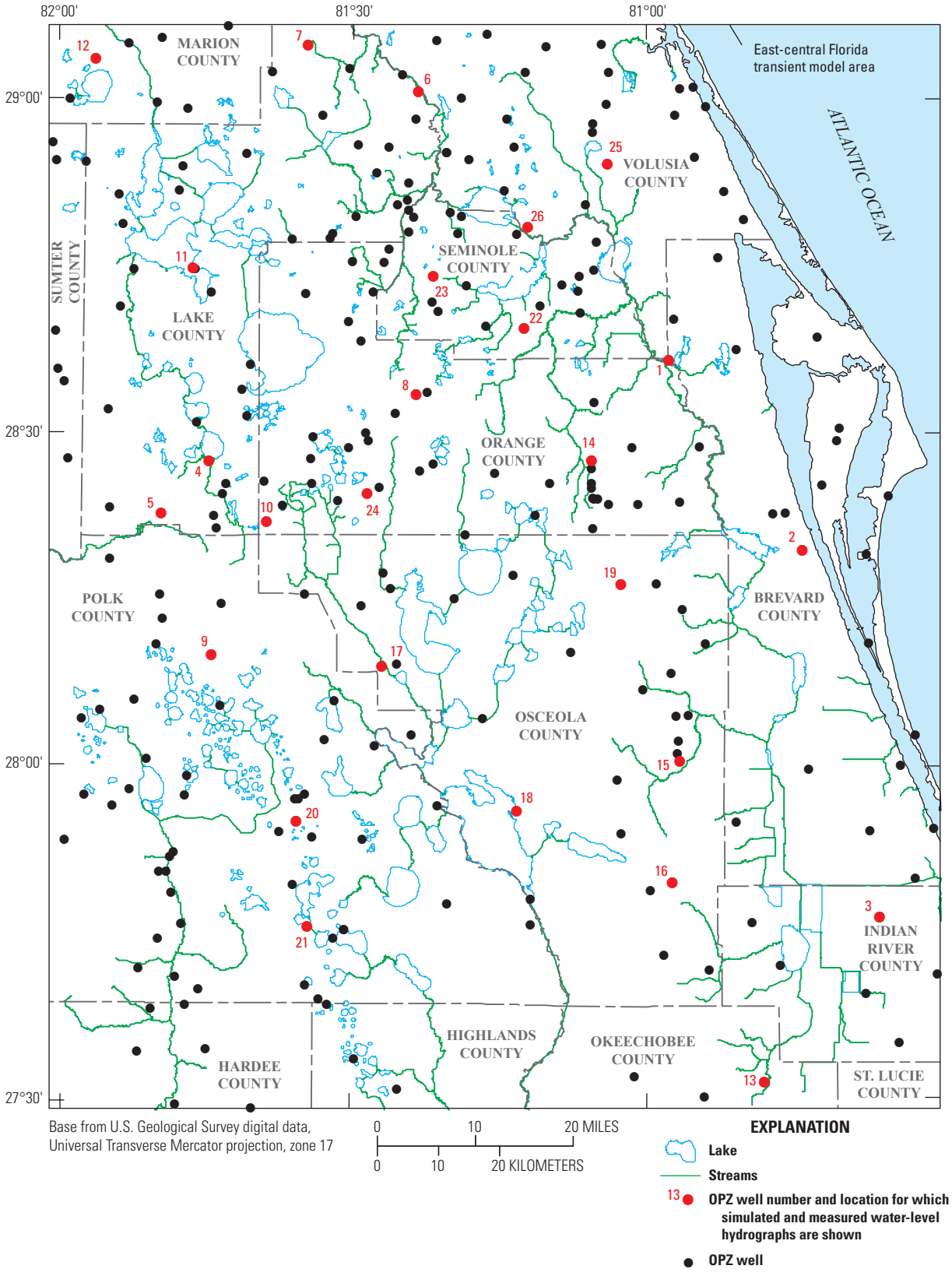

Figure 5–26. Selected Ocala permeable zone (OPZ) wells for which simulated and measured water-level hydrographs are shown.

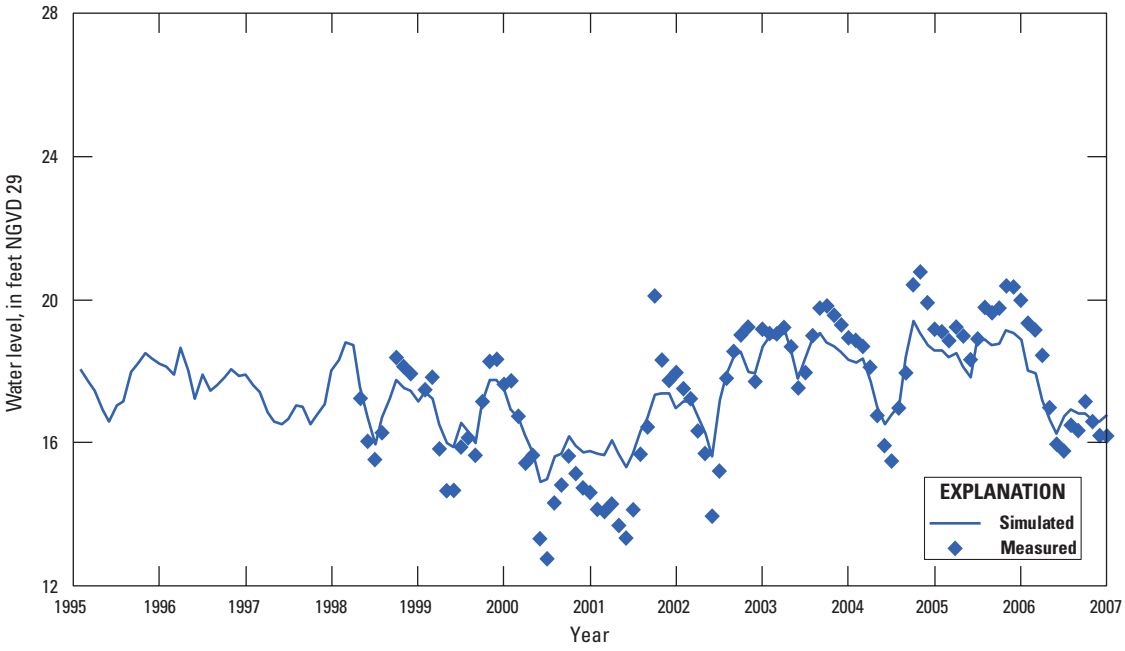

Figure 5–27. Measured and simulated water-level hydrographs for BR1526 at Seminole Ranch, well number 1 in figure 5–26.

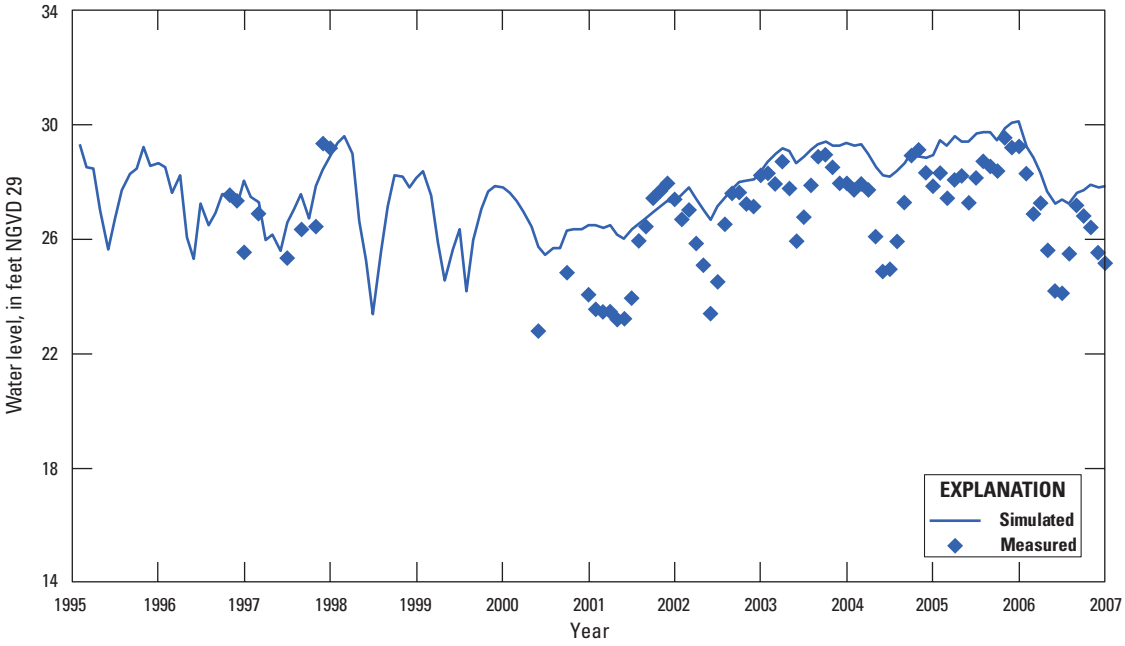

Figure 5–28. Measured and simulated water-level hydrographs for BR1558 at Kennedy Middle School, well number 2 in figure 5–26.

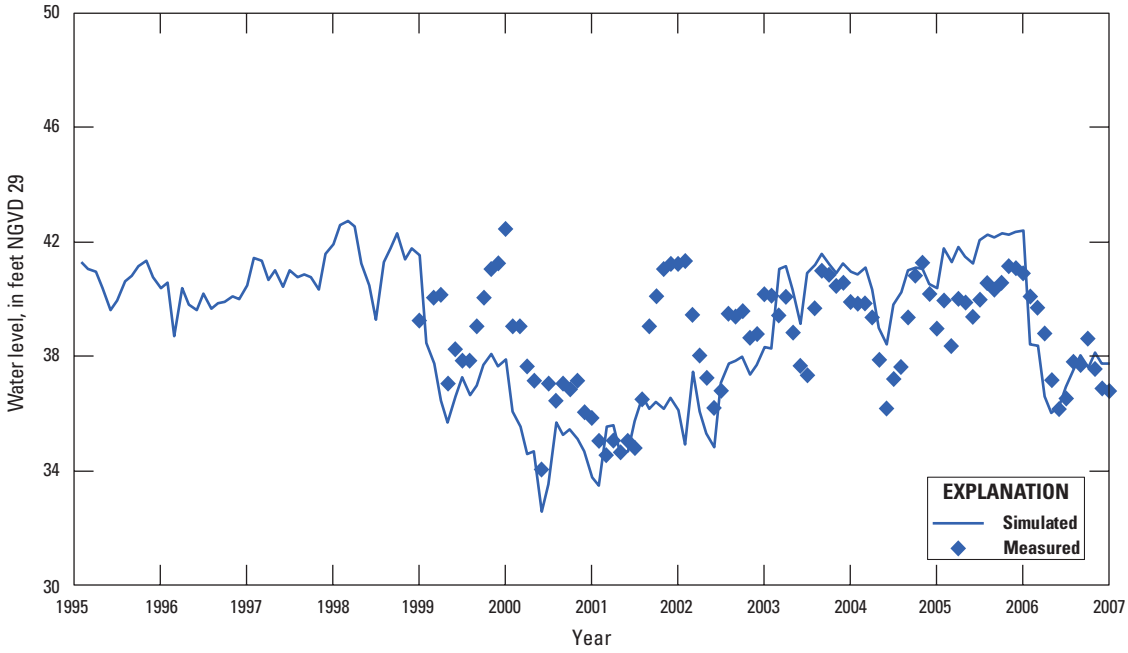

Figure 5–29. Measured and simulated water-level hydrographs for IR0921 Morrison at Fellsmere Farms, well number 3 in figure 5–26.

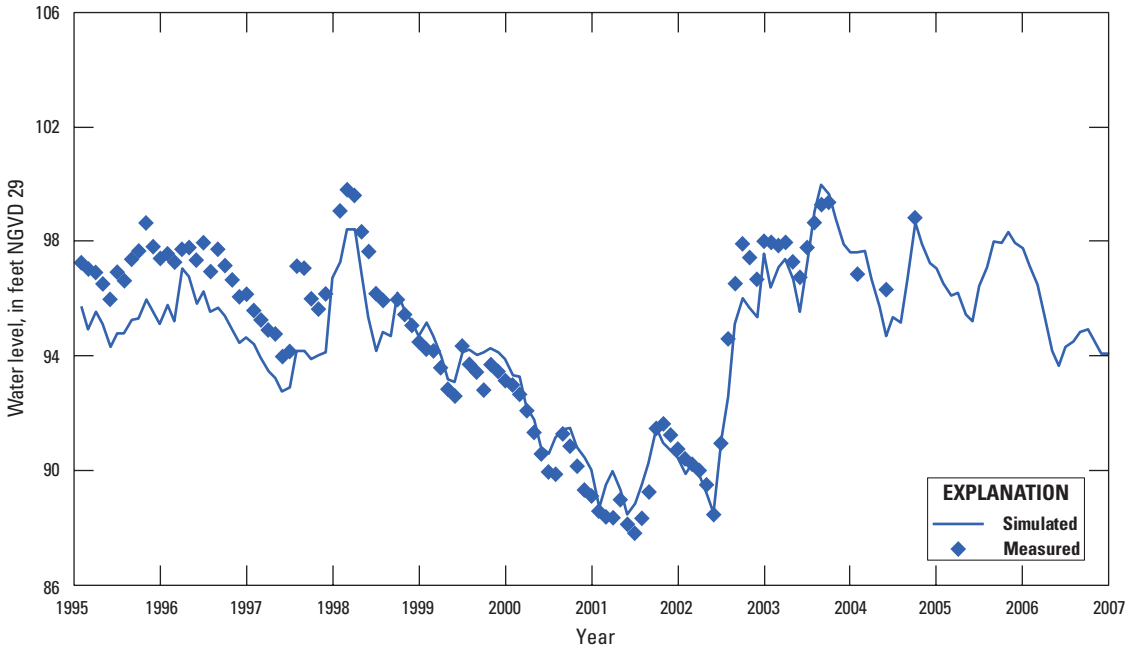

Figure 5–30. Measured and simulated water-level hydrographs for L–0053 at Lake Louisa State Park, well number 4 in figure 5–26.

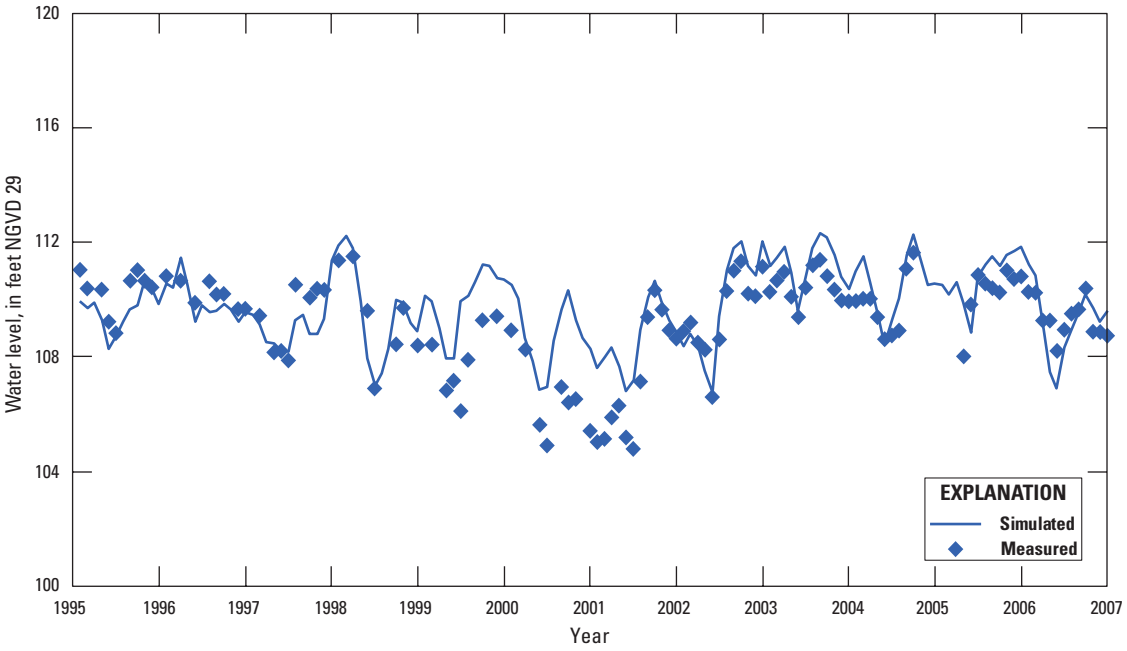

Figure 5–31. Measured and simulated water-level hydrographs for L-0057 Eva Deep, well number 5 in figure 5–26.

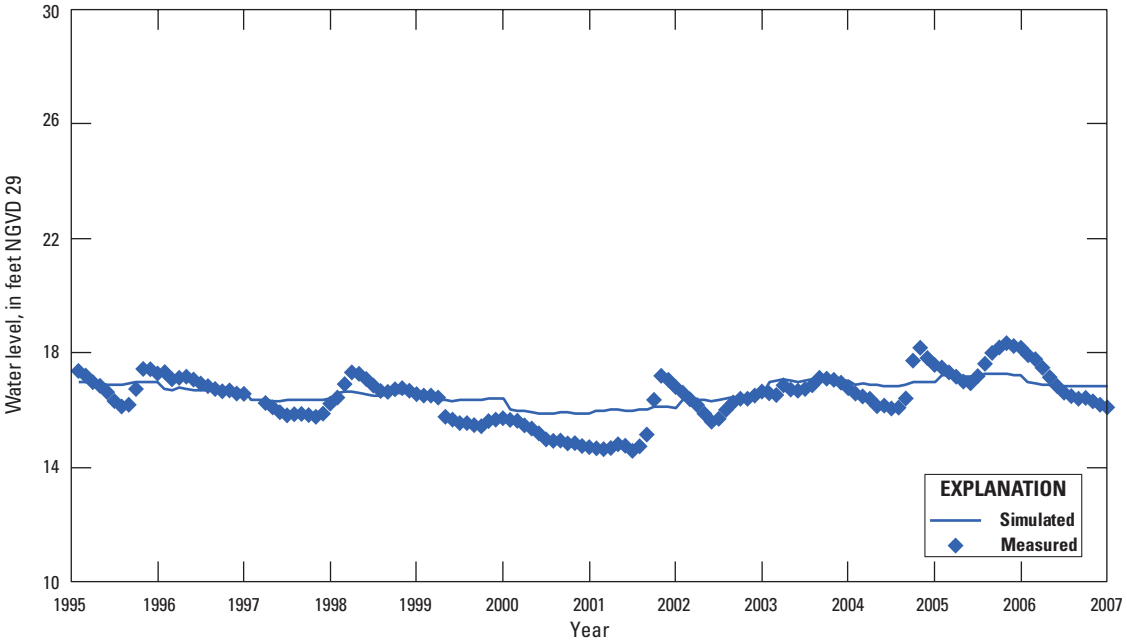

Figure 5–32. Measured and simulated water-level hydrographs for L-0066 at Alexander Springs, well number 7 in figure 5–26.

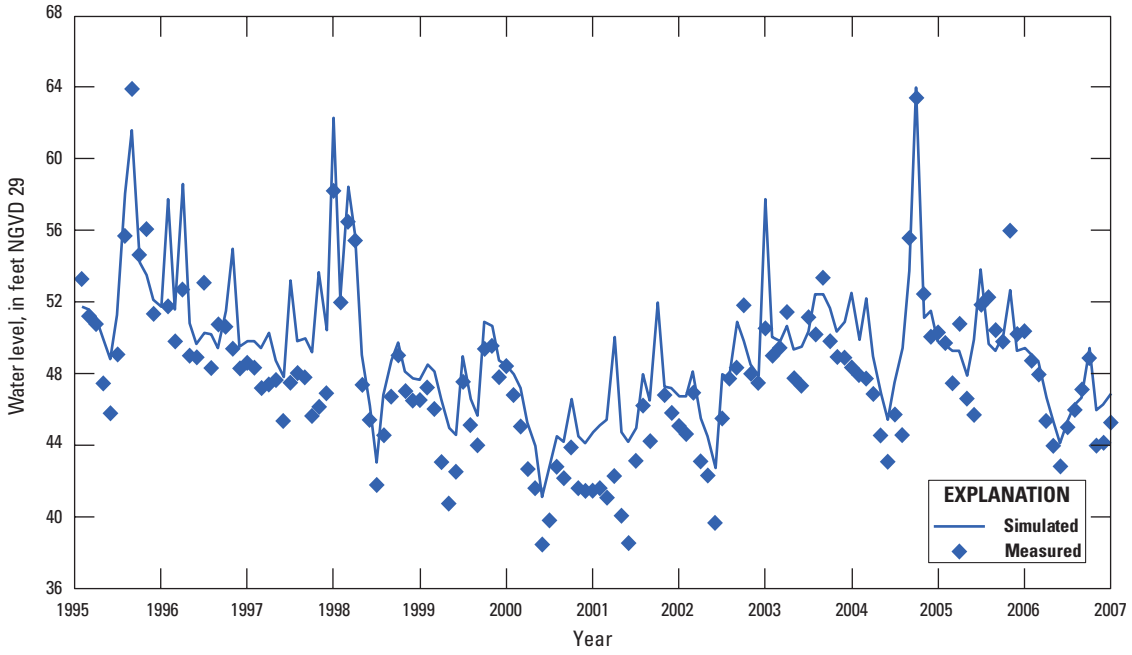

Figure 5–33. Measured and simulated water-level hydrographs for Lake Adair 10 Shallow, well number 8 in figure 5–26.

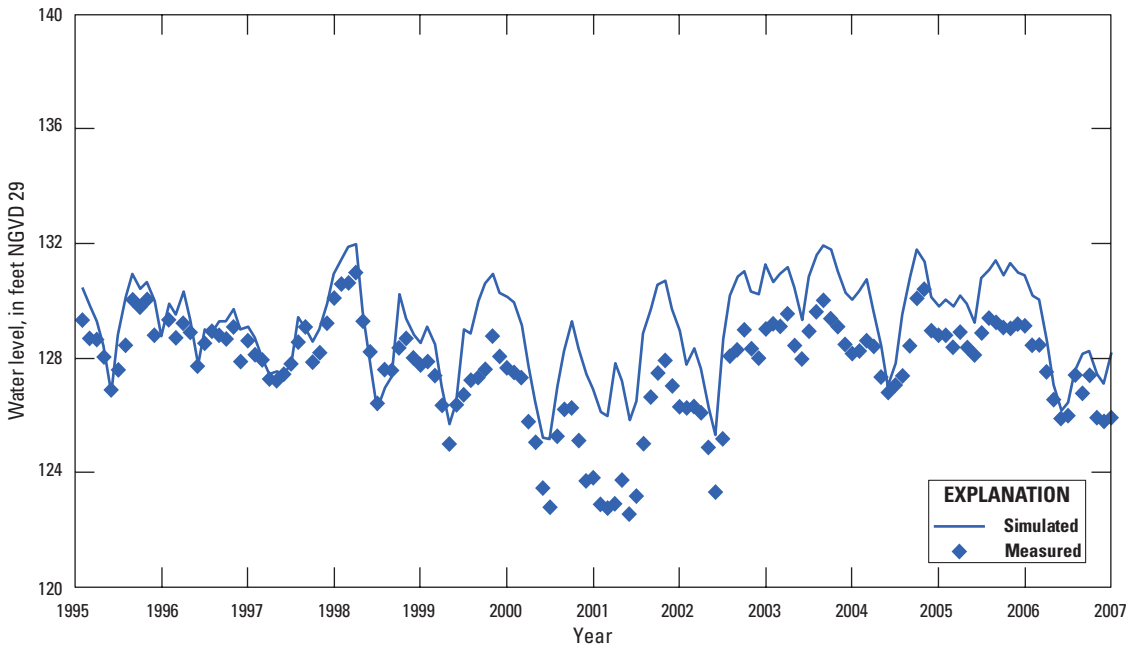

Figure 5–34. Measured and simulated water-level hydrographs for Lake Alfred deep, well number 9 in figure 5–26.

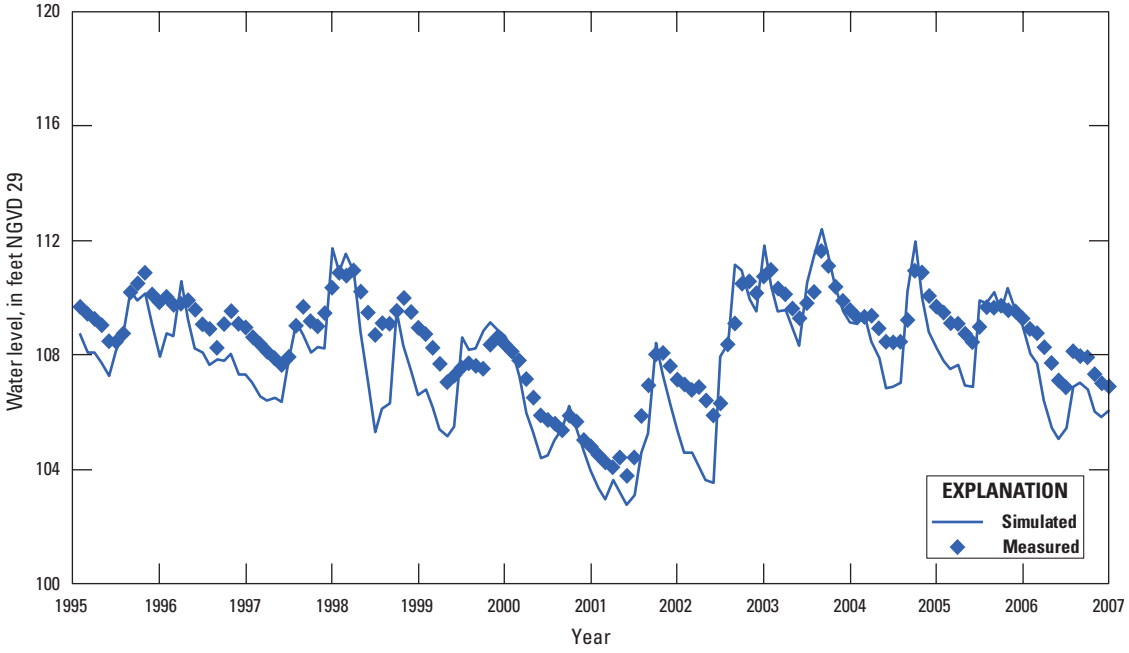

Figure 5–35. Measured and simulated water-level hydrographs for Lake Oliver deep, well number 10 in figure 5–26.

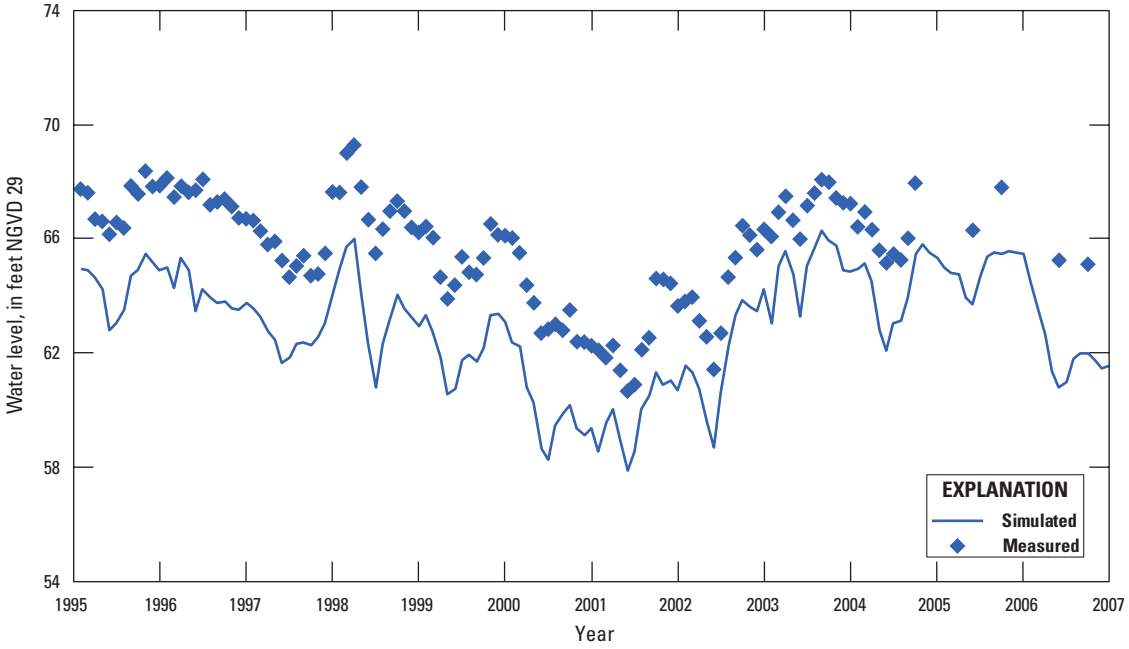

Figure 5–36. Measured and simulated water-level hydrographs for Lake Yale Groves, well number 11 in figure 5–26.

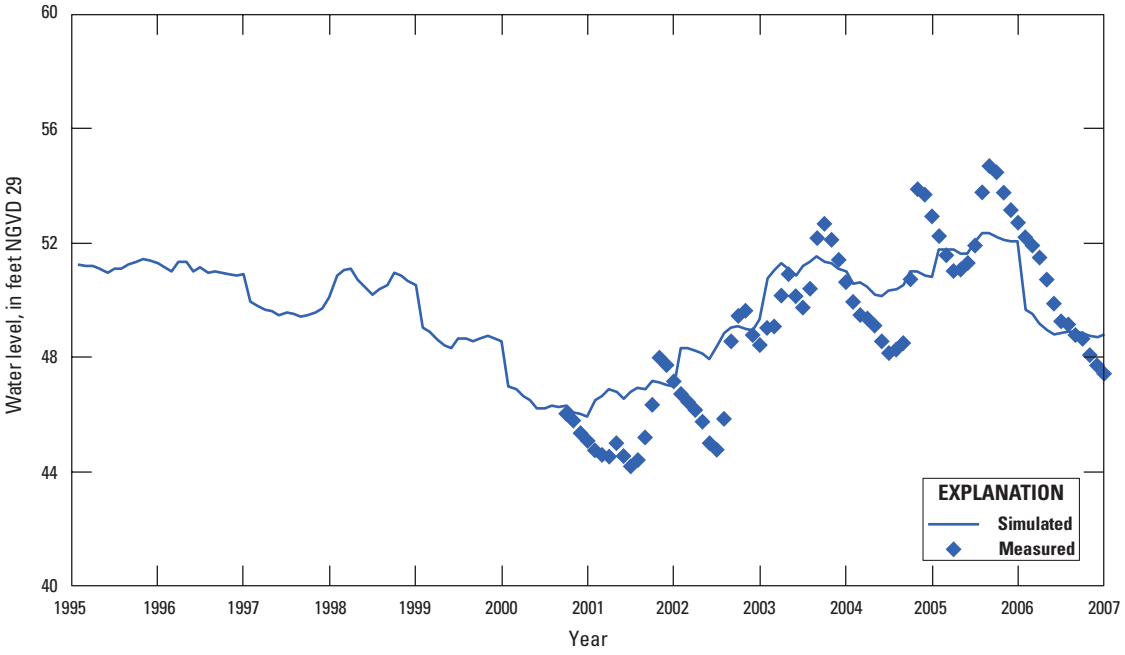

Figure 5–37. Measured and simulated water-level hydrographs for M-0445 Tiger Den Replacement, well number 12 in figure 5–26.

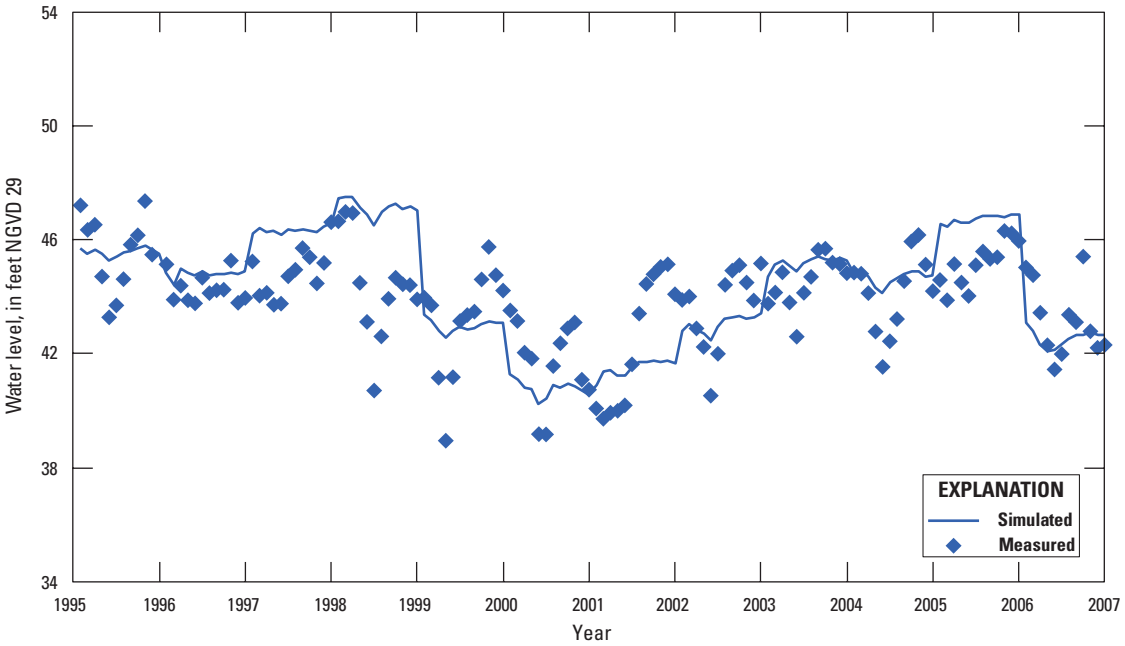

Figure 5–38. Measured and simulated water-level hydrographs for OK0001, well number 13 in figure 5–26.

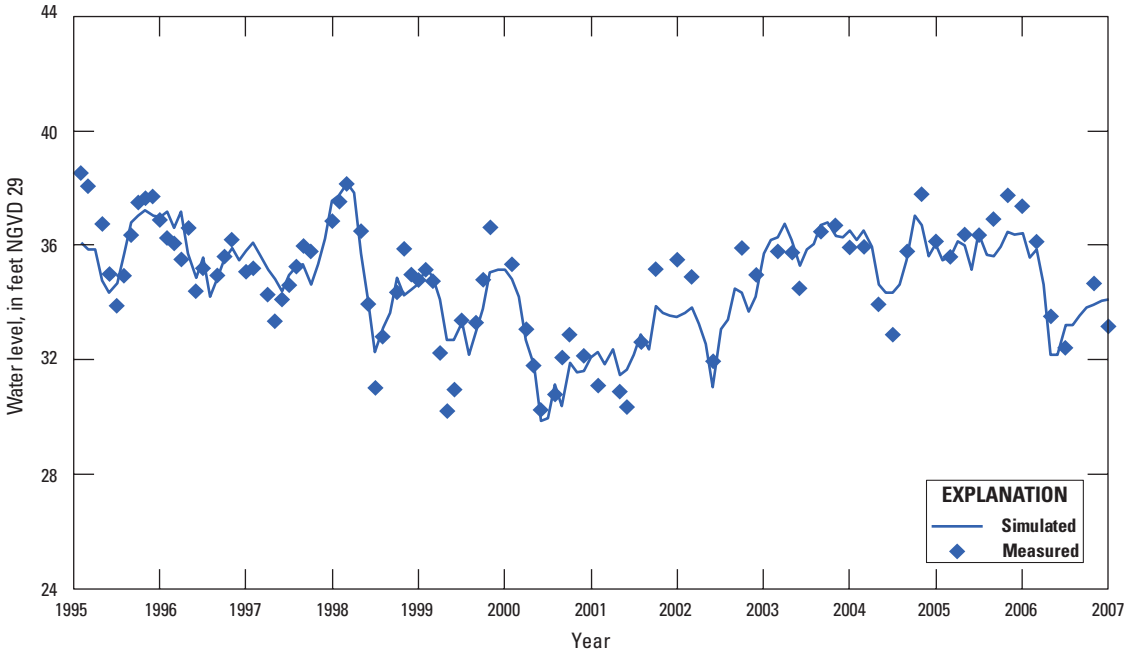

Figure 5–39. Measured and simulated water-level hydrographs for OR0265 Cocoa F, well number 14 in figure 5–26.

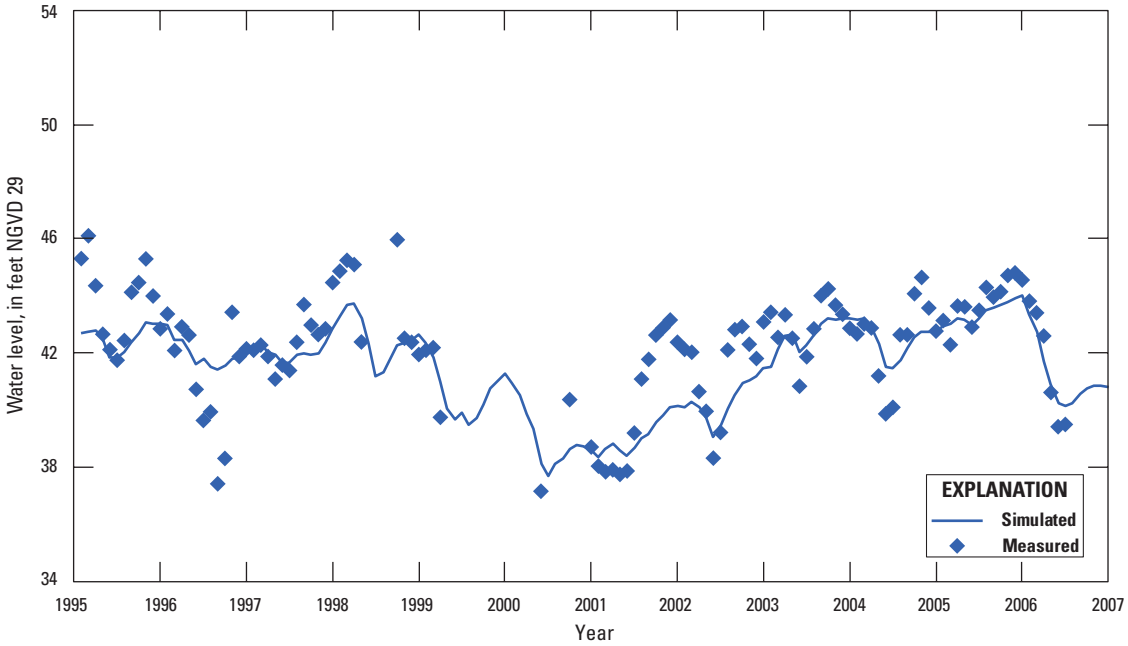

Figure 5–40. Measured and simulated water-level hydrographs for OS0019 Bull Creek Loop Rd SW, well number 15 in figure 5–26.

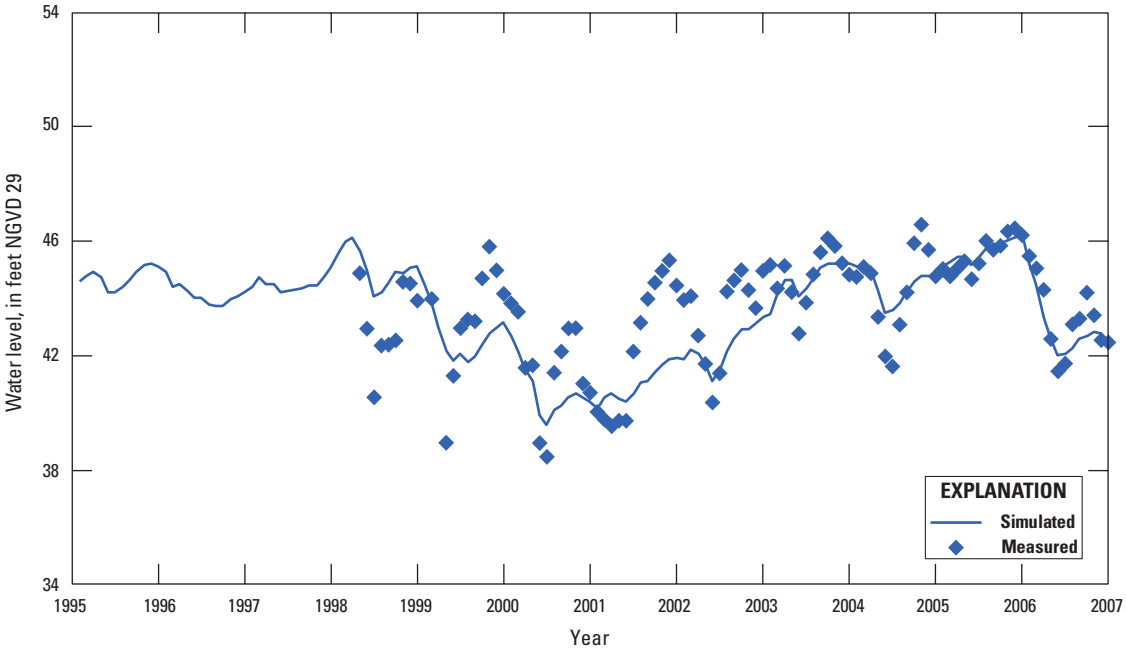

Figure 5–41. Measured and simulated water-level hydrographs for OS0231 Campbell Ranch, well number 16 in figure 5–26.

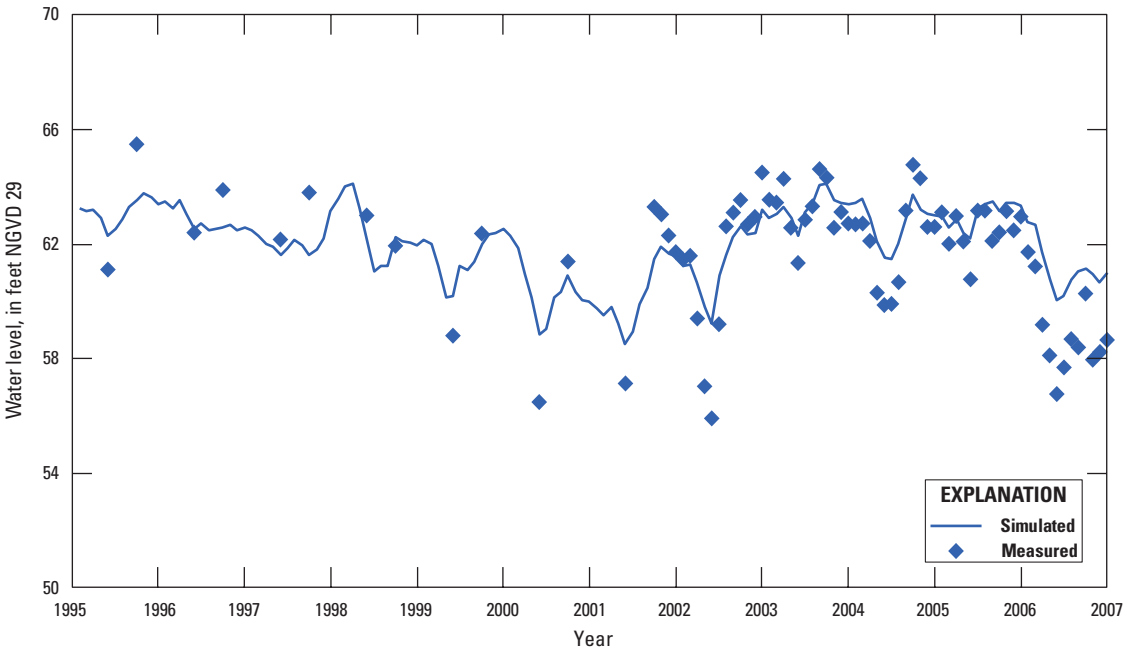

Figure 5–42. Measured and simulated water-level hydrographs for Reedy Creek OSF-11, well number 17 in figure 5–26.

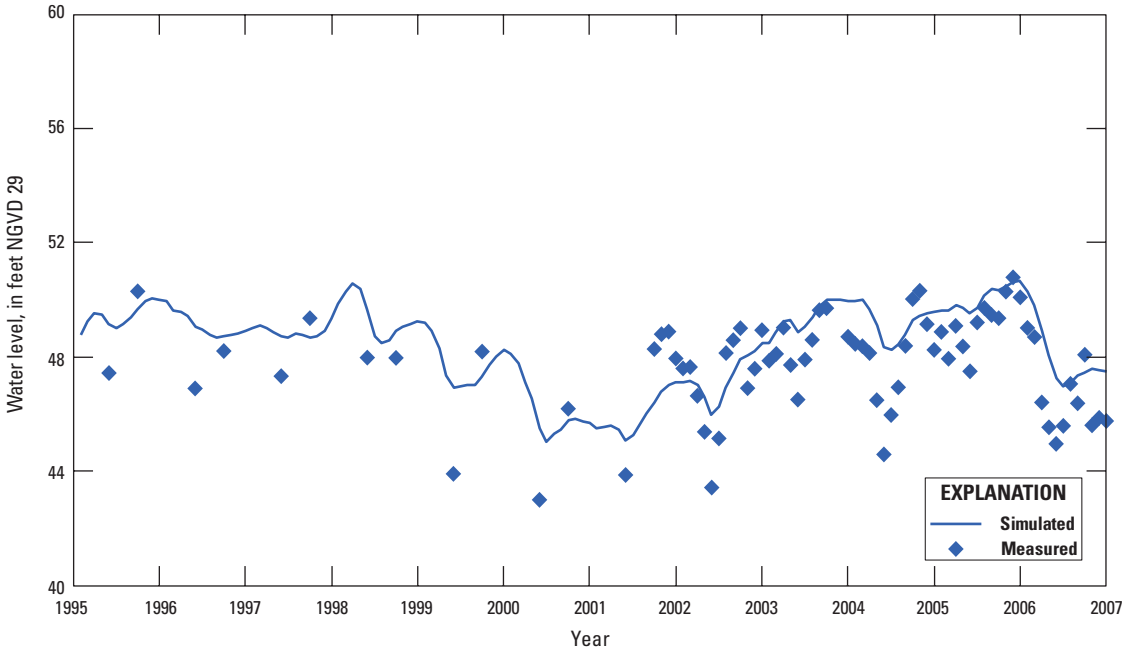

Figure 5–43. Measured and simulated water-level hydrographs for OSF–4 Joe Overstreet, well number 18 in figure 5–26.

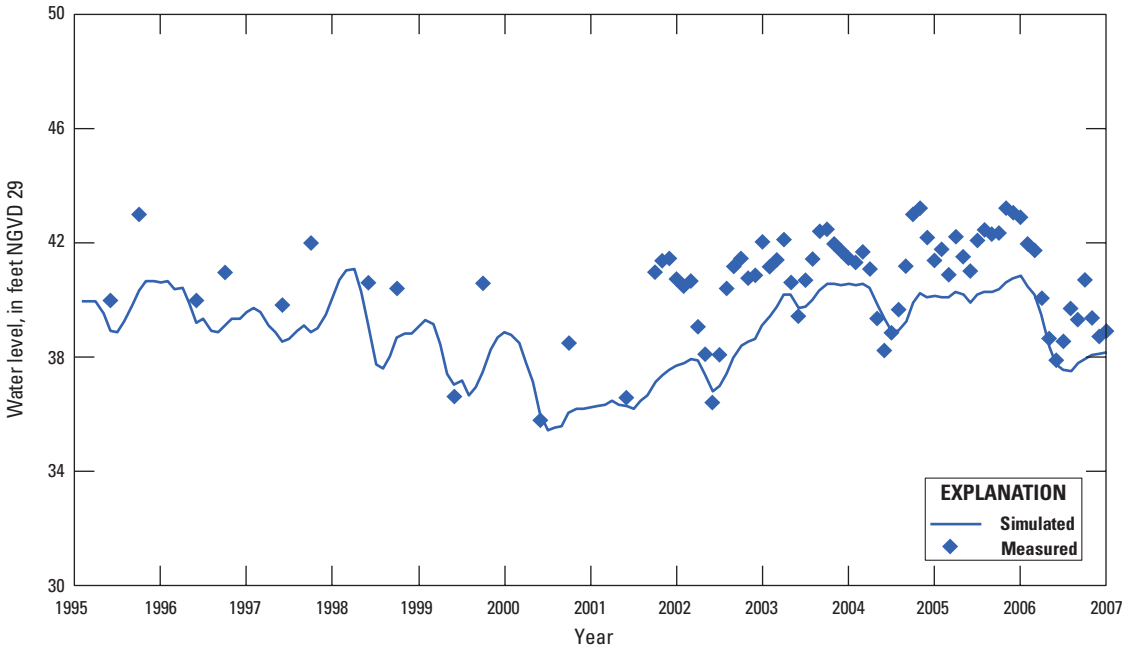

Figure 5–44. Measured and simulated water-level hydrographs for OSF-93 TH-9 Nova Road 532 West, well number 19 in figure 5–26.

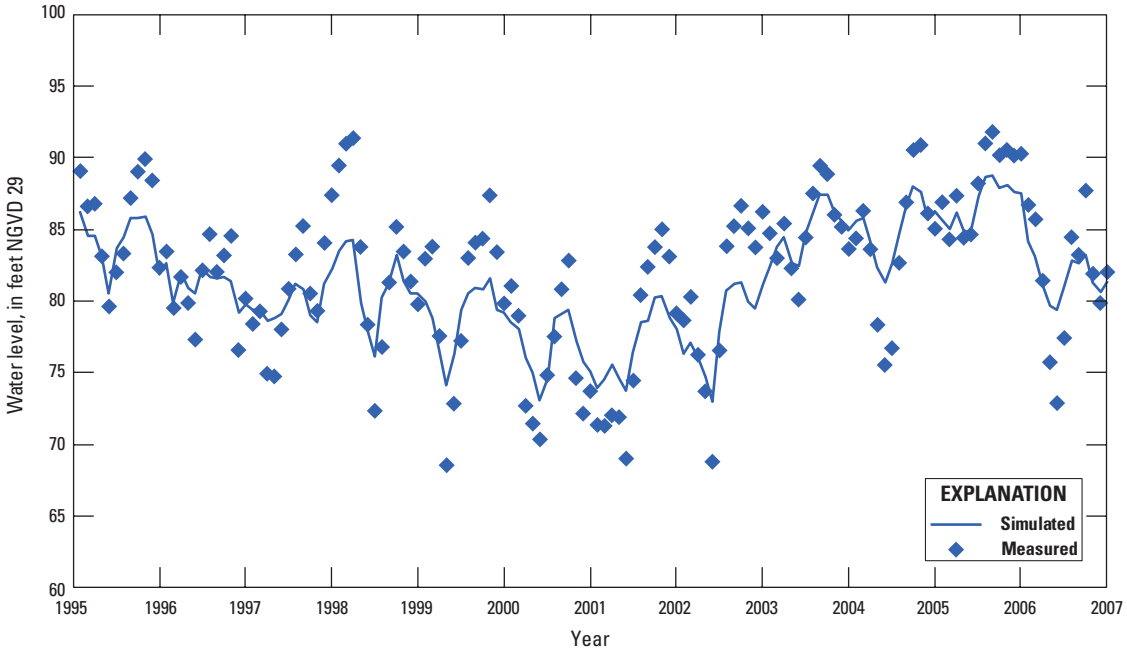

Figure 5–45. Measured and simulated water-level hydrographs for Regional Observation and Monitor-well Program CL-3 Floridan, well number 21 in figure 5–26.

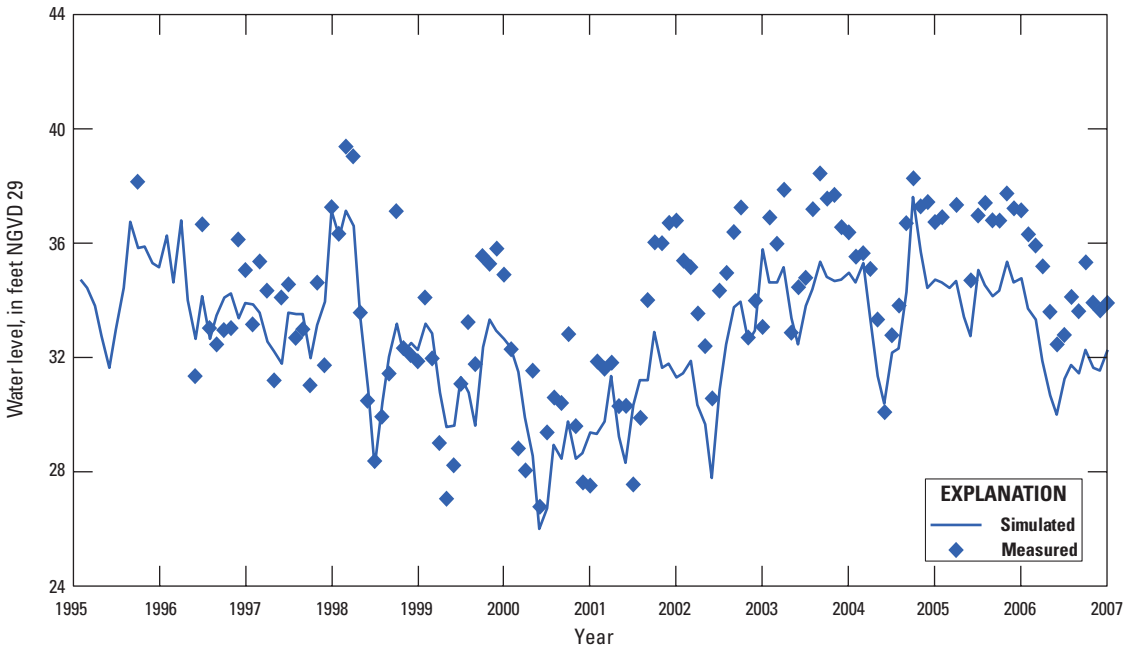

Figure 5–46. Measured and simulated water-level hydrographs for S-1193, well number 22 in figure 5–26.

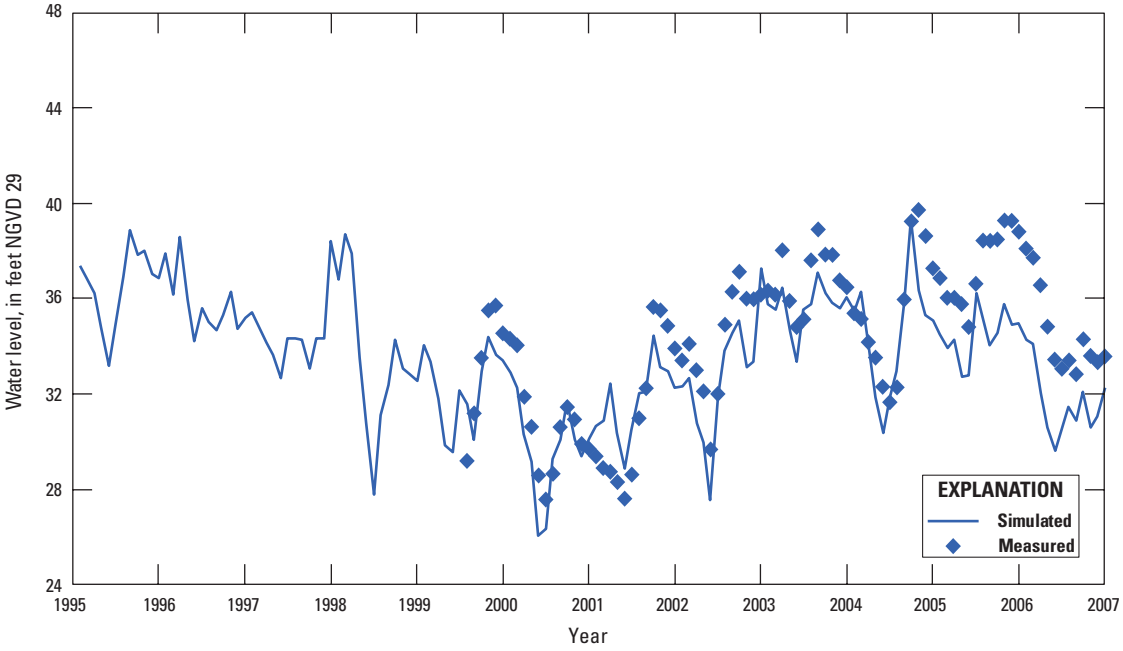

Figure 5–47. Measured and simulated water-level hydrographs for S-1408, well number 23 in figure 5–26.

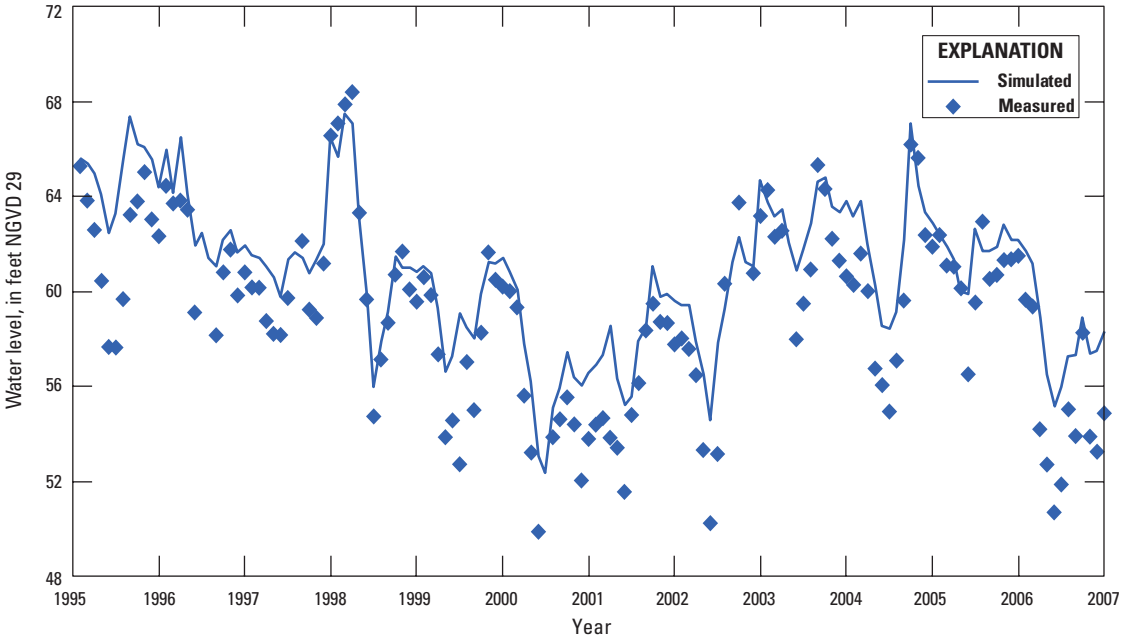

Figure 5–48. Measured and simulated water-level hydrographs for Sea World Drive replacement, well number 24 in figure 5–26.

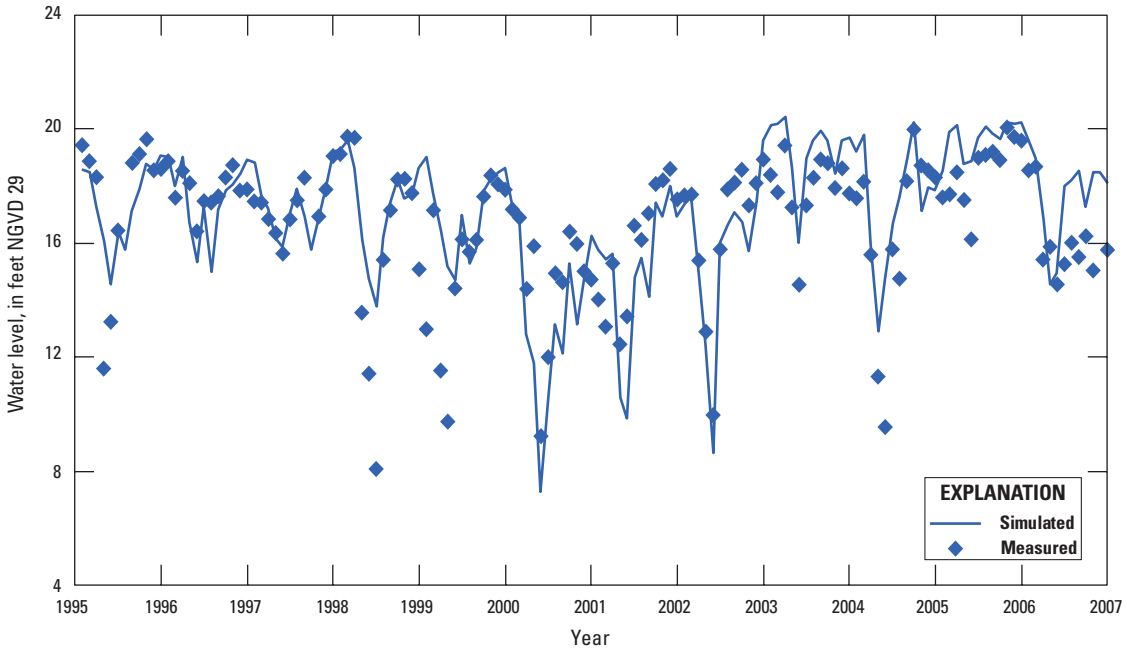

Figure 5–49. Measured and simulated water-level hydrographs for V-0198 at Lake Ashby Tower, well number 25 in figure 5–26.

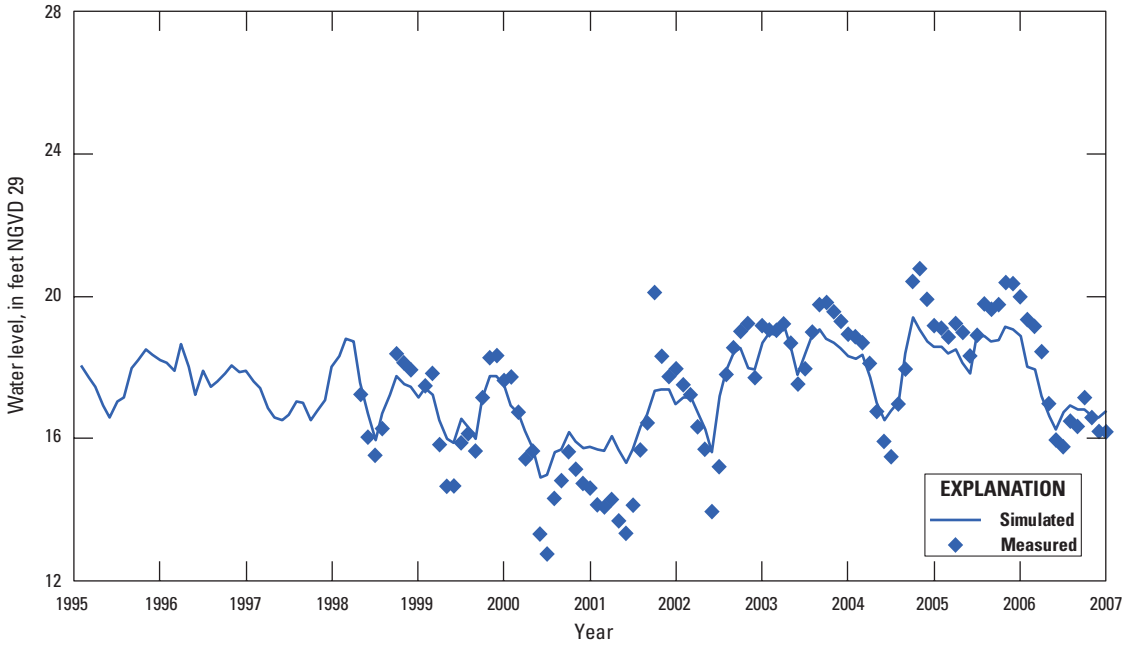

Figure 5–50. Measured and simulated water-level hydrographs for V-0818 Osteen Well, well number 26 in figure 5–26.

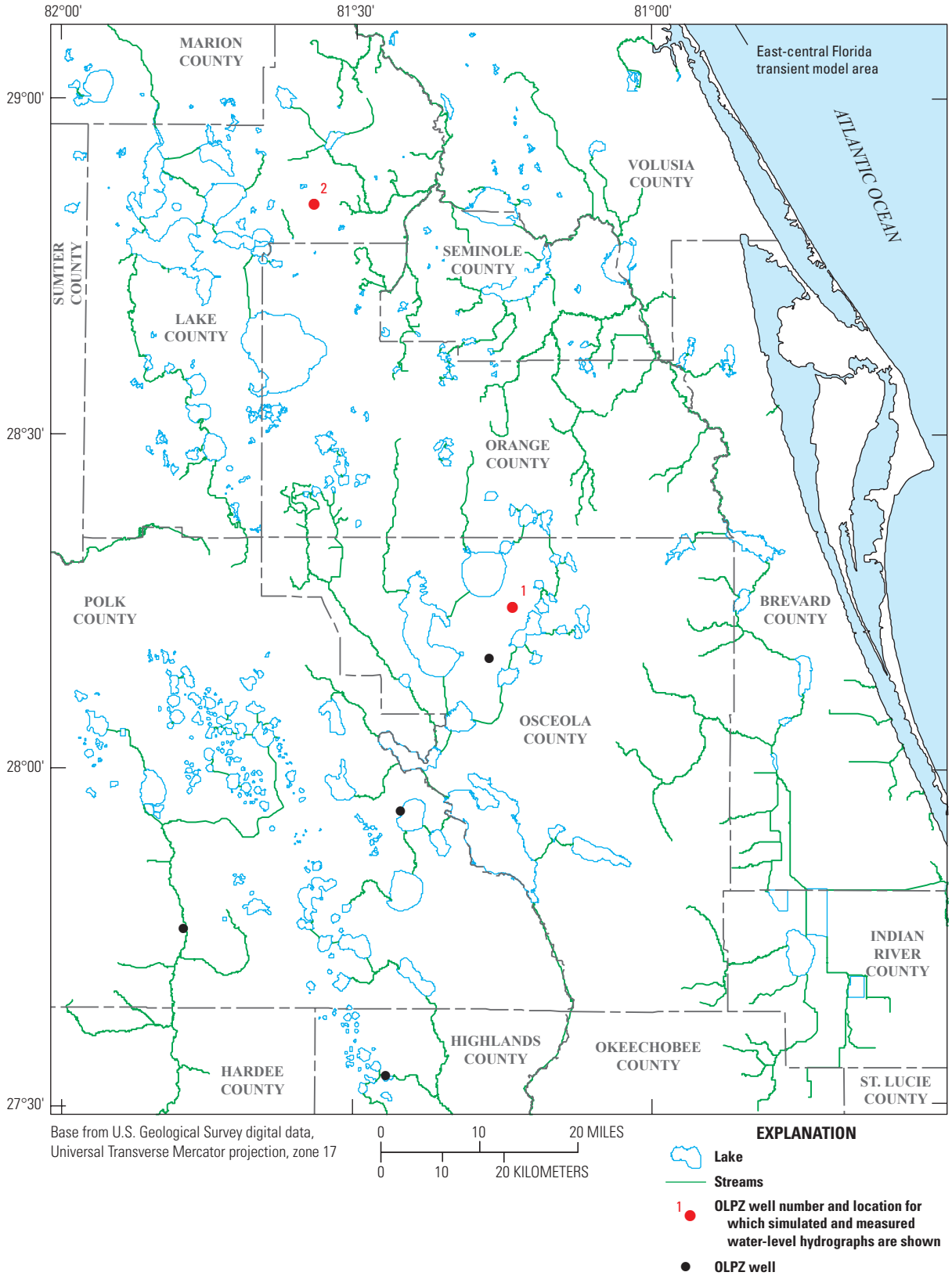

Figure 5–51. Selected Ocala low-permeable zone (OLPZ) wells for which simulated and measured water-level hydrographs are shown.

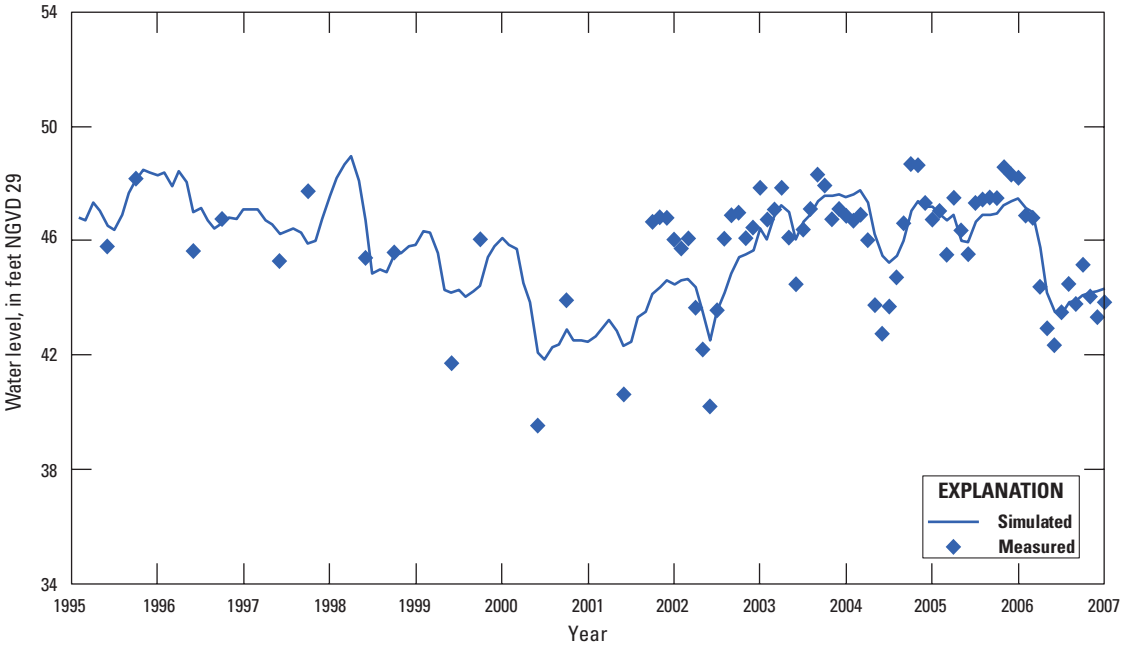

Figure 5–52. Measured and simulated water-level hydrographs for Ashton Forestry Tower, well number 1 in figure 5–51.

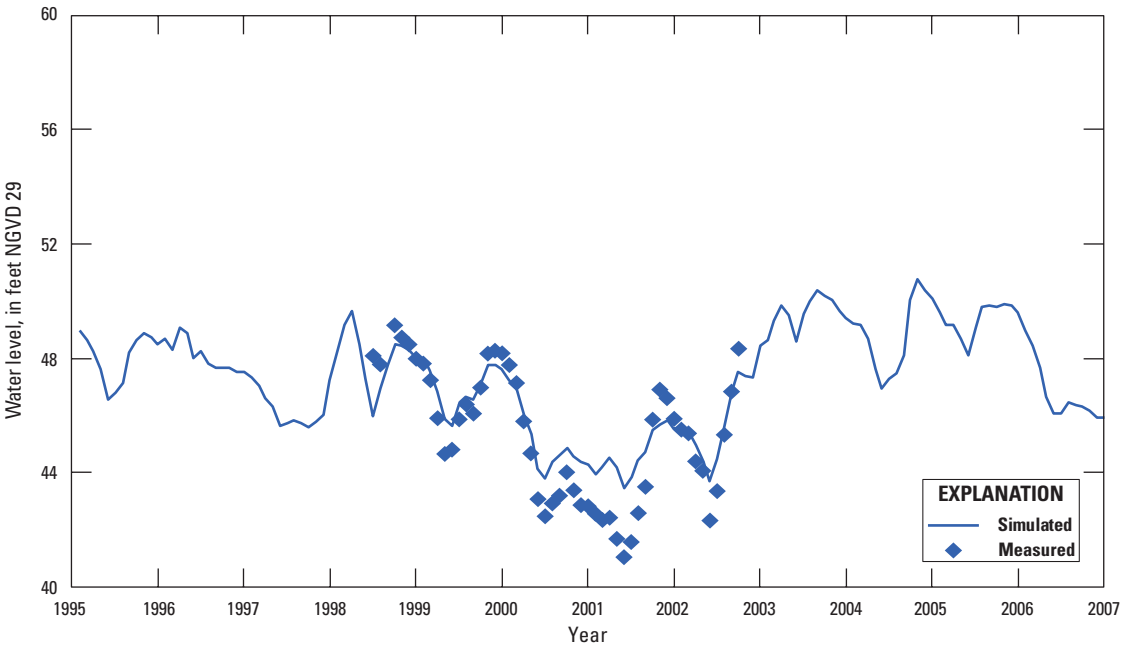

Figure 5–53. Measured and simulated water-level hydrographs for L-0704 Eustis Spray Field at Eustis, well number 2 in figure 5–51.

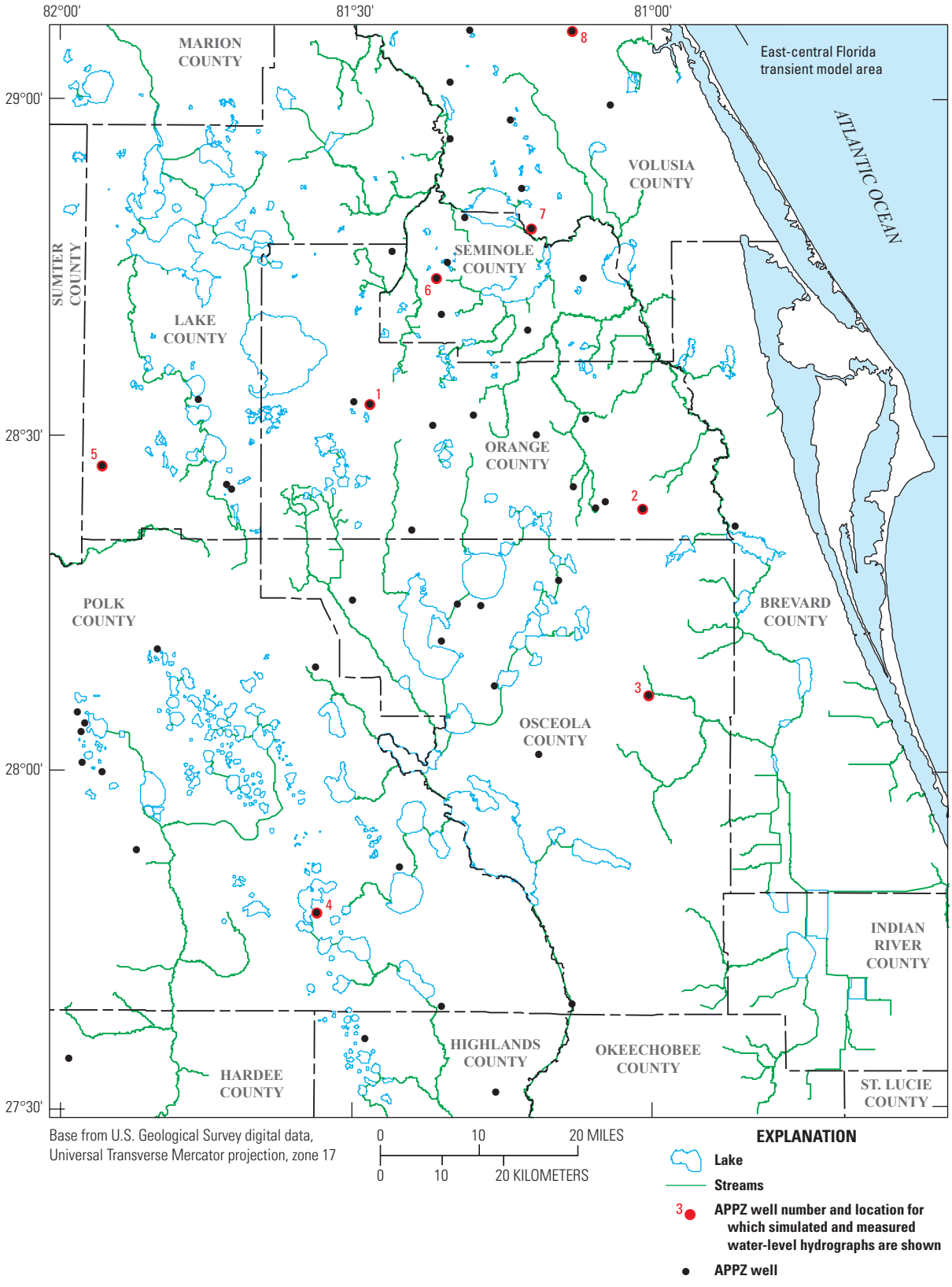

Figure 5–54. Selected Avon Park permeable zone (APPZ) wells for which simulated and measured water-level hydrographs are shown.

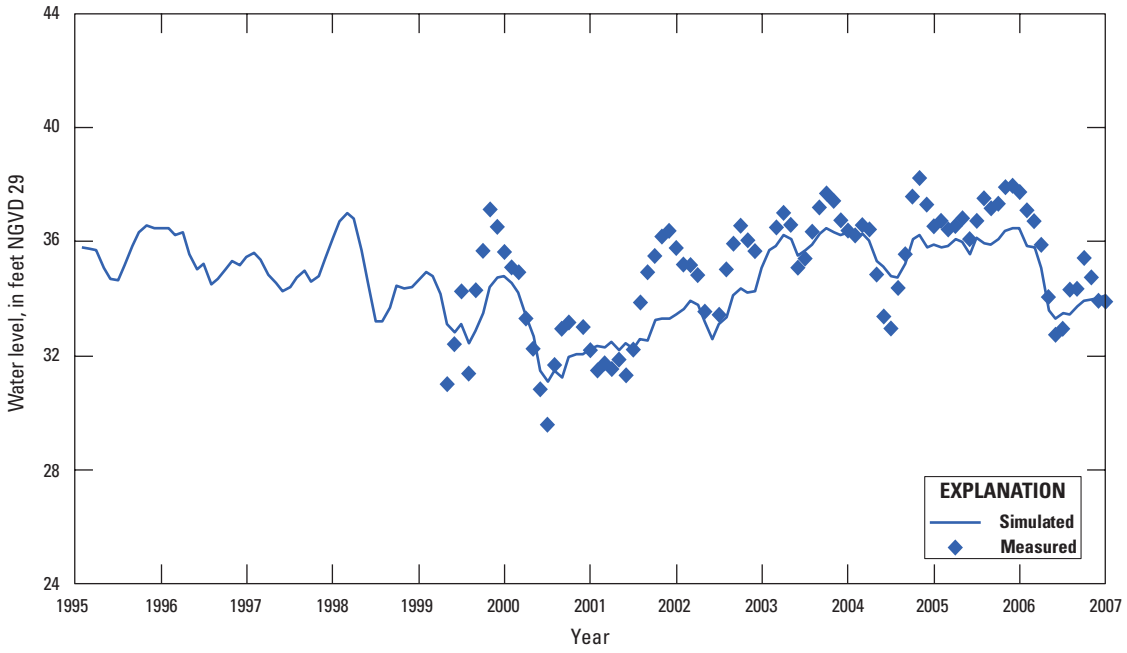

Figure 5–55. Measured and simulated water-level hydrographs for OR0673 Cocoa Well Field Site 13T, well number 2 in figure 5–54.

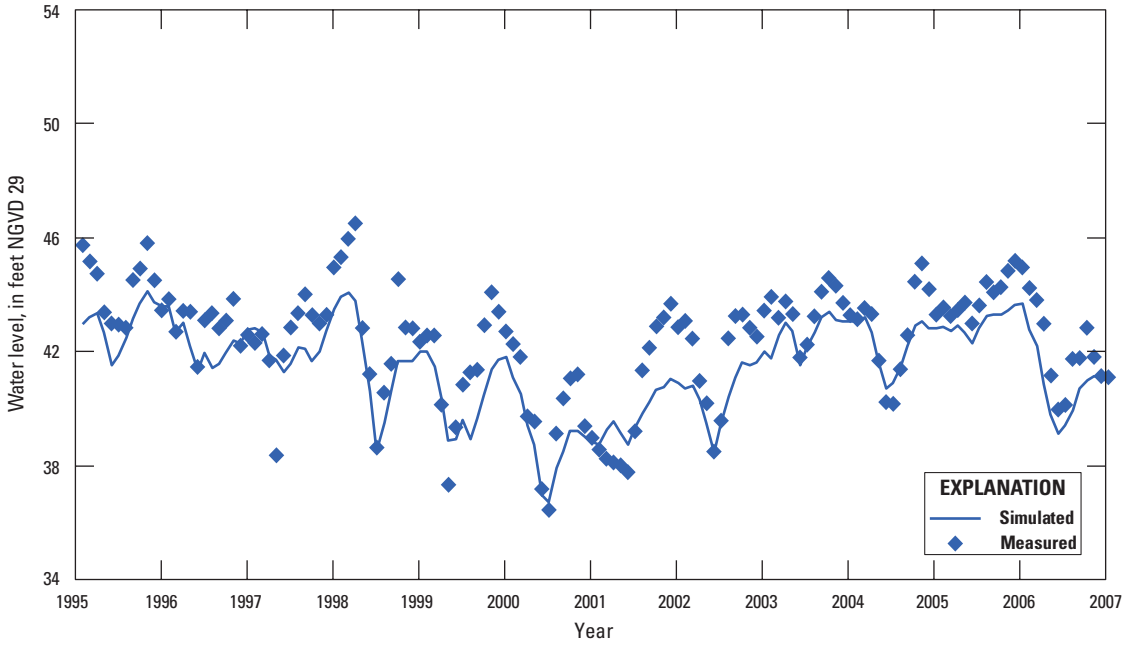

Figure 5–56. Measured and simulated water-level hydrographs for OS0022 Bull Creek APT Site 1, well number 3 in figure 5–54.

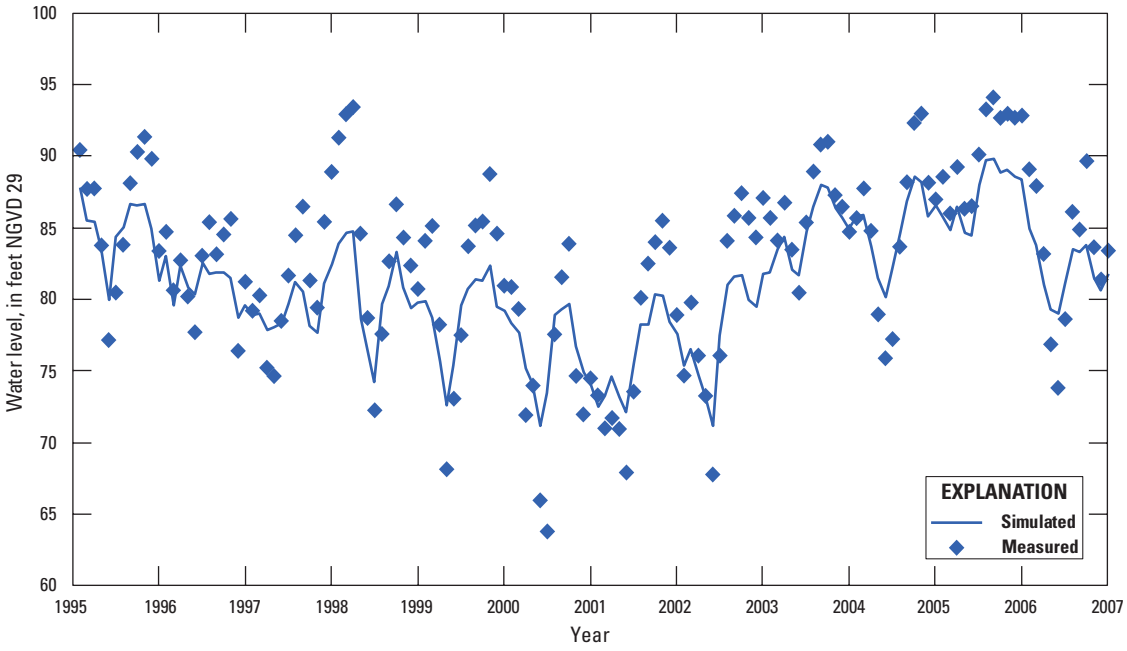

Figure 5–57. Measured and simulated water-level hydrographs for Regional Observation and Monitor-Well Program 55 Floridan, well number 4 in figure 5–54.

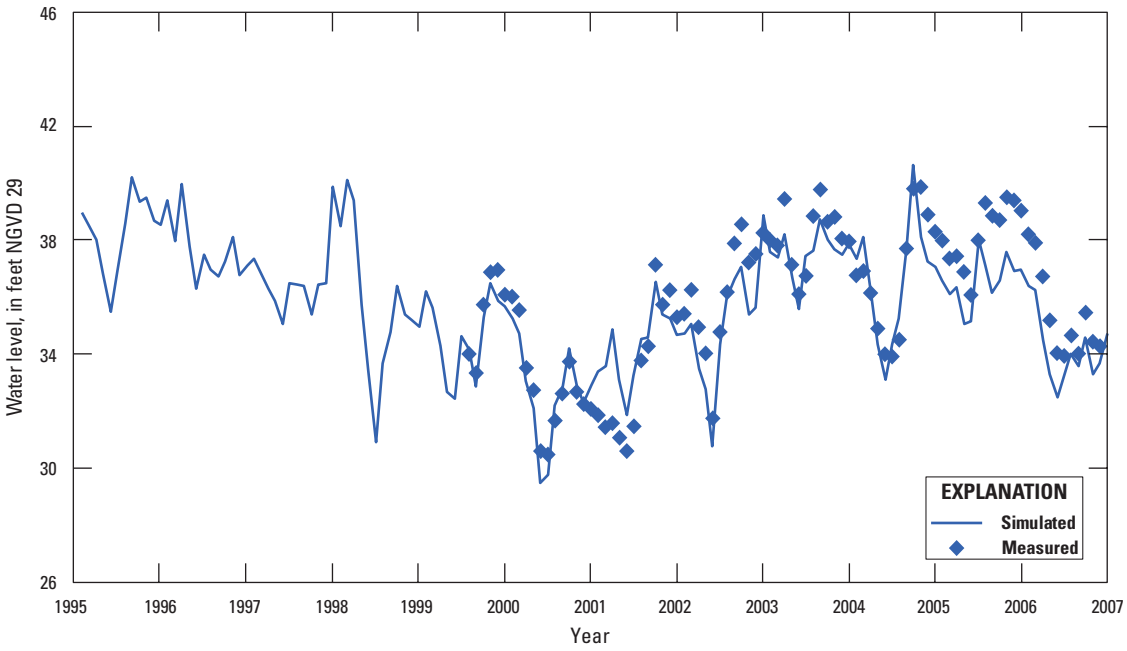

Figure 5–58. Measured and simulated water-level hydrographs for S-1407 Lake Mary Disposal, well number 6 in figure 5–54.

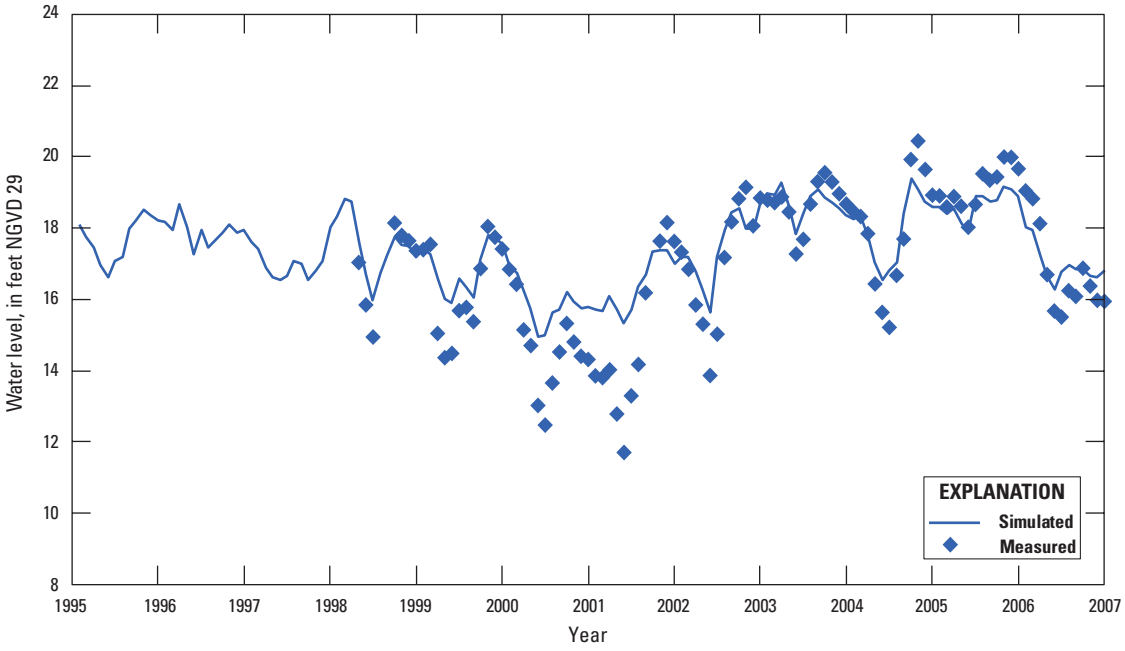

Figure 5–59. Measured and simulated water-level hydrographs for V-0801, well number 7 in figure 5–54.

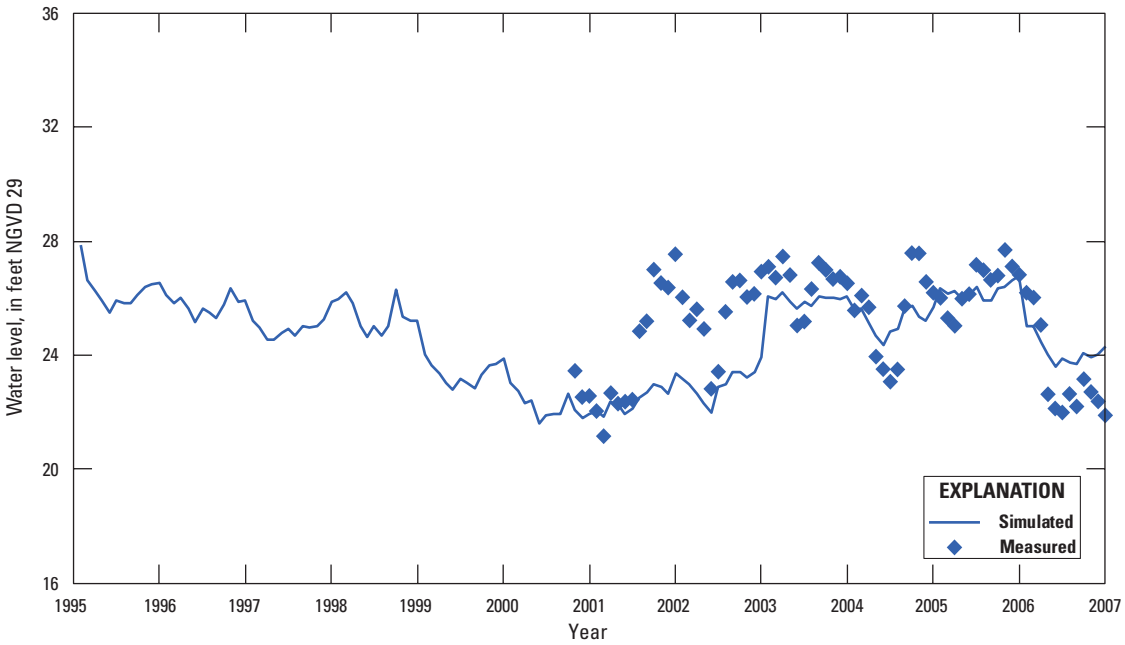

Figure 5–60. Measured and simulated water-level hydrographs for V-1098 Shunz Road, well number 8 in figure 5–54.

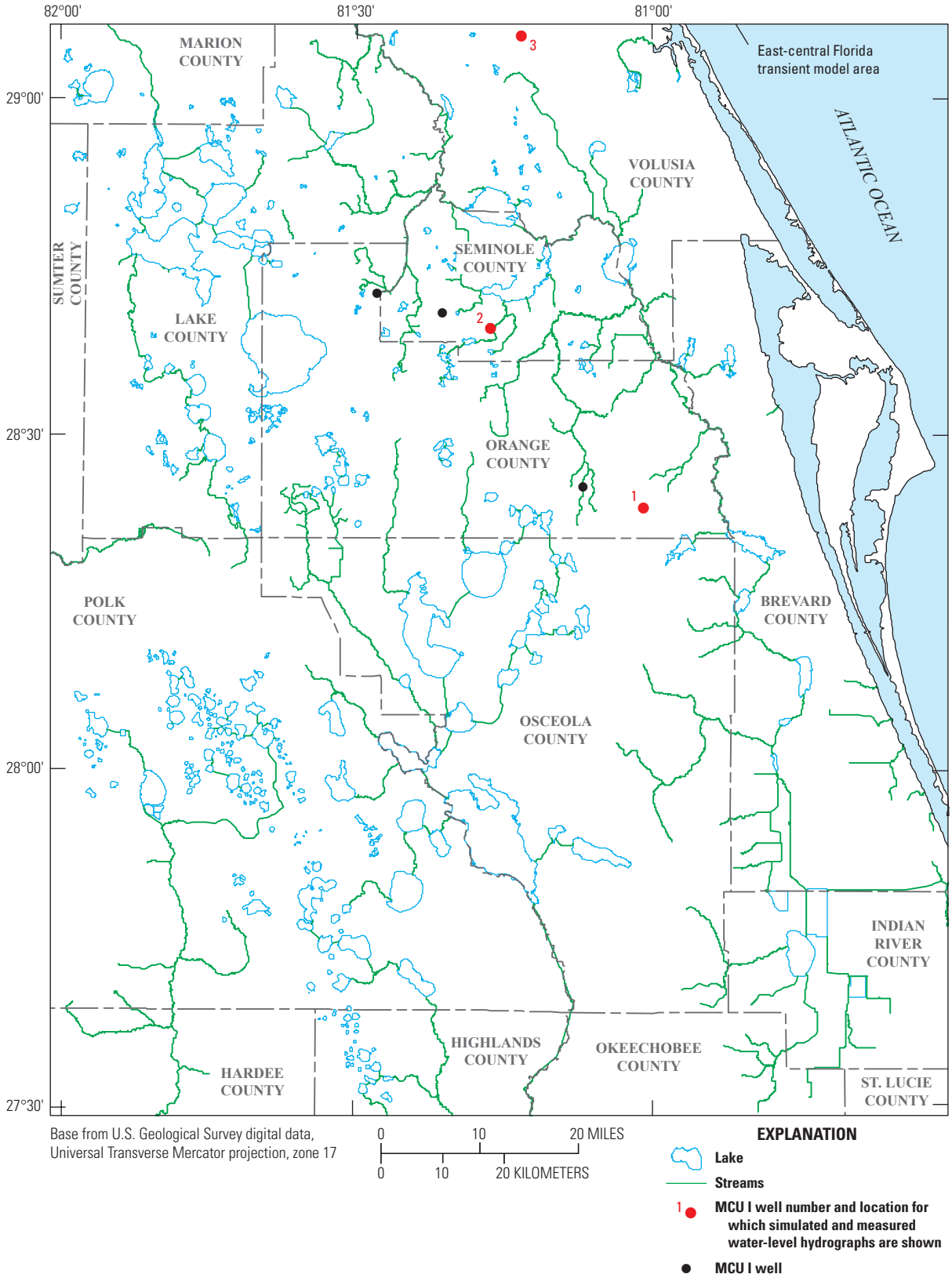

Figure 5–61. Selected middle confining unit I (MCU I) wells for which simulated and measured water-level hydrographs are shown.

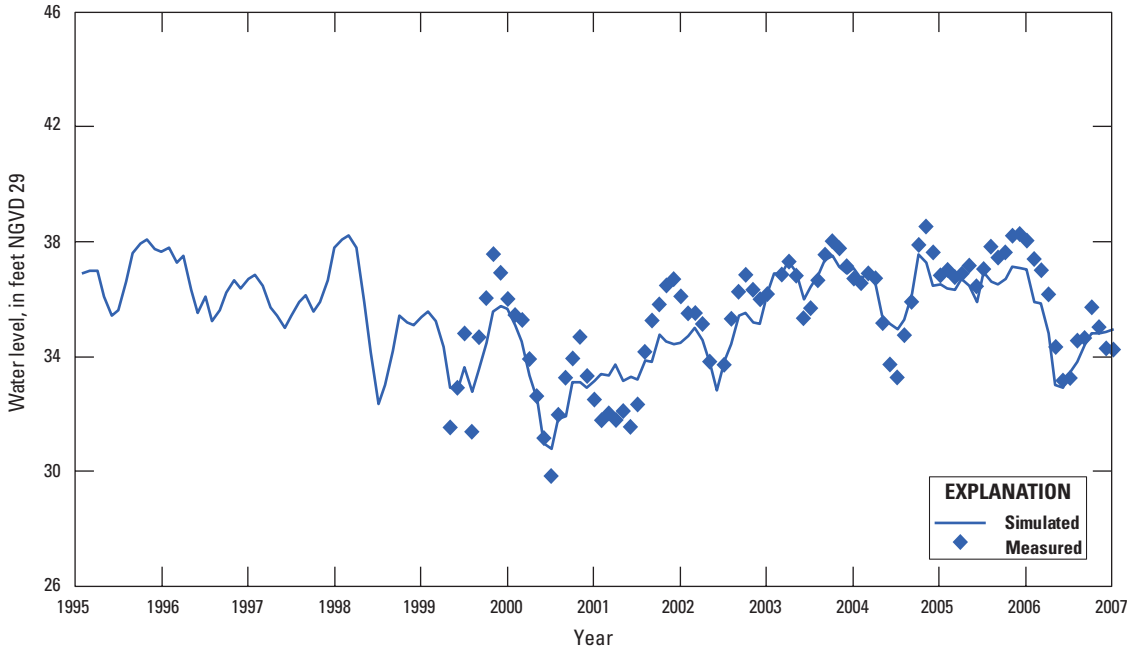

Figure 5–62. Measured and simulated water-level hydrographs for OR0675 Cocoa Well Field Site 13T, well number 1 in figure 5–61.

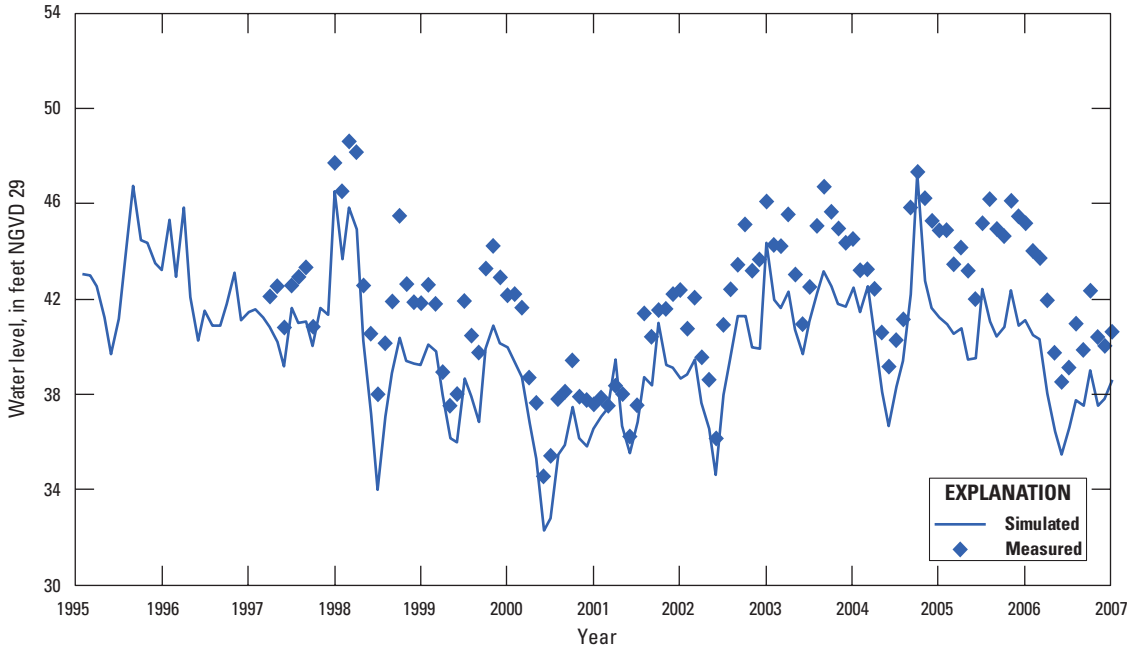

Figure 5–63. Measured and simulated water-level hydrographs for S-1257 Citrus Road Winter Springs, well number 2 in figure 5–61.

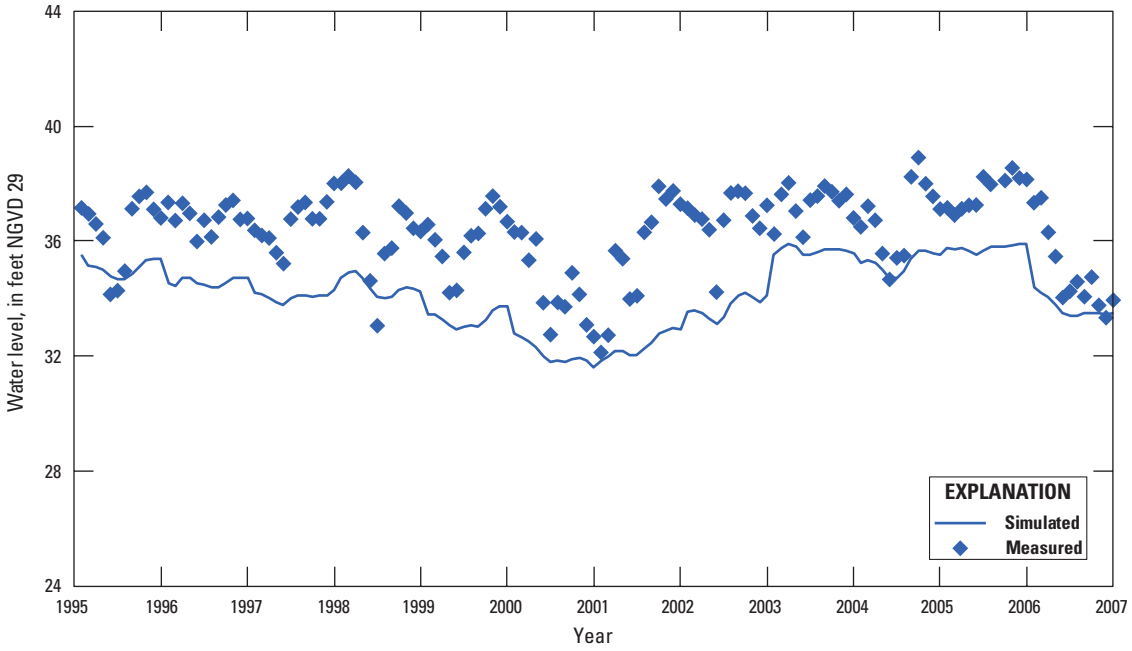

Figure 5–64. Measured and simulated water-level hydrographs for V-0081, well number 3 in figure 5–61.

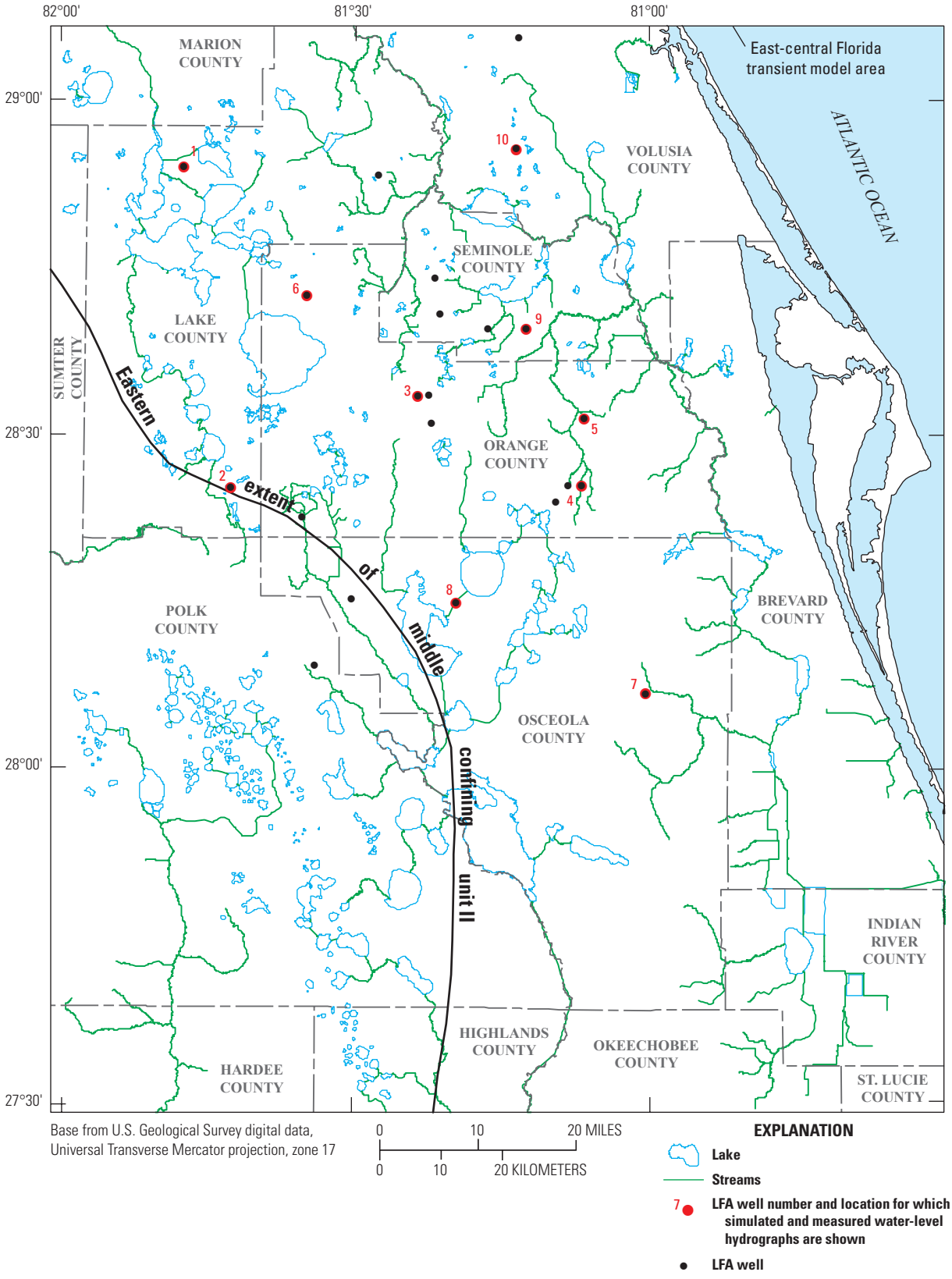

Figure 5–65. Selected Lower Floridan aquifer (LFA) wells for which simulated and measured water-level hydrographs are shown.

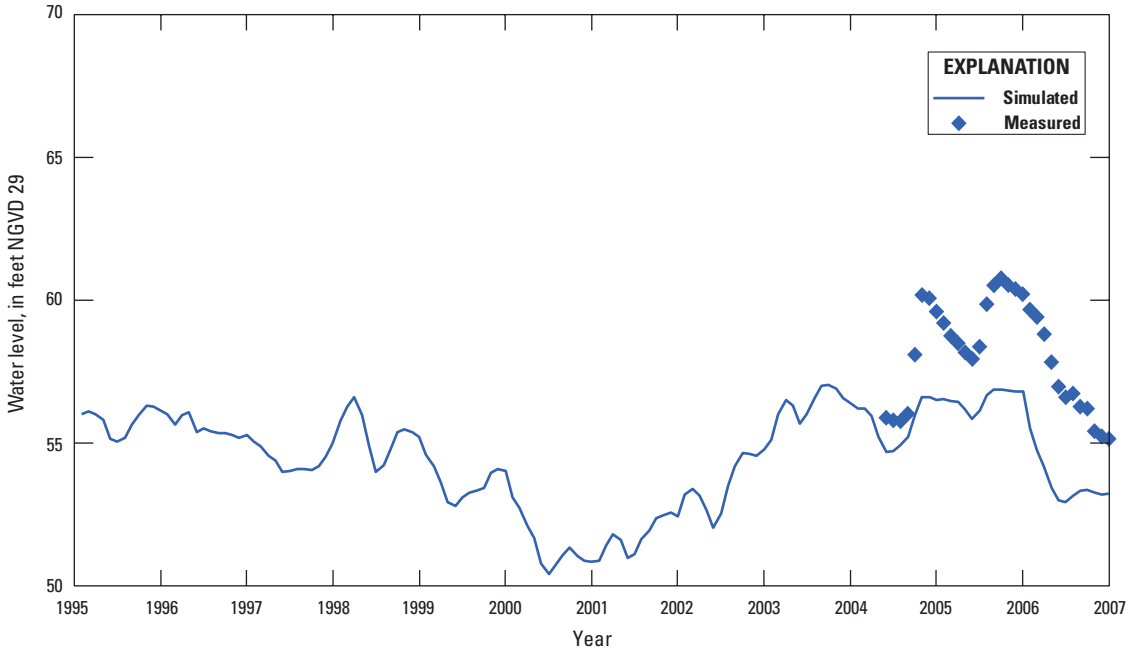

Figure 5–66. Measured and simulated water-level hydrographs for L-0599 Carrot Barn, well number 1 in figure 5–65.

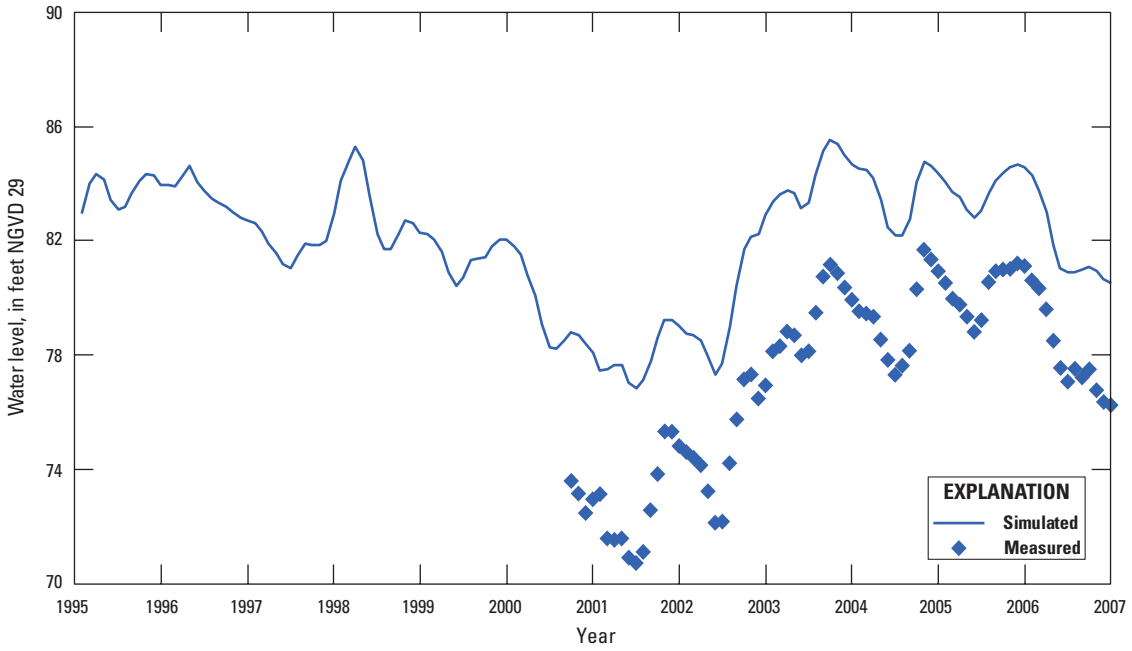

Figure 5–67. Measured and simulated water-level hydrographs for L-0729 Keene Lake, well number 2 in figure 5–65.

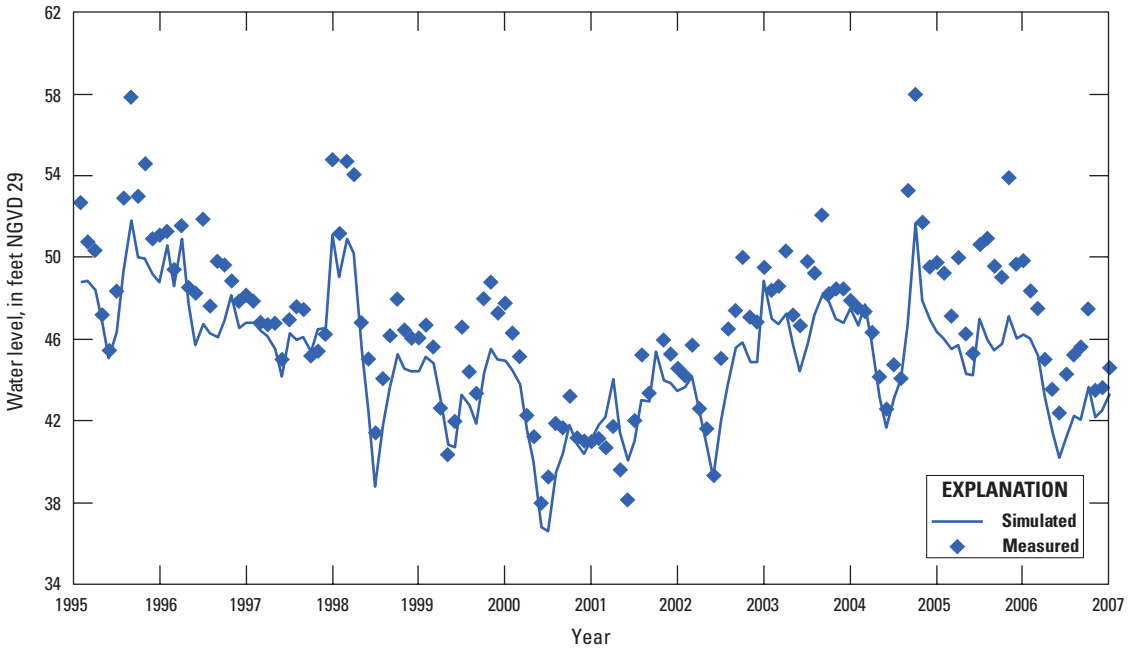

Figure 5–68. Measured and simulated water-level hydrographs for OR0009 Lake Adair 9, well number 3 in figure 5–65.

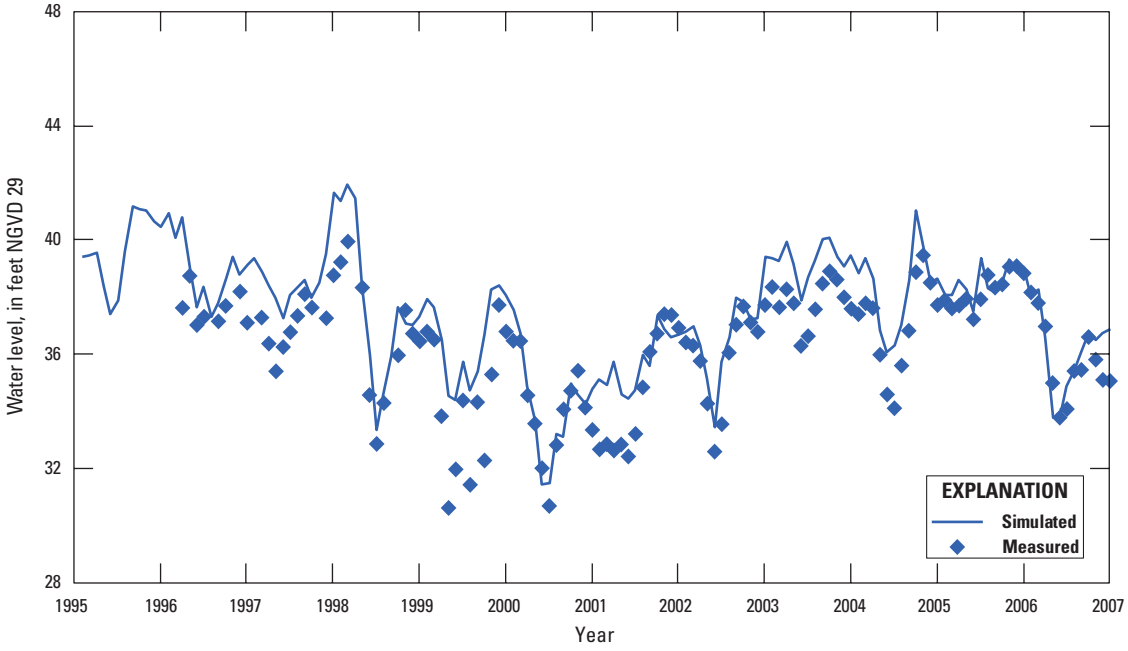

Figure 5–69. Measured and simulated water-level hydrographs for OR0618 Long Branch, well number 5 in figure 5–65.

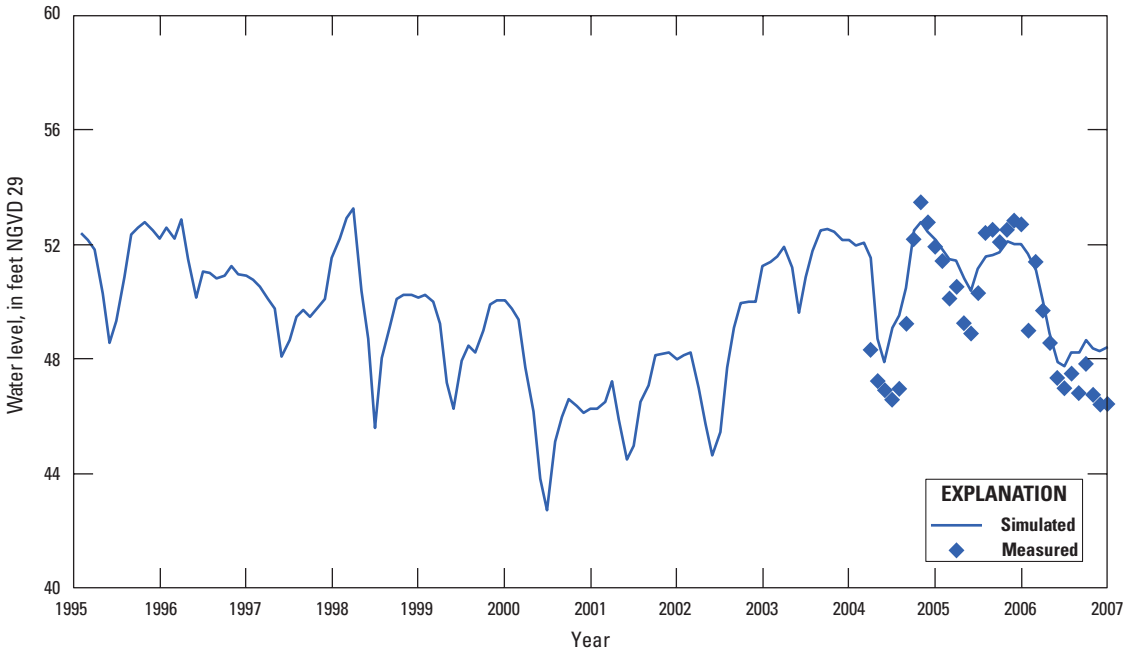

Figure 5–70. Measured and simulated water-level hydrographs for OR0794 Plymouth Tower, well number 6 in figure 5–65.

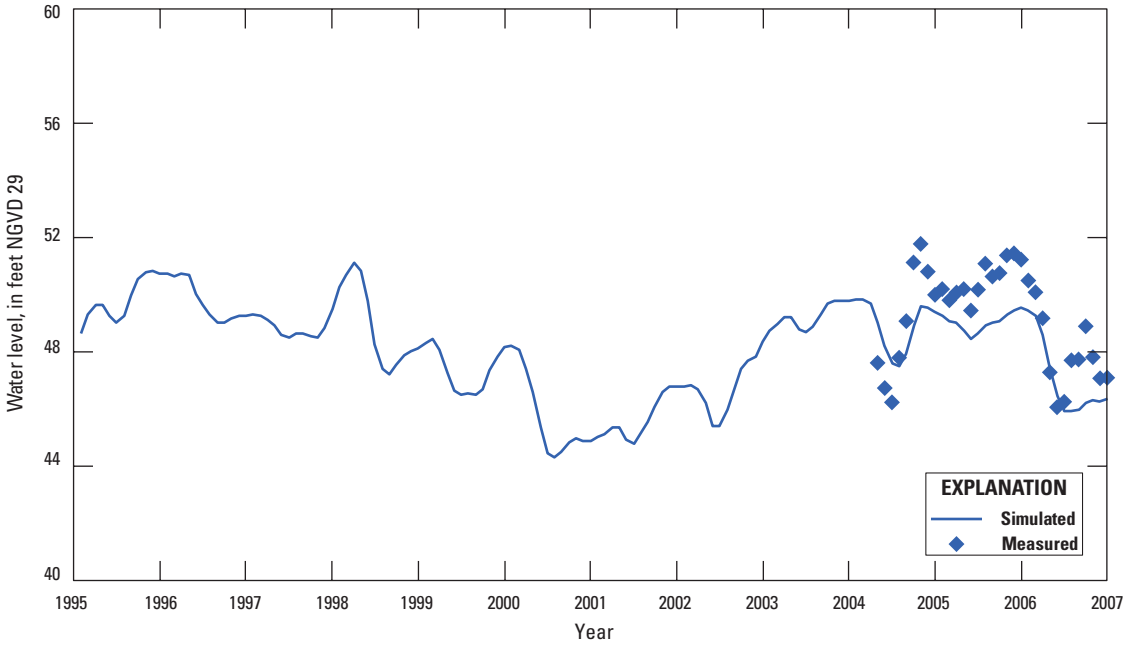

Figure 5–71. Measured and simulated water-level hydrographs for OSF-82L, well number 8 in figure 5–65.

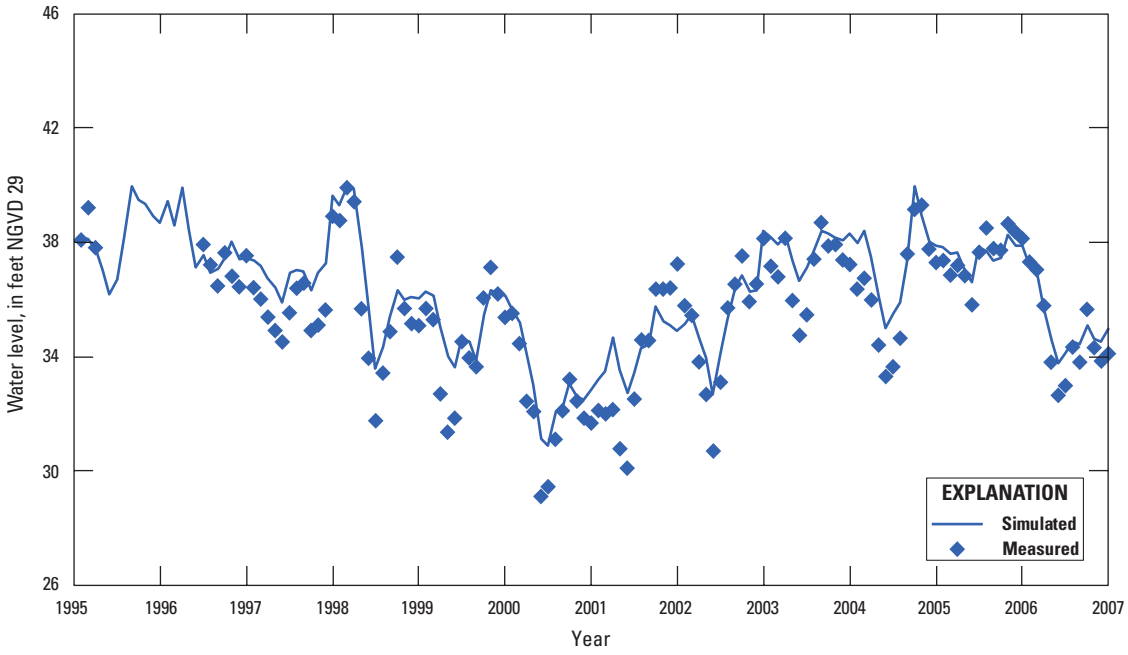

Figure 5–72. Measured and simulated water-level hydrographs for S-1078 Oviedo WTP, well number 9 in figure 5–65.

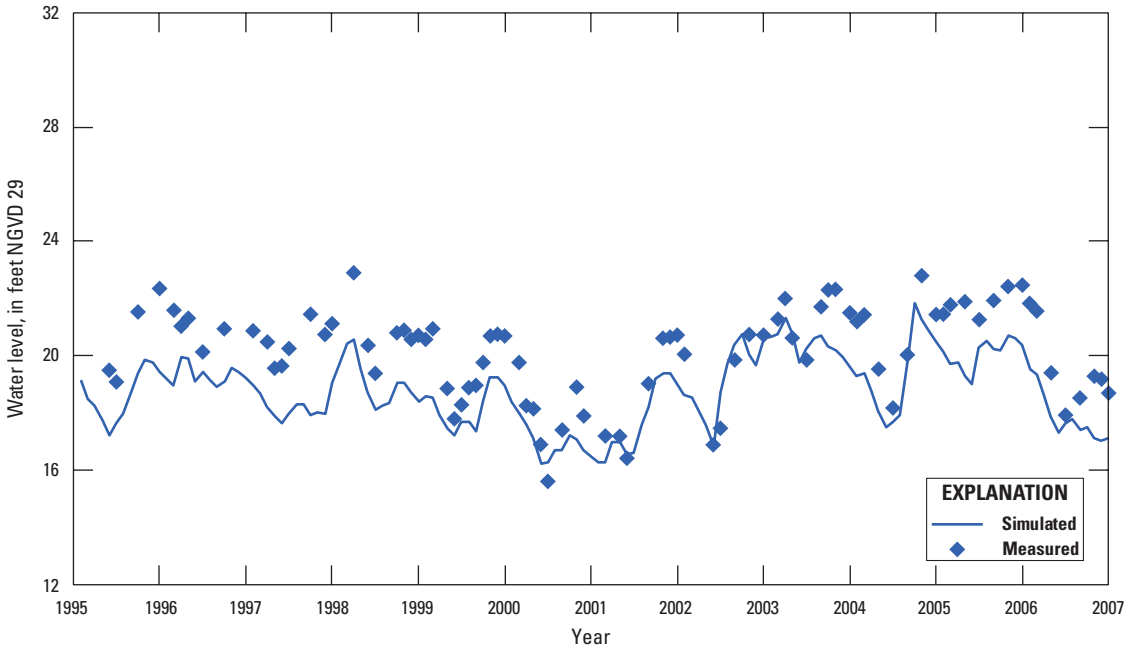

Figure 5–73. Measured and simulated water-level hydrographs for V-0774 Galaxy Middle School, well number 10 in figure 5–65.

Manuscript approved July 24, 2012

For more information about this publication, contact:
Nick Sepúlveda, Research Hydrologist
USGS Florida Water Science Center
12703 Research Parkway
Orlando, FL 32826
phone: (407) 803-5528
FAX: (407) 803-5501
e-mail: nsepul@usgs.gov

Or visit the Florida Water Science Center Web site at:
http://fl.water.usgs.gov

Prepared by the Raleigh Publishing Service Center
Edited by Mike G. Deacon
Illustrations by Kimberly A. Swidarski
Layout by Mike G. Deacon

A PDF version of this publication is available online at
http://pubs.usgs.gov/sir/2012/5161/